An Investigation of Reflective Cracking and Empirical Development of Design Specifications for Precast Composite Slab Span System (MnDOT PCSSS) Superstructures

A THESIS
SUBMITTED TO THE FACULTY OF THE GRADUATE SCHOOL
OF THE UNIVERSITY OF MINNESOTA
BY

David Michael Klaseus

IN PARTIAL FULFILLMENT OF THE REQUIREMENTS
FOR THE DEGREE OF
MASTER OF SCIENCE

Catherine W. French Carol K. Shield

March 2011

Acknowledgments

The research reported herein was sponsored by the National Cooperative Highway Research Program (NCHRP) under project 10-71 *Cast-in-Place Concrete Connections for Precast Deck Systems*. I would like to thank my advisors, Dr. Cathy French and Dr. Carol Shield, for their exceptional guidance and valuable advice. I would also like to thank all those who helped with the construction, instrumentation, and testing of the laboratory specimen constructed during this project, specifically Paul Bergson, Rachel Gaulke, Dan Sleigh, Eric Matzke, Roberto Piccinin, Brock Hedegaard, and Phil Cici. This project included the use of a laboratory specimen constructed by a previous student, Matthew Smith, who provided continued assistance regarding as-built details as necessary.

Several entities provided materials and guidance towards the completion of this project. As mentioned above, the NCHRP provided all of the funding for this project. The Minnesota Department of Transportation provided engineering insight regarding PCSSS design. County Materials of Roberts Wisconsin provided assistance in the design and fabrication of the precast inverted-T members. Gresser Construction Company of Eagan Minnesota provided the necessary concrete placement equipment during the construction of the laboratory specimens. Advance Shoring of St. Paul Minnesota also provided the shoring required for the disassembly and removal of the laboratory specimens from the University of Minnesota structures laboratory.

Finally, I would like to thank my parents, Steve and Corine Klaseus, whose continued support and assistance have been indispensible throughout my academic pursuits.

Abstract

The need to replace the deteriorating highway bridge infrastructure in the United States while minimizing the disruption to motorists has promoted the development of innovative construction techniques. To address this demand, a promising design has been developed by the Minnesota Department of Transportation (MnDOT) based on the French Poutre Dalle slab span bridge system. The MnDOT design, which is a precast composite slab span system (PCSSS), is practical for short to moderate spans up to approximately 65 ft. The PCSSS design requires no formwork or shoring during the construction process, while also making use of precast elements without the need for transverse post-tensioning.

A significant deterrent to the implementation of the PCSSS nationally was the lack of detailed design specifications and limited knowledge of the behavior of the system. To address these limitations, the current study involved the development of several large scale laboratory research specimens with the objective of investigating the development and control of reflective cracking at the discontinuities created by the longitudinal joints between adjacent precast panels. Also considered during this study included the effects and necessity of horizontal tie reinforcement on the development of composite action in the PCSSS.

This paper describes the laboratory investigation and analysis of the MnDOT PCSSS in reference to these behaviors and the development of a comprehensive design guide and code specifications for the AASHTO *LRFD Bridge Design Specifications*.

Table of Contents

List of Tables

List of Figures

Chapter 1: Introduction and Research Approach

1.0 Introduction

The aging highway bridge infrastructure in the United States is subjected to increasing traffic volumes and must be continuously renewed while accommodating traffic flow. Speed of construction, especially for the case of bridge replacement and repair projects, is a critical issue. Disruption of traffic and inconvenience to motorists, let alone major safety issues arising from detours, has encouraged the development of rapid construction methods. The issue of speed of construction, combined with higher labor costs and more variable quality control associated with on-site concrete casting, construction and motorist safety issues, political pressures, and environmental concerns, has paved the way for wider acceptance for the use of precast elements to speed construction.

Depending on the specific site conditions, the use of prefabricated bridge systems can minimize traffic disruption, improve work-zone safety, minimize impact to the environment, improve constructability, increase quality, and lower life-cycle costs. This technology is applicable and needed for both existing bridge replacement and new bridge construction. Over the past 50 years, thousands of short to medium span bridges have been built using precast concrete elements. Replacing an entire highway bridge including the substructure over a weekend has been accomplished through intense planning (Merwin 2003). In 1993, four bridges, each with spans ranging from 700 to 900 ft., were erected in less than 36 hours each including the substructures (Endicott 1993). Interestingly, the finished cost of the replacement project was significantly lower than the competing cast-in-place (CIP) alternatives. For many deficient bridges in the United States on the waiting list for replacement, it is imperative that new bridge construction be as economical as possible and yet be long lasting and nearly maintenance free (Tokerud 1979, Anderson 1972).

There are a large number of papers on the use of precast concrete elements in bridge systems including research on the use of precast elements such as deck panels for rapid deck replacement. On deck elements alone, there are nearly 200 references. The papers include research studies conducted at a number of universities including the University of Illinois, Chicago (Issa, 1995), and University of Nebraska (Tadros, 1998). Strong momentum exists for the growing use of precast construction; two recent projects to investigate precast decked systems include NCHRP 12-65 *Full-Depth, Precast-Concrete Bridge Deck Panel Systems* and NCHRP 12-69 *Design and*

Construction Guidelines for Long-Span Decked Precast, Prestressed Concrete Girder Bridges. The present project NCHRP 10-71 *Cast-in-Place Reinforced Connections for Precast Deck Systems* complements the work that was developed under those studies.

NCHRP 12-65 addressed the development of transverse and longitudinal connections between full-depth, precast-concrete bridge deck panels, with emphasis on systems without overlays and without post tensioning through the connection. NCHRP 12-69 addressed I-beam, bulb-tee, or multi-stemmed girders with integral decks cast and prestressed with the girder. The girders are erected abutting flanges of adjacent units, and load is transferred between the adjacent units using connections developed in the project.

The focus of the present project was to develop specifications, guidelines, and examples for the design and construction of durable CIP reinforced concrete connections for precast deck systems that emulate monolithic construction, considering issues including speed of construction, durability, and fatigue. The typical sequence of erecting bridge superstructures in the United States is to erect the precast prestressed concrete or steel beams, place either temporary formwork or stay-in-place formwork such as steel or concrete panels, place deck reinforcement, cast deck concrete, and remove formwork if necessary. This project focused on systems that reduce the need to place and remove formwork thus accelerating on-site construction and improving safety.

The system considered during this study to accomplish these objectives was identified during the 2004 Prefabricated Bridge Elements and Systems International Scanning tour (International Scanning Study Team (2005)). The scanning tour visited France, Belgium, Japan, and the Netherlands with eleven participants representing FHWA, State Departments of Transportation, National Association of County Engineers, industry, and academia. The study team developed a series of recommendations related to prefabricated elements and systems to be used for superstructure systems, along with substructure systems and movement systems for rapid replacement and construction. An example of this system included a French precast slab superstructure (Poutre Dalle) with overlapping looped reinforcement that extends into the longitudinal CIP connections. This superstructure, which is an entire bridge system, was specifically addressed in this project as a precast composite slab span system (PCSSS).

To implement these promising new systems, design guidelines and standard details were established. The developed guidelines also address the durability of the connection concepts including crack control. The PCSSS bridge design guidelines cover both component and system issues including “spalling” reinforcement, load distribution, effect of restraint moments,

composite action, and reinforcement to control reflective cracking; the research regarding end zone stresses (i.e., "spalling") and restraint moments were completed during separate research by Whitney Eriksson (2008) and Mathew Smith (Smith et. al., 2008), respectively.

The following sections summarize the objective and list of tasks associated with the NCHRP 10-71 project, *Cast-in-Place Concrete Connections for Precast Deck Systems*.

1.1. Scope of Study

The objective of this project was to develop guidance for the design and construction of durable CIP reinforced concrete connections for precast deck systems that emulate monolithic construction. This was accomplished through the following ten tasks.

1.1.1. Task 1 – Review relevant practice, performance, data, and research findings

Reviewed relevant practice, performance data, research findings, physical test results, and other information related to the design, fabrication, and installation of CIP reinforced concrete connections for precast deck systems that emulate monolithic construction. This information was gathered from technical literature and from unpublished experiences of engineers, bridge owners, and others. This review included the looped reinforcement details identified in Japan and France during the 2004 Prefabricated Bridge Elements and Systems International Scan.

1.1.2. Task 2 – Develop detailed design, fabrication, construction, and performance criteria

Developed detailed design, fabrication, construction, and performance criteria that were selected to provide durability, strength, fatigue resistance and rapid construction.

1.1.3. Task 3 – Develop conceptual designs for CIP reinforced concrete connections

Developed several conceptual designs for CIP reinforced concrete connections, including a comprehensive longitudinal connection detail for precast slab superstructures and three connection concepts for longitudinal or transverse connections between full-depth deck panels or deck flanges. The connection concepts were developed to not require overlays or post-tensioning.

Emphasis was placed on increasing construction speed while achieving durability and ride quality.

1.1.4. Task 4 – Develop an updated and detailed work plan

Developed an updated and detailed work plan for numerical and experimental evaluation of the conceptual designs based on the results of Tasks 2 and 3, including the development of large-scale connection test specimens.

1.1.5. Task 5 – Submit an interim report

The interim report was completed and submitted to seek approval to move forward with the work plan.

1.1.6. Task 6 – Execute the approved work plan for evaluation of the connections

This task represented the bulk of the effort for this project during which the approved work plan was executed for the evaluation of the connections.

1.1.7. Task 7 – Prepare a connection design, detailing guide, and construction guide

Prepared a comprehensive connection design and detailing guide, including a listing of all design steps with examples as needed for the connections that met the criteria established in Task 2.

1.1.8. Task 8 – Develop specification language and commentary

Developed specification language and commentary for recommended changes to the *AASHTO LRFD Bridge Design Specifications* and the *AASHTO LRFD Bridge Construction Specifications* as necessary to implement the recommended connection details.

1.1.9. Task 9 – Submit the products of Tasks 7 and 8 and the Draft Final Report

The products of Tasks 7 and 8 were submitted for panel review and comment.

1.1.10. Task 10 – Final Report

The research study has been documented in this final report. It includes the design and detailing guide with recommended modifications to the design specifications and a list of design steps and examples.

1.2. Introduction to Precast Composite Slab Span Systems (PCSSS)

Precast composite slab span systems (PCSSS) are a promising technology for the implementation of rapid construction techniques for bridge construction. The bridge systems are composed of precast, inverted-T sections, fabricated off-site and delivered to the jobsite ready for erection. The inverted-T sections are assembled such that no formwork is required prior to the placement of the CIP deck, which considerably reduces construction time related to the placement and removal of formwork. Transverse load transfer is achieved through the development of transversely oriented reinforcement protruding from the precast members. Furthermore, improved quality of the main superstructure can be achieved due to the rigid quality control associated with the fabrication of precast members, which may be difficult to achieve in cast-in-place (CIP) bridge construction.

The current study included an investigation of the literature related to precast composite slab span bridge systems and other relevant topics valuable in the development of PCSSS bridges. Included in this review was the work completed during a study commissioned by Mn/DOT (Smith et al., 2008) regarding a field and laboratory implementation of a PCSSS bridge. The laboratory bridge specimen utilized during the Mn/DOT study was subsequently made available for use with the NCHRP 10-71 project. The research conducted during the NCHRP 10-71 study included numerical parametric studies and further experimental studies of variables deemed to be important from the Mn/DOT study including the effects of reinforcement to control spalling, connection details for crack control, cyclic loading effects on crack development, and composite action between the precast and CIP.

Because of its similarity to slab-span bridge systems, the applicability of the AASHTO design provisions for slab-span systems were investigated in the study. The two primary considerations that distinguish PCSSS bridges from slab-span bridges are (1) the required reinforcement to control reflective cracking above the longitudinal joint between the precast flanges, and (2) the effect of restraint moments due to the composite nature of the system. With regard to the issue of reflective crack control, in addition to a numerical investigation regarding the effect of the transverse reinforcement, the issue was also studied in laboratory investigations of two large-

scale laboratory specimens (i.e., Concept 1 and 2 bridges), as well as in subassemblage test specimens specifically designed to investigate crack control. The effect of restraint moments in the PCSSS were investigated numerically and experimentally in a previous study by the researchers, the results of which can be found in Smith et al. (2008) and Eriksson (2008).

Other considerations for the design of the PCSSS investigated in the study included the composite action of the precast and CIP which was investigated through ultimate load tests of the Concept 1 and 2 bridges and the spalling reinforcement detail of the precast section. Current design requirements to control the end zone stresses in prestressed concrete members were developed for I-sections and are not directly applicable to the PCSSS precast inverted-T sections. The current design recommendations were found to be conservative for shallow inverted-T sections and unconservative for deeper inverted-T sections.

There were a few considerations not included in the laboratory research or numerical study such as the connection between the precast elements and the substructure. These details were investigated primarily by means of examination of structural plans for existing PCSSS structures.

1.3. Organization of Report

The chapters associated with the PCSSS bridge system are organized as follows. Chapter 2 provides a literature review of the system and associated parameters of interest including literature on crack control, composite action of cast-in-place (CIP) and precast systems, and spalling design requirements. Chapter 3 provides background on the system which was initially implemented in the U.S. by the Minnesota Department of Transportation (Mn/DOT). The chapter contains the results of a field and laboratory investigation sponsored by Mn/DOT which included an investigation of live load distribution and the effects of restraint moments. Chapter 4 presents a summary of a parametric study to investigate the range of applicability of PCSSS bridges. Numerical studies are summarized in this chapter, which were conducted to investigate a number of parameters including transverse reinforcement spacing for crack control, applicability of slab-span design recommendations for PCSSS in terms of live load distribution factors and skew effects. The chapter also summarizes the numerical and experimental results associated with end zone stresses in the inverted-T precast sections used to fabricate the PCSSS, and a review of support conditions that have been used for the systems in the field. The chapter concludes with the results of a numerical study used to determine the magnitude of the patch load to be applied in the laboratory investigations of the PCSSS Concept 1 and Concept 2 bridges. Chapter 5 presents a

summary and results of the tests on the Concept 1 and 2 laboratory bridges. Subassemblage tests used to investigate detailing of the joint region for crack control are summarized in Chapter 6. Conclusions of the PCSSS investigation are provided in Chapter 7.

Appendix A contains the recommended design recommendations including suggested changes to the AASHTO LRFD Bridge Design code and commentary that were developed during the study, in accordance with Task 8. Appendix B contains information on the instrumentation of one of the early implementations of the PCSSS in the State of Minnesota. Appendices C and D contain the information on the instrument locations in the Concept 1 and Concept 2 PCSSS laboratory bridge specimens, respectively. The coring analysis of the PCSSS laboratory bridge and subassemblage test specimens are contained in Appendix E. The subassemblage sectional design calculations and information on the instrumentation locations are contained in Appendices F and G, respectively.

Chapter 2: Literature Review

2.0 Introduction to Literature Review

The design and implementation of the experimental and numerical studies regarding precast composite slab span systems (PCSSS) associated with the NCHRP 10-71 project were completed after consideration of available previous research. Because the PCSSS was a relatively new concept, the existing literature associated with the system was limited. The system was based on the Poutre Dalle bridge system developed in France, but there were no published results regarding the performance of that system. The designs associated with the original implementation of the PCSSS in the U.S. were based on the AASHTO provisions for slab-span systems because of their many similarities. Major differences exist, however, between the PCSSS and slab-span bridge systems including the composite precast / cast-in-place (CIP) nature of the PCSSS which can result in the development of restraint moments in continuous bridges due to the different time-dependent properties of the component materials. In addition, the precast portion of the PCSSS had issues to be resolved regarding the applicability of AASHTO reinforcement provisions to control end cracking due to spalling stresses, and issues associated with the development of details to control reflective cracks that might develop above the interface between the precast flanges or the CIP-precast web interface.

2.1. Poutre Dalle System

During the FHWA/AASHTO 2004 International Scan Tour, rapid construction techniques used for prefabricated bridges in Europe were investigated (Hagen, 2005). The Poutre Dalle system used in France showed promise for rapid construction of short to moderate span bridges, shown in Figure 2.1.1. The system was designed to provide longitudinal moment capacity through the longitudinally oriented precast beams made composite with a CIP deck surface. Transverse load distribution was achieved through the development of transversely oriented reinforcement protruding from the precast section in the CIP concrete placed in the trough region created by adjacent panels.

The Minnesota Department of Transportation developed a precast composite slab span system (PCSSS), described in Chapter 3, that was based on the Poutre Dalle concept. Mn/DOT implemented the first two PCSSS bridges in 2005, both of which had been previously planned for

CIP slab construction. One of them was instrumented to be monitored in two ways: to investigate the magnitude and location of reflective cracking between adjacent inverted-T sections and to examine the conitnuity over the piers. Additionally four Mn/DOT PCSSS secctions were delivered to the University of Minnesota structures laboratory for additional study for possible refinements to the design and detailing of the system, described in Chapter 4.

Figure 2.1.1: Photograph of precast section used in Poutre Dalle System (Hagen, 2005)

2.2. Crack Control Reinforcement, Frosch et al., 2006

Cracking in bridge systems must be adequately controlled for aesthetic as well as performance and durability considerations. The presence of cracking in bridge superstructures introduces a means of ingress for chlorides and other contaminants which can be detrimental to the performance of the embedded reinforcement. This concern is especially applicable in regions with harsh environments, such as those with freeze-thaw cycles, which are also usually coupled

with the application of large amounts of salt to bridge superstructures. Crack control requires the use of adequately sized and spaced reinforcement.

Frosch et al. (2006) provided an extensive investigation of cracking in bridge decks and developed associated design recommendations for reinforcement to control cracking. Although Frosch's application was focused on the crack control of bridge decks, the findings of his research were applied to the NCHRP 10-71 study to investigate their applicability in the control of potential reflective cracking above the longitudinal joint between the precast flanges.

Frosch et al. (2006) completed an experimental research program through the observation of four highway bridge decks in Indiana, three of which were instrumented by the researchers. The fourth bridge was instrumented in a previous research study by Radabaugh (2001), the primary objective of which was to observe early age behavior of bridge decks exposed to field conditions. The bridges selected for the study included three two-span continuous bridges, with equal spans of 76, 101, and 123 ft. The fourth bridge was a five span bridge with spans of 39, 63, 77, 63, and 39 ft. The decks in the three two-span bridges were constructed with two layers of steel reinforcement for crack control, while the five span bridge was built with GFRP for the top layer of reinforcement and steel bars for the bottom layer of deck reinforcement. Characteristics of the four bridges selected for the field investigation are given in Table 2.2.1.

Table 2.2.1: Characteristics of Bridges in Field Investigation (Frosch et al., 2006)

Bridge	No. of Spans	Length of Spans (ft.)	Girder Type	Abutment Type	Skew (deg.)
I 65 over SR 25	2	76, 76	Steel	Integral	25
SR 18 over I 65	2	123, 123	Steel	Semi-Integral	30
SR 23 over US 20	2	101, 101	Precast/Prestressed Concrete	Integral	11
Thayer Rd over I 65	5	39, 63, 77, 63, 39	Steel	Rockers	5

The reinforcement selected in the bridge decks provided a range of longitudinal bar spacing values, between 6 and 18 in. The reinforcement size consisted of No. 4 or No. 5 bars. To facilitate the development of design recommendations related to crack control, the SR 18 bridge was constructed with different reinforcement details in the eastern and western spans, as illustrated in Table 2.2.2.

Table 2.2.2: Characteristics of deck reinforcement in field investigation (Frosch et al., 2006)

Bridge	Type of Reinforcement		Bar Size		Longitudinal Reinforcement Spacing (in.)	
	Top	Bottom	Top	Bottom	Top	Bottom
I 65 over SR 25	Steel	Steel	4	5	12	12
SR 18 over I 65 (Purdue Span)	Steel	Steel	4	4	6	6
SR 18 over I 65 (AASHTO Span)	Steel	Steel	5	5	18	12
SR 23 over US 20	Steel	Steel	5	5	6	6
Thayer Rd over I 65	GFRP	Steel	5	5	6	9

The Purdue span of the SR 18 bridge contained the reinforcement detail proposed by Frosch et al. for crack control, while the AASHTO Span was designed to conform to the requirements in the *Standard Specifications for Highway Bridges, 16th Edition* (AASHTO 1997) and the *INDOT Standard Specifications* dated 1999 (INDOT 1999).

Visual crack mapping, beginning as early as 15 days after the placement of the CIP deck with subsequent mappings completed as late as 799 days after the placement of the CIP deck, was utilized in conjunction with measured strains to evaluate the performance of each bridge deck. Table 2.2.3 compares the crack statistics for the two spans of SR18, as well as the results of the Thayer Road bridge, which had five shorter spans. Both of these structures were wet-cured for seven days.

As expected, for SR18 with the two different reinforcement details, the closer-spaced reinforcement tended to produce smaller cracks in greater numbers. The Purdue span was observed to have the most number of cracks; however the average crack width was the smallest, with a magnitude of 0.007 in., which was 30 percent less than the average crack width measured in the AASHTO span. Furthermore, less variation was observed in the crack widths, with a standard deviation of 0.005 in. compared to 0.008 in. for the AASHTO and Thayer Road spans.

Finally, the maximum crack width observed in the Purdue span was 28 and 31 percent smaller than that measured in the AASHTO and Thayer Road spans, respectively. The approximately 30 percent improvement in both the average and maximum crack widths, in combination with the reduction in variability among the crack widths, suggested that the design parameters utilized to develop the Purdue span in the SR 18 bridge should be considered as a superior alternative, in terms of performance, to the AASHTO (1997) and INDOT (1999) design parameters. Furthermore, the authors suggested that the performance of the Thayer Road spans, which was similar to that observed in the AASHTO span, was due to increased slip between the concrete and FRP reinforcement.

Table 2.2.3: Comparison of crack width statistics (Frosch et al., 2006)

Crack Statistics	SR 18		Thayer Rd
	AASHTO	Purdue	
Number of Cracks (Total)	15	22	19
Number of Cracks (per 100 ft.)	12.2	17.9	6.8
Average Crack Widths (in.)	0.010	0.007	0.010
Standard Deviation (in.)	0.008	0.005	0.008
Maximum Crack Width (in.)	0.025	0.018	0.026
Variance	3.11×10^{-5}	2.53×10^{-5}	5.56×10^{-6}

In addition to the experimental results obtained during the study, the researchers completed a numerical parametric study to further investigate the expected effects of various bridge design characteristics on the performance of bridge decks. The finite element method (FEM) model was developed using ANSYS (SAS Inc. 2004) and was calibrated using the results of the Radabaugh (2001) study to investigate the effects of restrained shrinkage. Radabaugh (2001) constructed two laboratory specimens to study the effects of shrinkage restraint due to stay-in-place (SIP) deck pans. The specimens were 9 ft. by 9 ft. square, and represented the positive moment region of the bridge decks in the I-65 bridge span over SR 25. The specimens were developed in an effort to investigate the level of restraint based on the type of formwork, where one specimen had SIP steel deck forms, and the second was constructed with plywood forms and two layers of 10-mil Teflon as a barrier between the plywood and concrete. The second specimen was expected to provide little shrinkage restraint and therefore was developed to represent a state of free-shrinkage. Four layers of solid elements were selected to model the deck, which provided insight into the behavior of the deck through its depth, while reinforcement was discretely modeled using

link elements. The materials were modeled as linear elastic, with the elastic modulus of the steel reinforcement and concrete of 29,000 ksi and 3,610 ksi, respectively. Uniform and linear concrete shrinkage profiles were considered, which were developed from the literature (Radabaugh, 2001 and Blackman, 2002).

The calibrated FEM model was utilized to complete a numerical parametric study to investigate the effects of a range of variables on cracking in bridge decks, outlined in Table 2.2.4. The variables considered included reinforcement type, size, and spacing, the girder superstructure depth and spacing, and the thickness and material strength of the CIP deck.

Table 2.2.4: Range of variables considered in parametric study (Frosch et al., 2006)

Variable		**Range**	**Control**
Reinforcement	Area (Bar Size)	#3-#7	#5
	Top Mat Spacing (in.)	3-18	12
	Bottom Mat Spacing (in.)	3-18	12
	Reinforcement Type	Steel, FRP	Steel
Girder	Depth (in.)	12-51	51
	Spacing (ft.)	6-10	7
Deck	Thickness (in.)	6-12	8
	f'_c (psi)	3,000-10,000	4,000

The results of the parametric study generally corroborated the results anticipated by the researchers, such as increasing the area of reinforcement in a section tended to reduce the crack widths and reinforcement stresses under a given load. The effects of reinforcement spacing were investigated by varying the spacing while simultaneously maintaining a constant reinforcement ratio among models. Using this method, the reinforcement spacing was observed to control two aspects of the behavior of the models: (1) the crack width was observed to be larger as the reinforcement spacing increased, and (2) the variation in the crack width between adjacent reinforcement was highly dependent on the bar spacing (i.e., an “unzipping” effect was observed between adjacent reinforcing bars).

For example, in the case of uniform shrinkage, with a steel reinforcement ratio of 0.65 percent, the following results were obtained. For the largest reinforcement spacing (i.e., 18 in.) considered in the study, the maximum difference between the crack width near a bar and half the distance to an adjacent bar was approximately 1.5 mils. Furthermore, the unzipping effect was dependent on the 3 in. mesh size, which was evinced by the fact that a change in crack width of approximately

1/2 mil was observed between measurements near and away from a bar in the 6 in. spacing model, while virtually no variation in the crack width was observed between adjacent bars in the model representing a 9 in. reinforcement spacing. A comparison of the performance of the different models was made by considering the maximum crack widths in each model, which subsequently corresponded to the crack width measured equidistant from adjacent reinforcement if a variation was observed between bars. A maximum crack width of approximately 2.4 mils was observed in the model with a 3 in. reinforcement spacing, while a maximum crack width of approximately 6.3 mils was observed in the model with an 18 in. reinforcement spacing; where the increase in the crack widths was observed to be linearly proportional to the bar spacing between these limits.

The authors suggested that if no slip is assumed to occur between the reinforcement and concrete, then when cracking occurs, the tensile stresses previously restrained by the concrete will be transferred to the reinforcement. If the concrete tensile strength is taken to be $6\sqrt{f'_c}$, then the stress in the reinforcement upon cracking can be determined as shown in Eqn. (2.2.1).

$$f_s = \frac{6\sqrt{f_c}}{\rho_g} \tag{2.2.1}$$

where f_c is the concrete compressive strength at the initiation of cracking in psi (and the units of $\sqrt{f_c}$ are in psi), and ρ_g is the gross reinforcement ratio. The researchers plotted the average reinforcement stresses versus the ratio $\sqrt{f_c} / \rho_g$, and found that a linear fit yielded a line with a slope of approximately 3, indicating that the average stress in the reinforcement bridging the crack was numerically determined to be about half of what would be expected if no slip occurred. The slip length utilized in the model was 2 in.

Furthermore, the authors discovered that, on average, the reinforcement stresses increased by approximately a factor of two between the simulated initial and final shrinkage states, where the initial state was when cracking first occurred ($6\sqrt{f_c}$) and the final was considered to be after a free shrinkage "load" of 1000 με was applied.

The researchers provided a recommended gross reinforcement ratio for crack control reinforcement based on the results from the FEM parametric study, outlined above. Because the concrete compressive strength at the time of cracking was unlikely to be known by the designer, the authors conservatively substituted the 28-day concrete compressive strength in the calculation. The recommended reinforcement ratio proposed by Frosch et al. (2006) is given in equation 2.2.2).

$$\rho_g = \frac{6\sqrt{f_c'}}{f_y} \quad (2.2.2)$$

Furthermore, the reinforcement spacing required to restrain crack growth was developed during the study and based on previous work. The reinforcement spacing, *s*, for Grade 60 bars is given as

$$s \leq 9\left(2.5 - \frac{c_c}{2}\right) \leq 9\ in. \quad (2.2.3)$$

where *s* is the reinforcement spacing (in.) and c_c is the depth of concrete cover measured from the extreme tensile fiber of the concrete to the face of reinforcement (in.).

2.3. Horizontal Shear Capacity of Composite Concrete Beams without Ties, Naito et al., 2006

Composite precast construction increases the efficiency of precast sections because it may reduce the section depth, as well as increase the load capacity, and the geometric stiffness of the system. A composite concrete system must be designed such that the horizontal compression and tension forces developed in the system can be transferred between the precast and CIP interface. Two design documents for concrete construction in the United States, AASHTO (2010) and ACI (318-08), include design parameters for horizontal shear transfer. ACI (318-08) allows for the design of composite sections without the use of horizontal shear reinforcement, and permits a maximum factored horizontal shear stress of 80 psi to be developed by a clean, roughened, surface with no ties crossing the shear plane. AASHTO (2010) requires that horizontal shear reinforcement be present in all sections in which composite action is to be achieved; however AASHTO provides a cohesion factor that may be interpreted, for the purpose of discussion, as a maximum allowable horizontal shear strength (Naito et al., 2006). The 2006 AASHTO LRFD design specification provided a cohesion factor of 100 psi for a clean, intentionally roughened surface to an amplitude of 1/4 in., while AASHTO (2010) increased the cohesion factor for a clean, intentionally roughened surface to 240 psi; which was not published at the time of designing the NCHRP 10-71 Concept 1 laboratory bridge specimen. Furthermore, research by Naito et al. (2006) suggests that sections without vertical ties for horizontal shear reinforcement can develop adequately large and reliable horizontal shear capacities.

The calculation of the horizontal shear demand in a section can be completed using many different methods. The researchers investigated three of these methods: (1) global force equilibrium, (2) simplified elastic beam behavior, and (3) classic elastic methods (Naito et al., 2006). Global force equilibrium considers a change in the compression force resultant over a

distance along the length of the beam, *l*. The horizontal shear strength is simply the change in the compression force divided by the horizontal shear area, or b_v *l, where b_v is the width of the horizontal shear plane. For simply-supported systems, the horizontal shear stress can be calculated using this method by dividing the total compressive force at midspan by half of the span length and the width of the horizontal shear plane. The second method considers flexural beam theory, which equates the horizontal shear demand to the vertical shear acting at a given section and is calculated as $V/(b_v d)$, where *d* is defined differently in ACI and AASHTO. ACI (318-08) defines *d* as the distance from the centroid of the longitudinal tension reinforcement to the extreme compression fiber of the section, while AASHTO (2010) defines *d* as the distance from the longitudinal tension reinforcement to the mid-thickness of the slab. The third method presented by the authors, the classic elastic method, considers the section properties of the beam; however, the method is applicable to uncracked sections only. The horizontal shear stress calculated using the classical elastic method is illustrated in Eqn. (2.3.1).

$$v_h = {}^{VQ}/_{Ib_v} \tag{2.3.1}$$

Naito et al. (2006) investigated the horizontal shear stress developed in composite girders without horizontal shear reinforcement. The researchers completed an experimental program with 19 test specimens to investigate the effects of surface roughness, concrete strength, and loading type (i.e., point loading versus uniform loading). Four variations in the surface roughness were considered, including as-placed (A), broom finish (B), 1/4 in. rake (R), and sheepsfoot (Sh). The concrete compressive strength in the flange was varied within a wide range of reasonably expected values, with measured concrete strengths of 3.11, 5.67, 8.75, and 9.71 ksi. Two-point and 5-point loading configurations were utilized during the study to simulate point loading and uniform loading, respectively. Load was applied through 12 in. neoprene bearing pads in an effort to reduce the localized bearing stress near the applied load. A summary of the research parameters and specimen characteristics is outlined in Table 2.3.1 (Naito et al., 2006).

The researchers provided instrumentation to determine the horizontal shear stress at the interface as well as to measure the slip that may occur along predicted failure planes. Two horizontally oriented strain gages were mounted on the surface of the CIP flange along the depth, to allow for the measurement of the horizontal shear stress with the use of known stress-strain relationships for the CIP concrete.

Table 2.3.1: Research parameters and specimen characteristics considered during the study (Naito et al., 2006)

Beam	Interface Finish	Loading Method	Interface Width (in.)	Web Steel Area (in.^{2})	Flange Strength (ksi)	Effective Prestress (ksi)
1	As-Placed	5 Point	5	0.2	5.67	141.3
2	Broom	5 Point	5	0.2	5.67	142.1
3	Monolithic	5 Point	5	0.0	9.71	139.9
4	Rake	5 Point	5	0.2	3.11	141.5
5	Rake	5 Point	5	0.2	5.67	143.1
6	Rake	5 Point	5	0.2	8.75	140.3
7	Sheepsfoot	5 Point	5	0.2	5.67	140.3
8	As-Placed	2 Point	2	0.2	5.67	140.2
9	As-Placed	2 Point	2	0.2	5.67	140.1
10	Broom	2 Point	2	0.2	5.67	140.2
11	Monolithic	2 Point	2	0.0	9.71	140.2
12	Monolithic	2 Point	2	0.0	9.71	140.2
13	Rake	2 Point	2	0.2	3.11	140.2
14	Rake	2 Point	2	0.2	3.11	140.2
15	Rake	2 Point	2	0.2	5.67	140.2
16	Rake	2 Point	2	0.2	5.67	140.2
17	Rake	2 Point	2	0.0	8.75	140.2
18	Rake	2 Point	2	0.0	8.75	140.2
19	Smooth	2 Point	2	0.2	5.67	140.2

Relatively large horizontal shear stresses were measured during both the 2-point and 5-point loading cases, and were always above the 80 psi allowed for sections without horizontal shear ties as specified by ACI (318-08) and the 240 psi cohesion value provided by AASHTO (2010). During the 5-point load tests, the horizontal shear stress was measured at the first indication of cracking in the section, generally flexure shear cracking, in an effort to investigate the shear stress

developed before cracking, which would generally be the case for a service condition, where cracking is generally avoided. The results of the 5-point load tests are illustrated in Table 2.3.2, with an average horizontal shear stress at cracking of 340.2 psi using the classic elastic method of calculation. The smallest average horizontal shear stress was 275.4 psi, calculated using the simplified elastic method provided by ACI (318-08).

Table 2.3.2: Horizontal shear stress at cracking (psi) during 5-point load tests (Naito et al., 2006)

Beam	**Interface Finish**	**Elastic VQ/Ib_v**	**ACI V/b_vd_p**	**AASHTO V/b_vd_v**
1	As-Placed	341.1	276.0	334.5
2	Broom	341.1	276.0	334.5
3	Monolithic	350.1	280.0	339.4
4	Rake	321.6	266.0	322.4
5	Rake	341.1	276.0	334.5
6	Rake	345.6	278.0	337.0
7	Sheepsfoot	341.1	276.0	334.5
	Average	340.2	275.4	333.9

The horizontal shear stresses developed during the 2-point load tests were calculated at the ultimate capacity of each specimen, and were subsequently considerably larger than those measured during the five-point load configurations. As illustrated in Table 2.3.3, the average horizontal shear stress measured at ultimate ranged from 828.4 psi to 1022.3 psi, depending on the method of calculation.

Table 2.3.3: Horizontal shear stress at ultimate (psi) during two-point load tests (Naito et al., 2006)

Beam	Interface Finish	From Strain C/Lb_v	Elastic VQ/Ib_v	ACI V/b_vd_p	AASHTO V/b_vd_v
8	As-Placed	482.2	863.2	698.4	846.6
9	As-Placed	814.0	1060.8	860.7	1043.2
10	Broom	915.6	993.2	804.6	975.3
11	Monolithic	1075.0	1067.0	848.4	1028.4
12	Monolithic	1288.0	1248.1	981.1	1189.2
13	Rake	639.0	850.6	703.7	852.9
14	Rake	1182.0	1015.1	840.2	1018.4
15	Rake	1348.0	1001.0	811.1	983.2
16	Rake	1245.0	1165.9	948.1	1149.2
17	Rake	1054.0	1141.3	934.3	1132.5
18	Rake	1194.0	1073.6	873.1	1058.3
19	Smooth	787.4	787.9	637.5	772.7
	Average	1002.0	1022.3	828.4	1004.1

The experimental results indicated that composite girders without horizontal shear reinforcement can develop significant horizontal shear stresses. The authors suggested that, with an average horizontal shear stress of 340.2 psi at the service state, which was more than three times the least conservative design estimate, the requirement for horizontal shear reinforcement in all sections by AASHTO (2005) be waived.

2.4. AASHTO (2007) Bursting Design Requirements

The AASHTO (2007) specifications required vertical reinforcement to resist four percent of the prestressing force in the end regions of precast beams over a horizontal distance of *h/4* from the face, where *h* is the section height. The provisions are for pretensioned anchorage regions and do not provide any distinction based on cross section. The AASHTO (2007) specifications resulted in the requirement of a large amount of vertical steel over a short distance for wide shallow members, such as the shallow inverted T sections used in PCSSS bridges. This created congestion of the vertical reinforcement in the end zones and provided an impetus for a review of the requirements and the end zone force demands for the case of shallow inverted-T sections.

In reviewing the literature, the origin of the AASHTO bursting requirements likely resulted from a Marshall and Mattock (1962) study on horizontal end zone cracking of pretensioned I-girders. The 1961 Interim AASHTO Specifications introduced bursting reinforcement requirements (in the AASHTO (2010) LRFD Bridge Design Specifications this is labeled "splitting resistance") for pretensioned I-beams stating, "Vertical stirrups acting at 20,000 psi to resist 4 percent of the prestressing force shall be placed within *d*/4 from the end of the beam with the end stirrup placed as close to end of beam as practicable," where *d* is the effective depth. By 1969, the above requirements were not limited to just I-beams, and instead were made applicable to end zones of all pretensioned beams. The AASHTO LRFD Bridge Design Specifications 1st edition (1994) had the same requirements as the 1969 version, but the 2nd edition (1998) stated that the vertical steel should be placed within *h/5* from the end face, where *h* is the height of the member. This specification was changed to *h*/4 from the end face in the 3rd edition (2004). The only difference between the 1969 provisions and the 4th edition (2007) of the AASHTO LRFD Bridge Design Specifications was that vertical steel could be placed within *h*/4 from the end face, rather than *d*/4. The 2008 Interim specifications relaxed the requirements for wide-shallow sections, by allowing the designer to spread the end zone reinforcement, termed "splitting" reinforcement over a larger distance. In the case of pretensioned solid or voided slabs, the designer can substitute the section width for "*h*," rather than using the section depth for "*h*."

Because the original AASHTO provisions were likely developed as a result of experimental testing performed on I-beams by Marshall and Mattock (1962), it is not clear whether the AASHTO requirements, developed for I-beam members, are applicable to other cross sections, particularly slab-span systems.

2.4.1. Bursting, Splitting and Spalling Stresses

The end regions of prestressed concrete sections have complicated states of stress. Beam theory is not applicable in the end regions of prestressed concrete beams because the longitudinal strain is not linearly distributed through the depth of the cross section due to the introduction of the prestress force. As the prestress force distributes through the section, various zones of compression and tension are created over a region assumed to extend a distance approximately equal to the depth of the section, in accordance with St. Venant's principle. The tensile stresses that develop in this region have been identified as bursting or spalling stresses, depending on their location. Splitting stresses are circumferential tensile stresses resulting from the radial

compressive stresses caused by bond. Splitting stresses occur along the transfer length and locally around the prestressing strand.

Bursting and spalling stresses are vertical tensile stresses that develop in the concrete from the distribution of the prestressing force as the force is transferred from the prestressing strand to the concrete at the ends of the member and can result in cracking at different locations in the beam. Spalling stresses are a maximum at the end face of the member, typically near the centroid of the section and result in cracking at the end face, which can propagate further into the member (Gergely et al., 1963). Bursting stresses occur along the line of the prestressing force, beginning a few inches into the beam and extending through the transfer length. Bursting and splitting stresses can result in strand slippage as cracking at the strand can eliminate bond between the strand and the concrete. Figure 2.4.1 shows the location of the bursting and spalling stresses in the end region of a section. Note that the AASHTO (2007) provisions (incorrectly labeled as bursting provisions) and the AASHTO (2010) provisions (incorrectly labeled as splitting provisions) are intended to resist spalling forces (i.e., vertical tensile forces occurring near the end face at the centroid of the member). AASHTO (2010) does not explicitly include provisions for vertical steel to resist bursting and splitting forces (i.e., vertical forces occurring along the line of the prestress in the transfer length region); however the AASHTO confinement reinforcement provisions fill this role.

Distribution of tensile stresses in the end region depends on the eccentricity of the prestressing force in the member, where eccentricity is the distance between the centroid of the prestressing force and the centroid of the member. In a centrally loaded member, forces distribute symmetrically through the vertical member height. Small spalling forces develop on the end face and a bursting force starts further into the member, as shown in Figure 2.4.1-a. In members with large eccentricity, there is greater area above the prestressing force in which the stresses need to distribute. This allows the prestressing force to spread through a greater vertical distance, making the curvature of the flow of stresses greater, creating a larger spalling force near the end region, as shown in Figure 2.4.1-b. This is consistent with previous experimental work which related the maximum tensile stress location to eccentricity. Gergely's (1963) study on post-tensioned I-girders and rectangular sections found members with small eccentricities had maximum tensile stresses in the bursting zone and members with large eccentricities had maximum tensile stresses in the spalling zone. Hawkins (1960) corroborated Gergely's findings and also found as eccentricity increased so did the magnitude of maximum tensile stress in the spalling zone.

The 12 in. deep precast inverted tee sections of the laboratory bridge specimen had slight eccentricities of 2.4 in. for the 3 in. flanged section and 2.5 in. for the 5.25 in. flanged section. Because it was unclear whether this shallow section would have a maximum tensile force in the bursting or spalling zone, tensile stresses in both zones were investigated.

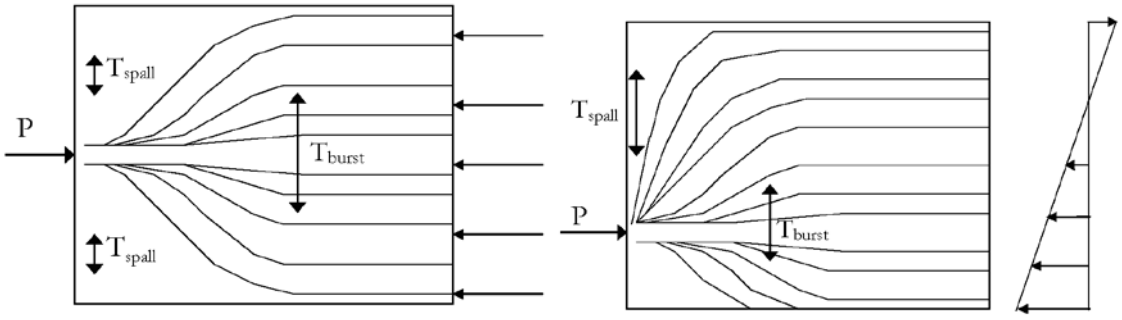

(a) Centrally prestressed member (b) Eccentrically prestressed member

Figure 2.4.1: Effects of eccentricity of distribution of compression and spalling forces

2.4.2. Stresses in End Regions of Post-Tensioned and Pretensioned Sections

Many previous studies investigated the effects of bursting and spalling stresses in post-tensioned members (Gergely et al., 1963; Hawkins, 1960). Only a few examined pretensioned members. The primary difference between post-tensioned and pretensioned systems is the means of introducing the distribution of the prestress force into the members. Post-tensioned systems transfer stress from the steel to the concrete at the end face, through bearing at the end plate, which spreads the force over the end of the member. In pretensioned systems, where the transfer of stress occurs through bond, the stress transfer is often assumed to vary linearly or uniformly until full transfer occurs. The distance needed to transfer the stress from steel to concrete is defined as the transfer length.

Research has shown that tensile stresses in end zones are affected by the transfer length (Base, 1958). Longer transfer lengths in pretensioned systems result in smaller bursting and spalling stresses. Shorter transfer lengths concentrate the transfer of forces, which result in larger bursting and spalling stresses, more similar to the case of post-tensioned systems (Uijl, 1983). Many theories developed from post-tensioned experiments can provide conservative estimates of the spalling and bursting stresses in pretensioned members, because they simulate the case of a very short transfer length.

Chapter 3: Background

3.0 Introduction to Background

Interest in the development of precast composite slab span system (PCSSS) bridges in Minnesota led to research on the topic at the University of Minnesota prior to the initiation of the NCHRP 10-71 project. The results were valuable in selecting appropriate design parameters for the laboratory portion of the NCHRP 10-71 project, and provided important information considered in the development of the comprehensive design guide for PCSSS bridges as part of the NCHRP project.

The first section of this chapter includes a summary of a phone survey that was completed at the outset of the current study. The primary focus of the survey was to identify the principle behaviors and concerns that engineers, contractors, fabricators, and researchers had with the precast slab span bridge system. The results of the phone survey proved very useful in the development of specific characteristics that the PCSSS should be expected to satisfy.

In addition, this chapter includes observations of an existing three-span PCSSS bridge (i.e., Bridge No. 13004) constructed in Center City, Minnesota, by the Minnesota Department of Transportation (Mn/DOT). This bridge was one of the initial implementations of the PCSSS in Minnesota, and was instrumented during construction to measure the load distribution and the potential for the development of reflective cracking. Near midspan of the center span of the bridge, three adjacent longitudinal joints were instrumented to investigate reflective cracking using a series of strain gages placed transversely above the joint. The instruments were monitored for several years following construction. The data collected from this bridge provided a useful data set regarding the behavior of an in-service PCSSS bridge, which was analyzed and utilized during the NCHRP 10-71 study to correlate the laboratory results with measured field data.

In addition to the Center City Bridge, Mn/DOT sponsored the construction and testing of a two-span laboratory specimen located at the University of Minnesota, referred to as the Concept 1 laboratory bridge elsewhere in the report. The Mn/DOT study included the investigation of the development of restraint moments in the Concept 1 laboratory bridge specimen. In addition, Eriksson (2008) completed a numerical and parametric study of restraint moments as part of the Mn/DOT investigation. Because of the previous research conducted regarding restraint moments on the PCSSS, no further investigation on the topic was conducted during the NCHRP 10-71 study, however the experimental data and other available resources from the previous studies

were analyzed to provide guidance regarding restraint moments that is included in the design guide developed during the NCHRP 10-71 study.

3.1. Introduction to Survey Results

This section provides a summary of the comments received from the individual respondents who participated in the phone survey that was used to gather information including the respondents' experience with similar systems, their input on important performance criteria, and their feedback on proposed connection concepts.

Nearly 60 people were interviewed during the phone surveys which were conducted in partial fulfillment of project Tasks 1 and 2. The individuals interviewed were selected through consultation with the project team, David Beal (Senior Program Officer, NCHRP), and interviewees who recommended others who should be contacted. The respondents represent bridge engineers (including many individuals who serve as State Bridge Engineers), consulting engineers, fabricators, material suppliers, industry representatives, and technical committee contacts. The distribution is presented in Table 3.1.1.

Table 3.1.1: Distribution of phone survey respondents

Bridge Engineer	Material Specialist	Fabricator	Researcher	Industry Rep	Contractor	Other
37	9	6	13	3	0	3

A few survey respondents were identified under multiple categories in Table 3.1.1, so the total number in the table (71) exceeds the number of survey respondents (59). Also note, that although there are no individuals listed under the "contractor" category, a number of bridge engineers and fabricators were able to provide firsthand experience on constructability issues encountered in the field. Attempts were made to include contractors in the survey, but because of the high level of activity with the contractors in the field towards the end of the construction season, and the difficulty in reaching the individuals in the field, this was not possible. The contractor on site during construction of the Mn/DOT implementation of the Poutre Dalle (PD) concept was queried by members of the project team regarding constructability issues, which influenced some of the decisions made in the concept development implemented in the University of Minnesota laboratory specimens described in Chapters 5 and 6.

The phone survey was primarily developed to provide insight into what the respondents considered to be the most important aspects and behaviors that should be considered for a rapid construction bridge system. In addition, respondents were provided with an overview and figure of the Poutre Dalle system as well as the modifications considered in the development o f the Mn/DOT PCSSS, and were asked to share their comments, concerns, and any changes they might consider if they were to implement a similar composite slab span system.

Some respondents (44) provided insight into the relative importance and prioritization of certain characteristics in regards to the PCSSS. The participating respondents were asked to provide a rank ordering, from one to eight (one being the most important), of the following categories: durability, strength, fatigue, seismic, constructability, rapid construction, serviceability/performance, and economy. Some participants did not rank all eight performance categories, and only ranked the one or two criteria considered to be most important. The category that received the highest number of votes was durability, with 91 percent of the 44 participants providing a ranking. A total of 75 percent of the respondents that provided a ranking in the durability category selected it as being the most important, with a ranking of one. The second and third most ranked categories were constructability and rapid construction, with a total of 68 and 57 percent of the respondents providing a ranking. Economy, serviceability/performance, and strength were the fourth, fifth, and sixth most ranked categories, with 45, 43, and 34 percent of the respondents providing a ranking, respectively. The two performance categories least likely to be ranked at all were fatigue and seismic, both with a total of 20 percent of the respondents providing a ranking.

The vast majority of the respondents considered durability to be the primary issue that must be considered with the PCSSS. Many respondents provided additional comments suggesting that reflective cracking between the precast panels would likely be a primary issue with the system. A primary concern among the respondents was in regards to the development of cracking and subsequent ingress of chlorides and the potential for corrosion of the reinforcement. One respondent suggested that the joints between the precast elements would be the weak link of the system, and should therefore be well designed and thought out. The overwhelming consensus that durability was a primary concern regarding the PCSSS was a major driver in the fact that the control of reflective cracking was an essential objective of the project.

3.1.1. Mn/DOT PCSSS and Poutre Dalle System

The survey respondents provided insightful comments and suggestions regarding the original PD system as well as the first implementation of the Mn/DOT PCSSS. Most, if not all, respondents liked the overall concept of the PCSSS, and furthermore thought it could be implemented by their DOT's. Some however, considered the system to be economical only in shorter spans, and did not envision the system as a highway bridge. Several respondents commented specifically on the applicability of the system in locations with vertical clearance requirements. The use of 90 degree hooked transverse reinforcement over the precast joint was favored strongly to the 180 degree version in the French Poutre Dalle system, especially as this allowed for the cage reinforcement to be pre-tied and dropped into position as one piece. A few respondents commented on the use of embedded transverse hooked bars, as it would require perforations of the formwork, which may not be favored by fabricators. One solution to perforated formwork would be the use of threaded bars, where the hooked reinforcement was threaded on after casting, which could therefore be done on-site. One respondent suggested that, if the embedded bars were selected for this system, that a standard bar spacing be selected. The bar spacing should either be constant, or an even multiple, thereby allowing fabricators to perforate their formwork in a given pattern which would not be expected to change.

The use of voids in the precast elements was brought up by a majority of the respondents, both for and against. Proponents of incorporating voids into the system suggested that the large dead weight of the system would be a hindrance, and that fabricating precast beams with voided elements had been successfully completed in the past (Grafton; Hyzak; Khalegi; Tadros). Several respondents however were opposed to the use of voids primarily due to previous performance issues, including durability issues reported by Minnesota and South Dakota.

The use of CIP concrete was discouraged by a number of respondents, primarily because they felt it would be difficult to achieve a significant benefit in terms of rapid construction, and can be costly and difficult to procure in rural areas. The use of CIP concrete in only the trough between each panel was suggested, where the top of the precast web could then be used as the driving surface, however limiting the quantity of CIP concrete was not expected to provide a significant savings. Furthermore, the use of a CIP deck overlay was favored by many respondents because it provided a uniform driving surface, regardless of differential camber in the precast elements, as well as covered the longitudinal joints and ensured the entire driving surface was a uniform color, which was considered to be important to several respondents.

3.2. Center City PCSSS Bridge

The first implementations of the Mn/DOT PCSSS began in 2005 with the design and construction of two precast composite slab-span structures. The first was in Beltrami County, Minnesota with three 45 ft. spans and a precast section depth of 16 in. The second implementation was Mn/DOT Bridge No. 13004 in Center City, Minnesota about 40 miles northeast of Minneapolis. The Center City Bridge was also a three-span bridge with 22, 27, 22 ft. spans and had a 12 in. precast section depth. The depth of the CIP concrete over the webs of the precast elements was 6 in. in both implementations. The CIP above the webs was reinforced with typical deck reinforcement in both the longitudinal and transverse directions. The plan view and construction stages of the Center City Bridge are shown in Figure 3.2.1.

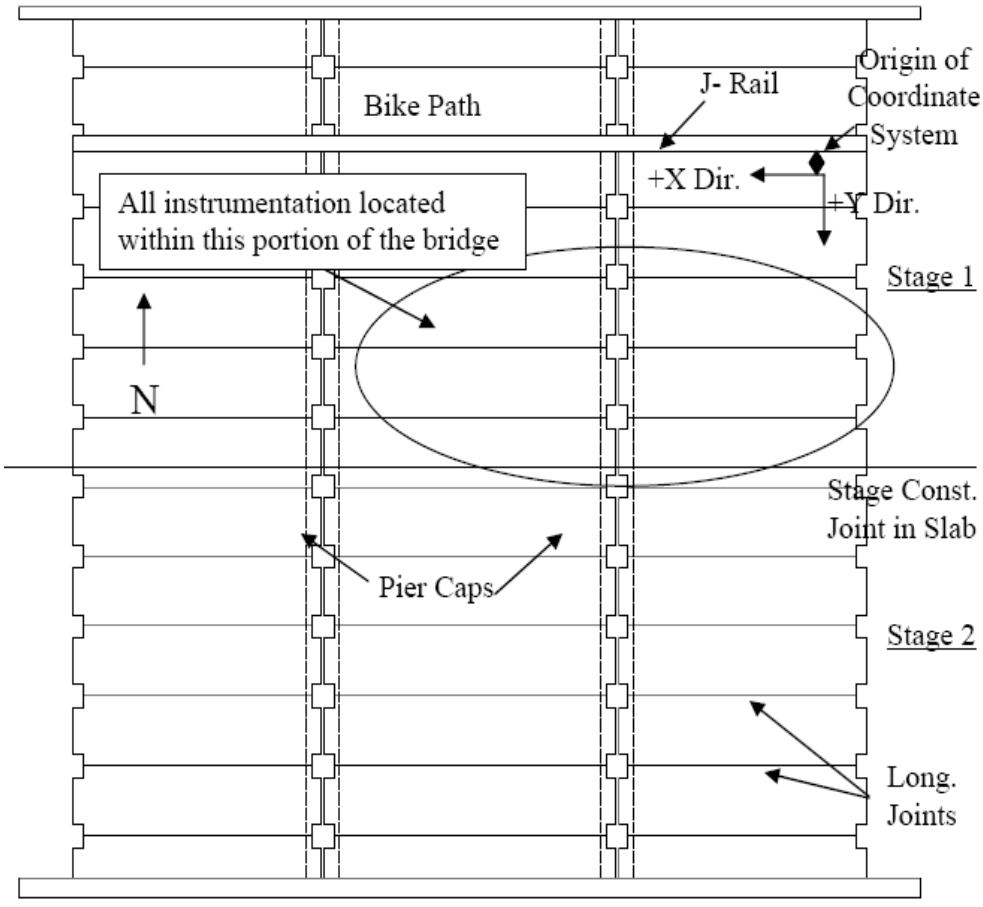

Figure 3.2.1: Plan view and construction stages of Mn/DOT Bridge No. 13004 in Center City, Minnesota (Bell et al. 2006)

The Center City Bridge was instrumented to investigate two primary behaviors, reflective cracking and live load distribution over a continuous pier. Reflective cracking was anticipated to originate from the discontinuity created by the joint between precast panels and/or at the corners of the precast webs near the top of the section, as illustrated in Figure 3.2.2. To facilitate the monitoring of reflective cracking and the overall performance of the structure, the bridge was instrumented with a total of 45 transversely oriented concrete embedment vibrating wire (VW) strain gages and 21 transversely oriented spot-weldable VW strain gages in the trough area between precast panels. The instrumentation to investigate reflective cracking was located solely in the center span of the bridge constructed during Stage 1, as shown in Figure 3.2.1. The instrumentation was distributed over three adjacent longitudinal joint regions, shown in Figure 3.2.3, to provide insight into the performance of each joint as well as the interaction between precast panels.

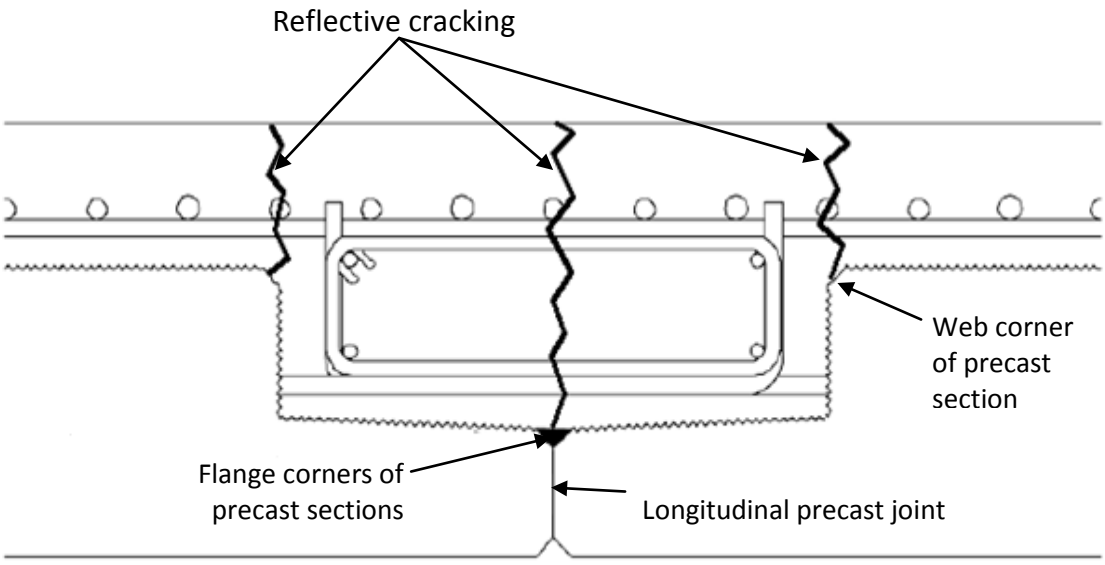

Figure 3.2.2: Anticipated locations of reflective cracking in Mn/DOT PCSSS (Bell et al. 2006)

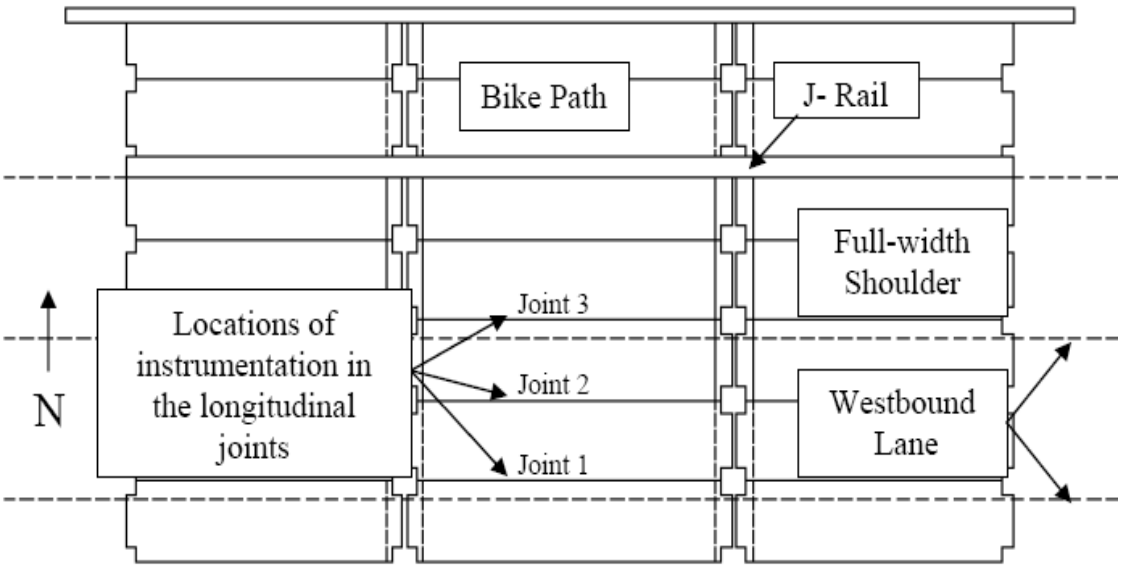

Figure 3.2.3: Location of instrumented joints in the Center City Bridge (Bell et al. 2006)

The concrete embedment gages provided a useful means of exploring the condition of the CIP concrete in the longitudinal trough region and were the primary instrumentation investigated during the NCHRP 10-71 study. All concrete embedment gages in the field bridge were nominally located at midspan of the center span in each of the three instrumented joints. The gages were oriented transversely in the precast trough in two vertical rows. The lower row, nominally placed at the same vertical location as the transverse hooks, contained five gages, while the upper row, placed just above the precast web consisted of ten gages. The instrumentation layout, which was identical at each of the instrumented joints, is shown in Figure 3.2.4. As shown in the figure, the instrumentation was overlapped to better determine the crack location to within a 2 in. region (i.e., gage length was 6 in., gage overlap was 2 in.). If an increase in strain was observed in two adjacent gages, it could be deduced that the crack developed in the region where the gages overlapped. The lower row of gages was embedded only in the CIP concrete and therefore cracking or separation along the vertical precast web interface could not be observed by the instrumentation, unless such a crack extended into the CIP topping.

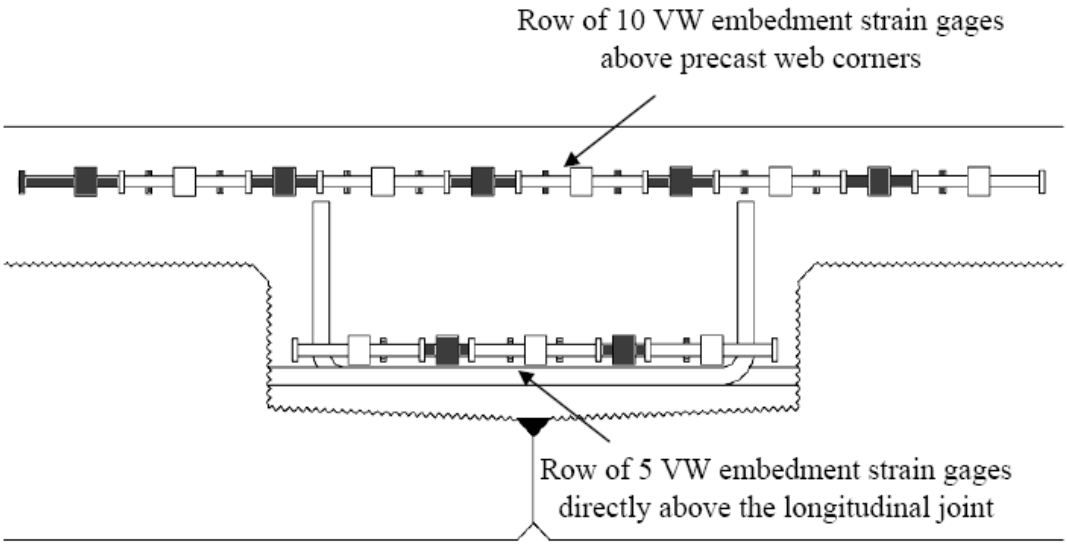

Figure 3.2.4: Location of transverse concrete embedment gages in each of the three instrumented joints at midspan of the center span of the Center City Bridge (Bell et al. 2006)

In addition, seven transversely oriented spot-weldable strain gages were included in each joint to provide insight into the stress demands on the reinforcement bridging the joint between adjacent precast members. The seven gages were installed on two immediately adjacent transverse hooked bars near the group of concrete embedment gages, as shown in Figure 3.2.5.

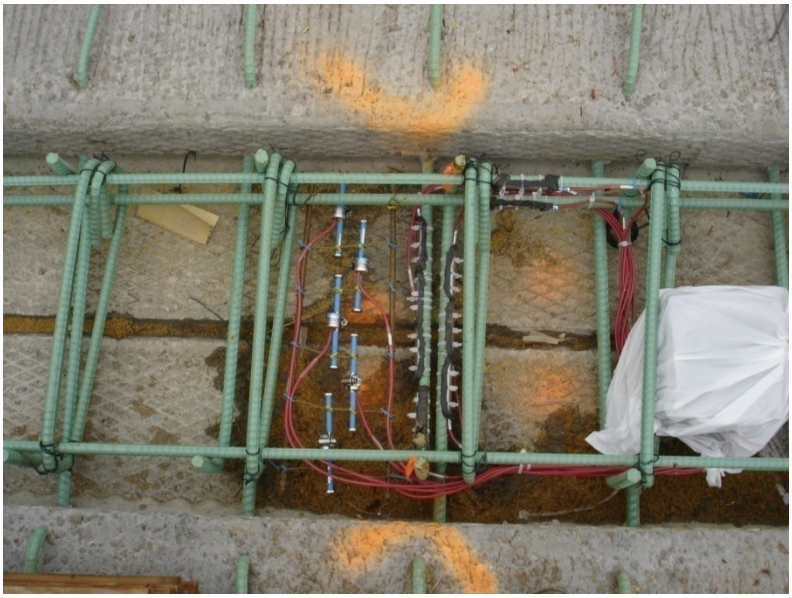

Figure 3.2.5: Lower level of concrete embedment and spot-weldable VW gages utilized in observation of reflective cracking in the Center City Bridge

Furthermore, the bridge was instrumented with longitudinally oriented spot-weldable gages to investigate the behavior of the structure in terms of longitudinal live load distribution over a continuous pier. Because of symmetry, only one pier was considered, as shown in Figure 3.2.1. The longitudinal instrumentation was selected to provide for the calculation of the longitudinal curvature at various cross sections on either side of the continuous pier. The longitudinal instrumentation layout is shown in Figure 3.2.6, where the vertical groups of gages are represented by either a diamond or circle. The gage groups represented by a diamond include three gages vertically distributed through the depth, with one gage on the lower No. 5 longitudinal cage bar, the second gage on the top No. 5 longitudinal cage bar, and the third was attached to the deck reinforcement. At cross sections near the pier, where the longitudinal cage reinforcement was not continuous, only two gages were present through the depth of the section, which is represented by the circle symbols. At these locations, the bottom gage was located on the longitudinal No. 8 bar that was provided near the precast flanges for positive restraint moments, and the top gage was located on the deck reinforcement. In addition, the deck reinforcement above two of the webs on the center span side of the pier were instrumented with single longitudinally oriented spot-weldable strain gages, represented by the triangle symbols in Figure 3.2.6.

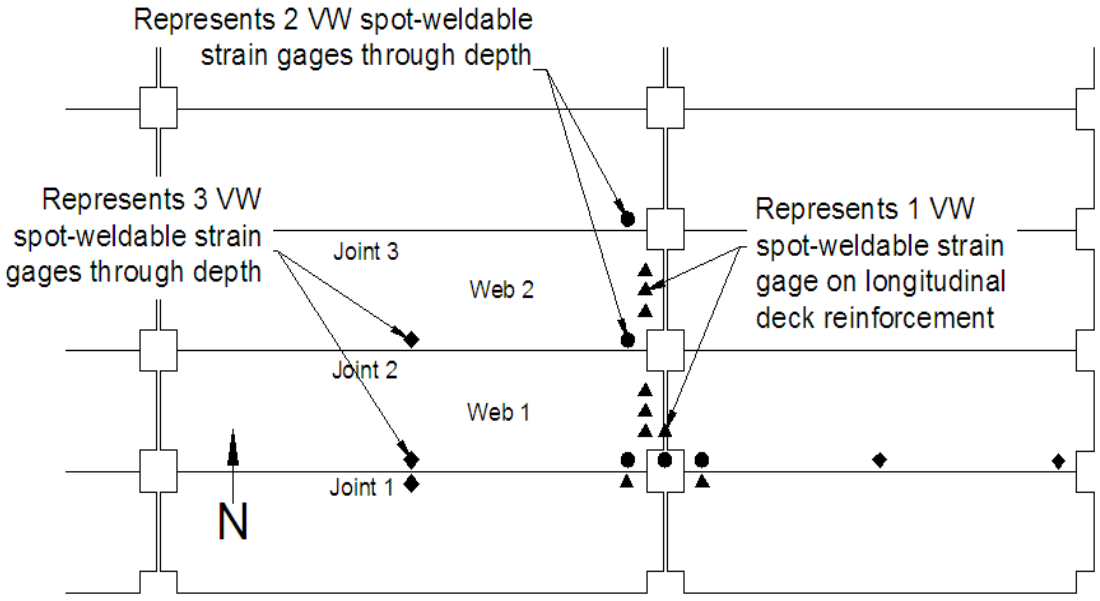

Figure 3.2.6: Plan view of longitudinal instrumentation locations for investigation of live load distribution over the continuous pier (Bell et al. 2006)

The Center City Bridge was constructed with a 5-1/4 in. thick precast flange, which controlled the depth of the transverse hooks and subsequently the vertical location of the instrumentation. The lower level of instruments were installed at a nominal depth, measured from the bottom of the section, of 8.5 in., while the upper row of instrumentation for monitoring reflective cracking was located at a nominal depth of 13.5 in. The nominal and measured instrumentation locations were tabulated by Smith et al. (2008). The nominal and as measured gage locations in the Center City Bridge are included in Appendix B.

The instrumentation naming scheme was described in detail by Smith et al. (2008), and is summarized here. The first two letters of the name refer to the type of gage and general location, "CJ" refers to a concrete embedment gage near the precast joint. The third digit refers to the joint number; therefore "CJ1" refers to instrumentation in joint 1. The fourth digit refers to the longitudinal location of the gage, "5" corresponds to midspan of the center span, which is where all concrete embedment gages were located to monitor the potential for developing reflective cracks (in conjunction with spot-weldable gages on transverse reinforcement). The fifth digit refers to the vertical depth of the gage, with "1" corresponding to the lower row of gages, and "3" corresponding to the top level of gages. Finally, the sixth digit corresponds to the individual gage number in a given row of instruments, and is incremented between one and five for the lower row of gages, and between one and ten for the top row of gages. Therefore, "CJ1-51-3" refers to a concrete embedment gage near the joint region in Joint 1 at midspan of the center span of the bridge, in the bottom layer of instruments and is the third gage in the row of five gages, which was centered directly over the joint.

The data from the instruments was recorded every two hours starting at 10:00am on October 1, 2005. The transverse strains measured at the three instrumented joints at midspan of the center span were monitored over the initial 24 month observation period during the study commissioned by Mn/DOT, as well as afterwards to augment data for the NCHRP 10-71 study. To provide insight into the mechanical strains observed in the bridge, the data collected from the concrete embedment gages was further analyzed. Due to the different values of the coefficient of thermal expansion between the concrete itself and the steel wire inside of the concrete embedment VW gages, taken to be 5.67 με/°F and 6.78 με/°F, respectively, a correction based on the difference between the values of the coefficients of thermal expansion was required to determine the mechanical strain, which was calculated as shown in Eqn. (3.2.1).

$$\varepsilon_{mechanical} = \varepsilon_{measured} + (6.78\ \mu\varepsilon/°F - 5.67\ \mu\varepsilon/°F) * \Delta T \quad (3.2.1)$$

where ΔT is the change in temperature, in degrees Fahrenheit, measured from the base temperature recorded when the initial readings of the strain gages were taken. No correction was necessary for the spot-weldable gages, as they measured the mechanical strain directly.

Large changes in strain observed in Joints 1 and 3 of the structure during the first spring after construction indicated reflective cracking initiated in Joints 1 and 3 on April 25, 2006. Figure 3.2.7 shows the data obtained for Joint 1 which was representative of the behavior of Joint 3 as well. The strain measured in the blue and red gages, which were located directly over and immediately next to the joint, show a large increase and divergence from the other gages starting on April 25, 2006. The blue and red gages correspond with a "3" and "2" as the last number in their name shown in the legend in Figure 3.2.7, respectively; the red gage data series is completely hidden from view by the blue gage data series. The behavior observed in Joints 1 and 3 suggested that cracking was initiated in these joints on April 25, 2006, which was attributed to the effects of solar radiation. Because the bridge was constructed in September of 2005, the bridge was not subjected to significant effects of solar radiation until the spring of 2006. Because the superstructure had been in service and instrumented for a total of 206 days before an increase in the transverse strain was observed, it is unlikely that traffic loading initiated the crack. In fact, strains measured in the transverse joints during subsequent truck load tests conducted in April 2007, as discussed in Section 3.2.1.1, were an order of magnitude smaller than those generated due to the solar radiation effects. Consequently, the reflective cracking was attributed to the effects of large daily variations in the thermal gradient encountered during the spring season due to solar radiation which produced large transverse tensile stresses between the precast panels. Also shown in the figure are the approximate changes in strain over the course of a day during a given summer, with values of 150με and 220με measured during the summers of 2008 and 2009, respectively.

A similar pattern of large measured strains and divergence of Gages 3 and 4 was observed in Joint 3 of the bridge. The approximate relative changes in transverse strain measured in Joint 3 during the summers of 2008 and 2009 were 230με and 300με, respectively. No sudden increase or divergence of the transverse strain was measured in any of the gages located in Joint 2 for the period between October 1, 2005 and July 14, 2009. The presence of cracking in both Joints 1 and 3 was expected to relieve the tensile stresses in the structure which may explain why cracking was not observed in Joint 2; that is, reflective cracking was not originally observed to develop in the adjacent joint.

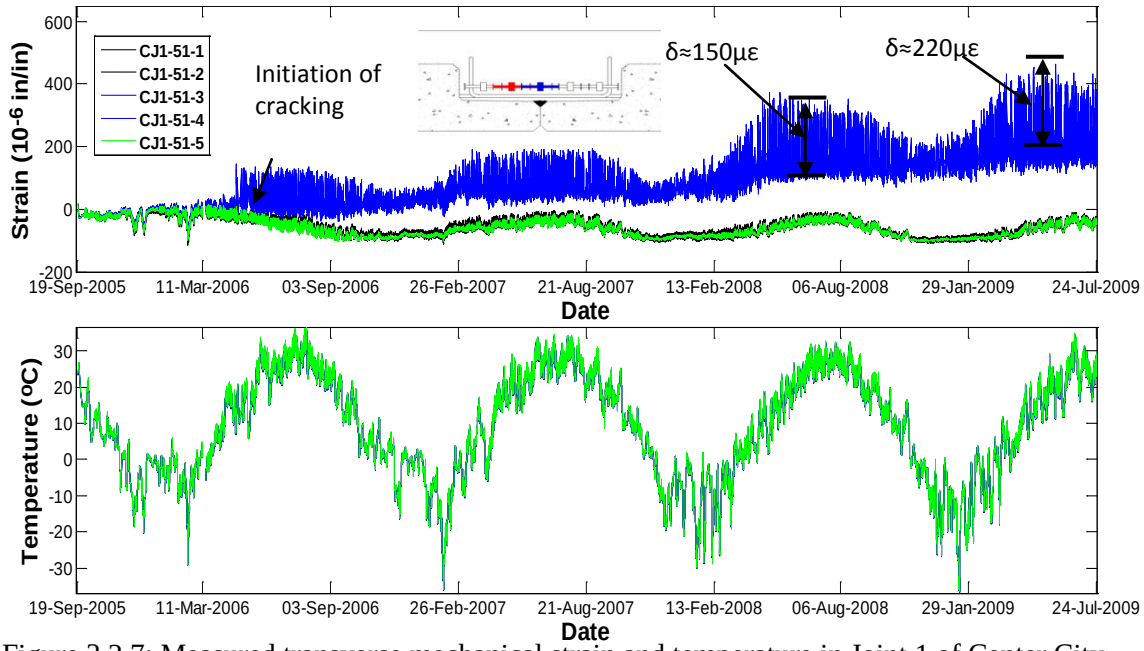

Figure 3.2.7: Measured transverse mechanical strain and temperature in Joint 1 of Center City Bridge [note results of red gage (black dashed line) are obscured by those of the blue gage (blue line) in the figure]

The transverse mechanical strains measured in the Center City Bridge, primarily the relative changes in the strain during a given summer outlined above, provided a quantitative measurement of the performance of an existing bridge in terms of reflective cracking. The measured transverse strains were utilized during the laboratory tests of the NCHRP 10-71 study as a means of determining adequate loading parameters in the laboratory and qualifying the results. The application of the data extracted from the Center City Bridge to the laboratory research specimens is discussed further in Chapters 4 and 5.

Smith et al. (2008) also observed large longitudinal strain readings on the reinforcement near mid-depth of the section at the east pier, which suggested that cracking due to positive restraint moment was present at that location. The daily strain changes of approximately 45 με prior to cracking increased to more than 700 με on April 23, 2006, which was two days before large increases in the daily strain fluctuations were observed in the transverse directions near the longitudinal precast joints at midspan of the center span. The crack at the east pier was monitored for a little over a year, however the monitoring did not continue past June 21, 2007, when the gage measuring the large daily strain changes began to malfunction. Two longitudinally oriented

strain gages located near the top of the section failed to record any large increases in strain over this period, which suggested that the crack had not propagated to the top of the section.

3.2.1. Live Load Distribution Tests at the Center City Bridge

A live load truck test at the Center City Bridge was completed by Smith et al. (2008). The objectives of the live load truck test were to evaluate the response of the structure to known static vehicle loads using the embedded instrumentation, which was subsequently analyzed to determine the applicability of the design assumptions made with respect to transverse live load distribution and continuity over the shared piers. A total of seven single truck and five paired truck configurations were selected for the truck tests, however due to time constraints associated with the single night test, the various configurations were prioritized, with the authors designating the primary test configurations with numbers, and the secondary configurations with letters. The locations of the centroid of the rear truck axles are shown in Figures 3.2.8a and 3.2.8b. The width of the truck axles was measured to be 6 ft.

As shown in Figure 3.2.8a, configurations 1, 2, 3, 4, A, and B were located at midspan of the center span of the bridge, and consisted only of single truck configurations, where the rear tandem of the single truck was centered at midspan of the center span for various lateral positions. The primary purpose of these test locations was to provide several load points across the width of the bridge, which would be useful in calculating longitudinal curvature profiles for many locations along the width of the bridge.

Furthermore, data from the transverse instrumentation collected during these test configurations was utilized to measure the transverse tensile strains in the trough region between the precast panels, where the potential for reflective cracking was a concern. The six truck configurations were selected such that the centroid of the wheels were located either over the precast web (i.e., configurations 2, 4, and A) or directly over the precast joint (i.e., configurations 1, 3, and B), which was expected to represent practical bounds for the minimum and maximum transverse tensile stress demands near the precast joint, respectively. An additional truck position was located at midspan of the outer span (configuration 6) to provide further insight into longitudinal continuity over the pier.

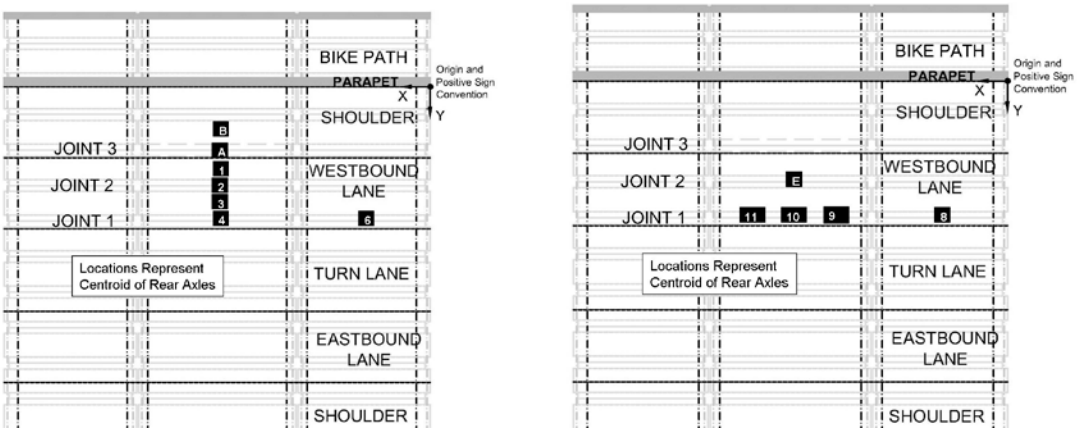

(a) Single truck positions (b) Paired truck positions

Figure 3.2.8: Single and paired truck positions during live load truck tests at the Center City Bridge (Smith et al. 2008)

Paired truck configurations are shown in Figure 3.2.8b which included configurations 8, 9, 10 and 11, in which cases, the two trucks were parked side by side as closely as possible. These configurations were centered over Joint 1, due to the abundance of longitudinal instrumentation near that joint, and were primarily used to investigate longitudinal continuity over the pier. A fifth configuration, designated E, had the rear tandem of the two trucks spaced laterally at 12 ft. on center at midspan of the center span. This orientation located the centroid of one truck directly over Joint 1 and the centroid of the other paired truck directly over Joint 3, thereby loading all three joints by wheel loads transversely located 3 ft. to either side of the three instrumented longitudinal joints. This configuration enabled evaluation of the transverse strains due to global plate bending without the effects of concentrated loads directly over the joints.

The researchers completed the live load tests overnight on April 18, 2007. A total of two tandem sand trucks were utilized, with measured gross vehicle weights of 52.0 and 51.7 kips, which were measured by the contractor away from the test site. Drive-on scales were utilized at the test site to determine the rear axle weights of the individual trucks, however fluctuations in the readings were observed during various weigh-ins due to the fact that the scales elevated the wheels being measured. Therefore, an average rear axle weight was calculated, which was estimated to be 18.6 kips and was applicable to both trucks. Complete tabulated strain measurements from the live load truck tests are given by Smith et al. (2008).

3.2.1.1. Observation of Reflective Cracking during Live Load Truck Tests

The transverse instrumentation located in the three joint regions at midspan of the center span was monitored while wheel loads were individually placed above each joint to investigate the effects of the static loading on the joint regions. When wheel loads were placed above each joint, an increase in the transverse mechanical strains of 19, 7, and 32 με were measured in Joints 1, 2, and 3, respectively. The results obtained for Joints 1 and 2 were calculated as an average over two tests, while three tests were completed over Joint 3. In all cases, the maximum transverse strain was recorded by the middle of the five concrete embedment gages that were located in the lower layer of instrumentation. The increase in the transverse mechanical strains observed during the various test configurations are shown in Table 3.2.1. Instrumentation designation and measured gage locations are given in Appendix B.

Table 3.2.1: Increases in transverse mechanical strains immediately over longitudinal joint during static live load truck tests on the Center City Bridge (Smith et al. 2008)

	Truck Configuration	**Strain Value(s) (με)**
Joint 1	3	19, 19
Joint 2	1	6, 6
Joint 2	3	8, 8
Joint 3	1	30, 31
Joint 3	B	34

When wheel loads were located directly above the longitudinal joints, the change in transverse strain was positive, indicating that there was an induced tensile stress in each joint, and therefore that loading tended to open the joint. Due to the fact that the three instrumented joints were designed identically, it was expected that each of the three joints should see similar increases in transverse strains under similar loading. Therefore, the results of the live load truck tests suggested that pre-existing cracking was likely to be present in Joints 1 and 3, because of the larger increases in transverse strain observed in those locations. This conclusion was also supported by the long term strain monitoring described in Section 3.2, where it was suggested that reflective cracking was observed in Joints 1 and 3. Furthermore the relative values of transverse strain observed during the live load truck tests were significantly less than the daily strain fluctuations observed in the same Joints during the long term observation, where, as discussed in Section 3.2, daily transverse strain fluctuations of more than 220 με were observed.

This suggests that transverse strains induced due to thermal gradients can be an order of magnitude larger than those observed due to traffic loading, and therefore should be considered carefully in the design of precast composite slab span systems.

Smith et al. also investigated the strains measured in the transverse hooked bars using seven spot-weldable strain gages placed on two adjacent hooked bars (i.e., three on one hooked bar and four on an immediately adjacent hooked bar) at midspan of the center span in each of the three Joints. The researchers observed that the strains measured in the transverse hooked bars were slightly smaller than those measured in the concrete embedment gages, despite the fact that the spot-weldable gages were located 1-¼ in. lower in the section. The authors suggested that the reduction in the measured strain in the transverse hooked bars may be due to slip between the transverse hooked bar and CIP concrete due to the size of the bar (No. 6) and epoxy coating. Another potential reason for the reduction in the measured strain may be due to localized slip due to reduced bond immediately near the strain gage as a result of the strain gage cover.

The measured increases in transverse mechanical strains in the adjacent hooked bars observed in Joint 1 under a wheel load during the live load tests are shown in Figure 3.2.9. It can be seen in the figure that each of the adjacent transverse hooked bars shared the load approximately equally, and the strain profile for each hooked bar was similar, regardless of the hook orientation, which suggested that the hooked end was equally effective as the embedded end of each bar.

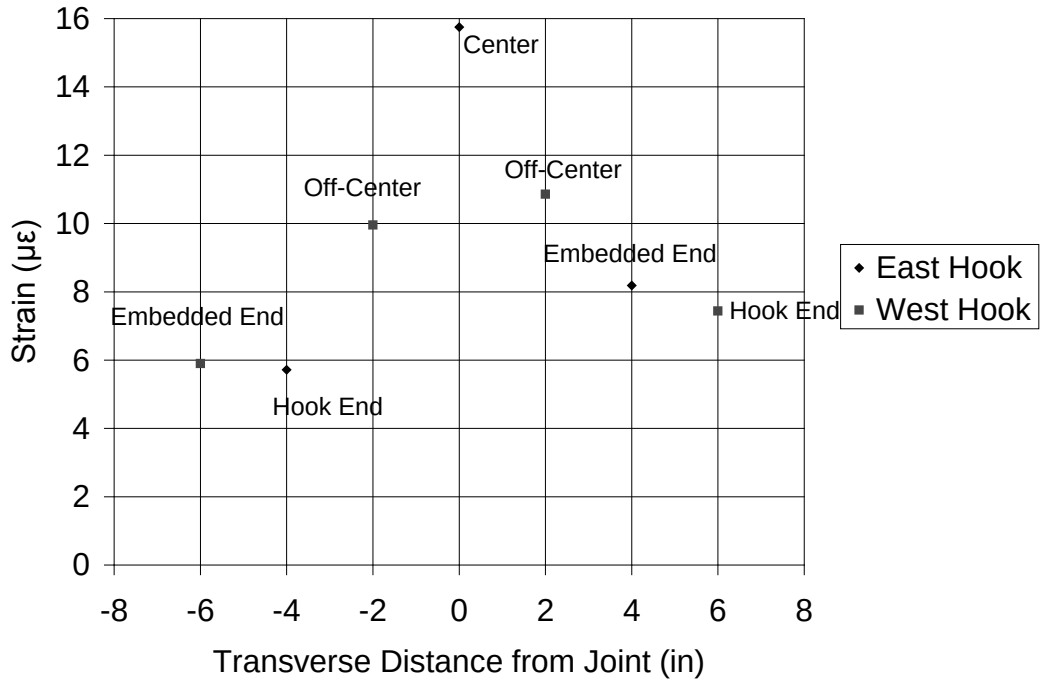

Figure 3.2.9: Change in mechanical tensile strain in transverse hooked bars at Joint 1 immediately under wheel load during live load truck tests on the Center City Bridge (Smith et al., 2008)

3.2.1.2. Transverse Load Distribution During Live Load Truck Tests

Smith et al. (2008) utilized the longitudinal curvature data collected during the live load truck tests to investigate the ability for the Center City Bridge to transfer live loads transversely to adjacent precast panels. In addition, the researchers were interested in the applicability of the AASHTO 2004 Specification Article 4.6.2.3 slab-type bridge load distribution factors, which were utilized in the design of the Center City Bridge (note that the AASHTO Article numbering and content has not changed between the 2004 and 2010 specifications). The authors subsequently utilized the effective width calculations for slab-type bridges to analyze the performance of the Center City Bridge during the truck tests. Configurations 1, 2, 3, 4, A, and B of the truck test were utilized to investigate live load distribution. In each case, longitudinal curvatures calculated at midspan of the center span were measured using the spot-weldable gages located on the longitudinal reinforcement in Joints 1 and 2. Using this procedure, the longitudinal curvature at each joint was calculated as the distance from the joint to the center of the truck load

was varied from 0 in. when the center of the truck was immediately over the joint, to as much as 180 in., which was the distance from the center of the truck to Joint 1 in Configuration B.

The longitudinal curvatures were estimated as the slope of the best fit line through three spot-weldable gages nominally located at 9, 12.5, and 15.5 in. from the bottom of the precast section, though measured locations were utilized in the calculation of the curvatures. The longitudinal curvatures measured as a function of the distance from the center of the truck load to Joints 1 and 2 are shown in Figure 3.2.10. Also included in the figure are the results of a finite element analysis assuming an isotropic flat plate with a smeared stiffness representing the composite section stiffness of the Center City Bridge. The authors included the parapets in their model, however found that the results were affected only locally by the parapets, and therefore were able to superimpose the data for each of the six configurations onto the single plot. Also included in the figure is a simple-span model, which was calculated assuming that the center span was modeled alone on roller bearings located at the center of each pier, thus providing a center to center of bearing simple span of 306 in. Finally, Figure 3.2.10 also illustrates the design equations provided by AASHTO LRFD (2004) Article 4.6.2.3, which provided the effective width factors for slab-type bridges.

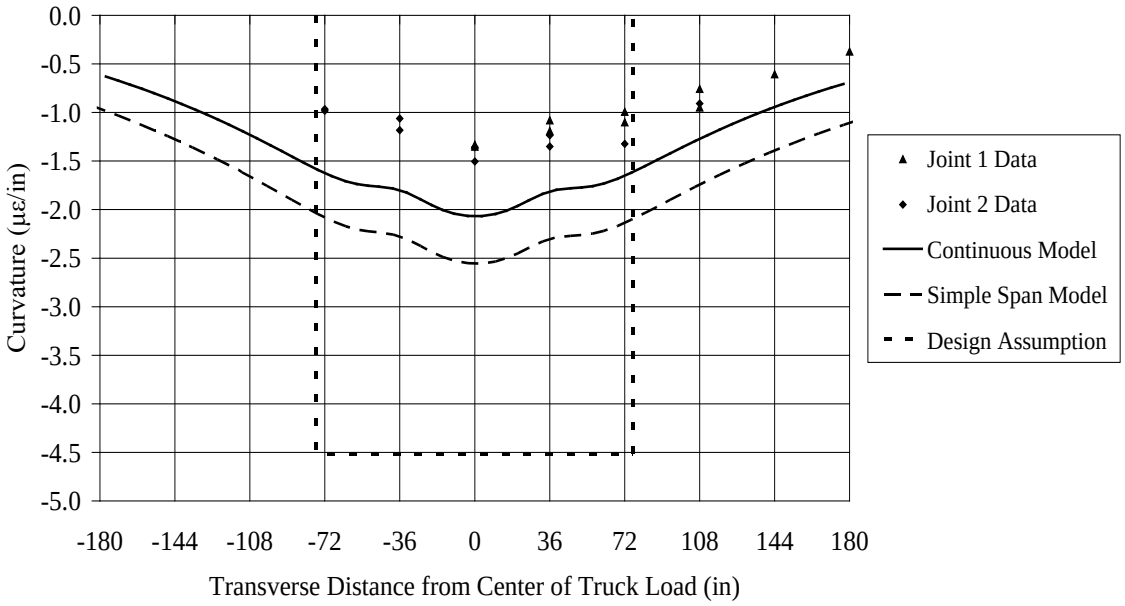

Figure 3.2.10: Longitudinal curvatures at midspan due to a single truck located at midspan of the center span of the Center City Bridge (Smith et al. 2008)

It is evident from Figure 3.2.10 that the measured longitudinal curvatures in the Center City Bridge followed the continuous isotropic model predictions well. Also observed from the figure are the relative similarities in the magnitudes of longitudinal curvatures at common distances from the center of the truck loads. This suggested that loads applied at various distances from Joints 1 and 2 tended to affect each joint similarly, despite suspected reflective cracking in Joint 1 (see Section 3.2). For this reason, the authors suggested that the PCSSS could be adequately modeled using an isotropic plate, which was expected to be simpler because it removed the need to model the discontinuity created by the longitudinal precast joint. Furthermore, the simple span model was found to be more conservative than the continuous model, and would also adequately serve as a method for numerical analysis of the PCSSS.

These results also provided significant insight into the applicability of the current design equations provided for slab-type bridges in the AASHTO (2004) LRFD Specification. As shown in the figure, the curvatures determined via the slab-type design equations were approximately three times larger than the curvatures measured in the Center City Bridge when the wheel load was centered directly over the longitudinal joint. For this reason, the slab-type effective lane widths presented in the AASHTO LRFD Specifications (2004) were deemed to be adequate and conservative for the design of precast composite slab span systems. It can be assumed that longer spans would behave similarly because they would have a deeper overall section, and the height of the gap at the flange tips would be unchanged, so longer span bridges should behave more like monolithic systems than shorter ones.

3.2.1.3. Continuity over the Continuous Piers during Live Load Truck Tests

Another behavior of interest considered by Smith et al. (2008) was the level of continuity achieved between the piers. For this case, midspan of the center span was loaded directly over Joint 1 and the longitudinal strains in the deck reinforcement of the adjacent span were recorded and compared to the values calculated using the isotropic continuous finite element model. When the center span was loaded, changes in longitudinal strains in the deck steel of the adjacent span were 1.2 and 1.5 με for single and double truck configurations, respectively. These values were slightly smaller than those predicted by the continuous FEM model, where values of 1.9 and 3.7 με were predicted for single and double truck configurations, respectively. A likely reason for the discrepancy between the measured and predicted values was attributed to moment transferred into the pier cap, whereas idealized rollers were assumed in the finite element model. In addition, the

midspan curvatures in the center span were observed to be smaller than those predicted in the model, as discussed in Section 3.2.1.2. The overall performance of the Center City Bridge during the truck tests suggested that the assumption of full continuity appeared to be conservative for the precast composite slab span system.

3.3. Restraint Moment

Multi-span precast composite bridge structures made continuous with CIP concrete develop time-dependent and thermal restraint moments at the continuous piers. The sign and magnitude of restraint moments are affected by shrinkage, creep, age of the precast members at the time of continuity, and thermal gradients. Positive and negative restraint moments are illustrated in Figure 3.3.1.

Negative restraint moments are caused by differential shrinkage of the CIP concrete, where the rate of shrinkage of the CIP concrete is larger than the rate of shrinkage and creep of the precast member. When the precast member is at a relatively old age, defined as greater than 90 days in AASHTO (2010) Article 5.14.1.4.4, the shrinkage of the newly placed CIP concrete will tend to "shorten" the top fiber of the bridge structure and subsequently induce longitudinal tensile stresses in the top of the bridge at the piers. The reinforcement included in the deck of the structure over the piers in continuous systems provides the tension ties necessary to counteract negative restraint moments.

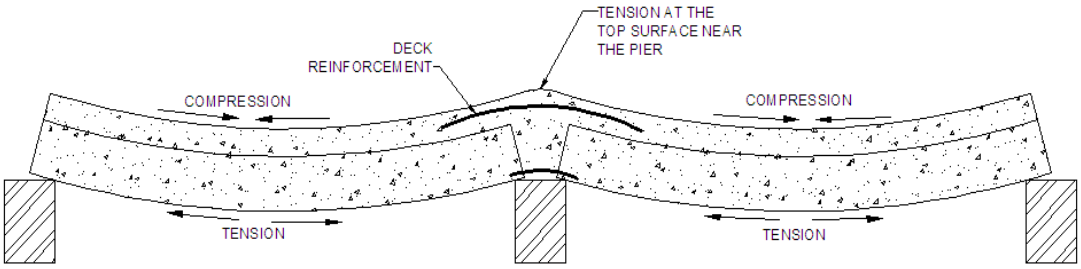

(a) Negative restraint moment induces tension near the top surface at the pier

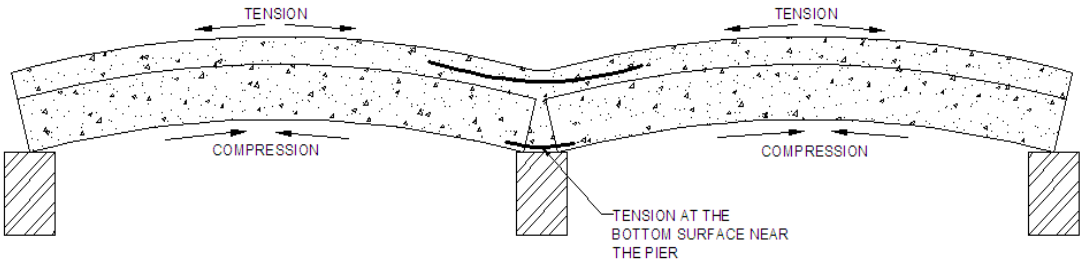

(b) Positive restraint moment induces tension near the bottom surface at the pier

Figure 3.3.1: Positive and negative restraint moments in continuous bridge superstructures (Molnau 2007)

Positive restraint moments at the piers in continuous systems may be due to both time-dependent and thermal effects. When the precast member is at a relatively young age at the time of continuity, the rate of shrinkage of the precast member and the CIP may be similar, however, the precast member would also undergo creep. The creep of the precast section would tend to "shorten" the bottom fiber of the bridge structure and subsequently induce longitudinal tensile stresses in the bottom of the bridge at the pier. In addition, thermal gradients in the section cause the top surface of the structure to expand, again inducing a positive restraint moment in the structure. For this reason, both time-dependent and thermal gradient effects must be considered in the design of positive restraint moments. Because positive restraint moments induce longitudinal tensile stresses near the bottom of the section, reinforcement must be provided to carry the tensile force at the piers. Because of the sectional geometry of the PCSSS, all reinforcement provided for positive restraint moments must be located within the longitudinal trough regions between precast panels. Consequently, this reinforcement must be placed in groups centered between panels, generally six feet apart, thereby prohibiting the distribution of the reinforcement along the face of the bottom surface.

Smith et al. (2008) monitored the Center City Bridge for evidence of cracking due to restraint moment. Gages located at the pier indicated that cracking initiated due to the effects of positive restraint moment. The crack was believed to develop as the bridge underwent its first large thermal gradient effects due to solar radiation in the spring. As a consequence, it was suspected that the behavior was driven by thermal gradients in the bridge superstructure where the solar radiation heated the top of the bridge. This caused the individual spans of the bridge to camber which generated positive restraint moments. Eriksson (2008, pp. 56) stated, "Because [the] time-dependent effects on [the day the crack was observed] should not have varied significantly from the previous day, researchers speculated thermal effects may have played a role in the crack development. Based on this conjecture, both time-dependent and thermal gradient effects on restraint moment were investigated analytically." Eriksson (2008) completed a parametric study to investigate the effects of differential shrinkage, creep, and thermal gradient effects on the development of restraint moments.

In an effort to predict the restraint moment in a section based on the time-dependent properties of the system, Eriksson completed a numerical parametric study using Pbeam, which is a fiber-based finite element code developed by Suttikan at the University of Texas in 1978 (Suttikan, 1978). The program allows for inputs including material strength, age, creep, shrinkage, steel relaxation, dead loads and support conditions. The program provides output in the form of stresses, strains, reactions and deformations at user specified time intervals (Suttikan 1978). Furthermore, Eriksson utilized a modified version of Pbeam created by Le (1998), called TPbeam, which enables incorporation of thermal gradient effects in the analysis. After finding that, when using functions based on measured quantities for the input values (i.e., creep, shrinkage, concrete strength gain with age, etc.), Pbeam predicted restraint moments that corresponded reasonably well with the measured results from the Concept 1 laboratory specimen, Eriksson utilized both Pbeam and TPbeam to conduct a parametric study to determine reasonable bounds for expected restraint moments in PCSSS bridges. In general, the purpose of the parametric study was to predict the maximum positive and negative restraint moments that would be expected in PCSSS bridges. Precast strengths of 6 ksi and 12.9 ksi were used with assumed continuity dates of 7, 28, 60, and 90 days to develop an expected envelope of the positive and negative restraint moments.

Because of the difficulty in providing reinforcement for positive restraint moment due to the geometry of the PCSSS, the necessity to design for such moments was of interest. Eriksson found that, “positive restraint moment cracking due to time-dependent effects is not expected for [PCSSS] for spans between 20 and 50 ft” as seen in Figure 3.3.2 where the ratio of positive restraint moment to cracking moment is always less than one when only time-dependent effects were included. Also, positive restraint moment generally induced at the pier was due to creep of the precast member, therefore increasing the age of the precast member at continuity will reduce the positive restraint moment due to time-dependent effects in the section. The thermal gradient due to solar radiation has the same effect as placing CIP on a young precast section. The results from TPbeam substantiate NCHRP 519 findings that state restraint moments due to thermal effects are significant (Miller et al. 2004). Eriksson (2008) found that the positive restraint moments caused by thermal effects induced restraint moments that were two to seven times larger than the positive restraint moments caused by time-dependent effects as shown in Figure 3.3.3. As a consequence, positive restraint moment cracking due to thermal gradient effects was expected to occur in nearly all of the designs studied, and therefore should be considered by the designer.

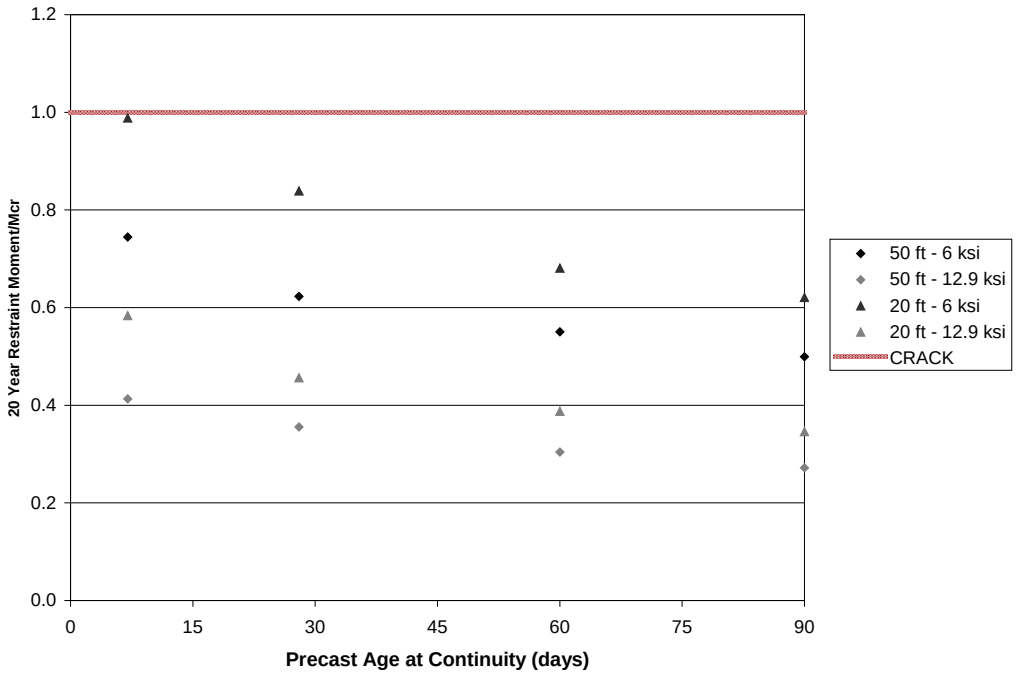

Figure 3.3.2: Ratio of 20-year positive restraint moment (due to time-dependent effects only) to cracking moment comparison

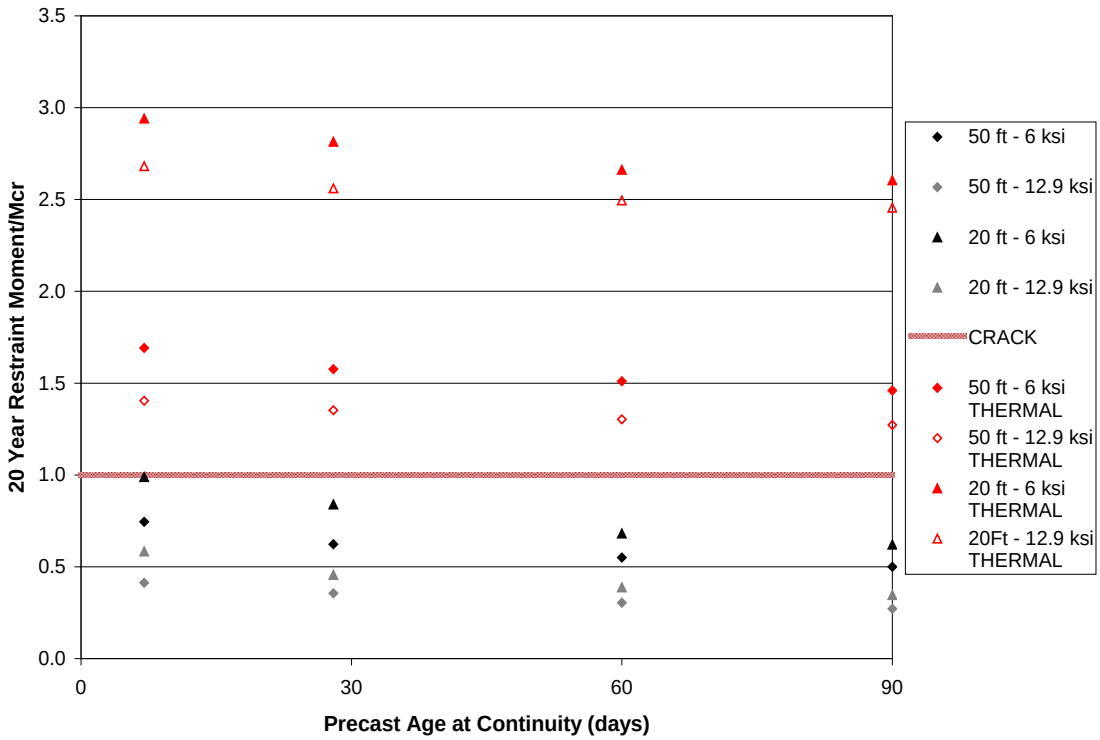

Figure 3.3.3: Ratio of 20-year positive restraint moment (due to time-dependent and thermal effects) to cracking moment comparison

AASHTO (2010) Article 3.12.3 provides general guidelines for design of thermal gradients based on regional zones, but indicates temperature gradient should be evaluated on a project specific basis. Judgment is reserved for experienced designers indicating thermal gradient can be neglected if previous structures have not experienced distress. These basic guidelines provide little guidance regarding when thermal gradients are important. Based on the fiber-based finite element model results from Pbeam and TPbeam and the suspected positive moment crack in the Center City Bridge, thermal effects have a significant effect on the development of positive restraint moments and should be considered in the restraint moment design.

Restraint moment design for time-dependent properties is complicated by the need to investigate the interaction of the variation in time-dependent effects over time. The PCA and P-method both provide options for how to design for restraint moments due to time-dependent effects. However, design for restraint moments caused by thermal effects does not include the time variation and should be summed with restraint moments due to time-dependent effects.

Barker and Puckett (2007) provide a hand calculation for determining the restraint moment due to thermal effects. Assuming the beam is a simple span between supports, the design thermal

gradient is applied to the section and used to calculate the resulting curvature in the beam. The curvature from a temperature gradient can be expressed as

$$\phi = \frac{\alpha}{I} \cdot \int T(y) \cdot y \cdot dA \tag{3.3.1}$$

where α is the coefficient of thermal expansion, *T(y)* is the temperature gradient (°F) through the depth *y* of the member (in.), and *I* is the moment of inertia of the entire cross section (in.^{4}) (Barker and Puckett, 2007). This equation is also found in AASHTO (2010) Article C4.6.6.

The end rotation (θ) can be found by integrating the curvature from midspan to the end of the span. Then, the restraint moment, or the moment restraining the rotation, can be found using the three-moment equation. The equation assumes pinned-end supports and is expressed as

$$M = 3 \cdot \theta \cdot \frac{E \cdot I}{L} \tag{3.3.2}$$

where θ is the rotation, *E* is the elastic modulus (for the composite system), and *L* is the span length.

The moment, *M*, is the restraint moment at the pier of a continuous system to resist the rotations induced by the thermal gradient. If the span lengths on each side of the pier are not equal, then the different spans will induce different moments at the pier (i.e., the rotation would be different, leading to different moments).The restraint moments induced by thermal gradients in each span can be calculated using Eqn. (3.3.2) and the design thermal gradient should be for the largest restraint moment. The effects of thermal gradients and time-dependent effects can be calculated independently and then combined with the appropriate load factors.

Using the above methodology for prediction of the thermally-induced restraint moments in the 20 and 50 ft. span beams in the parametric study conducted by Eriksson (2008) provided conservative results as compared to the TPbeam results, as shown in Figure 3.3.4. The hand calculations over-predicted the calculated positive restraint moment by a range of 20 to 40 percent. The calculations agreed with TPbeam results that the highest ratio of positive restraint moment induced by a thermal gradient to the cracking moment (i.e., 2.9) was for the 20 ft. span with 12.9 ksi concrete. The shorter span with greater concrete strength had the greatest stiffness and the least flexibility of the sections studied. The 50 ft. span with 6 ksi concrete, the most flexible section studied, had the lowest ratio of positive restraint moment induced by thermal gradient to cracking moment (i.e., 0.95).

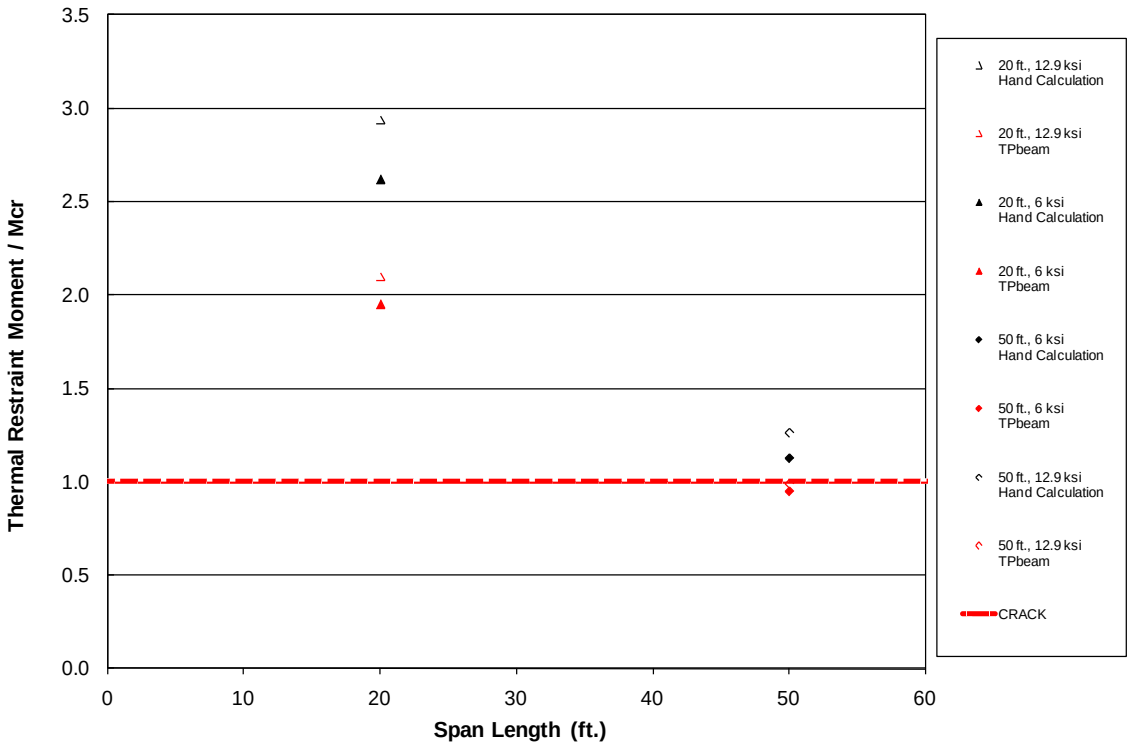

Figure 3.3.4: Comparison of calculated and TPbeam results for ratio of 20-year restraint moment (due to thermal effects only) to cracking moment

The magnitude of the positive restraint moments, with the inclusion of the effects of thermal gradient, may negate any benefit from continuity at service. In this case, if positive moment reinforcement steel is placed at the pier to tie the structure together, the possibility of developing a positive moment at the pier cannot be neglected and the restraint moment should be taken as the lesser of the calculated restraint moments and the moment that can be developed using the positive moment reinforcement placed at the pier.

Chapter 4: Numerical Studies of Practical Span Ranges, Applicability of Design Recommendations, and Other Issues

4.0 Introduction and Organization

A combined numerical and experimental approach was used to investigate issues associated with the development of design recommendations for the precast composite slab span system. In a few cases, where appropriate, design recommendations for the PCSSS were based on information obtained from the literature or previous studies conducted by the researchers (Smith et al. 2008, Eriksson 2008). Issues of interest included:

- Determination of range of applicability for PCSSS bridges (Section 4.1). Completed by Piccinin et. al. (2008)
- Control of reflective cracking across the longitudinal joint between precast flanges
    - Effect of transverse reinforcement spacing (Section 4.2). Completed by Hedegaard (2010)
- Applicability of slab-span design recommendations to PCSSS bridges
    - Live load distribution factors (Section 4.3). Completed by Hedegaard (2010)
    - Skew effects (Section 4.4). Completed by Hedegaard (2010)
- Composite action between the precast and CIP
- Effect of restraint moment due to time-dependent and thermal gradient effects
- End zone stresses in precast inverted tee sections (Section 4.5) (Eriksson 2008)
- Support conditions (Section 4.6)
- Determination of appropriate magnitude of patch load to be applied to laboratory specimens to represent range of possible span lengths (Section 4.7) (FEM Model by Piccinin (2010)

This chapter primarily focuses on the numerical investigations associated with these issues.

Regarding the range of applicability for the PCSSS, it was expected to be most efficient for relatively short to moderate span bridges. A parametric study was conducted over a range of span lengths for both simply-supported and continuous PCSSS models to provide greater insight into the range of spans that could be efficiently bridged using the PCSSS. Because of the shallow member depths associated with this type of superstructure, the service behavior and effective moment capacity of the section was largely dependent on the amount of prestress force, due to the

fact that the moment arm is relatively short in comparison to traditional girder-type bridges. For this reason, one of the primary limiting components of the precast inverted-T design was the level of prestress that could be achieved, while the appropriate stress limits in the specification were satisfied. The parametric study therefore was utilized to identify the appropriate span lengths that could be efficiently achieved, and the corresponding prestress force and member depths that would be required, which is summarized in Section 4.1.

A primary issue of importance for the NCHRP 10-71 study was the development of durable connection concepts. In the case of PCSSS bridges, the control of the development of potential reflective cracking is key to the achievement of a durable system. There is the potential for the development of reflective cracks in the CIP from stress raisers associated with the precast portion of the section (i.e., above the joint between the precast flanges and near sharp corners of the precast section). With regard to the issue of reflective crack control, numerical studies summarized in this chapter were used to investigate the effect of the transverse reinforcement spacing on reflective crack control, as well as on transverse load transfer. These studies are described in Section 4.2. Reflective crack control was also investigated extensively through the laboratory studies described in Chapters 5 and 6 which detail the results of the laboratory bridge and subassemblage tests, respectively.

PCSSS bridges are very similar to slab-span systems, with two exceptions. First, the adjacent flanges of the precast inverted-Ts used to create the PCSSS bridges cause discontinuities in the system along the interface of the adjacent flanges; and second, the composite nature of the PCSSS requires additional design considerations. To investigate the applicability of slab-span design recommendations to PCSSS bridges which feature the discontinuity along the adjacent flanges, numerical studies were conducted as described in Sections 4.3 and 4.4 regarding live load distribution and skew effects. Numerical models of the PCSSS featured discontinuities along the adjacent flanges which were compared to the results of models of monolithic systems. In some cases, additional models were developed to investigate the influence of potential reflective cracking on the performance of the systems. The PCSSS was expected to provide live load distribution in a similar manner to that of traditional monolithic slab-span superstructures, a conclusion that was supported by the numerical modeling. Furthermore, the effects of skew were expected to increase the magnitude of longitudinal shear stress in the region between the tips of the precast flanges, especially in the exterior joints between the members. Several FEM models were utilized to provide insight into the behavior of the system and the potential increases in

stress at various locations of the system due to skew, and to determine the applicability of the current specifications to the PCSSS.

The composite nature of the PCSSS required an investigation of the detailing requirements across the interface between the precast and CIP. In addition, the composite nature of the system required investigation of the potential for the development of restraint moments due to the time-dependent effects of creep and shrinkage. The required detailing across the interface between the precast and CIP to ensure composite action was investigated through a review of the literature, as well as through laboratory studies of the PCSSS Concept 1 and 2 bridges which were subjected to ultimate load tests as described in Chapter 5. The effect of restraint moments in the PCSSS were investigated numerically and experimentally in a previous study by the researchers, the results of which can be found in Smith et al. (2008) and Eriksson (2008). These results summarized in Section 3.3 provided the basis for the associated design recommendations in this study.

The precast inverted-T sections of the PCSSS also required review of associated design recommendations for the precast prestressed elements particularly for the development of detailing requirements associated with end zone stresses because current requirements were found to be developed considering I-sections rather than panel systems. This aspect was investigated numerically and experimentally as described in Section 4.5.

The connection between the precast elements and the substructure was investigated primarily by means of examination of structural plans for existing PCSSS structures. This review is summarized in Section 4.6.

Numerical analyses were also used to determine the patch load to be used for the laboratory investigations conducted on the Concept 1 and 2 PCSSS bridges discussed in Chapter 5. These analyses are summarized in Section 4.7.

4.1. Parametric Study to Investigate Practical Span Ranges and Associated Precast Sections

The work chronicled in Section 4.1 was completed by Piccinin et al. (2008).

The weight associated with the precast composite slab span system, like most slab bridges, was expected to limit the range of applicable spans to what may be considered short to moderate spans. The PCSSS was expected to be a practical system for bridges with spans up to approximately 60 ft. In an effort to clearly identify and document the range of spans and

associated section dimensions and design details for the PCSSS, a parametric study was completed. The study aimed to identify efficient span lengths, as well as the required prestress forces and to ensure that the compression and tension stress limits were satisfied in the inverted-T sections.

Span lengths of 20, 30, 50, and 65 ft. were identified as practical and efficient for the precast slab span system. The 20 ft. span length was chosen to represent the shortest practicable span length; the span range between 30 and 50 ft. was selected because of the large applicability of this system, while the 65 ft. span was chosen as a maximum feasible span length for the PCSSS. In addition, with the recommendation from K. Molnau (Mn/DOT), more representative configurations were considered, which included 20-30-20 ft., 30-50-30 ft., and 50-50-50 ft. three-span continuous systems. Because it was expected that a two-span 50-50 ft. would not differ significantly from the behavior of the 30-50-30 ft. three span bridge, a sole 65-65 ft. configuration was selected to investigate two-span systems.

Moment envelope curves were developed for the configurations listed above, and were considered for two dynamic load situations as specified by the AASHTO (2010) LRFD specifications, HL-93 and Tandem vehicles, in addition to a static uniformly distributed lane load of 640 lb/ft.^{2} patterned along the length of the system. A dynamic allowance factor equal to 0.33 was selected for the moving load cases. Live load distribution factors were calculated according to a modified version of the AASHTO (2010) specifications (Article 4.6.2.3), *Equivalent Strip Widths for Slab-Type Bridges,* as shown in Eqn. (4.1.1). The effective lane width was considered with two or more lanes loaded, and the limiting lane width factor of $12.0W/N_L$ was not considered.

$$E = 84.0 + 1.44\sqrt{L_1 W_1} \tag{4.1.1}$$

where E is the equivalent lane width when two or more lanes are loaded (in.), L_1 is the modified span length taken equal to the lesser of the span length or 60.0 (ft.), and W_1 is the modified edge-to-edge width of the bridge taken to be equal to the lesser of the width or 60.0 (ft.).

Initially positive and negative restraint moments were assumed to be zero during this portion of the study, which corresponded with the assumption that the CIP concrete was placed after the precast members were at a relatively old age. When the casting of the bridge deck is completed much later than the casting of the precast elements (i.e., 90 days as specified by the specification) the time-dependent drivers of positive restraint moments can be neglected (however the effects of thermal gradients should be considered).

Later consideration included the calculation of the restraint moments for two configurations, the 50-50-50 ft. and 65-65 ft. systems. In both cases, the age of the precast members was taken to be 14 days when continuity was established. The moments were calculated using the PCA method (Freyermuth, 1969). Depending on the age of the precast at which continuity is made and the amount of time since continuity, the PCA method is considered to predict accurate magnitudes for the maximum positive moments but generally overestimates the negative restraint moments. The method is based on both structural mechanics concepts and creep/shrinkage experimental data.

In this study, the positive restraint moments were more thoroughly considered because they were expected to influence the design of the system more significantly than the negative restraint moments. The positive restraint moments increase the magnitude of the positive moment at midspan at service, and are difficult to resist because of the limited locations available to include continuous reinforcement near the bottom of the section at the piers (i.e., in the troughs between the precast webs).

The material properties utilized in each model were identical. The concrete compressive strength of the CIP and precast concrete was taken to be 4 and 6 ksi, at 28-days, respectively. The precast concrete strength was assumed to be 5 ksi at transfer. A 6 in. thick composite CIP deck was identical in each model. The strands were assumed to be 0.5 in. diameter Grade 270 low relaxation strands pulled to a stress of 202.5 ksi (75 percent of f_{pu}). The flange thickness was kept constant at 3 in., and the standard width inverted-T sections of 6 ft. were used. The increased stiffness associated with the deck reinforcement was ignored during this study, which was consistent with similar calculations used by Mn/DOT during the design of bridge systems, and was conservative. Losses were calculated using the Zia method (1979).

The primary metrics utilized to determine the appropriate design parameters for each configuration were the stress limits specified by AASHTO (2010). Two limit states were investigated, transfer and service. The compression and tension stress limits for each are shown in Table 4.1.1.

Table 4.1.1[1]: Concrete stress limits utilized during parametric study

	PC Concrete	
	Limit	Value
Transfer		
Compression	$-0.6 \cdot f_{ci}$	-3 ksi
Tension	$0.24 \cdot \sqrt{f_{ci}}$	0.537 ksi
Service		
Compression	$-0.45 \cdot f'_c$	-2.7 ksi
Tension	$0.19 \cdot \sqrt{f'_c}$	0.465 ksi

[1]All units in Table 4.1.1 are in units of ksi, i.e., f'_c is entered into the equations in units of ksi (regardless of whether there is a square root function or not) and the results of each stress limit are in ksi

The design process was found to be governed by the stress limits at transfer at the ends of the beams, and the stress limits at service at midspan. In most cases, the tension limit for the bottom fiber at midspan at the service state was found to control.

Table 4.1.2 presents a summary of selected optimized sections for the individual span lengths. For each of the optimized sections, the table summarizes the total precast section depth; the assumed flange thickness, which was taken as 3 in. (76 mm) except in the case of one of the spans which was designed to replicate the short spans in the Center City field implementation of the bridge; cross-sectional area; required number of strands to meet the service stress limits; required concrete compressive strengths at transfer and service to meet the required stress limits; total prestress force assumed immediately after transfer; span configuration in which the section was assumed; and the limiting stress ratios in the design of the sections. In cases where the design stresses were exceeded, recommended changes were provided to alleviate the limit exceedance. In cases where the compressive stress limits were exceeded, the design concrete compressive strengths at release were increased; in cases where the tensile stress limits were exceeded, the required mild reinforcement to carry the full tensile force is listed.

As mentioned above, the bottom fiber tension stress limits controlled at service in most of the cases. Satisfying the bottom fiber tensile stress limits at service required increasing the number of tendons (total prestressing force) or increasing the depth of the section. An increase in the value of the maximum positive moment at midspan (longer spans), required a larger number of tendons to satisfy the stress limits and, when this was not feasible, the depth of the section was increased. When considering the effect of the positive restraint moments, the total positive moment acting at

midspan was increased and so it was necessary to increase the amount of prestress for the same section.

In considering the feasibility of the systems according to the different configurations described above, important issues were identified associated with the weight of the precast section that might be controlled by truck load capacities in transport or crane capacities at erection. For the truck load limits, the sections should be limited to 80 kips (350 kN) without requiring a special permit. Typical crane capacities can readily handle the 80 kip (350 kN) capacity (this value could be as high as 130 kips (580 kN) in some cases).

As an example, in the case of the 65 ft. (19.8 m) span section, an initial minimum depth of 20 in. (500 mm) was considered for the precast section, but it required three rows of tendons. The amount of prestress caused problems with the tensile and compressive stress limits at the ends at release and compressive stress limits at midspan at service. Increasing the depth of the precast section to 22 or 24 in. alleviated these issues to an extent. Using a 22 in. deep precast section with 54 tendons, required a concrete compressive strength at transfer of 6 ksi rather than the nominal value of 5 ksi. Using a 24 in. deep precast section with 46 prestressing tendons alternatively solved the problem but with this depth the weight of the precast section exceeded 80 kips, which could be an issue with transport.

Table 4.1.2: Precast section dimensions and results of parametric study

Span Length [ft.]	20	30	22[1]	22[1]	45	50	62	65
Depth of Precast [in.]	8	10	12	12	14	16	20	22
Flange Thickness [in.]	3	3	5.25	3	3	3	3	3
Cross-Sectional Area [in.^{2}]	460	560	710	650	750	840	1000	1100
Number of Strands	10	16	16	16	36	38	46	54
Concrete Strength at Transfer [ksi]	5	5	4.5	4.5	5.5	5.4	5.6	6
Concrete Strength at Service (ksi)	6	6	6	6	6	6	6	6
Prestress Force [kip]	306	500	500	500	1100	1200	1400	1700
Span Combination [ft.]	**20**[2]-30-**20**	20-**30**-20	**22-22**	**22-22**	**45**-62-**45**	**50-50-50**	45-**62**-45	**65-65**
Limiting Ratios in Design of Sections								
End stresses at transfer including mild reinforcement and f_{ci} modifications required to satisfy end stresses								
f_t /(0.24$\sqrt{f_{ci}}$ ksi)	<1	<1	<1	<1	1.51	1.73	2.04	2.11
Solution, A_s [in.^{2}]	--	--	--	--	6-#5	9-#5	10-#6	12-#6
f_c /(0.6f_{ci} ksi)	<1	<1	<1	<1	1.08	1.08	1.12	1.20
Solution, f_{ci} [ksi]	--	--	--	--	f_{ci}'=5.4	f_{ci}'=5.4	f_{ci}'=5.6	f_{ci}'=6
Midspan stresses at service Section depth and number of strands were chosen to satisfy end stresses								

[1]Represents the precast sections used in the Center City Bridge and Concept 1 and Concept 2 large scale laboratory specimens

[2]Bolded span lengths indicate the span utilized for the sectional design parameters in that column

In summary, the range of span lengths considered during this study was found to provide a reasonable bound for applicable span lengths for the PCSSS. The 65 ft. simply supported system would require 54 0.5 in. diameter strands. Because the prestressed strand is concentrated within the 4 ft. web width of the inverted-T section, it would take more than two layers of strands at 2 in. centers to accommodate 54 tendons. This would not be the most efficient use of the system because the short member depths require that the longitudinal reinforcement is grouped as low in

the member as possible to increase the eccentricity and moment arm. Also, at the lower bound, the 20 and 30 ft. spans provide a relatively economical design with the moderate member depth and number of tendons.

4.2. Parametric Study to Investigate Effect of Transverse Hook Spacing on Reflective Cracking

The work chronicled in Section 4.2 was completed by Brock Hedegaard (2010)

Finite element parametric modeling was used to investigate the influence of the spacing between transverse hooked reinforcement on the transverse load transfer and reflective crack controlling capabilities of the PCSSS. The geometry of the bridge specimen was similar to that used in the large-scale Concept 1 laboratory bridge, consisting of a two-span continuous bridge, however each span utilized in the model was 30 ft. Each span consisted of two adjacent 6 ft. wide precast panels. Several models were developed to investigate the range of transverse hooked bar spacing between 6 and 18 in. Each model was constructed using 20 node quadratic continuum elements with reduced integration. The boundary conditions were roller supports at the ends of the bridge and a perfectly frictionless pin at the continuous pier. Loading was applied to correspond with the magnitude and patch size utilized in the laboratory study, which was 35 kip and 10 by 20 in., respectively. The load was oriented such that the long direction of the patch was perpendicular to the direction of the longitudinal precast joint. Two load cases were considered, the first was with loading centered at midspan directly over the precast joint and the second was at midspan with the edge of the load aligned with the edge of the vertical precast web, as illustrated in Figure 4.2.1. A summary of the FEM test cases is given in Table 4.2.1.

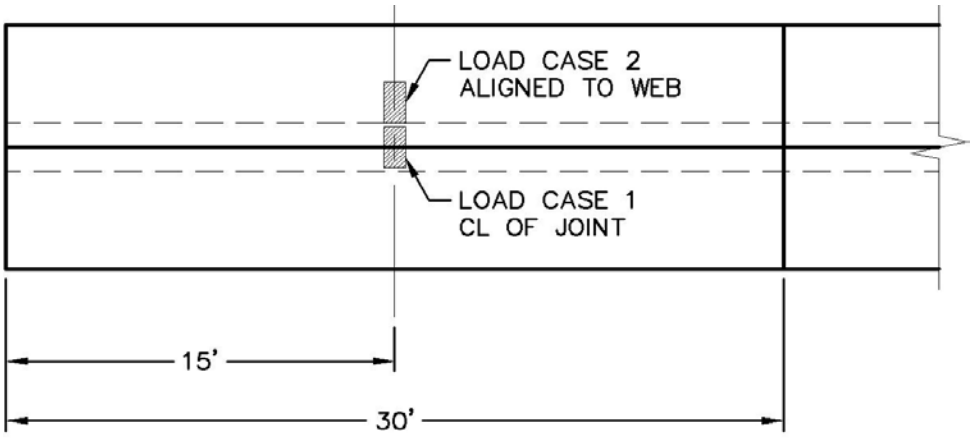

Figure 4.2.1: Location and orientation of loading in the loaded span of the two-span bridge model

Except for the transverse hooked bars crossing the longitudinal joint, rebar and prestressing strands were approximated as plates with negligible stiffness in all directions except axially in the orientation of the rebar. The transverse hooked bars were modeled as beam members with a 3/4 in. diameter circular cross section. The transverse hooked bars were debonded for 1-1/2 in. on either side of the longitudinal joint for a total debonded length of 3 in., which was selected as an approximation of the bond condition between the rebar and concrete in the joint area.

Four materials were used throughout the model. All CIP concrete was assumed to have an elastic modulus of 3,600 ksi, which was determined using AASHTO LRFD Article C5.4.2.4-1, assuming normal weight concrete with a compressive strength of 4,000 psi and Poisson's ratio of 0.2. All precast concrete was modeled assuming an elastic modulus of 4,600 ksi, which was calculated using the above equation and normal weight concrete with strength of 6.5 ksi and Poisson's ratio of 0.2. The plates used for modeling the rebar were assumed at have a modulus of elasticity of 1 psi and Poisson's ratio of 0.2; the low elastic modulus of the plates was selected to ensure that they did not contribute to the section stiffness globally. All rebar layers embedded within the plates (including mild steel and prestressing strands) were modeled with a modulus of elasticity of 29,000 ksi and Poisson's ratio of 0.3.

In model Runs 1, 2, and 3 the cast-in-place was bonded only to the sides and top of the precast panel webs. The precast flanges were assumed to be unbonded from the CIP concrete. The unbonded flanges were selected to simulate the separation of the flanges from the CIP above the longitudinal joints. These runs assumed reflective cracking to approximately the depth of the elastic neutral axis in transverse bending for the 12 in. hooked bar spacing. The crack was assumed to extend vertically a distance of 9 in. from the bottom of the section. The fourth run depicted a fully bonded slab, where the CIP was completely bonded to the precast panels and the joint between the tips of the precast panels was eliminated through the use of tied elements between the adjacent members. This fourth run simulated a monolithic slab span.

Table 4.2.1: Summary of FEM runs to investigate effects of transverse hooked bar spacing

Description	*Run Number*	*1*	*2*	*3*	*4*
	Run configuration	*PCSSS w/crack (6in. hook spacing, hooks lapped w/1in. stagger)*	*PCSSS w/crack (12in. hook spacing, hooks lapped w/1in. stagger)*	*PCSSS w/crack (18in. hook spacing, hooks lapped w/1in. stagger)*	*Solid slab, no crack (12in. hook spacing, hooks lapped w/1in. stagger)*
Geometry	*Spans:*	*2*	*2*	*2*	*2*
	#Panels wide	*2 (no outside flange) - 10ft wide*	*Same*	*Same*	*Same*
	Length	*30ft-30ft*	*Same*	*Same*	*Same*
	Depth of precast section	*3in.flange; 12in. web*	*Same*	*Same*	*Same*
	Depth of deck above precast web	*6in. CIP*	*Same*	*Same*	*Same*
	Supports	*Pin at center support, rollers on ends*	*Same*	*Same*	*Same*
Crack	*Simulated "crack" using contact elements.*	*Bottom of section to 9in. from bottom (half depth).*	*Same*	*Same*	*No Crack*
Material strength	*CIP Concrete*	*4ksi*	*Same*	*Same*	*Same*
	Precast Concrete	*6.5ksi*	*Same*	*Same*	*Same*
	Reinforcement	*60ksi*	*Same*	*Same*	*Same*
Reinforce-ment	*Deck steel*	*#8-#7-#7 @ 4in. oc* *Run along entire span length*	*Same*	*Same*	*Same*
	Transverse hooks in each direction (offset transversely by 1in.)	*#6@6in. (1" offset over joint)*	*#6@12in. (1" offset over joint)*	*#6@18in. (1" offset over joint)*	*#6@12in. (1" offset over joint)*
	Vertical location of transverse reinforcement	*4-5/8" center of #6 from bottom of form*	*Same*	*Same*	*Same*
	Prestressing strands	*16 in each PCSSS*	*Same*	*Same*	*Same*
	Transverse cage	*None*	*None*	*None*	*None*

In each model run, it was enforced that at least one solid element along the length of the bridge was unfilled with transverse hooked bars (i.e., in the case of the 18 in. spacing, two elements were often unfilled per transverse hooked bar). This causes the plots to appear "spiky", as elements

without rebar were free to open more than the reinforced elements. Figure 4.2.2 shows a comparison of the crack opening of runs where all elements were reinforced versus runs where at least every other element was unreinforced. The crack opening was measured directly above the precast joint, in the tension fiber of the CIP concrete. The case with all elements reinforced tended to fall between the bounds defined by the spikes in the plot for the case where not all elements had reinforcement. It was assumed that the case where not every element was reinforced better approximated the variations in the joint opening for a physical bridge, so the method of leaving every other element void of rebar was used throughout the analyses.

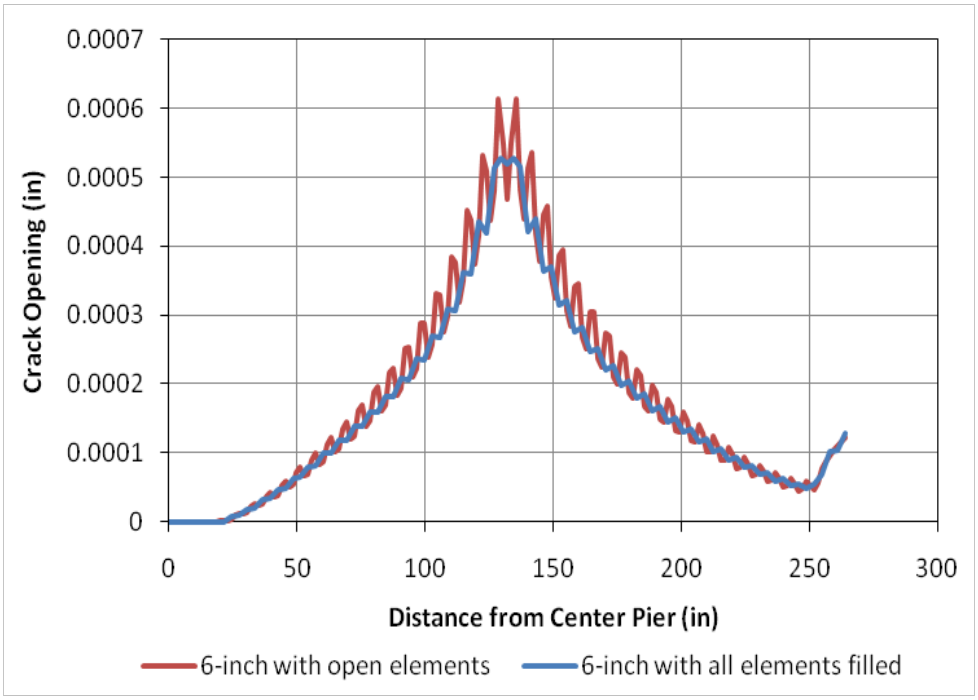

Figure 4.2.2: Crack opening in loaded span for 6 in. hooked bar spacing with or without one rebar per solid element

The measured bar stress and maximum crack opening in the loaded span for load case 1 (i.e., load at midspan with the edge of the load aligned with the edge of the vertical precast web) is plotted as a function of the transverse hooked bar spacing in Figure 4.2.3. A strong linear relationship was observed between the stress in the bar and the measured crack opening at the precast flange-CIP interface and the spacing between the transverse reinforcement, with a correlation coefficient between the three data points of 0.999 and 0.993, respectively. The linear relationship between the bar spacing and both the stress in the reinforcement and maximum opening suggests that the effectiveness of the reinforcement is not degraded as more reinforcement is added. The

proportional constant between the amount of reinforcement and the crack size/bar stress remained constant for the range of reinforcement spacing values considered during this study.

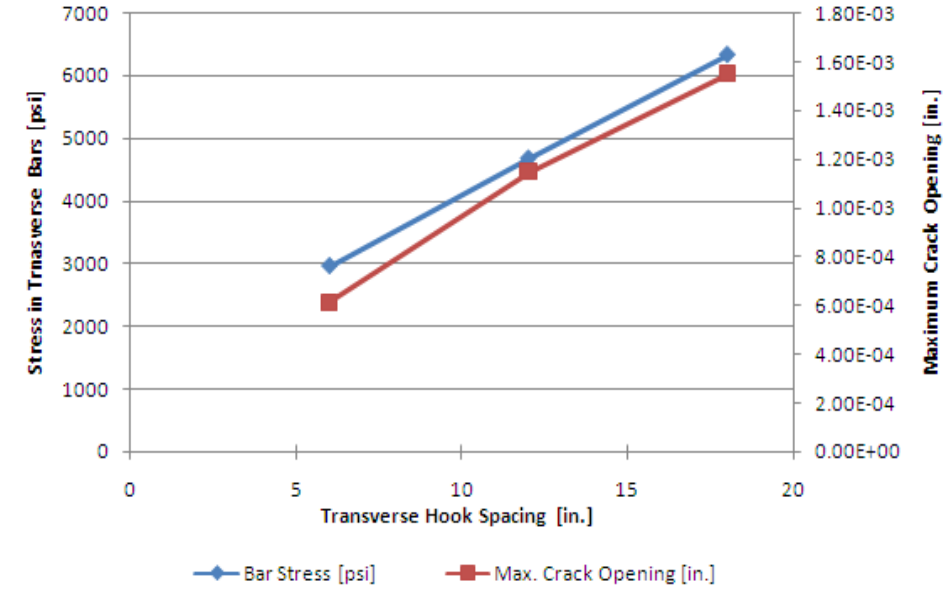

Figure 4.2.3: Maximum crack opening and transverse bar stress versus transverse hooked bar spacing in loaded span for load case 1

The effect of the spacing of the transverse hooked bars on transverse and longitudinal load distribution was also investigated during the parametric study. The transverse and longitudinal stress fields created by loading due to both load cases provided insight into the ability for each model to distribute the load throughout the structure. The transverse and longitudinal stress fields observed during the FEM runs for both load cases are shown in Figures 4.2.4-4.2.7. For the 6 and 12 in. spacing cases, the centerline of the patch load was centered over a pair of transverse hooks, while in the 18 in. spacing case the patch load straddles the hooks such that the edge of the patch load was relatively near the adjacent hooks. The center pier is illustrated in each model with the thick white line at the middle of each contour plot. Contour scales, which represent stress in units of psi, are also provided for each plot. For all cracked analyses (i.e., Runs 1 through 3), there was little variation in the overall distribution of the stresses, suggesting that the spacing of the transverse reinforcement had little effect on the ability for the PCSSS to distribute localized loading between adjacent panels and spans, which might be attributed to the proximity of the load to the reinforcement in all cases. As expected, noticeable variation in the transverse stress fields was observed between the cracked and uncracked model.

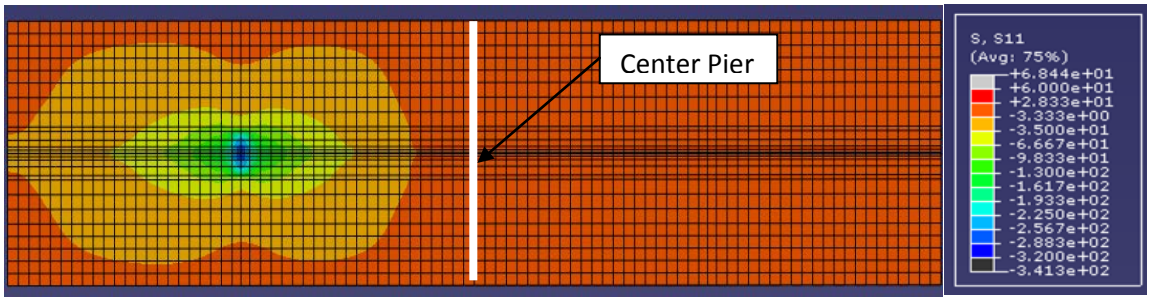

(a) 6 in. spacing (run 1)

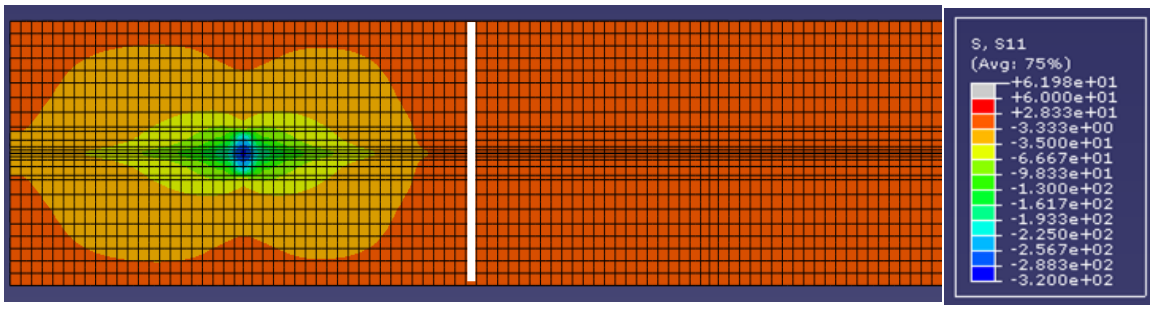

(b) 12 in. spacing (run 2)

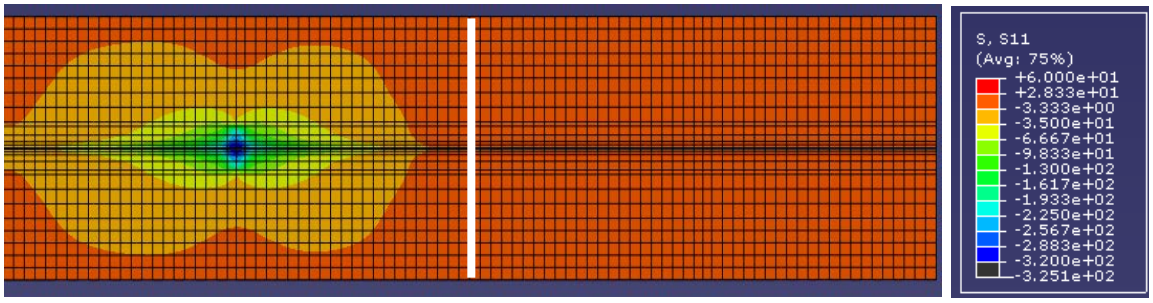

(c) 18 in. spacing (run3)

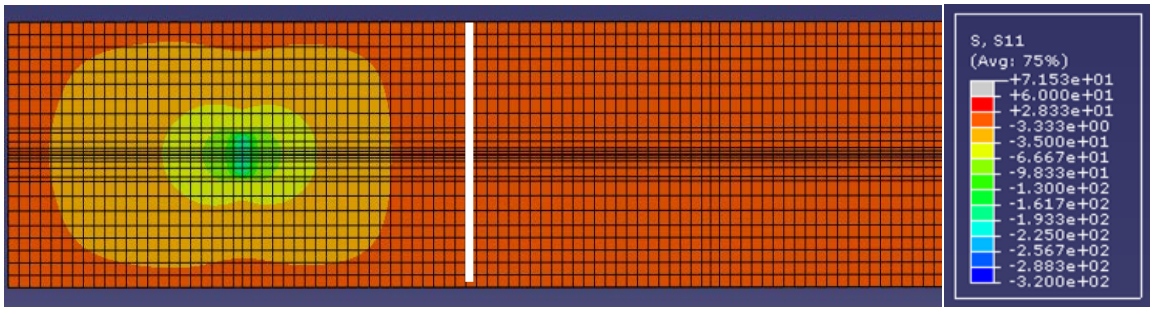

(d) Uncracked (run 4)

Figure 4.2.4: Transverse stress distribution in the compression (i.e., top) concrete fiber for load case 1 (units of stress are in psi)

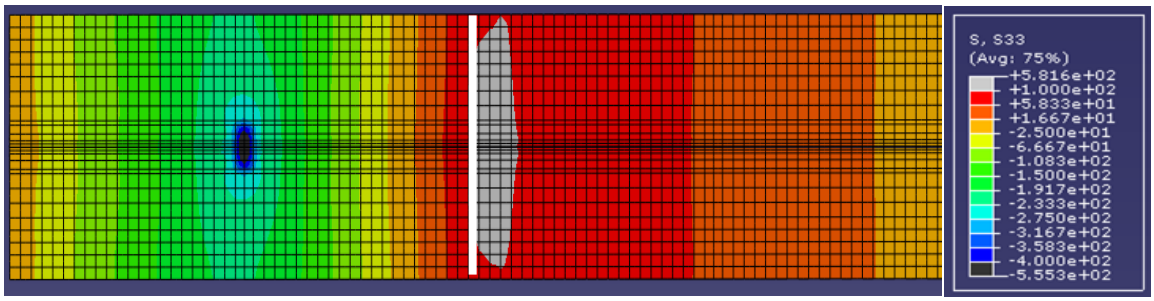

(a) 6 in. spacing (run 1)

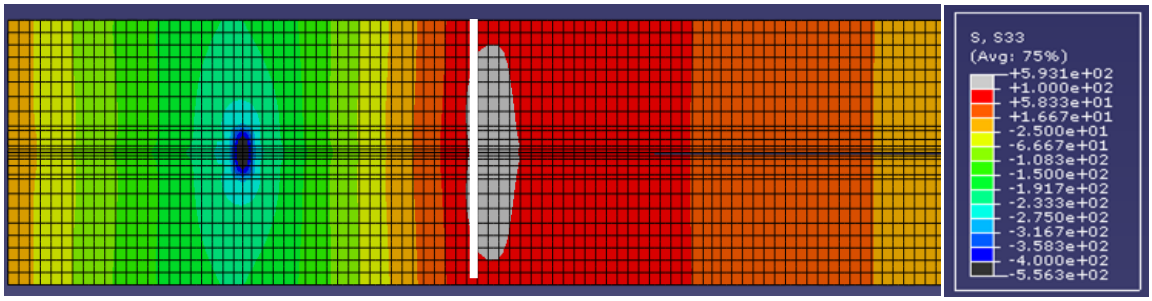

(b) 12 in. spacing (run 2)

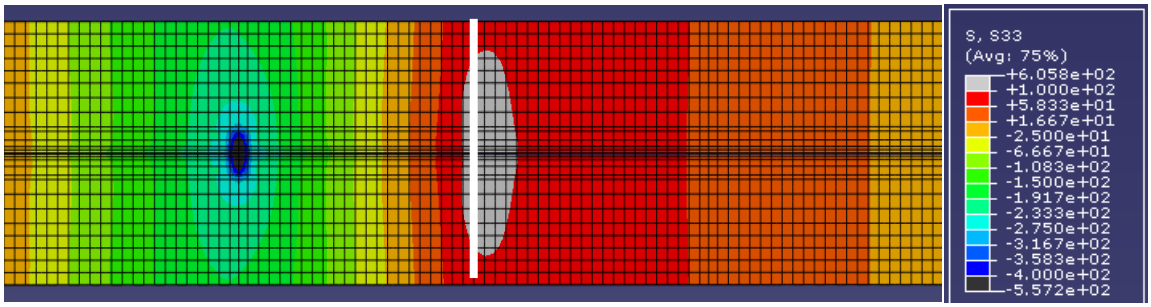

(c) 18 in. spacing (run 3)

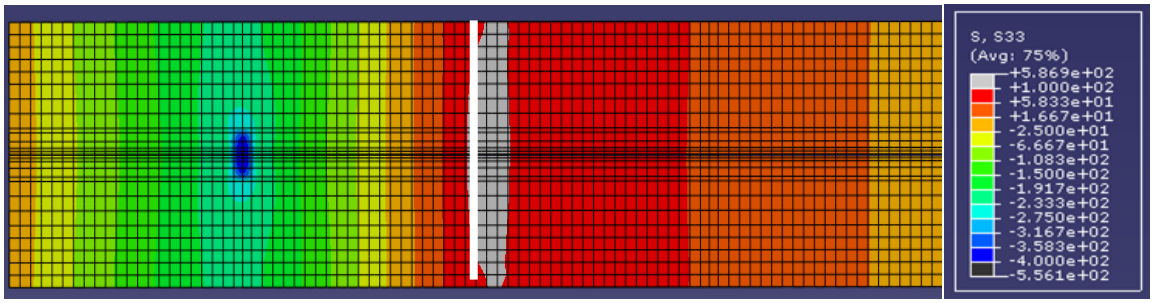

(d) Uncracked (run 4)

Figure 4.2.5: Longitudinal stress distribution in the compression (i.e., top) concrete fiber for load case 1 (units of stress are in psi)

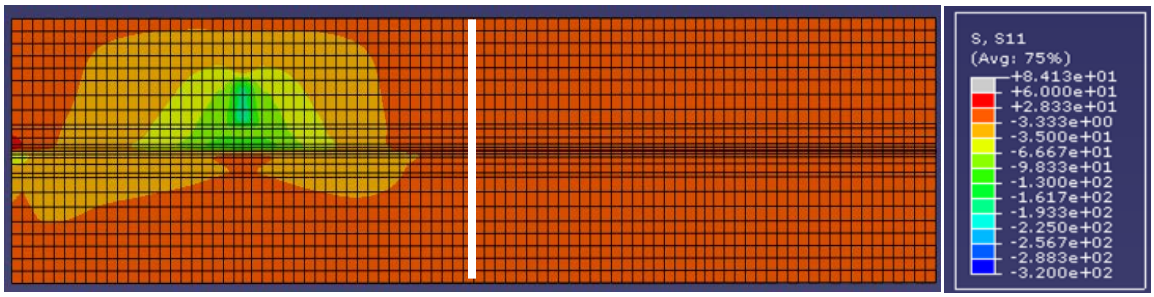

(a) 6 in. spacing (run 1)

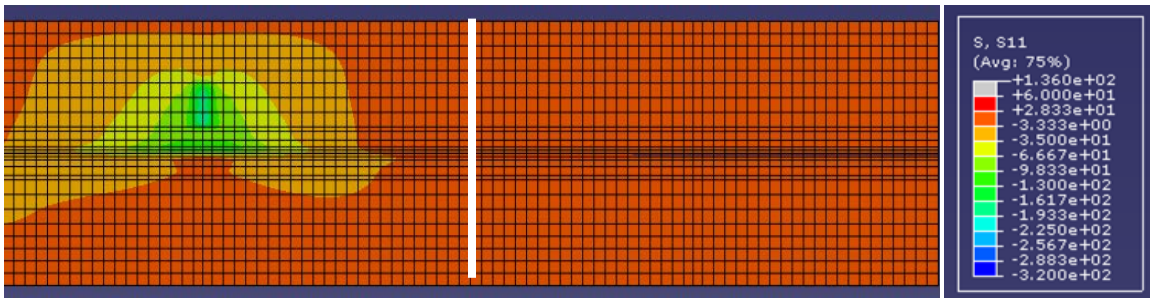

(b) 12 in. spacing (run 2)

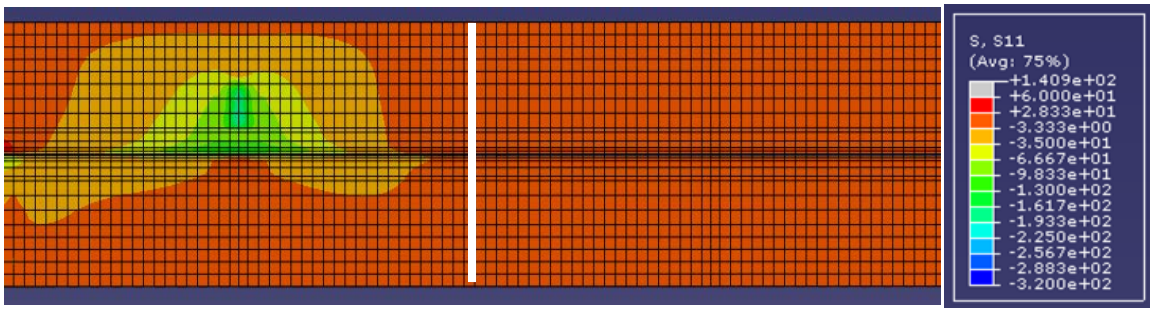

(c) 18 in. spacing (run 3)

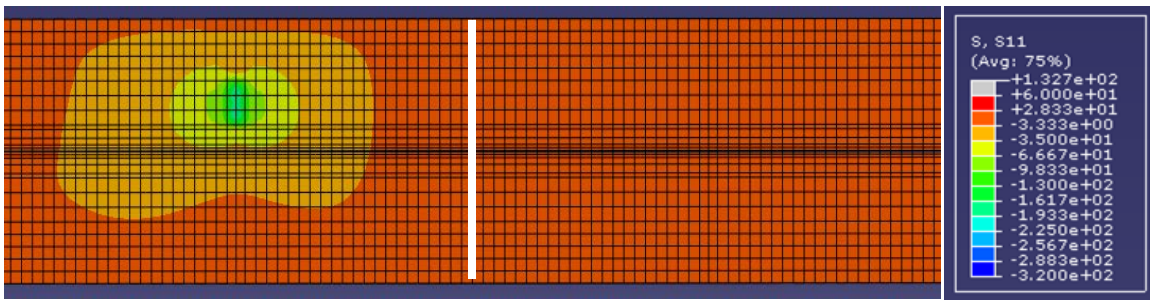

(d) Uncracked (run 4)

Figure 4.2.6: Transverse stress distribution in the compression (i.e., top) concrete fiber for load case 2 (units of stress are in psi)

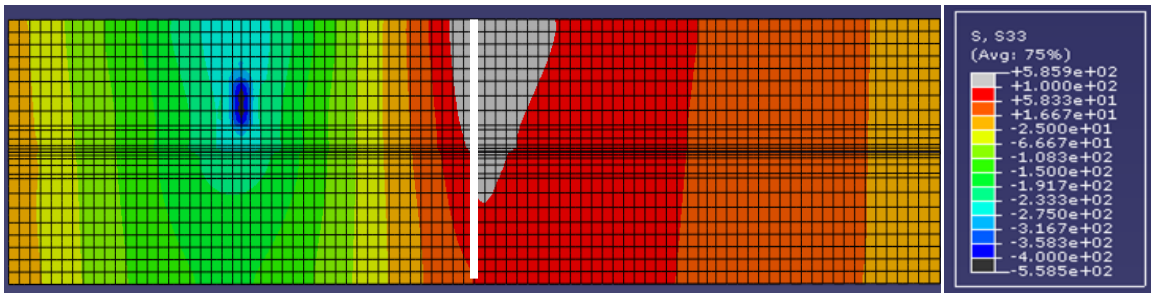

(a) 6 in. spacing (run 1)

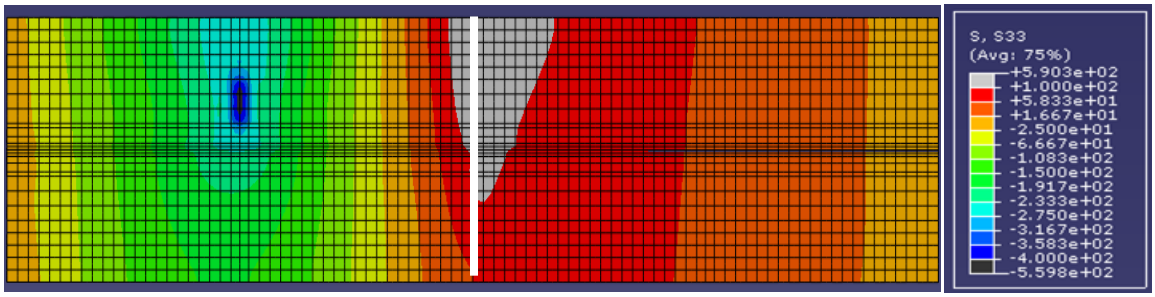

(b) 12 in. spacing (run 2)

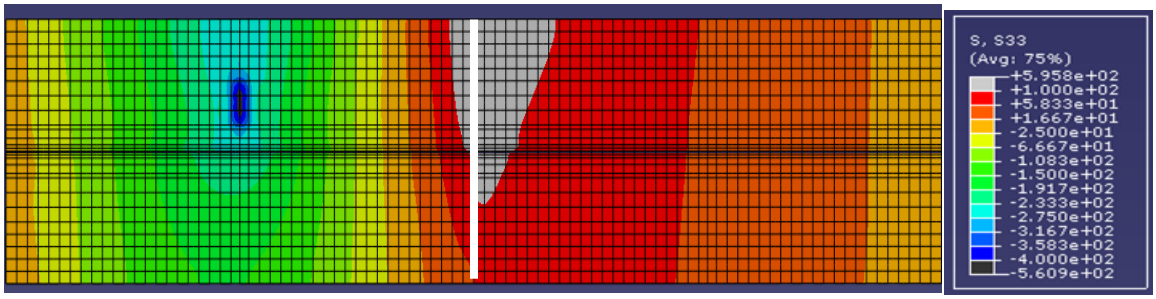

(c) 18 in. spacing (run 3)

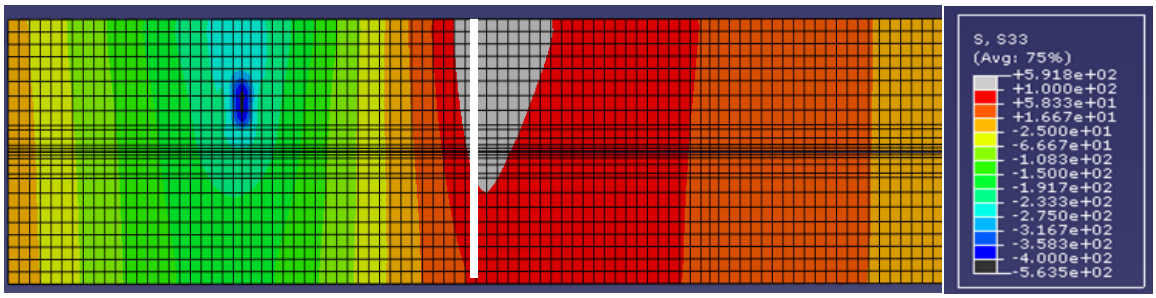

(d) Uncracked (run 4)

Figure 4.2.7: Longitudinal stress distribution in the compression (i.e., top) concrete fiber for load case 2 (units of stress are in psi)

4.3. Parametric Study to Investigate Live-Load Distribution Factors for PCSSS

The work chronicled in Section 4.3 was completed by Brock Hedegaard (2010).

The *Interim 2010 AASHTO LRFD Design Specification* provided design equations to determine the appropriate longitudinal moment demand for a given slab bridge system based on an effective lane width. The designer is then responsible for determining the proper amount and location of the longitudinal reinforcement and section geometry to satisfy the load demands. The specification provides further guidance in the design of the transverse reinforcement for slab bridges as a simple proportion of the total longitudinal tension reinforcement based on the span length of the structure, however the validity of this relationship when applied to the PCSSS was unknown.

A total of nine finite element models were constructed to investigate the effects of the longitudinal discontinuity between precast members on the longitudinal and transverse distribution of load. The models were constructed using the same material and modeling assumptions as stated in Section 4.2, however symmetry was utilized in this case to minimize computation time. Four unique specimen geometries were investigated, including two three-span bridges with equal spans of 30 and 50 ft., as well as two simply-supported bridges also with spans of 30 and 50 ft. Each of the specimens had ten 6 ft. precast panels across the width to accommodate four 12 ft. lanes and two 6 ft. shoulders. Several variations in the state of the specimen near the precast discontinuity were considered, including both a bonded and unbonded interface between the precast flange and CIP concrete, as well as a monolithic slab with no precast discontinuity present. The parameters of each of the nine models are given in Table 4.3.1. A tandem load was utilized for all models, with a total load of 12.5 kip distributed over a 10 by 20 in. patch, as shown in Figure 4.3.1. The 12.5 kip load represents the tire load from the AASHTO tandem load of 25 kip axles spaced 4 ft. apart, with the transverse spacing taken to be 6 ft., as specified in Article 3.6.1.2.3 (AASHTO 2010), and assuming that the axle load is equally distributed to each tire. No dynamic load allowance (per AASHTO 2010 Article 3.6.2) was used to magnify the loading, which was consistent with the assumed loading for the design moments that were used for comparison. The center spans were loaded in the continuous models. The joint and panel numbering is shown in Figure 4.3.2, which represents the center span of the continuous models as well as the simple span. Five variations in the applied tandem loading were considered for each run, as described below:

- Tandem 1 – tandem loading centered over webs of panels 5 and 6
- Tandem 2 – tandem loading centered over precast joints 4 and 5
- Tandem 3 – double tandem loading centered over webs of panels 4,5,6,7
- Tandem 4 – double tandem loading centered over precast joints 3,4,5,6
- Tandem 5 – double tandem loading with 12.5 kip patch loads over joints 4 and 6 and a double patch load (i.e., 25 kips) over joint 5

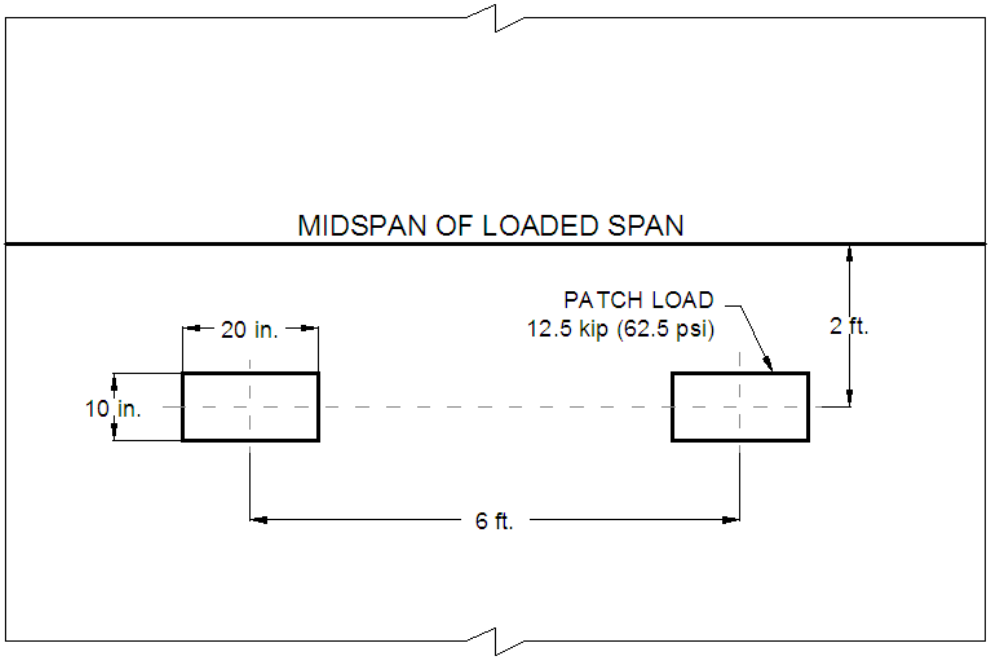

Figure 4.3.1: Tandem loading located 2 ft. from midspan utilized for FEM live-load distribution study

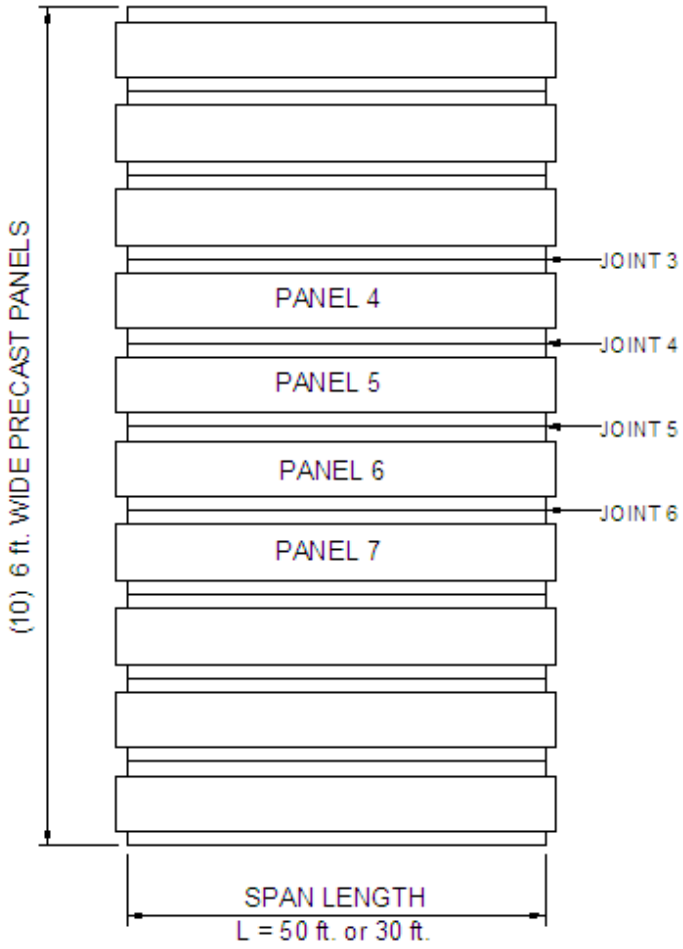

Figure 4.3.2: Panel and joint numbering used in the placement of tandem loading for the center span of the continuous models and the simple-span models

Table 4.3.1: Summary of FEM runs to investigate longitudinal and transverse live-load distribution factors

Description	Run Number	1	2	3	4	5	6	7	8	9
	Run configuration	PCSSS w/ 3" crack	PCSSS w/ 3" crack	PCSSS w/ 3" crack	PCSSS w/o crack	PCSSS w/ 3" crack	PCSSS w/ 3" crack	PCSSS w/ 3" crack	PCSSS w/o crack	PCSSS w/ 15" crack
Geometry	Spans:	3	Single	Single	Single	3	Single	Single	Single	Single
	#Panels wide	10—4lane bridge (12 ft. lanes + 6 ft. shoulders)\60ft.wide	Same	Same	Same	Same	Same	Same	Same	Same
	Length	30ft-30ft-30ft	30ft	30ft	30ft	50ft-50ft-50ft	50ft	50ft	50ft	30ft
	Depth of precast section	3in.flange; 12in. web	3in.flange; 12in. web	3in.flange; 12in. web	3in.flange; 12in. web	3in.flange; 16in. web	3in.flange; 16in. web	3in.flange; 16in. web	3in.flange; 16in. web	3in.flange; 12in. web
	Depth of deck above precast web	6in. CIP	Same	Same	Same	Same	Same	Same	Same	Same
	CIP to precast interface above flange	Unbonded	Unbonded	Bonded	Monolithic	Unbonded	Unbonded	Bonded	Monolithic	Unbonded
	Supports	Rollers	Same	Same	Same	Same	Same	Same	Same	Same
Crack	Simulated "crack" using contact elements.	Bottom of section to 3in. from bottom (precast joint).	Bottom of section to 3in. from bottom (precast joint).	Bottom of section to 3in. from bottom (precast joint).	No crack, monolithic	Bottom of section to 3in. from bottom (precast joint).	Bottom of section to 3in. from bottom (precast joint).	Bottom of section to 3in. from bottom (precast joint).	No crack, monolithic	Bottom of section to 15in. from bottom.
Mat'l strength	CIP Concrete	4ksi	Same	Same	Same	Same	Same	Same	Same	Same
	Precast Concrete	6.5ksi	Same	Same	Same	Same	Same	Same	Same	Same
	Reinforcement	60ksi	Same	Same	Same	Same	Same	Same	Same	Same
Reinforcement	Deck steel	#8-#7-#7 @ 4in. oc Run along entire span length	Same	Same	Same	Same	Same	Same	Same	Same
	Transverse hooks in each direction (offset transversely by 1in.)	#6@12in. Model as a continuous bar across the section rather than as lapped steel	Same	Same	Same	Same	Same	Same	Same	Same
	Location of transverse reinforcement	4-5/8" center of #6 from bottom of form	Same	Same	Same	Same	Same	Same	Same	Same
	Prestressing strands	16 in each PCSSS	16 in each PCSSS	16 in each PCSSS	16 in each PCSSS	38 in each PCSSS	38 in each PCSSS	38 in each PCSSS	38 in each PCSSS	16 in each PCSSS
	Transverse cage	None	None	None	None	None	None	None	None	None

In Runs 1, 2, 5, and 6 the CIP was bonded only to the sides and top of the panel webs while in Runs 3 and 7 the CIP was also bonded to the top of the precast flanges. In Runs 4 and 8 the system was assumed to be a monolithic slab with the discontinuity from the joint between the precast panels absent. Finally, Run 9 was similar to Run 2, except the crack was extended up to approximately the elastic neutral axis in transverse bending. In Run 9, the rebar crossing the cracked plane was debonded from the concrete a distance of 3 in. to either side of the cracked face.

The longitudinal design moments for slab bridges are calculated by applying the design load over an effective lane width, which is dependent on whether loading is applied to a single lane or multiple lanes, per AASHTO (2010) Article 4.6.2.3. The two variations of effective lane widths account for multiple presence factors in that the effective strip width for single lane loading has been divided by a factor of 1.20. The factors do not represent a physical change in loading, but instead account for the likelihood of multiple vehicles traveling together; they are statistical factors to promote conservative design (in the case of single lane loading). The multiple presence factors were ignored in the modeled scenarios. The longitudinal design moments and associated curvatures are shown in Table 4.3.2 for both single and multiple lane loadings for the various runs.

Table 4.3.2: AASHTO (2010) longitudinal design moments and curvatures

	Moment (kip-ft./ft. span)		Curvature (με/in.)	
Run	Single[1]	Multiple[2]	Single	Multiple
1	16.1	17.7	7.37	8.13
2	24.4	26.9	11.17	12.32
3	24.4	26.9	11.17	12.32
4	24.4	26.9	11.17	12.32
5	22.9	28.6	5.64	7.05
6	33.9	42.4	8.34	10.43
7	33.9	42.4	8.34	10.43
8	33.9	42.4	8.34	10.43
9	24.4	26.9	11.17	12.32

[1]"Single" is associated with all loading applied to a single lane
[2]"Multiple" is associated with loading applied to two or more lanes

The maximum longitudinal curvatures obtained from the FEM model with the Tandem 2 loading (patch load applied over joints 4 and 5) and Tandem 5 loading (patch load applied over joints 4 and 6 and double patch load applied over joint 5) are compared with the design curvatures in Table 4.3.3. The Tandem 5 loading was considered to be a worst case loading scenario with respect to expected lane loading because the tandems were spaced much closer than would be physically possible.

In comparing the results of the FEM to design ratios, the PCSSS resulted in slightly higher values in comparison to those of the monolithic systems (e.g., for the Tandem 2 Load Case: 0.43 [Run 2] for PCSSS vs. 0.39 [Run 4] for the monolithic 30 ft. span sections, and 0.41 [Run 6] for the PCSSS vs. 0.39 [Run 8] for the monolithic 50 ft. span); however the results were still conservative. The ratio of the maximum longitudinal curvature to the design curvature among the nine runs loaded with the Tandem 5 load case ranged from 0.57 to 0.84 for run 8 and 9 respectively. This suggests that, even when reflective cracking was assumed to have progressed vertically to within 3 in. of the extreme compression fiber, as in run 9, the design effective lane widths provided by AASHTO (2010) Article 4.6.2.3 prove to be conservative, and should therefore be utilized for the design of precast composite slab span bridge systems.

Table 4.3.3: FEM and design longitudinal curvatures under Tandem 2 and Tandem 5 load cases

	Tandem 2 Load Case Curvature (με/in)			Tandem 5 Load Case Curvature (με/in)		
Run	Max FEM	Design	FEM/Design	Max FEM	Design	FEM/DESIGN
1	3.72	7.37	0.50	6.76	8.13	0.83
2	4.76	11.17	0.43	8.81	12.32	0.72
3	4.41	11.17	0.39	8.25	12.32	0.67
4	4.35	11.17	0.39	8.14	12.32	0.66
5	2.68	5.64	0.48	NM[1]	7.05	NM
6	3.4	8.34	0.41	NM	10.43	NM
7	3.26	8.34	0.39	6.03	10.43	0.58
8	3.23	8.34	0.39	5.97	10.43	0.57
9	5.18	11.17	0.46	10.38	12.32	0.84

[1]Not measured

Shaded rows indicate monolithic models

4.4. Parametric Study to Investigate Skew Effects

The work chronicled in Section 4.4 was completed by Brock Hedegaard (2010).

Several additional challenges are present in the design of bridges with skewed supports, such that the primary axis of the substructure is not aligned perpendicularly to the longitudinal axis of the superstructure. The primary effects of skewed bridge construction are geometric, with some effect on moments, shears, and live-load distribution. A plan view of the pier details for a skewed PCSSS bridge is shown in Figure 4.4.1. According to the PCI Bridge Manual (2001), in solid slab-span bridge systems with skewed supports, the load tends to take a "short cut" between the obtuse corners of the span, while the load in skewed bridges supported by longitudinal I-girders tends to flow along the length of the supporting members (PCI 2001). The PCSSS was expected to be bounded by these behaviors, and would subsequently tend to exhibit the characteristics of longitudinal stringer bridges as the precast joint is degraded due to reflective cracking.

Another primary concern regarding skewed PCSSS bridges was the effect of the skew angle on the maximum horizontal shear induced above the precast joint. Several FEM models were developed to investigate the relationship between the skew angle and the resulting magnitude of this stress.

A total of eight FEM models were constructed for this portion of the study, with skew angles ranging from 0 to 45 degrees. For each of the skew angles selected, two corresponding FEM models were created, one with the presence of the 3 in. discontinuity between the precast joints and an unbonded surface between the top of the precast flanges and the CIP concrete and a second with a monolithic thickness and the absence of the precast joint. Each model was constructed as a single 30 ft. simple-span bridge structure. The material and other modeling parameters were identical to the previous runs, described in Section 4.2. The parameters of each of the eight FEM models are given in Table 4.4.1.

Three load cases were considered for this portion of the study, outlined below. Each load case included a 35 kip load applied over a 12 by 12 in. patch. An illustration of the model and applied load cases is shown in Figure 4.4.2.

- Load Case 1 – loading applied at quarter span at center of outside panel near acute angle support
- Load Case 2 – loading applied at midspan at center of outside panel
- Load Case 3 – loading applied at quarter span at center of outside panel near obtuse angle support

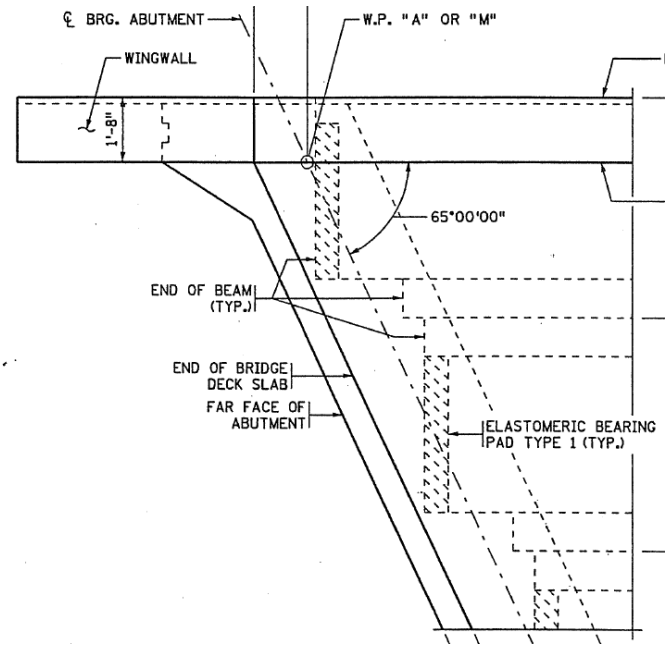

Figure 4.4.1: Placement of precast slab span panels at a skewed support

Table 4.4.1: Summary of FEM runs to investigate performance of skewed PCSSS

Description	Run Number	1	2	3	4	5	6	7	8
	Run configuration	PCSSS w/ 3" crack - 0 skew	PCSSS w/ 3" crack - 15 skew	PCSSS w/ 3" crack - 30 skew	PCSSS w/ 3" crack - 45 skew	PCSSS w/o crack - 0 skew	PCSSS w/o crack - 15 skew	PCSSS w/o crack - 30 skew	PCSSS w/o crack - 45 skew
Geometry	Spans:	Single	Single	Single	Single	Single	Single	Single	Single
	#Panels wide	3 panels /18ft.wide	Same	Same	Same	Same	Same	Same	Same
	Length	30ft	Same	Same	Same	Same	Same	Same	Same
	Skew Angle	0 deg	15 deg	30 deg	45 deg	0 deg	15 deg	30 deg	45 deg
	Depth of precast section	3in.flange; 12in. web	Same	Same	Same	Same	Same	Same	Same
	Depth of deck above precast web	6in. CIP	Same	Same	Same	Same	Same	Same	Same
	CIP to precast interface above flange	Unbonded	Unbonded	Unbonded	Unbonded	Monolithic	Monolithic	Monolithic	Monolithic
	Supports	Rollers	Same	Same	Same	Same	Same	Same	Same
Crack	Simulated "crack" using contact elements.	Bottom of section to 3in. from bottom (precast joint).	Bottom of section to 3in. from bottom (precast joint).	Bottom of section to 3in. from bottom (precast joint).	Bottom of section to 3in. from bottom (precast joint).	No crack, monolithic	No crack, monolithic	No crack, monolithic	No crack, monolithic
Mat'l strength	CIP Concrete	4ksi	Same	Same	Same	Same	Same	Same	Same
	Precast Concrete	6.5ksi	Same	Same	Same	Same	Same	Same	Same
	Reinforcement	60ksi	Same	Same	Same	Same	Same	Same	Same
Reinforcement	Deck steel	#8-#7-#7 @ 4in. oc Run along entire span length	Same	Same	Same	Same	Same	Same	Same
	Transverse hooks in each direction (offset transversely by 1in.)	#6@12in. Model as a continuous bar across the section rather than as lapped steel	Same	Same	Same	Same	Same	Same	Same
	Location of transverse reinforcement	4-5/8" center of #6 from bottom of form	Same	Same	Same	Same	Same	Same	Same
	Prestressing strands	16 in each PCSSS	Same	Same	Same	Same	Same	Same	Same
	Transverse cage	None	None	None	None	None	None	None	None

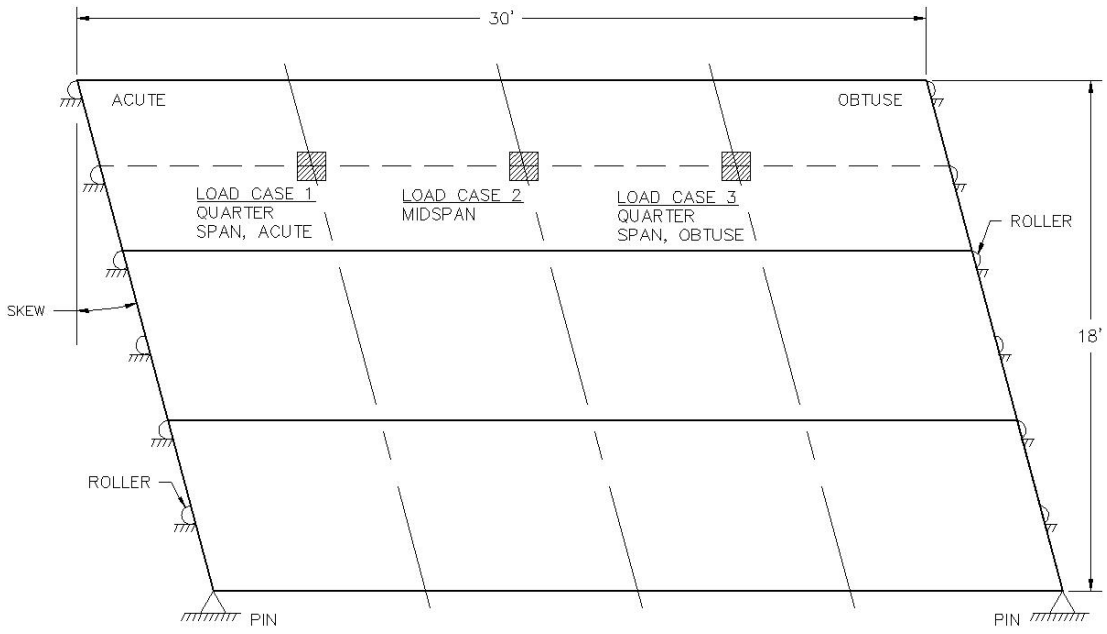

Figure 4.4.2: Simply supported, three panel wide bridge and location of loading used for FEM models

For all cases, the horizontal shear stress in the cast-in-place concrete was measured along the entire length and depth of the structure in the plane of the precast joint adjacent to the loading. The maximum horizontal shear stress in this plane was investigated for a range of skew angles for each of the load cases. The maximum horizontal shear stress measured in the models with a 3 in. deep precast joint and the associated monolithic models are shown in Figure 4.4.3 (a) and (b), respectively.

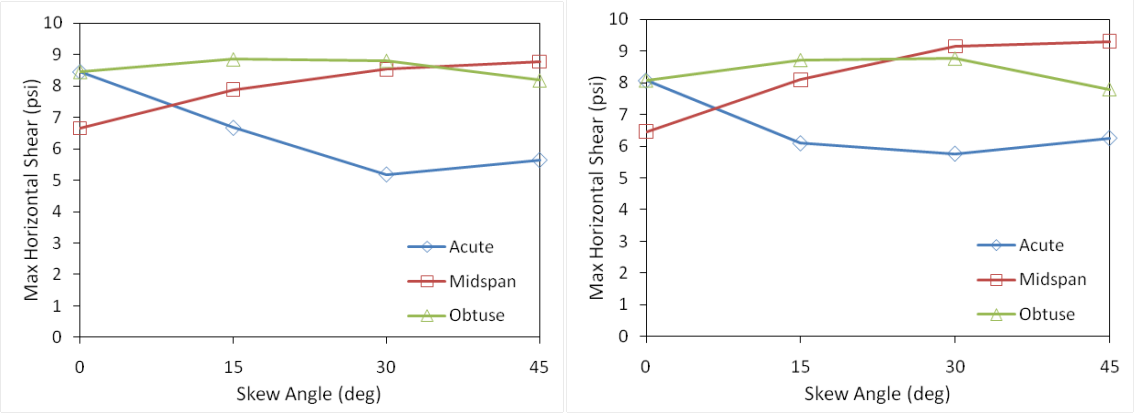

(a) 3 in. precast joint (b) Monolithic

Figure 4.4.3: Maximum horizontal shear stress measured in the cast-in-place concrete above the precast joint measured under the acute, midspan, and obtuse load cases

The horizontal shear stress in the models considered with load case 1, which had load applied near the acute pier connection, was observed to be reduced with increasing skew angles for both the section with the 3 in. flange joint as well as the monolithic model. The horizontal shear stress caused by load case 3, representing loading near the obtuse pier connection, for both the jointed and monolithic models remained relatively constant through the range of skew angles considered. For both model types, the midspan load case produced the most significant increase in horizontal shear stress, with an approximately 1/3 increase in the stress observed in both the jointed and monolithic models.

The maximum shear stress from these three load cases defined stress envelopes for the jointed and monolithic models that varied with skew angle, shown in Figure 4.4.4. This maximum horizontal shear stress envelope remained relatively constant through the range of skew angles considered for both jointed and monolithic models. With increasing skew angle, the shear stress envelope increased by approximately 15% for the monolithic models and by less than 10% for the jointed models. The small variation and consistency between the models considering a 3 in. precast joint and a monolithic structure suggested that the effect of the precast joint in precast composite slab span construction was not expected to significantly affect the performance of the system in skewed applications.

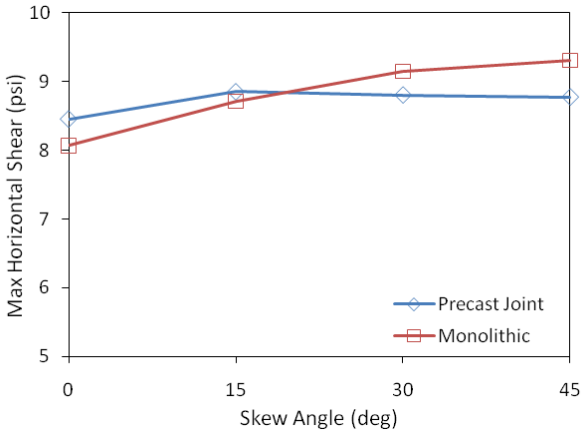

Figure 4.4.4: Maximum horizontal shear stress envelope above longitudinal precast joint considering all load cases for precast joint models and monolithic slab models.

4.5. End Zone Stresses in Precast Inverted Tee Sections

The work chronicled in Section 4.5 was completed by Whitney Eriksson (2008).

Horizontal cracking frequently forms in the end region of prestressed concrete members when the prestressing strand is released and the prestress force is transferred to the concrete section. These cracks, which result from the vertical tension created by the transfer of prestress force, are defined as “spalling” cracks, though often incorrectly labeled as “bursting” or “splitting” cracks (Gergely et al., 1963). If unrestrained, these cracks can extend into the precast member and may negatively impact both the flexural and shear strength and durability of the section.

Previous studies have suggested that these cracks cannot be eliminated, however vertically oriented reinforcing steel can limit crack width and propagation (Fountain, 1963). The first design parameters related to end zone stresses in prestressed members were introduced in the 1961 AASHTO Design Specification (AASHTO, 1961), that specified a minimum vertical reinforcement requirement for pretensioned member end regions. This specification remained virtually unchanged since its introduction until the 2008 interim AASHTO LRFD specification incorporated changes to the specification, which included a change in the terminology of the end zone stresses from “bursting” to “splitting” resistance of the pretensioned anchorage zones.

The placement of large amounts of vertical reinforcement in the end regions of shallow inverted-T precast members caused congestion and difficulty in the placement of prestressing strand and concrete when 4 percent of the total prestressing force was used (i.e., AASHTO LRFD 2010). A historical study of the development of reinforcement designs for vertical end zone stresses

indicated that the original design parameters were likely developed from a Marshall and Mattock (1962) study on horizontal end zone cracking in pretensioned I-girders, suggesting that design parameters provided in the specification may not be applicable to precast inverted-T sections. Also included in the modifications to the 2008 interim AASHTO LRFD specification was specific language for solid and voided slabs, as well as pretensioned box and tub girders.

Variations in the spalling reinforcement details were investigated experimentally with the Concept 1 and 2 laboratory bridge specimens by varying the vertical end region reinforcement in the ends of the precast panels used in the laboratory bridges, which are discussed under the unnumbered heading “experimental study,” included in this section.

Because of the complicated state of stress near the end regions of prestressed members, two similar but unique modes of cracking may be observed. To limit the ambiguity regarding these stresses, the vertical tensile stresses which occur along the line of the prestressing forces were labeled as bursting stresses, while the vertical tensile stresses located away from the line of the prestressing force were labeled as spalling stresses, as illustrated in Figure 4.5.1.

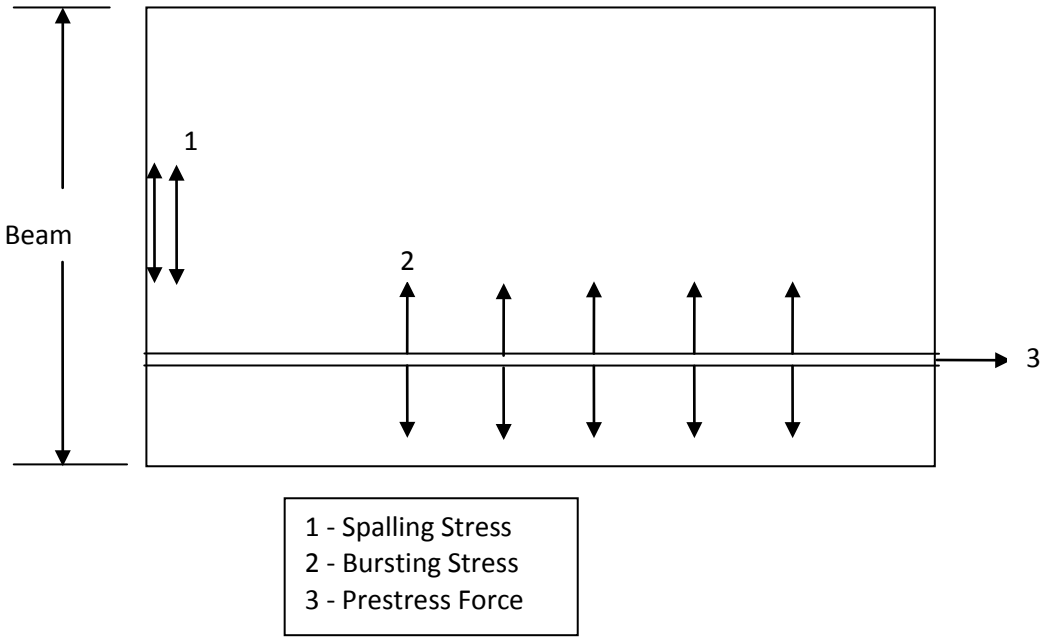

Figure 4.5.1: Spalling and bursting stresses near the end zone of prestressed members

Beam theory is not applicable in the end regions of prestressed concrete beams because the longitudinal strain is not linearly distributed through the depth of the cross section due to the

introduction of the prestress force. Spalling stresses are a maximum at the end face of the member, typically near mid-height of the section and result in cracking at the end face which can propagate further into the member (Gergely et al., 1963). Bursting stresses occur along the line of the prestressing force, beginning a few inches into the beam and extending throughout the transfer length. Bursting stresses can result in strand slippage as cracking along the strand can eliminate bond between the strand and the concrete.

Distribution of tensile stresses in the end region depends on the eccentricity of the prestressing force within the member. When the prestress acts at the centroid of the section, force is distributed symmetrically through the vertical member depth; in members with large eccentricity there is greater area above the prestressing force for stresses to distribute. This prestressing force is allowed to spread through a greater vertical distance which subsequently increases the spalling force near the end region. This is consistent with previous experimental work which related the maximum tensile stress location to eccentricity. Gergely's (1963) study on post-tensioned I-girders and rectangular sections found members with small eccentricities had maximum tensile stresses in the bursting zone and members with large eccentricities had maximum tensile stresses in the spalling zone. Hawkins (1960) corroborated Gergely's findings and also found that the eccentricity of the prestressing strand and the magnitude of maximum tensile stress in the spalling zone were positively related.

Numerical Study

FEM modeling was also performed to determine the magnitude and location of spalling and bursting stresses in the end region of precast inverted-T sections. Several simplifications were considered during the analysis to reduce the complexity and computational requirements of the model. The flanges were neglected to allow for the system to be modeled as a two-dimensional (2D) rectangular slab. Furthermore, the concrete was modeled as perfectly linearly elastic, which was appropriate up to the initiation of cracking. The transfer of the prestressing force was simulated by incrementing the force in the strand, from zero at the face of the section to the full magnitude at the transfer length (L_t), in 1/4 in. increments. Slip occurring between the strand and concrete was ignored. The transfer length was conservatively taken as 40 strand diameters (i.e., 20 in. for 1/2 in. strand), which was two-thirds of the transfer length specified by AASHTO (2010). The reduction in the transfer length from the AASHTO (2010) specification was selected to be conservative, as shorter transfer lengths are associated with higher vertical end zone stresses. Uniform and linear bond stress models were utilized, with the linear distribution

decreasing with distance from the end face of the member. A total of 57 runs were completed during the numerical study, as documented in Table 4.5.1.

Although the FEM model was not verified with experimental results from pretensioned beams, the models were compared to the results from Gergely's (1963) experimental study on a 6 by 12 in. post-tensioned rectangular beam. A 2D elastic model was created to simulate the physical experiment, with adequate correlation between the experimental and FEM model results, as shown in Figure 4.5.2, where the vertical axis represents the vertical tensile strains measured at midheight along the edge of the section and the horizontal axis corresponds to the distance from the end face of the specimen.

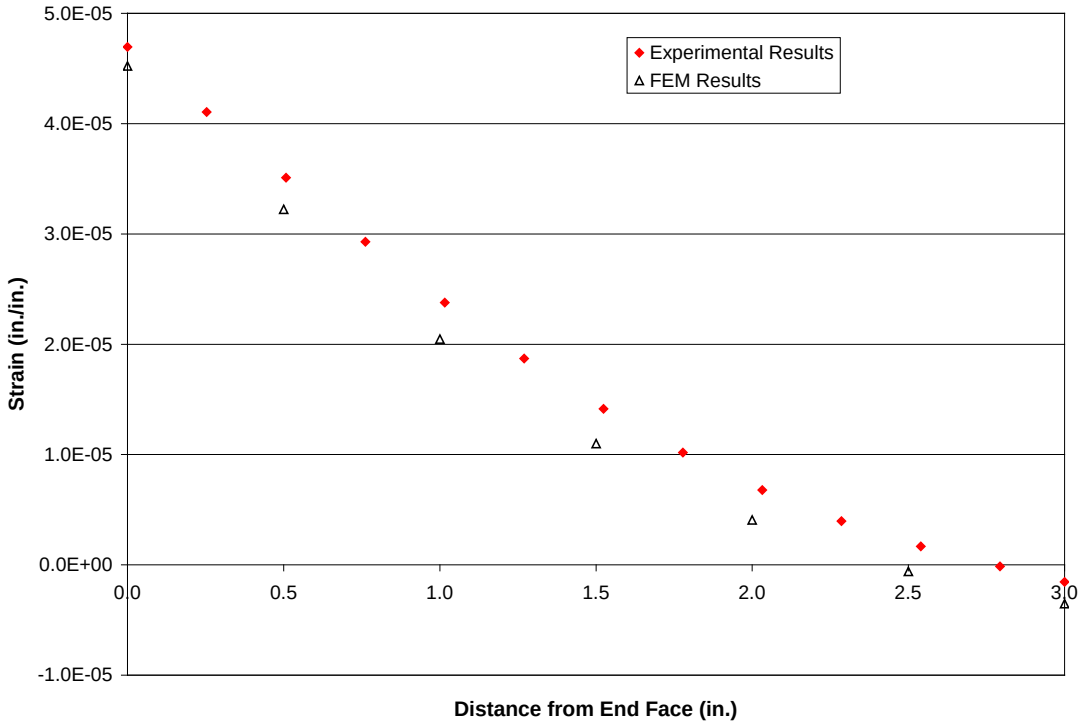

Figure 4.5.2: Validation of FEM model with experimental results from Gergely (1963)

Table 4.5.1: Description of models run during parametric study

Run #	h (in.)	L_t (in.)	e (in.)	e/h	Bond Stress Distribution		Run #	h (in.)	L_t (in.)	e (in.)	e/h	Bond Stress Distribution
1	12	20	5	0.42	Uniform		**30**	6	20	2	0.33	Uniform
2	12	20	4	0.33	Uniform		**31**	18	20	6	0.33	Uniform
3	12	20	3.5	0.29	Uniform		**32**	24	20	8	0.33	Uniform
4	12	20	3	0.25	Uniform		**33**	30	20	10	0.33	Uniform
5	12	20	2.5	0.21	Uniform		**34**	36	20	12	0.33	Uniform
6	12	20	2	0.17	Uniform		**35**	42	20	14	0.33	Uniform
7	12	20	0	0.0	Uniform		**36**	6	20	2	0.33	Linear
8	12	20	5	0.42	Linear		**37**	18	20	6	0.33	Linear
9	12	20	4	0.33	Linear		**38**	24	20	8	0.33	Linear
10	12	20	3.5	0.29	Linear		**39**	30	20	10	0.33	Linear
11	12	20	3	0.25	Linear		**40**	36	20	12	0.33	Linear
12	12	20	2.5	0.21	Linear		**41**	42	20	14	0.33	Linear
13	12	20	2	0.17	Linear		**42**	8	20	1.6	0.20	Uniform
14	12	20	0	0.0	Linear		**43**	10	20	2.5	0.25	Uniform
15	12	6	4	0.33	Uniform		**44**	12	20	2.5	0.21	Uniform
16	12	10	4	0.33	Uniform		**45**	12	20	2.4	0.20	Uniform
17	12	12	4	0.33	Uniform		**46**	14	20	3.7	0.26	Uniform
18	12	16	4	0.33	Uniform		**47**	16	20	4.6	0.29	Uniform
19	12	20	4	0.33	Uniform		**48**	20	20	6.3	0.31	Uniform
20	12	24	4	0.33	Uniform		**49**	22	20	6.8	0.31	Uniform
21	12	28	4	0.33	Uniform		**50**	8	20	1.6	0.20	Linear
22	12	0	4	0.33	End[1]		**51**	10	20	2.5	0.25	Linear
23	12	6	4	0.33	Linear		**52**	12	20	2.5	0.21	Linear
24	12	10	4	0.33	Linear		**53**	12	20	2.4	0.20	Linear
25	12	12	4	0.33	Linear		**54**	14	20	3.7	0.26	Linear
26	12	16	4	0.33	Linear		**55**	16	20	4.6	0.29	Linear
27	12	20	4	0.33	Linear		**56**	20	20	6.3	0.31	Linear
28	12	24	4	0.33	Linear		**57**	22	20	6.8	0.31	Linear
29	12	28	4	0.33	Linear							

[1]All force assumed to be applied at the end face to simulate post-tensioned case

The spalling force magnitude and stress distribution into the beam was found to depend on many factors. The assumption of linear bond distribution (where bond stress decreases linearly into the section) creates larger spalling stresses which extend a shorter distance into the member than uniform bond distribution. As the ratio of eccentricity (*e*) and height (*h*) increases, the magnitude of the spalling stresses increase and extend further into the member. A shorter transfer length distributes the prestress over a shorter distance resulting in larger spalling stresses extending over a shorter distance into the member. As height increases, the spalling force increases and the distribution of the stress extends further into the member because of the greater vertical area over which to distribute the prestress.

Bursting force magnitude and location is affected by eccentricity, transfer length, and height. Bursting forces increase with smaller *e/h* ratios and start further into the member. Shorter transfer lengths distribute forces over a shorter distance which results in larger bursting stresses and a smaller length over which bursting stresses act. As member height increases, the magnitude of the bursting forces increase and the length over which the bursting stress acts is increased slightly. The length which bursting stresses extend is mostly based on transfer length but larger heights and smaller *e/h* values also increase the ratio of the length over which bursting stresses act to height.

For smaller *e/h* values, bursting force is significantly larger than the spalling force. However, although the total force generated from the bursting stresses is larger than the total force generated from the spalling stresses, the bursting force acts over a much larger area. This provides a greater amount of concrete to resist the tensile forces.

Figure 4.5.3 compares the bursting and spalling stresses for a member 12 in. in height with 2.4 in. eccentricity and a 20 in. transfer length. The maximum stress is larger for spalling than for bursting. Also, the maximum spalling stress occurs on the end face which is only restrained on one side making it more likely for a crack to form there. In the majority of historical studies on end zone cracking, detrimental cracking initiates on the end face of members. If cracks are found along the line of load, they are likely caused by a combination of bursting and radial stresses, as expressed in Uijl's (1983) hollow core slab study.

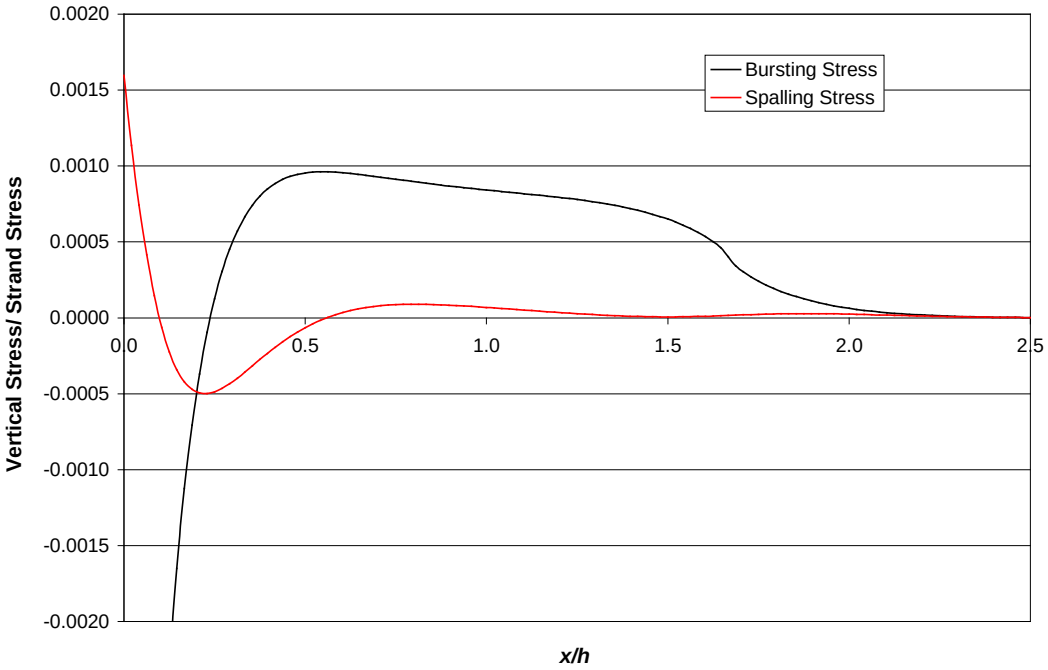

Figure 4.5.3: Comparison of Bursting and Spalling Stresses for Member *e/h*=0.20

The ratio of the predicted spalling force to the prestress force of slabs with a constant depth of 12 in. is shown in Figure 4.5.4. Table 4.5.2 shows the ratio of predicted spalling force to strand force as found through FE modeling of slabs with the same *e/h* ratio as the feasible precast inverted tee sections in Table 4.1.2. The spalling force ranged from 0.3 to 8.5 percent of the prestressing force.

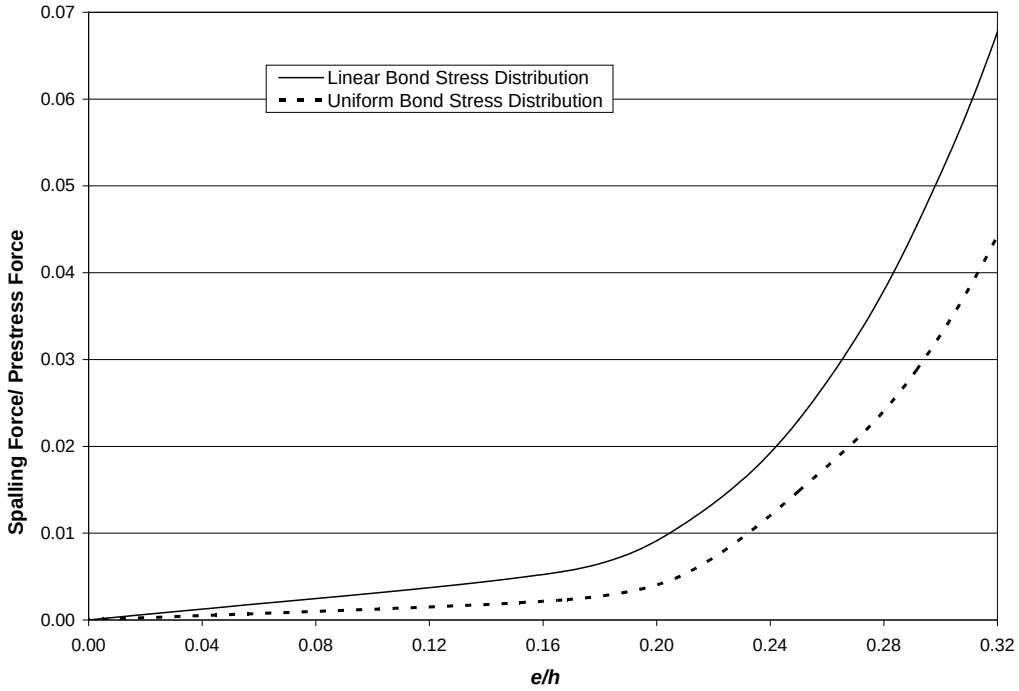

Figure 4.5.4: Ratio of spalling force to prestress force as a function of ratio of eccentricity to precast member depth for linear and uniform bond stress distributions, with h= 12 in and L_t = 20 in.

Table 4.5.2: Ratio of Spalling Forces to Prestress Forces as Predicted by FE Models for Slabs with Equivalent *e/h* as Feasible Precast Inverted Tee Sections, using both Uniform and Linear Bond Stress Distributions, varying *h* and *e/h* and constant L_t=20 in.

Depth of Precast (in.)	8	10	12[1]	12[2]	14	16	20	22
e/h (in.)	0.20	0.25	0.20	0.21	0.26	0.29	0.31	0.31
Spalling Force assuming uniform bond stress distribution/ Total Strand Force	0.003	0.011	0.004	0.005	0.019	0.033	0.065	0.067
Spalling Force assuming linear bond stress distribution/ Total Strand Force	0.006	0.021	0.009	0.011	0.030	0.052	0.085	0.085

[1]Laboratory Bridge Specimen with 5.25 in. flange height
[2]Laboratory Bridge Specimen with 3.0 in. flange height

Experimental Study

Four different variations in the vertical steel configurations were considered during the laboratory study, with each configuration repeated twice. The reinforcement details for each configuration are shown in Table 4.5.3. The vertical reinforcement in configurations 1 and 2 provided less than half of the 1.0 in.^{2} required by the AASHTO (2010) specification. The area of vertical reinforcement provided in configuration 4 was sufficient according to the specification; however it did not meet the placement requirements because the reinforcement extended farther into the section than the larger of 3 in. or one quarter of the total member depth (i.e., the reinforcement was not adequately grouped near the end of the beam). The vertical reinforcement in configuration 3 met all requirements of the specification, and consisted of No. 5 four legged stirrups spaced at 2 in. An additional No. 5 four legged stirrup was also placed a distance of 4 in. from the face in configuration 3.

Table 4.5.3: Vertical reinforcement in configurations 1-4 of the precast members utilized in experimental study

Configuration	**Description of Vertical End Zone Reinforcement**	**Cross Section View of Stirrup**	**Elevation View of Reinforcement Spacing**
1	#3 stirrup at 2 and 4 in. total area = 0.44 in^2		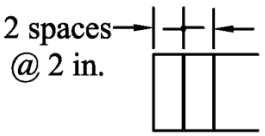
2	#4 stirrup at 2 in. total area = 0.40 in.^{2}		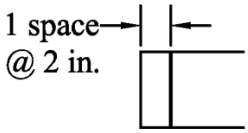
3	#5 four legged stirrup at 2 and 4 in. total area = 2.5 in.^{2}	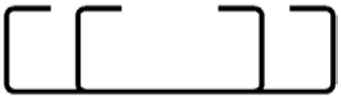	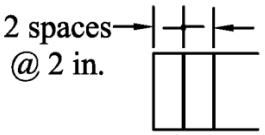
4	#5 stirrup at 2 and 4 in. total area = 1.2 in.^{2}	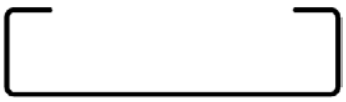	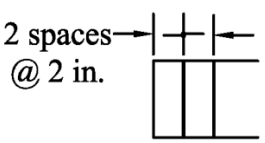

The end regions of the panels used in the Concept 1 laboratory bridge were well instrumented to investigate the state of stress immediately after release. On the side face of each section, rosettes were placed at midheight, 2 in. from the end face. A single strain gage was attached to each vertical stirrup with vertical placement ranging from 5.5 in. to 7.5 in. from the bottom of the precast section. The concrete and steel gages were monitored before, during, and after transfer. Readings were taken every minute, starting at 56 minutes before release and until 88 minutes after release. The average of the strain readings taken in the fifteen minutes before release was used to zero the remaining measurements.

The measured strains in each end section of the precast members used for the Concept 1 laboratory bridge are recorded in Table 4.5.4. The magnitudes of the strains observed in the end sections of the inverted-T sections were negligible, and no signs of cracking were detected, visually or via the instrumentation. The results from the experimental study suggested that the precast concrete at the time of transfer, which was measured to have a compressive strength of 7410 psi at an age of 1 day (Smith et al., 2008), was sufficient to resist vertical tensile stresses in the end zones regardless of the reinforcement details.

Table 4.5.4: Maximum of the measured strain values in end regions of precast members used for Concept 1 laboratory bridge in the 88 minutes after transfer of prestress force

	Span 1				**Span 2**			
Stirrup Location from End Face	2 in.		4 in.		2 in.		4 in.	
Northwest								
Vertical Stirrup Size	#3		#3		#3		#3	
Steel Gages (με)	3.5		-3.6		19		-4.8	
Concrete Gages (Vertical Leg of Rosette) (με)	-21		n/a		7.2		n/a	
Northeast								
Vertical Stirrup Size	#4		n/a		#4		n/a	
Steel Gages (με)	-1.1		n/a		16		n/a	
Concrete Gages (Vertical Leg of Rosette) (με)	3.0		n/a		35		n/a	
Southwest								
Vertical Stirrup Size	2 - #5		2 - #5		2 - #5		2 - #5	
	Inner[1]	Outer[2]	Inner	Outer	Inner	Outer	Inner	Outer
Steel Gages (με)	-3.7	16	-4.2	0.8	-8.7	6.2	-7.2	-1.9
Concrete Gages (Vertical Leg of Rosette) (με)	0.4		n/a		17		n/a	
Southeast								
Vertical Stirrup Size	#5		#5		#5		#5	
Steel Gages (με)	-1.1		-7.1		-20		-8.6	
Concrete Gages (Vertical Leg of Rosette) (με)	1.4		n/a		24		n/a	

[1] Inner – inner stirrup of four-legged stirrup

[2] Outer – outer stirrup of four-legged stirrup

Summary and Application to Design

Results from the finite element study revealed that the relationship between $e^2/(h*d_b)$ to the ratio of tensile spalling force to prestress force is reasonably approximated by a straight line as shown

in Figure 4.5.5. Because the true bond stress distribution is somewhere between uniform and linear bond stress, an average between these two assumptions was developed, as shown in Figure 4.5.5. The equation for this straight line approximation is

$$T = P\left(0.02\frac{e^2}{hd_b} - 0.01\right) \geq 0 \tag{4.5.1}$$

where T is the spalling force and P is the strand force.

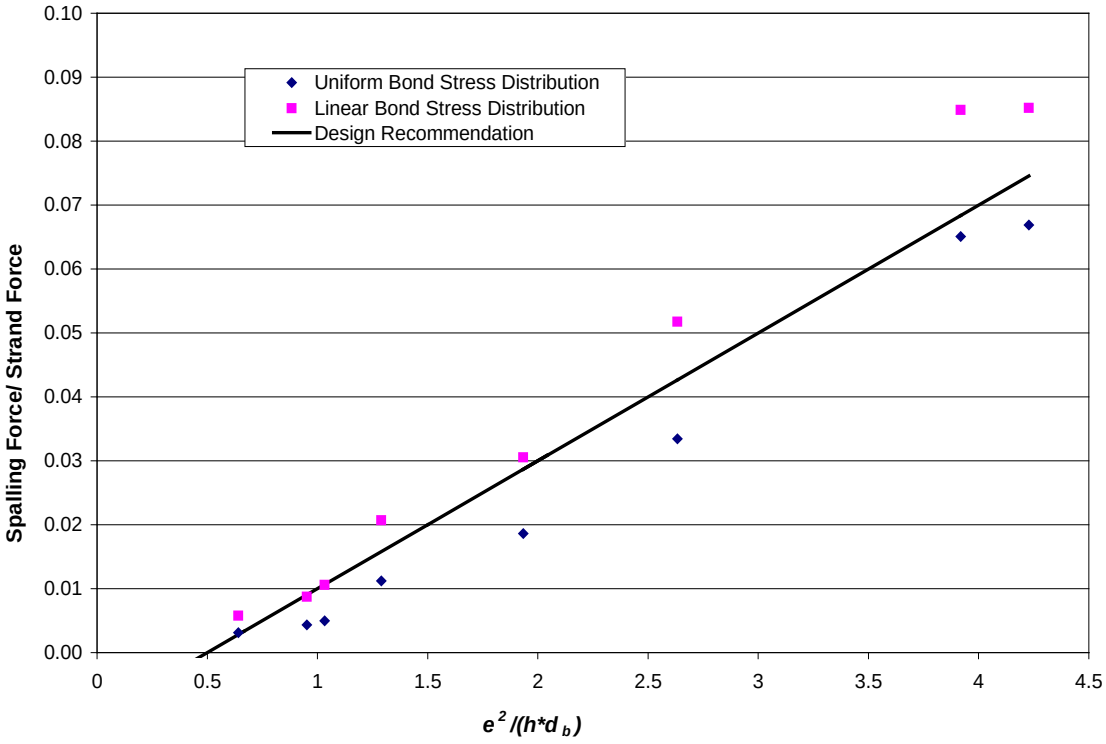

Figure 4.5.5: Ratio of Spalling Force to Prestress Force for varying $e^2/(h*d_b)$

Vertical steel reinforcement does not carry the vertical tensile stress until the concrete cracks. If the spalling stresses are small enough in a member for the concrete tensile strength to prevent cracking, vertical tensile steel is not necessary for the member.

To calculate the concrete area to be considered in providing tensile resistance, the area over which spalling forces act must be determined. Based on the slab span sections studied, the shortest distance into the member the spalling stress extends is $h/12$. This becomes a conservative estimate as the section increases in height and e/h. The area of concrete to resist this tensile strength is conservatively estimated as the product between $h/12$ and the distance between the outermost prestress strands (b_s) and can be written as

$$T_c = 0.24\sqrt{f_c}\frac{h}{12}b_s \ , \tag{4.5.2}$$

where T_c is the tensile force that can be resisted by the concrete, f_c is the concrete compressive strength at 28 days, h is the height of the member, and b_s is the distance between the outermost pretension strands. If the design tensile force is smaller than the tensile force resisted by concrete ($T < T_c$), it is reasonable to assume cracking will not occur and vertical tensile steel is not needed in the end region to resist the spalling force. Otherwise, steel must be placed within the end region of the member to resist the tensile force found in Eqn. (4.5.1). The area of steel needed to resist the predicted spalling force is given by

$$A_s = \frac{T}{f_s} \ , \tag{4.5.3}$$

where A_s is the area of steel and f_s is the allowable working stress of vertical reinforcement.

Application of these recommendations to the designs resulting from the parametric study described in Section 4.1 result in the end zone reinforcement identified in Table 4.5.5. The last line of the table includes the AASHTO 2010 requirements for comparison, which are incorrectly referred to as splitting resistance rather than spalling resistance requirements in AASHTO.

Table 4.5.5: Spalling reinforcement for Precast Inverted-T Sections

Height (in.)	8	10	12	12	14	16	20	22
Number of Strands	12	16	16	16	36	38	46	54
Strand Diameter (in.)	0.5	0.5	0.5	0.5	0.5	0.5	0.5	0.5
Total Prestress Force at Jacking (k)	370	500	500	500	1100	1200	1400	1700
Concrete Compressive Strength at Transfer (ksi)	5.0	5.0	4.5	4.5	5.5	5.5	5.6	6.0
e (in.)	1.6	2.5	2.4	2.5	3.7	4.6	6.3	6.8
T (k) (Eqn. 4.5.1)	1.0	7.5	4.6	5.4	32	51	97	126
T_c (k) (Eqn. 4.5.2)	17	21	24	24	32	36	45	51
Vertical Steel Needed?	No	No	No	No	No	Yes	Yes	Yes
A_s (in.^{2}) (Eqn. 4.5.3)	--	--	--	--	--	2.6	4.9	6.3
h/4	--	--	--	--	--	4.0	5.0	5.5
Stirrup Bar Size	--	--	--	--	--	#6	#6	#6
A_s (in^2) per AASTHO Article 5.10.10.1	0.74	1.0	1.0	1.0	2.2	2.4	2.8	3.4

4.6. Connection Details between Superstructure and Substructure

The bearing and connection details between the bridge superstructure and the supporting substructure were investigated by a review of existing PCSSS bridges constructed by the Minnesota Department of Transportation. Because no problems have been encountered in the existing field bridges, the same details may be deemed appropriate in future applications of PCSSS bridges. Some modifications are recommended to reduce the potential for restrained shrinkage in the transverse direction.

Figure 4.6.1 shows an elevation view of the bearing detail at one of the two continuous supports for the Center City Bridge, one of the original field implementations of the PCSSS. The pile caps in this particular bridge were precast, and the elevation view is shown through one of the sections featuring a vent hole through the pile cap into which dowels were placed prior to casting the CIP concrete.

As shown in the figure, the main bearing support was provided by a 6 in. wide by 1/2 in. thick neoprene bearing pad, with the center of bearing located 12 in. from the edge of the pier. Polystyrene was utilized in the 9 in. between the edge of the pier and the neoprene, as well as the 4 in. between the neoprene and the end of the beam; the polystyrene was selected because it would prevent the egress of concrete during the closure pour and was crushable and would therefore not significantly affect the bearing geometry of the system.

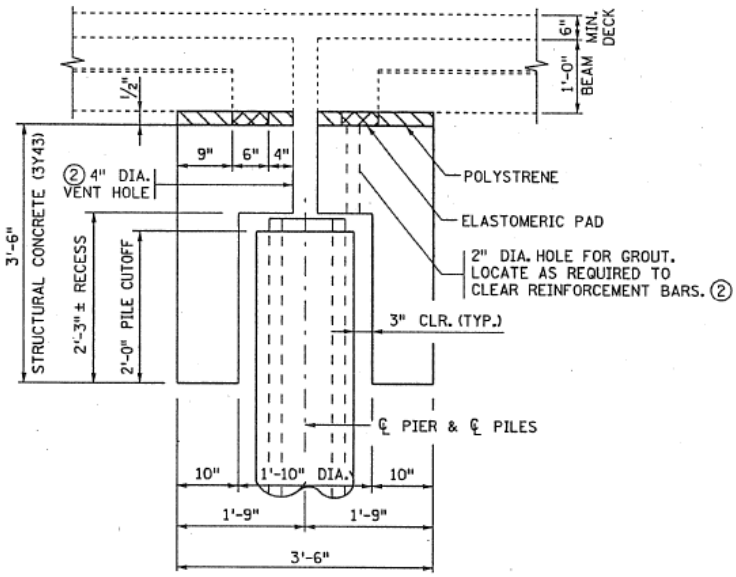

Figure 4.6.1: Bearing detail at continuous pier in Mn/DOT Bridge No. 13004 in Center City, Minnesota

The neoprene and polystyrene were not located in the transverse joint between the precast sections nor in the regions beneath the flange cutouts. This enabled the CIP concrete to fill those regions to facilitate the negative moment resistance of the bridge by enabling the transfer of compressive forces low in the section across the pier.

Vertical dowels were provided in the Center City Bridge to ensure that a mechanical connection was present between the substructure and superstructure. The vertical reinforcement was epoxied into holes drilled between the ends of the adjacent precast members at the continuous piers, and were subsequently embedded in the CIP closure pour. The vertical dowels consisted of No. 5 bars at 12 in.

The placement of the vertical reinforcement in these locations was found to be difficult in some of the subsequent applications of PCSSS bridges, because the 4 in. gap between the ends of the precast panels does not always provide sufficient tolerance for the precast panel span lengths. For this reason, the placement of the vertical dowels in the 10 in. flange cutout region may be preferred; however eccentricity of the vertical dowels from the centerline between precast panels will allow for the introduction of a moment between the superstructure and substructure in plan, and should therefore be avoided. It is recommended that the vertical dowels be oriented along a single line bisecting the area between adjacent precast panels at continuous piers. Because the reinforcement is not provided to prevent cracking, and is simply to provide dowel action in the case of differential displacement between the superstructure and substructure, it may be acceptable to place the reinforcement as a group in the 24 in. space between precast webs, however still along the line bisecting the specimens.

A method considered by the Minnesota Department of Transportation to reduce the potential for the restraint of transverse shrinkage was to encase the vertical dowels in foam. The foam will likely only be beneficial if the CIP is debonded from the pier via a bond breaker. Consequently, in future applications of PCSSS bridges, it is recommended that a debonding material, such as a sheet of plastic be used, to prevent the CIP concrete from bonding to the substructure.

4.7. Numerical Determination of Laboratory Loading

The finite element models described in Section 4.7 were developed by Roberto Piccinin (2010)

Mechanical loading was utilized in the laboratory to simulate traffic loading on the laboratory specimens (i.e., Concept 1 and Concept 2), described in Chapter 5. The Concept 1 specimen was developed based on the Center City Bridge, with some parameter variations (e.g., investigation of

different flange thicknesses: 3 in. flange thickness in one span versus the 5-¼ in. flange thickness in the other span which emulated the Center City Bridge). The laboratory bridge specimens were fabricated with 12 in. thick precast panels and 6 in. cast-in-place topping. The approximately 22 ft. span lengths represented the outer spans of the Center City Bridge, which were a lower practical bound of PCSSS bridge spans. The same 18 in. deep section was used in all three spans (22-27-22 ft.) of the Center City Bridge, and could be used in even longer spans as indicated by Table 4.1.2. The use of the 18 in. deep section led to relatively low service stresses particularly in the end spans.

In an effort to improve the relevance of the laboratory tests to longer spans, the magnitude of the patch load was selected after a numerical analysis of longer PCSSS bridges. The 35 kip value was expected to induce the same levels of transverse tensile stress in the joint region of the 22 ft.-5 in. laboratory bridge span as would be expected in a 30 ft. three-span continuous system. The 30 ft. continuous bridge was selected because it represented a reasonable value for the design span of a slab span system with 12 in. deep precast panels (although as shown in Table 4.1.2, it might be possible to use something as shallow as a 10 in. deep precast section for a 30 ft. span). The 35 kip patch load was applicable to both the two-span Concept 1 and simply-supported Concept 2 laboratory bridges, coincidentally, because loading was applied at the quarter points of the simply-supported Concept 2 specimen, which featured different transverse reinforcement details in each half of the bridge span.

The numerical model was developed assuming an unbonded constraint between the precast flanges and CIP concrete, as illustrated in Figure 4.7.1. This was done to ensure that convergence would be achieved at the interface immediately above the precast joint. Figure 4.7.2 illustrates a modified four point AASHTO tandem design load on the three span 30 ft. continuous bridge, which consists of four 25 kip patch loads spaced in a 4 by 6 ft. grid. This modified tandem load pattern was based on twice the design tandem load, as specified in Article 3.6.1.2.3 (AASHTO 2010). The design tandem was doubled to provide an expected worst case scenario near the joint region, which represented two truck wheel loads placed as closely as possible directly over a longitudinal joint. The image is shown from the end span looking in the direction of traffic. The 6 ft. wide patch loads are placed directly above the precast joints, which represented the worst load case for the system.

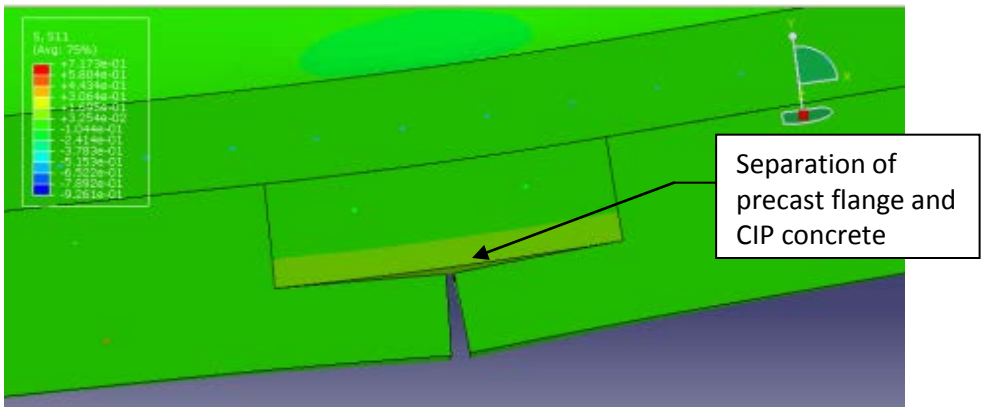

Figure 4.7.1: Separation of top of precast joint from CIP concrete in 30 ft. continuous and laboratory bridge models

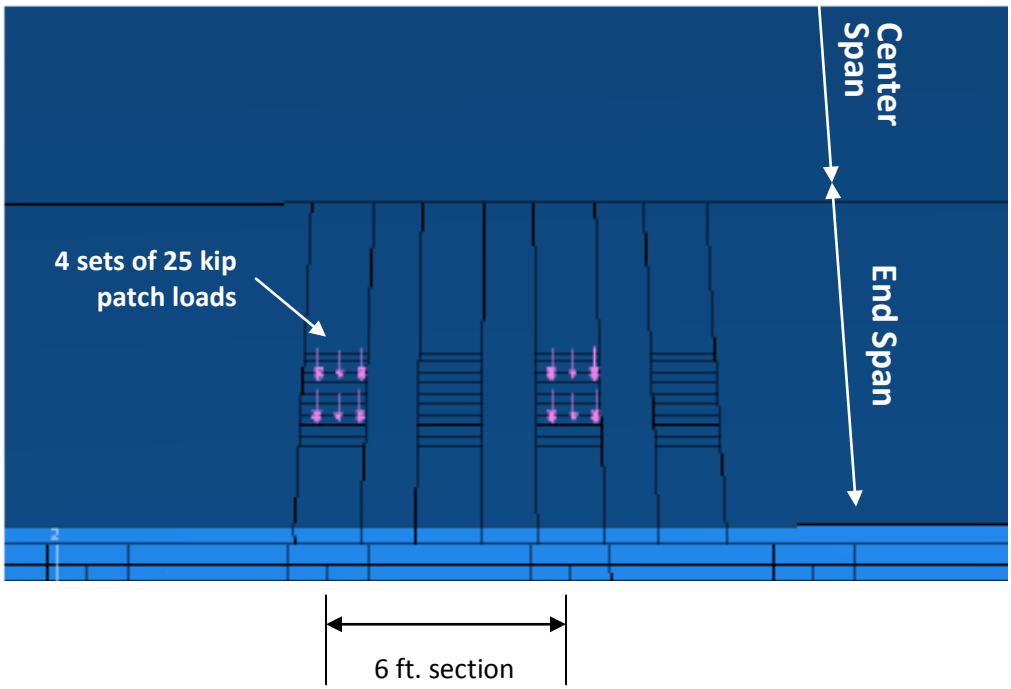

Figure 4.7.2: Three span 30-30-30 ft. continuous bridge with AASHTO tandem loading, increased by a magnitude of two to account for two trucks side by side with adjacent wheels applied over the joint, applied for the numerical calculation of a patch load demand in laboratory bridge.

The numerical models utilized for the Concept 1 and Concept 2 laboratory specimens are shown under deformation in Figure 4.7.3a-b, respectively. The Concept 1 model was analyzed with the patch load centered at midspan of both spans, while the Concept 2 model was loaded at the quarter points. The same numerical model was utilized to analyze the effect of the patch load for both specimens. For the Concept 2 bridge, which was a simply-supported span, the same two-span model was used with an assumed modulus of elasticity of the CIP and precast concrete in the span with the 5-¼ in. thick flange set to be 1/100 of the modulus of elasticity of the CIP used in the loaded span modeled with a 3 in. flange, effectively creating a simply-supported boundary condition at the end of the bridge connected to the adjacent span.

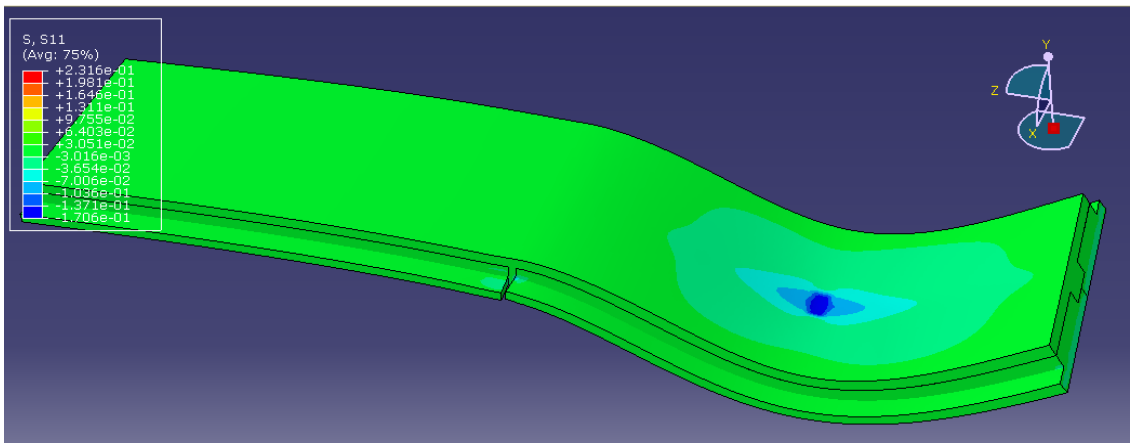

a) Concept 1 laboratory specimen – patch loading at midspan

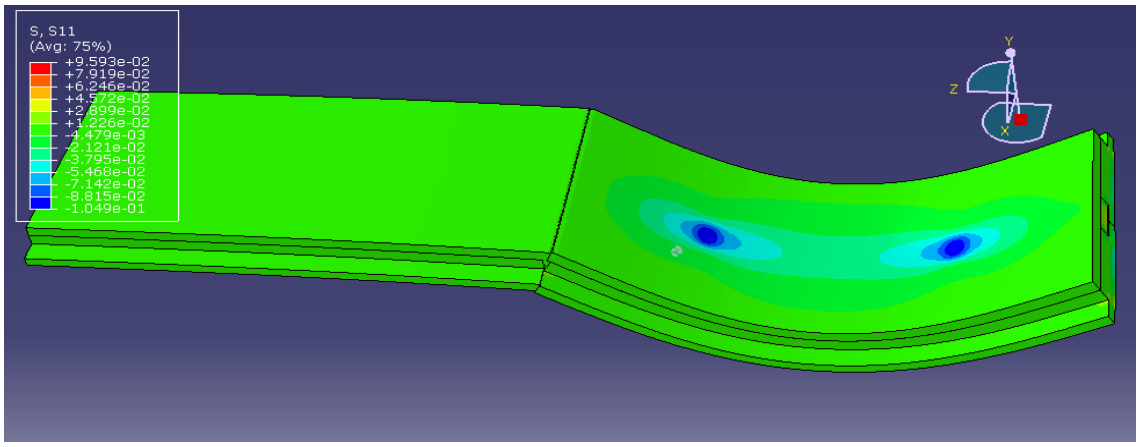

b) Concept 2 laboratory specimen – patch loading at quarter points. Second span modeled with modulus of elasticity of CIP equal to 1/100 CIP modulus of elasticity of loaded span

Figure 4.7.3: Deflected numerical models of (a) Concept 1 specimen and (b) Concept 2 specimen for determination of patch loading in laboratory specimens

The analyses suggested that the load required to induce similar levels of transverse tensile stresses in the 30 ft. continuous bridge and the loading cases of the laboratory bridge varied by less than two kips, and therefore, with a patch load of 26.7 kips required to induce similar levels of transverse stress in the laboratory bridge as the 30 ft. continuous bridge. Furthermore, the dynamic loading effects were considered through the use of a 33 percent increase in the static load, as specified in Article 3.6.2.1 of the AASHTO specification (2010). Therefore, the calculated load to be applied to the laboratory bridge to simulate a tandem vehicle loading on a 30 ft. continuous bridge was determined to be 35 kips (26.7 kips * 1.33).

Chapter 5: Large-Scale Laboratory Bridge Investigation of System Behavior

5.0 Introduction

The performance of the precast composite slab span system in a global sense depends on the interaction between neighboring precast panels as well as panels in the adjacent spans. This interaction between components of the PCSSS warranted the development of two large-scale laboratory test specimens constructed and tested in the University of Minnesota Structures Laboratory. The first bridge, Concept 1, was developed as a continuous two-span system with two adjacent precast panels per span. A number of variables were investigated with this bridge, which are discussed in detail in Section 5.1.1. A portion of the Concept 1 specimen emulated one of the first implementations of PCSSS bridges in the State of Minnesota, Mn/DOT Bridge 13004 built in Center City. The second bridge, designated as the Concept 2 specimen, was a simply-supported bridge with two adjacent precast panels. The Concept 2 laboratory bridge was developed to augment the information obtained from testing of the Concept 1 laboratory bridge specimen, and is discussed in detail in Section 5.1.2. This chapter discusses the development, testing, and results of the large-scale laboratory testing.

5.1. Selection and Design of Laboratory Bridge Specimens

The Concept 1 specimen which was based on the Center City Bridge with modifications as required to investigate variations in some of the parameters, was constructed as part of a Mn/DOT research project which consisted of a companion field and laboratory investigation described by Smith et al. 2008. The results of the field study are summarized in Section 3.2. At the conclusion of the Mn/DOT study, the Concept 1 laboratory bridge was made available to the NCHRP 10-71 study, which included cyclic tests to simulate fatigue, investigation of initiation of reflective cracking simulated to emulate observed crack initiation in the Center City field bridge, as well as tests to investigate the ultimate strength of the system and composite action. The Concept 2 laboratory bridge, developed at the conclusion of laboratory testing on the Concept 1 laboratory bridge, was designed to incorporate information accrued from the Concept 1 tests, as well as to investigate variations in additional parameters. Relevant design details for both specimens are discussed in the following sections.

Many of the design details associated with the Concept 1 and Concept 2 large-scale laboratory bridge specimens, as well as the subassemblage specimens discussed in Chapter 6, include variations in the size and spacing of the transverse reinforcement traversing the longitudinal precast joint in the trough region created by adjacently abutted precast sections. To provide a means of qualifying the reinforcement in this region, a transverse reinforcement ratio was defined. The presence of transverse reinforcement for both transverse load transfer and reflective crack control warranted separate definitions for the reinforcement ratio in each case.

In the case of transverse load transfer, the area of reinforcement considered was only that which was embedded or mechanically anchored through the precast web in the lowest region of the CIP trough such that all load developed in the reinforcement could be adequately transferred through the adjacent panels. For a given longitudinal joint, the reinforcement protruding from a single precast panel was considered (i.e., for each pair of transverse embedded bars, only one was considered in the reinforcement ratio). It was assumed that the load was transferred from the bars protruding from one panel to the bars protruding from the adjacent panel through lap splices. Furthermore, the area of concrete considered in the calculation was taken as that between the top of the precast flanges and the top of the section. An illustration of the area of steel and concrete considered for the calculation of the reinforcement ratio for transverse load transfer is highlighted in yellow in Figure 5.1.1.

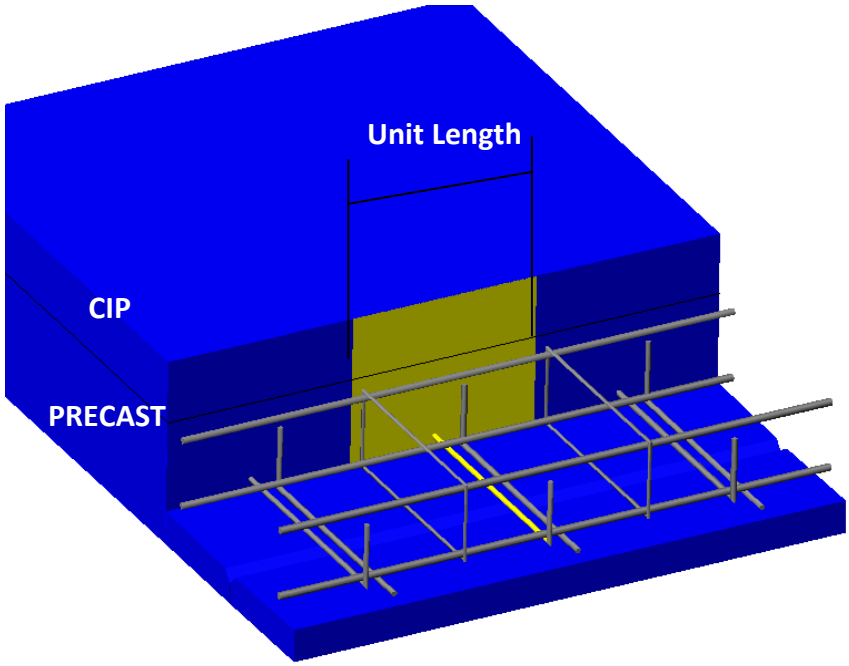

Figure 5.1.1: Reinforcement and depth of concrete considered in the calculation of the reinforcement ratio for transverse load transfer (highlighted in yellow)

The reinforcement ratio for crack control, on the other hand, considered the area of all reinforcement crossing the precast joint near the bottom of the CIP trough. Therefore, the bottom leg of the cage stirrups and all of the embedded transverse reinforcement was included in the calculation (i.e., for each pair of transverse embedded bars, both were included in the calculation because both were assumed to be effective above the longitudinal joint between the adjacent flanges). Furthermore, the area of concrete used in the calculation was only that which was located between the top of the precast flanges and the top of the precast webs. An illustration of the area of steel and concrete considered in the calculation of the reinforcement ratio for crack control is highlighted in yellow in Figure 5.1.2. It should be noted that this crack control reinforcement would only be effective in the region above the longitudinal joint between adjacent precast panels. For potential cracks that may develop at the precast web-CIP interface, only the reinforcement protruding from the precast webs would be effective.

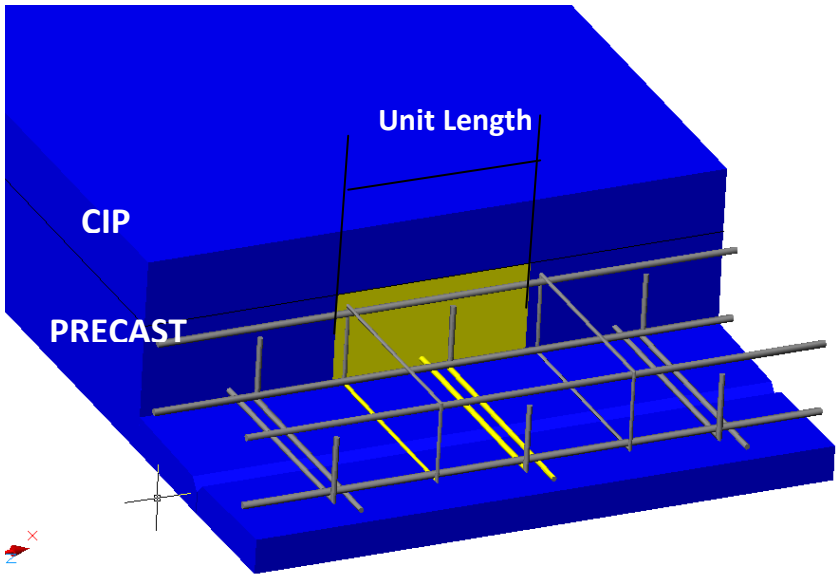

Figure 5.1.2: Reinforcement and depth of concrete considered in the calculation of the reinforcement ratio for reflective crack control (highlighted in yellow)

5.1.1. Concept 1 Laboratory Bridge

The continuous two-span Concept 1 laboratory bridge specimen was selected to provide insight into the effects of restraint moment developed at the pier, load distribution, and the effect of a number of variations in parameters. Restraint moments will develop at continuous piers due to both time-dependent effects (i.e., creep and shrinkage) and thermal gradients. Because the

laboratory bridge was constructed and tested within the temperature-controlled environment of the University of Minnesota Structures Laboratory, restraint moments due to thermal effects were not experimentally studied in the laboratory specimen, however an effort to induce a longitudinal curvature due to a uniformly applied thermal heat source was implemented on Span 2 of the Concept 1 laboratory bridge, which is discussed later in this chapter.

Variables investigated in the two-span Concept 1 laboratory bridge are summarized in Table 5.1.1. The variables included the precast flange thickness, flange surface roughness, and reinforcement detailing, in addition to the amount of CIP deck reinforcement. Span 2 of the bridge was constructed identically to the exterior spans of the Center City Bridge, allowing for a relative comparison between observed results in the field and laboratory bridges. Span 1 of the bridge specimen was constructed with the application of the variables of interest, such as a reduced flange depth; the reduction in flange depth from 5.25 to 3 in. was introduced in an effort to reduce the distance between the transverse hooked bars and the precast flange, which would help to intercept a potential reflective crack at the precast joint region at a lower depth as well as increase the transverse moment capacity. Additionally, a smooth flange surface was used in Span 1. The smooth flange was designed to reduce the stress concentration above the flanges directly at the joint, as well as aid in the removal of the formwork during fabrication. The stirrup spacing for horizontal shear reinforcement was increased to 24 in. on center in Span 1, primarily because the 12 in. stirrup spacing utilized in Span 2 was expected to be overly conservative. The horizontal shear reinforcement was also detailed with increased clear spacing below the hooked bars in Span 1, as the 1/4 in. nominal clear spacing provided in Span 2 was expected to inhibit bond development between the CIP concrete and the stirrup hook. The longitudinal and transverse deck reinforcement was also considered during the study, with the north half of the bridge consisting of a reduced longitudinal reinforcement scheme. The transverse deck reinforcement was reduced to No. 4 bars at 12 in. in Span 1, from No. 5 bars at the same spacing in Span 2. The four precast panels used in the Concept 1 laboratory bridge provided eight regions (i.e., one region at each end of each precast panel) that were used in the end zone stress study, discussed in Section 4.5. The bursting reinforcement locations in the Concept 1 laboratory bridge are shown in Figure 5.1.3, and were identical for Spans 1 and 2.

The behaviors of interest to this study are discussed herein; additional results pertinent to the Concept 1 laboratory bridge have been documented by Smith et al. (2008) in association with the previous Mn/DOT study.

Table 5.1.1: Original and modified design criteria in Spans 1 and 2 of the Concept 1 laboratory bridge

Span 1 (Modified Section)	**Span 2 (Original Section)**
Decreased flange thickness (3 in.)	Original flange thickness (5-¼ in.)
Smooth flange surface	Original roughened flange surface
Increased stirrup spacing for horizontal shear reinforcement (No. 5 Stirrups at 24 in.)	Original stirrup spacing for horizontal shear reinforcement (No. 5 Stirrups at 12 in.)
Increased clear spacing under hooks (1-3/8 in. nominal clear spacing between horizontal shear reinforcement stirrups and precast section)	Original clear spacing under hooks (1/4 in. nominal clear spacing between horizontal shear reinforcement stirrups and precast section)
Decreased transverse deck reinforcement (No. 4 bars at 12 in.)	Original transverse deck reinforcement (No. 5 bars at 12 in.)
The longitudinal deck steel in the south half of the bridge was two No. 7 and one No. 8 bars per 12 in. at the continuous pier (Original design)	
The longitudinal deck steel in the north half of the bridge was reduced to No. 6 bars at 6 in. spacing at the continuous pier (Modified design)	

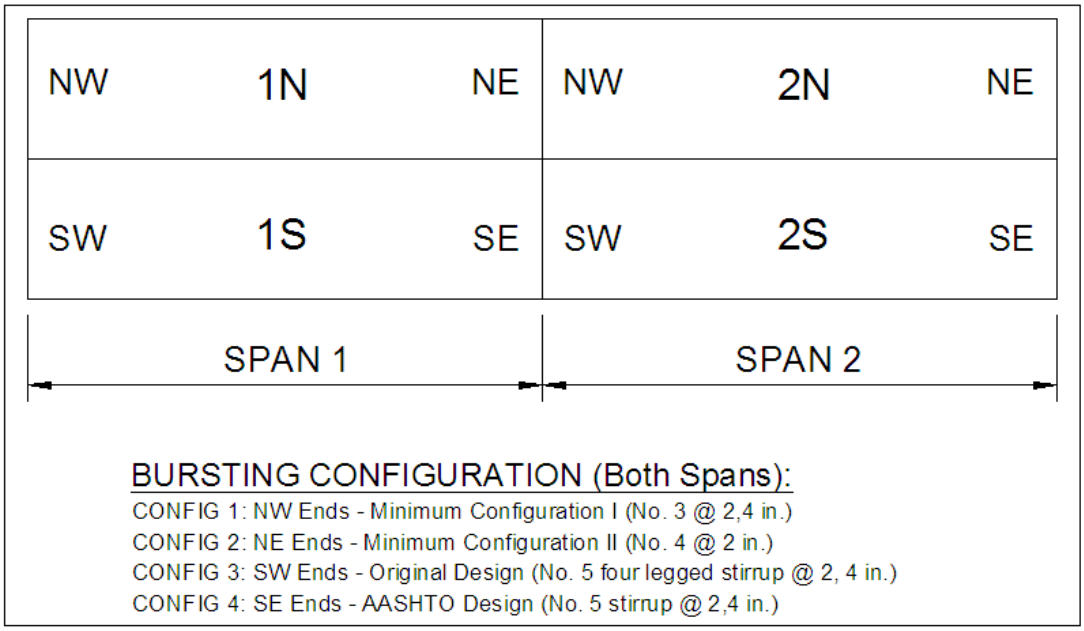

Figure 5.1.3: Bursting reinforcement details used in the Concept 1 laboratory specimen. Configuration numbers correspond to the discussion on bursting in Section 4.5

A simplified plan view of the Concept 1 laboratory bridge, including support locations and relevant dimensions is included in Figure 5.1.4; the transverse reinforcement near the longitudinal precast joint region is not shown for clarity. The reinforcement present in each unique cross section (i.e., east, west, or midspan) of each precast panel (i.e., 1N, 1S, 2N, 2S), as well as an elevation and layout views illustrating the location of reinforcement along the length of each beam are shown in Figures 5.1.5 through 5.1.20; four figures are included for each precast panel, in the following order: east cross section, west cross section, midspan cross section, and elevation/plan. A photograph of the Concept 1 laboratory bridge shortly after the completion of the continuity deck pour is shown in Figure 5.1.21.

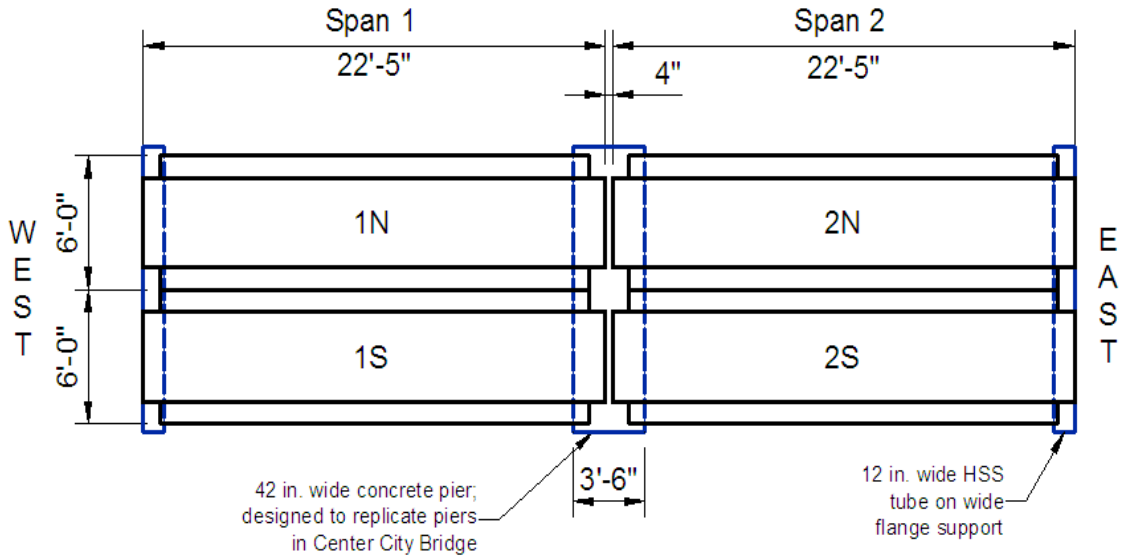

Figure 5.1.4: Plan view of the Concept 1 laboratory bridge, including support locations and relevant dimensions. Transverse reinforcement near longitudinal precast joint is not included for clarity

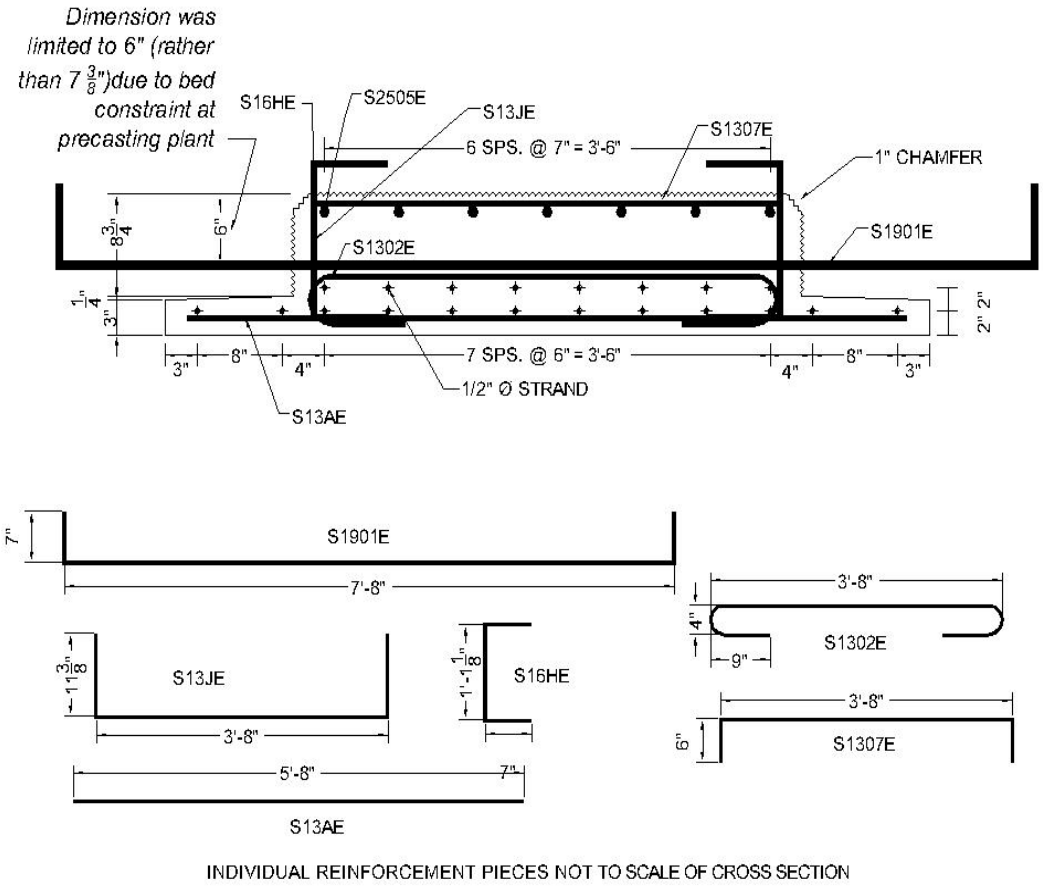

Figure 5.1.5: Cross section and individual reinforcement details for the east end of precast beam 1N

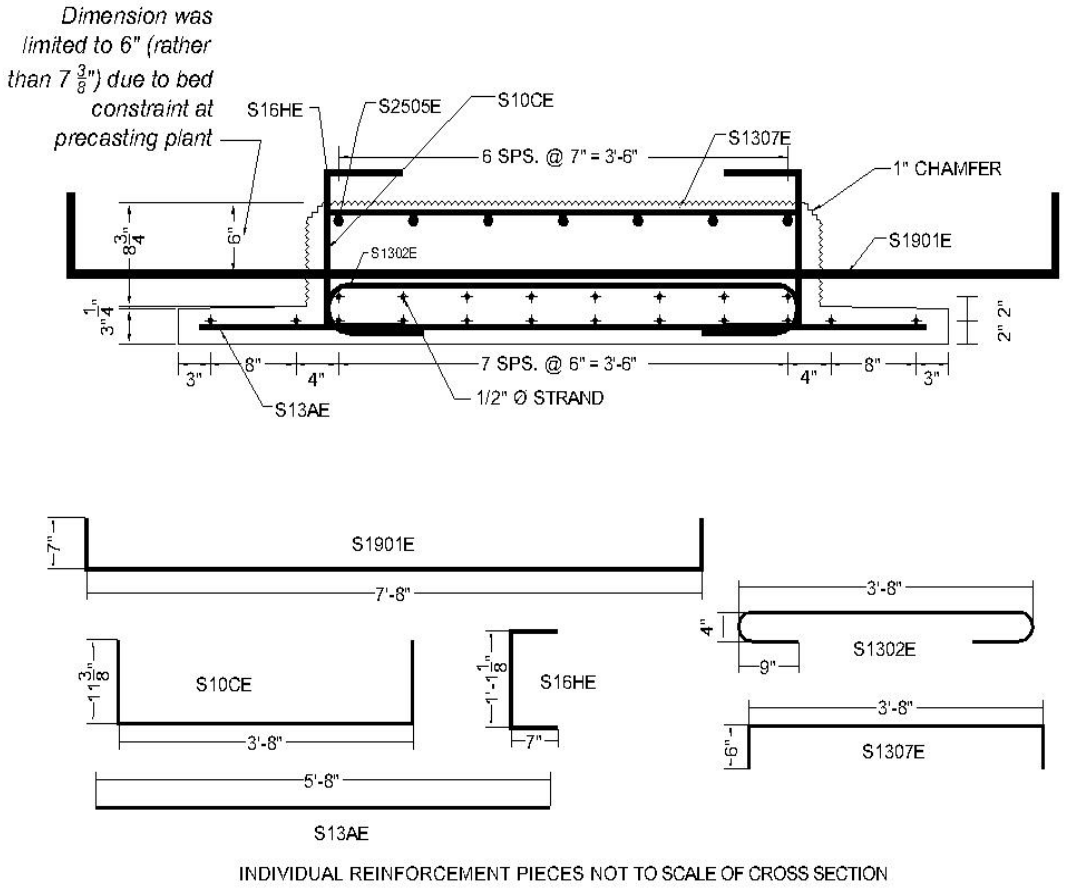

Figure 5.1.6: Cross section and individual reinforcement details for west end of precast beam 1N

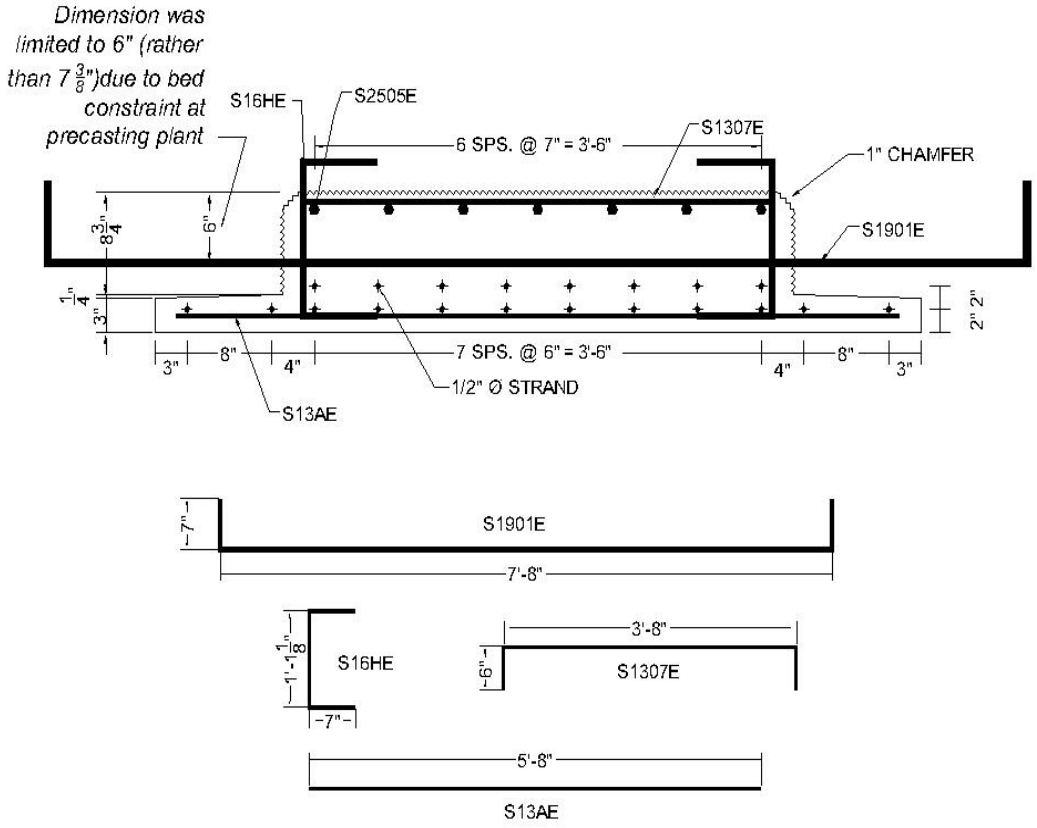

Figure 5.1.7: Cross section and individual reinforcement details for midspan of precast beam 1N

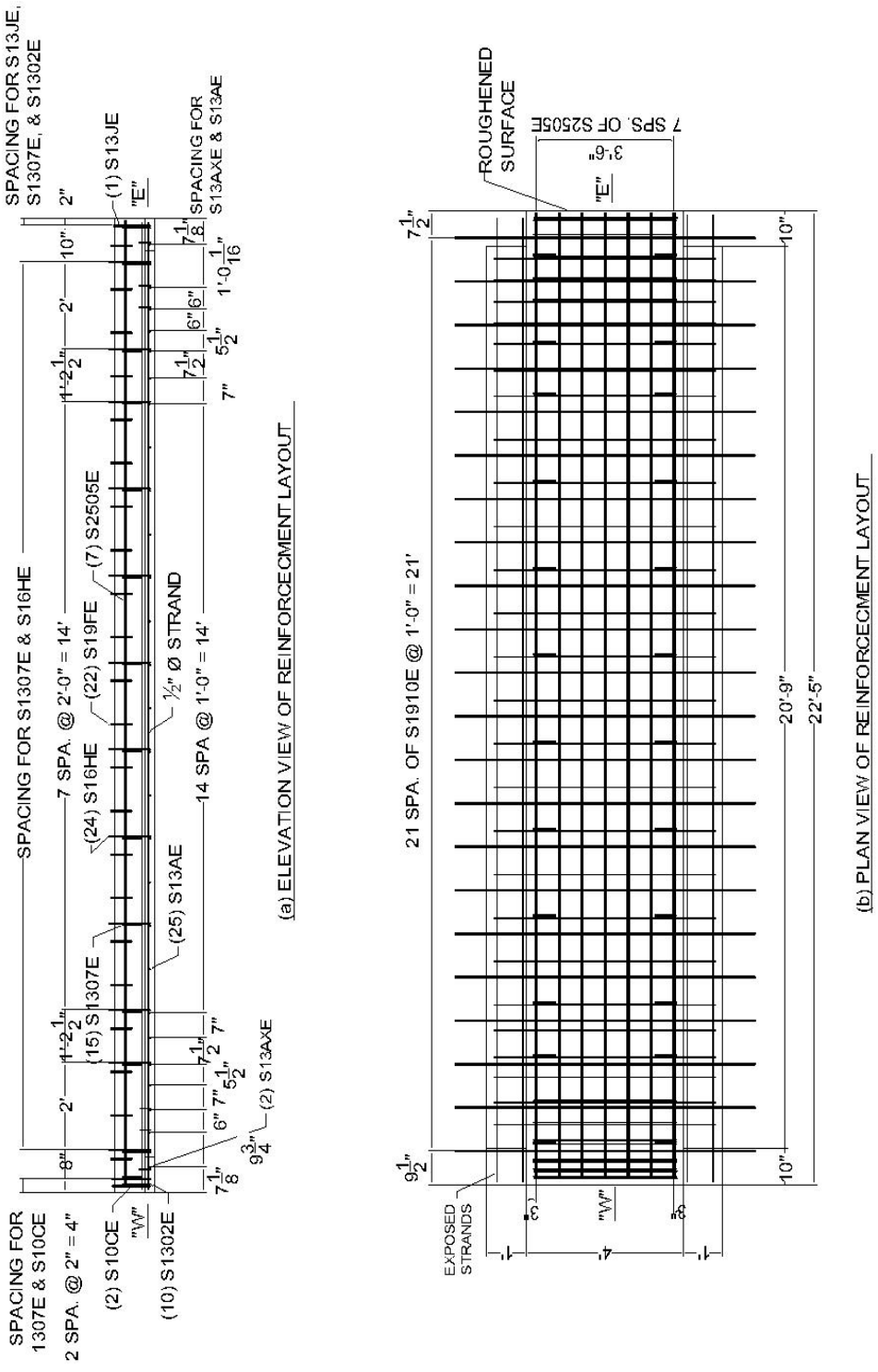

Figure 5.1.8: Elevation and plan views of reinforcement layout for precast beam 1N

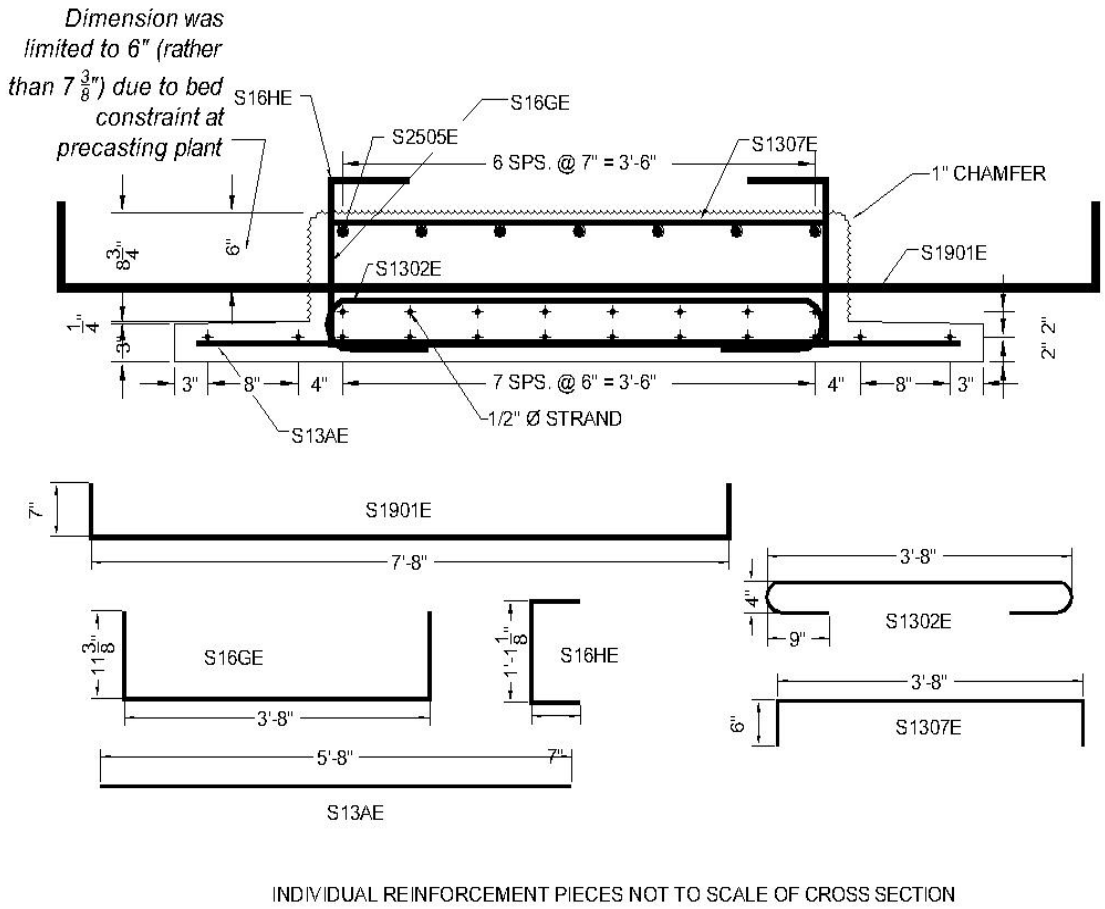

Figure 5.1.9: Cross section and individual reinforcement details for east end of precast beam 1S

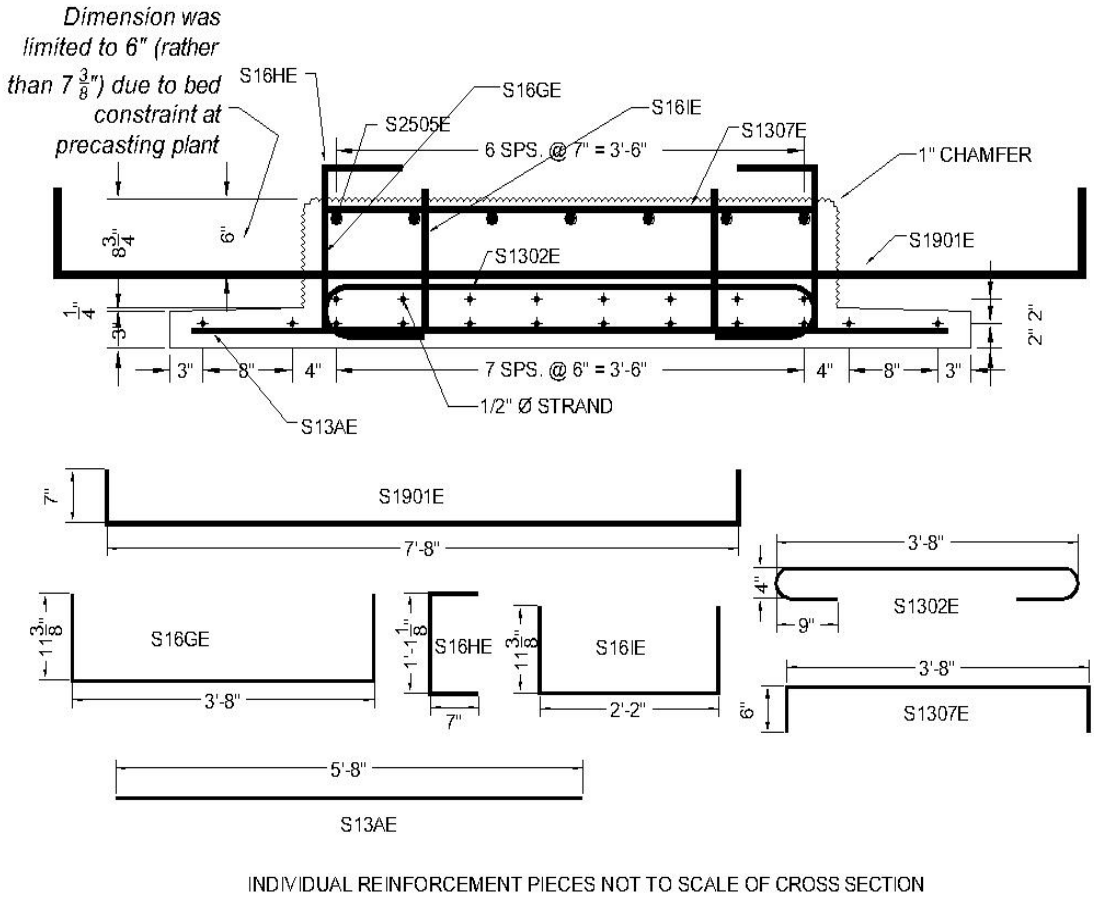

Figure 5.1.10: Cross section and individual reinforcement details for west end of precast beam 1S

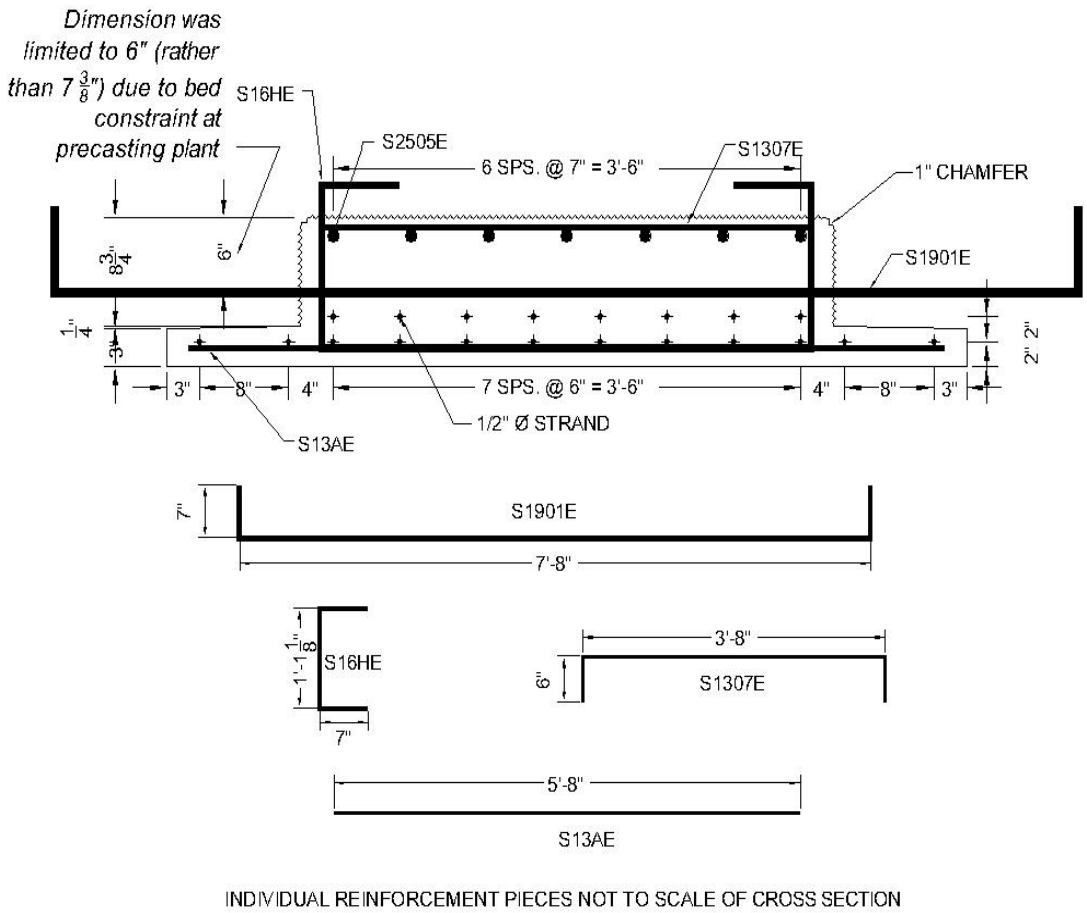

Figure 5.1.11: Cross section and individual reinforcement details for midspan of precast beam 1S

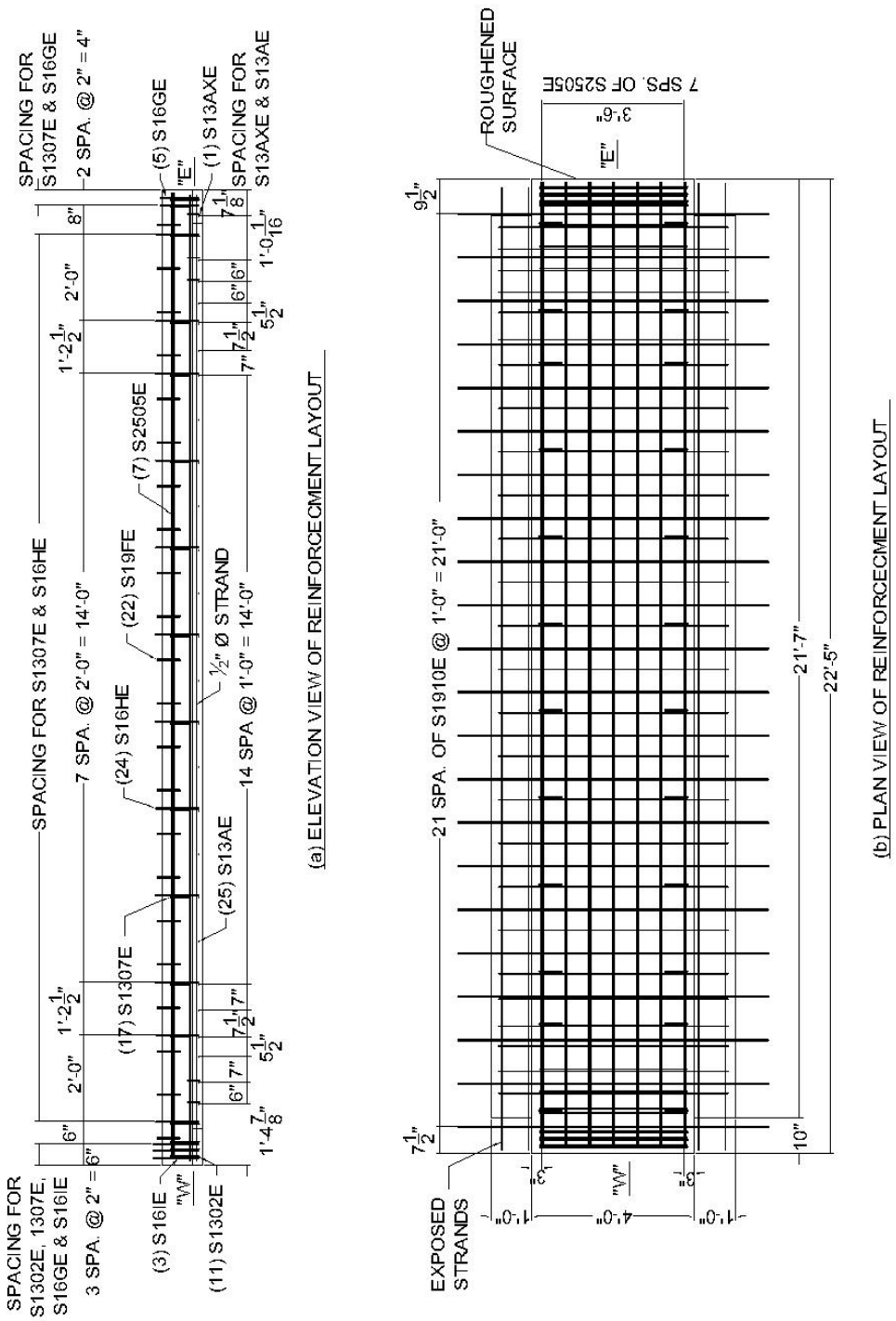

Figure 5.1.12: Elevation and plan views of reinforcement layout for precast beam 1S

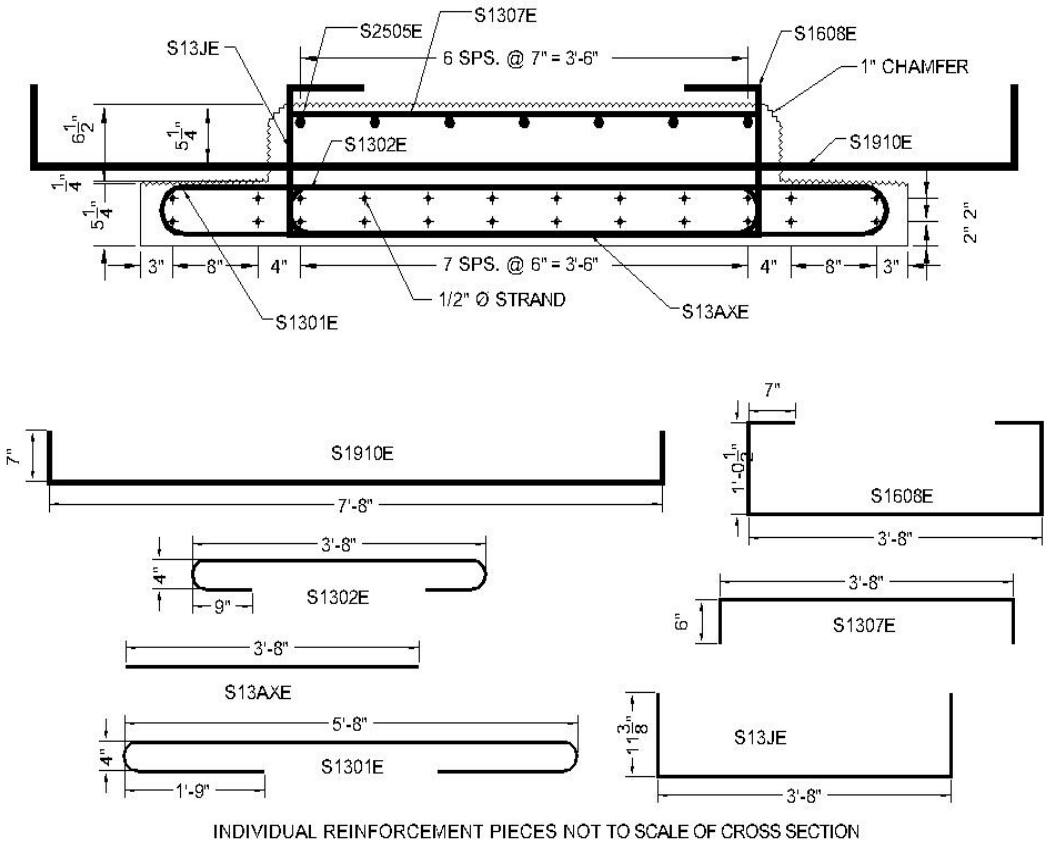

Figure 5.1.13. Cross section and individual reinforcement details for east end of precast beam 2N

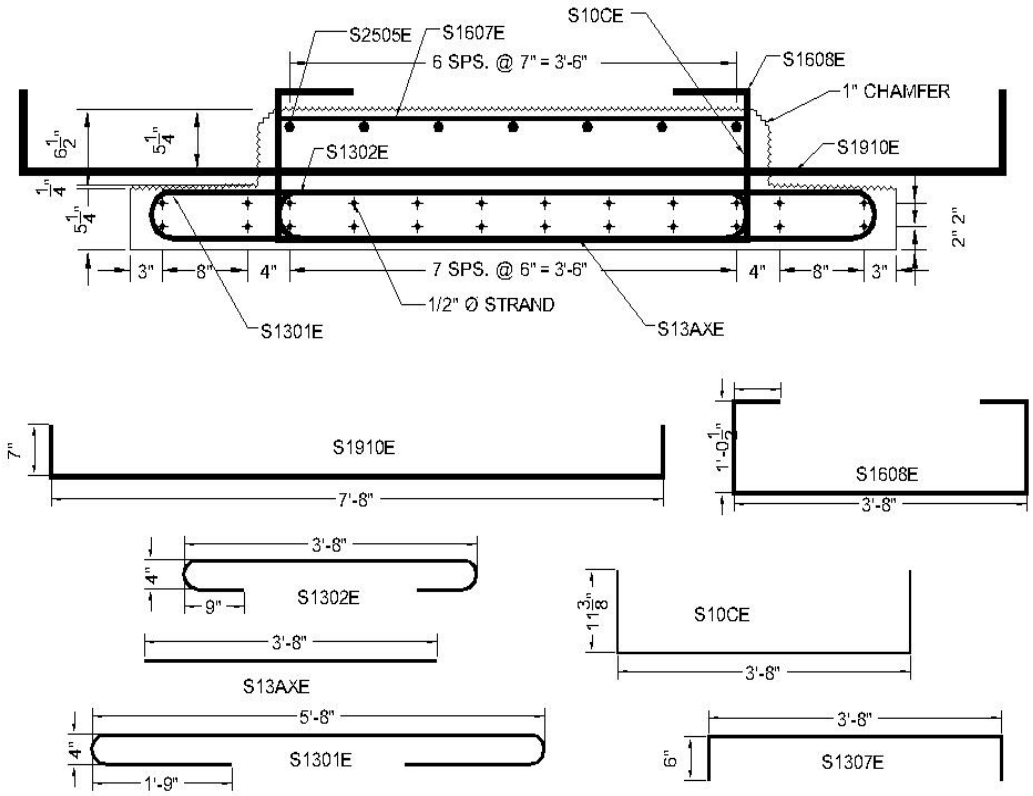

INDIVIDUAL REINFORCEMENT PIECES NOT TO SCALE OF CROSS SECTION

Figure 5.1.14: Cross section and individual reinforcement details for west end of precast beam 2N

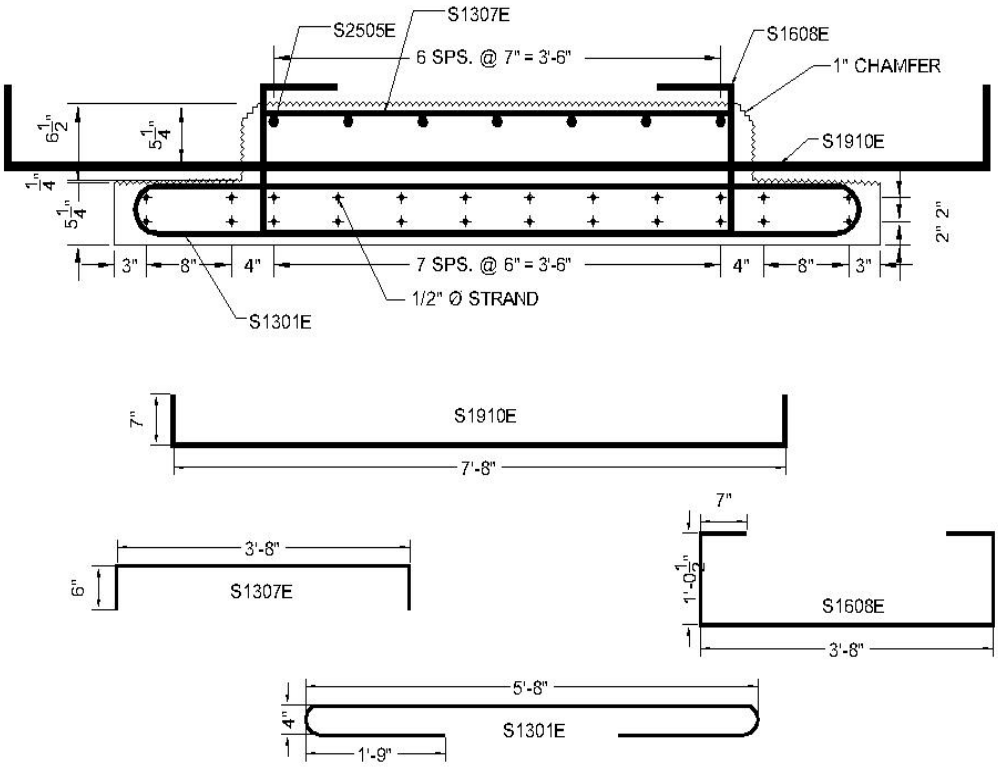

Figure 5.1.15: Cross section and individual reinforcement details for midspan of precast beam 2N

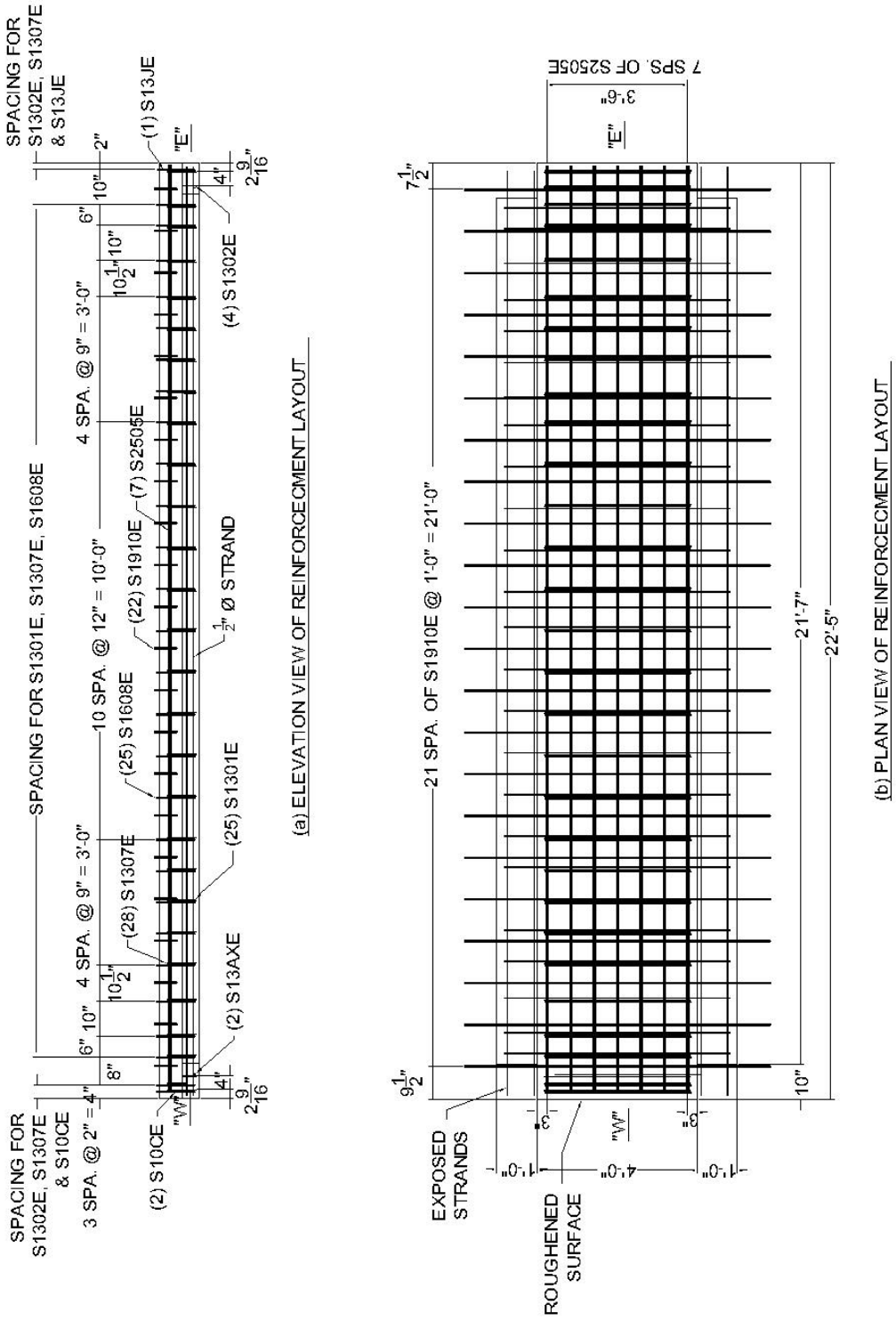

Figure 5.1.16: Elevation and plan views of reinforcement layout for precast beam 2N

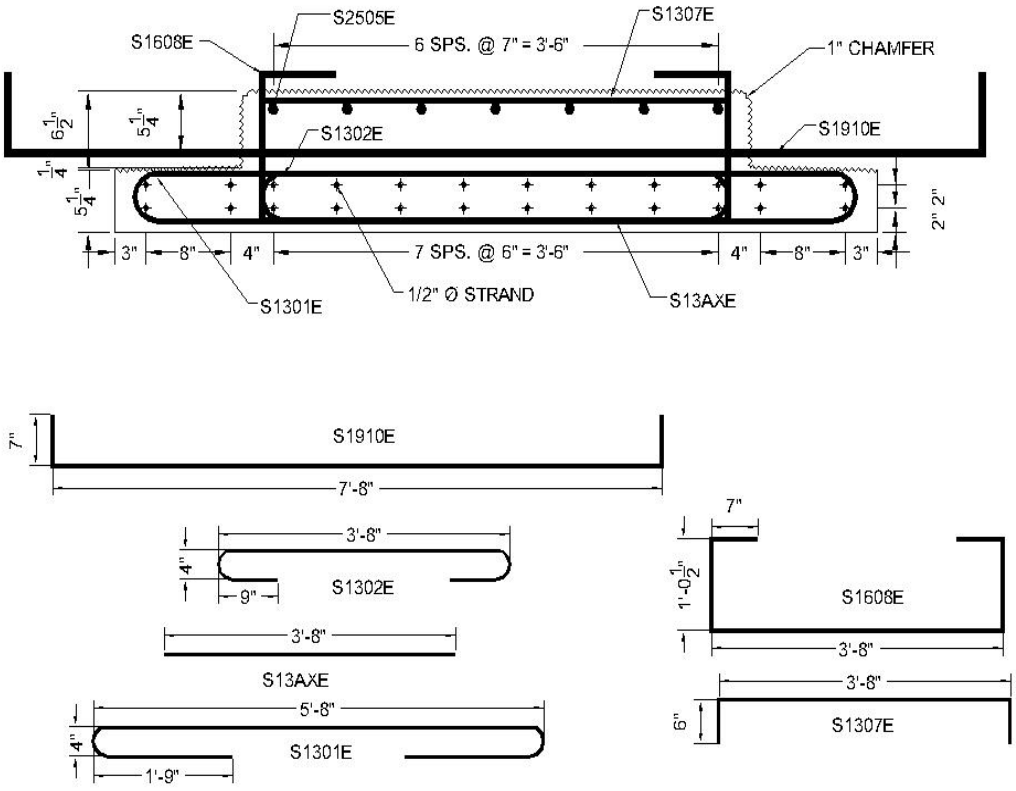

Figure 5.1.17: Cross section and individual reinforcement details for east end of precast beam 2S

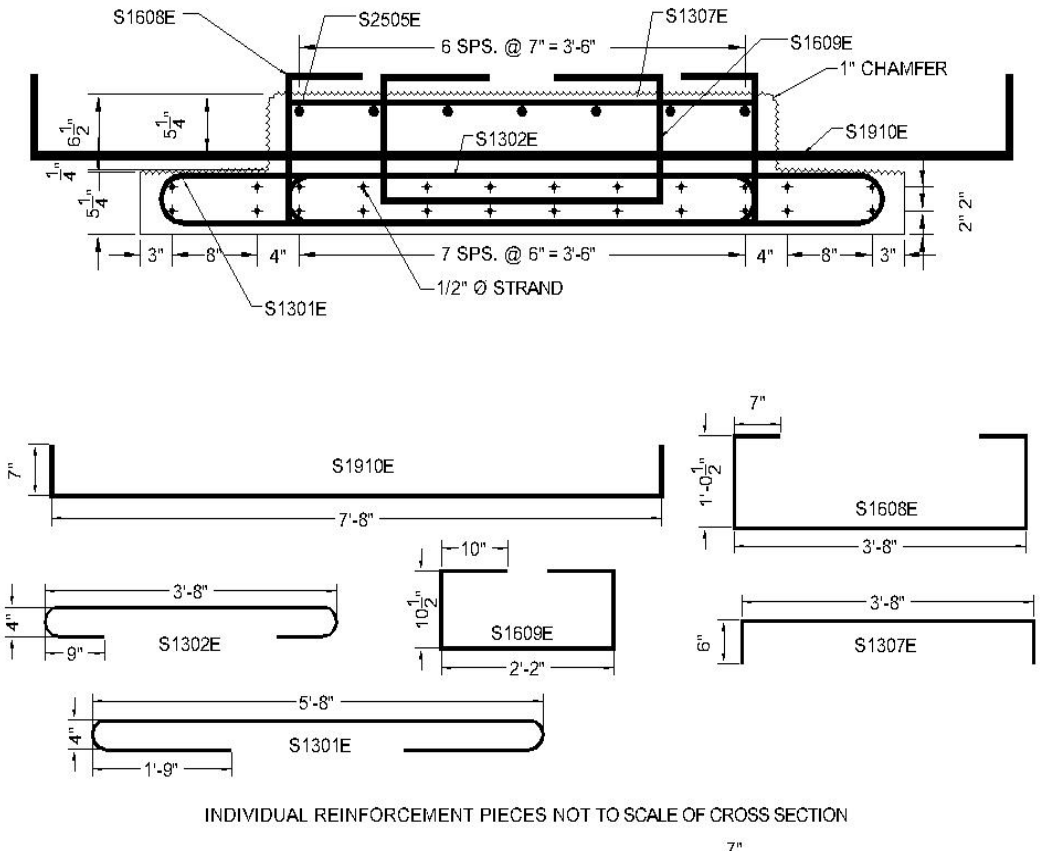

Figure 5.1.18: Cross section and individual reinforcement details for west end of precast beam 2S

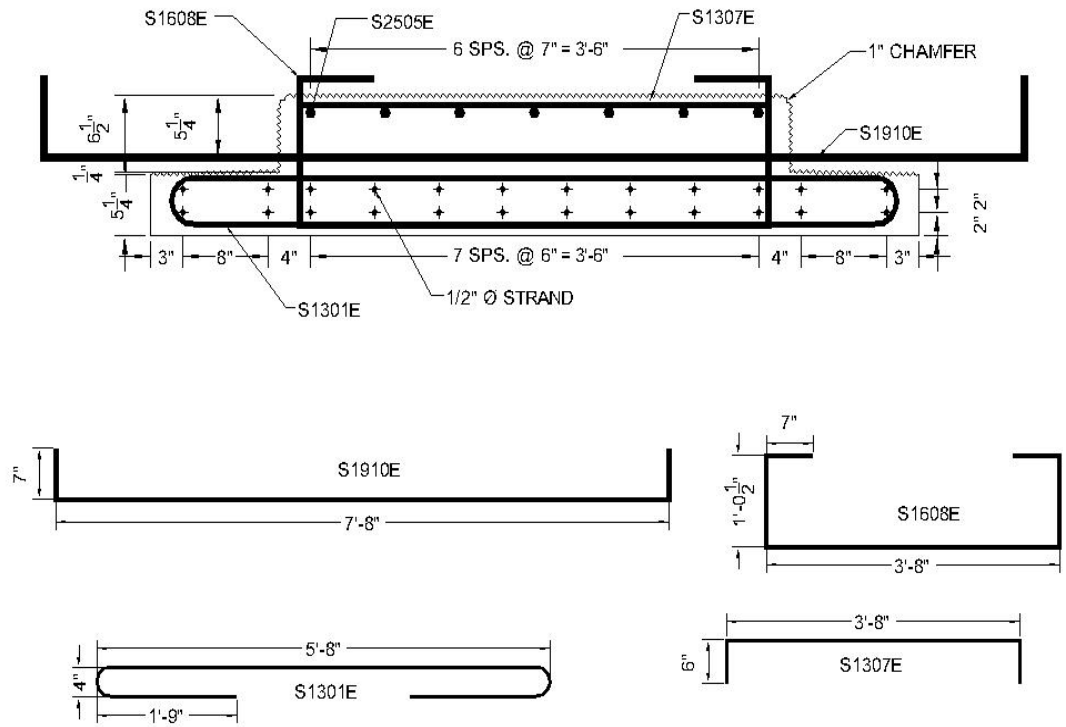

Figure 5.1.19: Cross section and individual reinforcement details at midspan of precast beam 2S

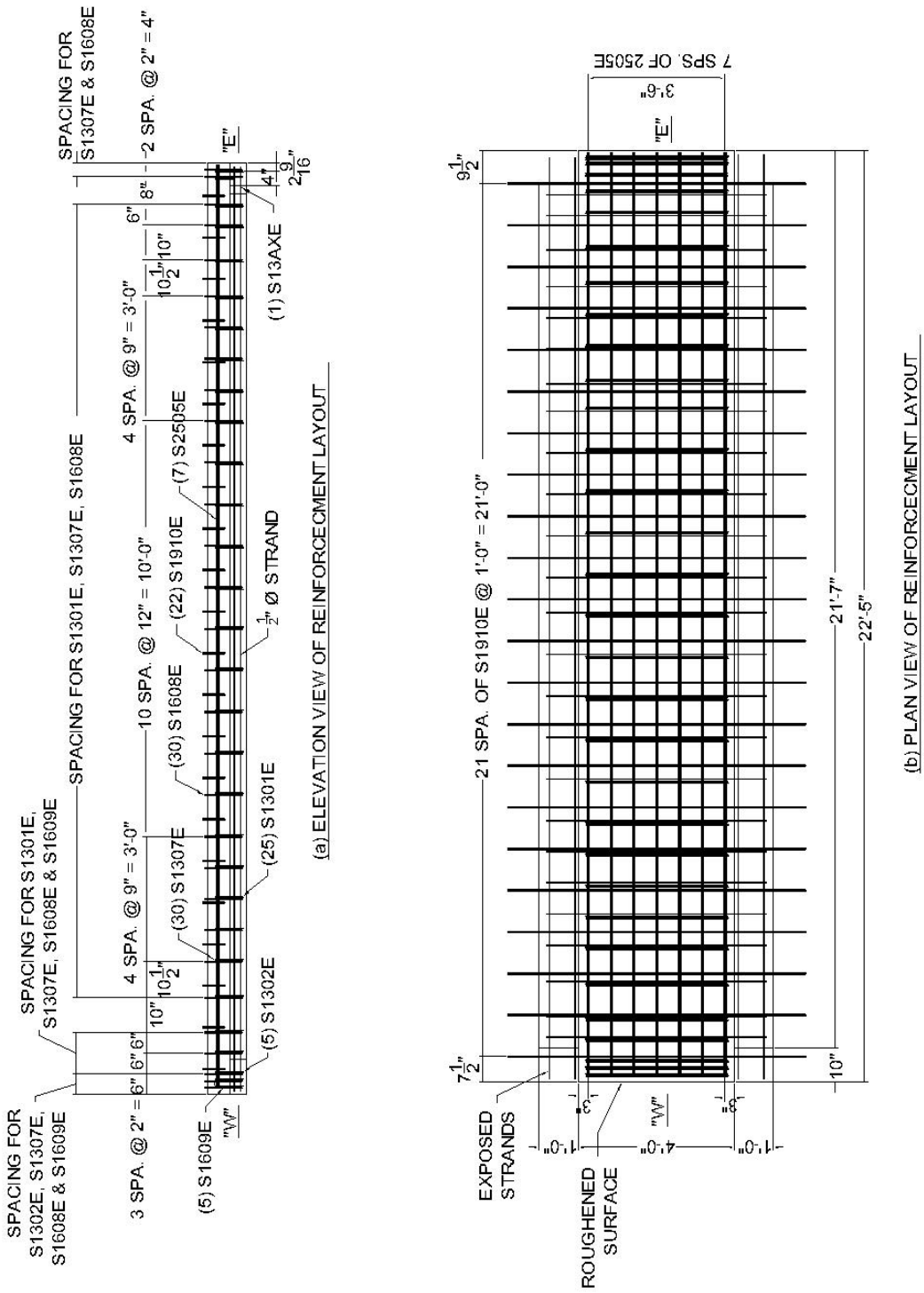

Figure 5.1.20: Elevation and plan views of reinforcement layout for precast beam 2S

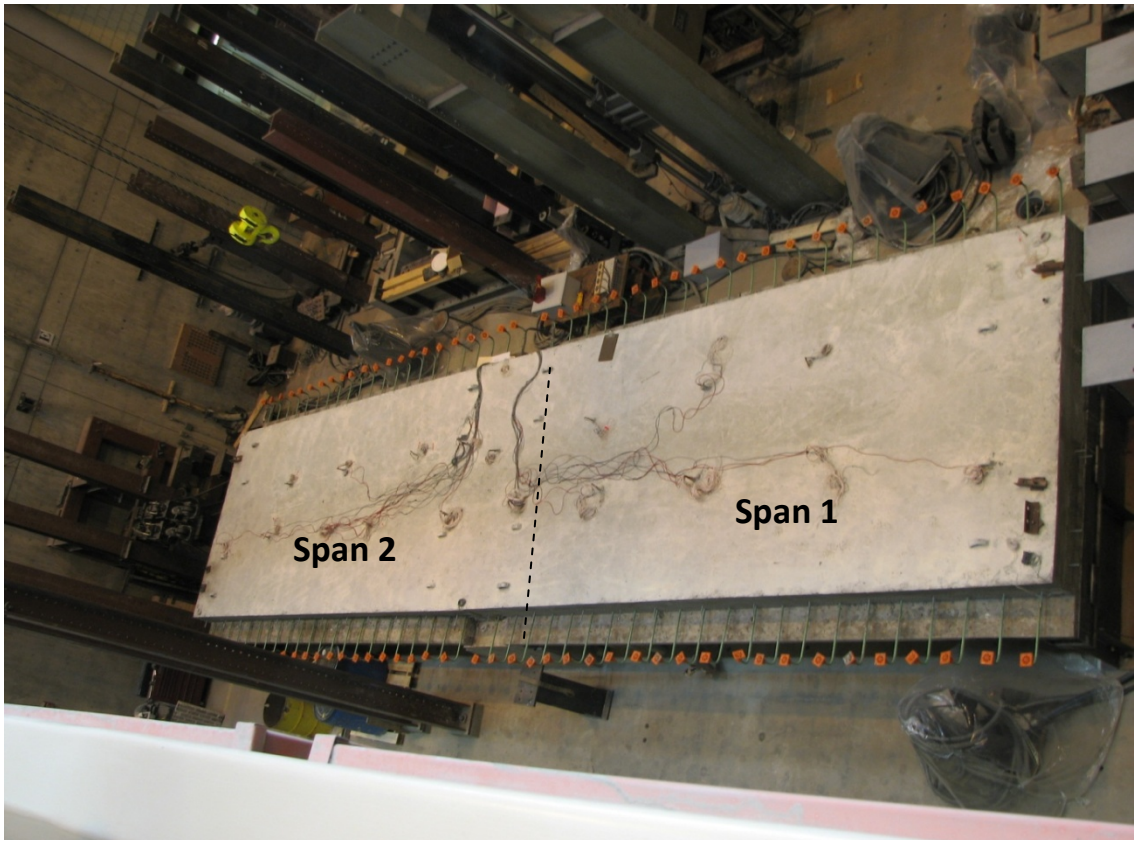

Figure 5.1.21: Photograph of the Concept 1 laboratory bridge shortly after completion of the continuity pour

The reinforcement ratios for each span were not identical because of the reduction in the flange thickness in Span 1. The reinforcement ratio for transverse load transfer and crack control in Span 2 (which was similar to the Center City Bridge) was 0.0029 and 0.0147, respectively; whereas the reinforcement ratio for transverse load transfer and crack control in Span 1 was 0.0024 and 0.0110, respectively.

The center pier supporting the Concept 1 laboratory bridge was designed to replicate the piers present in the Center City Bridge (see Figure 4.6.1 for the bearing and pier detail in the Center City Bridge). The pier cap extended 42 in. in the direction corresponding to the longitudinal direction of the bridge, identified hereafter as the width of the pier. A 6 in. wide by 1/2 in. thick elastomeric bearing pad provided the primary bearing at the pier, with the bearing pad occupying the area between 4 and 10 in. from the ends of the precast beams. The remaining area between the pier cap and precast beams was filled with 1/2 in. polystyrene foam, which was selected to

prevent the egress of CIP concrete during the closure pour, while also remaining relatively crushable to allow the elastomeric bearing pad to act as the primary means of bearing.

The supports at the free ends of the bridge were constructed with a 12 in. wide HSS tube section resting on a wide flange section. A 1/2 in. thick by 12 in. wide elastomeric bearing pad was provided between the HSS tube and precast inverted-T. The end support detail was selected to provide little rotational restraint, and therefore simulate a roller connection. Lateral stability at the end supports was provided via bracing between the wide flange sections and the strong floor, as shown in Figure 5.1.22.

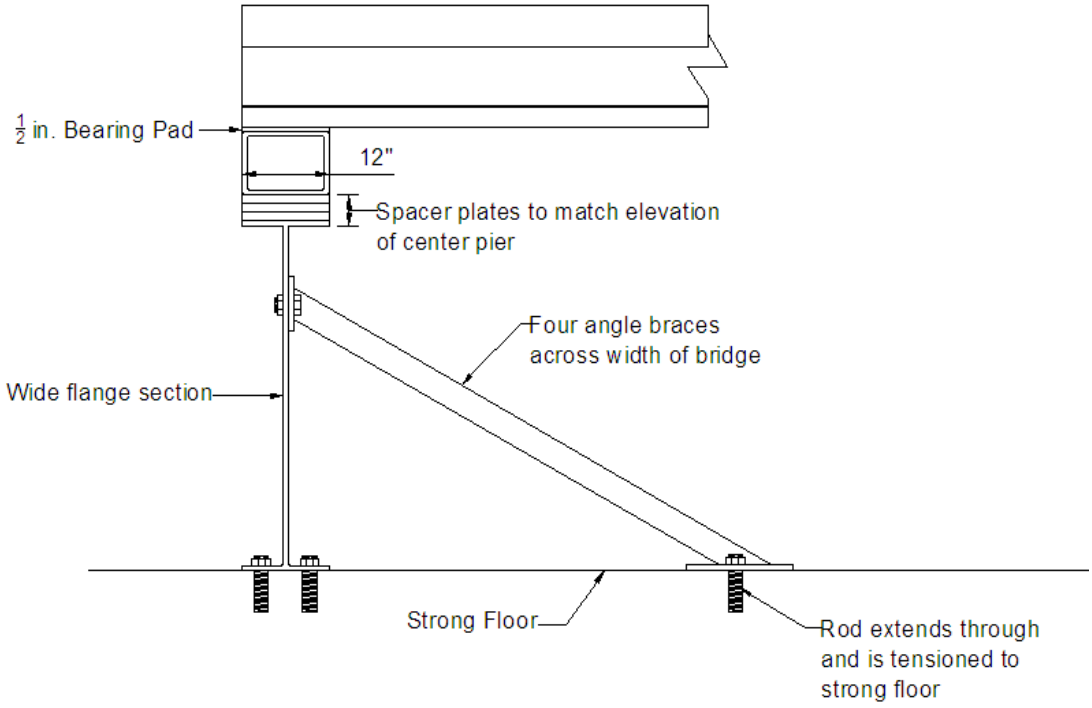

Figure 5.1.22: Support and bearing detail of the end supports of the laboratory bridge specimens

5.1.2. Concept 2 Laboratory Bridge

The Concept 2 laboratory bridge was developed to address issues that remained unanswered at the conclusion of the Concept 1 tests. A statically determinate simply-supported bridge specimen was selected to provide a direct means of determining the applied moment during testing. The symmetrical nature of the simply-supported structure enabled investigation of two unique design parameters in each half span of the bridge. Table 5.1.2 highlights the variations in parameters in the Concept 2 laboratory bridge relative to those of Span 1 of the Concept 1 laboratory bridge.

Both half spans of the Concept 2 laboratory bridge were constructed with No. 4 transverse bars spaced at 18 in. protruding from the precast sections. The west half span of the bridge was constructed using traditional hooked bars as defined by AASHTO (2010) Article 5.10.2.1. The east half span of the Concept 2 laboratory bridge was constructed with threaded transverse bars without a hook return or headed feature, as shown in Figure 5.1.23, extending approximately 22.5 in. from the face of the web, which left approximately 1.5 in. clear to the face of the adjacent precast web. The use of hooked threaded bars were deemed impractical due to the difficulty in ensuring the hooked portion of the bar would be oriented vertically upward when the threaded portion of the bar was fully tightened into the anchor; positional threaded inserts that could resolve this issue would be costly. Headed bars were considered as an alternative to hooked bars, but the clearance required around the head would require the transverse bars to be raised higher in the section to accommodate the required clearance of the head to the horizontal precast flange face. As a consequence, it was decided to use straight transverse bars threaded into the anchors embedded in the precast sections. The development length of the straight bars was calculated to be 28.5 in. using ACI 318-08 Section 12.2.2, with an assumed concrete compressive strength of 4,000 psi and ψ_t=1.2, suggesting that approximately 80 percent of the yield strength of the straight bars would be developed over the distance between the free end of the bar and the vertical precast web.

The transverse reinforcement (both the hooked and straight bars) in the trough region provided the primary mechanism for transverse load transfer between adjacent precast panels. For this reason, it is imperative that the transverse reinforcement be continuous through the precast member. In the case of the mechanically anchored reinforcement, continuity was provided using straight bars embedded in the web region of each precast member, which were threaded half way into the mechanical anchor at the interior longitudinal precast joint, as shown in Figure 5.1.24; a vertical hook was maintained over the outside precast flange to assist with the location of the internal reinforcement during the study. When mechanical anchors are used in a real world application, the embedded continuous reinforcement could be connected to mechanical anchors at the vertical web faces on both sides of the precast member. Note that in Figure 5.1.24 the transverse reinforcement to be mechanically anchored across the joint region is not shown for clarity.

Table 5.1.2: Comparison of design parameters between Span 1 of Concept 1 and Concept 2 laboratory bridge specimen

Span 1 of Concept 1 Laboratory Bridge	**Concept 2 Laboratory Bridge**
No 6 transverse hooks spaced at 12 in.	No. 4 transverse bars spaced at 18 in.
No. 5 cage spaced at 12 in., in line with hooks	No. 3 cage spaced at 18 in., offset 9 in. from bars
2 1/2 in. clear from face of flange to bottom of transverse hook	1 in. clear from face of flange to bottom of transverse bar
All transverse bars embedded into web and terminated with a standard hook	East half span included threaded straight bars West half span included embedded hooked bars
No. 5 stirrups at 24 in. for horizontal shear reinforcement	No reinforcement for horizontal shear transfer

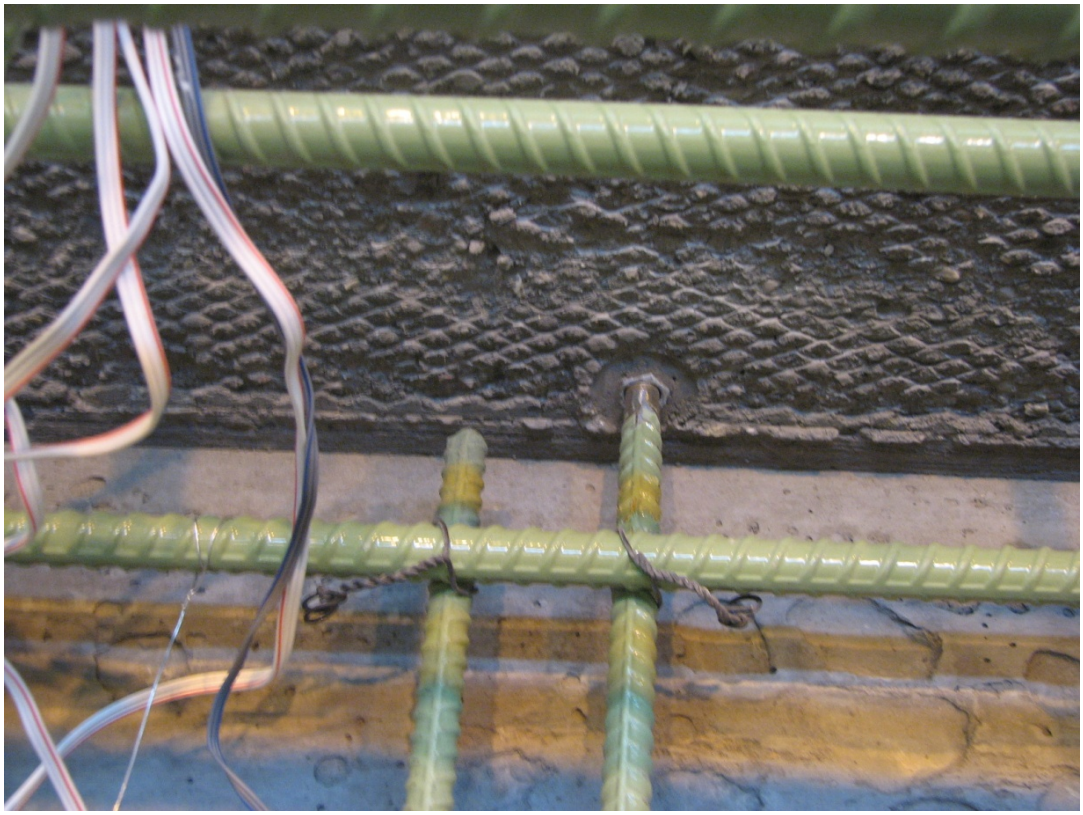

Figure 5.1.23: Threaded connection and adjacent termination detail of straight bars in east half span of the Concept 2 laboratory bridge specimen

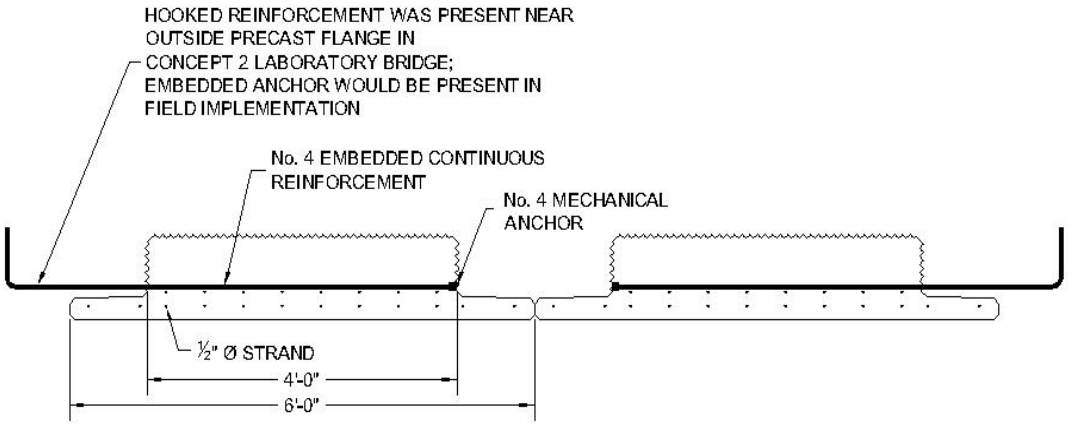

Figure 5.1.24: Conceptual section illustrating continuous nature of embedded reinforcement utilized in conjunction with mechanical anchors when threaded transverse reinforcement is present; figure shown represents configuration in east half span of the Concept 2 laboratory bridge specimen (transverse reinforcement in joint region to be mechanically anchored to reinforcement in precast web is not shown)

As for the Concept 1 specimen, a supplementary cage was used in the joint region to control potential reflective cracks that could originate over the longitudinal joint between the adjacent precast flanges. The reinforcement cage in the Concept 2 laboratory bridge was reduced in size to No. 3 stirrups and increased in spacing to 18 in. in comparison with that of the Concept 1 laboratory bridge. The cage reinforcement was offset from the protruding transverse bars by 9 in. to ensure that the maximum spacing of the transverse reinforcement across the joint did not exceed 9 in. The reinforcement ratio of the transverse section for crack control was 0.0031. The specimen was intended to provide a lower bound design based on the ACI (318-08) and AASHTO (2010) specifications for potential crack control reinforcement, specifically satisfying a spacing limit of 18 in. and a minimum reinforcement ratio of 0.0018. The reinforcement ratio of the section for transverse load transfer was 0.0007. The reinforcement ratios for both the Concept 1 and Concept 2 laboratory bridges are summarized in Table 5.1.3.

Table 5.1.3: Transverse load transfer and crack control reinforcement ratios for the Concept 1 and Concept 2 large-scale laboratory bridge specimens

Specimen description	Reinforcement ratio for crack control	Reinforcement ratio for transverse load transfer
Concept 1, Span 1	0.0110	0.0024
Concept 1, Span 2	0.0147	0.0029
Concept 2	0.0031	0.0007

Another modification implemented in the Concept 2 laboratory bridge included the removal of all horizontal shear reinforcement, leaving only the roughened surface of the precast web to provide all necessary horizontal shear transfer. This modification was selected to address the required minimum horizontal shear reinforcement in the AASHTO (2010) LRFD specification, as the literature suggested that requirement was overly conservative (see review of work by Naito et al. (2006) in Section 2.3). Furthermore, the large horizontal interface between the top of the precast webs and the CIP deck provided a horizontal shear interface area that was considerably larger than is generally provided by traditional girder bridges, where the width of the top flange is relatively narrow. The sectional capacity of the Concept 2 laboratory bridge was calculated using the measured concrete compressive strength of 5,800 psi, which resulted in the determination of the largest expected internal compression and tension forces for the specimen, which were equal to approximately 2450 kips. Using the global force equilibrium method for calculating the horizontal shear demand, the total change in compression force was divided by the area over which that change occurs. Because the Concept 2 laboratory bridge was simply supported, the compression force was assumed to be a maximum of 2450 kips at midspan, and 0 kips at the center of bearing. The shear area was therefore calculated as the product of half of the center to center of bearing (256 in. / 2 = 128 in.) multiplied by the full width of the web in compression, or 10 ft.; the area over the longitudinal trough region was included in the width of the shear area, as this area was expected to provide horizontal shear resistance as effectively as the horizontal precast-CIP interface [Note that CIP was not placed over the exterior flanges, only in the trough region between the two adjacent precast sections.]. Using this method, the horizontal shear demand at the predicted ultimate capacity of the Concept 2 laboratory bridge was calculated to be approximately 160 psi. The cohesion factor for a horizontal shear interface that is clean and intentionally roughened provided in Article 5.8.4.3 of the AASHTO LRFD specification (2010) was 240 psi, suggesting that the largest horizontal shear stress that was expected to be developed in the Concept 2 laboratory bridge was unlikely to result in loss of composite action.

A simplified plan view of the Concept 2 laboratory bridge specimen, including support locations and relevant dimensions is included in Figure 5.1.25; the transverse reinforcement near the longitudinal precast joint region is not shown for clarity. The Concept 2 laboratory bridge was designed with the same overall dimensions as a single span in the Concept 1 laboratory bridge. Therefore, the Concept 2 laboratory bridge was placed to the east of the center pier, with the west bearing being located on the concrete pier, and the east bearing located on the 12 in. HSS tube. Based on the work outlined in Section 4.5, no bursting reinforcement was necessary in the precast elements utilized in the Concept 2 specimen. The reinforcement present in each cross section (i.e., east, west, and midspan), as well as elevation and layout views documenting the location of reinforcement along the length of each beam is shown in Figures 5.1.26 through 5.1.32. A photograph of the Concept 2 laboratory bridge specimen is shown in Figure 5.1.33.

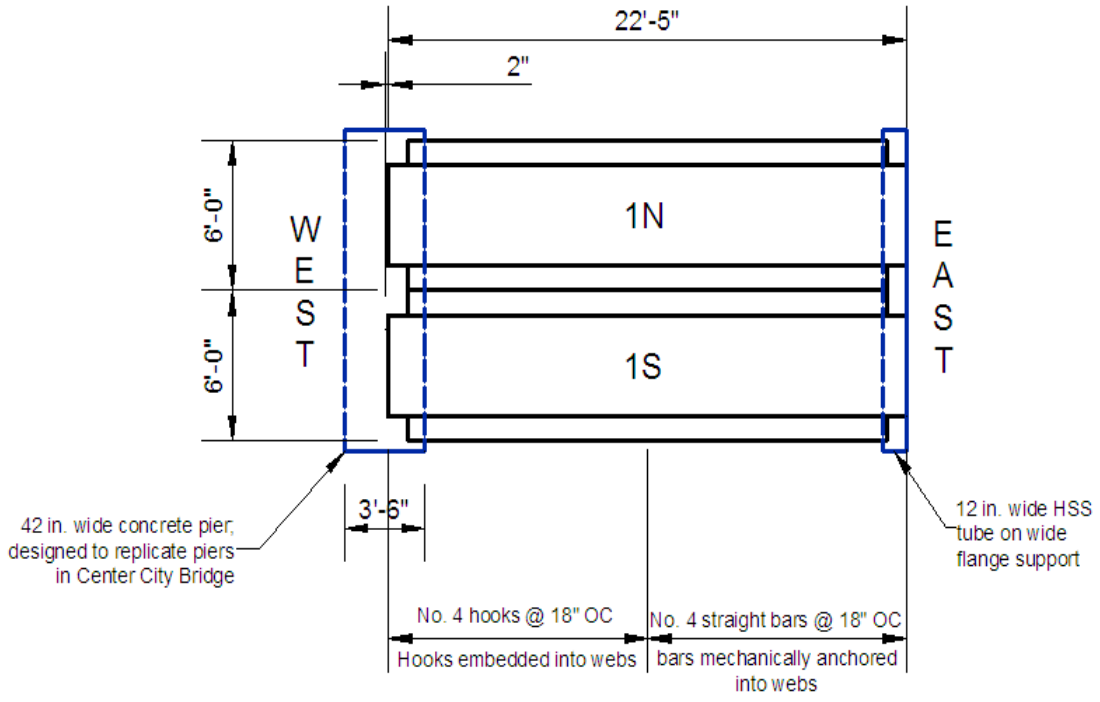

Figure 5.1.25: Plan view of the Concept 2 laboratory bridge specimen, including support locations and relevant dimensions. Transverse reinforcement near longitudinal precast joint is not included for clarity

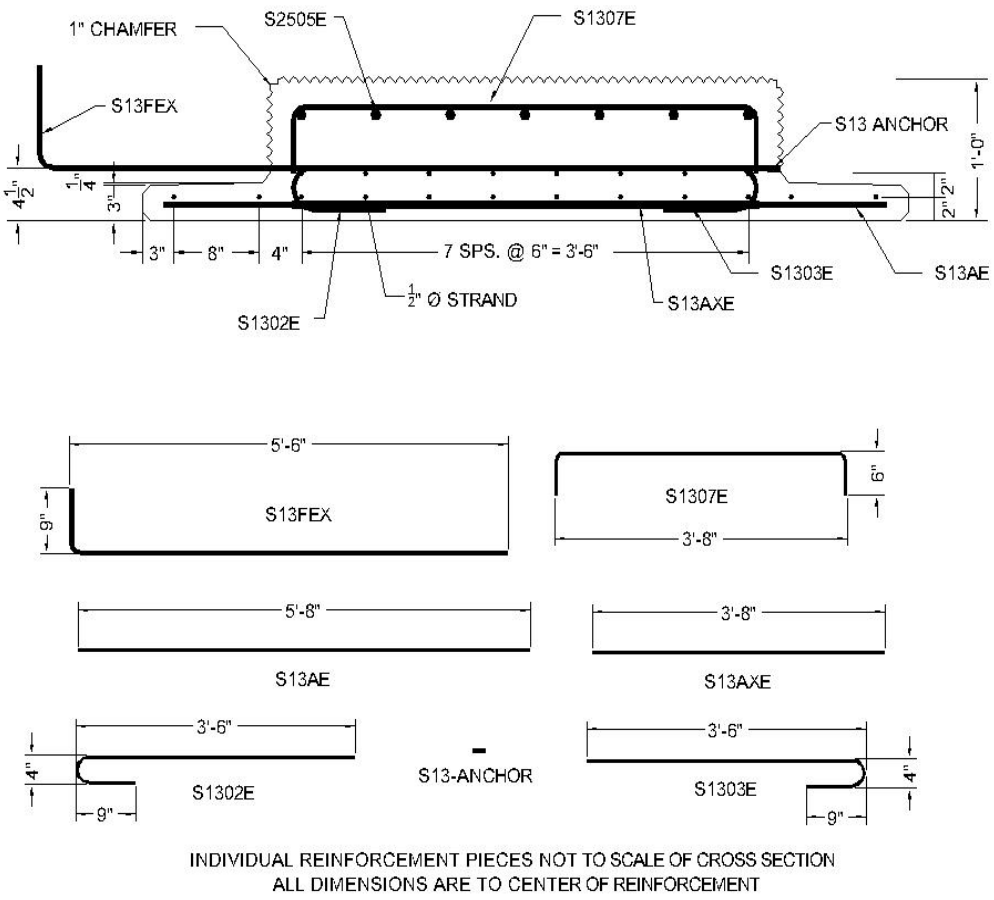

Figure 5.1.26: Cross section and individual reinforcement details for the east end of the precast beam 1N in the Concept 2 laboratory bridge specimen

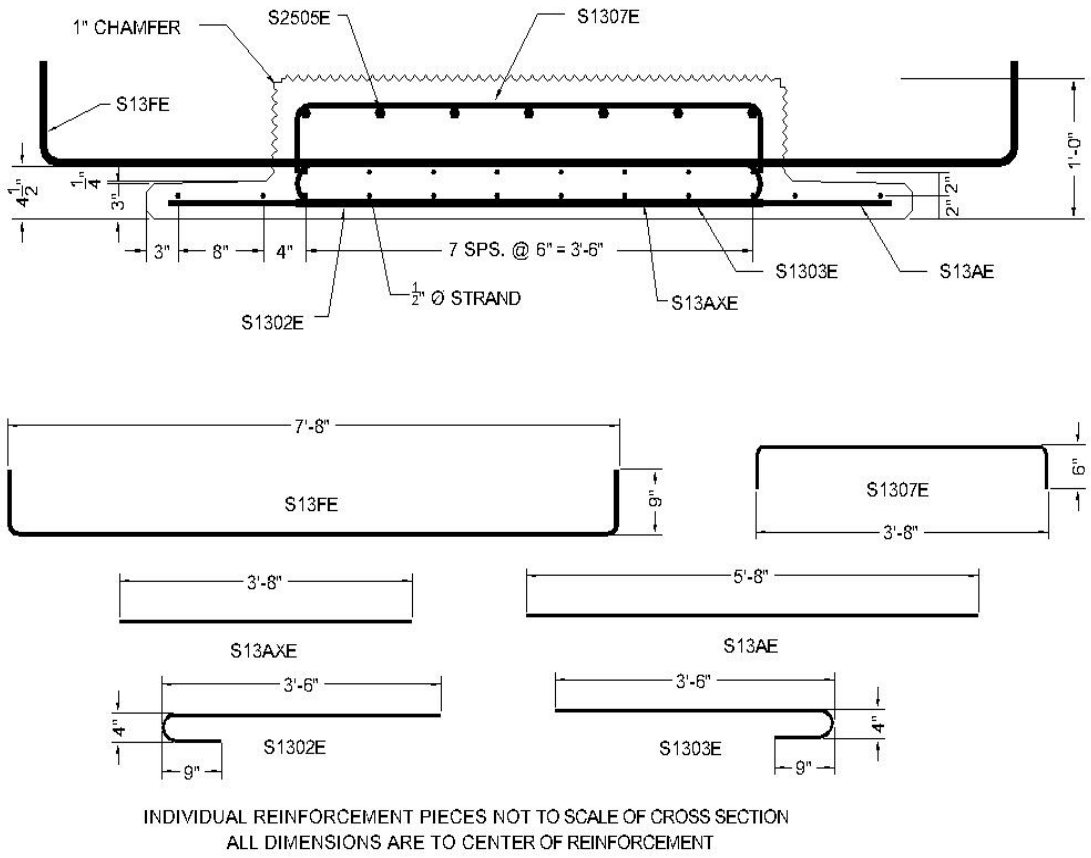

Figure 5.1.27: Cross section and individual reinforcement details for the west end of the precast beams 1N and 1S in the Concept 2 laboratory bridge specimen

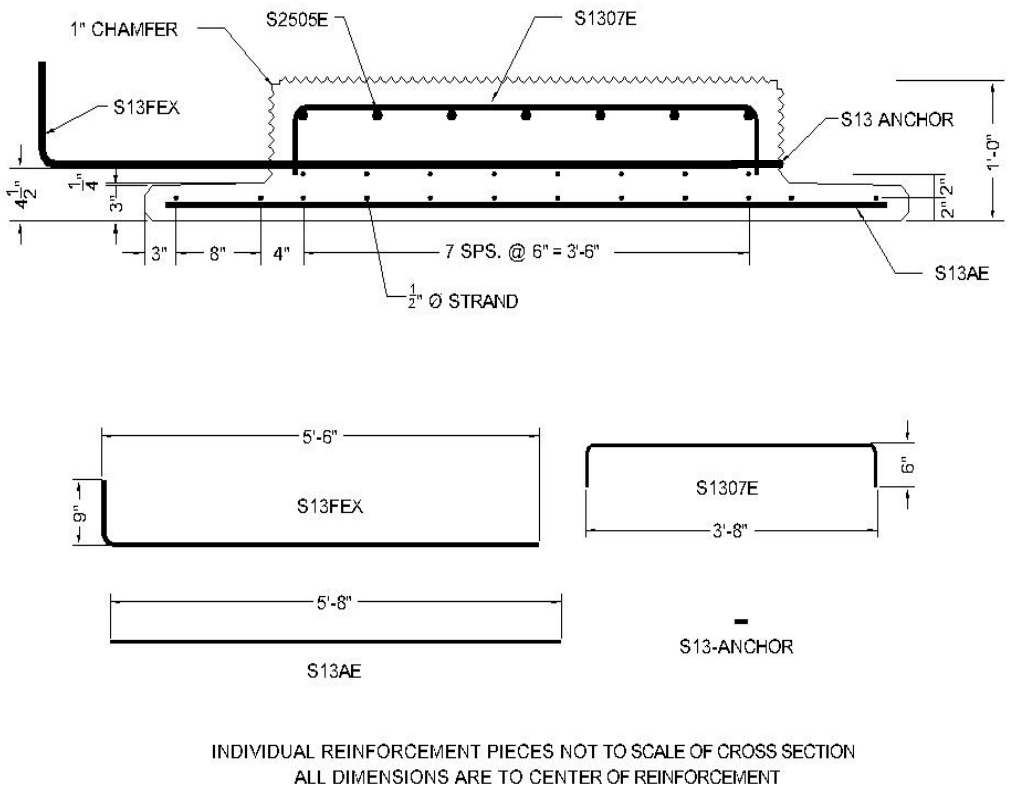

Figure 5.1.28: Cross section and individual reinforcement details at midspan of precast beam 1N in the Concept 2 laboratory bridge specimen

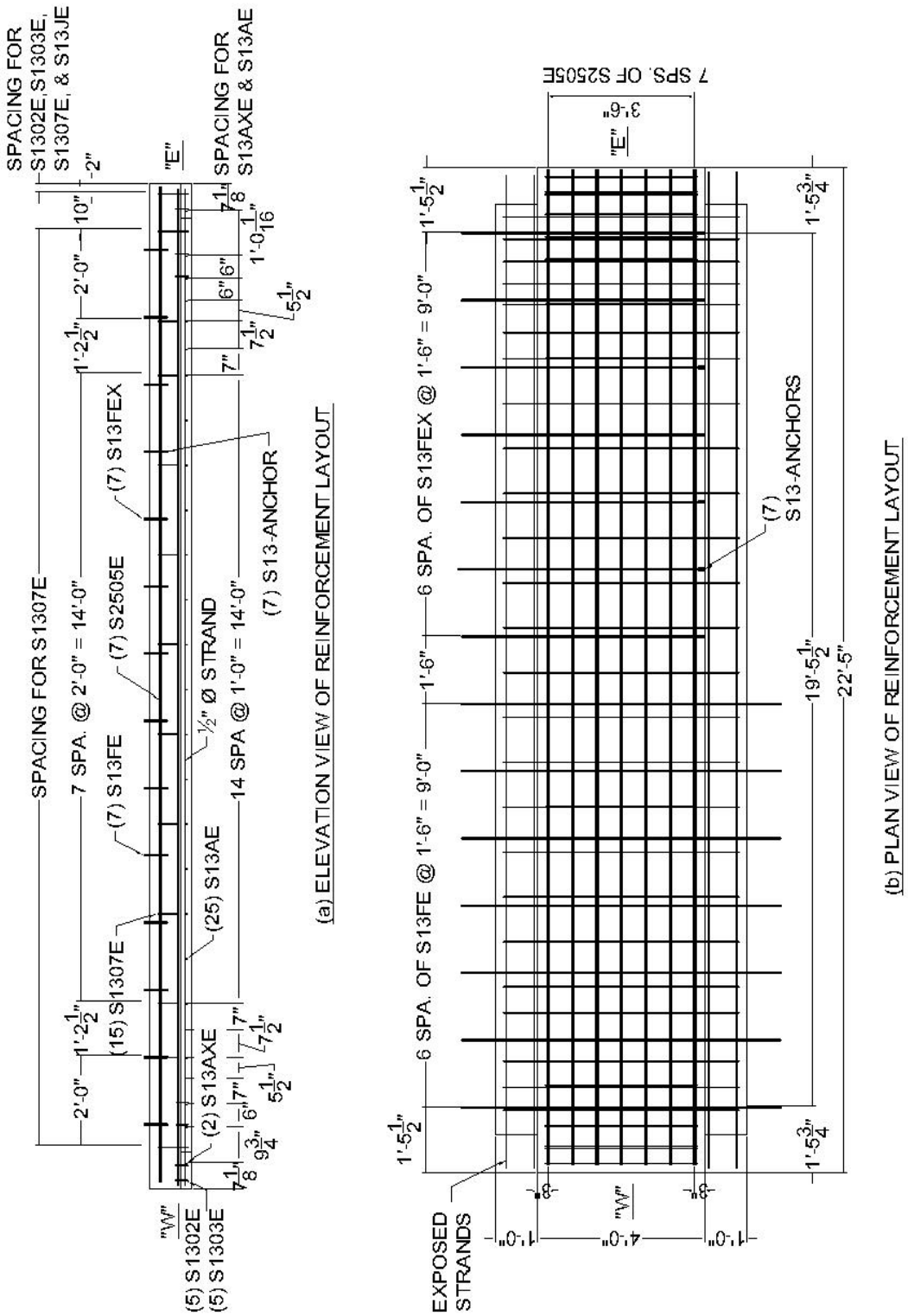

Figure 5.1.29: Elevation and plan views of the reinforcement layout for precast beam 1N in the Concept 2 laboratory bridge specimen

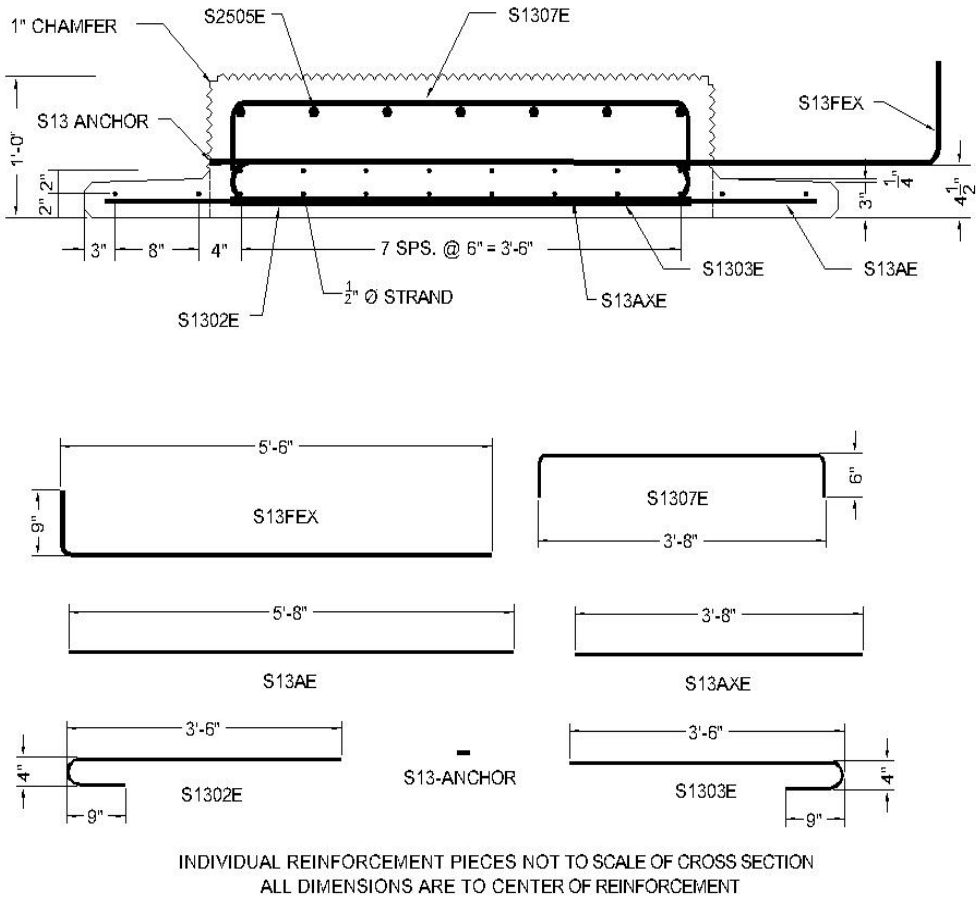

Figure 5.1.30: Cross section and individual reinforcement details for the east end of the precast beam 1S in the Concept 2 laboratory bridge specimen

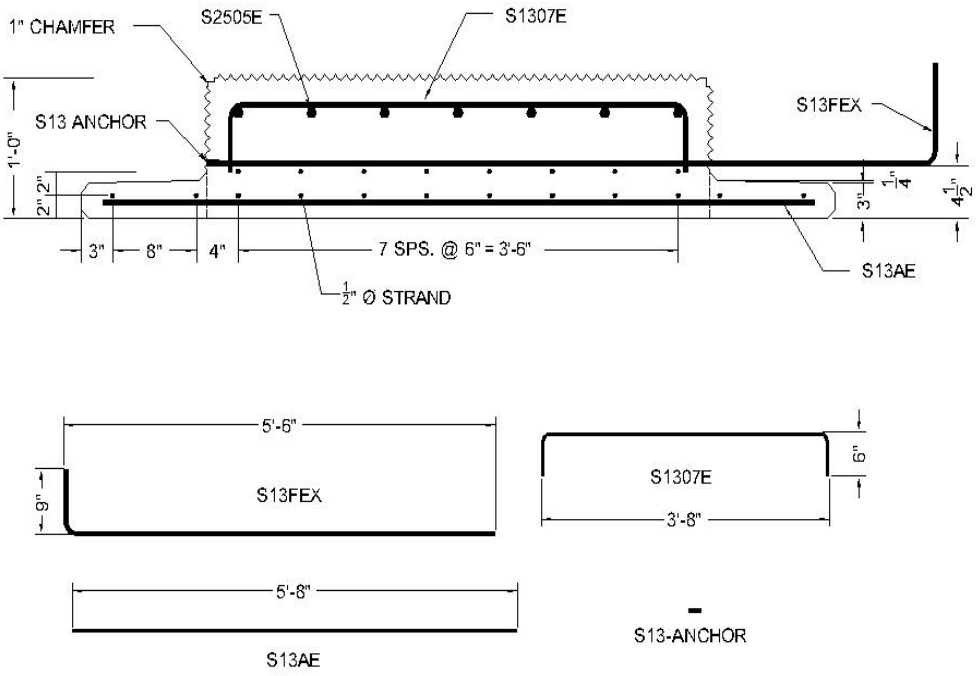

Figure 5.1.31: Cross section and individual reinforcement details at midspan of precast beam 1S in the Concept 2 laboratory bridge specimen

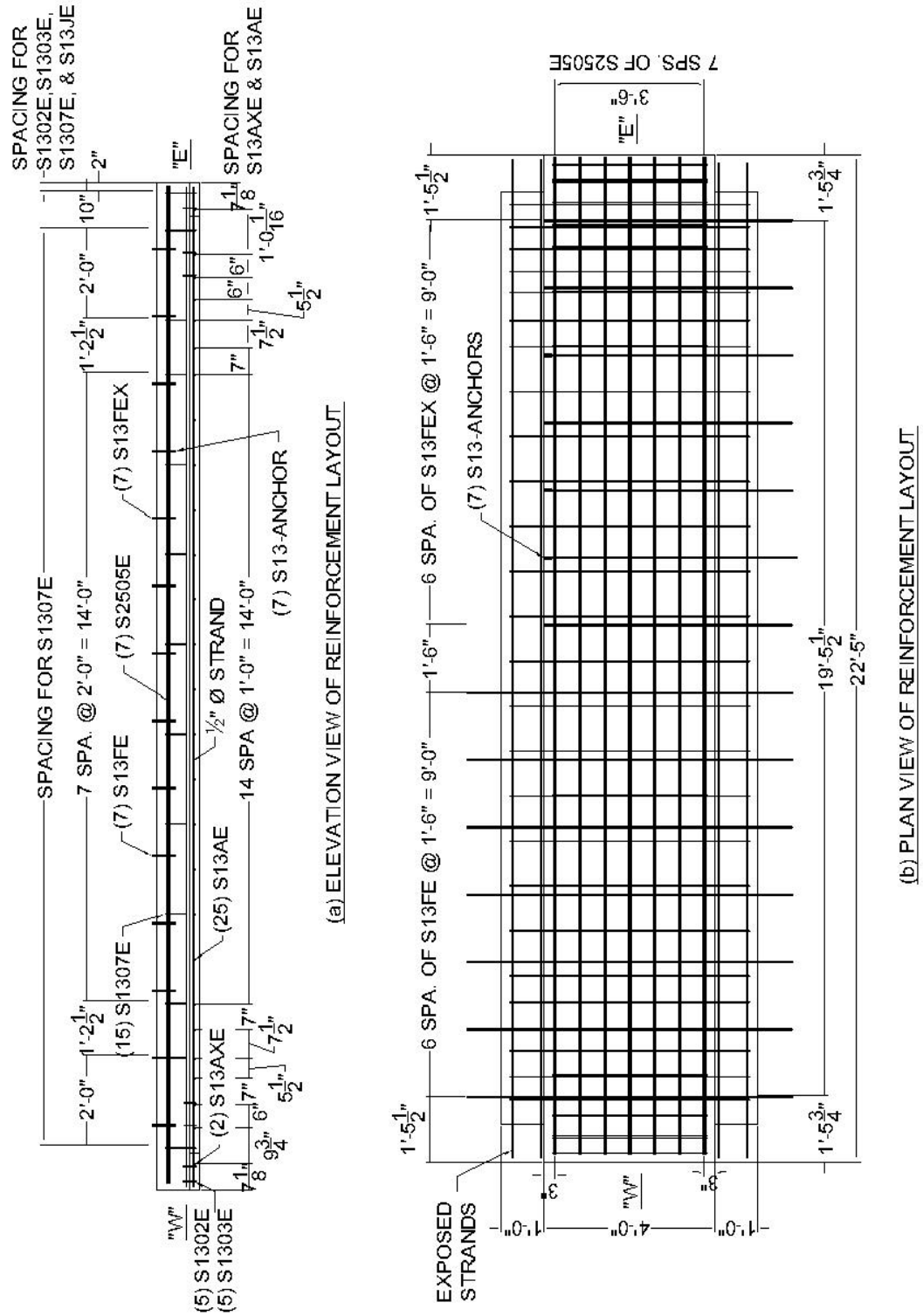

Figure 5.1.32: Elevation and plan views of the reinforcement layout for precast beam 1S in the Concept 2 laboratory bridge specimen

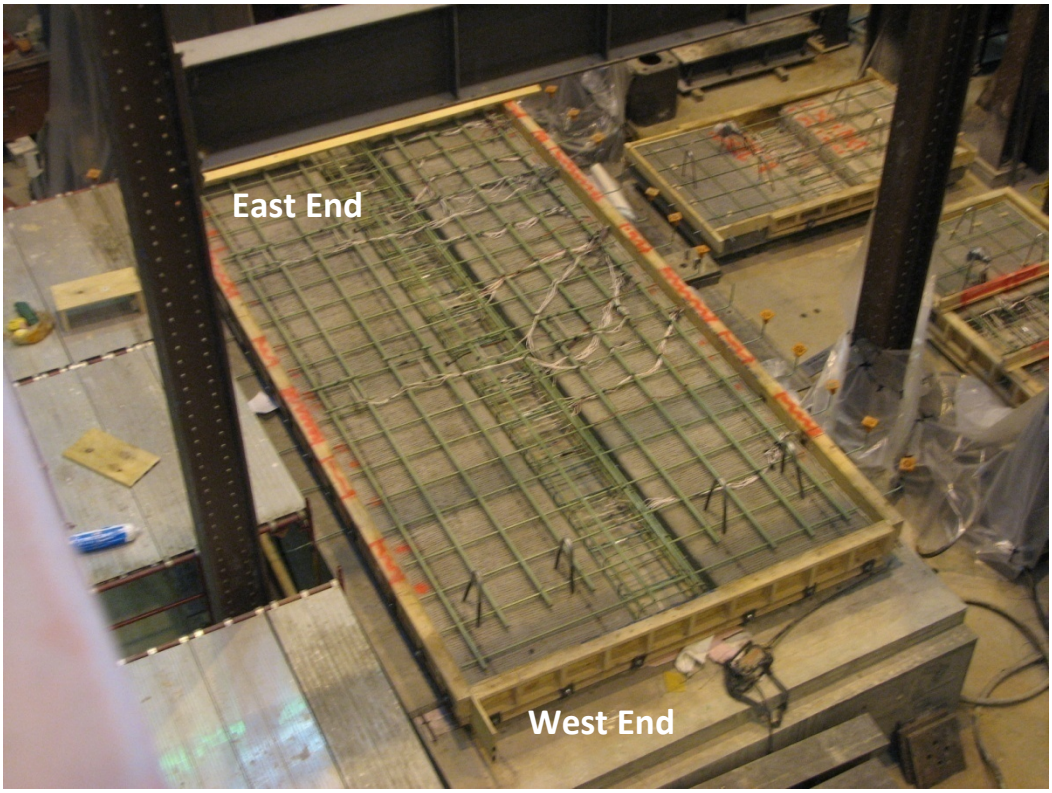

Figure 5.1.33: Photograph of the Concept 2 laboratory bridge specimen prior to placement of CIP concrete

The Concept 2 laboratory bridge specimen occupied the same space in the University of Minnesota Structures Laboratory as Span 2 of the Concept 1 laboratory bridge specimen. The west end of the Concept 2 laboratory bridge specimen was located a distance of 2 in. from the center of the concrete pier, with the east end of the specimen bearing completely on the 12 in. HSS tube/wide flange support. See Figure 4.6.1 and 5igure 5.1.22 for details on the concrete and steel supports, respectively.

5.1.3. Instrumentation of Concept 1 and Concept 2 Laboratory Bridge Specimens

The instrumentation schemes used in the Concept 1 and Concept 2 laboratory bridge specimens facilitated the monitoring of the transverse behavior and health of the joint region between precast panels. In addition, vertical sets of longitudinally oriented instrumentation were provided as a means of calculating the longitudinal curvature during load transfer and ultimate tests. The primary instrumentation type was concrete embedment resistive strain gages due to their relatively inexpensive cost, which allowed for an adequately dense instrumentation field. A small

number of longitudinally oriented concrete embedment VW strain gages were also used to allow for the measurement of prestress losses, as well as to provide an estimate of the absolute levels of strain in the section without the effects of gage drift. Transversely oriented concrete embedment VW and spot-weldable VW strain gages were also included to provide an estimate of the strain due to transverse shrinkage near the precast joint, as well as to provide an estimate of the absolute levels of transverse strain throughout the laboratory tests.

The instrumentation layout for the Concept 1 laboratory bridge specimen is shown in Figure 5.1.34 (Smith et al. 2008). Each span had a set of transversely oriented instruments at each end, each quarter point, and at midspan. At each section, five transversely oriented concrete embedment resistive gages were located near the precast flange equally dispersed between adjacent precast webs. Some cross sections had an additional ten transversely oriented concrete embedment resistive gages located above the precast web corners. The presence of the gages above the precast web is indicated by the longer transverse line extending over the webs in Figure 5.1.34. A representative cross-sectional view of the fully instrumented section is shown in Figure 5.1.35; the aspect ratio of the instrumentation has been modified for clarity. In addition, adjacent transverse gages overlapped (not shown in figure) to provide redundancy and a means to better refine the determination of crack locations by investigating whether a crack may have intersected a single gage or two adjacent gages. The nominal and measured gage locations in the Concept 1 laboratory bridge are given in Appendix C.

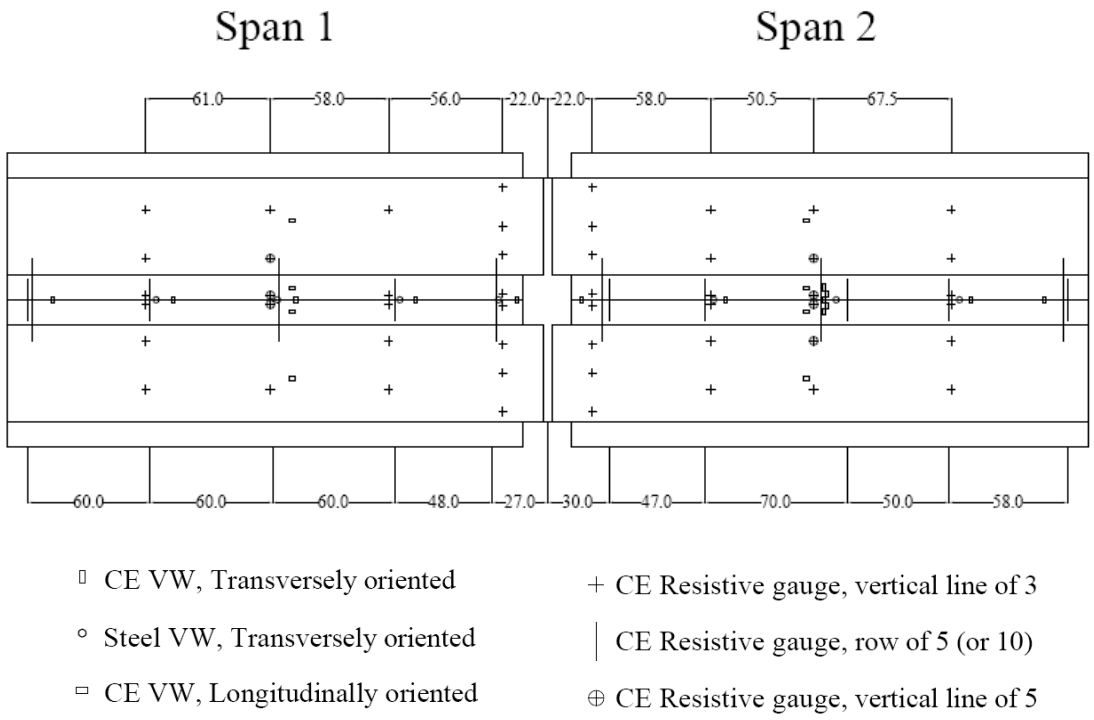

Figure 5.1.34: Instrumentation layout for Concept 1 laboratory bridge specimen (Smith et al. 2008)

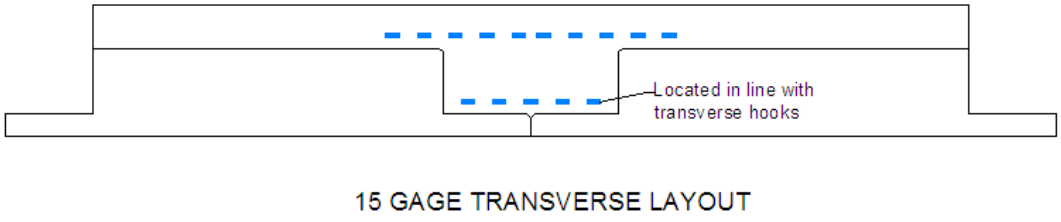

Figure 5.1.35: Typical instrumentation layout near precast joint in the Concept 1 laboratory bridge specimen

The instrumentation layout developed for the Concept 2 laboratory bridge closely followed the original instrumentation plan for the Concept 1 laboratory bridge. Additional transversely oriented instruments were added at the eighth points to allow for increased refinement in detection of the extent of longitudinal reflective cracking. Similarly, an additional layer of transversely oriented concrete embedment strain gages was added through the depth of the cross

section to improve the accuracy of the measurement of the depth of the crack in the section. The number of gages across the width of the joint region was reduced in response to the localized behavior of the crack observed in the Concept 1 laboratory bridge near the precast joint. Furthermore, fewer vertical sets of instruments were selected for longitudinal instrumentation, while five gages were included in each vertical set to improve the accuracy of the curvature calculation, especially in the case of faulty or broken instrumentation due to construction. The instrumentation layout for the Concept 2 laboratory bridge and the standard cross sections are shown in Figure 5.1.36 and Figure 5.1.37, respectively. The nominal and measured gage locations for the Concept 2 laboratory bridge are given in Appendix D.

The origin and positive *x* and *y* ordinate directions for the placement of the instrumentation for the Concept 1 and Concept 2 laboratory bridges is shown in Figure 5.1.38. The origin was located at the center of the concrete pier for both bridges. The positive *x* ordinate was directed towards the east wall of the lab, with the positive *y* ordinate towards the north. The vertical ordinate, *z*, was measured from the bottom of the precast sections.

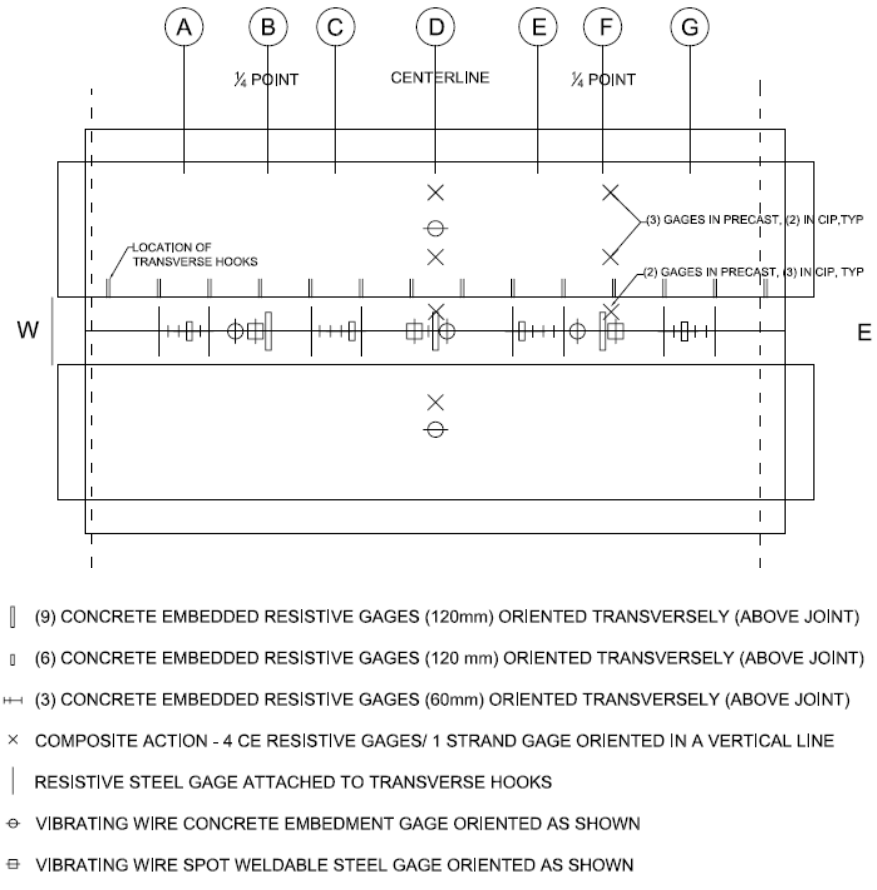

Figure 5.1.36: Instrumentation layout for the Concept 2 laboratory bridge specimen

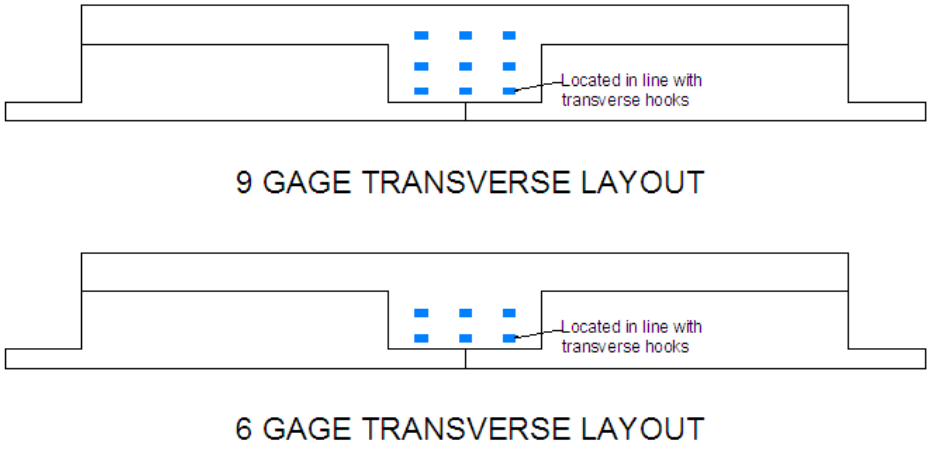

Figure 5.1.37: Typical 9 and 6 gage transverse instrumentation layout in Concept 2 laboratory bridge specimen

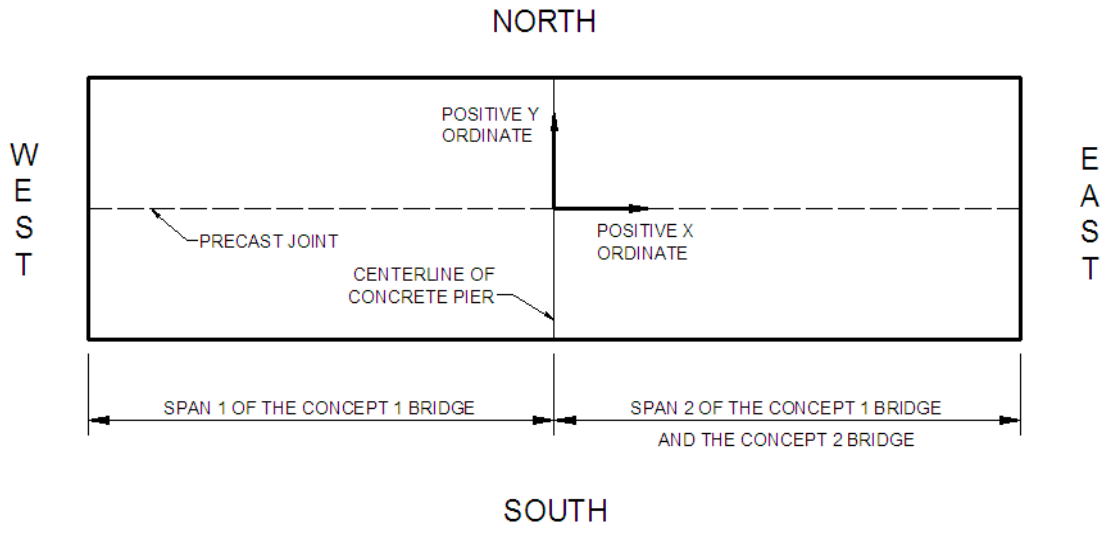

Figure 5.1.38: Location of origin and definition of positive x and y ordinates for instrumentation layout in the Concept 1 and Concept 2 laboratory bridge specimen

5.2. Construction of Laboratory Bridge Specimens and Material Properties

Fabrication of the precast panels for both bridges was completed at County Materials in Roberts, Wisconsin. The CIP concrete selected for the project was a standard Mn/DOT bridge design mix, designated as 3Y33H68, with a nominal compressive strength of 4,000 psi at 28 days. Due to the

interest in the effects of restraint moment on the system, the CIP concrete was placed on the Concept 1 laboratory bridge when the precast panels were at a young age of 7 days. Material testing was completed on the Concept 1 laboratory bridge to determine measured concrete compressive strengths, tensile strengths, and elastic modulus, and was tabulated by Smith et al. (2008), which is summarized in Table 5.2.1 and Table 5.2.2 for the CIP and precast concrete, respectively.

A more relaxed construction schedule was sufficient for the Concept 2 laboratory bridge because of the simply-supported design. The CIP concrete for the Concept 2 laboratory bridge was poured when the precast panels had reached an age of 83 days. The concrete 28-day CIP concrete compressive strength was measured to be 5750 psi, measured according to ASTM C36 *Test Method for Compressive Strength of Cylindrical Concrete Specimens* (ASTM C36, 2009). The CIP concrete tensile strength was measured to be 640 psi at an age of 28 days, measured according to ASTM C78 *Standard Test Method for Flexural Strength of Concrete (Using Simple Beam with Third-Point Loading)* (ASTM C78, 2009). The elastic modulus of the CIP concrete at an age of 28 days was measured to be 4,020 ksi, which was measured in accordance with ASTM C469 *Standard Test Method for Static Modulus of Elasticity and Poisson's ratio of Concrete in Compression* (ASTM C469, 2002). The measured material properties are summarized in Table 5.2.1 and Table 5.2.2 for the CIP and precast concrete, respectively.

Table 5.2.1: Measured CIP material properties at an age of 28 days

Specimen Description	Compressive Strength, f_c'	Modulus of Rupture, f_r	Elastic Modulus, E
Concept 1, Span 1	4160 psi	411 psi	3540 ksi
Concept 2, Span 2	4590 psi	457 psi	3780 ksi
Concept 2	5750 psi	640 psi	4020 ksi

Table 5.2.2: Measured precast concrete material properties for the Concept 1 and Concept 2 bridges

Specimen Description	Compressive Strength, f_c'	Modulus of Rupture, f_r	Elastic Modulus, E
Concept 1, both spans	12,900 psi	927 psi	6160 ksi
Concept 2	12,150 psi	783 psi	6029 ksi

The surfaces of the precast panels were not pre-wetted prior to the placement of the CIP concrete for either of the bridge specimens. No deleterious behavior appeared to result in casting the CIP on non-wetted precast surfaces; however, it is recommended in future applications of constructing PCSSS bridges in the field, that the precast surfaces be pre-wetted prior to casting the CIP. Both specimens were moist-cured for 8 days based on the ACI 308.1-98 *Standard Specification for Curing Concrete*.

The yield strength of the No. 4 hooked bars that provided transverse reinforcement continuity and crack control reinforcement above the longitudinal joint between the precast panels in the Concept 2 laboratory bridge specimen was found to be approximately 70 ksi through the testing of three representative samples.

5.3. Laboratory Testing Program and Results

An extensive laboratory testing program was developed for each specimen. The requirements for the testing plan included simulated fatigue loading, reproducing levels of strain in the precast joint region as observed in the Center City Bridge, as well as the introduction of reflective cracking, monitoring load transfer between precast panels in common spans, and loading to the ultimate capacity of the bridge specimens or the maximum capacity of the load frame. Because the tests used on the Concept 1 and Concept 2 laboratory bridges were similar, the testing plans and results of the laboratory tests are discussed below based on the controlling behavior, rather than by laboratory specimen. The results of the tests presented herein were all associated with the NCHRP 10-71 study. The previous tests conducted on the Concept 1 laboratory bridge specimen as part of a Mn/DOT study are summarized in Smith et al. (2008).

5.3.1. Simulated Traffic Loading

Good fatigue performance of any highway structure is essential to ensure stable behavior over extended periods of time. Traffic loading was simulated on the Concept 1 and 2 bridge specimens using a representative patch load of dimensions 10 by 20 in. oriented with the long direction perpendicular to the joint. Two million cycles of fatigue loading were completed on each span of the laboratory bridge specimens. The loading was placed at midspan of both spans of the Concept 1 laboratory bridge. The complete two million cycles of fatigue loading were completed on Span 2 prior to the implementation of fatigue loading on Span 1, while equal patch loads were cycled at the quarter points of the Concept 2 laboratory bridge using a spreader beam. The nominal patch

load used for all fatigue loading was 35 kips (i.e., Concept 1 laboratory bridge: 35 kips was applied to midspan; Concept 2 laboratory bridge: 35 kips was applied to each quarter point simultaneously); the development of the magnitude of the laboratory patch loading was discussed in Section 4.7.

The magnitude of the patch load was developed to replicate the magnitude of transverse stress at the precast flange-CIP interface in the laboratory specimen as was expected in a 30-30-30 ft. three-span continuous bridge with twice the AASHTO (2010) tandem design load applied. A magnitude of twice the AAHSTO tandem load was selected to account for the possibility of two truck wheel loads being located directly above a longitudinal joint and situated immediately adjacent to one another. As discussed in Section 4.7, the stress developed near the precast flange at midspan of the Concept 1 laboratory bridge and at the quarter points of the Concept 2 laboratory bridge were nearly identical, which accounts for the equal patch loads used in both specimens. Also note that the maximum moment developed due to a single patch load at midspan was equal to the maximum moment developed due to two equal patch loads placed at the quarter points.

During the fatigue and all associated patch loading, the load was cycled between 2 and 35 kips. A minimum load of 2 kips was maintained during all tests to prevent the actuator from "walking" during cycling. Steel angles were also adhered to the surface of the deck to help constrain the movement of the actuators during testing. Load distributed to the quarter points of the Concept 2 laboratory bridge using the spreader beam was cycled between 4 and 70 kips.

As discussed in Section 3.2 reflective cracking was observed in two of the three instrumented joints in the Center City Bridge via transversely oriented concrete embedment VW strain gages located at midspan of the center span. Furthermore, cracking in the field bridge was observed to occur during the first spring after construction was completed, revealing the potential for reflective cracking to be present during the majority of the service life for the precast composite slab span system (PCSSS) bridge. In an effort to investigate the fatigue performance of the PCSSS both with and without the presence of reflective cracking, the fatigue study for each specimen was conducted in two parts. As mentioned above, the fatigue study for each span of the Concept 1 laboratory Bridge (Span 2 first, followed by Span 1) was conducted in series; followed by the tests of the Concept 2 laboratory bridge after completion of the Concept 1 laboratory bridge tests. The subsequent discussion of the fatigue testing is relevant to each span separately.

The first portion of fatigue loading consisted of the completion of one million cycles of fatigue loading on the virgin laboratory specimens, with no reflective cracking observed prior to the

initiation of fatigue loading. At the conclusion of each 100,000 cycles, fatigue loading was suspended to allow for a quasi-static 35 kip patch load to be applied to the section at the same location as the fatigue patch load (i.e., Concept 1 laboratory bridge: 35 kips was applied to midspan; Concept 2 laboratory bridge: 35 kips was applied to each quarter point simultaneously).

During the quasi-static loading, data from the complete set of transversely oriented strain gages was collected. A minimum of three quasi-static cycles were completed during this process to provide redundancy. This process provided a sample of the condition of the longitudinal joint in 100,000 cycle increments.

At the completion of the first million cycles of loading, a longitudinal reflective crack was introduced near the precast joint by increasing the applied loads until target strain values were reached to replicate the levels of transverse strain measured via concrete embedment VW strain gages located near the precast flange in the Center City Bridge. The target transverse strain value of 160 με was selected to represent the maximum daily change in strain observed in Joint 1 during the first summer after construction. The target strain value of 160 με is hereafter referred to as part of the environmental effect simulation, which is discussed in further detail in Section 5.3.2.

During the initiation of the reflective crack in the laboratory study, mechanical loading was applied to the same 10 by 20 in. patch dimension utilized during the fatigue study while the transverse strains measured via the concrete embedment resistive strain gages located nearest the precast flanges were monitored in real time, until a change in strain of approximately 160 με was observed, which was also generally associated with observed nonlinearity in the strain measurements, suggesting that a crack was generated. For Span 2 of the Concept 1 laboratory bridge, the crack was initiated at midspan (i.e., same location as during fatigue tests). In Span 1 of the Concept 1 laboratory bridge and the Concept 2 laboratory bridge, the crack was first initiated at the same longitudinal location as the fatigue tests (i.e., midspan of Span 1 and at the quarter points of the Concept 2 laboratory bridge, though cracking at the west quarter of the Concept 2 laboratory bridge was not clearly observed, which is discussed in Section 5.3.2. For these two spans, the crack was extended longitudinally using a 10 ft. long spreader beam, as it was expected that the uniform nature of a thermal gradient induced in a field bridge would tend to extend the crack along the length of the span. Bearing plates were placed a distance of 2.5 and 5 ft. to either side of midspan (corresponding with an effective 5 and 10 ft. spreader length). The locations of the applied patch loads for fatigue loading and locations of the patch loads used to extend the

length of the reflective crack, where applicable, are shown in Figures 5.3.1 and 5.3.2 for the Concept 1 and Concept 2 laboratory bridge specimens, respectively.

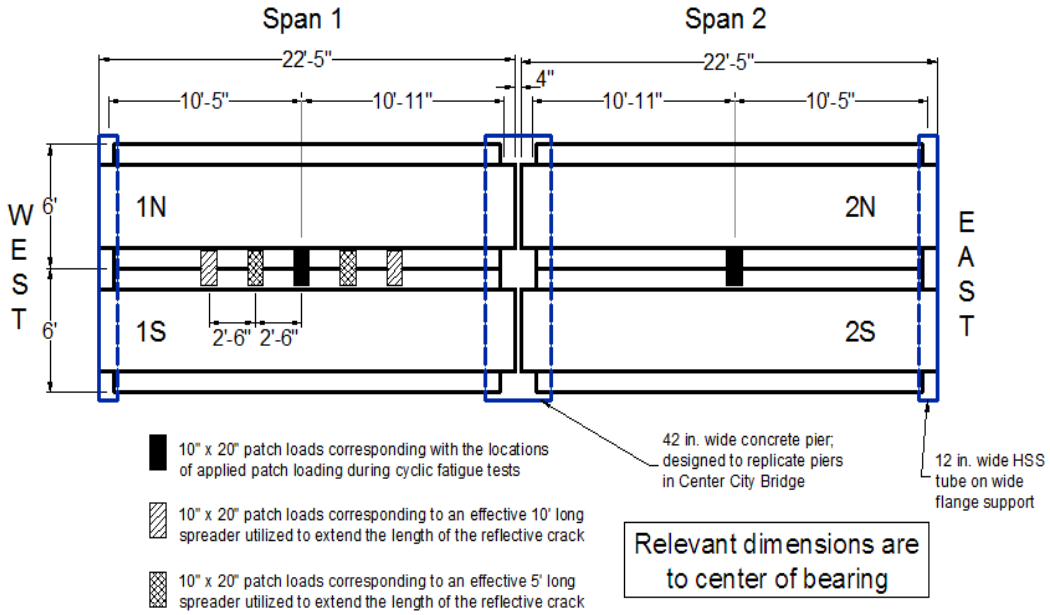

Figure 5.3.1: Placement of patch loads during fatigue loading and extension of longitudinal reflective cracking (applicable in Span 1 only) for the Concept 1 laboratory bridge specimen

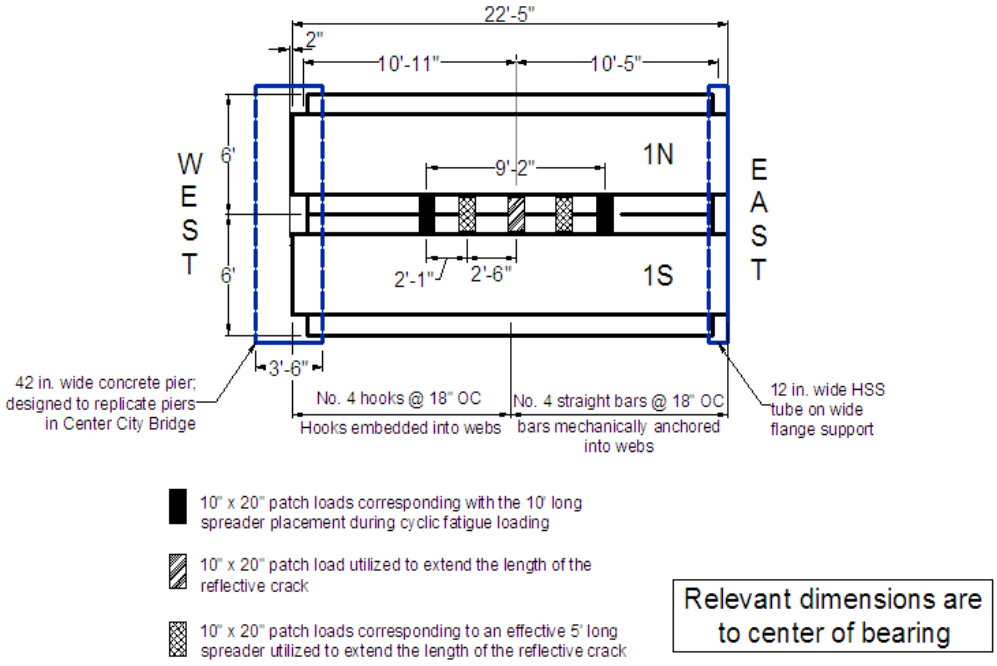

Figure 5.3.2: Placement of patch loads during fatigue loading and extension of longitudinal reflective cracking for the Concept 2 laboratory bridge specimen

The vertical location of the transversely oriented concrete embedment resistive strain gages varied between each span of the Concept 1 laboratory bridge and the Concept 2 laboratory bridge due to the variations in the thickness of the precast flange and the vertical depth of the transverse reinforcement traversing the longitudinal precast joint. The measured vertical locations of the bottommost layers of transversely oriented strain gages that were monitored during initiation of cracking in the laboratory bridge specimens, as well as the relative instrumentation in the Center City Bridge, are given in Table 5.3.1. Because of the variations in the depths of the instrumentation, the transverse strain observed in the Center City Bridge was not simulated exactly in the laboratory specimens. The target strain was not modified for each span based on the relative depth of the instrumentation because a relatively consistent magnitude of strain was desired to be induced in the transverse reinforcement (which was vertically collocated with the instrumentation).

The transverse strains measured during the introduction of reflective cracking in each span are shown in Table 5.3.2, along with the total applied load required to achieve each level of strain. The transverse strains reported here were the largest strains measured at the cross sections associated with fatigue loading (i.e., midspan for Concept 1 laboratory bridge, and quarter points for the Concept 2 laboratory bridge). When cracking was completed using the spreader load, the applied load shown in Table 5.3.2 represents the total load applied to the spreader. The distribution of load to symmetrically placed patch loads was measured via load cells and was found to be approximately equal.

Table 5.3.1: Measured vertical locations of transversely oriented strain gages that were utilized in the observation of reflective cracking in the Center City Bridge and laboratory bridge specimens

Specimen Description	Type of Instrumentation	Vertical depth of instrumentation, measured from the bottom of PC section
Center City Field Bridge	Concrete embedment VW strain gage	8.25 in.
Concept 1, Span 1 laboratory bridge	Concrete embedment resistive strain gages	6 in.
Concept 1, Span 2 laboratory bridge	Concrete embedment resistive strain gages	7.25 in.
Concept 2 laboratory bridge	Concrete embedment resistive strain gages	4 in.

Table 5.3.2: Measured transverse strains during introduction of reflective cracking after the completion of one million fatigue cycles in each specimen

Specimen Description	Load applied to patch or spreader	Measured transverse strain	Associated applied load
Concept 1, Span 1	Patch load	161 με	89 kip
Concept 1, Span 2	Patch load	200 με	95 kip
Concept 2, east quarter point (straight bars)	Spreader load	150 με	210 kip
Concept 2, west quarter point (hooked bars)	Spreader load	85με	210 kip

The largest strain that was developed in the west quarter point of the Concept 2 laboratory bridge was 85 με, when a total load of 210 kips was applied to a spreader beam and a transverse strain of 150 με was measured at the east quarter point.

A second million cycles of fatigue loading were subsequently completed on each specimen after reflective cracking was introduced in each section. As before, cyclic loading was suspended every 100,000 cycles to investigate the condition of the longitudinal precast joint via the measurement of the transversely oriented strain gage data during application of a quasi-static 35 kip patch load.

The behavior of the large-scale bridge specimens subjected to the fatigue loading is summarized in Table 5.3.3, which illustrates the change in strain measured under the quasi-static 35 kip patch load at relevant points during the two million cycles of loading. The first column of the table identifies the specimen designation. For the Concept 2 specimen, fatigue loading was completed at the quarter points using a spreader beam; in addition, a 35 kip quasi-static load was applied at midspan to investigate the performance of the joint at that location, and is included in the table. The initial strain was the strain measured prior to the fatigue tests (at zero cycles). Because little variation in the transverse strain was observed during the first and second million cycles, only the end points of these loading periods are shown.

The transverse instrumentation used to ascertain the results in Table 5.3.3 was determined after the introduction of cracking at one million cycles. During and after cracking, only one or two transversely oriented concrete embedment resistive strain gages located at the loaded cross section recorded a crack with a significant permanent strain increase, suggesting that, at those cross sections, the crack traversed those gages. For all cases, this instrumentation was located in the lowest level of gages, near the precast flanges, and was coincident with the location of loading

(i.e., at midspan if loading was applied at midspan or at the quarter points when loading was applied there). Figure 5.3.3 illustrates the gages that were used to create Table 5.3.3 for each specimen. Note that for the Concept 1 specimen, gage number 3 corresponded to the gage centered over the precast joint; whereas, in the Concept 2 specimen, gage number 2 corresponded to the gage centered over the precast joint.

Table 5.3.3[1]: Change in transverse strain measured at 35 kips throughout the course of 2M cycles of fatigue loading in each span of Concept 1 and Concept 2 laboratory specimens

Specimen	Initial Strain (με)	Change from initial strain (με)[2]		
		Before Cracking	After Cracking	After 2M Cycles
Concept 1, Span 1	18	0	24	25
Concept 1, Span 2	23	1	26	24
Concept 2, Midspan	33	-2	9	9
Concept 2, East Quarter span (straight bars)	33	-1	32	30
Concept 2, West Quarter span (hooked bars)	30	-3	5	6

[1]The instrumentation used to measure the values in this table is illustrated in Figure 5.3.3
[2]The initial strain was measured at zero cycles. The data taken to represent the before cracking state was recorded immediately after the completion of one million cycles. The data representing the after cracking state was recorded immediately after cracking with no cycling completed between.

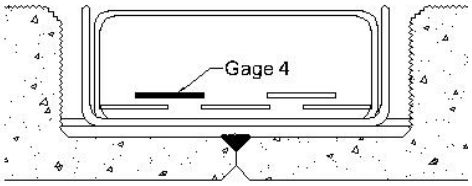

(a) Concept 1 Span 1; patch load at midspan

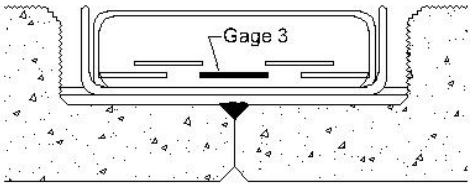

(b) Concept 1 Span 2; patch load at midspan

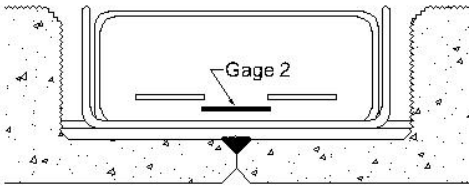

(c) Concept 2; patch load at midspan

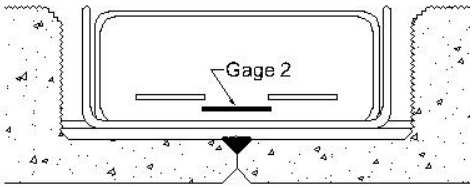

(d) Concept 2; patch load at west quarter point

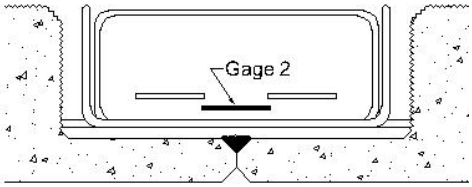

(e) Concept 2; patch load at east quarter point

Figure 5.3.3: Transversely oriented concrete embedment resistive gages located nearest the precast flange[1]. Instrumentation locations which detected reflective cracking and were used for measurement of transverse strain values during fatigue loading are highlighted in black and annotated

[1]The instrumentation is shown in two layers to illustrate the overlap between gages, however the gages were nominally located in the same vertical layer and at the same depth as the horizontal legs of the embedded transverse reinforcement. Extent of overlap between gages is shown to scale

Good fatigue behavior was observed for both the Concept 1 and Concept 2 laboratory bridge specimens. No significant degradation of the joint was observed. The transverse strains remained stable throughout the two million cycles of load regardless of the presence of the longitudinal reflective crack that was imposed near the precast joint. The performance of each specimen during the second million cycles of fatigue loading can be inferred from Table 5.3.3 by subtracting the measured strain values in the two rightmost columns. The largest increase in the strain measured during the second million cycles of loading was observed to be 2 με in both Span 2 of the Concept 1 laboratory bridge and the east quarter of the Concept 2 laboratory bridge. Because the resistive gages were considered accurate to approximately +/- 6με, this small increase in strain was considered negligible. Furthermore, the increase in the transverse strain due to the introduction of the longitudinal reflective crack (calculated by subtracting the after cracking strain value from the before cracking strain value in Table 5.3.3) varied slightly depending on the specimen. The increase in strain in Span 1 and 2 of the Concept 1 laboratory bridge was 24με and 25με, respectively, while the increase under the spreader load in the Concept 2 laboratory bridge was approximately 33με and 8με for the east and west quarters, respectively. The increase in strain due to cracking under the midspan patch load in the Concept 2 laboratory bridge was approximately 11με. The similar performance level attributed to the Concept 1 laboratory bridge and Concept 2 laboratory bridge in regards to reflective crack control under traffic loading suggested that the reinforcement details from either span were adequate for the design of PCSSS bridges.

5.3.2. Environmental Effect Simulation

As mentioned in Section 5.3.1, transverse strain measurements in the Center City Bridge suggested that a reflective crack initiated in the joint region during the first spring after construction. Of the three adjacent instrumented joints at midspan of the center span of the field bridge, the two outermost joints showed evidence of cracking. The transverse strains measured in the bridge immediately after construction in October 2005 until July 2009 are shown in Figure 3.2.7. The instruments directly over the joint and in the position immediately next to the joint (blue and red series, respectively) illustrated the presence of a reflective crack, initiating on April 25th, 2006. The ranges of strains observed during the summer of 2008 and summer of 2009 were approximately 150με and 220με respectively. The seasonal fluctuation of the strain measurements, in addition to the fact that the 35 kip patch load used for fatigue testing had induced a transverse strain of only approximately 40με in the laboratory bridge, further

substantiated that the large strains observed in the transverse joints of the field bridge were likely due to environmental effects rather than due to traffic load.

The increase in transverse strains from the summer of 2008 to the summer of 2009 warranted the investigation of the degradation of the joint region under large strains. It was expected that the increase in strains was caused by one of three sources: (1) fatigue traffic loading on the cracked system caused the degradation of the joint, (2) the cyclic influence of the thermal gradient change between day and night caused the increase in transverse strain, or (3) a larger thermal gradient may have been experienced that caused the crack to extend. Therefore, as mentioned in Section 5.3.1, a crack was induced in the laboratory bridge at the conclusion of one million traffic fatigue cycles to allow for the investigation of traffic fatigue loading on the cracked system.

At the conclusion of the second million cycles of traffic fatigue loading, additional cyclic loading was applied to the laboratory bridge specimens at larger strain levels to simulate cyclic strains due to environmental effects observed in the Center City Bridge. The strain cycles simulated the large daily strain fluctuations observed in the field bridge that occurred during the seasons that experienced the largest effects of solar radiation. For each level of strain considered, a total of 15,000 cycles were applied. The 15,000 cycles were selected to simulate approximately 100 years of significant temperature fluctuations, assuming that a total of 150 days a year were expected to induce considerable thermal gradients. Each of the three test spans were subjected to similar levels of transverse strains throughout the testing procedure. Two qualitative levels of transverse strain were considered during the environmental study, specified from here forward as environmental simulation strain level A, which corresponded to a target strain of approximately 180 με, and environmental simulation strain level B, which corresponded to a target strain of approximately 300 με. Target level A was selected based on the observed daily fluctuations in the transverse strain in Joints 1 and 3 of the Center City Bridge soon after reflective cracking was observed. Target level B was defined during the environmental simulation tests on Span 1 of the Concept 1 specimen; a strain of approximately 300 με was measured in the transverse instrumentation near the precast joint when a total patch load of 210 kips, which was the maximum practically available load to the 210 kip actuators, was applied at midspan of Span 1. This magnitude of transverse strain was comparable to the daily transverse strain fluctuations observed in Joint 3 of the Center City Bridge during the summer of 2008.

At both levels of strain to simulate environmental effects, quasi-static and cyclic loading was applied. As with the initiation of reflective cracking in the specimens after the first million fatigue cycles, quasi-static loading was applied to each specimen, while the instrumentation designated in

Figure 5.3.3 (same instrumentation that was utilized during the fatigue tests) was monitored in real time, until a change in strain approximately equal to the target levels was reached. The full range of transversely oriented instrumentation was also monitored during this process, however only the gages that had previously indicated cracking exhibited large increases in strain with load, suggesting that no new cracks developed during this process. Quasi-static loading was applied using a load controlled program, with load applied at a rate of approximately 6 kips per minute until a strain of 80 percent of the target strain was observed, at which point load was applied at a rate of 1 kip per minute. All quasi-static and cyclic loading associated with environmental simulation strain level A was completed prior to the initiation of quasi-static and cyclic loading to strain level B. A spreader beam was also employed in each of the spans to help increase the longitudinal extent of the reflective crack. Because the methodology utilized in the environmental effect simulation evolved during the tests, the specific spreader orientation for each span is discussed later in this section.

Cyclic loading during the environmental simulation was completed using a displacement-controlled test program, which effectively ensured that the level of strain induced near the precast joint during each cycle was approximately equal to the target strain level. Displacement limits were determined during the preceding quasi-static load-control tests at both target levels. The displacement limits were selected such that each cycle ranged from a maximum displacement which approximately induced the level of strain selected, while the minimum displacement was selected to ensure that a compressive force of no less than 2 kips was present at each patch load, which was primarily to keep the loading actuator from “walking” during testing. The magnitude of strain in the selected instrumentation (i.e., Figure 5.3.3) and the minimum load was monitored throughout each test. The displacement limits were modified in real time as necessary to maintain the desired values, though this process was seldom required.

The maximum levels of strain achieved in the joint region in each of the specimens throughout the environmental effect simulation are tabulated in Table 5.3.4. For both spans of the Concept 1 specimen, the cyclic loading to induce the target strain levels was applied at midspan through a single patch load, though both quasi-static patch and spreader loads were first utilized to induce and extend the longitudinal crack. For the Concept 2 laboratory bridge, the cyclic environmental loading to induce the target-level strains was applied using a spreader beam, with the patch loads placed at the quarter points of the span, though both quasi-static patch and spreader loads were utilized to induce and extend the crack prior to cyclic loading. The column designated by ‘P/S’ in Table 5.3.4 represents the use of a patch load, spreader load, or both (in which case the order

shown is that applied to the specimen) during the quasi-static cracking process. Generally, the use of the spreader test did not affect the strains measured at midspan, and vice-versa, which indicated that the effects of loading were relatively localized and did not affect the measurements 1/4 span away. The number of cycles completed at each load, if applicable, is represented in parentheses immediately following the respective strain level to which the sections were cycled. The column headers in Table 5.3.4 represent the target environmental simulation strain levels. Deviations from the measured strain and target strain at each level were generally due to limitations in the capacities of the loading actuators used during the study, as was observed for the Concept 2 specimen at the 300με target strain.

Table 5.3.4: Maximum transverse strains and number of cycles completed at given strain level during laboratory environmental effect simulation

Max. strain observed in joint regions and (number of cycles completed at that strain)	Prior to cracking at 1M cycles[1]	P/S[2]	Cracking at 1M Cycles	P/S[2]	Environmental simulation strain level A	P/S[2]	Environmental simulation strain level B	P/S[2]
Approximate target strain value			160 με		180 με		300 με	
Concept 1, Span 1	18με	P	161με	S,P	213με (15,000)	S,P	303με (15,000)	S,P
Concept 1, Span 2	23με	P	200με	P	183με (15,000)	S,P	233με (15,000)	S,P
Concept 2, east quarter	33με	S	150με	S,P	177με (15,000)	S,P	253με (15,000)	S,P
Concept 2, west quarter	30με	S	85με	S,P	81με (15,000)	S,P	104με (15,000)	S,P
Concept 2, midspan	33με	P	174με	S,P	176με (15,000)	S,P	256με (15,000)	S,P

[1]Measured strain was induced due to applied 35 kip patch load at midspan of the Concept 1 laboratory bridge spans, and at each quarter span, simultaneously, in the Concept 2 laboratory bridge

[2]Patch (P) or spreader (S) load orientation utilized to apply initial quasi-static cracking load, prior to cyclic loading

Span 2 of the Concept 1 laboratory bridge (which emulated the Center City Bridge section) was the first specimen to undergo loading to simulate environmental effects and as a result was subjected to the most unique loading procedure of all of the bridge specimens. Specifically, the

use of a 110 kip capacity actuator initially limited the loading capabilities on the specimen. Also unique to the environmental simulation history on Span 2 of the Concept 1 laboratory bridge was that a preliminary load test was completed which induced a transverse strain of approximately 160με near the joint at which 200 cycles were completed. This process was completed to investigate the performance of the joint to the 160με level after the completion of the second million cycles of fatigue load. The specimen was subsequently cycled for an additional 15,000 cycles to the environmental simulation levels A and B each. The reflective crack introduced in the section after the completion of the first million cycles of fatigue load was developed using a quasi-static patch load at midspan, and was not extended with use of a spreader beam. Cracking induced in the section to correlate with the environmental simulation strain levels A and B was generated with the use of both spreader and patch loading. The reflective crack was extended to the outer (i.e., east) quarter point of Span 2, however the crack was not observed to have extended to the instrumentation at the interior quarter point, which may have been attributed to transverse restraint provided by the proximity to the nearby interior support. Figure 5.3.4 illustrates the performance of Span 2 of the Concept 1 laboratory bridge during the environmental loading simulation. The diamond, square, and triangle data series represent strain measurements at midspan, the outer quarter point and the inner quarter point, respectively, with the data measured from the gages centered over the precast joint at each cross section. The vertical axis represents the magnitude of the transverse strain measured under a 35 kip patch load applied at midspan. The number of cycles completed, the strain that was induced in the section and the load required to induce that strain has been tabulated for Span 2 of the Concept 1 laboratory bridge in Table 5.3.5.

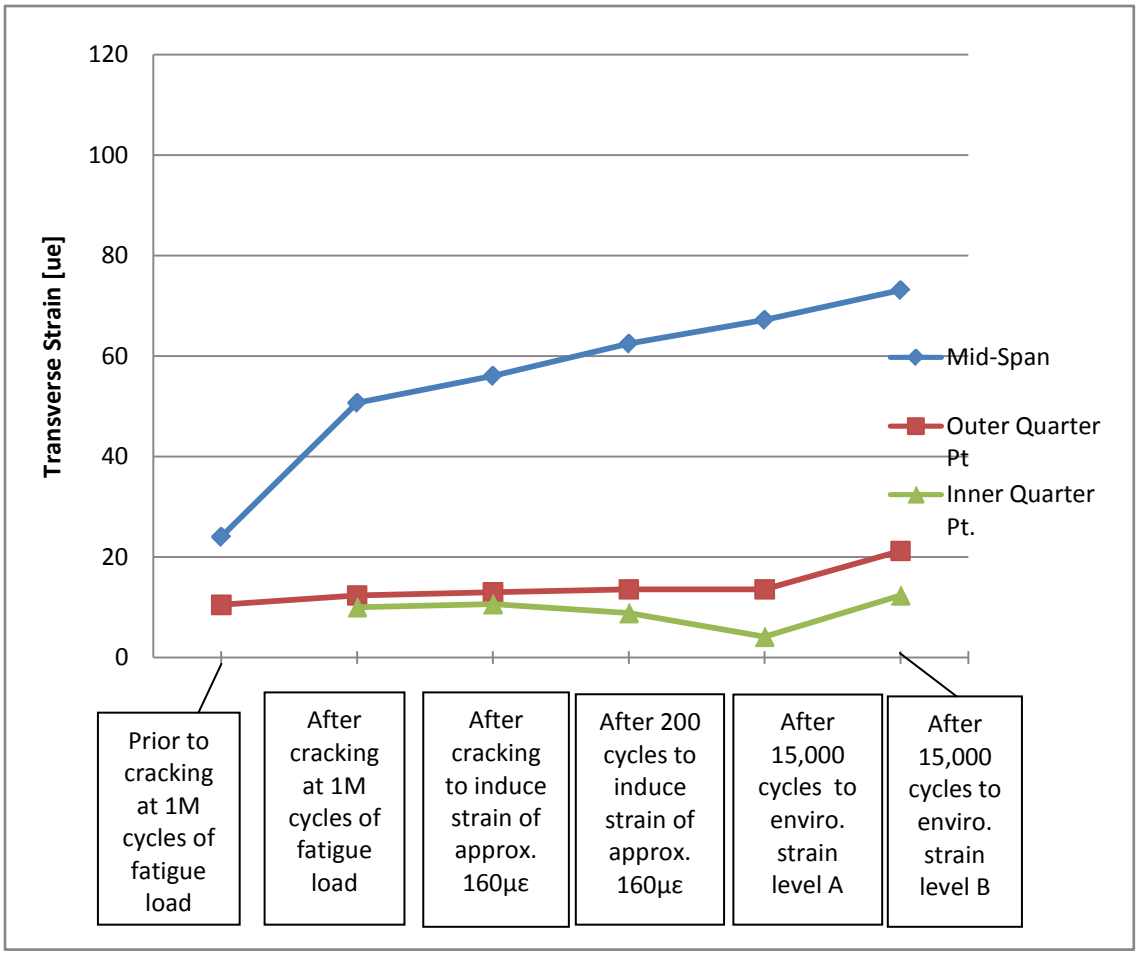

Figure 5.3.4[1]: Transverse strains measured with a 35 kip patch load applied at midspan during environmental effect simulation in Span 2 of Concept 1 laboratory bridge

[1]Figure 5.3.4 shows the transverse strain measured at midspan, the outer quarter point and the inner quarter point under a 35 kip patch load applied at midspan of Span 2. The horizontal axis contains a description of the behavior and qualitative target strain values. For example, the data points labeled “After 15,000 cycles to enviro. strain level A” represent the transverse strain measured with a 35k patch load applied at midspan after a load to induce a strain of 183με (from Table 5.3.4) was applied quasi-statically, and a spreader beam was utilized to extend the crack.

Table 5.3.5: Measured load and transverse strain, and number of cycles completed during environmental effect simulation on Span 2 of the Concept 1 laboratory bridge specimen

Concept 1, Span 2	Prior to cracking at 1M cycles of fatigue load	After cracking at 1M cycles of fatigue load	After cracking to target strain of 160με	After cycling to target strain of 160με	After cycling to enviro. strain level A	After cycling to enviro. strain level B
Magnitude of target strain	NA[1]	160με	160με	160με	180με	300με
Number of cycles completed at each stage	3	3	3	200	15000	15000
Max. transverse strain achieved	23με	200με	160με	160με	183με	233με
Load required to achieve strain	35k[2]	95k[2]	95k[2]	95k[2]	108k[2]	155k[3]

[1]The first column of Table 5.3.5 represents the strain measured during the fatigue loading. Fatigue loading was not based on strain levels, but rather was based on an applied patch load of 35 kip, therefore no target strain was applicable to fatigue loading
[2]The load recorded represents the patch load applied at midspan.
[3]The load recorded represents the total load applied to the 10 ft. longitudinal spreader beam. The load applied at each quarter point was half of this value.

Span 2 of the Concept 1 laboratory bridge indicated degradation of the joint due to the static and cyclic application of loads after reflective cracking was first introduced into the span (which corresponds to the data point labeled as “After cracking at 1M cycles of fatigue loading”). Degradation of the joint is evident in Figure 5.3.4 in that the transverse strain measured at midspan with a 35 kip patch load applied at midspan increased as the environmental effect simulation progressed from initially cracking the joint after the first million cycles of fatigue load to the last environmental simulation test of applying cyclic loading to induce strains on the order of the environmental simulation strain level B. The increase in strain under the 35 kip patch load applied at midspan, however was relatively small after the crack was first introduced in the section. The increase in transverse strain at midspan under the 35 kip patch load due to the initiation of the crack after the first million cycles was approximately 25με (i.e., 50με - 25με). Increases in the transverse strain due to cracking and cyclic loading to induce strains on the order of the environmental target levels A and B were observed to be between 5-8με (i.e., difference in

measured strains between the second and third data points, the third and fourth data points, etc.). Furthermore, a total increase in strain at the 35 kip patch load of about 15με at midspan due to the application of 30,000 cycles to simulate environmental loading (i.e., 77με after cycling to strain level B - 62με after 200 cycles to strain level A), suggests a relatively stable joint region when loaded to strains on the order of 200με. Recall that the application of 15,000 cycles was assumed to represent approximately 100 years of thermal effect loading, where there was assumed to be 150 days in a year with a significant thermal gradient.

A similar environmental simulation process was completed on Span 1 of the Concept 1 laboratory bridge. The primary difference in testing Span 1 involved the early use of an actuator with a 220 kip capacity. The reflective crack introduced in the section after the completion of the first million cycles of fatigue load was developed using a quasi-static patch load at midspan, and was also extended with use of a spreader beam during two separate load cycles, the first with bearing points symmetrically located 2.5 ft. from midspan, and the second with bearing points symmetrically located 5 ft. from midspan (referred to as 5 and 10 ft. spreader tests, respectively). Cracking induced in the section to correlate with the environmental simulation strain levels A and B was generated with the use of both the 5 and 10 ft. spreader layout as well as patch loading; however, cyclic loading was always applied through a patch load at midspan. The reflective crack was extended to the outer (i.e., west) quarter point of Span 2, however the crack was not observed to have extended to the instrumentation at the interior quarter point, which was attributed to the transverse restraint provided by proximity to the nearby interior support, and was similar to the observed results from Span 1 of the Concept 1 laboratory bridge.

The results of the environmental effect laboratory test on Span 1 are shown in Figure 5.3.5. In addition, Table 5.3.6 outlines the number of cycles completed, the strain that was induced in the section and the load required to induce that strain for Span 1 of the Concept 1 laboratory bridge.

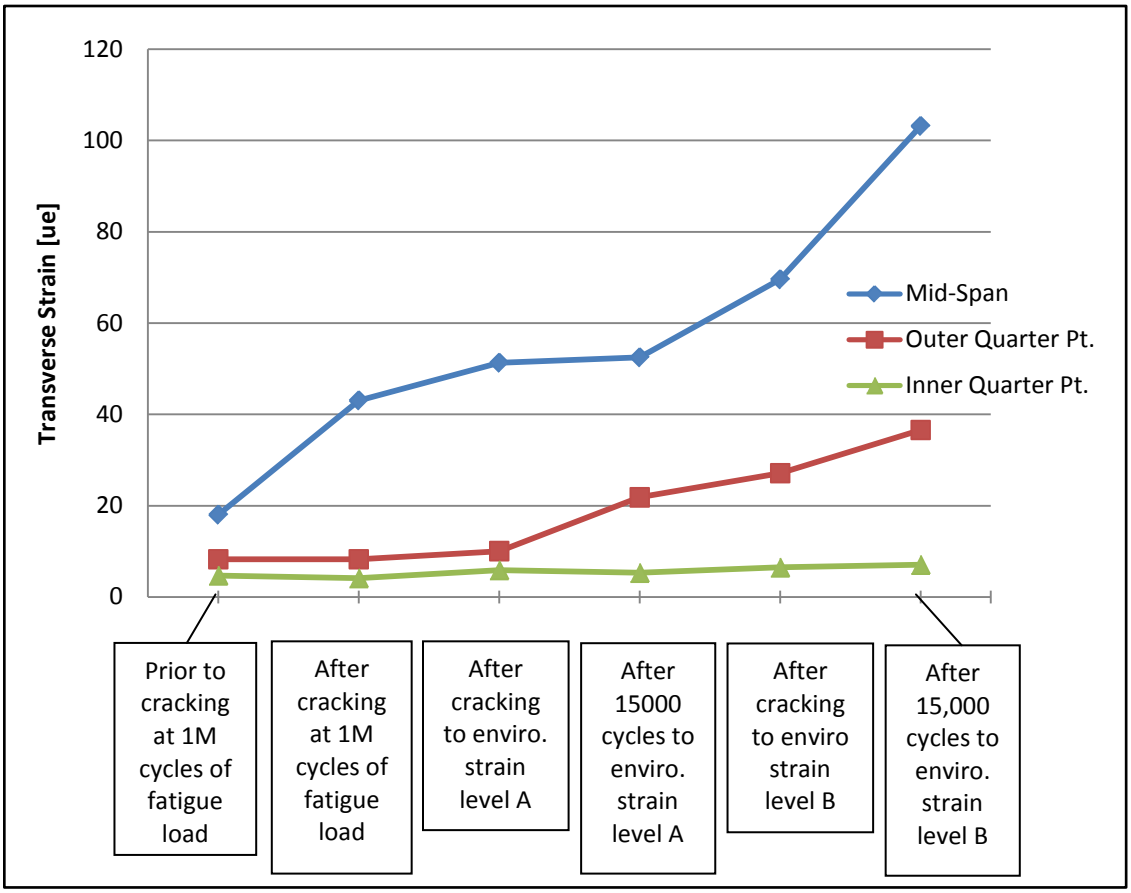

Figure 5.3.5: Transverse strains measured with 35 kip patch load applied at midspan during environmental effect simulation in Span 1 of Concept 1 laboratory bridge

Table 5.3.6: Measured load and transverse strain, and number of cycles completed during environmental effect simulation on Span 1 of the Concept 1 laboratory bridge specimen

Span 1, Concept 1	Prior to cracking at 1M cycles of fatigue load	After cracking at 1M cycles of fatigue load	After cracking to enviro. strain level A	After cycling to enviro. strain level A	After cracking to enviro. strain level B	After cycling to enviro. strain level B
Magnitude of target strain	NA[1]	160με	180με	180με	300με	300με
Number of cycles completed	3	3	3	15000	3	15000
Max. transverse strain achieved	18με	161με	213με	213με	280με	303με
Load required to achieve strain	35k[2]	89k[2]	160k[3]	105k[3]	206k[3]	210k[3]

[1]The first column of Table 5.3.6 represents the strain measured during the fatigue loading. Fatigue loading was not based on strain levels, and but rather was based on an applied patch load of 35 kip, therefore no target strain was applicable to fatigue loading
[2]The load recorded represents the patch load applied at midspan.
[3]The load recorded represents the total load applied to the 10 ft. longitudinal spreader beam setup.

Somewhat significant degradation of the joint with the application of the 35 kip patch load was observed due to both cracking and cycling at approximately 210 kips, or a measured strain of approximately 300με. Furthermore, degradation of the outer quarter point at the environmental strain level A and above suggested that the use of the 10 and 5 ft. spreader beam for the application of the quasi-static patch loads reduced the stiffness toward the exterior support along the joint. It should be noted that although degradation was observed under the application of loading, a forensic examination of the specimen discussed in Section 5.4 indicated negligible residual damage in the unloaded specimen.

The Concept 2 laboratory bridge consisted of two half spans of interest. For this reason, simulation of environmental effects was completed at the quarter points and at midspan separately, with the tests for environmental simulation strain level A completed first at the quarter points and then at midspan, with the same order of testing used at environmental simulation strain level B. The spreader setup consisted of load applied quasi-statically and dynamically through a 10 ft. long spreader beam centered at midspan. The reflective crack introduced in the section after

the completion of the first million cycles of fatigue load was developed using a quasi-static patch load at the quarter points through the use of the 10 ft. spreader beam, and was also extended to midspan via a single patch load at that location, though cracking was observed only between midspan and just beyond the east quarter point, which corresponded to the half span constructed with straight transverse reinforcement in the trough region. Cracking induced in the section to correlate with the environmental simulation strain levels A and B was generated with the use of both a 5 and 10 ft. spreader layout as well as patch loading at midspan, though for all tests cracking was not observed in the instrumentation in the west half span of the specimen. An additional load test was designed with a spreader beam bearing a distance of 2.5 ft. towards the west half span, and 5 ft. towards the east half span, in an effort to increase the reaction force in the west half span and subsequently induce cracking near that location. Loading was applied in a quasi-static load controlled load test, however the transverse strains measured at the midspan cross section reached the target values prior to the indication of the cracking at the west quarter point, and therefore no additional load was applied in this modified setup.

The lack of observed cracking was attributed to three possible explanations. The west half span corresponded to the half span of the bridge bearing on the concrete pier (i.e., corresponding to the interior half spans in the Concept 1 laboratory bridge), in which cracking was also not observed attributed to transverse restraint provided by the support. The natural roughness of the concrete pier may have provided additional restraint to the transverse expansion of the joint at the pier, which may have reduced the transverse stress demands in the CIP concrete near the joint. The west half span was also constructed with hooked reinforcement rather than the straight bars in the adjacent half span, though cracking was observed in the previous specimens where larger diameter hooked bars at closer spacing were used. A third possibility was that a potential reflective crack in the west half span was not observed by the instrumentation. This may have been the case especially if the crack propagated along the precast flange-CIP interface to the vertical web interface of the precast section, where instrumentation was not present (A forensic examination of the specimen following testing did not reveal a crack at the vertical web interface; however, the forensic exam was conducted under no load such that cracks that had opened under loading may have closed upon unloading.).

Figure 5.3.6 illustrates the behavior of the Concept 2 laboratory bridge under a 35 kip quasi-static patch load applied at the quarter points (i.e., a load of 70 kips applied to a 10 ft. spreader beam from midspan) at various times during the environmental simulation. Even though the Concept 2 laboratory bridge specimen had a single simply-supported span, the three data series in Figure

5.3.6 are named in the same way as for the Concept 1 laboratory bridge: the inside quarter was located nearest the concrete pier (i.e., west end of the Concept 2 laboratory bridge), while the outside quarter was located nearest the steel pier (i.e., east end of the Concept 2 laboratory bridge). Table 5.3.7 outlines the number of cycles completed, the strain that was induced in the section at both the east and west quarter points, and the associated load required to induce that strain for the Concept 2 laboratory bridge specimen.

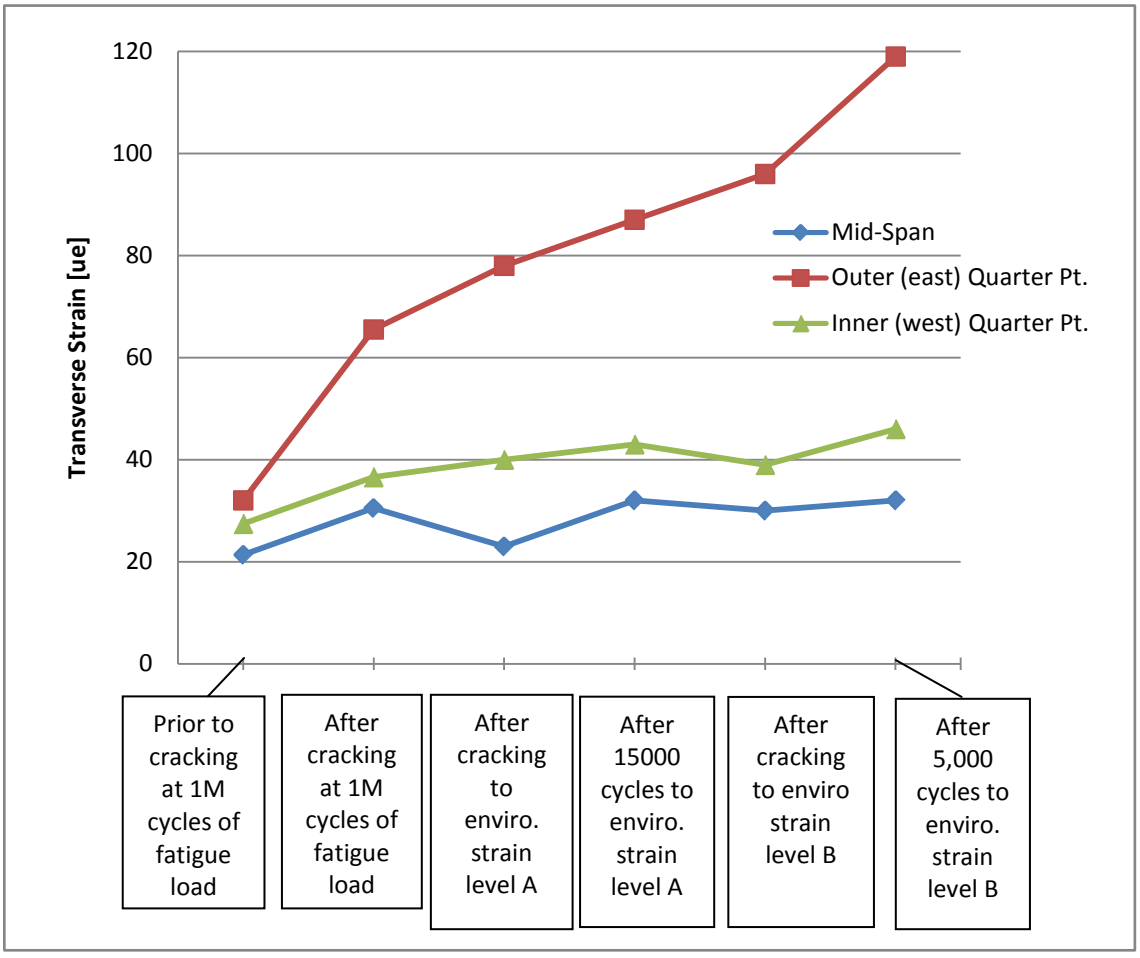

Figure 5.3.6: Transverse strains measured with 35 kip patch load applied at quarter points during environmental effect simulation in the Concept 2 laboratory bridge

Table 5.3.7: Measured load and transverse strain, and number of cycles completed during environmental effect simulation at the quarter points of the Concept 2 laboratory bridge specimen

Concept 2, load applied at quarter points	Prior to cracking at 1M cycles of fatigue load	After cracking at 1M cycles of fatigue load	After cracking to enviro. strain level A	After cycling to enviro. strain level A	After cracking to enviro. strain level B	After cycling to enviro. strain level B
Magnitude of target strain	NA[1]	160με	180με	180με	300με	300με
Number of cycles Completed	3	3	3	15000	3	5000
Max. transverse strain measured at the east quarter point	33με	150με	177με	177με	253με	253με
Max. transverse strain measured at the west quarter point	30με	85με	81με	81με	104με	104με
Load required to achieve strain[2]	70k	210k	195k	153k	210k	207k

[1]The first column of Table 5.3.7 represents the strain measured during the fatigue loading. Fatigue loading was not based on strain levels, but rather was based on an applied patch load of 35 kip, therefore no target strain was applicable to fatigue loading

[2]The load recorded represents the total load applied to the 10 ft. longitudinal spreader beam setup

Relatively similar levels of degradation were observed in the Concept 2 laboratory bridge compared to Span 1 of the Concept 1 laboratory bridge. At the conclusion of cracking and cycling to a load that induced a strain representative of the environmental target strain level A, the strain measured when a 35 kip patch load was applied to each quarter point had increased by 22με (i.e., 87με - 65με), compared to 9με (i.e., 52με - 43με) and 17με (i.e., 67με - 50με) for Spans 1 and 2 of the Concept 1 laboratory bridge, respectively. Furthermore, when loaded to the maximum capacity of the 220 kip actuator, which was limited to 210 kips due to the available system hydraulic pressure at the time of testing, and cycling to induce a strain of 253με at the east quarter point, the strain measured with an applied 35 kip quasi-static patch load at each quarter point increased by 32με (i.e., 119με - 87με), compared to a 51με (i.e., 103με - 52με) increase in Span 1 of the Concept 1 laboratory bridge. Note however that the Concept 2 bridge only underwent 5000

cycles at that strain level as opposed to the 15000 cycles subjected to the Concept 1 bridge spans and the magnitude of strain induced in each span during the environmental simulation varied. The absence of cracking near the west quarter span was further supported by the minimal increase in the strain measured at that location over the duration of the environmental simulation.

Cyclic loading was applied at midspan of the Concept 2 laboratory bridge after the completion of loading at the quarter points for both environmental simulation strain levels A and B (i.e., cyclic loading to level A was applied at quarter points, then midspan, followed by cyclic loading to level B at the quarter points, then midspan). The target strain level at the environmental simulation level B was modified for the midspan tests, with the revised target strain to be the maximum transverse strain measured at the quarter points (i.e., 253με at the east quarter point). The behavior of the specimen under a 35 kip quasi-static patch load at midspan through the duration of the environmental simulation is shown in Figure 5.3.7. The three data series in Figure 5.3.7 are named in the same way as for the Concept 1 laboratory bridge(i.e., the inside quarter is located nearest the concrete pier (west end of the Concept 2 laboratory bridge), while the outside quarter was located nearest the steel pier (east end of the Concept 2 laboratory bridge)). Table 5.3.8 outlines the number of cycles completed, the strain that was induced in the section at midspan, and the associated load required to induce that strain for the Concept 2 laboratory bridge.

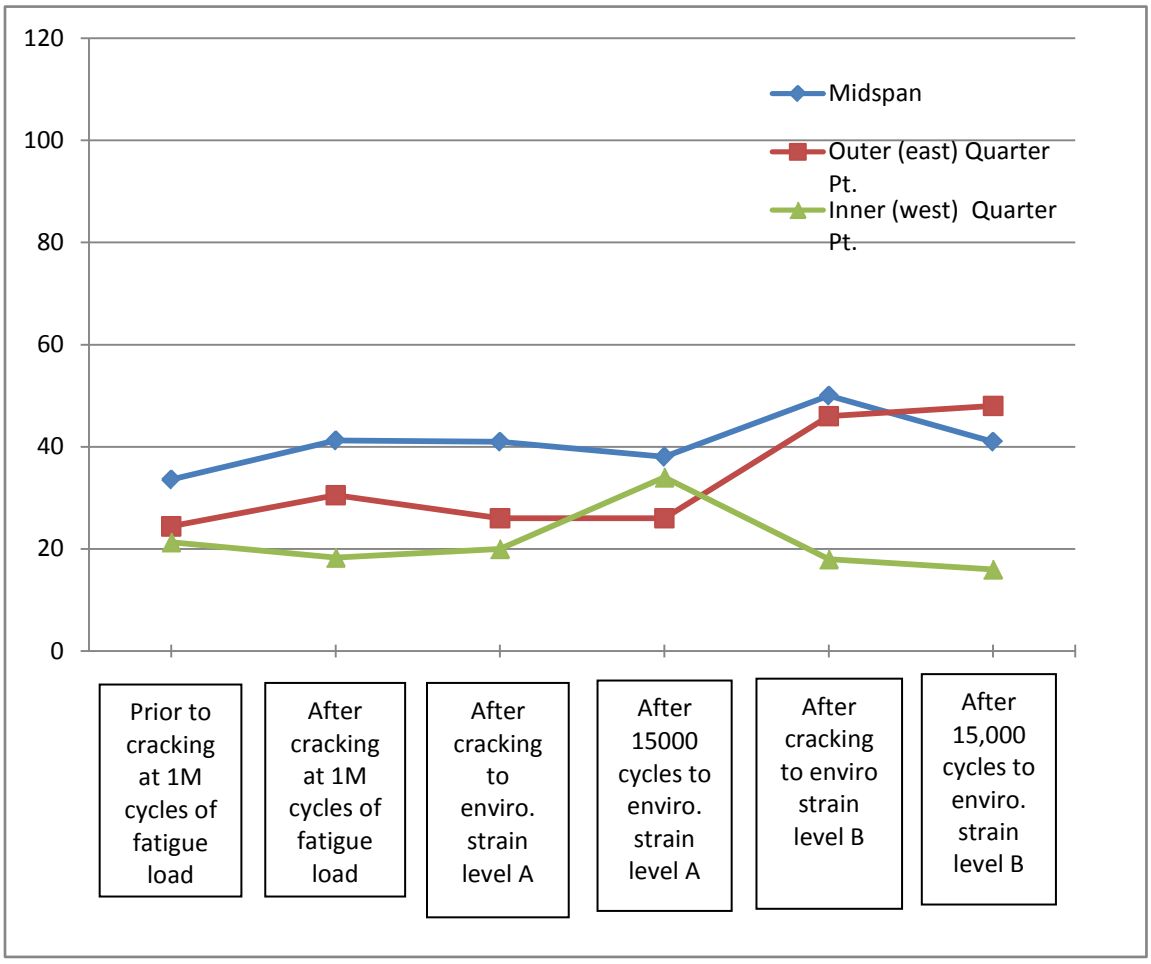

Figure 5.3.7: Transverse strains measured with 35 kip patch load applied at midspan during environmental effect simulation in the Concept 2 laboratory bridge

Table 5.3.8: Measured load and transverse strain, and number of cycles completed during environmental effect simulation at midspan of the Concept 2 laboratory bridge specimen

Concept 2, load applied at midspan	Prior to cracking at 1M cycles of fatigue load	After cracking at 1M cycles of fatigue load	After cracking to enviro. strain level A	After cycling to enviro. strain level A	After cracking to enviro. strain level B	After cycling to enviro. strain level B
Magnitude of target strain	NA[1]	160με	180με	180με	300με	300με
Number of cycles Completed	3	3	3	15000	3	15000
Max. transverse strain measured at midspan	33με	174με	176με	176με	256με	256με
Load required to achieve strain	35k	136k	116k	116k	124k	134k

[1]The first column of Table 5.3.8 represents the strain measured during the fatigue loading. Fatigue loading was not based on strain levels, but rather was based on an applied patch load of 35 kip, therefore no target strain was applicable to fatigue loading.

Little degradation of the longitudinal joint was observed at midspan of the Concept 2 laboratory bridge during the environmental effect simulation. Note that despite the fact that loading was applied at midspan in Figure 5.3.7, a larger increase in the transverse strain was measured at the outer (east) quarter point than at midspan after cracking and cycling to simulate the environmental strain target level B, which suggested that the level of degradation achieved near the east quarter point was more severe than that at midspan. The resiliency of the joint region at midspan was likely due to the limited success in extending the reflective crack into the west half span of the specimen.

The rate of degradation of the joint during cycling was also monitored during the environmental simulation on the Concept 2 laboratory bridge. Figure 5.3.8 illustrates the strain measured at midspan periodically with the 35 kip patch load located at midspan throughout the 15000 cycles that were completed to the maximum capacity of the actuator.

The cycling portion of the environmental simulation to induce a strain to the target level B was ended at after the completion of 5,000 cycles because of a fracture failure of the steel spreader beam used for the test. The rate of degradation of the joint at the outside quarter point was

observed to be larger during the early cycles and tended to taper off between 2,000 and 5,000 cycles. The increase in strain at the outer quarter point measured with the application of the 35 kip patch load over the first 2,000 cycles was 22με, while an additional 3,000 cycles increased the strain by only 10με. This suggested that the 5,000 cycles applied for the environmental simulation of the Concept 2 specimen provided an adequate estimate of the degradation that might be expected under the cyclic loads to a given strain condition.

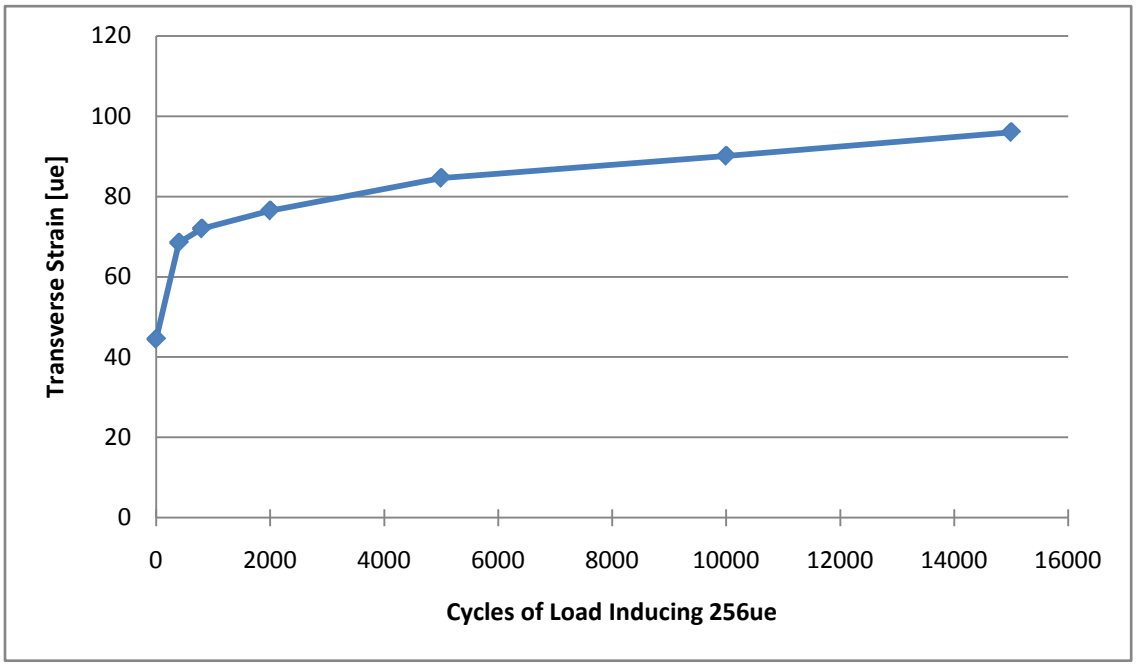

Figure 5.3.8: Transverse strains measured at midspan under the 35 kip patch load applied at midspan during the 15,000 cycles completed during the environmental effect simulation

In summary, Span 2 of the Concept 1 laboratory bridge showed excellent crack control during the cycling procedure at the environmental simulation strain level B, which corresponded to a measured value of approximately 233με. Span 1 of the same bridge, which would be expected to have superior crack control capabilities because of the reduced flange depth, showed a degradation of the joint under the same target strain level, which corresponded to an approximate transverse strain of 303με. Finally, the Concept 2 laboratory bridge, which was cycled to a maximum strain level of approximately 256με, measured at the east quarter point, also showed degradation of that portion of the joint region during cycling. The Concept 2 span was constructed with less total reinforcement, however with a tighter spacing. In addition, the Concept

2 laboratory bridge was constructed with a 3 in. flange, which would be expected to outperform Span 2 of the Concept 1 laboratory bridge. Because of the similarity in the performance of the two bridge concepts, the details from either were expected to be acceptable for PCSSS bridge construction. Furthermore, the adequate performance of the Concept 1 laboratory bridge (with 12 in. maximum transverse reinforcement spacing) indicated that a maximum spacing of 12 in. was suitable for the design of PCSSS bridges based on this research. Recall that the variations in the depths of the instrumentation utilized to measure the transverse strains (see Table 5.3.1) in each specimen prevented direct comparison of the relative magnitudes of measured strain among the specimen. Assuming that the transverse strain varied linearly between the compression and tension fibers of the section, instrumentation that was located lower in the section was associated with a smaller transverse curvature than instrumentation that was located higher in the section when both gages measured identical strains. A forensic exam was completed on each of the laboratory bridge specimens in an effort to visually identify reflective cracking by means of an investigation of core samples. After saw cutting the specimens into several sections, as discussed in detail in Section 5.4, negligible evidence of reflective cracking was observed in the forensic exam, despite the fact that many locations selected for core samples coincided with the location of concrete embedment instrumentation which reported large, inelastic strains during the load tests. Because the forensic exam was conducted following the tests, the cracks may have closed due to the load removal.

In addition to the environmental effect simulation using the procedures described above with the application of mechanical loading, a setup using commercial grade heated thermal blankets was applied to Span 2 of the Concept 1 laboratory bridge in an attempt to induce the same thermal gradient in the laboratory bridge as measured in the Center City Bridge. This method was found to be incapable of inducing the required thermal gradient in the specimen, and was not considered feasible in the future.

5.3.3. Load Transfer Between Precast Panels

The ability of the section to effectively transfer load between adjacent precast panels was expected to depend on the condition of the longitudinal joint and therefore was expected to change throughout the extent of laboratory testing as cracking was induced along the longitudinal joint. To investigate the load transfer between adjacent panels, patch loading was applied at the middle of the south precast panel, approximately 36 in. from the precast joint, directly at midspan of Span 2 of the Concept 1 laboratory bridge as well as separate tests at midspan and the quarter

points of the Concept 2 laboratory bridge. The locations of the applied load for the load transfer tests are shown in Figure 5.3.9. Load transfer was not investigated during testing of Span 1 of the Concept 1 laboratory bridge. Load transfer tests were completed on Span 2 prior to traffic fatigue or introduction of cracking, as well as at the conclusion of all fatigue loading and environmental simulations. Several load transfer tests were completed on the Concept 2 laboratory bridge throughout the series of traffic fatigue cycles as well as intermittently during the environmental simulation. Monitoring of the longitudinal instrumentation during the load transfer tests allowed for the calculation and comparison of the longitudinal curvature in the loaded and unloaded panels.

Span 2 of the Concept 1 laboratory bridge was first loaded on the south panel prior to any fatigue or cracking loading in November 2007. The second load test on the south panel was completed at the conclusion of all fatigue, cracking, and environmental simulation on both spans in October 2008 at the completion of roughly 2,030,200 cycles of fatigue and environmental loading on Span 2. Figure 5.3.10 illustrates the measured longitudinal curvature in the north and south panels at midspan in Span 2 of the Concept 1 laboratory bridge. The gages utilized through the depth in both panels were nominally located at midspan approximately 21 in. from the precast joint.

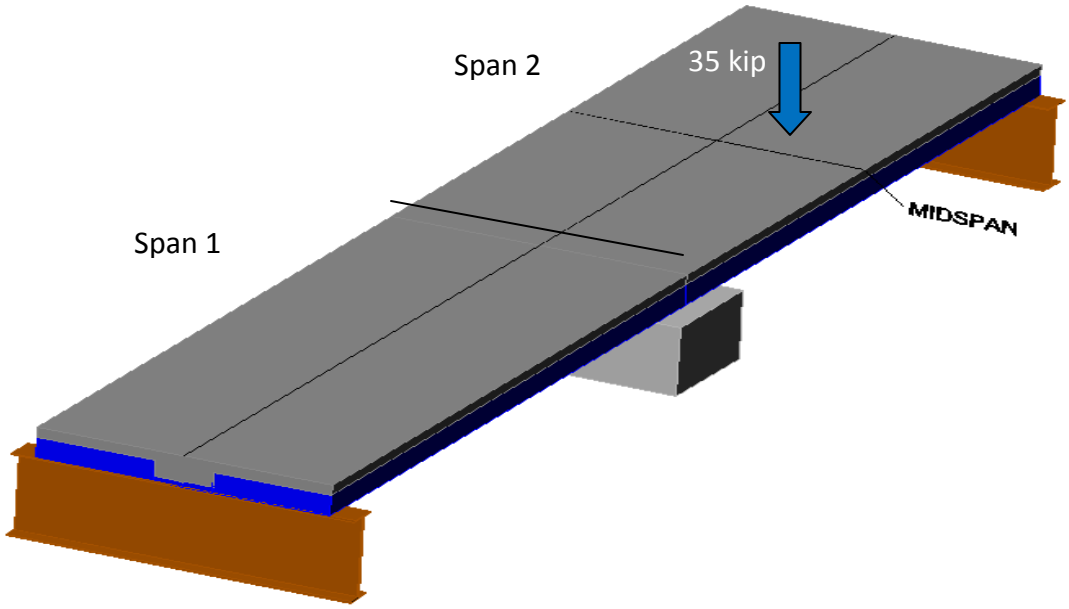

(a) Load placement during transverse load distribution tests for Concept 1 laboratory bridge

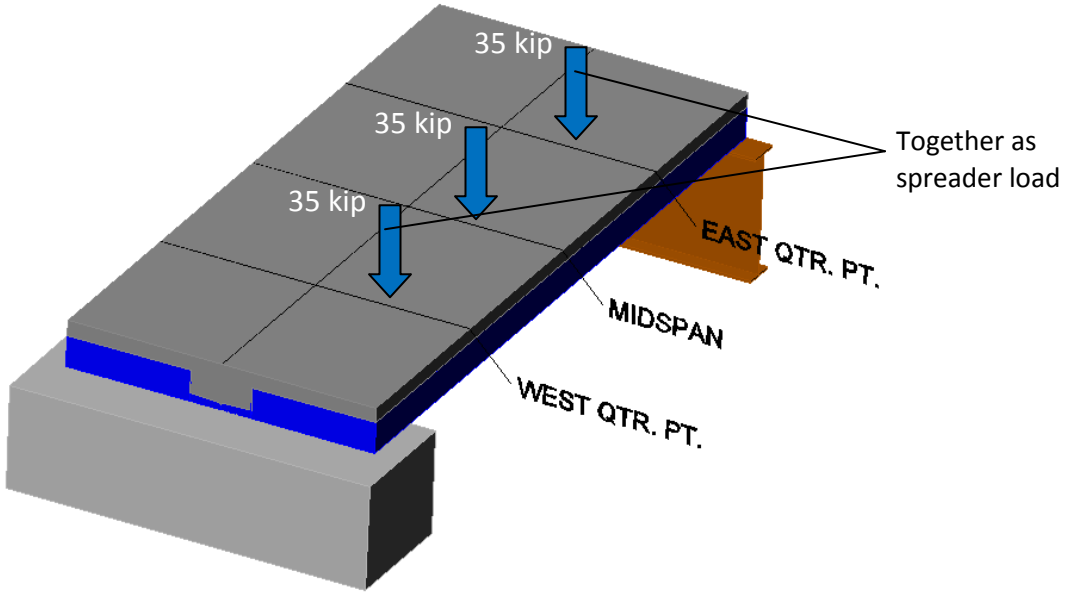

(b) Load placement during transverse load distribution tests for Concept 2 laboratory bridge

Figure 5.3.9: Load placement during transverse load distribution tests for Concept 1 and Concept 2 laboratory specimens

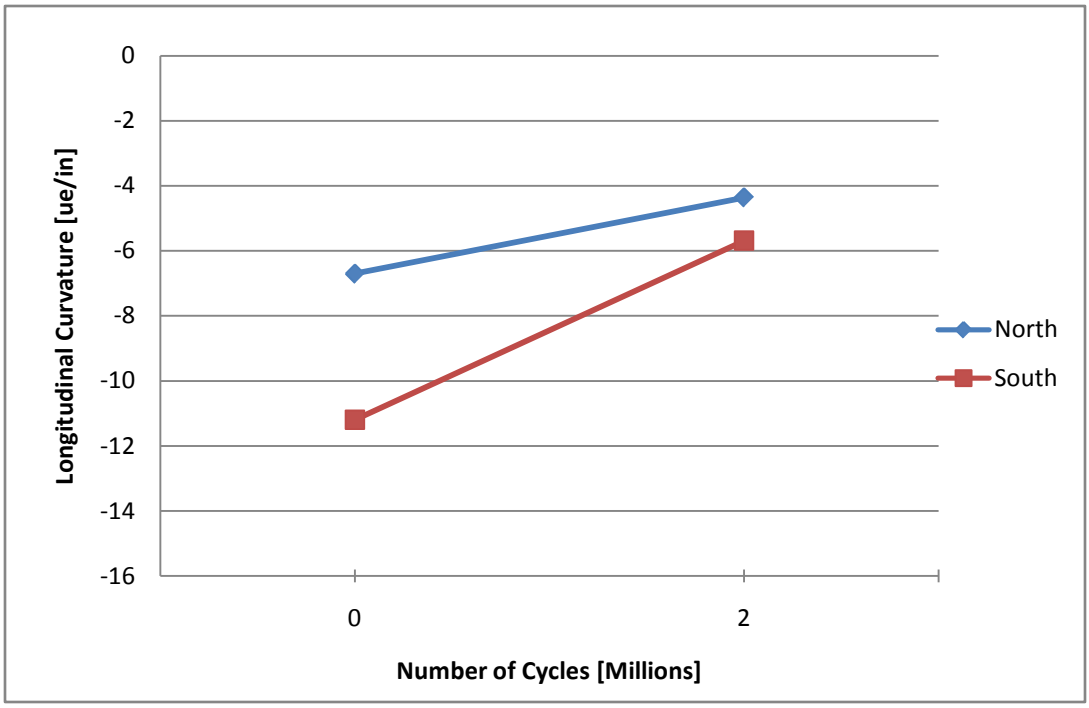

Figure 5.3.10: Longitudinal curvature in north and south panels in Span 2 of Concept 1 laboratory bridge under 35 kip patch load applied at midspan centered over south panel

The curvature at each data point was calculated using three longitudinally oriented strain gages in a vertical line. The coefficient of variation (R^2) value for the curvature ranged from 0.961 to 0.988 for the four data points shown in Figure 5.3.10. The reduction in measured curvature between the tests at zero and two million cycles might be attributed to variations in the loading and instrumentation setup between the two measurements, as the zero and two million cycles were completed by different personnel.

Load transfer was more thoroughly investigated in the Concept 2 laboratory bridge, with the longitudinal curvature measured several times throughout the laboratory tests conducted by the same personnel. As for the tests on Span 2 of the Concept 1 laboratory bridge, the south panel of the Concept 2 laboratory bridge was loaded both at midspan as well as at the quarter points with a 35 kip patch load at each location. Figure 5.3.11 illustrates the curvature calculated throughout the fatigue and environmental cycles with a 35 kip patch load applied to each quarter point through a longitudinal spreader. The last data points in the figure were taken after completion of environmental cycling to the 160με strain level. The longitudinal curvature was not obtained after the environmental simulation cycles to the 250με strain level due to failure of the spreader beam during those tests.

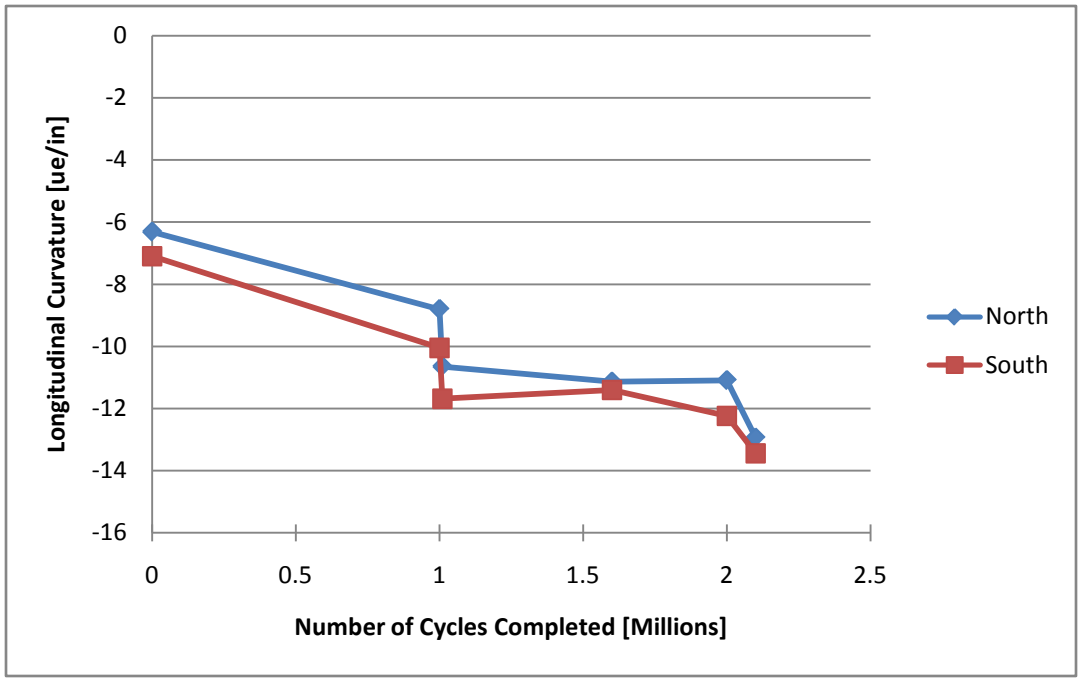

Figure 5.3.11: Longitudinal curvature in north and south panels in Concept 2 laboratory bridge under 35 kip patch load applied at the quarter points centered over south panel.

The longitudinal curvatures were observed to increase in the Concept 2 laboratory bridge. The increase in curvature observed in the Concept 2 laboratory bridge was not suspected to be a result of longitudinal flexural cracking, as the predicted cracking loads for Span 2 of the Concept 1 laboratory bridge and the Concept 2 laboratory bridge were 271 and 224 kips, respectively, while the largest loads applied to Span 2 of the Concept 1 laboratory bridge and the Concept 2 laboratory bridge were 155 and 210 kips, respectively.

It was expected that the longitudinal curvatures measured in the north precast panels would decrease as reflective cracking was introduced and extended near the precast joint because of reduced ability for the section to transfer load across the joint region, though this was not observed. Rather, good transverse load transfer was observed across the longitudinal joint regardless of the application of fatigue loading to simulate traffic loads, the introduction of reflective cracking, or even the application of cyclic loading to simulate the large daily strain fluctuations observed in the Center City field bridge due to environmental effects.

5.3.4. Composite Action

Each of the three bridge spans (i.e., Concept 1 Span 1 and 2, and Concept 2) provided an opportunity to investigate the effects of variations in horizontal shear reinforcement on composite action. Span 2 of the Concept 1 laboratory bridge was constructed with horizontal shear ties spaced at 12 in., though the hook returns provided a nominal 1/4 in. of clearance to the top of the precast web, which was unlikely to provide adequate clearance for proper bond. The horizontal shear reinforcement in this span reflected that used in the Center City Bridge, where, according to Article 5.8.4.1 of the AASHTO LRFD specification (2004), the maximum stirrup spacing at the ends of the precast beam was 15 in., which could be reduced to 24 in. at locations away from the ends (where the shears were smaller). The horizontal shear reinforcement spacing was doubled to 24 in. in Span 1 of the Concept 1 laboratory bridge and the clearance between hook returns and the top of the precast web was increased to 1-3/8 in., while no horizontal shear reinforcement was provided in the Concept 2 laboratory bridge. The 2010 AASHTO LRFD specification required the presence of a minimum area of horizontal shear reinforcement, though Naito et al. (2006) suggested that this requirement was overly conservative (see Section 2.3), which prompted the investigation of the performance of the PCSSS in the absence of horizontal shear reinforcement. In all three cases, a roughened surface was provided by means of raking, which created a surface roughness amplitude of approximately 1/4 in, and was provided on the horizontal top web surface as well as both vertical web faces in each specimen. The top surface of the precast flanges was also roughened in Span 2 of the Concept 1 laboratory bridge. A photograph of the surface condition of one of the precast members utilized in the Concept 2 laboratory bridge is shown in Figure 5.3.12.

Figure 5.3.12: Intentionally roughened surface, by means of raking, of top web of precast beam used for the construction of Concept 2 laboratory bridge specimen

The ability of the precast slab span system to maintain composite action throughout all loading scenarios warranted investigation of composite action at the largest possible load levels available in the laboratory. For this reason, load tests were conducted on each span to determine the maximum capacity of each specimen, and subsequently to determine whether composite action was maintained throughout each test. A total of between 3 and 6 longitudinally oriented concrete embedment resistive gages aligned vertically in the CIP and precast concrete at several cross sections in each specimen were utilized to calculate the longitudinal curvature during the ultimate tests. An analysis of the curvatures provided an assessment of the state of continuity between the precast and CIP concrete.

The application of load during the ultimate tests was expected to create an artificially compressed region near the location of applied load, which was likely to increase the horizontal shear friction (due to the localized increase in the normal force) at that location. Therefore, the location of the applied loading during the ultimate tests was modified in an effort to reduce the artificial effects

of loading on the longitudinally oriented instrumentation. In both spans of the Concept 1 laboratory bridge, the instrumentation utilized for the investigation of composite action was located within a longitudinal distance of 3 in. from the application of load at midspan. The load frame was therefore modified, and relocated 20 in. closer to the center pier, which provided a center to center distance of 17 in. from the load beam to the instrumentation. The longitudinally oriented instrumentation in the Concept 2 laboratory bridge was designed to allow for the load frame to remain in the same position for the ultimate loading as was utilized for the fatigue and environmental studies, with a center to center distance of 21 in. between the instrumentation and load beam.

Each test was preceded by the construction of an even grouted surface between the top of the bridge and the loading beam, which extended across the entire width of the bridge and had a flange width of 12 in. Three actuators, a 220 kip in the center with a 110 kip actuator to each side, were used to apply load to the transverse load beam. Load was applied to each specimen using a displacement-controlled program, primarily to prevent the rapid collapse of the specimens, if applicable. The displacement rate was selected such that the load was increased by approximately 2 kips per minute. A photograph of the loading system utilized for the ultimate tests is provided in Figure 5.3.13.

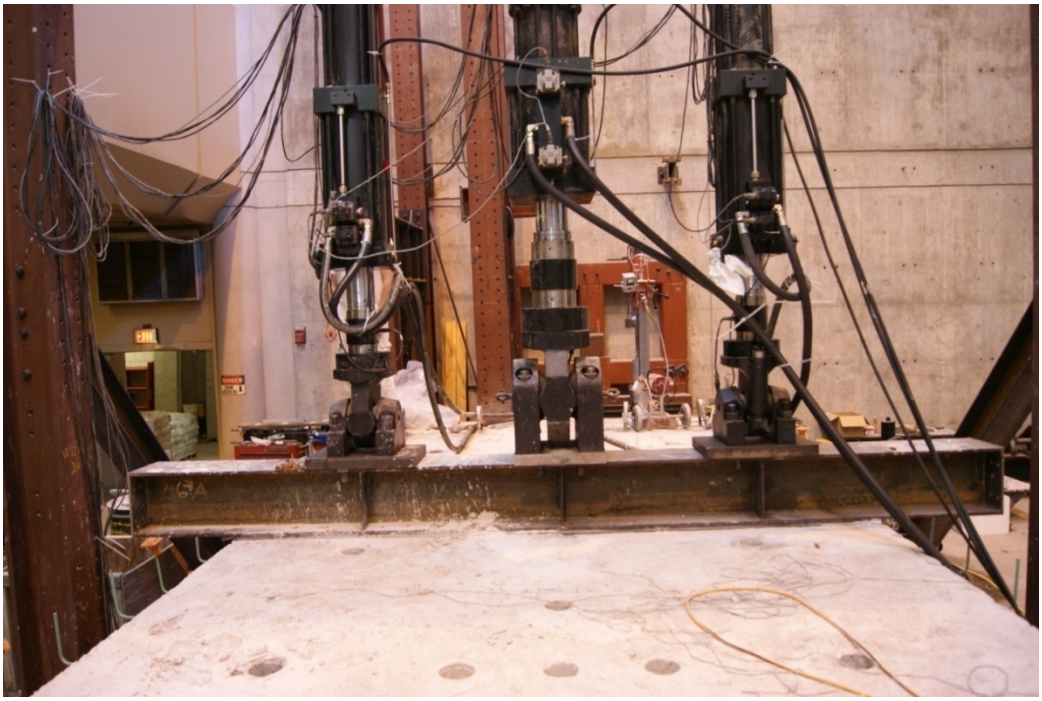

Figure 5.3.13: Photograph of tri-actuator load setup and transverse loading beam utilized during ultimate load tests; shown for the Concept 2 laboratory bridge test

The calculation of the sectional ultimate moment capacity for each span was completed using Response-2000. The assumed tensile strength of the prestressing strand was taken to be 270 ksi, the yield strength of the mild reinforcement as 60 ksi, and the concrete compressive strain at crushing was assumed to be 0.003.

The ultimate sectional moment capacity of each section varied slightly, due to the depths of the longitudinal cage reinforcement based on the flange thickness, number of strands in each span, as well as variations in the CIP concrete compressive strength and the finished depth of each span due to construction tolerances. The maximum measured depth of the Concept 1 laboratory bridge was 19.25 in., with concrete compressive strengths of 4.47 ksi and 4.55 ksi at an age of 432 days in Spans 1 and 2, respectively. The measurement of the compressive strength at 432 days suggests that the value should reasonably represent the maximum strength and reasonably predict the strength during ultimate loading, which occurred when the CIP concrete was 855 and 784 days old in Spans 1 and 2, respectively. The maximum measured section depth in the Concept 2 laboratory bridge was 18.5 in. with a CIP concrete compressive strength of 6.9 ksi measured 10 days prior to ultimate loading on the Concept 2 laboratory bridge.

The ultimate sectional moment capacity of Span 2 of the Concept 1 laboratory bridge was calculated to be 2544 ft.-kip, and the calculated capacity of Concept 1 Span 1 was 2256 ft.-kip. The sectional capacity of the Concept 2 laboratory bridge was calculated to be 2313 ft.-kip.

A numerical analysis of the continuous two-span Concept 1 laboratory bridge suggested that the ultimate capacity of the specimen would not be reached, as the maximum load available during the Concept 1 ultimate tests was approximately 420 kips, which corresponded to an applied maximum moment of 1272 ft.-kips, which was considerably less than the ultimate sectional capacities of either Span 1 or 2. The continuous bridge was modeled as a three-span system, with the center span modeled with an 18 in. span length (i.e., the distance between the center of bearing of Spans 1 and 2 at the center pier). The center span was modeled with a moment of inertia that was an order of magnitude larger than that of the exterior spans, to simulate the stiffness provided by the pier.

Ultimate loading was initiated on Span 2 of the Concept 1 laboratory bridge, with a maximum applied load of approximately 420 kips. The ultimate capacity of the section was not observed to be imminent, which corresponded with the previously stated predictions. In an effort to reach the ultimate capacity of Spans 1 and 2, saw cutting was completed at the center pier in an attempt to reduce the continuity in the bridge (i.e., create approximately simple-support conditions) to reach the maximum flexural capacity of the laboratory bridge specimens with the available actuators.

The cutting blade had a usable cutting radius of approximately 5 in, and therefore only the longitudinal deck reinforcement was severed, while the longitudinal reinforcement for continuity at the bottom of the reinforcing cage through the joint remained intact. Spans 1 and 2 of the Concept 1 laboratory bridge after continuity was modified at the center pier are referred to as semi-simple spans hereafter.

The ultimate capacities of the two semi-simple spans in the Concept 1 laboratory bridge and the simple span in the Concept 2 laboratory bridge were not achieved during testing due to limitations of the actuators. The maximum load available during the Concept 1 tests was approximately 420 kips, while an applied load of 458 kips was achieved during the Concept 2 test, due to an increase in available hydraulic pressure. The applied loads and respective moments, as well as the calculated sectional capacities of each specimen are given in Table 5.3.9.

Table 5.3.9: Maximum loads applied to laboratory bridge specimens during ultimate loading, calculated applied moments, and predicted moment capacities

Specimen	Max. applied load	Calculated max. applied moment	Predicted ultimate sectional capacity
Concept 1, continuous span	420 kip	1272 ft.-kip	2256 ft.-kip for Span 1 2544 ft.-kip for Span 2
Concept 1, Span 1, semi-simple span	420 kip	2158 ft.-kip	2256 ft.-kip
Concept 1, Span 2, semi-simple span	420 kip	2158 ft.-kip	2544 ft.-kip
Concept 2	458 kip	2450 ft.-kip	2313 ft.-kip

In all cases, ultimate failure of the specimens was not observed to be imminent. Loading was conducted at a displacement controlled rate; no reduction in applied load was observed during the tests, suggesting that composite action was maintained throughout the applied load range. In addition, visual inspections of the CIP-precast interface did not reveal any indication of slippage between the CIP and precast section on the external faces.

A composite section should experience linearly varying strains through the full depth of the section, while loss of composite action would be evinced if distinct curvatures were observed in each section (i.e., the CIP top section and the precast bottom section). Therefore, an analysis of the longitudinal curvatures in each section was conducted.

The Concept 2 laboratory bridge specimen was well instrumented for the calculation of longitudinal curvature. At least three longitudinally oriented instruments were included in both the precast and CIP concrete. Good linear correlation through the section was observed among the instruments used to calculate the curvature at most locations. The change in curvature, measured between an applied load of 0 kips and 458 kips, and correlation coefficients, among other quantities determined during the ultimate test on the Concept 2 laboratory bridge are summarized in Table 5.3.10.

Table 5.3.10: Longitudinal curvature and relevant values during ultimate loading on Concept 2 laboratory bridge specimen

Location[1]	**Number of Gages**	**Load [kip]**	**Curvature [1/in.]**	**NA Depth [in.]**	**R^2**
N-Mid-40”	7	458	-454.5	14.0	0.991
N-Mid-20”	6	458	-341.3	12.8	0.977
N-Mid-3”	6	458	-476.2	14.3	0.930
S-Mid-20”	6	458	-416.7	12.9	0.975
N-Qtr-20”	6	458	-201.0	13.0	0.995
N-Qtr-40”	7	458	-196.1	13.0	0.981
N-Qtr-3”	5	458	-213.2	12.4	0.954

[1]The instrumentation location was designated as follows: North/South precast panel – Mid-span/Quarter point – Distance to gage set from precast joint

As an example, the longitudinal curvature measured at midspan of the north panel, 20 in. from the precast joint (i.e., N-Mid-20”) is shown in Figure 5.3.14. The curvature measured at this location reasonably represents the results of the ultimate load test at all locations. The linear trend line appears to provide a good fit to the instrumentation both above and below a vertical depth of 12 in. measured from the bottom of the precast, the location of the top of the precast web-CIP interface, suggesting that composite action was maintained at the applied load of 458 kips. The measured curvature was calculated based on the linear trend line, where the curvature was the reciprocal of the slope of the line.

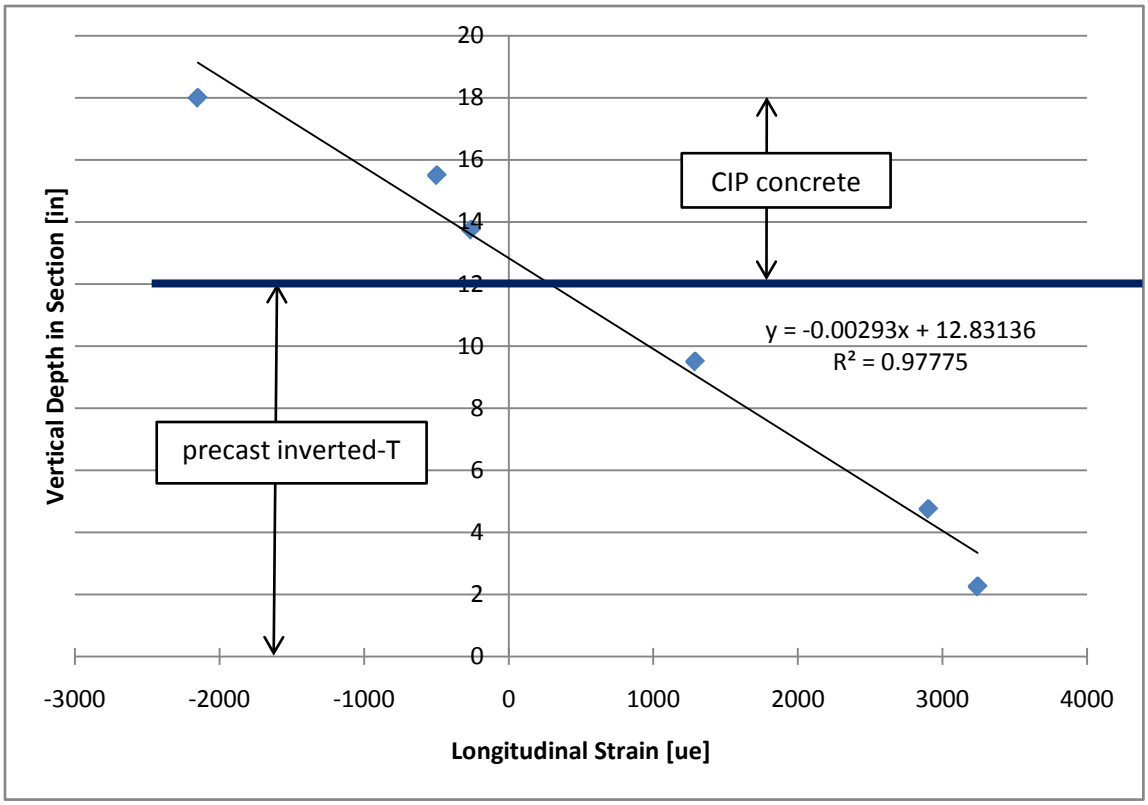

Figure 5.3.14: Longitudinal strains measured through the section depth at midspan of north panel 20 in. from precast joint with 458 kip applied Load in Concept 2 laboratory bridge specimen

The compression force developed in the section was calculated by integrating the stress profile using the measured strain profile and assuming the modified Kent and Park (Park et al., 1982) concrete stress-strain model with a nominal concrete compressive strength, f'_c, of 5865 psi, which was equal to 85 percent of the measured concrete compressive strength of 6.9 ksi, and $\varepsilon_0 = 0.002$. Eighty-five percent of the measured concrete compressive cylinder strength was utilized to provide an estimate of the unconfined concrete compressive strength in a structural member. Integrating the compressive stress above the neutral axis and multiplying by the deck width, the total compressive stress developed in the Concept 2 laboratory bridge was 2134 kips. The reduction in compressive force transferred through the composite surface due to the concrete in tension must also be considered. Using the measured modulus of rupture, the uncracked concrete in tension was assumed to provide a tensile force of 46 kips in the CIP. Therefore, the compressive force transferred between the CIP and precast concrete was 2088 kips. Dividing the total force by the width of the deck, including the area above the longitudinal trough, and half of the center to center of bearing span length, the measured stress transferred through the

unreinforced composite surface was determined to be 135 psi. Because the unreinforced Concept 2 laboratory bridge span provided good horizontal shear capacity throughout loading to the maximum load of the actuators, which was nearly the ultimate capacity of the section, it was recommended that AASHTO Article 5.8.4 be modified to allow sections unreinforced for horizontal shear to develop a nominal horizontal shear strength of up to 135 psi.

5.4. Destructive Testing of Large-Scale Laboratory Specimens

At the conclusion of the tests, cores were taken at locations of interest through the laboratory bridge specimens to investigate the location and extent of cracks that were believed to have developed during the tests based on the strain measurements. The information obtained from the cores is summarized in Section 5.4.1. The specimens were also sliced into segments small enough such that they could be removed from the laboratory with the overhead crane. The information obtained from a visual inspection of the sliced surfaces to determine the extent of any residual cracking is summarized in Section 5.4.2.

5.4.1. Inspection of Cores taken from Laboratory Bridge Specimens

The inspection of core specimens was completed by Phil Cici (2010).

At the conclusion of laboratory testing a series of cores were removed from both the Concept 1 and Concept 2 laboratory bridges to provide a means of physical investigation of the cracking behavior near the precast joint. The cores were utilized to document a maximum crack width and length in each core, the magnitude of the crack width was dependent on the maximum loading and specific boundary conditions in each span, and therefore would not be directly comparable between spans.

The diameter of cores ranged between 2, 3, and 4 in. Each of the core specimens was examined both with the naked eye and the aid of an Olympus SZX12 stereo-microscope to find cracks on the core surface. The level of magnification used to examine the cores ranged between 2.1X to 27X, which was the full capacity of the microscope. All cracking that was identified in each core was tabulated, regardless of the size or anticipated origin. The observed crack widths were documented in classification categories, defined in Table 5.4.1. The vertical depth of the cracking identified in the cores was referenced from the line created by the horizontal precast flange-CIP interface, as shown in Figure 5.4.1. A complete description of the characteristics and measured values obtained from each core sample is tabulated in Appendix E.

Table 5.4.1: Crack width classification categories for analysis of core specimens

Crack Classification	Crack Width (W)
0.002	W < 0.002 in.
A	0.002 in. ≤ W < 0.008 in.
B	0.008 in. ≤ W < 0.023 in.
C	0.023 in. ≤ W < 0.200 in.
D	W ≥ 0.200 in.

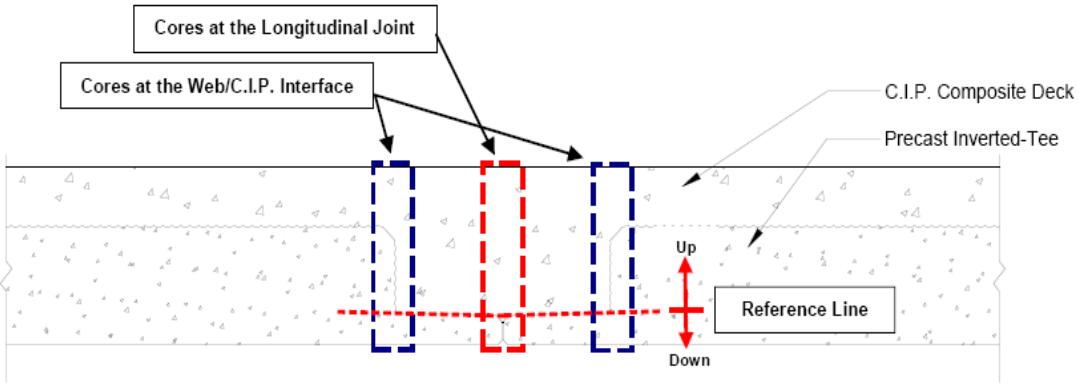

Figure 5.4.1: Location of reference line for measurement of vertical location of cracking in core specimens

Core samples were extracted from both spans of the Concept 1 large-scale laboratory bridge. A total of five cores were removed from Span 1, while four cores were extracted from Span 2. All the cores from the Concept 1 laboratory bridge specimen were nominally located directly over the longitudinal precast joint (corresponding to the red core outline in Figure 5.4.1), at various locations along the length of each span. Table 5.4.2 shows the core description and location, as well as observed crack width and depth. The specimen identification consists of the bridge concept number-span number-core number. The *x*-coordinate of the core location corresponds to the coordinate system with the origin at the center of the pier, in accordance with the locations of the instrumentation; a negative *x*-coordinate corresponds to Span 1; while a positive *x*-coordinate corresponds with Span 2. After the first core was removed from Span 1 of the Concept 1 laboratory bridge, a saw cut was completed along the entire length of the bridge near the precast

joint, after which specimens C1-S1-2 through C1-S1-5 were removed from the span. These cores therefore consisted of two half cylinders. The thickness of the cylinder removed due to the saw cut was approximately 1/8 in. wide through the length of the core near where the precast joint was located. Because of this, evidence of cracking in these specimens may have been removed from the saw cut, however the only core from the Concept 1 laboratory bridge where a crack was clearly measured was in a core specimen that had been cut. The other potential cracks were too small to be seen even with the magnification of the microscope.

Table 5.4.2: Summary of maximum height and width of cracks measured in core specimens from the Concept 1 laboratory specimen

Specimen	*x*-Coordinate of Core (in.)	Saw Cut?	Diameter of Core (in.)	Maximum height of crack[1] (in.)	Maximum width of crack[2] (in.)
C1-S1-1	-194.5	No	1.75	Undefined[4]	Undefined
C1-S1-2	-26	Yes	2.75	NO[3]	NO
C1-S1-3	-134	Yes	2.75	NO	NO
C1-S1-4	-192	Yes	2.75	NO	NO
C1-S1-5	-197.5	Yes	2.75	2.75 (up)	A
C1-S2-1	74	No	1.75	NO	NO
C1-S2-2	146	No	1.75	NO	NO
C1-S2-3	195.5	No	1.75	NO	NO
C1-S2-4	198	No	1.75	NO	NO

[1]The height of crack was measured from the reference line, defined in Figure 5.4.1; only "upward" values are recorded in this table
[2]The width of crack was documented by crack classification, as defined in Table 5.4.1
[3]"NO" represents "No reflective cracks observed"
[4] "Undefined" represents that the reflective crack was continuous with a shrinkage crack from the deck surface, therefore beginning and end points were undefined

The only evidence of internal cracking observed via the investigation of the core samples was in specimen C1-S1-5, which was in the outer quarter of Span 1, despite clear evidence from the instrumentation that cracking occurred at several other locations. Strain increases as large as 303 με and 233 με were measured in Spans 1 and 2, respectively, via the concrete embedment resistive gages under loading. Considering the 4.7 in. gage length, a maximum associated crack width of 0.0011 and 0.0014 inches might be expected in all the core samples except C1-S1-2 because of the proximity to the continuous pier. While the expected crack widths of

approximately 0.001 inches were smaller than the 0.002 inch minimum reading on the crack gage, the use of the microscope allowed for significantly smaller cracks to be identified, especially those on the order of 0.001 inches. From the forensic examination, it appears that the cracks may have closed upon unloading.

The Concept 2 laboratory bridge was similarly cored at the conclusion of testing. In this case, eight cores were removed from the specimen, four from each quarter point. At each quarter point, two cores were removed from above the joint, 4 in. apart, while the remaining two were centered over the vertical precast webs. Cores were taken from the web areas to document any cracks or separation at the CIP-precast web interface at those locations, which should be avoided because the cage reinforcement provides no benefit near the vertical web interfaces. Table 5.4.3 includes a summary of the measured crack widths and depths in the cores from the Concept 2 specimen. No saw cutting was present in the Concept 2 laboratory bridge specimen prior to the removal of the core samples. The measured core locations in the Concept 2 laboratory bridge corresponded with the origin and sign convention utilized for the placement of the instrumentation.

Table 5.4.3: Summary of maximum height and width of cracks measured in core specimens from the Concept 2 laboratory specimen

Specimen	*x*-Coordinate of Core (in.)	*y*- Coordinate of Core (in.)	Diameter of Core (in.)	Maximum height of crack[1] (in.)	Maximum width of crack[2] (in.)
C2-S1-1	193	0	3.75	NO[3]	NO
C2-S1-2	189	0	3.75	2.25	0.003
C2-S1-3	193	+12	3.75	3.5	A
C2-S1-4	193	-12	3.75	NO	NO
C2-S1-5	76	0	3.75	NO	NO
C2-S1-6	80	0	3.75	NO	NO
C2-S1-7	76	+12	3.75	NO	NO
C2-S1-8	76	-12	3.75	NO	NO

[1]The height of crack was measured from the reference line, defined in Figure 5.4.1; only "upward" values are recorded in this table
[2]The width of crack was documented by crack classification, as defined in Table 5.4.1
[3]"NO" represents "No reflective cracks observed"

Reflective cracking was observed in one of the four cores located over the joint in the Concept 2 laboratory bridge specimen, and was located in the east half span (C2-S1-2). In addition, a vertical crack was also observed at the vertical CIP-precast web interface (C2-S1-3), also located in the east half span. It is unclear if the discontinuity observed at this location was truly a crack, or was separation of the precast web and CIP concrete due to poor bond, or was simply an illusion due to the interface between the two types of concrete, however it was expected that cracking or separation at the vertical web interface would relieve transverse stresses at the longitudinal joint, which would likely hinder crack growth over the joint, however cracking was measured extensively near the east quarter point of the span, suggesting that the vertical web face cracking was unlikely. Furthermore, the fact that no cracking or separation of vertical CIP-precast web interface at the west quarter point suggested that it was unlikely that the lack of observed cracking indicated by the instrumentation over the joint in the west half span of the Concept 2 specimen was due to cracking at the vertical web interface and subsequent relief of transverse stresses near the longitudinal precast joint.

The largest transverse strain measured during load testing on the Concept 2 laboratory bridge was approximately 256 με, measured near midspan, which over the 4.7 in. gage length of the concrete embedment resistive gage would correspond to a maximum crack width of approximately 0.0014. This was a strain measured under loading to simulate the environmental effects. A likely reason that the cracks were not identifiable with the microscope was because the cores were removed from the bridge upon unloading and examined under no load conditions.

5.4.2. Visual Inspection of Internal Surfaces after Sectioning the Laboratory Bridge Specimens by Means of Saw Cutting

Capacity constraints of the overhead crane system present in the University of Minnesota Structures Laboratory necessitated that both the Concept 1 and Concept 2 laboratory specimens be split into segments of no more than 30,000 lbs in total weight for removal. This created an opportunity to visually inspect the internal cut faces of the specimens for signs of cracking. For this reason, the laboratory bridge specimens were segmented such that the locations of the cuts were near locations of expected cracking, as determined via the data analyses.

The two span Concept 1 laboratory bridge specimen was cut into a total of eight sections, as shown in Figure 5.4.2.

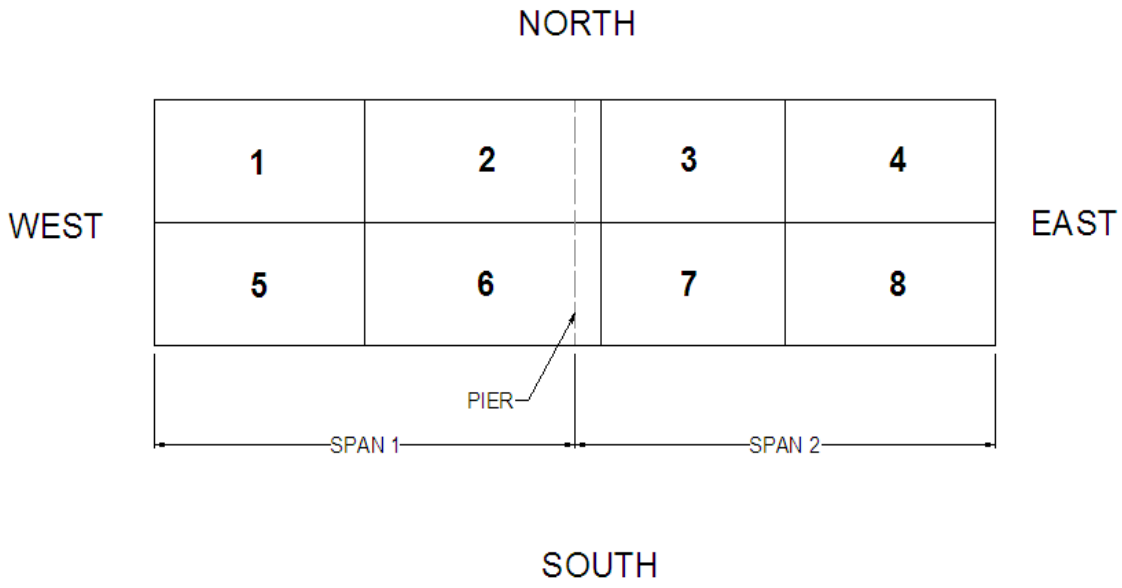

Figure 5.4.2: Concept 1 laboratory bridge specimen partitioning for saw cutting procedure

The longitudinal saw cut, which ran the length of the Concept 1 laboratory bridge specimen was nominally located directly through the precast joint, though drift of the saw during the cutting process caused the cut to vary between +/- 1 in. to either side of the precast joint. Unfortunately, the location of the cut line near the precast joint allowed for the possibility of the saw kerf to remove the evidence of reflective cracking in the section.

No signs of reflective cracking were observed on any of the cut faces in the Concept 1 laboratory bridge specimen, despite the use of a wetting and drying process in the region where reflective cracking was expected (i.e., the precast trough region) in which water was sprayed on the surface and allowed to air dry. This process was expected to highlight small cracks, where the ingress of water into the cracks would emphasize any cracking on the cut surfaces.

The vertical and horizontal interfaces between the precast concrete and CIP concrete however tended to feature unique characteristics. In the case of the horizontal precast – CIP interface, delamination of the PC flanges from the CIP concrete was observed, as shown in Figure 5.4.3. This documented evidence of delamination at the horizontal interface was observed in all cross-sectional cuts, regardless of the presence of the smooth or roughened precast flange. No evidence of delamination or cracking was observed at the vertical PC web interface on any of the cut surfaces of the Concept 1 laboratory bridge.

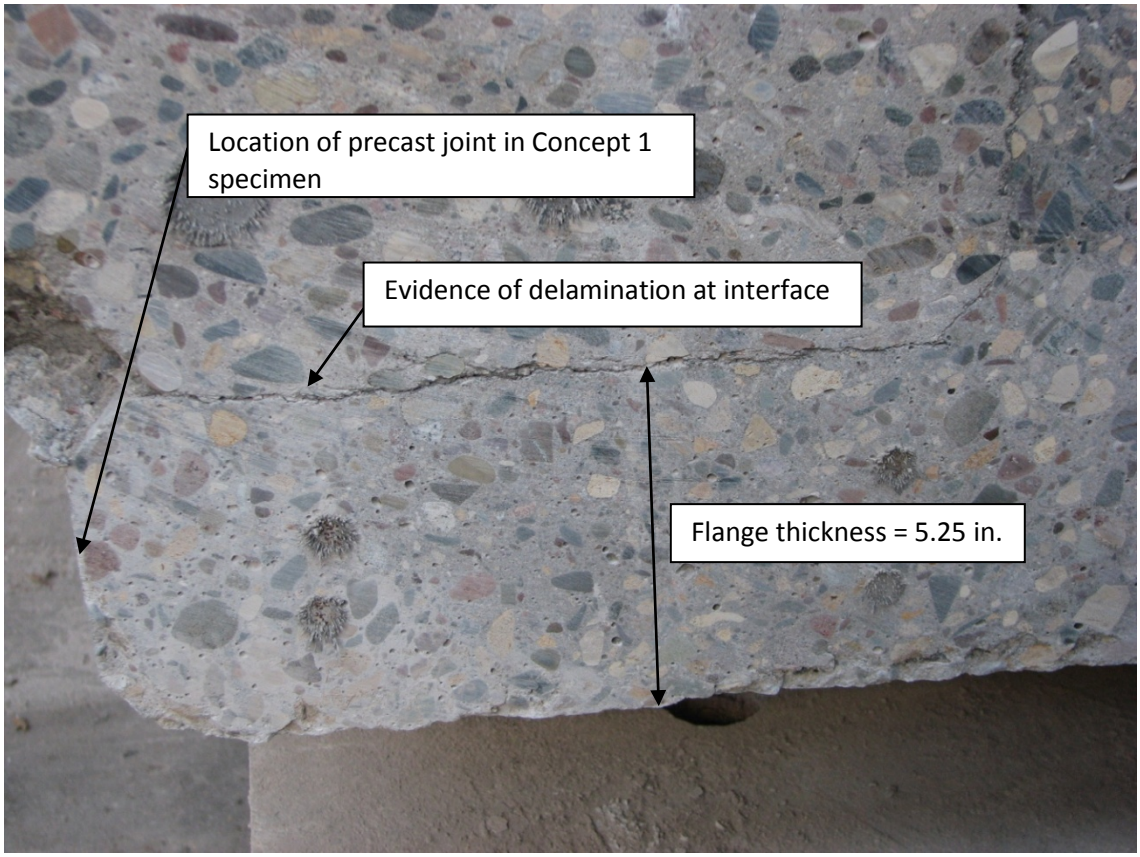

Figure 5.4.3: Delamination at the PC – CIP interface in the East transverse face of section number 7 of the Concept 1 Laboratory bridge specimen

The Concept 2 laboratory bridge specimen was similarly sectioned to accommodate removal from the laboratory. The cutting plan for this specimen included a total of three transverse cuts, at each quarter point of the span. Recall that the quarter points of the span coincided with the locations of the loading during the tests. The cutting plan and numbering convention is shown in Figure 5.4.4.

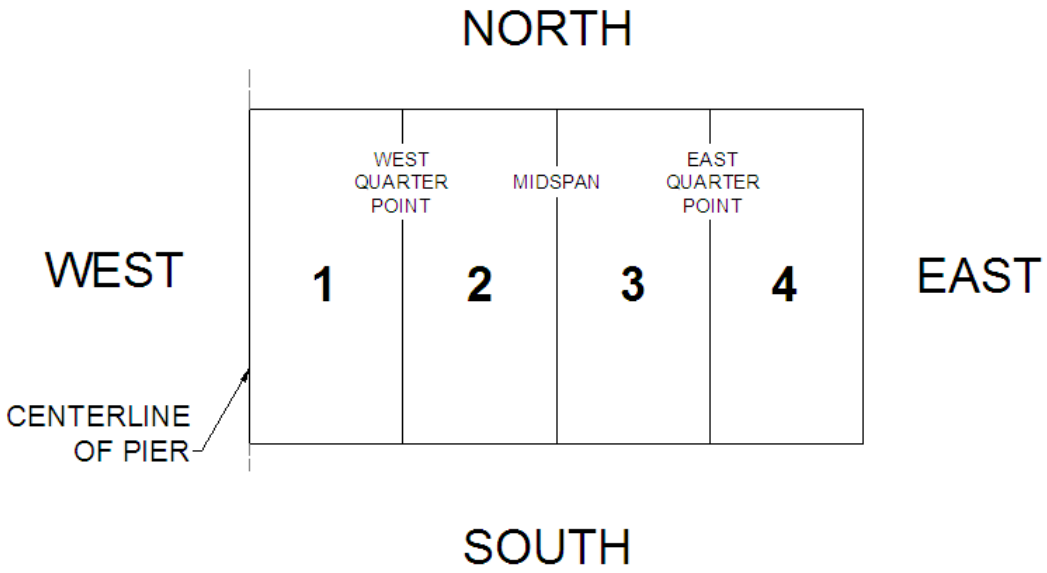

Figure 5.4.4: Concept 2 laboratory bridge specimen partitioning for saw cutting procedure

Evidence of reflective cracking was not observed in any of the cross sections in the Concept 2 laboratory bridge specimen. As observed in the Concept 1 laboratory bridge specimen, some delamination of the horizontal PC – CIP interface was observed at midspan on both the west face of panel 3 and the east face of panel 2, as illustrated in Figure 5.4.5. In addition, a diagonal crack was observed on the east face of panel 2 originating near the precast flange interface and propagating towards the corner of the precast section, as shown in Figures 5.4.6 and 5.4.7. The crack was measured to be approximately 0.006 in. As discussed in Section 5.4, cracking was observed in the east quarter of the Concept 2 laboratory bridge north of the joint via the core analysis, though was not detected via the analysis of the cut faces at the corresponding location.

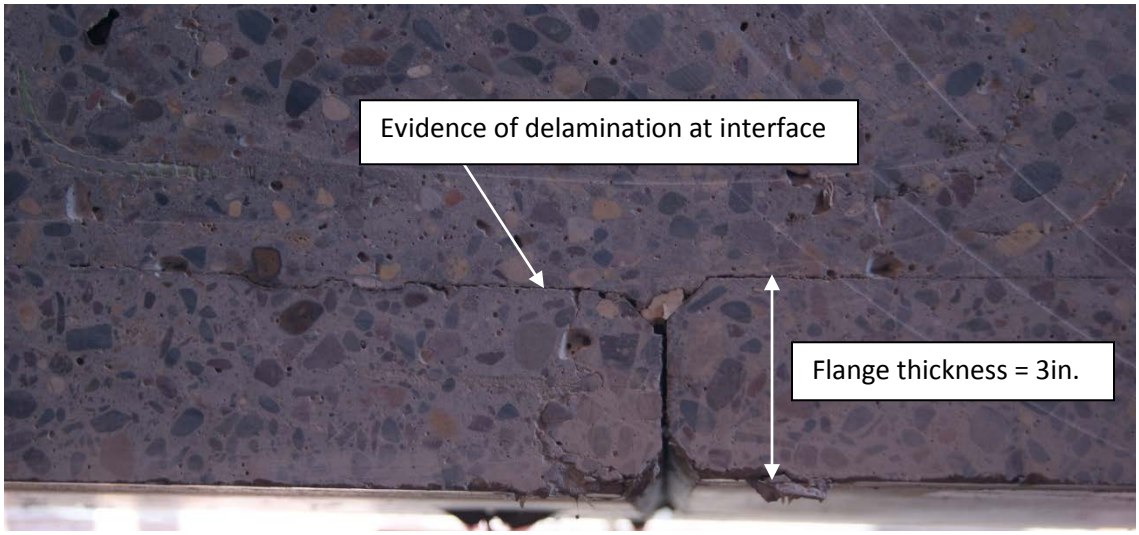

Figure 5.4.5: Delamination at the PC – CIP interface observed on the West face of section number 3 of the Concept 2 laboratory bridge specimen

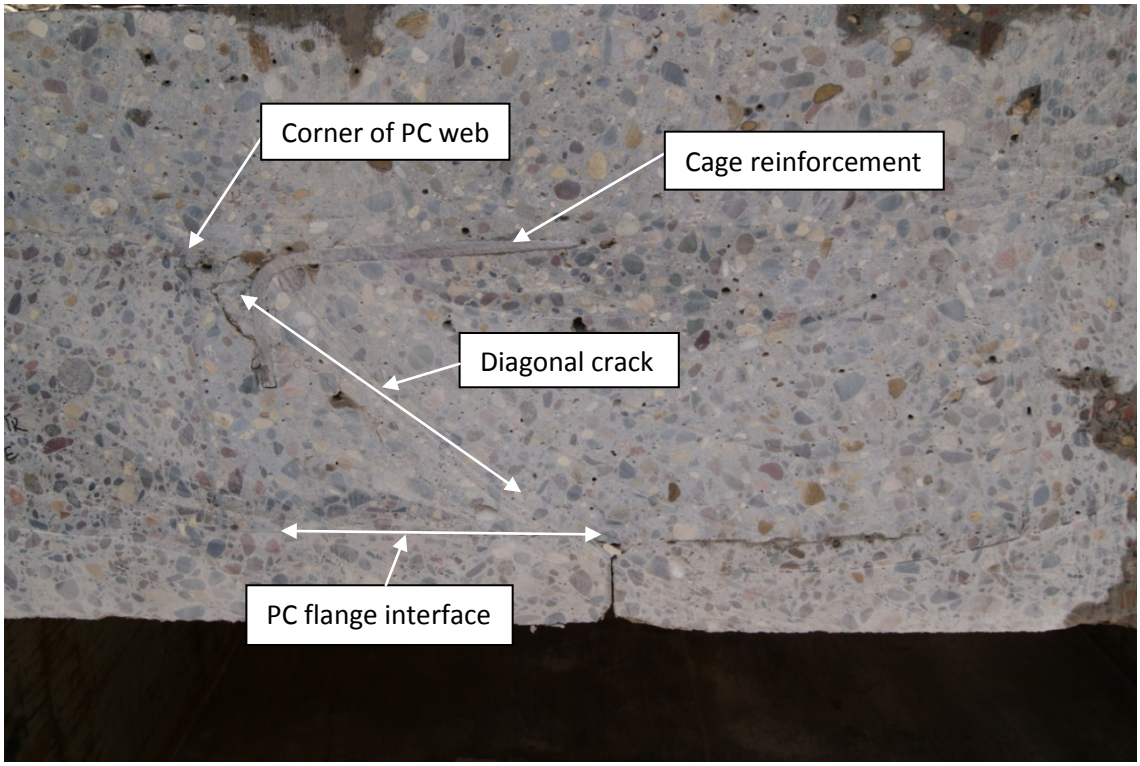

Figure 5.4.6: Evidence of diagonal cracking in the trough region on the east face of panel 2 in the Concept 2 laboratory bridge

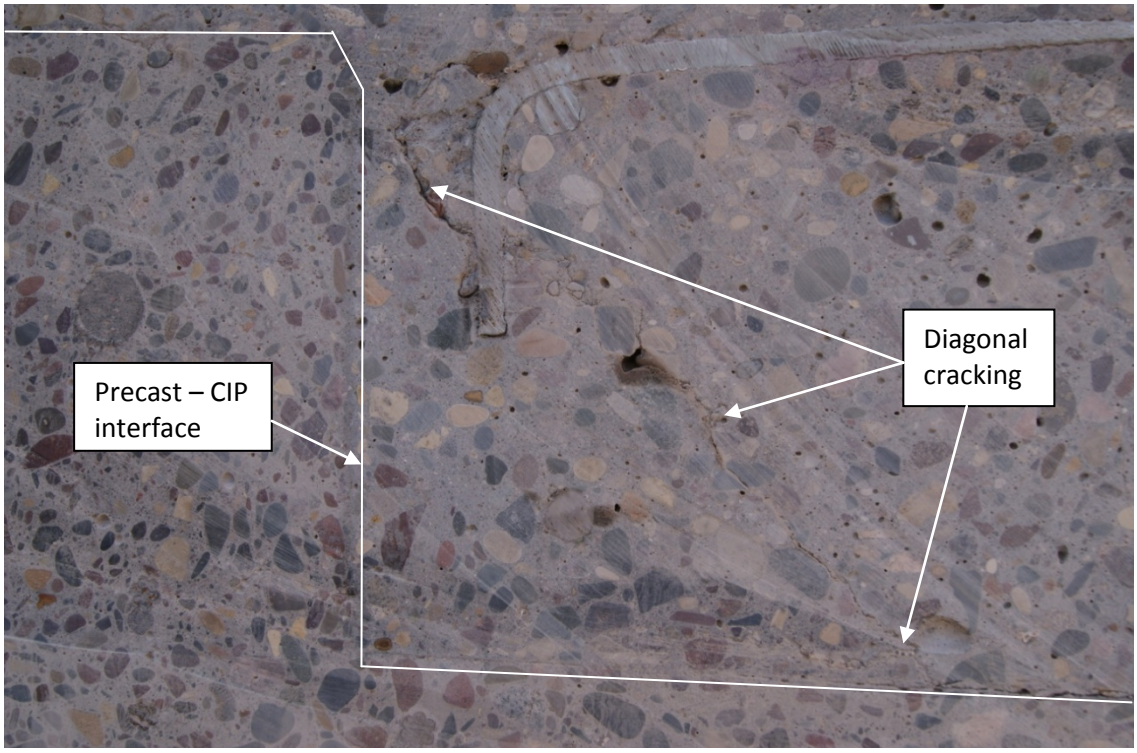

Figure 5.4.7: Close up view of diagonal crack identified on east face of panel 2 in the Concept 2 laboratory bridge

Chapter 6: Subassemblage Investigation of Crack Control Reinforcement

6.0 Introduction

Seven specimens were designed to investigate the effect of spacing, size, and placement of transverse reinforcement on the development and propagation of reflective cracking in the precast composite slab span system. This chapter describes the design and cracking behavior of these seven subassemblage specimens. Each specimen in this section is generally referenced by the specimen number and representative design parameter, i.e., Specimen 1, the first control specimen, is commonly referenced as: SSMBLG1-Control1.

6.1. Selection and Design of Laboratory Subassemblage Specimens

Each subassemblage specimen was selected to investigate a single attribute (e.g., spacing of transverse reinforcement, bar size, absence of reinforcement cage, specimen depth) that was expected to influence the crack control performance of the system. The specimens were designed as simply-supported panel elements with a 10 ft. span with the precast joint located at midspan, as illustrated in Figure 6.1.1. The widths of the specimens (i.e., in the direction parallel to the precast joint) ranged from 62.75 to 67.25 in. and was dependent on the transverse reinforcement spacing. Each specimen was designed such that the center of the transverse reinforcement closest to one face was located a distance of 3.5 in. from that face, defined as the origin face, except for in SSMBLG6-Frosch where the center of the hoop reinforcement was located 3.25 in. from the face. The specimen width was selected such that the opposite face, designated as the end face, was located a distance of half of the transverse reinforcement spacing from the center of the nearest transverse hooked pair, or in the case of SSMBLG6-Frosch it was the distance from the end face to the center of the nearest cage hoop. This configuration enabled the investigation of crack width both at a constant distance from the interior reinforcement, as well as an estimate at the maximum crack width, which was expected to occur at midpoint between adjacent bars.

The specimen supports were parallel to the longitudinal joint between the precast elements, rather than transverse to the joint, in order to flexurally crack the specimens along the joint. It was found during the testing of the first specimen, that the stiff flanges of the precast section rotated and caused delamination between the precast flange and CIP concrete, resulting in propagation of

a crack at the precast-CIP concrete interface. The test setup was modified to clamp the precast flanges to the CIP concrete a distance of approximately 1.25 in. from the longitudinal joint in both directions. This test setup with the clamping system was believed to more realistically emulate the field conditions because in a bridge system, the pier supports are normal to the longitudinal joint and would constrain the relative rotation between the precast flange tips and the CIP at the ends of the span.

The selection of the reinforcement details for each specimen was completed using a range of sources, primarily Frosch (2006), AASHTO (2010), and ACI (318-08). The design parameters of each subassemblage specimen are summarized in Table 6.1.1. The reinforcement ratio shown in Table 6.1.1 is the reinforcement ratio defined for crack control. This value accounts for all reinforcement traversing the longitudinal joint located near the bottom of the trough area near the precast flanges, which accounts for contribution from both the transverse hooked bars and the reinforcing cage. The reinforcement ratios for load transfer and crack control are discussed in detail in Section 5.1.

The subassemblage specimens were designed to provide insight into the relative performance of variations in the transverse reinforcement details for crack control and load transfer. For this reason, the specimen designs were limited to the transverse reinforcement selection. The primary depth of the precast members used for the subassemblage specimens was selected to be 12 in. to maintain consistency with the bridge specimens. The depth of the deck was minimized in an effort to reduce the transverse cracking moment of the specimens so that yielding of the transverse reinforcement immediately at cracking could be avoided. A minimum deck thickness of 2 in. was used to provide concrete cover over the deck reinforcement placed to resist potential shrinkage cracking at the surface. The reinforcement to control shrinkage cracking consisted of a total of five No. 3 bars, oriented perpendicular to the precast joint, in the deck region of each of specimen, in addition to eight No. 3 bars oriented parallel to the precast joint. The deck reinforcement was placed a clear distance of 1/4 in. from the precast members in all specimens except for SSMBLG3-HighBars, where the deck reinforcement was placed a clear distance of 3/4 in., due to a localized increase in the section depth away from the joint, which is discussed in more detail in Section 6.1.3. A photograph illustrating the deck reinforcement is shown in Figure 6.1.2.

Each subassemblage specimen was designed to include four sets of transverse hooked bars to ensure at least two sets of interior transverse hooked bars were present, while the cage reinforcement design and placement was varied among the specimens. The specific design

parameters of each subassemblage specimen are described in the following sections. The design and section calculations for each of the subassemblage specimens are given in Appendix F, which utilize the measured material properties, as documented in Section 6.4. Two spatial relationships were used throughout the construction and testing of the subassemblage specimens. The North direction was defined to originate from the origin face and point in the direction of the precast joint. In addition, a three-dimensional grid, with the origin located at the bottom of the section, at the precast joint, on the origin face, was used. The *x*-direction corresponded to the north direction and pointed along the direction of the precast joint and was therefore always positive. The *y*- and *z*- directions followed the right hand rule, thus *y* pointed in the west direction, with zero at the precast joint, and *z* pointed upwards, with zero at the bottom of the section.

Table 6.1.1: Subassemblage specimen design details

Specimen Identification	Width	Depth	Transverse Bars (Load Trans.)			Cage (Crack Control)			Max Spacing[2]	R/F Ratio[3]
	[in]	[in]	Size	Spacing	Depth[1]	Presence	Size	Spacing		ρ_{cr}
SSMBLG1-Control1	62.75	14	#4	18 in. OC	4 1/2 in.	Cage	#3	18 in. OC	9	0.0031
SSMBLG2-NoCage	67.25	14	#4	18 in. OC	4 1/2 in.	No Cage	0	0	18	0.0025
SSMBLG3-HighBars	62.75	14	#4	18 in. OC	7 in.	Cage	#3	18 in. OC	9	0.0031
SSMBLG4-Deep	62.75	18	#4	18 in. OC	4 1/2 in.	Cage	#3	18 in. OC	9	0.0022
SSMBLG5-No.6Bars	62.75	14	#6	18 in. OC	4 1/2 in.	Cage	#3	18 in. OC	9	0.0061
SSMBLG6-Frosch	64	14	#4	18 in. OC	4 1/2 in.	Cage	#3	4.5 in. OC	4.5	0.0052
SSMBLG7-Control2	62.75	14	#4	18 in. OC	4 1/2 in.	Cage	#3	18 in. OC	9	0.0031

[1]The depth of the transverse reinforcement was taken from the bottom of the precast section to the center of the reinforcement

[2]The maximum spacing was the maximum nominal distance between reinforcement traversing the longitudinal joint, regardless of type (i.e., transverse hooked bars or cage)

[3]The reinforcement ratio shown is that corresponding to crack control, see above and Section 5.1

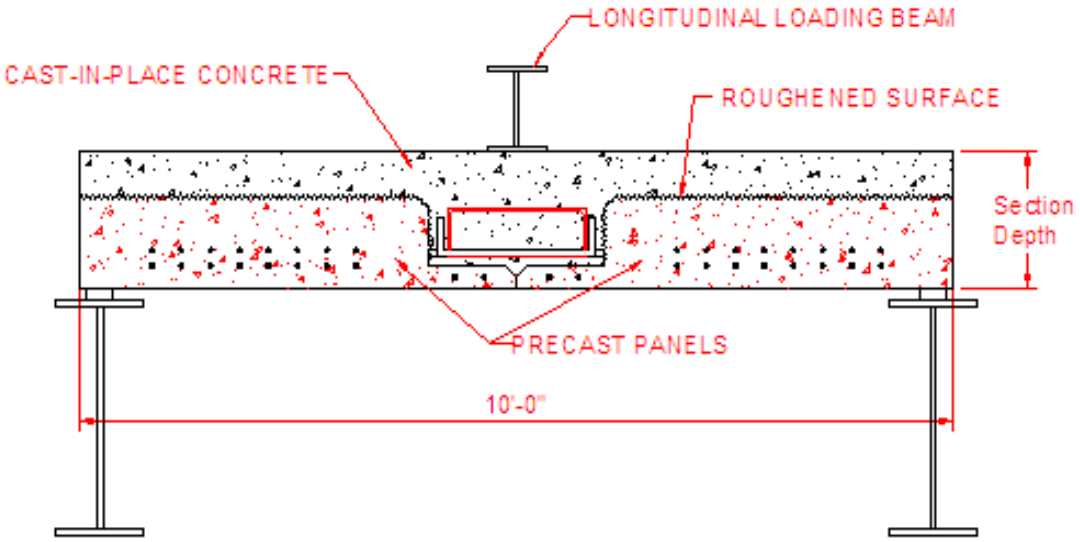

(a) Elevation view of subassemblage specimens

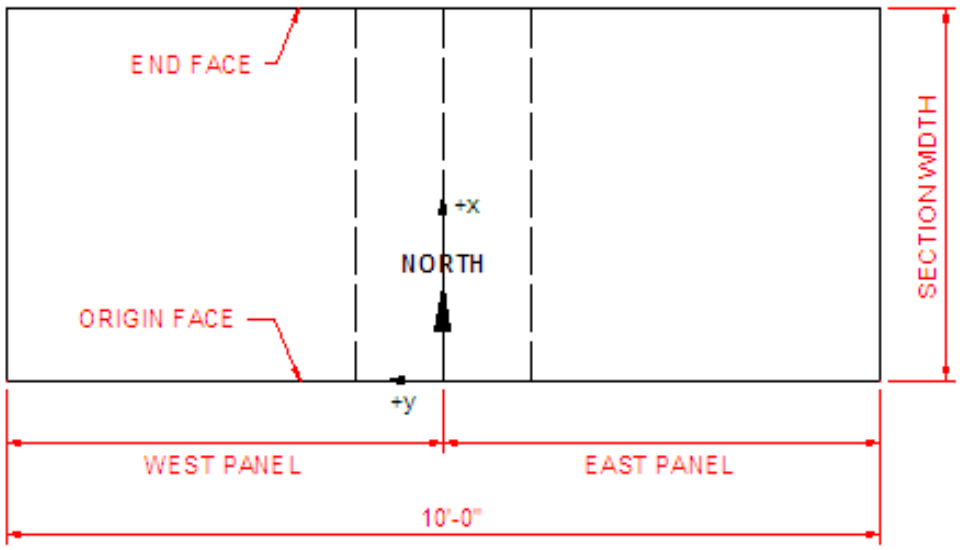

(b) Plan view and directional orientation of subassembalge specimens

Figure 6.1.1: Elevation and plan views of subassemblage specimen. The *x*-axis was aligned along the North direction and corresponded with the longitudinal joint. Positive *x* pointed North, positive *y* pointed West, positive *z*, was vertically upward

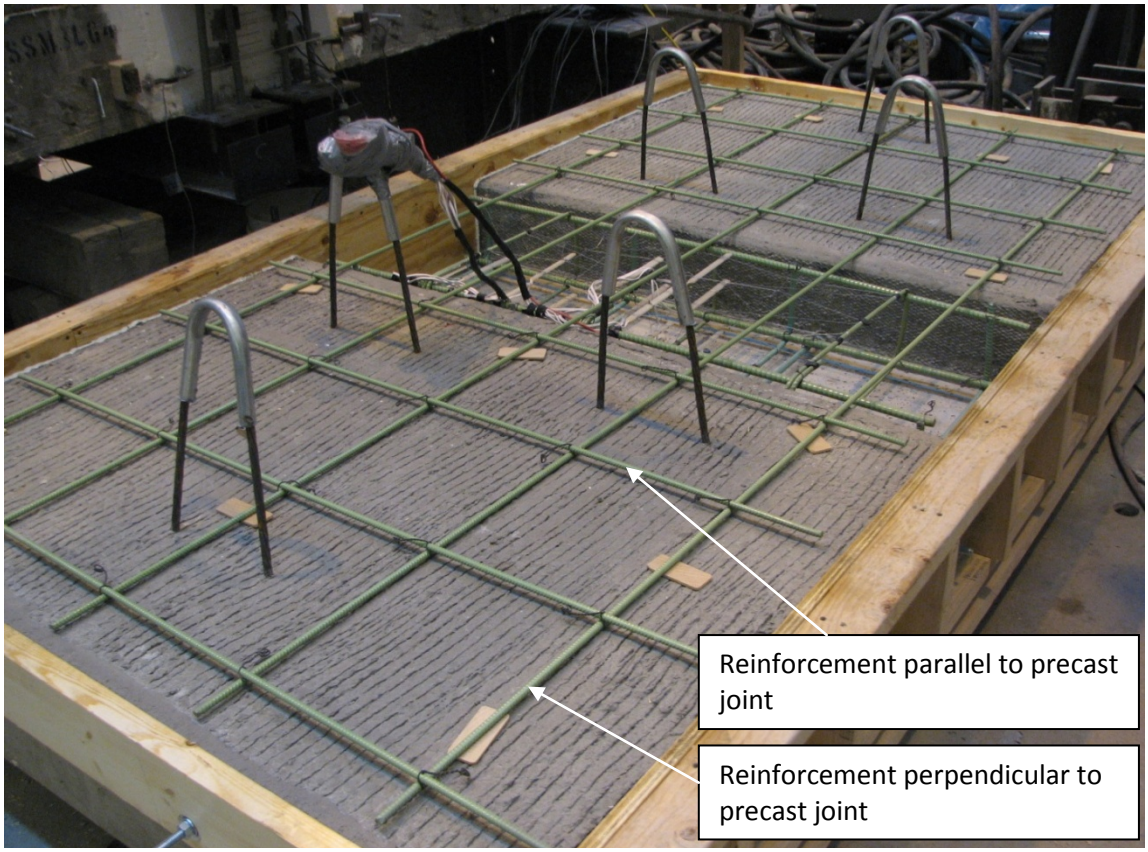

Figure 6.1.2: Photograph of deck reinforcement utilized for the subassemblage specimens

6.1.1. Subassemblage 1 – Control Specimen 1

The first subassemblage was deemed the control specimen because it had detailing similar to that of the transverse hooked reinforcement in the Concept 2 laboratory bridge specimen. The control specimen had a reinforcement ratio for transverse load transfer of 0.0010, while the cage and additional transverse hooked bar provided a reinforcement ratio of 0.0031 for crack control. This crack control reinforcement ratio was considered a practical lower bound value for the system when constructed with a cage, as constructability issues may arise if reinforcement smaller than No. 4 transverse hooked bars and No. 3 cage hoops are selected. The maximum spacing between transverse reinforcement was reduced to 9 in. by offsetting the cage reinforcement from the transverse hooked bars. The reinforcement layout for SSMBLG1-Control1 is shown in Figure 6.1.3. The cage reinforcement is shown in green. The portion of the transverse hooked bars protruding into the CIP concrete is shown in blue. For simplicity, the part of the hooked bars embedded in the precast elements is not shown.

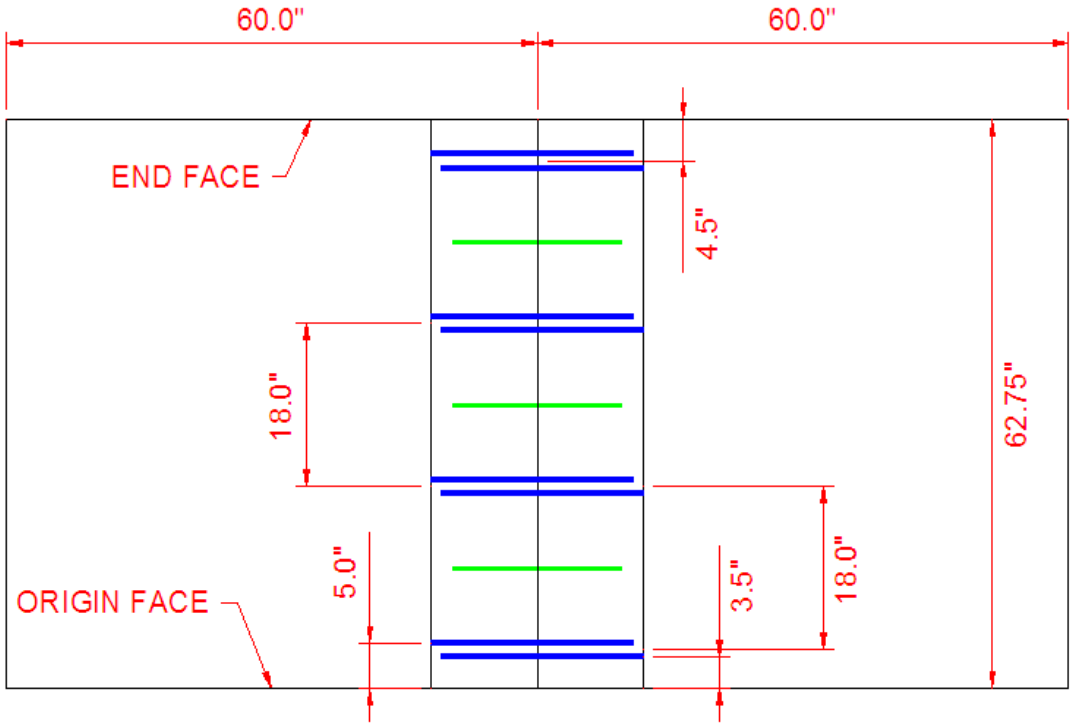

Figure 6.1.3: Layout for SSMBLG1-Control1, SSMBLG3-HighBars, SSMBLG4-Deep, SSMBLG5-No.6Bars, and SSMBLG7-Control2. Transverse hooked bars are shown in blue; cage reinforcement is shown in green

6.1.2. Subassemblage 2 – No Cage Reinforcement

The reinforcement cage was intended to provide additional reinforcement for reflective crack control above the longitudinal joint. In order to be able to evaluate the effectiveness of the presence of the cage with the test series, one of the specimens, SSMBLG2-NoCage, was designed without cage reinforcement. The overall width of the specimen was increased to 67.25 in. to allow for the end transverse hooked bar to be half of the maximum spacing (9 in.) away from the end face. The reinforcement ratio for transverse load transfer was equal to 0.0010, while the reinforcement ratio for crack control was equal to 0.0025, which corresponded to the lower bound reinforcement ratio for crack control investigated during the study. The absence of the reinforcement cage increased the maximum spacing to 18 in. The specimen layout is shown in Figure 6.1.4.

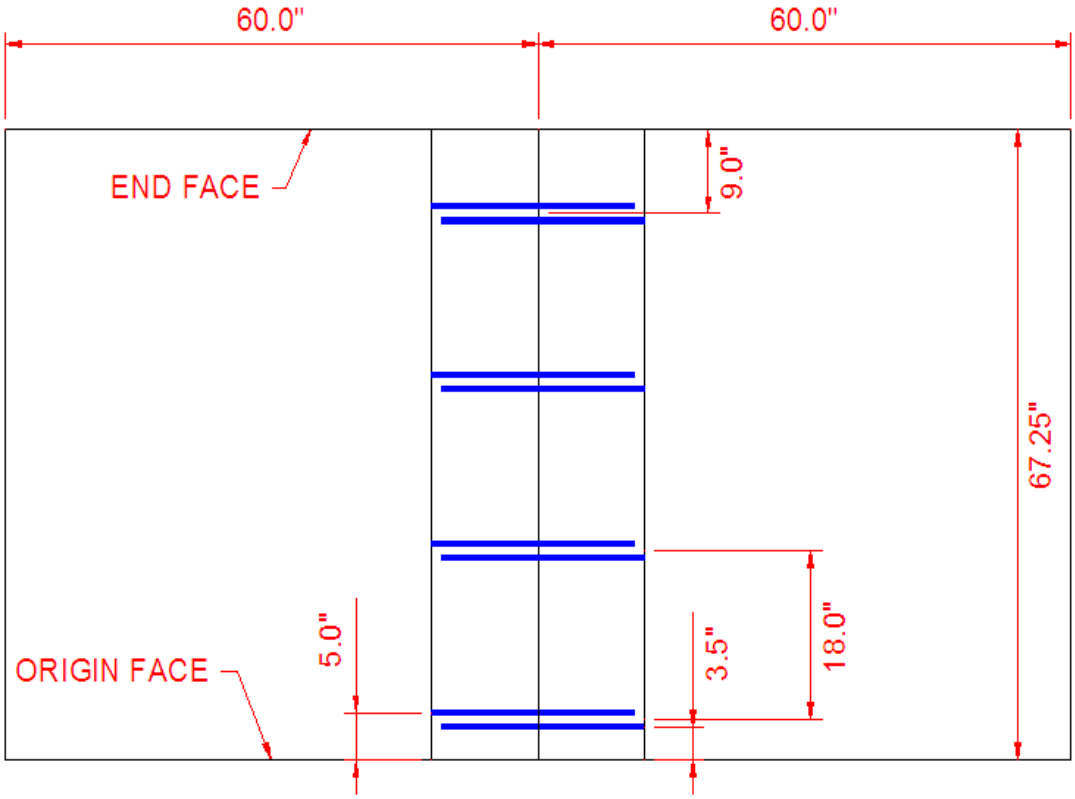

Figure 6.1.4: Layout for SSMBLG2-NoCage. Transverse hooked bars are shown in blue

6.1.3. Subassemblage 3 – Increased Distance Between Transverse Hooks and Precast Flange

The third subassemblage specimen was designed with the centroid of the transverse hooked bars located higher in the section than for the other specimens. In SSMBLG3-HighBars, the reinforcement was located 7 in. from the bottom of the section, which placed the hooked bars 55 percent higher than those in the other specimens. The proximity of the transverse hooked bars to the precast flange was expected to alter the performance of the system in two primary ways. The transverse moment of inertia of the cracked section decreased as the distance between the compression fiber and the reinforcement was decreased. The reduced moment of inertia of SSMBLG3-HighBars was expected to increase the curvature, and subsequently the stress demands on the transverse reinforcement of the section relative to the control specimen. Secondly, the lower in the section that the transverse reinforcement intercepts the reflective crack, the more effective that reinforcement was expected to be in controlling the crack. As a consequence, it was expected that SSMBLG3-HighBars would be less effective in controlling the

crack than the control specimen. The specimen layout for SSMBLG3-HighBars was identical to that shown in Figure 6.1.3 for the control specimen. The only difference was the vertical position of the transverse hooked bars and cage.

Because SSMBLG3-HighBars was constructed and tested first, and the capability of the 2 in. deep deck to develop adequate bond for the shrinkage reinforcement used in the deck was unknown, this specimen was constructed with an increased section depth away from the precast joint. The depth of the section near the joint was maintained at 14 in., and increased to 15-½ in. starting at 15 in. from the joint in both directions. An elevation view of SSMBLG3-HighBars with the increased depth of the deck is shown in Figure 6.1.5. The reinforcement ratios for crack control and load transfer were equal to 0.0031 and 0.0010, respectively.

Figure 6.1.5: Elevation view of SSMBLG3-HighBars and increased deck depth to provide additional cover for the shrinkage reinforcement in the deck

As previously noted, SSMBLG3-HighBars was tested first, and delamination of the precast-CIP interface was observed early in the test, before cracking was observed near the precast joint. Though subsequent use of a clamping assembly was anticipated to better emulate the expected restraint of a real structure, the presence of delamination at those locations greatly influenced the behavior near the precast joint, and subsequently, data collected during testing on this section is not considered to be reliable, and therefore is not included in the analysis of the data from the remaining specimens. Because little information was expected to be learned from the specimen after delamination of the joint, SSMBLG3-HighBars was utilized as a general test specimen to investigation the behavior of the overall subassemblage concept in the load frame. Therefore, the specimen was loaded in a wide range of sequences and load levels, so much so that the specimen failed by fracturing of the transverse hooks near the CIP - precast web interface at an applied load of approximately 111 percent of the predicted cracking load, or 32 kips. The specimen after failure is shown in Figure 6.1.6.

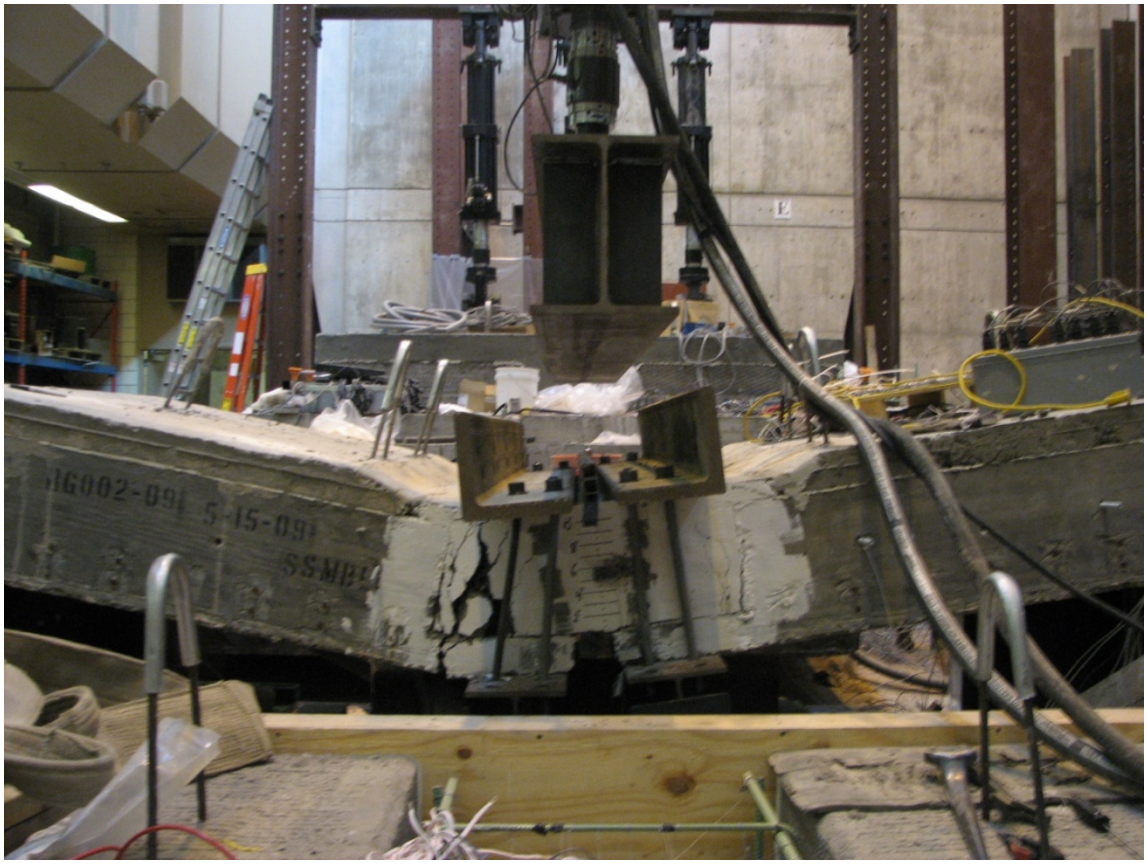

Figure 6.1.6: Failure of SSMBLG3-HighBars due to fracture of the transverse hooked reinforcement near the CIP - precast web interface

6.1.4. Subassemblage 4 – Increased Depth of Precast Section

As the span length of the PCSSS increases, the depth of the precast section also needs to increase in order to meet stress requirements at transfer and service. The 12 in. deep precast section was expected to perform well for moderate spans. The maximum practical span of the system was estimated to be approximately 65 ft., requiring a precast section depth of approximately 22 in. SSMBLG4-Deep was designed with an identical reinforcement plan as that of the control specimen, such that the effects of the deeper section could be investigated with an unchanged reinforcement design, although the depth of the cage stirrups was increased to the same relative depth as in the 12 in. deep precast sections (i.e., the top of the cage stirrup was aligned with the top of the precast web). The load transfer and crack control reinforcement ratios of the section were reduced to 0.0007 and 0.0012, respectively, due to the increase in the area of concrete considered in the calculation. The specimen layout of SSMBLG4-Deep was identical to that shown in Figure 6.1.3 for the control specimen.

6.1.5. Subassemblage 5 – Increased Transverse Hook Size

The size of the reinforcement used for transverse load transfer must be sufficient to provide adequate flexural capacity after cracking. Article 5.7.3.3.2 of the *2010 AASHTO LRFD Design Specification* requires that the nominal flexural moment capacity of the section be at least 120 percent of the cracking moment. No. 6 transverse hooked bars represented the minimum bar size that could satisfy this requirement while maintaining a hook spacing of 18 in. The specimen layout of SSMBLG5-No.6Bars was also identical to that shown in Figure 6.1.3. The cage remained unchanged from the control specimen; the only difference was that No. 6 hooked bars were used rather than No. 4 hooked bars. The reinforcement ratio for crack control and load transfer was 0.0033 and 0.0061, respectively, both of which represented the upper bounds investigated during the study.

6.1.6. Subassemblage 6 – Frosch Design Recommendations

Frosch et al. (2006) provided relevant design recommendations for crack control reinforcement in bridge decks which is summarized in Section 2.2. Frosch et al. provided guidelines for both the spacing and reinforcement ratio required for crack control via an experimental and numerical parametric study. The spacing limits were developed to provide sufficient reinforcement such that the crack widths would remain less than 0.021 in. The crack width selected represented a 1/3 increase in the maximum crack width of 0.016 in. suggested by ACI 224 (2001) for aesthetics. The authors stated that the increase in the selected maximum crack width was done due to the wide scatter generally observed in crack widths. The reinforcement spacing design proposed by Frosch et al. when grade 60 mild steel reinforcement was used is given in Eqn. (6.1.1).

$$s < 9 * \left(2.5 - \frac{c_c}{2}\right) \leq 9in \tag{6.1.1}$$

where c_c is the depth of concrete cover from the extreme tensile fiber of the concrete to the center of reinforcement in inches.

The depth of cover, c_c , considered in Eqn. (6.1.1) was calculated to the bottom of the CIP concrete above the flanges, thus disregarding the depth of the precast flange. This was deemed a reasonable assumption because of the discontinuity between the precast flanges along the longitudinal joint where the flanges in the adjacent precast panels abutted. The precast flanges themselves were reinforced as part of the design of the precast inverted-T sections.

Frosch provided a recommended reinforcement ratio for crack control reinforcement, as given in Eqn. (6.1.2). The reinforcement ratio was developed to ensure that sufficient reinforcement is present upon the introduction of cracking such that all tensile loads can be transferred through the reinforcing bars.

$$\rho = 6\frac{\sqrt{f_c'}}{f_y} \tag{6.1.2}$$

where *fc*' is the specified concrete strength and f_y is the specified reinforcement yield strength.

With the depth of cover assumed to be 1.5 in., the maximum spacing was determined to be the 9 in. bound of Eqn. (6.1.1), and with grade 60 reinforcement and a 28-day concrete compressive strength of 4000 psi, the reinforcement ratio for crack control reinforcement was determined to be 0.0063 from Eqn. (6.1.2).

The reinforcement design for SSMBLG6-Frosch was selected such that the transverse reinforcement for load transfer (i.e., hooked bars protruding from the precast webs) was identical to that of the control specimen. Therefore, the cage reinforcement was modified to meet the above limits; however the cage bar size was maintained at No. 3 hoops to provide consistency among the specimens. The hoop spacing for the SSMBLG6-Frosch specimen was provided at 4.5 in. because an even multiple of 18 in. (i.e., the hook spacing) was desired, primarily to avoid interference between the cage and transverse hooked reinforcement, and a cage design requiring closer spacing, or spacing that caused intermittent interference between the cage and hooked bars, would be expensive and difficult to implement in the field. The 4.5 in. spacing was well within the maximum 9 in. spacing recommended by Frosch et al. (2008), but because of the design constraints associated with spacing the cage reinforcement to facilitate constructability, the reinforcement ratio for crack control provided in the SSMBLG6-Frosch specimen (i.e., 0.0052) was smaller than that strictly required by Frosch et al. (2008) (i.e., 0.0063 for Grade 60 steel and a concrete compressive strength of 4,000 psi). The specimen reinforcement ratio was considered sufficient to explore the increased benefit of the design recommendations provided by Frosch et al. (2008). The reinforcement ratio for load transfer was 0.0010. The specimen layout of SSMBLG6-Frosch is shown in Figure 6.1.7. It should be noted that the specimen SSMBLG5-No.6Bars had a reinforcement ratio (i.e., 0.0061) that was closer to that of the Frosch requirements.

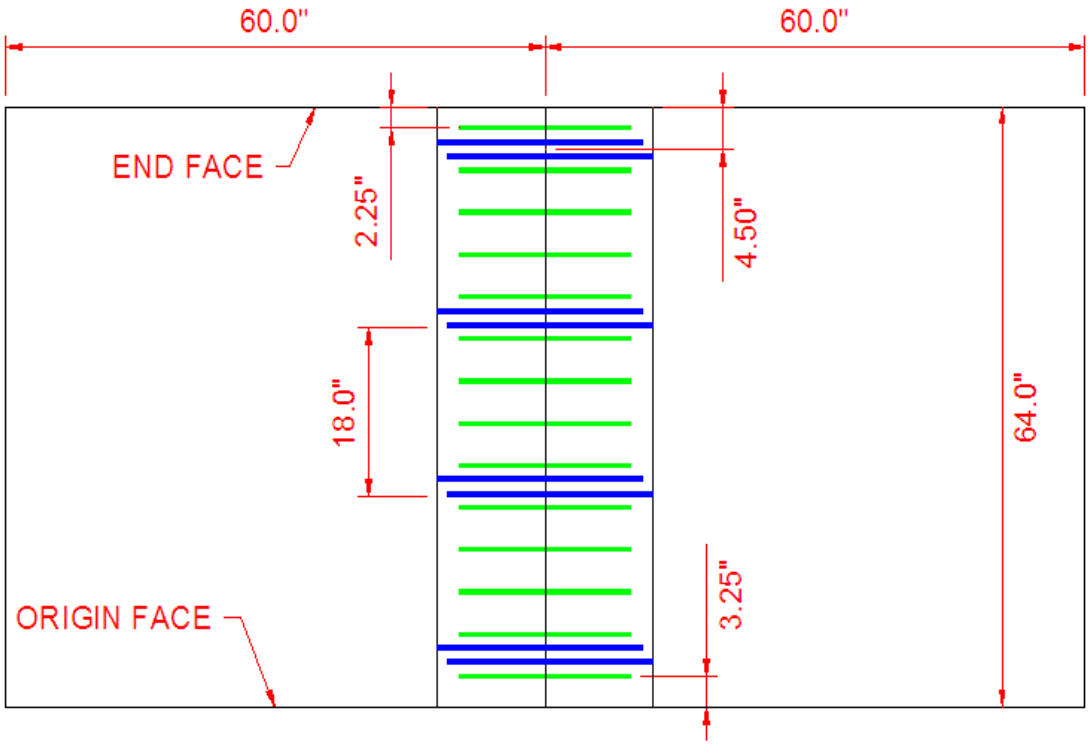

Figure 6.1.7: Specimen layout for SSMBLG6-Frosch. Transverse hooked bars are shown in blue; cage reinforcement is shown in green

6.1.7. Subassemblage 7 – Control Specimen 2

The seventh subassemblage specimen was originally designed to provide means to investigate a debonded flange surface. Observations of the performance of SSMBLG3-HighBars and SSMBLG5-No.6Bars, which were constructed and tested prior to the construction of the remaining five specimens, suggested that inadequate bond of the precast flange and CIP concrete could hinder the performance of the subassemblage specimens and limit their value by promoting the formation of a crack at the CIP-precast web interface. The intent of the subassemblage specimens was to investigate the crack control characteristics of the transverse reinforcement and cage above the longitudinal joint above the interface of the adjacent precast flanges. No instrumentation was located across the CIP-precast web interface, and only the transverse hooked bars could provide crack control at that location rather than the combined effect with the cage. For these reasons, the seventh subassemblage specimen was developed as a redundant control specimen. The reinforcement ratios for crack control and load transfer were identical to SSMBLG1-Control1, with values of 0.0031 and 0.0010, respectively.

The specimen geometry of SSMBLG7-Control 2 was identical to SSMBLG1-Control1, however the flange surfaces of this specimen had been patched to provide a smooth surface in an effort to minimize the bond at the interface before the decision to abandon the debonded specimen was made. This represented the only difference in the design and construction between SSMBLG7-Control2 and SSMBLG1-Control1. The specimen layout for SSMBLG7-Control2 is shown in Figure 6.1.3. The flange surface before and after the surface irregularities were patched is shown in Figure 6.1.8, which illustrates the representative level of smoothness present in this specimen.

(a) Prior to patching (b) After patching

Figure 6.1.8: Precast flange surface condition in SSMBLG7-Control2 before and after patching of the flange to provide a smooth surface condition

A manufacturing error was observed after the fabrication of the precast elements for SSMBLG7-Control2 was completed. The second set of transverse hooked bars, measured from the origin face, was constructed with the bars protruding from the adjacent precast members in reverse order, as shown in Figure 6.1.9. Because of this, two adjacent bars protruding from one precast member were spaced slightly larger than 18 in., and the two respective bars from the opposite member were spaced at slightly less than 18 in., however the center to center distance between adjacent sets of transverse hooked bars remained constant, at 18 in.

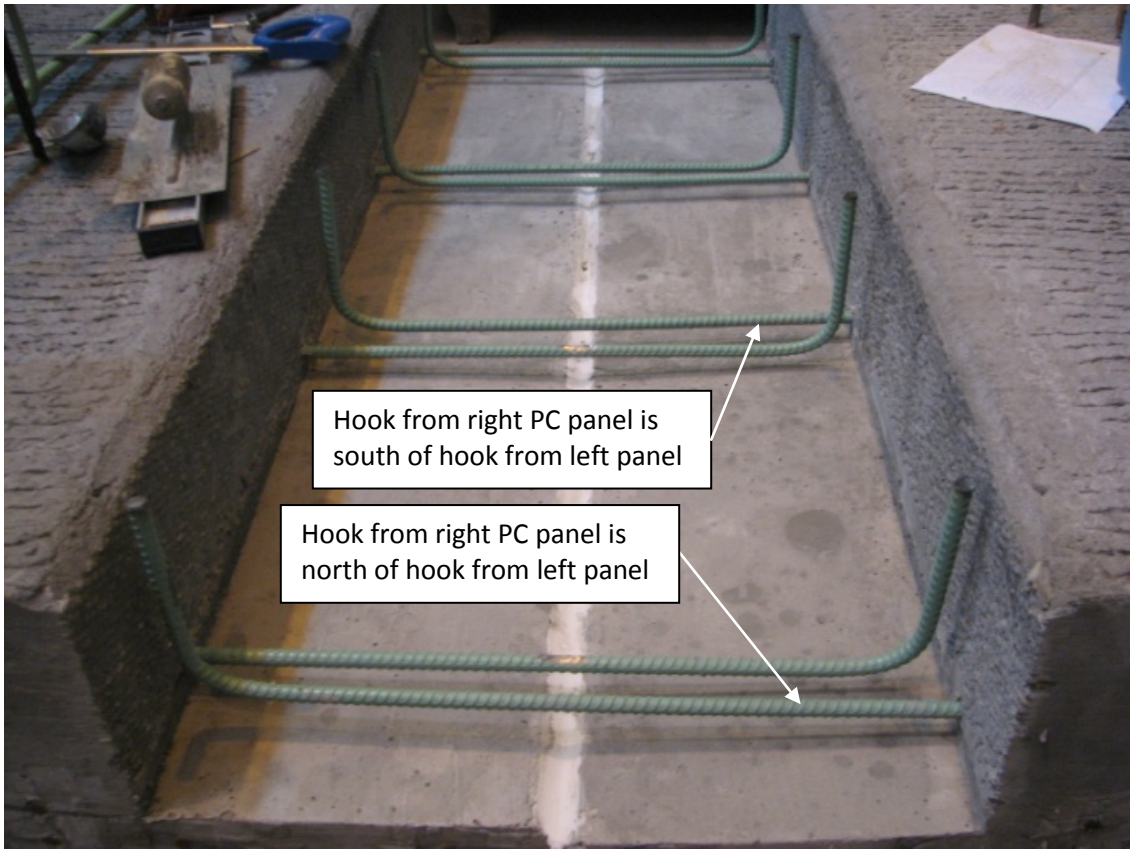

Figure 6.1.9: Photograph of SSMBLG7-Control2 to illustrate manufacturing error in placement of transverse hooked bars

6.2. Instrumentation of Subassemblage Specimens

Each of the seven subassemblage specimens were instrumented similarly, with the only exception being the presence of additional instrumentation in SSMBLG3-HighBars to provide adequate comparison among specimens. Each specimen had a concrete embedment VW strain gage oriented perpendicular to the joint near the middle of the specimen directly over the precast joint at the same vertical depth as the transverse hooked bars (i.e., a nominal distance of 4.5 in. from the bottom of the precast section). Because vibrating wire gages do not drift over time, these were selected to monitor the effects of shrinkage as well as provide an absolute value of strain at the joint to quantify any potential shrinkage or cracking during handling of the specimens in the laboratory (see Section 6.6). An analysis of the shrinkage strains measured via the concrete embedment VW strain gages is included in Section 6.6.1.

Each specimen contained a total of 17 concrete embedment resistive strain gages oriented perpendicular to the joint, near the joint. The 17 gages were split between two cross sections.

Nine of the gages were located near the middle of the specimen, with the remaining eight gages located near the origin face of the specimen. The instrumentation layout for the subassemblage specimens is shown in Figure 6.2.1. Each vertical layer of gages consisted of three concrete embedment resistive gages, with one centered over the precast joint and the remaining two centered 4.5 in. to either side of the precast joint.

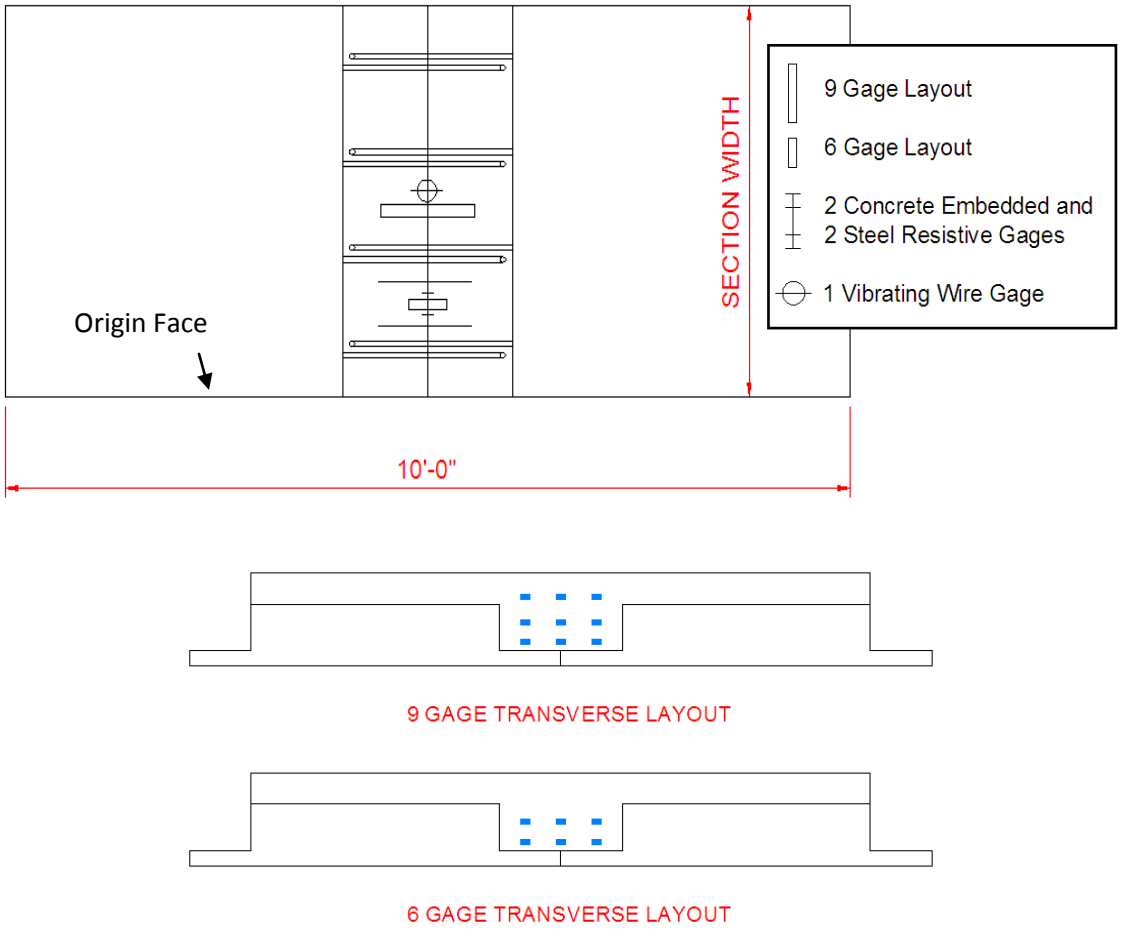

Figure 6.2.1: Instrumentation layout for subassemblage specimens. Overlap of gages not shown for clarity

The nine and six gage layouts were installed to track the height of the crack from the precast – CIP concrete interface above the flange. All instruments in the nine and six gage layouts were 120 mm concrete embedment resistive strain gages. The bottom three strain gages were located at the same depth as the transverse hooked bars. The second layer was located midway through the depth of the reinforcement cage, while the third layer, where present, was located at the top of the reinforcement cage. The additional instrumentation near the origin face included two 60 mm

concrete embedment resistive strain gages oriented perpendicular to the joint, one to either side of the six gage layout; 60 mm gages were chosen for this location because they were available from a past project. A 1 mm strain gage was attached to the transverse hooked bar nearest the origin face with a second gage attached to the hooked bar located 18 in. away; both were located directly over the precast joint. The two resistive steel gages and three concrete embedment resistive gages across the joint allowed for the transverse strain to be measured at five locations between adjacent transverse hooked bars. The instrumentation at the origin face of SSMBLG7-Control2, which was representative of all specimens, is shown in Figure 6.2.2.

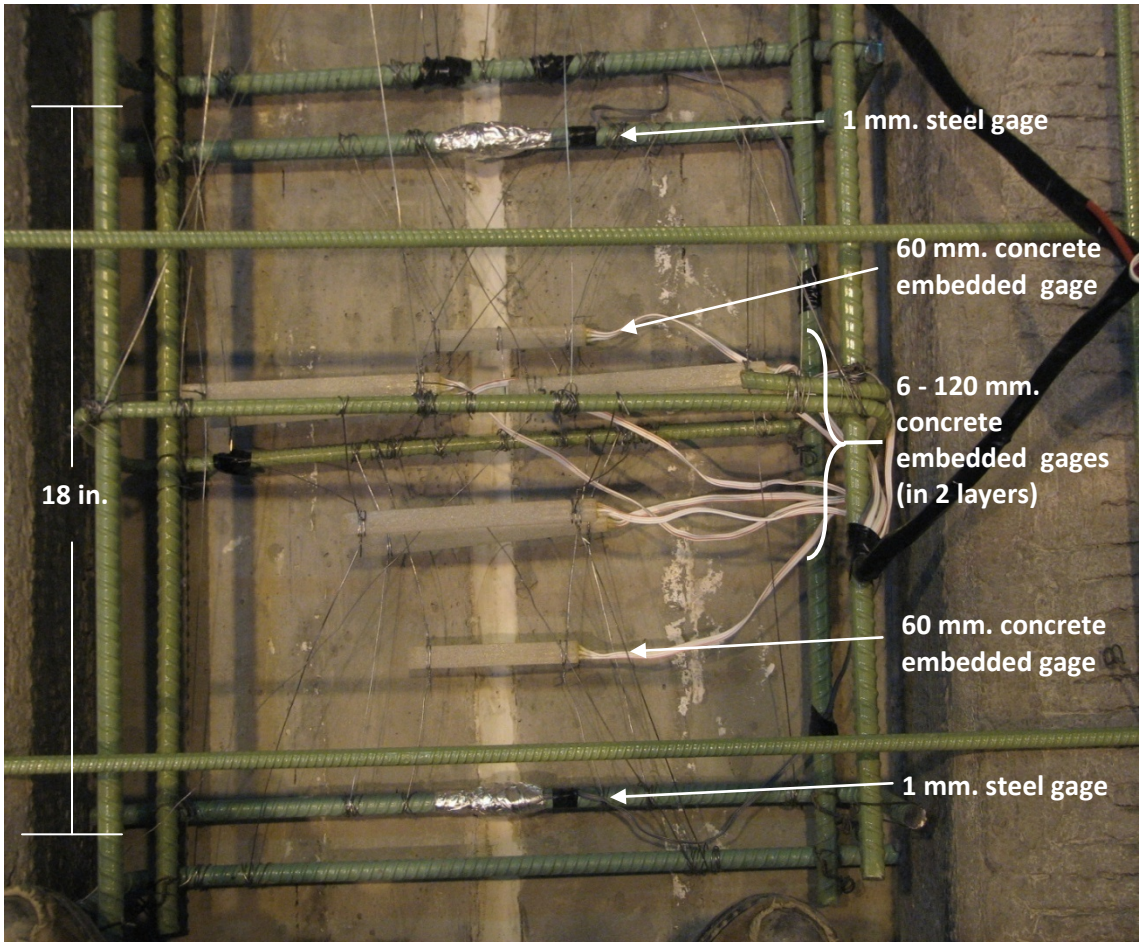

Figure 6.2.2: Plan view of instrumentation near origin face of subassemblage specimens

Two additional strain gages were added to SSMBLG3-HighBars to facilitate comparison among the specimens. The two additional strain gages were located 1.5 in. up from the precast flange centered over the joint, one at each instrumented cross section, to correspond with the lower level

of gages in the other specimens. The instrumentation naming scheme and nominal and as-placed locations for the instrumentation in each specimen are tabulated in Appendix G.

In addition to the embedded instrumentation, external LVDT's were utilized to monitor the joint opening. Four LVDTs were placed on both the origin and end faces of the specimen, and were located such that the center of the gage length of each LVDT was vertically aligned with the precast joint. The vertical locations of the LVDT instrumentation was measured from the bottom of the 45 degree, 1 in. chamfer near the horizontal precast-CIP interface, as shown in Figure 6.2.3. Three LVDTs were utilized to measure displacement locally near the precast joint, each with a nominal range of ±0.050 in., except for SSMBLG5-No.6Bars, which was instrumented with LVDTs with a nominal range of ±0.1 in. (referred to as LVDT050 or LVDT100 hereafter) and a relatively constant gage length of 9.5 in, which was measured from the center of the anchor block that secured the LVDT to the center of the corresponding anchor block to which the core was attached, and varied by no more than 1/4 in. The three LVDT050s were located a distance of -0.75 in. (Low LVDT), 2 in. (Mid LVDT), and 5 in. (High LVDT) from the bottom of the 1 in. precast chamfer. A fourth LVDT spanned between the adjacent vertical precast webs, which was selected to provide a measurement of the total opening associated with the vertical web interfaces, as well as entire CIP region. The fourth LVDT had a nominal range of ±0.5 in. (referred to as LVDT500 hereafter), a gage length of 30 ±1/4 in., and was located a nominal distance of 3 in. from the bottom of the precast chamfer.

Also included on both the origin and end faces was a vertical grid to assist with the documentation of cracking expected on those faces. The grid was also measured from the bottom of the precast chamfer, and consisted of solid horizontal lines in increments of 1 in., along with dots in increments of 1/2 in. The dots were located along a vertical projection of the precast joint. The LVDT layout and vertical grid on the origin face of SSMBLG6-Frosch, which was representative of both faces on all of the specimens, is shown in Figure 6.2.4.

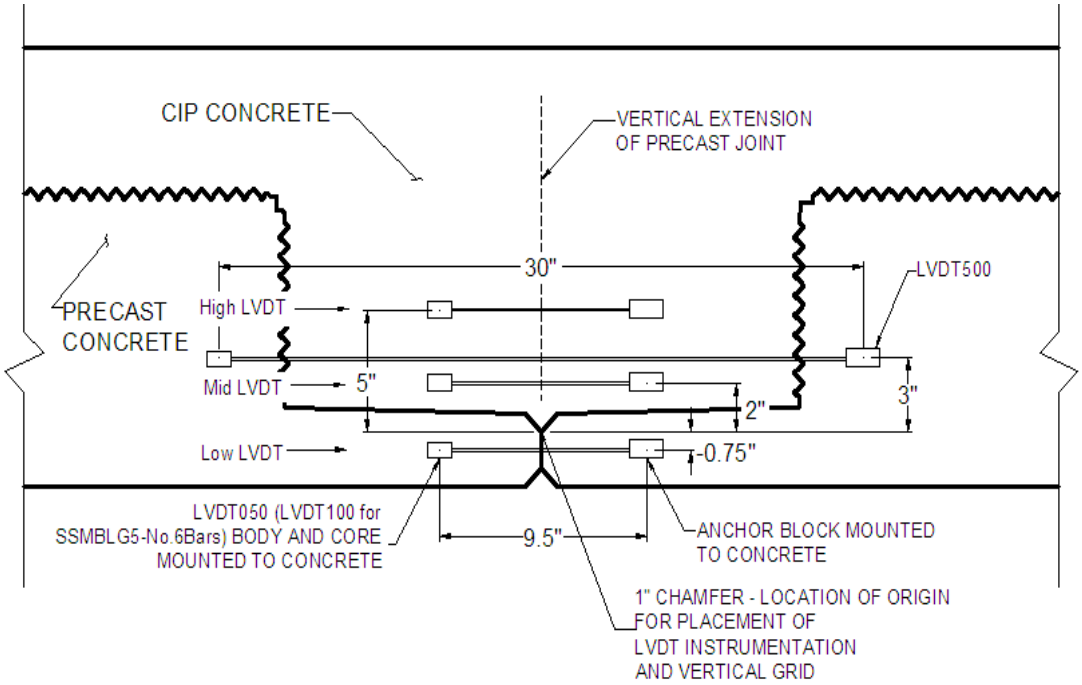

Figure 6.2.3: Location of LVDT instrumentation utilized for subassemblage tests. Vertical measurements for placement of instrumentation originated from bottom of 1 in. precast chamfer

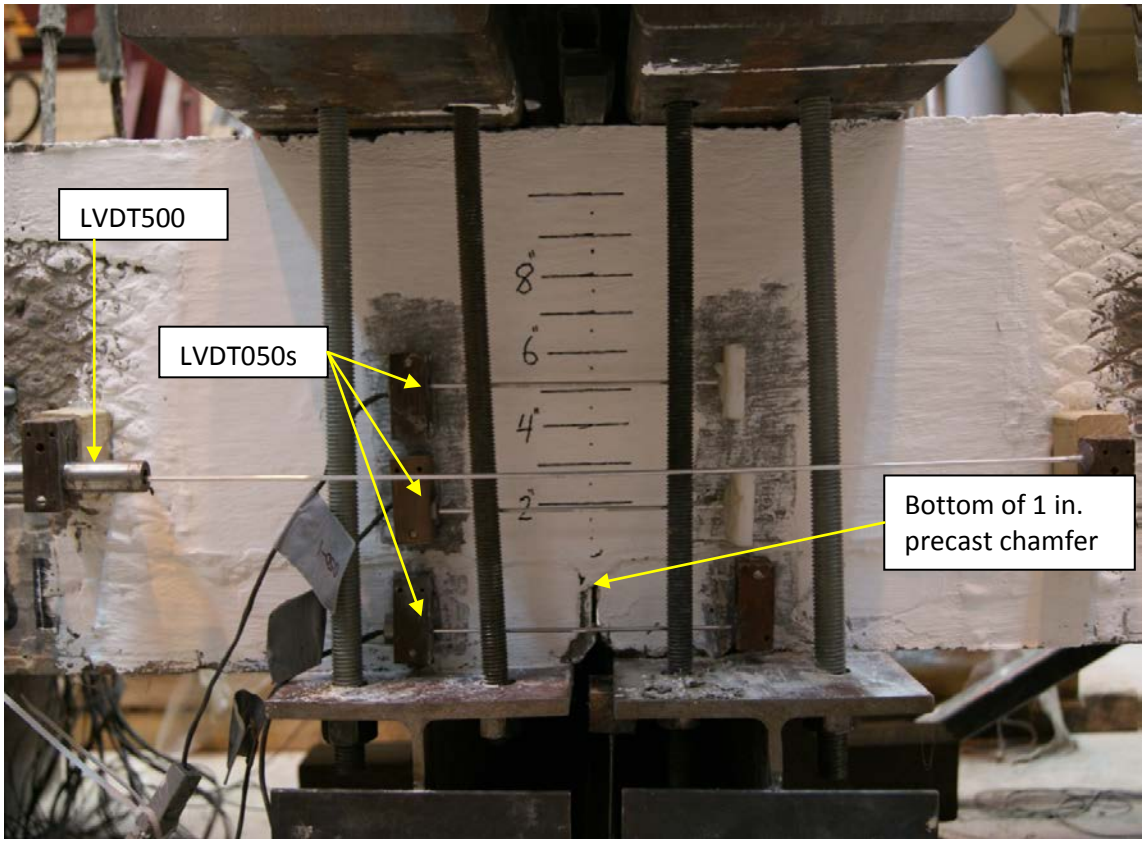

Figure 6.2.4: LVDT layout on origin face of SSMBLG6-Frosch. Vertical line above precast joint is shown by series of dots; measurements were taken from bottom of the precast chamfer

6.3. Clamping System

Each subassemblage specimen was considered to represent a portion of a PCSSS bridge. The specimens were essentially 5 ft. “long” bridge sections, two panels “wide”; however the panels were supported parallel to the longitudinal joint between the precast panels to facilitate investigation of the effectiveness of the transverse reinforcement in controlling flexural cracks that could be induced along the longitudinal joint with the test setup.

As described in Section 6.1, it was found during the testing of the first specimen, that the stiff flanges of the precast section rotated and caused delamination between the precast flange and CIP concrete, resulting in propagation of a crack at the precast-CIP concrete interface. The test setup was subsequently modified by developing a system to clamp the precast flanges to the CIP concrete on either side of the longitudinal joint. Although the test setup induced compressive forces through the depth of the section at the faces, it was believed to better emulate the field conditions because in a bridge system, the pier supports would be normal to the longitudinal joint,

preventing the relative rotation of the precast flanges with respect to the CIP in the trough above the precast flanges at the ends of the sections.

The vertical rods that connected the top and bottom steel members used to clamp the section were located a clear distance of between 2 and 3 in. from the face of the specimen. Consequently, curvature was induced in the longitudinal clamping members, which tended to concentrate the compressive force at the ends of the members. This served to better simulate the effects of restraint in the bridge system (i.e., clamping the subassemblage specimens near the ends simulated the effect of the bridge supports transverse to the longitudinal joint, and relieved the compressive stress across the subassemblage). An illustration of the clamping system, viewed in elevation perpendicular to the precast joint, is shown in Figure 6.3.1, while a cross section (i.e., section AA in Figure 6.3.1) parallel to the precast joint with the curvature of the clamping system shown exaggerated, is shown in Figure 6.3.2.

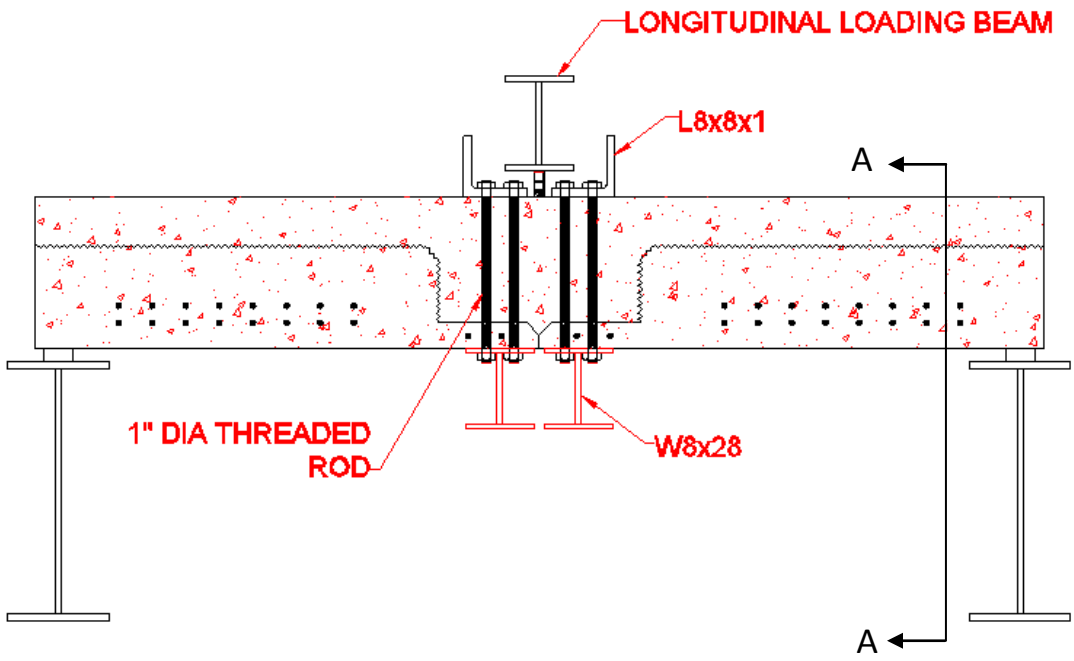

Figure 6.3.1: Clamping system developed to simulate restraint near joint region on subassemblage specimens. Section AA is shown in Figure 6.3.2

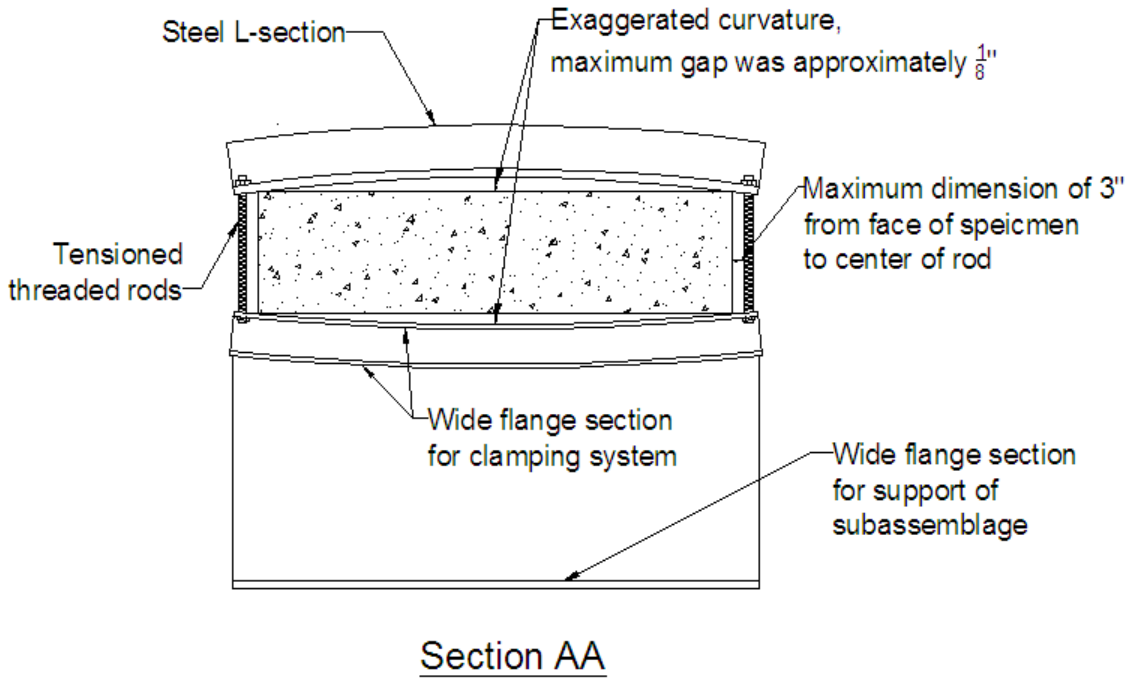

Figure 6.3.2: Section view of clamping assembly and subassemblage specimen, parallel to joint, illustrating exaggerated curvature of L-section (top) and wide flange section (bottom) due to eccentricity of tensioned threaded rods

The clamping system was developed with structural steel members, as shown in Figure 6.3.1 placed as near the precast joint as possible, while providing sufficient clearance for the loading strip between the clamps. A total of four 1 in. diameter threaded rods connected the upper and lower steel members near each face. The rods were tightened using an 18 in. long standard spud wrench. The concrete surfaces at the top and bottom of the specimens were adequately smooth and level such that the longitudinal steel clamping members were placed directly on the specimens as constructed without the addition of a grout bed.

As mentioned previously, the clamping assembly was not initially utilized during the testing of the first specimen, SSMBLG3-HighBars. The necessity for the clamping system was quickly realized, as the separation of the horizontal precast flange – CIP concrete interface and the vertical web interface was observed early in the test, shown in Figure 6.3.3. Cracking and/or separation at these locations greatly reduced the applicability and value of the tests because the crack was not able to develop above the longitudinal joint where the crack control reinforcement and instrumentation was located. In the field study of Center City PCSSS bridge (No. 13004) documented in Smith et al. (2008), instrumentation had indicated the initiation of reflective cracking above the longitudinal joint between the precast flanges. While instrumentation was not

present in that bridge at the vertical CIP-precast web interface, it would be unlikely that a crack would be present both at the joint and web face, because the presence of one crack would tend to relieve tensile stresses at the other locations. For these reasons, it was necessary to provide the clamping system to ensure that the boundary conditions imposed on the subassemblages were adequately representative of the conditions observed in the implementation of the PCSSS in the field. The clamped assembly fully installed with the HSS sections and neoprene bearing pad in place is shown in Figure 6.3.4.

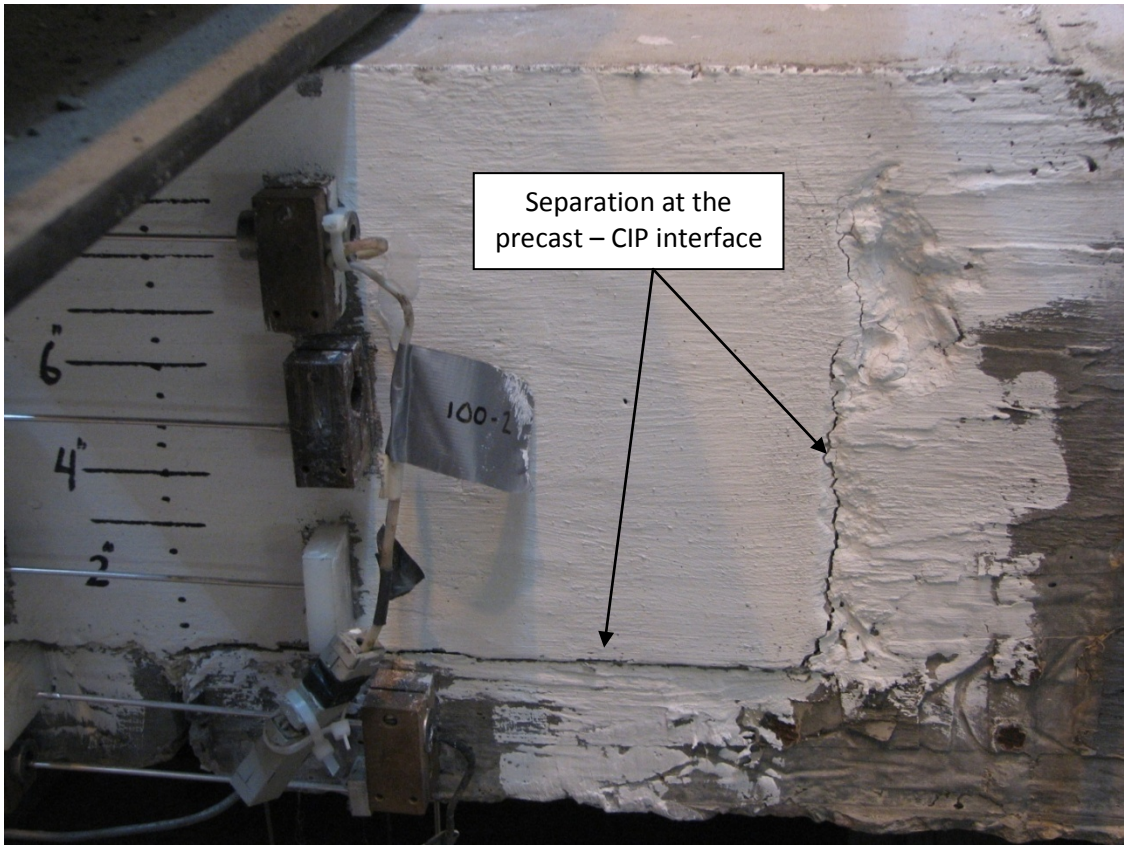

Figure 6.3.3: Separation of East precast section from CIP concrete during testing of SSMBLG3-HighBars before the implementation of the vertical clamping assembly

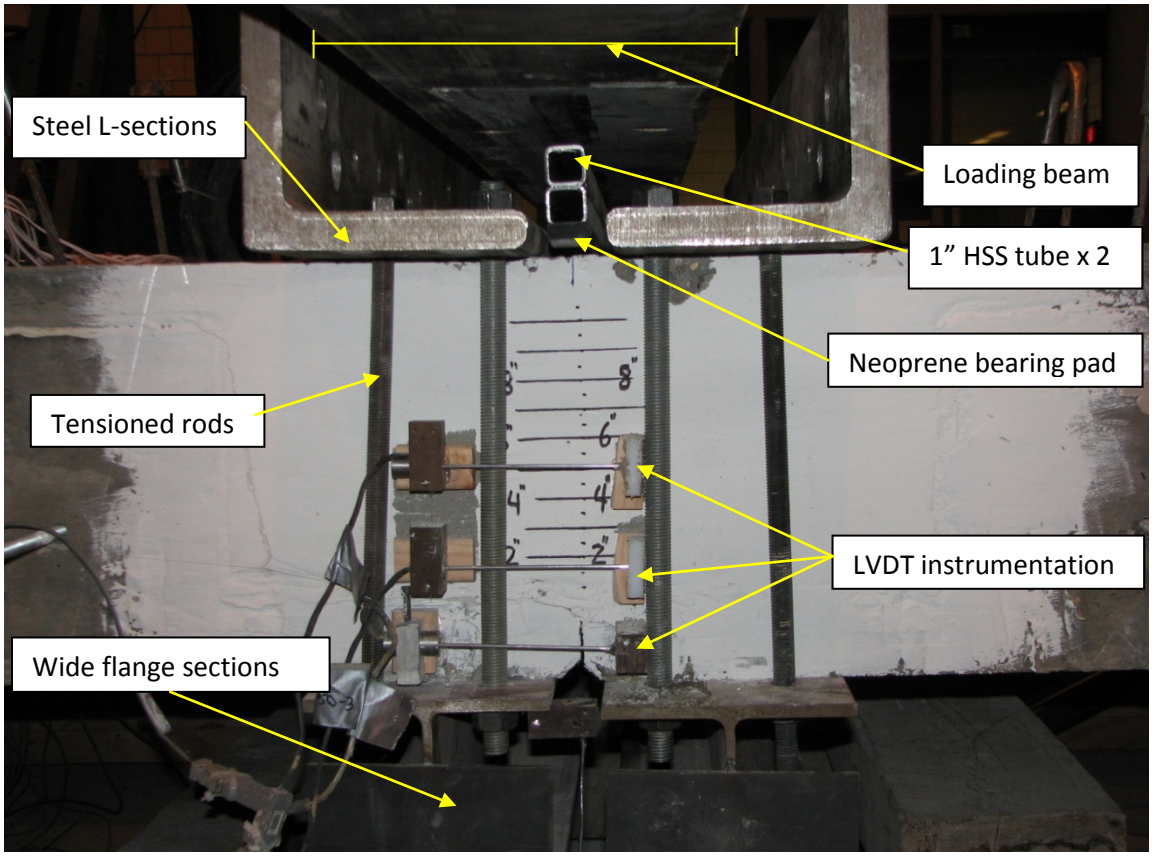

Figure 6.3.4: Clamping system used to provide rotational restraint of the precast members from the CIP concrete during the subassemblage tests and loading apparatus consisting of 1 in. HSS and neoprene bearing pad

6.4.Construction of Subassemblage Specimens and Material Properties

The seven subassemblage specimens were constructed in two groups. The CIP concrete for SSMBLG3-HighBars and SSMBLG5-No.6Bars was placed on July 27th, 2009. The remaining five specimens were cast on October 1st, 2009. The CIP concrete used in all specimens was Mn/DOT state mix 3Y33HE, which had a nominal 28-day strength of 4,000 psi and was provided by a single supplier.

The two specimens constructed during the first pour were built with concrete from two separate ready-mix trucks to allow for sufficient time between pours to finish each specimen. The vertical precast webs near the joint were not prewetted prior to placement of the CIP concrete.

The five specimens constructed during the second pour used concrete from a total of three ready-mix trucks. SSMBLG2-NoCage and SSMBLG6-Frosch used concrete from the same truck, while SSMBLG1-Control1 and SSMBLG7-Control2 used concrete from the second truck, and

SSMBLG4-Deep used concrete from the third truck. All the specimens were prewetted with water and allowed to reach a surface dry condition prior to the placement of the CIP concrete.

All seven specimens were moist cured for 8 days immediately after placement of the CIP concrete according to ACI 308.1-98 *Standard Specification for Curing Concrete* (ACI 308.1-98). The curing process consisted of the placement of prewetted burlap against the concrete surface, with a 4 mil plastic sheet above. The burlap was wetted in 12 hour increments to ensure the surface was continuously moist during the 8 day period.

The material properties of each specimen were measured at two key times. The concrete compressive strength was measured via 4x8 in. concrete cylinders 28 days after the concrete was placed and on the day testing was initiated for each specimen. Furthermore, the tensile strength of the concrete was measured both via 6x6x24 in. beams and 6x12 in. concrete cylinders on the first day of testing for each specimen. In addition, the modulus of elasticity of the concrete was measured on the first day of testing using 4x8 in. concrete cylinders. The measured material properties for the specimens when the CIP concrete was at an age of 28 days are included in Table 6.4.1. Note that the order of the specimens listed in the table is the order in which the specimens were cast; consequently, they are not listed in numerical order. For the sets of specimens cast with the same batch of concrete (i.e., specimens 1 and 7, and specimens 2 and 6), a single value is listed in the table for the 28-day strength. The material properties measured on the first day of testing for each specimen are given in Table 6.4.2. The order in which the specimens were tested was: SSMBLG3-HighBars, SSMBLG5-No.6Bars, SSMBLG1-Control1, SSMBLG6-Frosch, SSMBLG7-Control2, SSMBLG2-NoCage, and lastly SSMBLG4-Deep.

Table 6.4.1: Measured subassemblage CIP concrete material properties at an age of 28 days

Specimen #	Description	f_c' [psi]
3	High Bars	4714
5	No. 6 Bars	5201
1	Control 1	5670
7	Control 2	
2	No Cage	6238
6	Frosch	
4	Deep Section	6326

Table 6.4.2: Measured subassemblage CIP concrete material properties on first day of specimen testing

Specimen #	Description	CIP age on 1st day of testing	f_c [psi]	f_t -Beam [psi]	f_t – Split Cylinder [psi]	E_c [ksi]
1	Control 1	95 days	6552	840	594	4740
2	No Cage	122 days	6577	746	521	5633
3	High Bars	37 days	4726	678	497	3933
4	Deep Section	127 days	7151	757	546	4703
5	No. 6 Bars	53 days	5204	609	501	4112
6	Frosch	103 days	6898	806	529	5270
7	Control 2	113 days	7005	732	548	4194

The transverse hooked reinforcement utilized in the subassemblage specimens was tested using the exterior transverse hooks in the Concept 2 laboratory bridge. The No. 4 reinforcing bars embedded in the precast panels for the Concept 2 bridge and subassemblage tests was procured by County Materials at the same time, was of the same bar size, and was epoxy coated; therefore it was expected that the embedded reinforcement in the Concept 2 bridge adequately represented the embedded #4 bars in the subassemblage specimens. Three tensile tests were completed to measure the yield strength of the reinforcement, with average yield strength of approximately 70 ksi. Note that the reinforcing bars were specified as standard Grade 60 steel. Tensile tests were not conducted on the No. 6 bars.

6.5. Laboratory Testing Program

An extensive laboratory testing program was developed to investigate the performance of each subassemblage specimen. The primary concern regarding the design of the testing program was to create a testing plan that would not be heavily influenced by the age of the specimen or the differences in the material strengths and properties of each specimen at the time of testing. The primary objective of the testing plan was to provide a means to investigate the effectiveness of the transverse reinforcement above the longitudinal joint between the precast flanges in controlling the crack growth generated through both static and cyclic load tests. Therefore, the test plan was constructed to monitor crack growth, especially at loads above those which initiated flexural cracking near the joint.

In an effort to minimize the variations of the concrete strengths and other material properties on the results of the tests, the modulus of rupture of the CIP concrete in each specimen, measured on the first day of testing, according to ASTM C78-09 *Standard Test Method for Flexural Strength of Concrete (Using Simple Beam with Third-Point Loading)* (ASTM C78-09), was used to determine the predicted transverse cracking moment of the subassemblage specimen. The modulus of rupture of each specimen is repeated in Table 6.5.1 along with the respective predicted cracking moment, M_{crack} , and predicted cracking load, P_{crack} , for each specimen.

Table 6.5.1: Subassemblage specimen measured modulus of rupture and predicted cracking moment and load

Specimen #	Description	f_t [psi]	$M_{CR\text{-}pred}$ [in-kip]	$P_{CR\text{-}pred}$ [kip]
1	Control 1	840	1117	33.0
2	No Cage	746	1050	30.8
3	High Bars	678	872	28.9
4	Deep Section	757	1855	56.9
5	No. 6 Bars	609	851	22.7
6	Frosch	806	1121	32.2
7	Control 2	732	972	28.2

The testing plan for the subassemblage specimens was based on the load at which cracking was observed to occur. Because effects such as restrained shrinkage in the test specimens may have reduced the cracking load from the predicted value, loading was conducted in small increments, followed by cyclic loading, in order to capture the initiation of visual cracking. After the specimen was taken to each increased load level and held at the peak, the specimen was examined at each face (i.e., origin and end face) for evidence of visual cracking. After cracking was observed, the specimens were subjected to cyclic loading at a lower load level to investigate the stability of the crack (i.e., potential durability of the test specimens) under repeated loads. The specimens were subsequently subjected to increased levels of static load to grow the crack, and the process of cycling the specimen at a lower load level continued.

The specific testing plan, which was consistent for each specimen (with the exception of SSMBLG3-HighBars), consisted of an initial load to 15 percent of the predicted cracking load, $P_{CR\text{-}pred}$, followed by an increase of 5 percent of the predicted cracking load during each

subsequent load step. At each load step, the load was applied and removed at a quasi-static rate three times; followed by 1,000 cycles to the displacement that occurred concurrent with load applied at the current load step at a dynamic rate of 0.7 Hz via a displacement-controlled test. The displacement limits were selected such that the range of load that was applied at each load step was initially between 2 kips at the lower bound up to the load applied during the quasi-static loading at each step. A quasi-load controlled testing scheme was used in the initial cracking phases of the tests to better control the crack propagation. Upon observation of a visual crack at either the origin or end faces, the load was recorded as the observed cracking load, $P_{CR\text{-}meas}$, after which the specimen was subjected to 5,000 cycles of displacement-controlled loading to the displacement that occurred concurrent to the load level previously reached. As previously mentioned, displacement limits were selected such that the applied load was cycled between 2 kips and the target load at that particular load step. The specimens were subsequently subjected to an additional 2,000 displacement-controlled load cycles with the displacement limits selected such that they initially occurred concurrent with the "base" level load. The displacement limits were periodically adjusted during the completion of cyclic loading at each load step such that the applied load range was kept relatively constant; thereby producing a load-controlled type testing environment with the benefit of a controlled lower bound displacement to prohibit sudden collapse of the specimens. The base load was taken as approximately 55 percent of $P_{CR\text{-}meas}$ (i.e., "BASE" $\approx 0.55*P_{CR\text{-}meas}$), rounded to the nearest 5 percent of $P_{\text{CR-pred}}$, because the applied load values were tabulated and plotted as percentages of the predicted cracking load. The use of 55 percent of the observed cracking load was selected to provide an adequately small base level (i.e., small enough such that initial cracking was reasonably expected not to have occurred prior to exceeding the base level load) which would allow for the investigation of degradation of the specimen due to cyclic loading at the base load while not inducing large levels of strain.

The load was incremented above the observed cracking load, $P_{\text{CR-meas}}$, in load step increments of 5 percent of $P_{\text{CR-pred}}$ consisting of both quasi-static and 1,000 cycles of quasi-load-controlled fatigue load at each load step, until the crack length observed on either the origin or end face reached a length of 8 in., measured from the origin of the vertical grid on each face (i.e., the bottom of the chamfer at the precast joint, see Figure 6.2.3 for additional details). A total of 5,000 quasi-load-controlled cycles were then completed at a displacement consistent with the load required to grow the crack to a length of 8 in., and the base-level load was repeated. Load was then incremented until the maximum load, P_{max}, was achieved, which was selected as the lesser of: (1) a proportion of the predicted cracking load, taken as approximately 195 percent of $P_{\text{CR-meas}}$

(i.e., $P_{max} \approx 1.95*P_{CR\text{-}meas}$), rounded to the nearest 5 percent of the predicted cracking load, or (2) when delamination was observed at the vertical precast – CIP web interface. Because the subassemblage tests were designed to induce a maximum moment at the longitudinal precast joint, data measured near the precast joint after the observation of cracking or delamination at the vertical precast-CIP web interface was considered to be irrelevant. Therefore, P_{max} was selected based on when cracking was observed at the vertical precast-CIP web interface during testing on SSMBLG5-No.6Bars, which was at an applied load of approximately 195 percent of $P_{CR\text{-}meas}$. The maximum applied load, P_{max}, was then followed by 2,000 cycles of quasi-load-controlled loading at the base level. The loading procedure for an example specimen with a predicted cracking load of 40 kips is given in Table 6.5.2. The only specimen to deviate from this plan was the first one tested, SSMBLG3-HighBars, where the initial load step was 50 percent of the predicted cracking load, and the lack of the clamping assembly allowed separation at the precast flange-CIP concrete interface.

During each load step, visual observations were recorded. The crack width and general observations were documented after the application of the third quasi-static load cycle with the load applied. In addition, after the completion of all cyclic loading at a given load step, the crack widths and other observations were again recorded with the magnitude of load equal to that which was applied during the cyclic tests at that load step.

Table 6.5.2: Subassemblage loading plan for example specimen with predicted cracking load of 40 kips

Predicted Cracking Load $P_{CR\text{-}pred}$ = 40 k	Applied load when cracking was observed $P_{CR\text{-}meas}$= 24 k (= 60% of $P_{CR\text{-}pred}$)
Base ≈ 0.55*$P_{CR\text{-}meas}$ = 0.55(24 k) = 13.2 k = 33% of $P_{CR\text{-}pred}$ rounded to 35% of $P_{CR\text{-}pred}$ = 14 k	
Reflective crack width reached length of 8 in. during load step to 105% of $P_{CR\text{-}meas}$	
Maximum Load ≈ 1.95*$P_{CR\text{-}meas}$ = 47 k = 117% of $P_{CR\text{-}pred}$ rounded to 120% of $P_{CR\text{-}pred}$ = 48 k	

Load Step	Applied Load [% of $P_{CR\text{-}pred}$]	Applied Load [kip]	# Cycles Completed at applied load
1	15	6	1000
2	20	8	1000
3	25	10	1000
4	30	12	1000
5	35	14	1000
6	40	16	1000
7	45	18	1000
8	50	20	1000
9	55	22	1000
10[1]	60 (100% of $P_{CR\text{-}meas}$)	24	5000
11 "base" load	35 (≈55% of $P_{CR\text{-}meas}$)	14	2000
12	65	26	1000
13	70	28	1000
14	75	30	1000
15	80	32	1000
16	85	34	1000
17	90	36	1000
18	95	38	1000
19	100	40	1000
20	105	42	5000
21 "base" load	35 (≈55% of $P_{CR\text{-}meas}$)	14	2000
22	110	44	1000
23	115	46	1000
24	120 (≈195% of $P_{CR\text{-}meas}$)	48	1000
25 "base" load	35 (≈55% of $P_{CR\text{-}meas}$)	14	2000

[1]cracking visually observed at this load level

6.5.1. Data Acquisition

The primary instrumentation utilized during the subassemblage tests were resistive-type concrete embedment strain gages and LVDTs, and also included a single transversely oriented concrete embedment VW gage. All data from the resistive and LVDT instrumentation were collected via a single National Instruments data acquisition (DAQ) system. The DAQ collected data at all times during the testing process at a rate of 15 Hz. The DAQ was equipped with a low pass filter which produced readings of satisfactory quality, with an approximate total gage noise of ±6 με for the 120 mm concrete embedment resistive strain gages at a steady state condition. Data from the concrete embedment VW gages was collected via a CR10X data logger from Campbell Scientific at 2 minute intervals. The approximate noise of the concrete embedment VW gages instrumentation was approximately ±0.5 με.

6.6. Results of Laboratory Testing

A thorough analysis of the data collected both visually and via the DAQ was completed at the conclusion of the laboratory testing of each specimen. Seven metrics were developed in an effort to quantitatively and qualitatively characterize the performance of the subassemblage specimens relative to each other. Three of the seven metrics were defined based on visual observations and crack measurements during each test, which consisted of the documentation of general observations related to cracking observed during testing, and the measurement of the width and length of the crack observed on the origin and end faces of each specimen. Three metrics were determined through analysis of the data collected with the DAQ during the tests, and included an analysis of the strain due to shrinkage and placement of the subassemblage specimens in the load frame, width of opening of the joint measured via the LVDT instrumentation, and an analysis to investigate the vertical and horizontal generation and propagation of reflective cracking internally. The seventh metric consisted of the investigation of the predicted transverse reinforcement stress demands in the specimens. In all cases, the results were tabulated in terms of the predicted cracking load, $P_{CR\text{-}pred}$. The section is organized as follows:

- Investigation of transverse strain due to shrinkage and handling of the specimens (Section 6.6.1)
- General observations regarding cracking observed during load tests (Section 6.6.2)
- Analysis of visually observed crack widths on the origin and end faces of each specimen (Section 6.6.3)

- Analysis of opening of joint region measured at the origin and end faces via LVDT instrumentation (Section 6.6.4)
- Analysis of the rate of increase in the vertical length of cracking measured with a crack gage on the origin and end faces of each specimen (Section 6.6.5)
- Investigation of the vertical and horizontal generation and propagation of reflective cracking near the longitudinal joint between the precast flanges measured via concrete embedment resistive strain gages (Section 6.6.6)
- Predicted transverse reinforcement stress demands through range of loading (Section 6.6.7)

6.6.1. Transverse Strains Near Joint Region due to Shrinkage and Handling of Subassemblage Specimens

The transverse strain near the joint region was monitored during the curing process, as well as during handling of the specimens, to provide an estimate of the state of strain near the joint at the initiation of load testing. A single transversely oriented concrete embedment VW strain gage was installed near the middle of each section (measured along the precast joint), as shown in Figure 6.2.1. The strain in each gage was recorded in two hour increments from 1 hour after placement of the CIP concrete until the conclusion of all load testing.

The initial state of strain, defined to be the strain at the initiation of load testing, was of interest because the introduction of cracking due to applied load was a critical element of the testing plan, and therefore a record of existing cracking present prior to the start of testing was of interest. The transverse mechanical strains measured via the concrete embedment VW strain gages as a function of the number of days after placement of the CIP concrete, up until the first day of laboratory testing for each specimen, is shown in Figure 6.6.1. The horizontal axis represents the number of days between the placement of the CIP concrete and the first day of load testing for each specimen, and ranged from 37 days (SSMBLG3-HighBars) to 127 days (SSMBLG4-Deep). The transverse strains given in the figure originate at zero strain, and increase quickly over a short period of time, giving the illusion that the initial strain was nonzero. In addition, the DAQ was initiated at the same absolute time for all of the specimens, therefore there was a variation of several hours between when the CIP concrete was placed in the first and last specimen of the day, resulting in a small relative difference in the age of the specimens at what is referred to as zero time (when the DAQ was initiated). The vertical offsets among the readings may be attributed to the different stages of hydration occurring in the different specimens when the DAQ was

initiated. Each specimen was transferred from a construction staging area (where the CIP concrete was placed) to a loading frame, which is shown in the figure by the positive (i.e., tensile) increase in strains near the rightmost point of most of the data series.

The specimens were cured and stored in the University of Minnesota Structures Laboratory. The maximum temperature variation measured via the thermistors in the concrete embedment vibrating wire gages was +/- 7 degrees Fahrenheit. No sudden change in temperature was observed during the time between casting and testing of the specimens, which suggested that the mechanical strains reported in Figure 6.6.1 were primarily due to shrinkage.

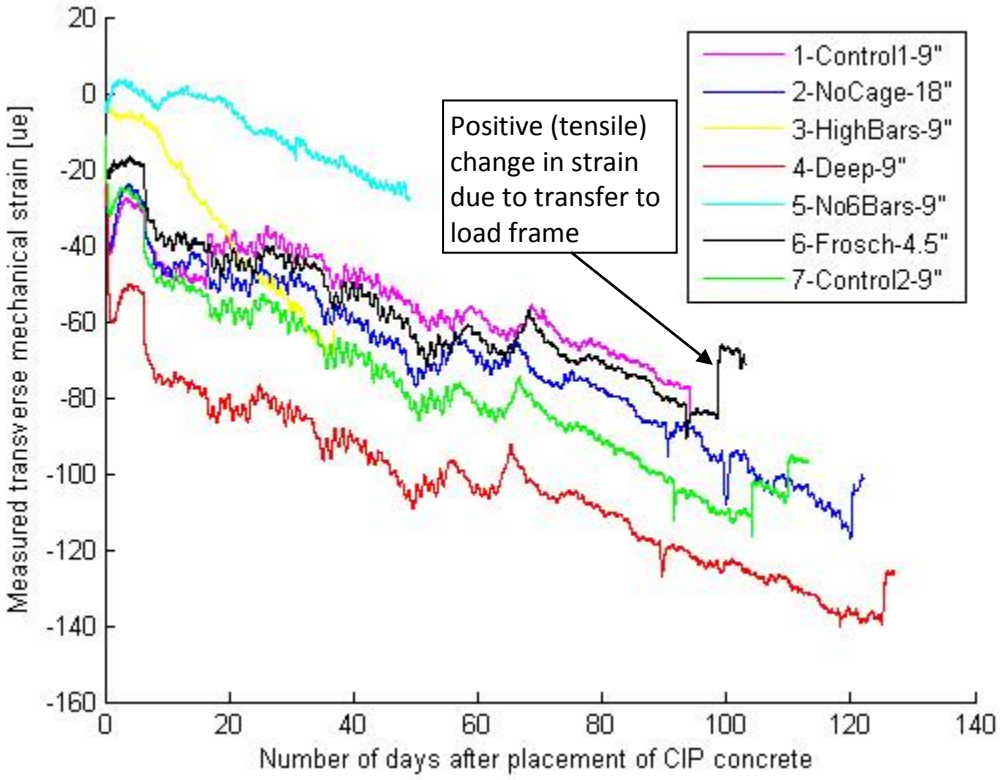

Figure 6.6.1: Measured transverse mechanical strains in the subassemblage specimens based on the number of days after the placement of the CIP concrete

The sign of the transverse strain data remained “compressive” indicating shortening or shrinkage throughout the curing and handling periods for each specimen. No evidence of cracking was

visually observed on either the origin or end faces of the specimens after placement of each subassemblage into the load frame.

6.6.2. General Observations of Cracking Behavior during Load Testing

Cracking was induced in the CIP region near the precast joint in each of the seven subassemblage specimens as a result of applied mechanical loading in accordance with the testing program. In addition, cracking was also observed at the vertical precast web-CIP interface, and occurred after the initiation of cracking near the joint in each of the specimens except SSMBLG3-HighBars, due to the absence of the clamping assembly on that specimen. Of the remaining six specimens, a single primary vertical crack was observed on both the origin and end faces throughout the range of applied loads on all but SSMBLG6-Frosch, where two distinct vertical cracks were observed on both faces. For this specimen, a second vertical crack was observed at an applied load of approximately 49.0 k (152 percent of $P_{CR\text{-}pred}$) and 41.9 k (130 percent of $P_{CR\text{-}pred}$) on the origin and end faces, respectively. A photograph of the dual vertical cracks observed on the origin face of SSMBLG6-Frosch, which is representative of both faces, is shown in Figure 6.6.2. In the discussion regarding visually measured crack widths and lengths in the following sections, the crack width was taken to be equal to the largest observed crack on each face when two cracks were present (i.e., when the load was large enough such that a second crack had formed), and the recorded crack length was taken to be the longest crack among the two, though little variation was observed in either the crack widths or crack lengths after the second 5 percent increase in applied load above the load step in which the secondary cracks were initiated.

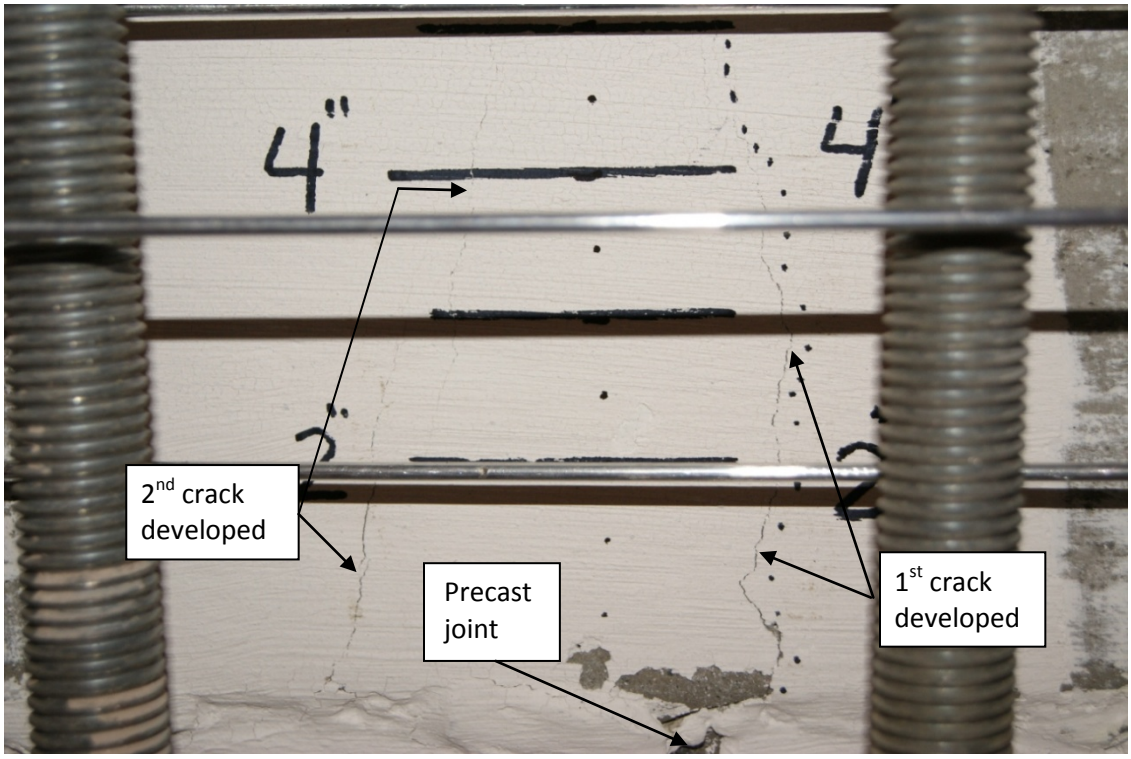

Figure 6.6.2: Photograph of development of two primary vertical cracks near the precast flange on origin face of SSMBLG6-Frosch. Applied load was 49.0 k (152 percent of $P_{CR\text{-}pred}$)

Cracking was also observed near the vertical precast web-CIP interface at large levels of applied load. Cracking at these locations generally initiated at the bottom of the precast section, near the embedded end of the precast flange, as illustrated in Figure 6.6.3. The observed cracking near the bottom of the precast flanges was likely primarily due to the added restraint provided by the clamping assembly, whereas if the clamps were not present delamination of the horizontal precast flange-CIP interface was expected, as observed during testing of SSMBLG3-HighBars before the installation of the clamping mechanism. The introduction of cracking was generally observed at the vertical web interfaces on both sides of the precast joint, and tended to initiate at roughly the same applied load.

In some cases, at loads near the maximum applied to each specimen, diagonal cracking was also observed in the CIP region, initiating at the outside edge of the bottom wide flange section of the clamping assembly, and extending to the vertical precast web-CIP interface, as noted in Figure 6.6.3.

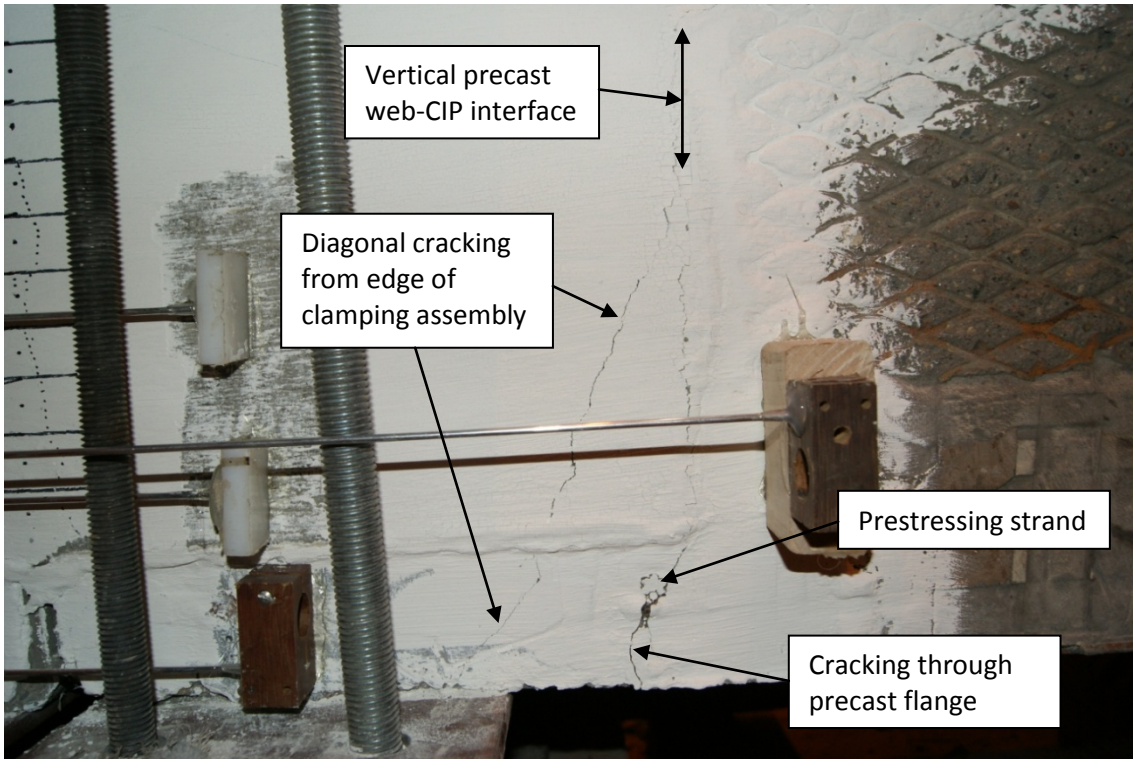

Figure 6.6.3: Photograph of cracking near the vertical precast web-CIP interface, including cracking through the precast flange and diagonal cracking due to the clamping assembly in SSMBLG6-Frosch

6.6.3. Width of Cracking Near Joint Region Measured with Crack Gage

The crack widths observed on both the origin and end faces of each subassemblage were documented throughout the majority of the tests. The procedure for visually documenting the crack growth in the subassemblage specimens was finalized during testing of the second specimen, or SSMBLG5-No.6Bars. For this reason, crack widths obtained for the SSMBLG3-HighBars test and crack widths from the origin face of SSMBLG5-No.6Bars are not compared with those of the other specimens. For the remaining specimens, the crack width was measured at each 5 percent increment relative to the predicted cracking load on both faces. A standard crack gage with a range of 0.002 to 0.032 in., inclusive, was used to measure the crack width at the lowest possible location in the CIP concrete in each specimen. The crack width was measured directly at the interface between the silicone caulk and CIP concrete, or as close as possible, and was recorded in association with the loading that corresponded to the respective load step applied to the section. The width of observed cracking on the faces of the specimens generally tended to be reduced with the removal of the applied load.

The detail near the joint and location of crack measurement is shown in Figure 6.6.4. A representative image of the crack width measurement is shown in Figure 6.6.5.

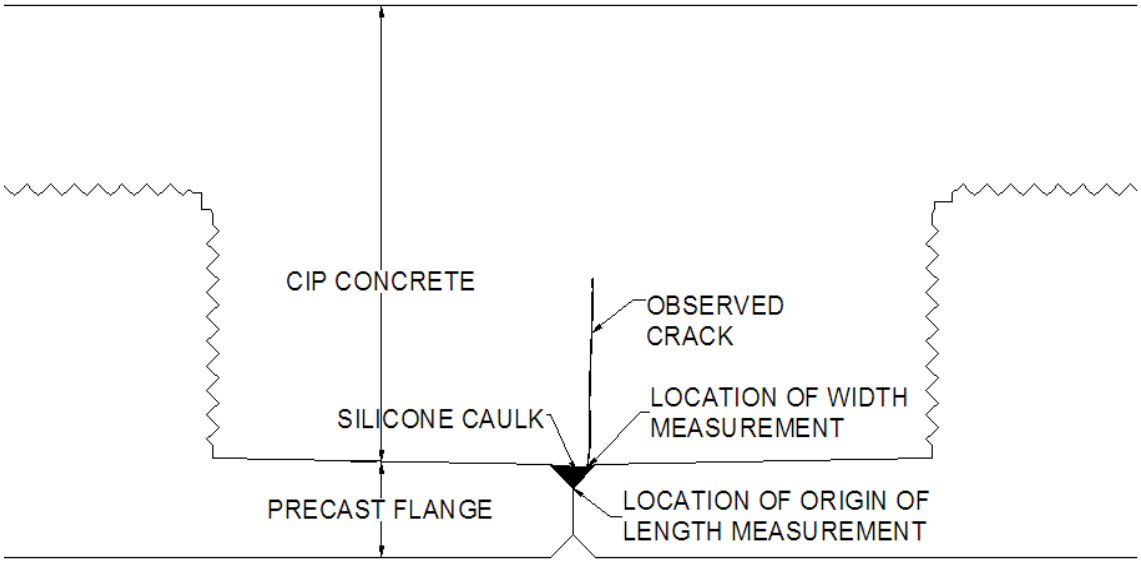

Figure 6.6.4: Location of measurement of width and length of crack observed on origin and end faces of subassemblage specimens

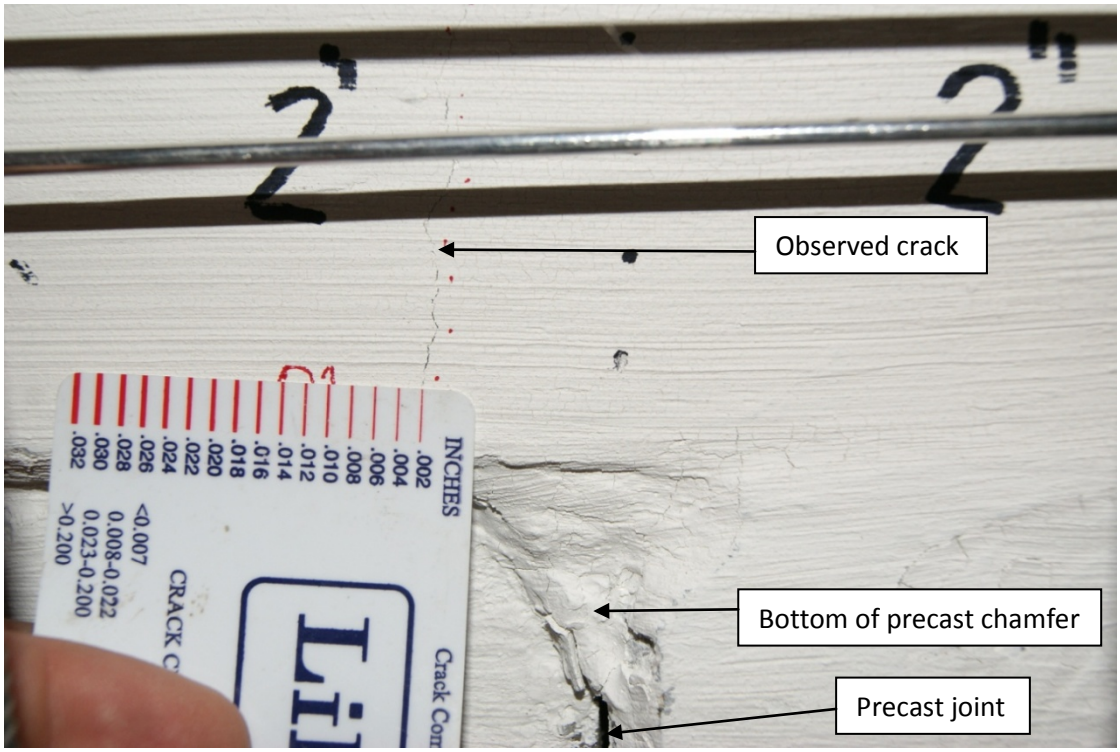

Figure 6.6.5: Measurement of crack width during subassemblage testing

Because the performance of the transverse hooked bars and cage reinforcement was of primary interest in the subassemblage specimens, and the presence of cracking near the vertical precast web face was undesirable and could have an influence on the crack width measurement above the longitudinal joint between the precast flanges, the observed crack widths were tabulated up to and including the load step in which the first crack or separation of the vertical precast web was observed. Figure 6.6.6 shows the width of the crack observed near the joint on the origin face before each set of cycles in the selected specimens. Each specimen is labeled in the legend using the specimen number, descriptive name, and transverse reinforcement spacing (considering both the transverse hooked bars and cage as transverse reinforcement). The horizontal axis illustrates the measured crack width in inches, while the percent of predicted cracking load is shown on the vertical axis. It is to be noted, that the percent of the predicted cracking load at which the crack width is indicated as “0 in.” corresponds to the visually observed cracking load. In other words, for 6-Frosch-4.5”, visual cracking was observed at 65% of the predicted cracking load. One of the reasons for the observed cracking load being less than the predicted cracking load was attributed to potential restrained shrinkage effects in the subassemblages. The crack was observed to originate at roughly the same percentage of predicted cracking load, with the exception of SSMBLG6-Frosch, which required an additional increase of approximately 15 percent of the predicted cracking load before cracking was first observed. Subsequent analysis of the internal strain data (see Section 6.6.6) suggested that small crack widths of SSMBLG6-Frosch hindered early visual detection of the crack, which caused the observed results to be inaccurately recorded at higher loads. Because of the larger perceived measured cracking load, SSMBLG6-Frosch was consistently loaded to higher levels of load in comparison with some of the other test specimens. This was also the case for the SSMBLG5-No.6Bars, for which results are not present in Figure 6.6.6 because crack width measurements were not recorded on the origin face of that specimen.

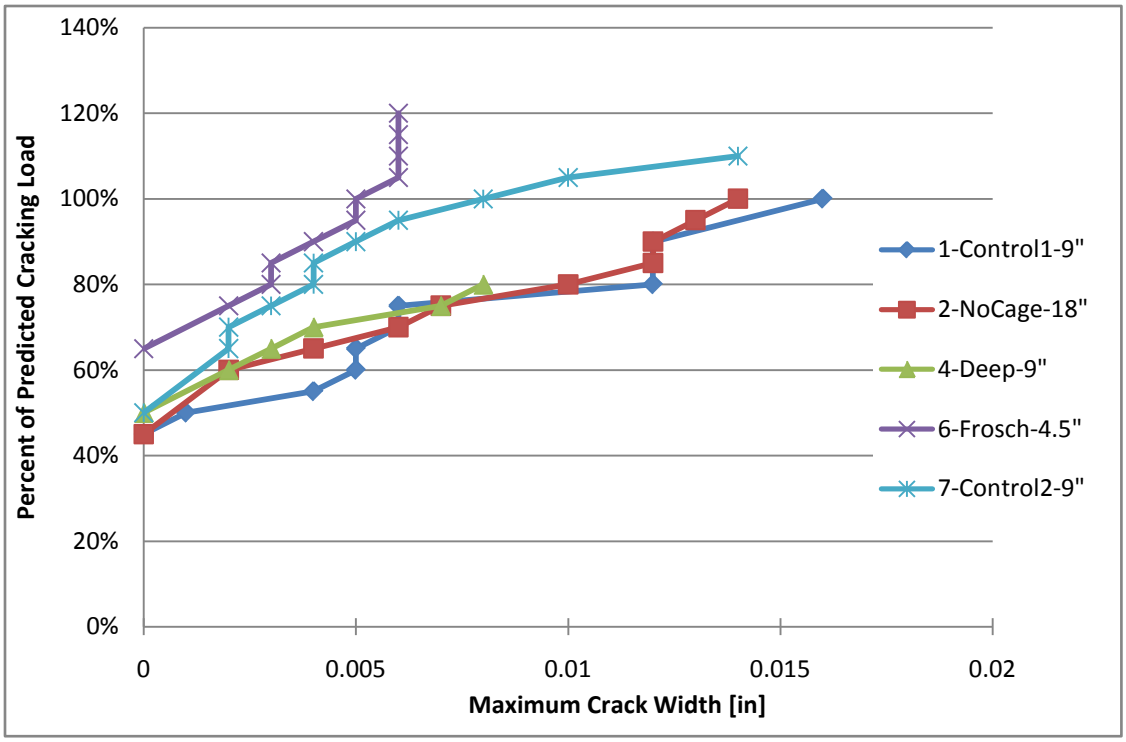

Figure 6.6.6: Maximum[1] crack widths measured on the origin face[2] of selected specimens[3] before each set of cycles

[1]Maximum crack width was measured at the horizontal precast-CIP flange interface
[2]Clear distance from origin face to first transverse bar was approximately 3.1 in. for SSMBLG5-No.6Bars and SSMBLG6-Frosch, and 3.25 in. for the other specimens
[3]SSMBLG5-No.6Bars is not shown because crack widths were not measured on the origin face of that specimen. SSMBLG3-HighBars is also not shown because the clamping apparatus was not installed prior to testing and therefore those results are not comparable to the remaining specimens

The performance of each specimen can be deduced from Figure 6.6.6 by selecting a value for the percent of the predicted cracking load and comparing the measured crack widths at that load. As expected, the observed crack widths tended to be bounded by the specimens with the closest (Frosch) and sparsest (No Cage) maximum reinforcement spacing. The variation in the observed crack widths between the two control specimens, SSMBLG1-Control1 and SSMBLG7-Control2 might be attributed to the smooth surface condition achieved in the SSMBLG7-Control2 specimen. The smooth flange surface was expected to better distribute the tensile stresses across the width of the CIP concrete in the trough between the precast webs (transverse to the longitudinal joint) reducing the effect of the discontinuity created by the interface between the adjacent precast flanges. A smooth or debonded surface however may not support an improved

overall PCSSS because if a reflective crack would initiate at the vertical precast web-CIP concrete interface, the cage reinforcement would not contribute to the crack control resistance. The only reinforcement crossing such a crack would be the transverse hooked bars protruding from the precast webs. Figure 6.6.6 clearly shows that SSMBLG6-Frosch outperformed the other specimens at high loads.

The crack widths on the end face of the specimens were documented at increased load levels prior to the subsequent cycling, and the values are plotted in Figure 6.6.7 with respect to the percentage of the cracking load applied. The crack widths measured on the end face followed a similar trend to those documented on the origin face. The transverse reinforcement terminated a distance of half of the maximum spacing from the end face of each specimen, essentially providing an estimate of the crack width at the point farthest from adjacent transverse reinforcement in the specimen; whereas on the origin face, the clear distance to the transverse reinforcement was approximately 3.1 in. for SSMBLG5-No.6Bars and SSMBLG6-Frosch and 3.25 in. for the remaining specimens. As observed near the origin face, the Frosch and Control2 specimens performed well, however the inclusion of the results from SSMBLG5-No.6Bars also showed very good performance of this specimen. As stated earlier in this section, the relatively higher initial visual cracking loads recorded for SSMBLG5-No.6Bars and SSMBLG6-Frosch were found to be much larger than those identified with the embedded instrumentation which was attributed to the relatively smaller crack widths generated in these specimens (see Section 6.6.6). The SSMBLG5-No.6Bars and SSMBLG6-Frosch were subjected to relatively higher levels of subsequent loads than the other specimens because the applied load history was associated with the visual crack initiation.

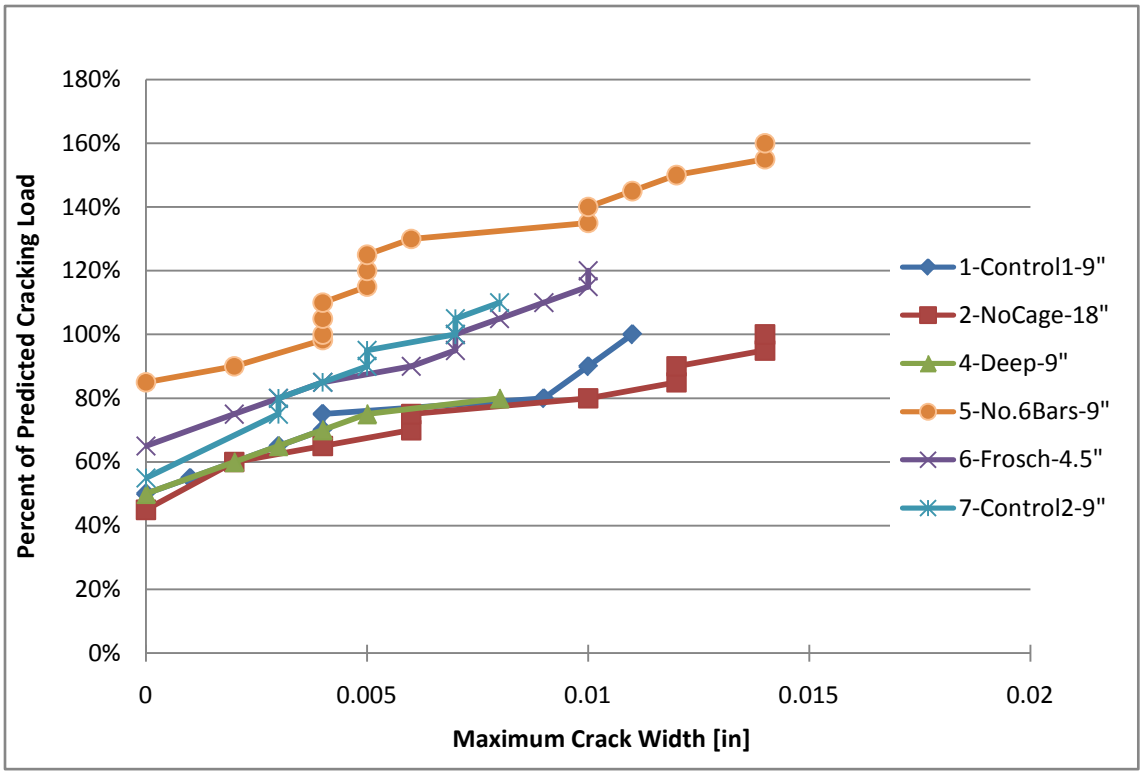

Figure 6.6.7: Maximum[1] crack widths measured on the end face[2] of selected specimens before each set of cycles

[1]Maximum crack width was measured at the horizontal precast flange -CIP interface; and in the case of SSMBLG6-Frosch, where two vertical cracks were observed at high loads, the largest crack width was recorded

[2]Reinforcement spacing from end face of specimen was half of the maximum reinforcement spacing

According to Figure 6.6.7, SSMBLG5-No.6Bars, SSMBLG6-Frosch, and SSMBLG7-Control2 appeared to outperform the other specimens, especially at higher levels of load in the case of SSMBLG6-Frosch and SSMBLG7-Control2. Also, in the case of SSMBLG6-Frosch, recall two vertical cracks were observed on each face of the specimen, which was generally preferred because the development of many, smaller cracks is often favored to the development of few, larger cracks, especially when the ingress of water and corrosive materials are of concern. Also observed from the figure, SSMBLG2-NoCage showed large increases in the measured crack width with each 5 percent increase in the applied load, especially at higher levels of load, highlighting the faster rate of degradation of this specimen compared to the others that were well reinforced for crack control. Furthermore, it is evident that an increased area of reinforcement can also provide satisfactory crack control performance, as shown by SSMBLG5-No.6Bars.

The section constructed with a deeper precast beam, SSMBLG4-Deep, was observed to perform relatively well, especially considering that the reinforcement ratio for crack control in this section was smaller than the other specimens due to the increase in member depth while the section contained similar reinforcement details as were used in the control specimens.

The overall performance of the six subassemblage specimens based on the crack widths measured using a crack gage was good. Note that at an applied load of 100 percent of $P_{CR\text{-}pred}$, the worst performing specimen was SSMBLG2-NoCage, with a measured crack width of approximately 0.014 in. An estimate of acceptable crack widths was determined based on recommendations from ACI Committee 224, which recommended a maximum crack width of 0.007 in. for structures exposed to corrosive environments, and 0.016 in. as a maximum limit for aesthetics (ACI 224, 2001). Also recall that Frosch et al. selected a target maximum crack with of 0.021 in. during their study (Frosch et al., 2006).

The crack widths were also measured after the completion of all cyclic loading at each load step. The potential durability of each specimen subjected to cyclic loading might be inferred by examining the change in measured crack width on the end face before and after the completion of cyclic loading at a given load step, as illustrated in Table 6.6.1. Negligible to small increases in measured crack widths after cyclic loading at each load step indicated good performance. Many specimens showed no increase or only small increases in crack width (i.e., 0.001 in.) due to the application of cyclic loading. The four largest increases in the measured crack widths are highlighted in yellow.

Table 6.6.1: Increase in the measured crack width on the end face as a result of cyclic loading at each load step

Increase in measured crack width (in.)	Subassemblage Specimen					
Percent of $P_{cr\text{-}pred}$	1-Control1	2-NoCage	4-Deep	5-No.6Bars	6-Frosch	7-Control2
45	NCO[1]	0	NCO	NCO	NCO	NCO
50	0	0	0			
55	0	0.001	0.001			
60	0.001	0.002	0.001			0
65	0.001	0.002	0		0	0
70	0	0	0.003		0	0
75	0.004	0.002	0.003		0	0.001
80	0.001	0	0.002		0.001	0
85	NA[2]	0	Delam	0	0.001	0.001
90	0	0.001		0	0	0
95	NA	0		0	0	0
100	0.002	0.001		0	0	0.002
105	Delam[3]	Delam		0	0.001	0.001
110				0	0	0.002
115				0	0	Delam
120				0	0	
125				0.001	Delam	
130				0.003		
135				0		
140				0.001		
145				0.001		
150				0		
155				0		
160				0		

[1]No cracking was visually observed at associated load step
[2]Measurements were not available at given load step due to error in data collection
[3]Delamination was observed at vertical precast web – CIP interface

The relative performance between each face of a given specimen was also of interest. Each face had reinforcement located a specified distance away. The reinforcement near the origin face was a clear distance of 3.1 in. away in SSMBLG5-No.6Bars and SSMBLG6-Frosch and 3.25 in. in the remaining specimens, while the center of the reinforcement or paired hooks near the end face was half of the maximum spacing away, ranging from ideally 2.25 to 9 in. Figure 6.6.8 shows the difference in the measured crack widths between the origin face and the end face; a positive value

in Figure 6.6.8 indicates that the crack width measured on the origin face was larger than that measured on the end face. For all specimens shown other than SSMBLG6-Frosch, the proximity of the reinforcement to the origin face (3.1 in.) was smaller than the proximity of the reinforcement to the end face, and therefore the crack widths on the origin face would be expected to be smaller than those on the end face, resulting in negative values in Figure 6.6.8. On the contrary, SSMBLG6-Frosch data showed a negative trend, suggesting that the crack width at the end face, where the reinforcement was nearest the face of the specimen was larger than on the origin face; however, there was very little difference in the distance from the reinforcement to the origin and end faces in the SSMBLG6-Frosch specimen. Both control specimens showed a trend towards positive differences in the crack widths, again suggesting that the face with the reinforcement located closer exhibited larger crack widths. Furthermore, contrary to expected results, SSMBLG2-NoCage, which had the largest difference between the proximity of the reinforcement on each face at 5.75 in. (9 in. on end face – 3.25 in. on origin face), showed the least variation in the crack widths measured between the faces.

Because the crack width could only be measured at the external faces, and only one measurement was taken on each face, potential variations in the measured crack widths with respect to the distance from the reinforcement were expected, which may correspond to some of the unexpected trends documented in Figure 6.6.8.

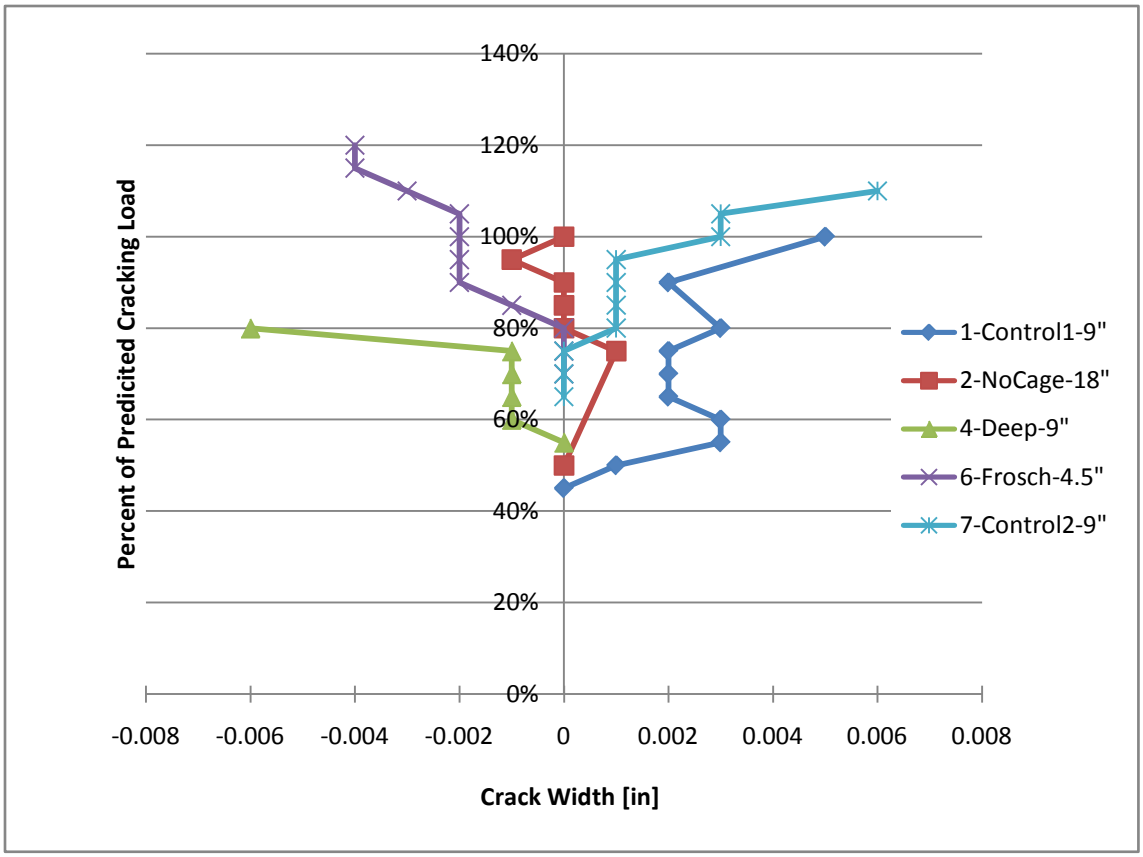

Figure 6.6.8[1]: Difference in crack width between the origin and end face (origin minus end)

[1]Measured crack widths were not available on the origin face of SSMBLG5-No.6Bars

6.6.4. Width of Cracking Near Joint Region Measured with LVDTs

The origin and end face of each specimen was instrumented with LVDTs oriented across the joint to measure the total displacement, or opening, within their gage lengths. The placement and LVDT size used was included in Section 6.2.

The Mid LVDT displacement measurements (from LVDT050, or LVDT100 for SSMBLG5-No.6Bars) located a distance of 2 in. from the bottom of the precast chamfer on the origin and end faces are shown in Figures 6.6.9 and 6.6.10, respectively. The figures illustrate the measured LVDT displacement as a function of the applied load; therefore improved performance can be identified by data closer to the upper left corner of the plot, and steeper slope. As before, the specimens exhibiting smaller crack widths were SSMBLG6-Frosch, SSMBLG7-Control2, and SSMBLG5-No.6Bars, especially at larger levels of load, which was especially evident by the steeper slopes of those three data series, compared to the slopes of the SSMBLG1-Control1, SSMBLG2-NoCage, and SSMBLG4-Deep data series.

The displacements measured with the Mid LVDTs correlated relatively well with the visually recorded crack widths measured with a crack gage at the intersection of the chamfers at the joint, documented in Section 6.6.3. It was generally expected that the displacements measured with the LVDTs would be slightly larger than the crack widths measured with a crack gage because the LVDT measurements included the concrete strains across the gage length, as well as the widths of each of the vertical cracks, where multiple cracks were present (i.e., SSMBLG6-Frosch), though this was not generally observed. Note however that the Mid LVDTs were located a vertical distance of 2 in. above the horizontal precast – CIP interface (which is where the visual observations were recorded). Because the specimens were subjected to flexural stresses, it was expected that the strain would vary linearly with the depth, which suggested that the Mid LVDTs could measure a smaller crack width than what was visually observed, depending on the amount of straining and additional cracking occurring between the gage blocks of the LVDT instrumentation. The maximum crack width measured with a crack gage and maximum displacement measured with the LVDT instrumentation are given for both the origin and end faces in Table 6.6.2. The measured LVDT displacements correlated relatively well to the crack widths measured visually using a crack gage.

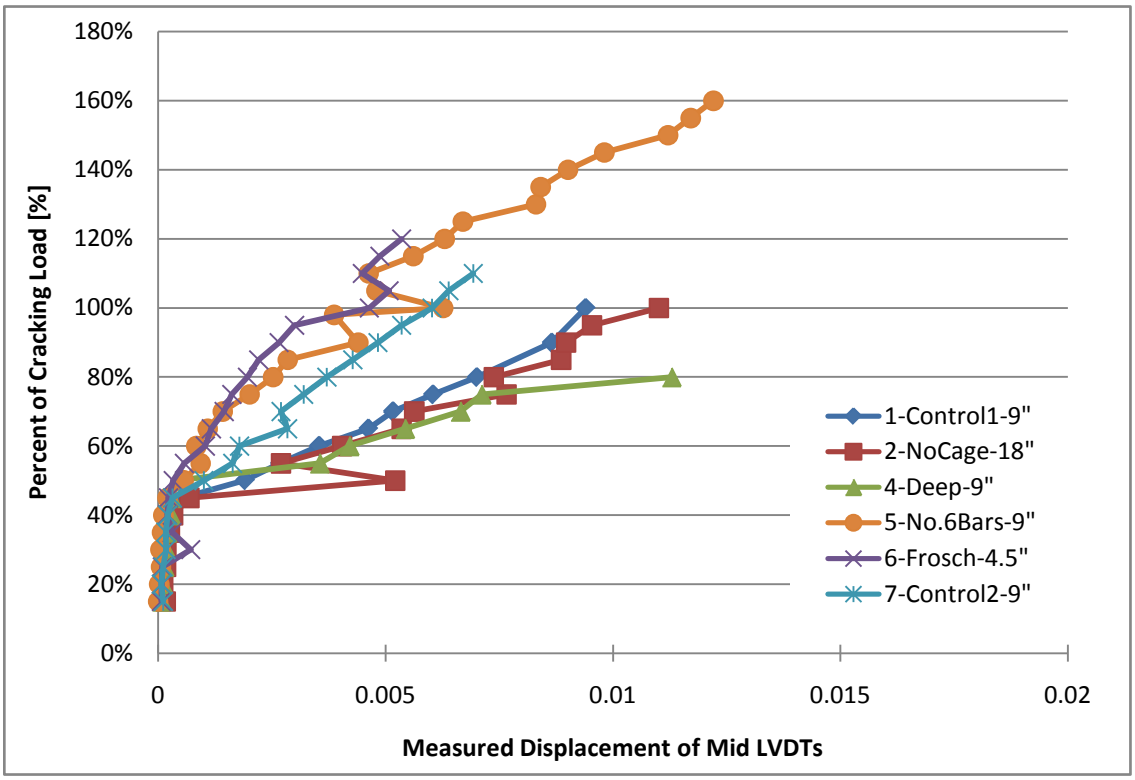

Figure 6.6.9: LVDT displacement measured via the Mid LVDT at the origin face

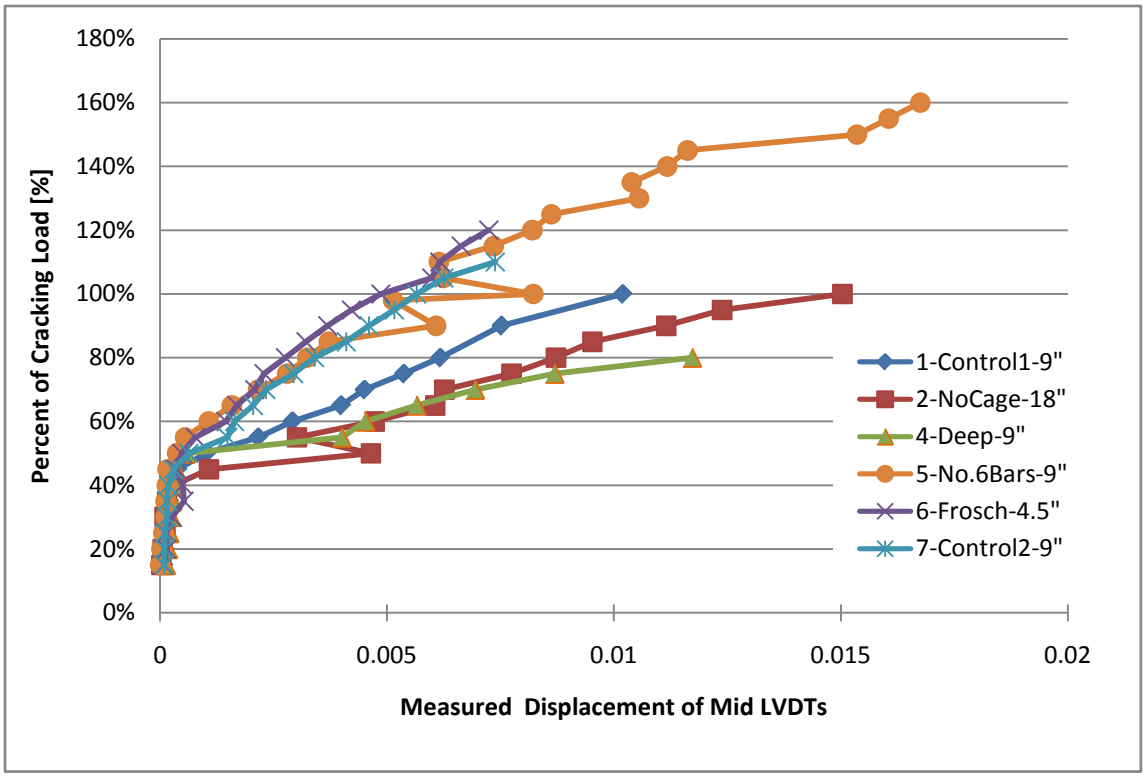

Figure 6.6.10: LVDT displacement measured via the Mid LVDT at the end face

Table 6.6.2: Maximum crack widths via crack gage (from Section 6.6.3) and LVDT displacements measured on the origin and end faces[1]

Specimen Description	Percent of predicted cracking load applied[2]	**Origin Face**		**End Face**	
		Measured with crack gage	Measured with LVDTs	Measured with crack gage	Measured with LVDTs
1-Control1-9"	100%	0.016 in.	0.009 in.	0.011 in.	0.010 in.
2-NoCage-18"	100%	0.014 in.	0.011 in.	0.014 in.	0.015 in.
4-Deep-9"	80%	0.008 in.	0.011 in.	0.008 in.	0.012 in.
5-No.6Bars-9"	160%	NA[3]	0.012 in.	0.014 in.	0.017 in.
6-Frosch-4.5"	110%	0.006 in.	0.005 in.	0.01 in.	0.007 in.
7-Control2-9"	120%	0.014 in.	0.007 in.	0.008 in.	0.007 in.

[1]Note that the locations of measurements were inconsistent between the crack gage and LVDT measurements (see Section 6.2)

[2]The tabulated applied percentage of the predicted cracking load was the largest applied load prior to cracking at the vertical precast web-CIP interface

[3]Crack widths measured with a crack gage were not available on the origin face of SSMBLG5-No.6Bars

The difference in the measured LVDT displacements between the origin and end faces at each load step was investigated in a similar method to that used in Section 6.6.3. Recall that all reinforcement near the origin face was a clear distance of 3.1 in. away from the face in SSMBLG5-No.6Bars and SSMBLG6-Frosch and 3.25 in. from the face in the remaining specimens, while the center of the hooked pair or center of the cage hoop reinforcement was half of the maximum spacing away from the end face, nominally ranging from 2.25 to 9 in. Figure 6.6.11 shows the difference in the LVDT displacements between the origin face and the end face; a positive value in Figure 6.6.11 indicates that the LVDT displacement measured on the origin face was larger than that measured on the end face. For all specimens other than SSMBLG6-Frosch, the proximity of the reinforcement to the origin face was less than that to the end face, therefore, it was expected that the results for these specimens would have a negative sign because crack widths were expected to increase as the distance from the nearest reinforcement increased, which generally corresponded with the observed results. Also note that SSMBLG6-Frosch was expected to have the least variation in the measurements from opposite faces because the difference in the proximity to the reinforcement to the exterior faces was the smallest for that specimen. Furthermore, the observed relative LVDT displacements between the origin and end faces matched the expected results better than the same analyses of the crack widths measured with a crack gage, which highlighted the variability in those measurements.

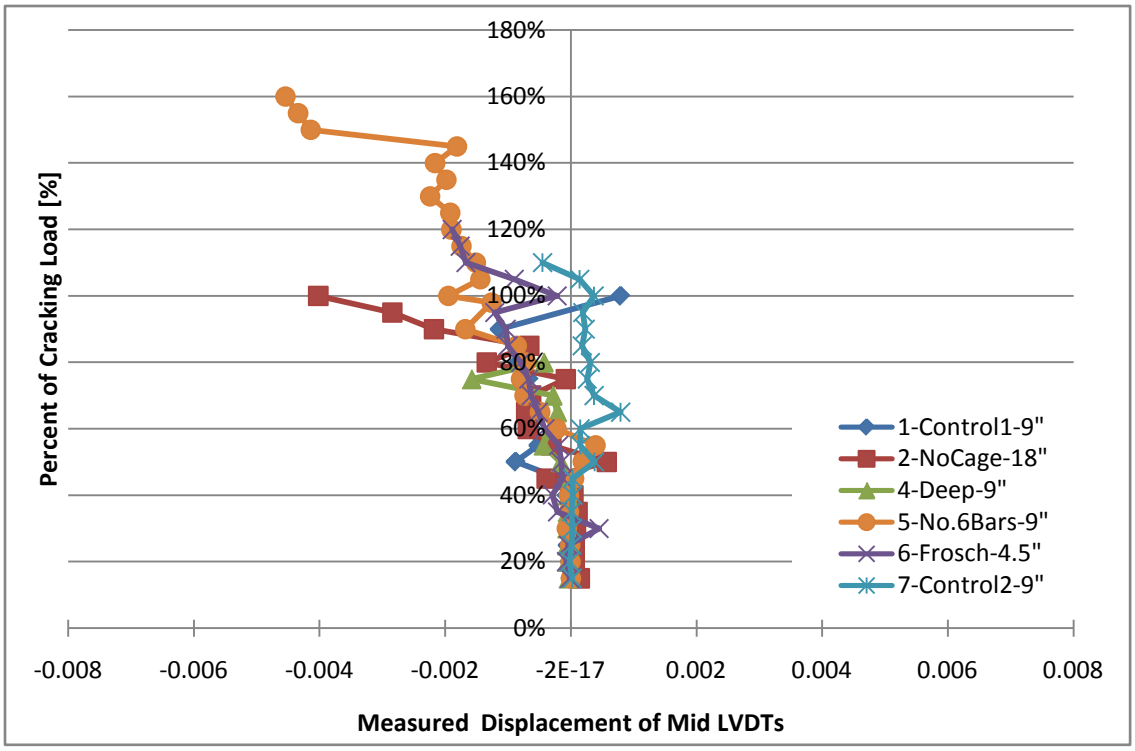

Figure 6.6.11: Difference in LVDT displacements between the origin and end face (origin minus end)

6.6.5. Rate of Increase in the Length of Cracking Near Joint Region via Visual Observation

The vertical length of the reflective crack near the joint region was also recorded during the subassemblage tests. The origin of the measured crack length was taken at the intersection of the chamfers at the joint in the precast flanges, as shown in Figure 6.6.4. As before, crack lengths were not documented for SSMBLG3-HighBars (which underwent delamination between the precast flange and the CIP concrete without the clamping system rather than developing a crack above the adjacent precast flange tips); crack lengths were also not documented on the origin face of SSMBLG5-No.6Bars using the same methodology as for the other specimens; therefore, those locations are not included in the specimen comparison. The length of the crack was measured using either the grid that was transferred onto each specimen, a tape measure, or both. Measurements were generally taken with a precision to within ¼ in. A representative image of the measurement of the length of the crack is shown in Figure 6.6.12. The measured crack length, normalized by the total section depth of each specimen (to include analysis of the deep section in the comparison), versus the applied load in terms of a percent of the predicted cracking load

before each set of cycles measured on the origin and end face is shown in Figure 6.6.13 and Figure 6.6.14, respectively. Also included is the range of the predicted cracked neutral axis locations for the specimens shown in the figures, with the specimens representing the upper and lower bounds annotated on the plots. The predicted cracked neutral axis locations are also tabulated in Table 6.6.3. The location of the cracked neutral axis was calculated using measured concrete compressive strengths and the measured modulus of rupture for each specimen.

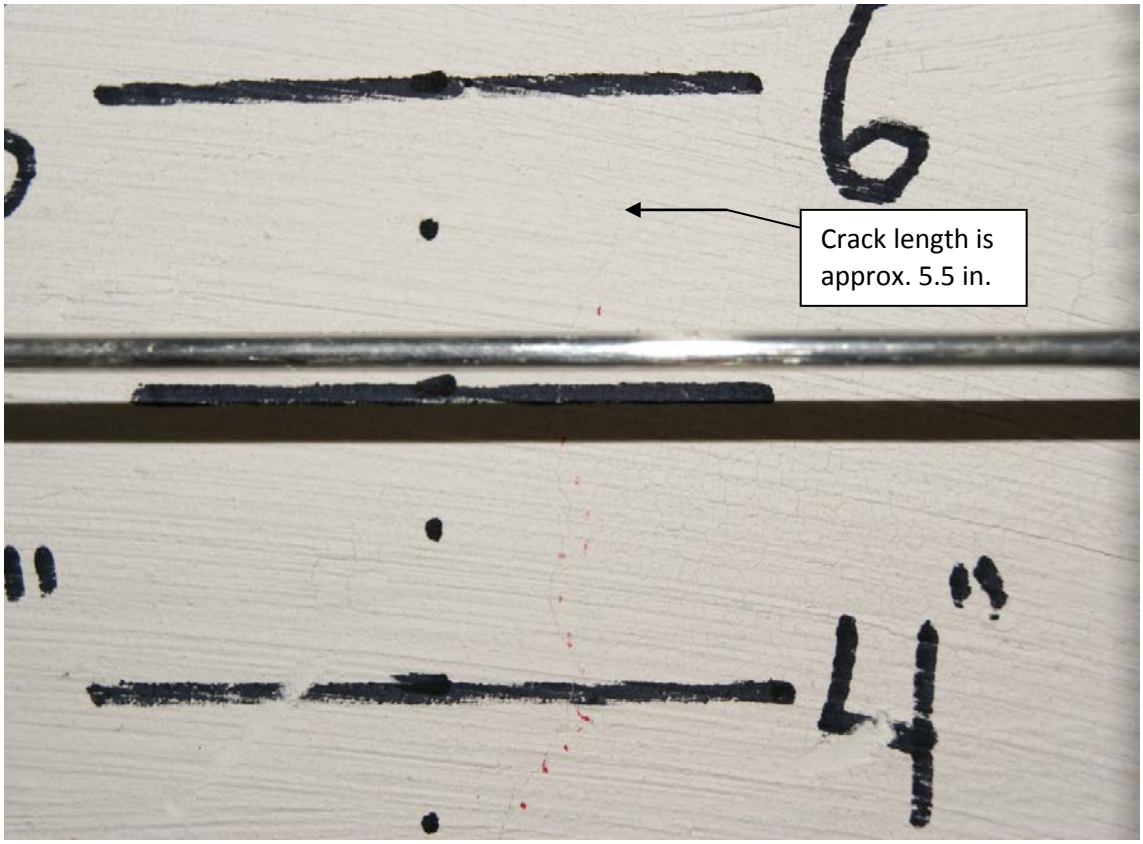

Figure 6.6.12: Measurement of the length of crack during subassemblage testing. Red dots illustrate path of crack

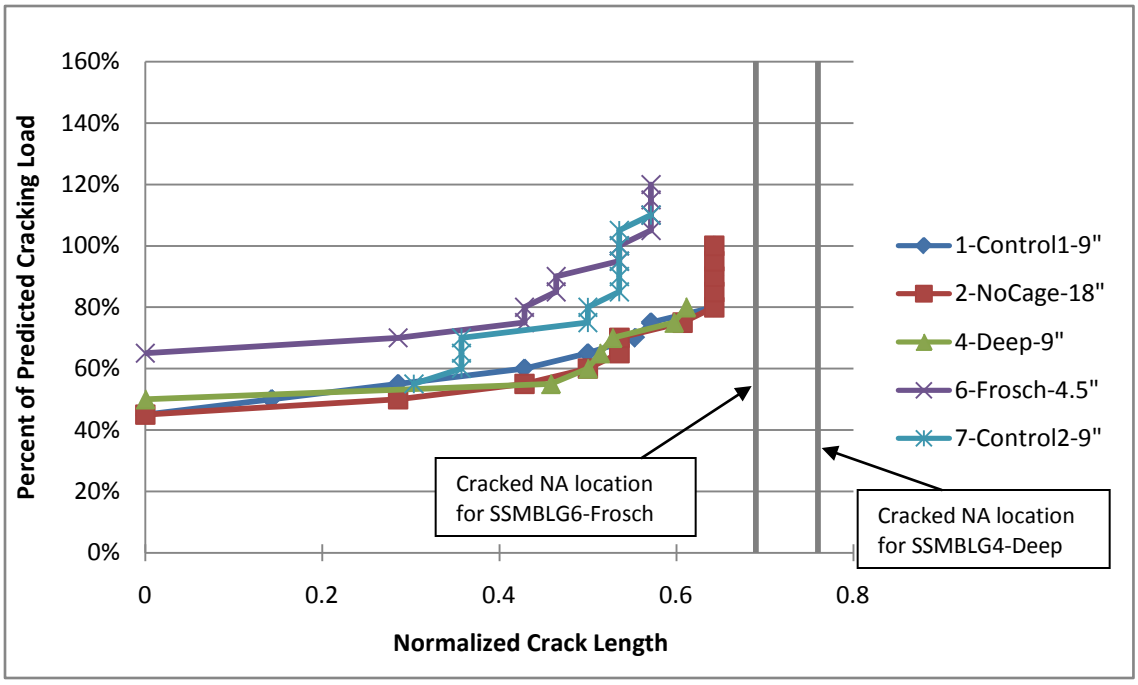

Figure 6.6.13: Normalized crack length on the origin face of selected specimens before each set of cycles

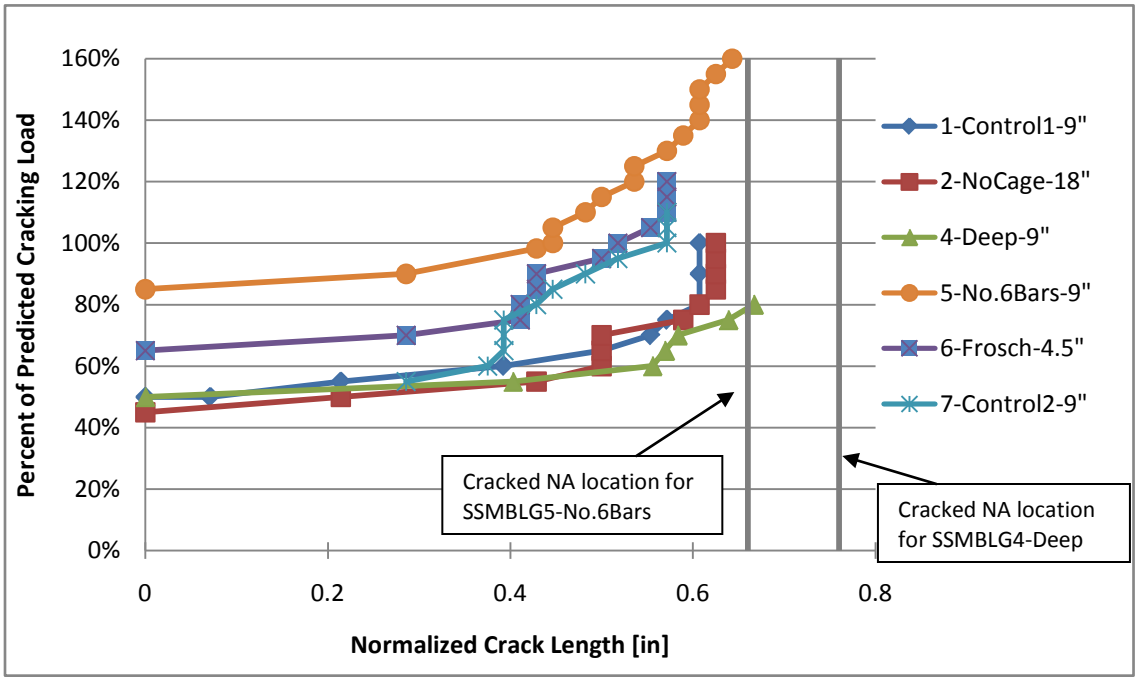

Figure 6.6.14: Normalized crack length on the end face of selected specimens before each set of cycles

Table 6.6.3: Predicted locations of the subassemblage cracked section neutral axes

Specimen	Cracked Section Neutral Axis Depth measured from the compression fiber	Normalized Depth of Cracked Section Neutral Axis (measured from bottom of section)
1-Control1	1.74 in.	0.71
2-NoCage	1.43 in.	0.73
4-Deep	2.09 in.	0.76
5-No.6Bars	2.48 in.	0.66
6-Frosch	2.01 in.	0.69
7-Control2	1.84 in.	0.71

For each of the specimens, normalized crack length increased to a maximum of between 50 and 65 percent of the total section depth (i.e., precast depth plus depth of the deck). The primary behavior of interest regarding the length of the crack was its rate of increase relative to increases in the applied load, or the slope of each data series, particularly over a select range of applied loads. The final, or maximum, crack length was of little significance because the crack length was expected to be driven up to the cracked neutral axis (NA) in each case, though the results for each specimen showed that the maximum visually observed length of the crack did not reach the location of the cracked neutral axis As illustrated in Figures 6.6.13 and 6.6.14, the well reinforced sections (i.e., SSMBLG5-No.6Bars and SSMBLG6-Frosch controlled the length and rate of increase in the length of the crack, especially at high loads. Note however, that the predicted neutral axis locations suggest that the maximum length of the crack in the well reinforced sections would be lower than in the remaining specimens.

The variation in the crack length measured on the origin face and end face before each set of cycles provided further insight regarding the effect of reinforcement spacing. The difference in the normalized crack length on the origin and end faces (origin minus end face) is illustrated in Figure 6.6.15; a positive value implies that the crack length on the origin face was greater than that on the end face at a given load step. As before, all specimens other than SSMBLG6-Frosch had reinforcement located closer to the origin face (3.1 in. clear from face) than the end face (2.25 in. from center of reinforcement to end face), suggesting that the difference in the normalized crack length should be negative for these specimens. However, for the majority of the specimens, the difference in the crack length between the origin and end faces was almost always positive, suggesting that the proximity of transverse reinforcement to a face for the situations investigated did not directly affect the length of the crack. This further supports the notion that the crack

length is better controlled by the amount of reinforcement for crack control as opposed to the spacing of the reinforcement for the spacings included in this study.

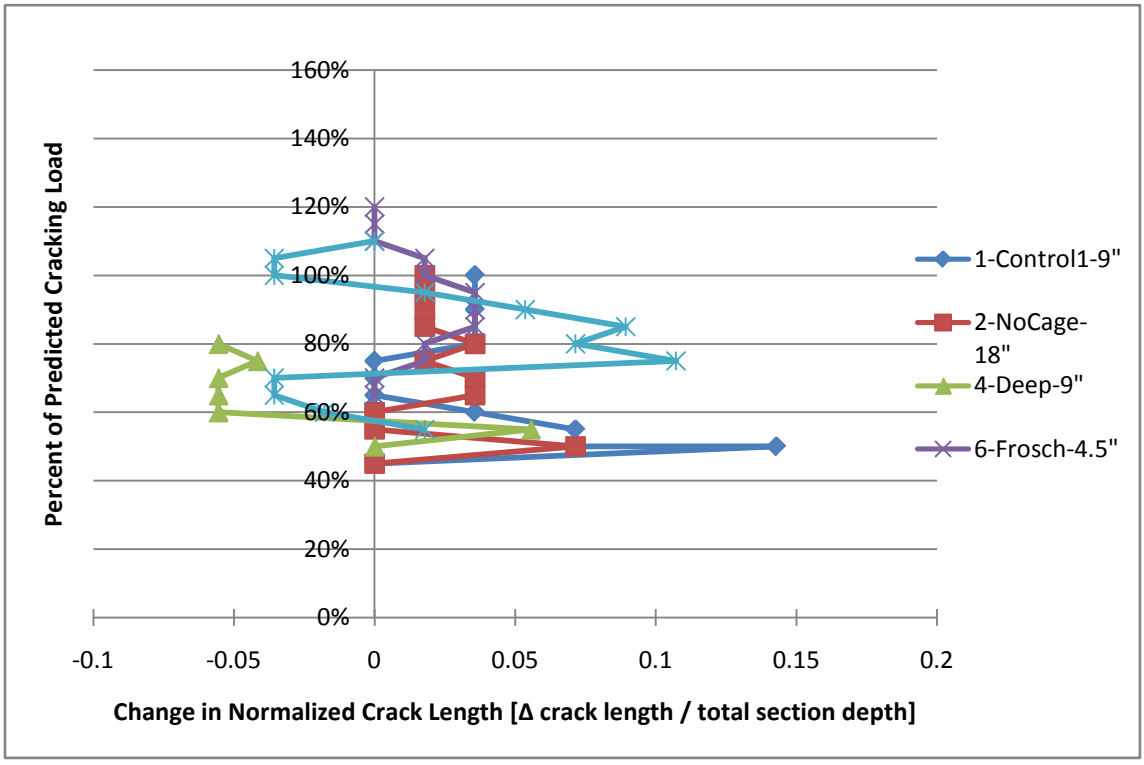

Figure 6.6.15: Difference in normalized crack length between the origin and end face (origin minus end) of selected specimens

6.6.6. Investigation of the Vertical and Horizontal Generation and Propagation of Reflective Cracking near the Precast Joint Measured via Concrete Embedment Resistive Strain Gages

The concrete embedment resistive strain gages provided a quantitative means to determine the internal crack initiation and propagation within the subassemblage specimens. The presence of cracking at a particular gage was identified based on the slope of the load versus strain relationship for each gage, which is illustrated in Figures 6.6.16 through 6.6.20. Using this method, the location of the crack could be determined using an "on-off" type of metric. Furthermore, when the load was small (i.e., when the percent of cracking load was on the order of 40 or 45 percent) large increases in the measured strain were also considered to be representative of cracking. As an example, consider the slope of the load versus strain data for SSMBLG1-Control1, as shown in Figures 6.6.16 through 6.6.20. Each figure illustrates the slope of the load versus strain data for each of the three transversely oriented concrete embedment resistive gages

across the width of the CIP region near the precast joint at each vertical level (i.e., 1.0, 1.5, and 2.0). The figures are also annotated with the load at which load cracking was assumed to have occurred, which included some level of subjectivity.

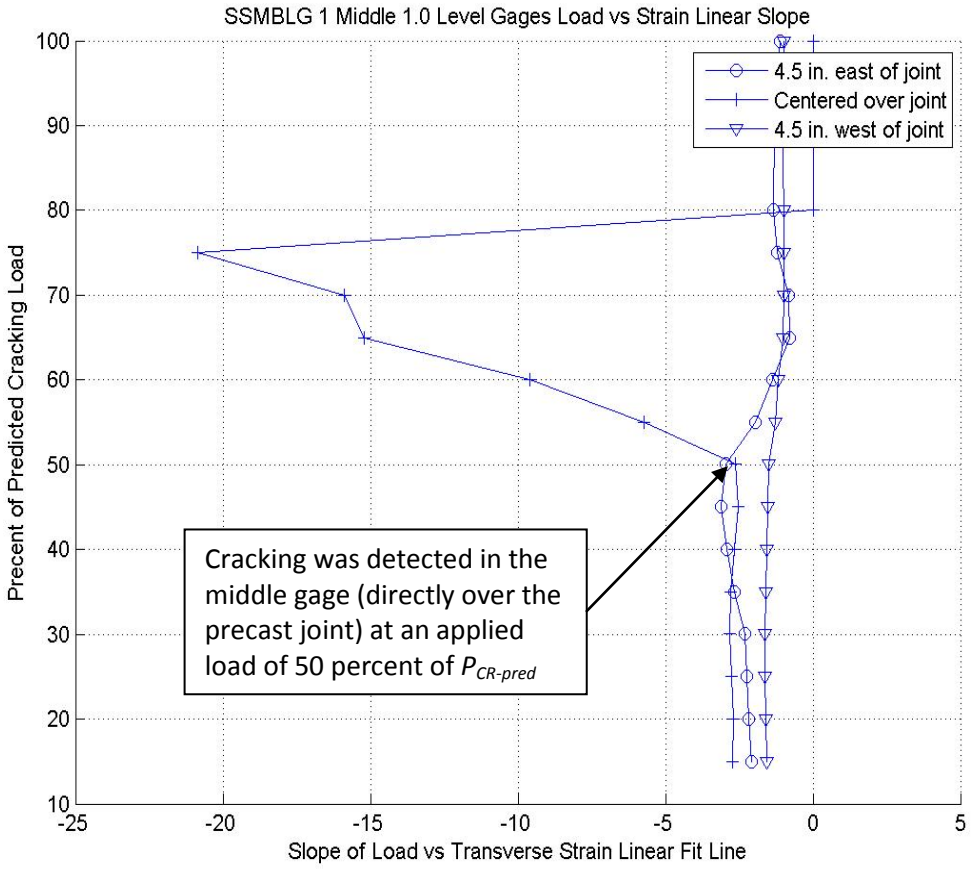

Figure 6.6.16: Slope of linear fit line for load versus 1.0 level strain data at middle cross section in SSMBLG1-Control1

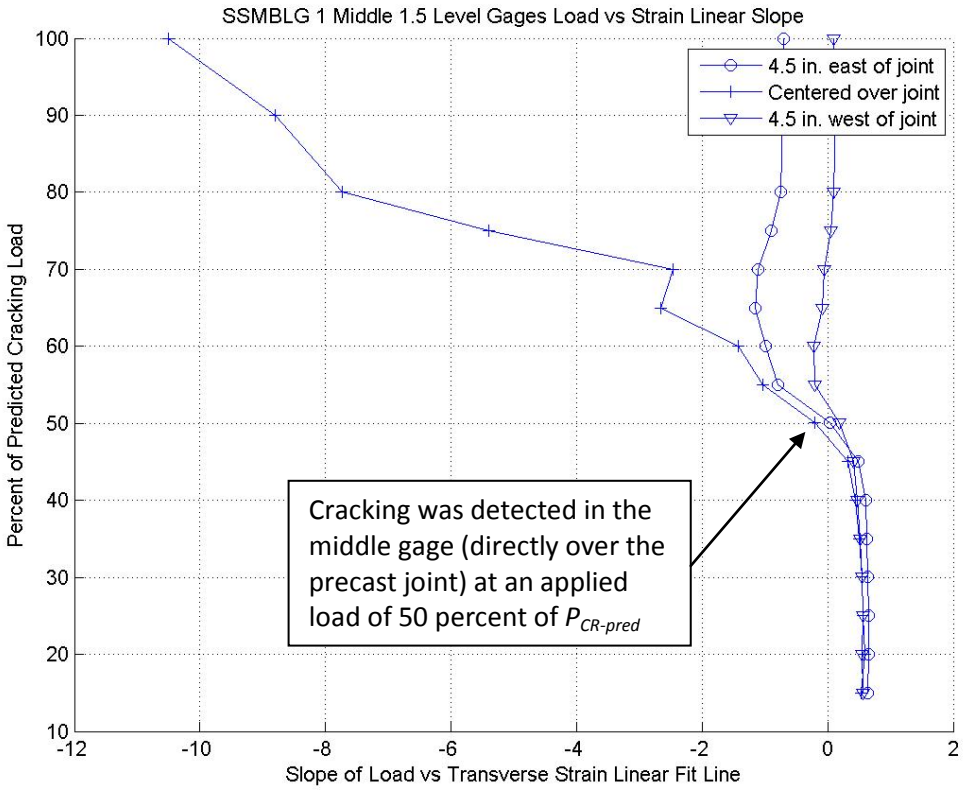

Figure 6.6.17: Slope of linear fit line for load versus 1.5 level strain data at middle cross section in SSMBLG1-Control1

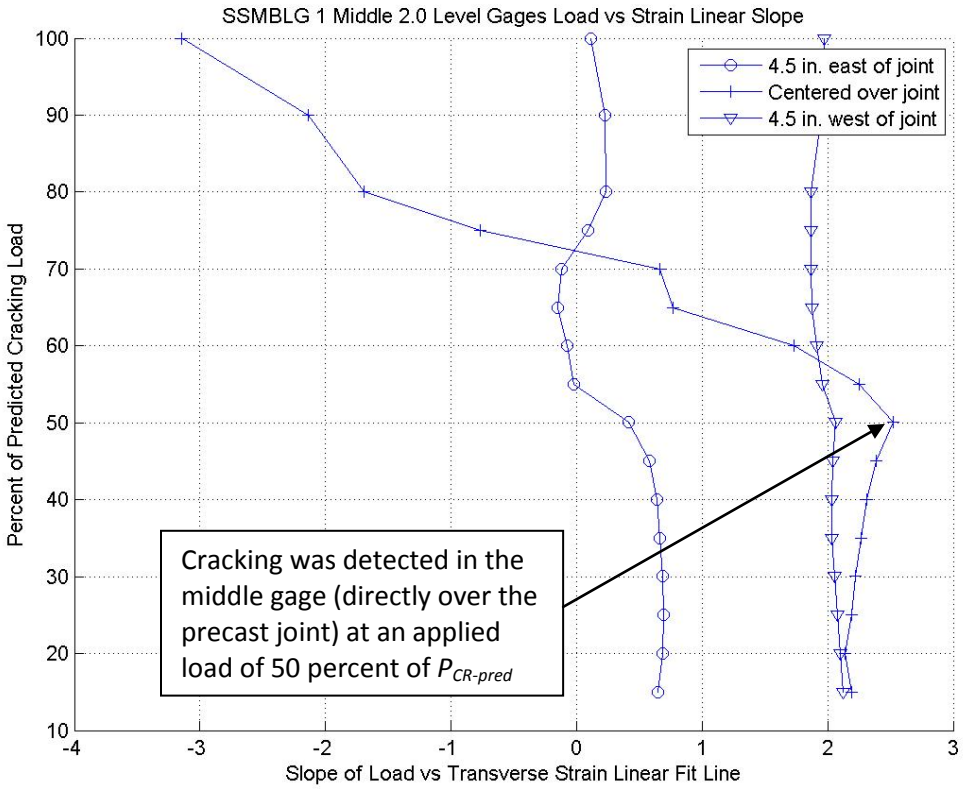

Figure 6.6.18: Slope of linear fit line for load versus 2.0 level strain data at middle cross section in SSMBLG1-Control1

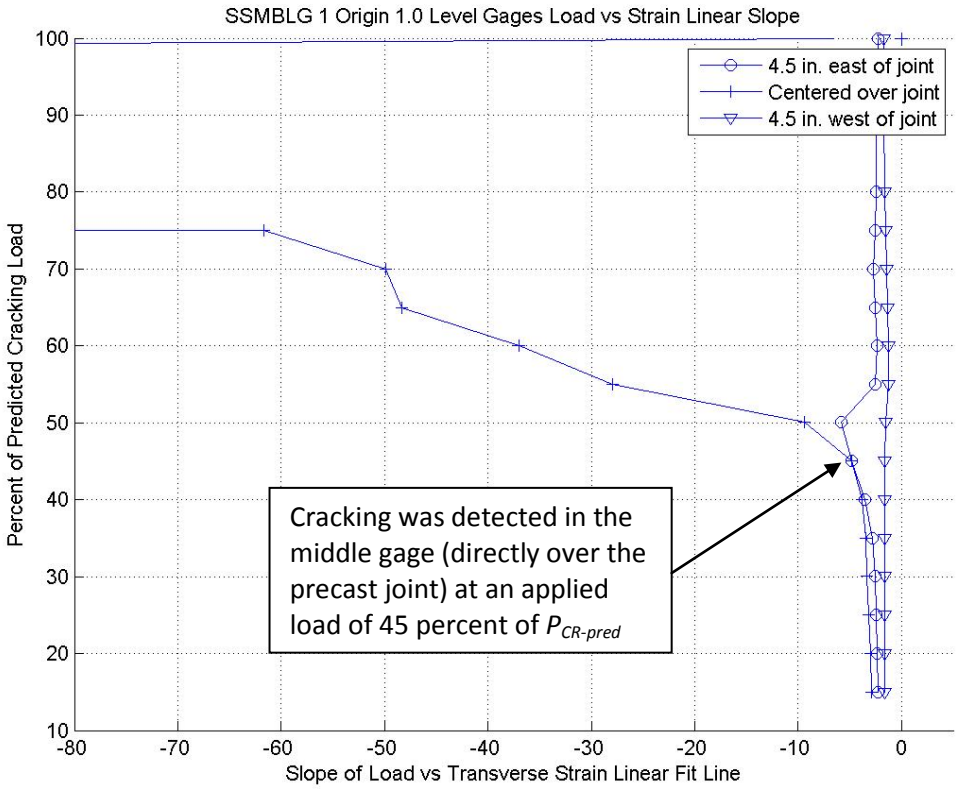

Figure 6.6.19: Slope of linear fit line for load versus 1.0 level strain data at origin cross section in SSMBLG1-Control1

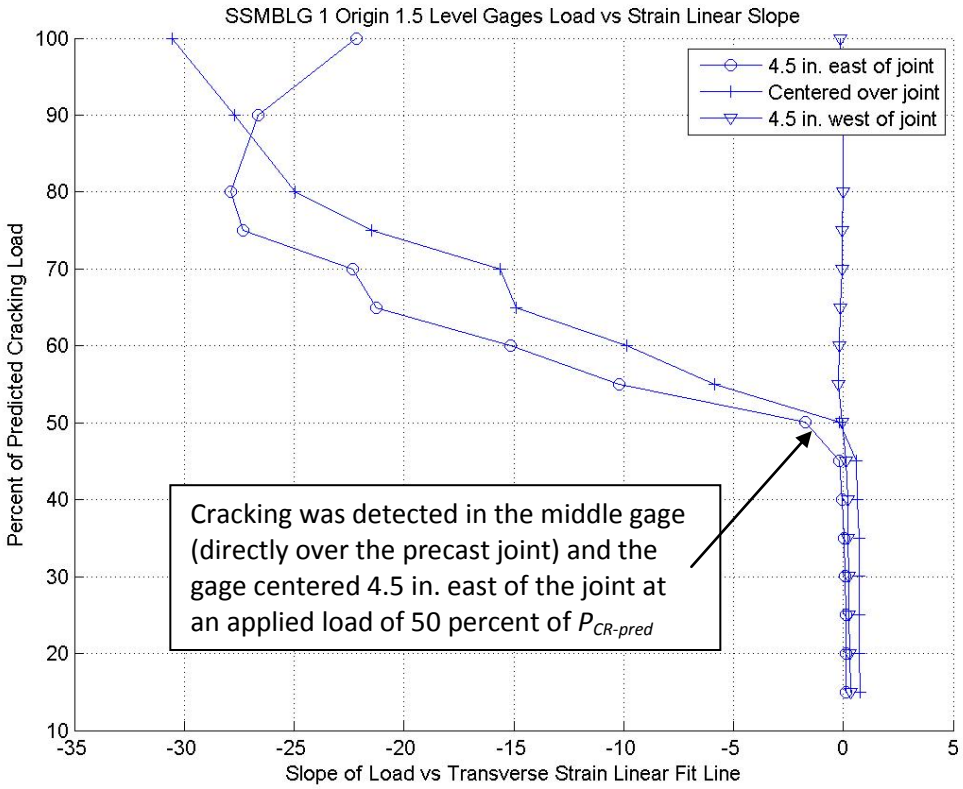

Figure 6.6.20: Slope of linear fit line for load versus 1.5 level strain data at origin cross section in SSMBLG1-Control1

The load at which cracking was first observed was taken as the first data point where a clear difference in the slope of the data occurred. For example, in Figure 6.6.16, the crack was assumed to be present at the 1.0 location at the midspan cross section at a load of 50% of the cracking load, with cracking observed only in the gage centered over the joint. Furthermore, when cracking was observed in two adjacent gages at similar levels of applied load, it was more likely that a single crack was developed in the region of overlap between the gages as opposed to two independent cracks.

Using this process, the load required to drive a crack to the various vertical levels of each specimen was determined. Recall (from Section 6.2) that the concrete embedment resistive gages were placed at three vertical locations designated 1.0, 1.5 and 2.0. The 1.0 level gages coincided with the depth of the transverse hooked bars which were nominally located 4-½ in. from the bottom of the specimen (for all but SSMBLG3-HighBars). The 1.5 level gages were located 8 in. from the bottom of the section (10 in. for SSMBLG4-Deep), and the 2.0 level gages coincided

with the top of the cage (i.e., top of the precast web) at 12 in. from the bottom of the section (16 in. for SSMBLG4-Deep). The middle cross section contained the 1.0, 1.5, and 2.0 level gages, while the origin cross section contained only the 1.0 and 1.5 level gages.

Figure 6.6.21 and Figure 6.6.22 illustrate the load at which cracking was observed for each specimen at the gages through the depth at the midspan and origin cross sections, respectively.

A specimen exhibiting superior performance would have a steeper slope at each gage level, that is, larger levels of load would be required to drive a crack to a given depth. Better performance was observed in SSMBLG6-Frosch and SSMBLG5-No.6Bars, which corresponded with expected results, as the transverse reinforcement details of these two specimens included an increased area of reinforcement (achieved either through tighter spacing or larger bars, respectively). Also pertinent to these specimens was the fact that the cracked section neutral axis was slightly lower in the section than in the other members, as outlined in Table 6.6.3, though the variation in cracked neutral axis depth normalized to the total section depth was relatively small. An analysis of the remaining four specimens suggested that little to no increase in load was required to drive a crack from the lowest level of gage to the highest, indicating a less than ideal reinforcement design. As with the other analyses, SSMBLG3-HighBars were not included in this analysis because this specimen was initially tested with the absence of the clamping system.

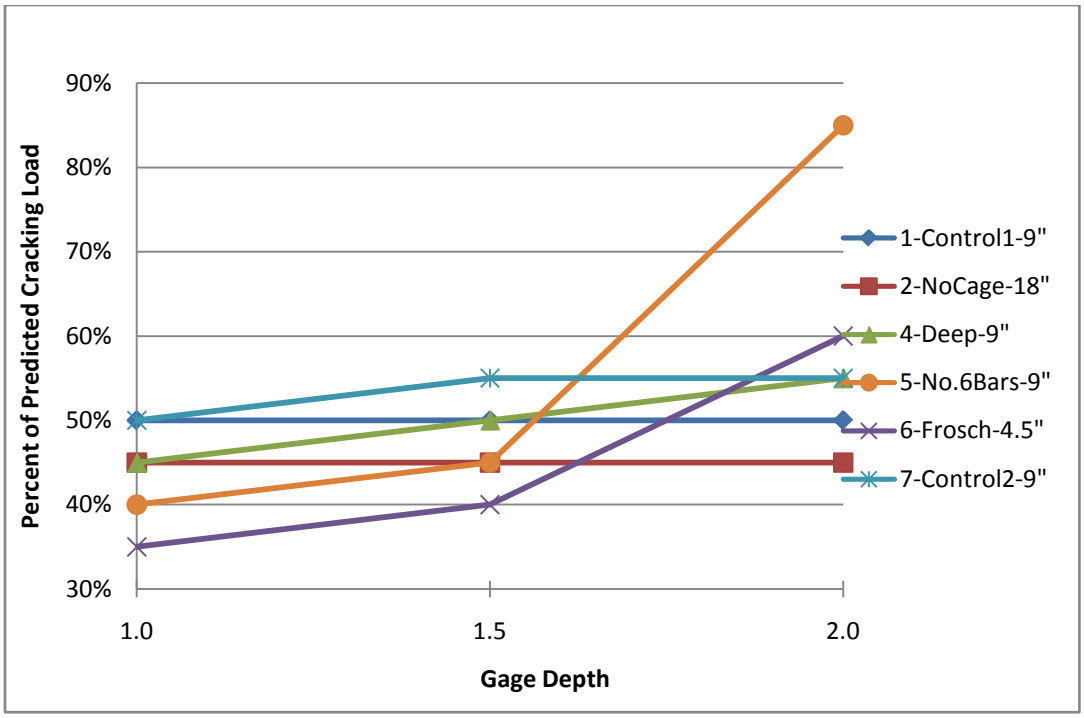

Figure 6.6.21: Load at which cracking was first observed in gages at middle cross section as determined from concrete embedment resistive strain gages

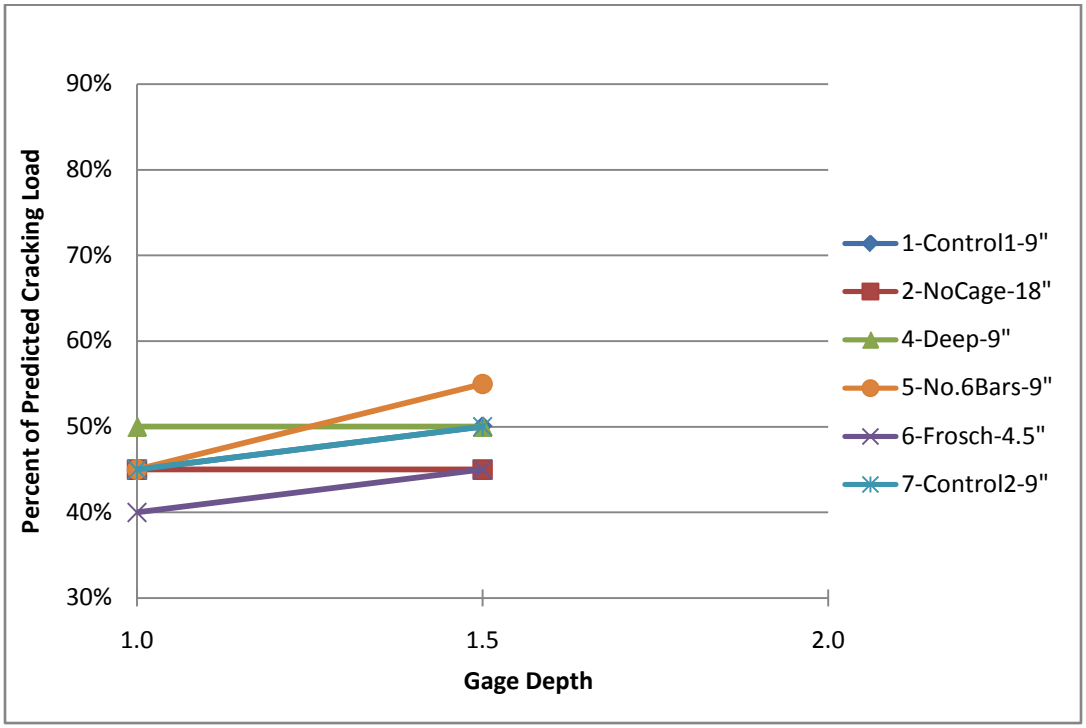

Figure 6.6.22: Load at which cracking was first observed in gages at origin cross section as determined from strain gages

The improved performance of SSMBLG5-No.6Bars and SSMBLG6-Frosch based on the analysis of the strain gage data supported the results from the previous sections. Furthermore, SSMBLG5-No.6Bars outperformed the Frosch specimen as larger levels of load were applied as the crack was driven up towards the top level of instrumentation. The specimen with larger reinforcing bars, which had a slightly larger overall reinforcement ratio for crack control, at 117 percent of the crack control reinforcement ratio of the Frosch specimen, further supported the notion that increased reinforcement area was superior to reduced reinforcement spacing when working to limit the depth of reflective cracking in the sections studied (although the reinforcement ratio provided in SSMBLG5-No.6Bars was closer to that specified by Frosch et al., 2006, because of the desire to maintain the same transverse bar sizes and hook spacing among the specimens). This may have resulted because the reinforcement spacings used in the study were all no larger than 9 in. with the exception of SSMBLG2-NoCage. With adequate reinforcement spacing, the dominant factor observed in controlling the cracking was the amount of reinforcement.

In addition to the investigation of the vertical propagation of cracking, the horizontal propagation was also considered. A longitudinally oriented spreader beam (i.e., parallel to the precast joint) was utilized to apply load during the subassemblage tests to provide a relatively uniform transverse stress gradient (i.e., stresses perpendicular to the precast joint) along the length of the precast joint. The spreader loading was designed to provide a stress field that was constant along the length of the precast joint over which the reinforcement details of each particular specimen could be investigated. Furthermore, uniform loading applied along the structure above the longitudinal joint between the precast elements was necessary to provide an unbiased investigation of the crack mapping completed on the origin and end faces of each specimen, where the influence of the proximity of the embedded reinforcement on surface cracking was monitored. In addition, the investigation of horizontal crack propagation (both along the joint and transverse to the joint) provided a useful metric to identify details that promoted the development of more cracks, which were expected to be smaller in size.

Several transversely oriented concrete embedment and steel resistive strain gages were installed in each subassemblage specimen at various locations along the precast joint, as outlined in Section 6.2. The largest number of gages in a single layer were vertically located at approximately 1.5 in. from the horizontal precast – CIP interface, which corresponded to the vertical location of the center of the transverse hooked bars (in all cases except SSMBLG3-HighBars). A total of ten transversely oriented gages were located at this depth, and were distributed between the middle of the section near the precast joint, and towards the origin face.

The behavior of cracking along the length of the precast joint was investigated using these ten gages, which provided insight into the uniformity of loading as well as a means of comparing the results from the visual observations and DAQ analysis. A plan view of the ten strain gages discussed in this section is shown in Figure 6.6.23. The 120 mm concrete embedment resistive strain gages over the joint, and to the east or west of the joint are illustrated using a square, circle and x symbol, respectively. The 60 mm concrete embedment resistive strain gages over the joint are shown with a star. The steel resistive strain gages are illustrated using a diamond symbol, while cracks observed visually on the end and origin faces of each specimen are denoted by a triangle.

The results of the analysis for each subassemblage specimen are presented in two complementary plots. In both plots, only gages in which cracking was detected are shown, and subsequently the number of data points in each plot varied. The first plot illustrates the load at which cracking was detected by the internal instrumentation or visually on each face versus the location along the precast joint where each of the ten strain gages of interest were located. The horizontal axis corresponds with the "*x*" axis dimension utilized for the duration of the subassemblage tests, and therefore a distance of zero corresponded to the origin face and the end face was located at either 67.25 in. (SSMBLG2-NoCage), 64 in. (SSMBLG6-Frosch), or 62.75 in. (remaining specimens). The first plot provides a means of identifying how uniform cracking was along the length of the precast joint in terms of the level of applied load required to induce cracking, and also provided insight into the uniformity of applied loading using a spreader beam.

The second plot presented for each specimen provides a means of visualizing the geometric location of the crack in terms of approximate lateral distance from the longitudinal joint between the precast flanges. The horizontal axis matches the previously described plot, and corresponds with the length of the precast joint. The vertical axis represents the width of the precast trough region, which is 24 in. Both plots also indicate the transverse hook and cage reinforcement in blue and green vertical lines, respectively. In this case, the gages near the middle and origin face of the specimen provided insight into where the crack was detected internally. The reported location of the crack represents the center of the gage in which cracking was detected, and therefore the location of the crack was given as the nominal "*y*" dimension for the gages, which corresponded to +/- 4.5 in. and 0 in. for the three gages located at each of the two cross sections. Also because of the overlap between adjacent gages, cracking detected in two adjacent gages at similar levels of load suggested that the crack was located in the region of overlap.

The results of the above analysis for each of the subassemblage specimens are shown in Figures 6.6.24 – 6.6.29.

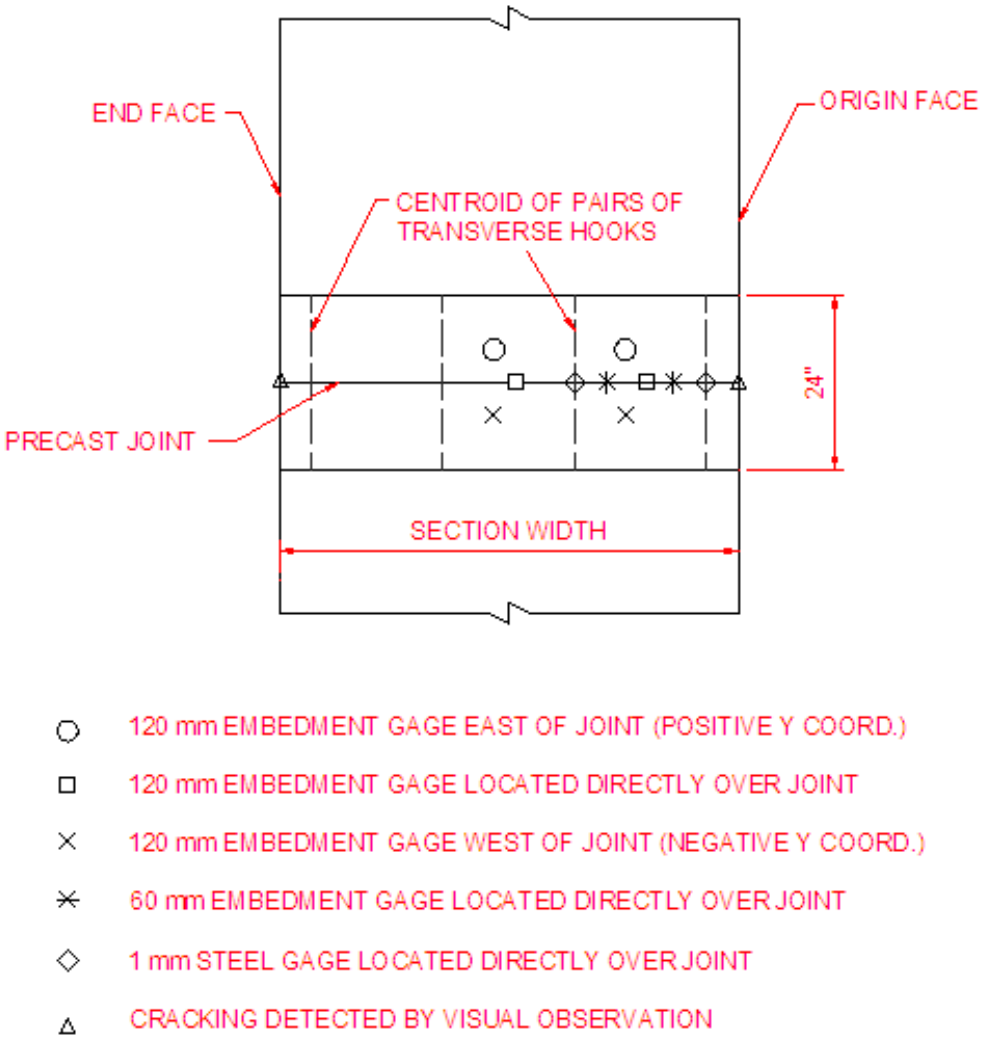

Figure 6.6.23: Strain gage identification utilized for investigation of uniformity of cracking along the length of the precast joint. Pairs of hooks spaced at 18 in. and the cage reinforcement are not shown in the drawing for clarity

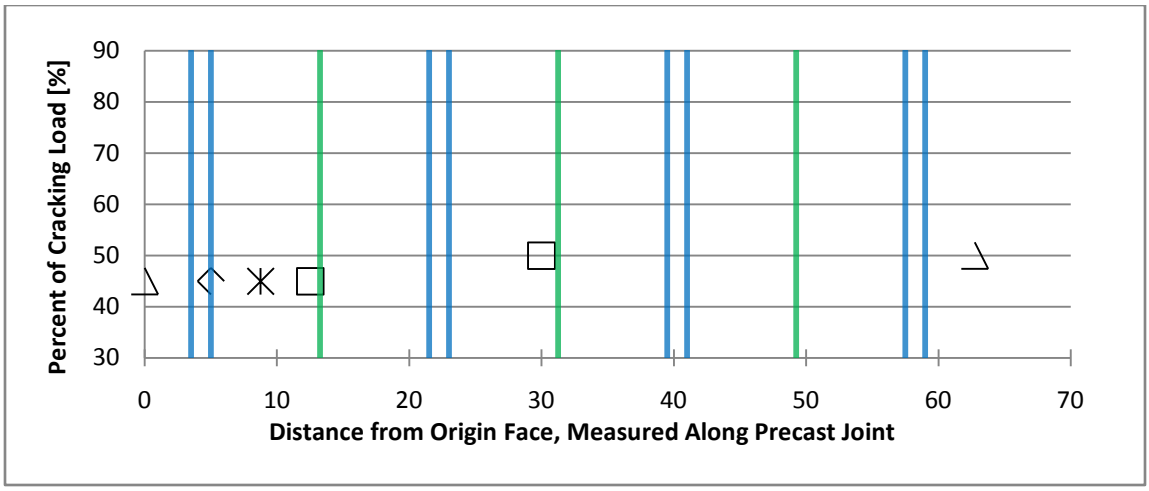

(a) Load at which cracking was detected at various locations along the length of the precast joint

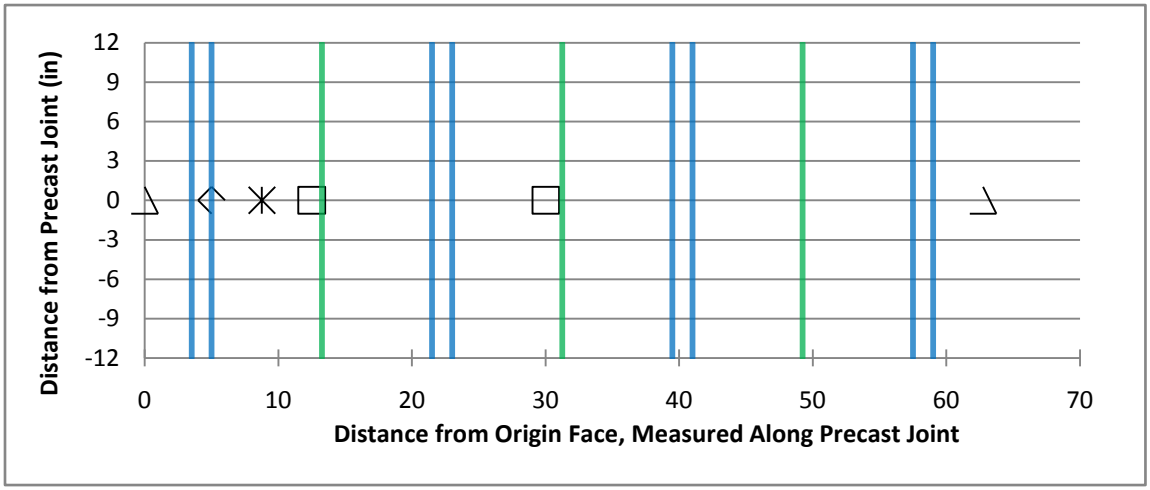

(b) Lateral location of instrumentation in which cracking was detected at various locations along the length of the precast joint

Figure 6.6.24: Load and location at which cracking was detected for SSMBLG1-Control1

The results from SSMBLG1-Control1 showed relatively good uniformity in the location and load at which cracking was observed. The load at which cracking was detected near the origin cross section and the middle cross section varied by only one load step, or 5 percent of the predicted cracking load. Cracking was detected internally near the origin cross section at 45 percent of the predicted cracking load, while not visually observed on the origin or end face until the following load step, at 50 percent of the predicted cracking load. Also, as shown in Figure 6.6.24(b), the

instrumentation in which the crack was detected was that which was centered over the longitudinal joint between the precast flanges.

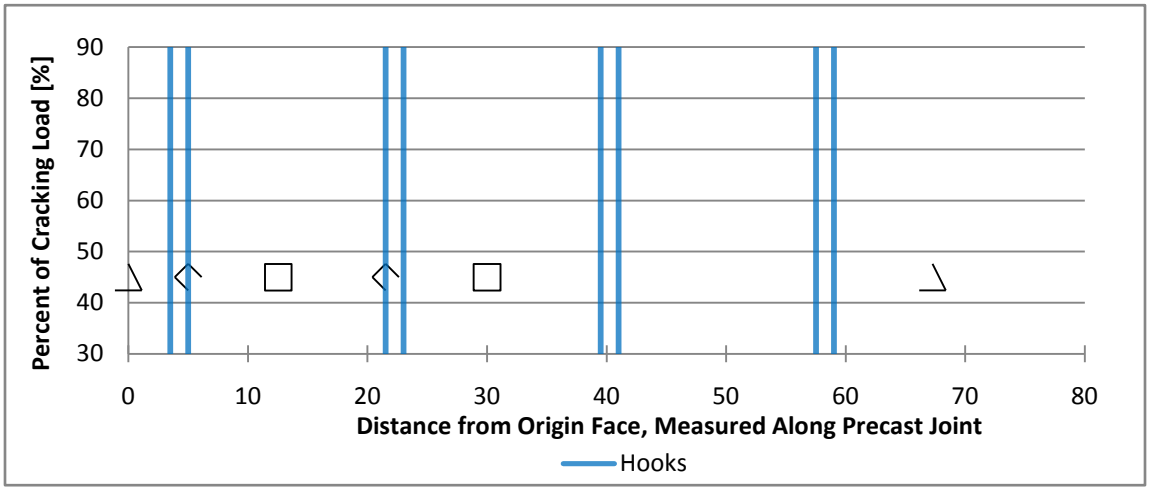

(a) Load at which cracking was detected at various locations along the length of the precast joint

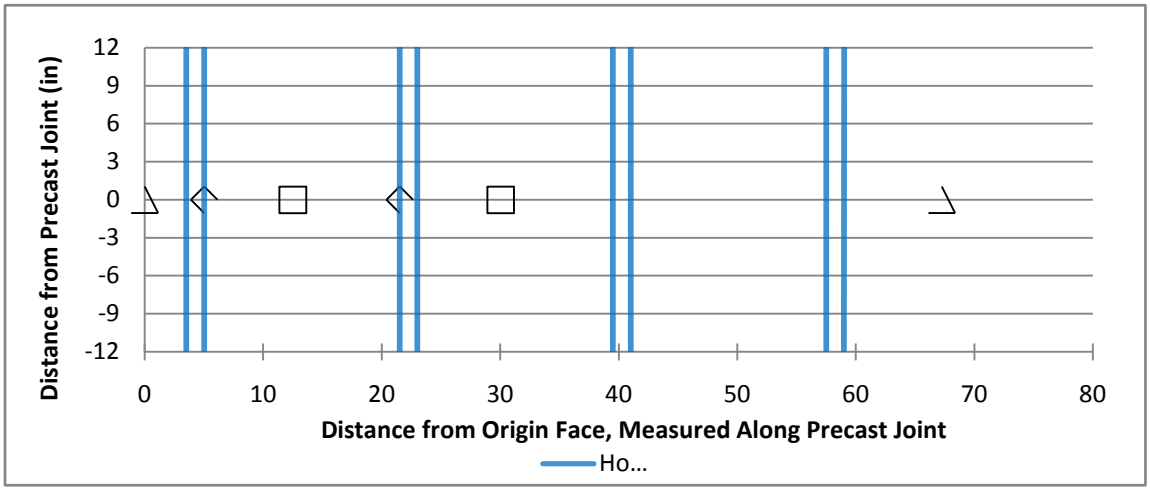

(b) Lateral location of instrumentation in which cracking was detected at various locations along the length of the precast joint

Figure 6.6.25: Load and location at which cracking was detected for SSMBLG2-NoCage

Relatively good uniformity in the location and load at which cracking was detected was also observed for SSMBLG2-NoCage. As with the first specimen, cracking was observed via the embedment instrumentation one load step prior to the visually observed cracking load. Also,

cracking was detected solely in the instrumentation which was centered directly over the longitudinal joint between the precast flanges.

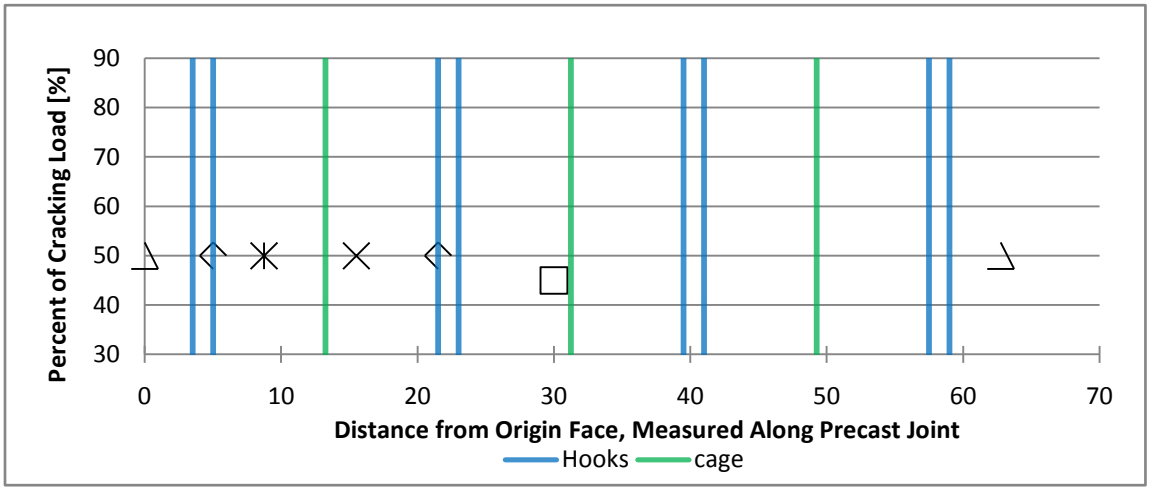

(a) Load at which cracking was detected at various locations along the length of the precast joint

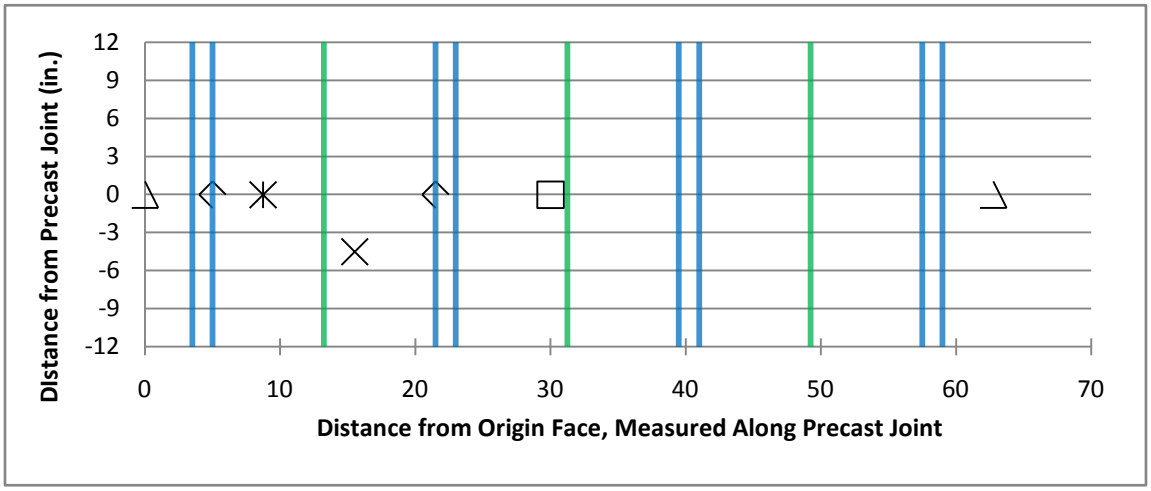

(b) Lateral location of instrumentation in which cracking was detected at various locations along the length of the precast joint

Figure 6.6.26: Load and location at which cracking was detected for SSMBLG4-Deep

As observed in the previous two specimens, the visually observed cracking load was larger than the load at which cracking was detected via the embedded instrumentation for SSMBLG4-Deep. Cracking was relatively uniform along the length of the longitudinal joint between the precast flanges, and varied by 10 percent of the predicted cracking load between the internal and visually

observed results. Cracking at the set of three concrete embedment resistive strain gages near the origin face was detected in the gage centered 4.5 in. west of the precast joint, though the remaining gages near the origin face (which were all centered over the precast joint) also detected the crack.

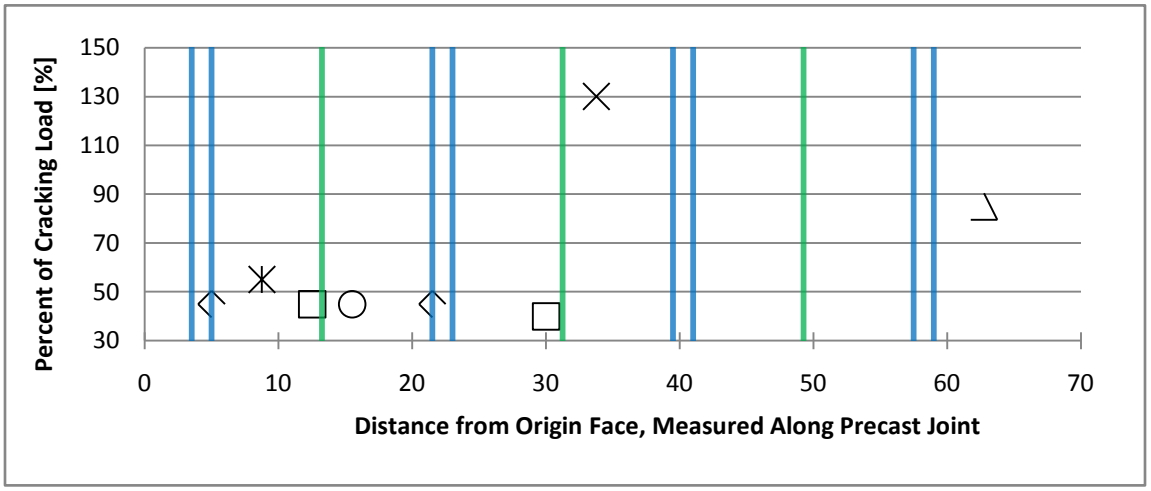

(a) Load at which cracking was detected at various locations along the length of the precast joint

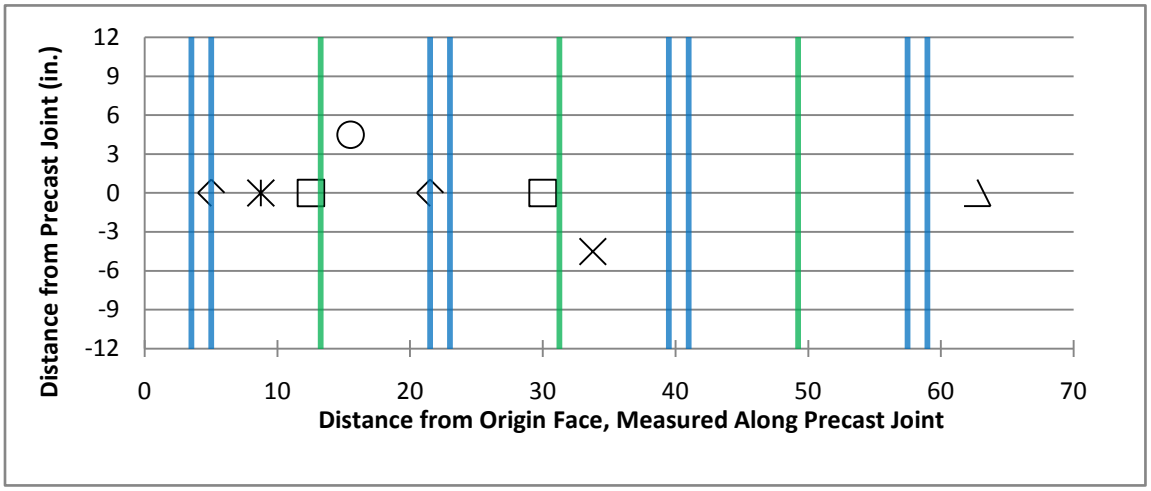

(b) Lateral location of instrumentation in which cracking was detected at various locations along the length of the precast joint

Figure 6.6.27: Load and location at which cracking was detected for SSMBLG5-No.6Bars

The results for SSMBLG5-No.6Bars are shown in Figure 6.6.27. For this specimen, visual observations were not recorded on the origin face of the specimen, and are therefore not present

in the figure. Cracking was first detected in SSMBLG5-No.6Bars with the internal instrumentation at an applied load of approximately 45 percent of the predicted cracking load, which was observed at both the origin and middle cross sections; however the load at cracking detected by the internal gages did not correlate with the load at which cracking was visually observed on the end face, which was approximately 85 percent of the predicted cracking load. The discrepancy between the DAQ and visually observed data is likely due to an error in the load at which cracking was visually observed, possibly as a result of the crack not being immediately identified. This might be attributed to crack widths being smaller in this specimen than those of other specimens where the internal instrumentation and external visual measurements better correlated in terms of crack initiation.

Also observed in SSMBLG5-No.6Bars was that the crack traversed two gages at each of the two multi-instrumented cross sections. Near the origin face, the crack traversed the gage centered over the joint first, and then at the next load step was detected in the gage 4.5 in. west of the joint. This may have indicated that the crack was slightly offset from the longitudinal joint between the precast flanges. At the middle cross section the crack was detected in the gage centered over the joint at roughly the same load as other locations in the section, and then cracking was detected in the gage 4.5 in. east of the joint at a significantly higher load (i.e., a approximately 130 percent of the predicted cracking load). The indication of cracking on the opposite side of the joint compared to the other gage that had previously indicated cracking, at a much later time in the test after the load had been increased significantly, suggests that multiple cracks developed in the section. The presence of multiple cracks was expected to be a beneficial characteristic of PCSSS bridges, because more cracks near the joint suggested that the crack widths may be smaller, and cracks located in the region of the cage reinforcement was preferred to cracking occurring near the vertical precast web, where the cage provided no benefit.

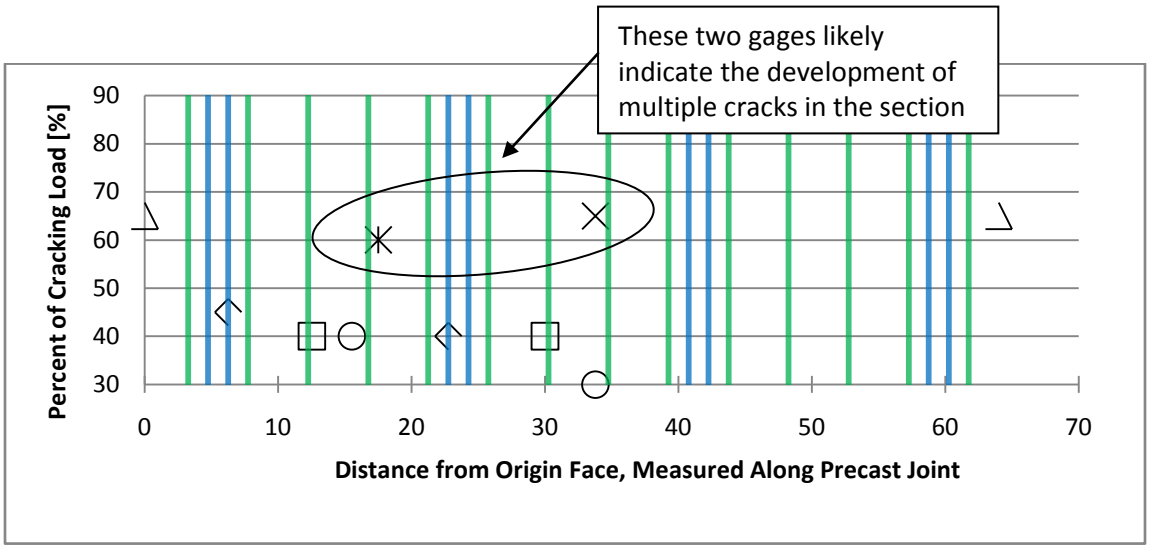

(a) Load at which cracking was detected at various locations along the length of the precast joint

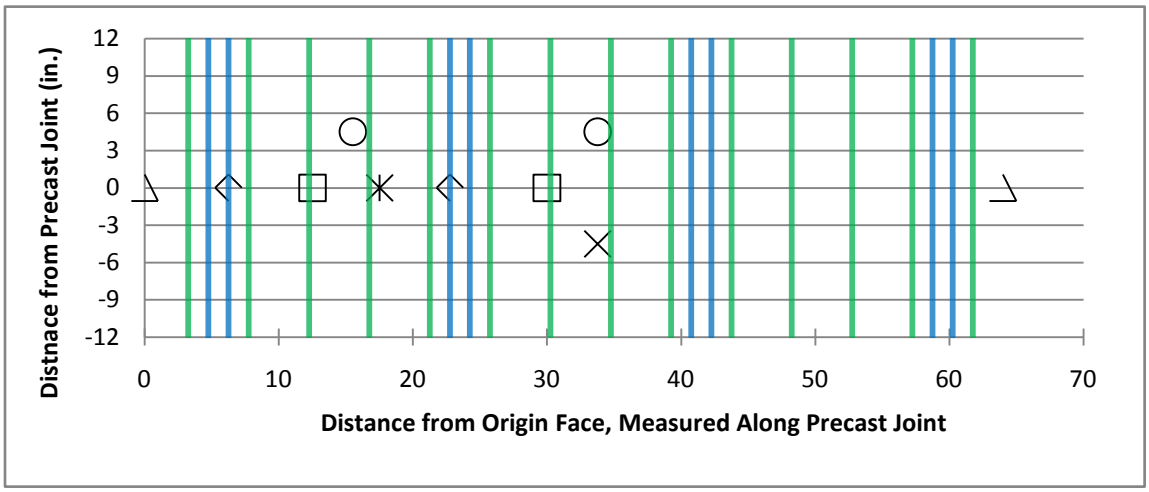

(b) Lateral location of instrumentation in which cracking was detected at various locations along the length of the precast joint

Figure 6.6.28: Load and location at which cracking was detected for SSMBLG6-Frosch

Cracking in SSMBLG6-Frosch was detected in the most number of gages, a total of eight, among the specimens. There was a relatively large variation in the load at which cracking was detected, though the grouping of data points near 40 and 65 percent of the predicted cracking load suggested that multiple cracks were present in the section. Also, as discussed in Section 6.6.2, two cracks were observed near the longitudinal joint between the precast flanges on both the

origin and end faces of this specimen, with the secondary cracks observed visually at approximately 140 percent of the predicted cracking load. These observations suggest that the relatively large reinforcement ratio provided in SSMBLG6-Frosch (which was accomplished through a tight spacing of No. 3 cage stirrups) encouraged the development of more, smaller cracks, as for the case of SSMBLG5-No.6Bars. The presence of multiple cracks was further supported by the results shown in Figure 6.6.28, specifically at the middle cross section, where cracking was detected in the gages centered directly over the joint, as well as the gages centered 4.5 in. in either direction of the joint at different load levels.

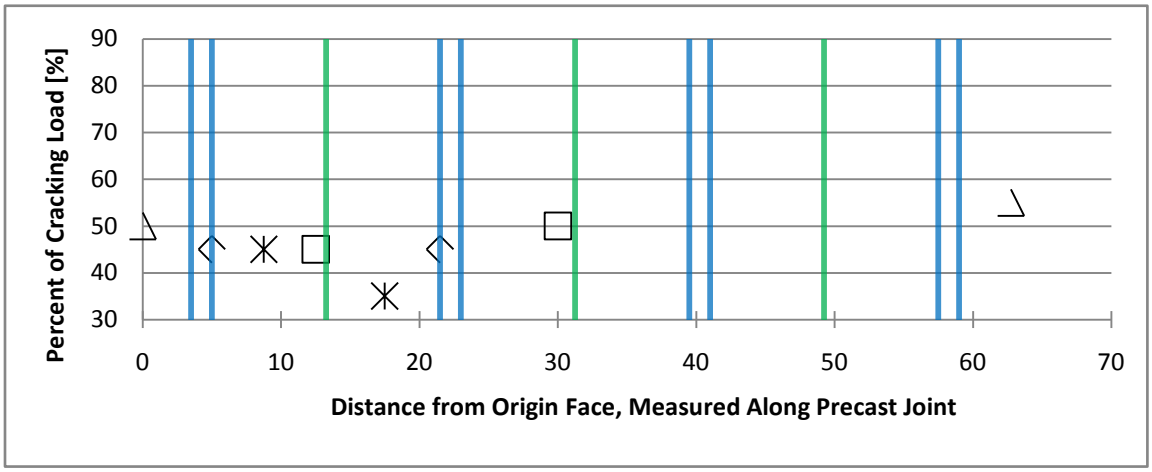

(a) Load at which cracking was detected at various locations along the length of the precast joint

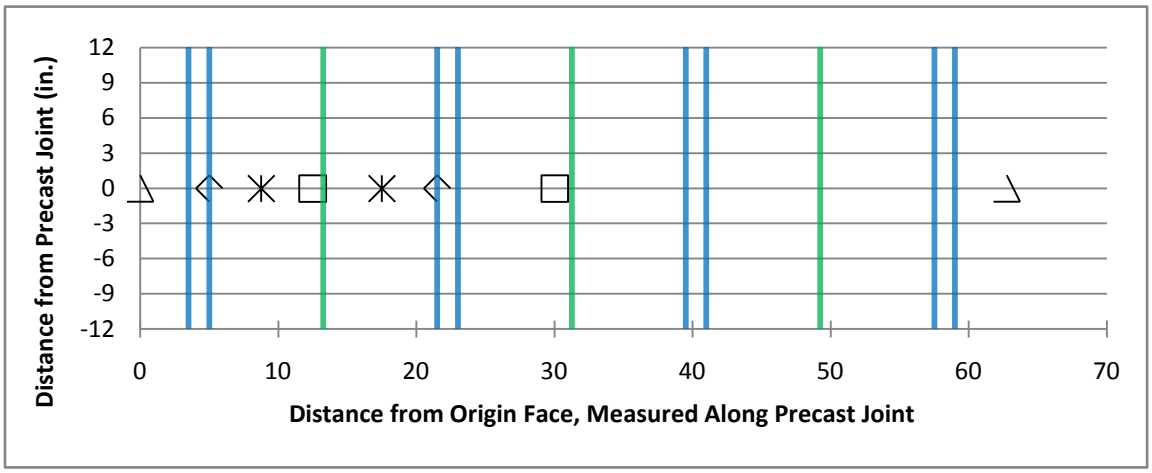

(b) Lateral location of instrumentation in which cracking was detected at various locations along the length of the precast joint

Figure 6.6.29: Load and location at which cracking was detected for SSMBLG7-Control2

The second control specimen exhibited behavior similar to SSMBLG1-Control1, SSMBLG2-NoCage, and SSMBLG4-Deep, in that a single crack was detected along the length of the longitudinal joint between the precast flanges, as shown in Figure 6.6.29(b), at roughly the same applied load despite the presence of the smooth surface condition.

In general, the behavior of the specimens as categorized in this section can be divided into two categories, based on the relative area of reinforcement provided for crack control. SSMBLG1-Control1, SSMBLG2-NOCage, SSMBLG4-Deep, and SSMBLG7-Control2, which had similar amounts of reinforcement for crack control, had cracking that was observed at nearly the same applied load at the various locations along the longitudinal joint between the precast flanges. Furthermore, cracking was generally detected in the gages that were centered over the precast joint. Visual cracking loads observed for these specimens also correlated well with the internal strain measurements. This behavior provided confirmation that the loading setup shown in Figure 6.3.4 adequately induced a region of maximum moment uniformly along the precast joint.

The two specimens with relatively larger reinforcement areas for crack control, SSMBLG5-No.6Bars and SSMBLG6-Frosch appeared to develop multiple cracks in the precast joint region based on the results from the embedded instrumentation. In the case of SSMBLG6-Frosch, this was confirmed with the visual observation of two unique cracks observed on both the origin and end faces of the specimen, as discussed in Section 6.6.2. The introduction of more cracks, each of which was expected to have smaller crack widths, was expected to provide an improved system because the smaller crack widths tend to be more resistant to the ingress of chlorides. The visual cracking loads recorded for these specimens were significantly larger than the cracking loads identified with the embedded instrumentation, which indicates that the crack widths generated in these more heavily reinforced specimens were much smaller than those generated in the more lightly reinforced specimens (SSMBLG1-Control1, SSMBLG2-NOCage, SSMBLG4-Deep, and SSMBLG7-Control2).

6.6.7. Calculation of Expected Tensile Reinforcement Stress in Subassemblage Specimens

An analytical investigation of the stress demands on the tensile reinforcement in each subassemblage specimen was conducted to investigate the expected reinforcement stress ranges among the specimens during loading. The sectional analysis tool BIAX (Wallace, 1989) was utilized to construct moment-curvature diagrams for each specimen. Two models were

constructed for each specimen, one with the concrete tensile strength included in the analysis – which was utilized to identify the cracking moment and stress in the reinforcement before cracking, while the second model neglected the effects of the concrete tensile strength and was utilized to model the behavior after cracking. The stress-strain model for the reinforcement included the effects of strain hardening, which was based on the equation presented by Saenz (1964). The ultimate strength of the reinforcement was assumed to be 100 ksi, with a fracture strength of 90 ksi. The strain at the onset of strain hardening was assumed to be 1 percent. The strain at the ultimate stress was assumed to be 8 percent, with an assumed fracture strain of 10 percent. The initial modulus of elasticity for the strain hardening region was assumed to be 1500 ksi. The measured 28-day concrete compressive strengths, concrete tensile strengths, and reinforcement yield strengths were utilized in the program inputs. The reinforcement yield strength was measured to be approximately 70 ksi for the No. 4 bars, and was assumed to be similar for the No. 6 bars. The reinforcement stress was calculated for increasing moment until a concrete compressive strain of 0.003 (inclusive) was achieved, which was assumed to represent the maximum available concrete compressive strain before crushing occurred.

The predicted tensile reinforcement stress in each specimen is shown in Figure 6.6.30. The vertical axis represents the applied loading, and is given as the ratio of the applied load to the predicted cracking load.

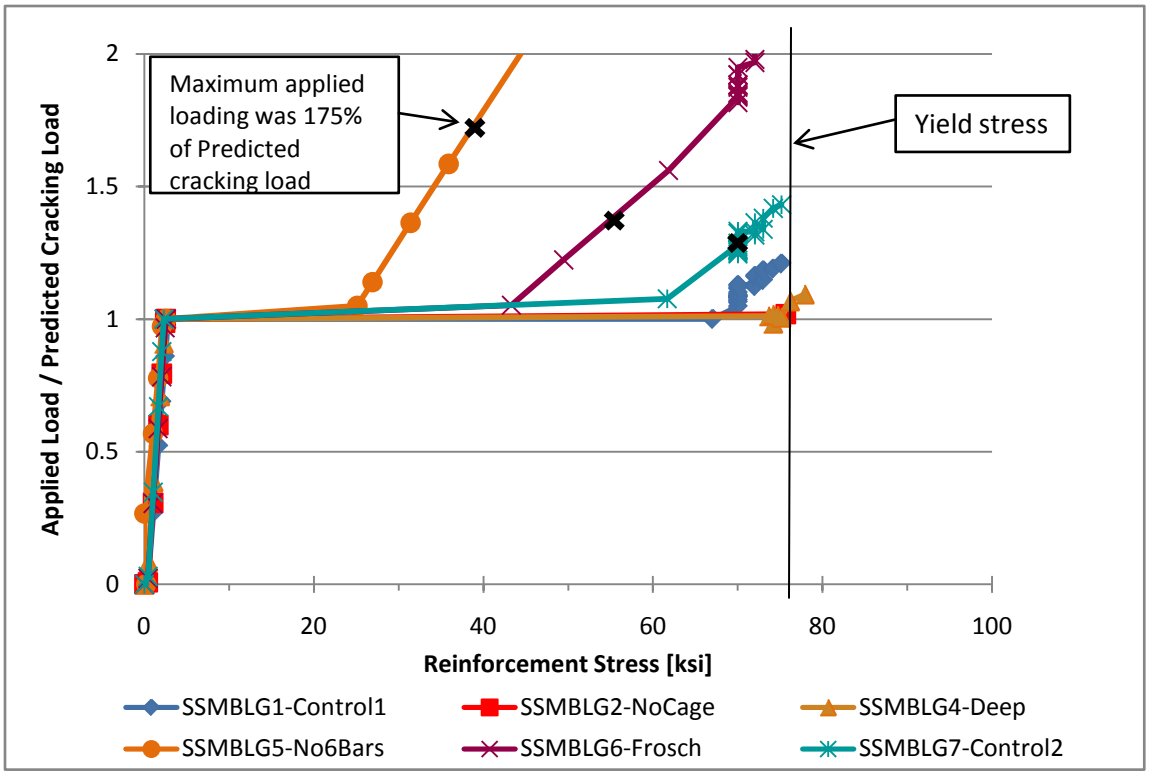

Figure 6.6.30: Predicted tensile reinforcement stress demands as a function of applied loading in subassemblage specimens[1]

[1]The black 'x' symbols indicate the maximum applied load for each specimen during testing. The 'x' symbol was not shown for each specimen for clarity; the maximum applied load for each specimen is given in Table 6.6.4.

The plot shown in Figure 6.6.30 represents the expected tensile reinforcement stress range in each subassemblage specimen for increasing load up to when concrete crushing in compression was expected according to the analysis. The plot is truncated at a ratio of applied load to predicted cracking load of 2, which cuts off the load at which crushing would have been observed for SSMBLG5-No.6Bars. All of the tests were terminated before concrete crushing was observed. Test terminations are denoted by the black "x" symbols for three of the specimens. For clarity, these symbols were left off the plot for the specimens that were expected to undergo concrete crushing near the cracking load. Table 6.6.4 summarizes the maximum tensile reinforcement stress predicted for each of the specimens associated with the maximum loads applied during each of the tests.

Table 6.6.4: Maximum applied loading and associated predicted tensile reinforcement stresses in subassemblage specimens

Specimen	Tensile Reinforcement Area, including cage [in^2]	Ratio of Maximum Applied Load/Predicted Cracking Load	Predicted Tensile Reinforcement Stress [ksi]
SSMBLG1-Control1	1.93	1.0	67.0
SSMBLG2-NoCage	1.60	1.0	75.7
SSMBLG4-Deep	1.93	1.05	76.0
SSMBLG5-No6Bars	3.85	1.75	39.3
SSMBLG6-Frosch	3.03	1.35	54.1
SSMBLG7-Control2	1.93	1.25	70.0

As illustrated in Table 6.6.4, the tensile reinforcement was expected to yield in subassemblage specimens 2 (NoCage), 4 (Deep), and 7 (Control2). As shown in Figure 6.6.30, the reinforcement stresses immediately after cracking in the two specimens with the significantly larger tensile reinforcement areas, SSMBLG5-No6Bars and SSMBLG6-Frosch, were expected to be considerably smaller than yield. This is consistent with the conclusions of the previous sections that the more heavily reinforced specimens exhibited smaller crack widths.

6.7. Destructive Testing of Subassemblage Specimens

The inspection of core specimens was completed by Phil Cici (2010).

At the conclusion of the testing program, three or more cores were removed from each specimen to investigate the physical crack length. Three total cores were taken from each specimen, unless more were deemed necessary to locate a crack. The three cores were removed from the middle of the specimen on a line perpendicular to the joint, with one core centered over the joint, and the remaining two centered over each vertical precast web, as illustrated in Figure 6.7.1. The core locations were selected to facilitate measurement of the reflective crack at the joint and the depth of cracking or separation at the vertical precast web-CIP concrete interface.

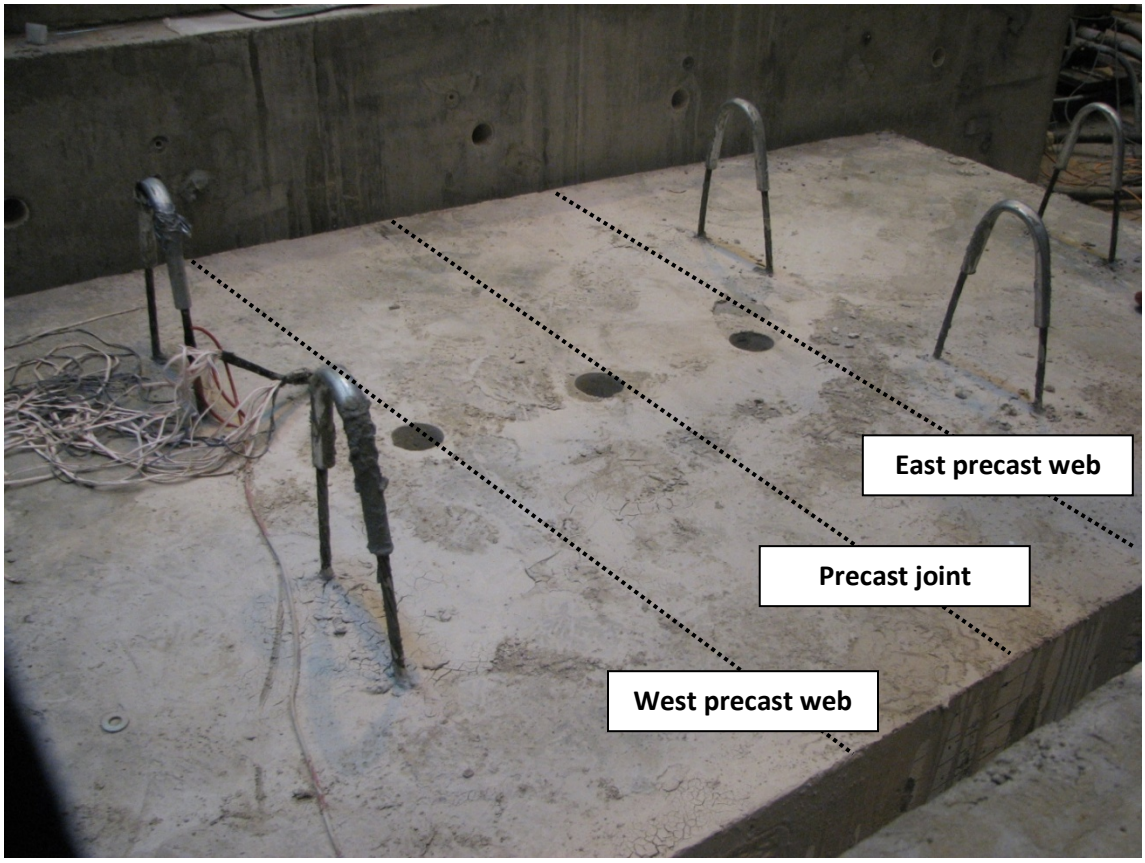

Figure 6.7.1: Coring locations in subassemblage specimens

Each of the core specimens was examined both with the naked eye and the aid of an Olympus SZX12 stereo-microscope to identify the extent of cracking on the core surface. The level of magnification used to examine the cores ranged between 2.1X to 27X, which was the full capacity of the microscope. Any and all cracking that was identified in each core was tabulated, regardless of the size or anticipated origin. The observed crack widths were documented in classification categories, defined in Table 6.7.1. The vertical depth of cracking identified in the cores was referenced from the line created by the horizontal precast flange-CIP concrete interface, as shown in Figure 6.7.2. The characteristics of each core specimen and the measured crack widths and locations for each subassemblage specimen are tabulated in detail in Appendix E.

Table 6.7.1: Crack width classification categories for analysis of core specimens

Crack Classification	Crack Width (W)
0.002	W < 0.002 in.
A	0.002 in. ≤ W < 0.008 in.
B	0.008 in. ≤ W < 0.023 in.
C	0.023 in. ≤ W < 0.200 in.
D	W ≥ 0.200 in.

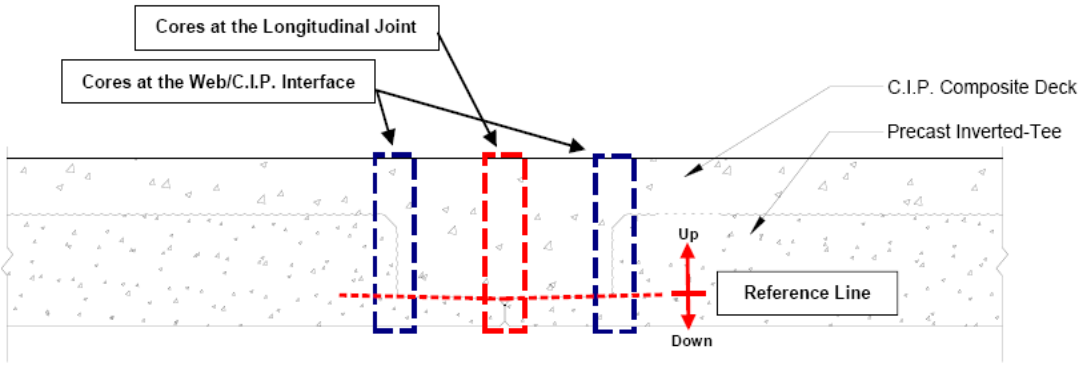

Figure 6.7.2: Location of reference line for measurement of vertical location of cracking in core specimens

The maximum height of the crack, measured vertically upwards from the reference line, and the maximum width of the crack are summarized in Table 6.7.2. Also shown in the table are the maximum crack length and width that were measured on the origin and end faces of the specimens during the tests. The crack length and width correspond to the length and width of the cracks under the applied load in the load step immediately preceding the first observed cracks at the vertical web interface. The maximum values recorded here are the largest of the measured crack widths and lengths documented in Appendix E. Because the cores were removed after the completion of all loading, the observed cracked condition of the core specimens corresponded to the maximum level of loading applied to each subassemblage specimen. Because the cores were subsequently examined under no load, the potential cracks present in the cored samples may have been reduced in size in comparison with the maximum lengths and widths measured at the origin and end faces under load. This was corroborated by the fact that the observed crack widths on the faces of the specimens were reduced after the removal of load.

Table 6.7.2: Summary of maximum height and width of crack measured in core specimens

Specimen	Location of Core	Maximum height of crack[1]	Maximum width of crack[2]	Crack length measured on face[3]		Crack width measured on face[4] (class designation)	
				Origin Face	End Face	Origin Face	End Face
1-Control1-9”	Joint	7.5 in.	C	8.3 in	7.8 in.	0.016 in. (B)	0.011 in. (B)
	East Web	7 in.	B				
	West Web	NO[5]	NO				
2-NoCage-18”	Joint	7.25 in.	B	8.3 in.	8.1 in.	0.014 in. (B)	0.014 in. (B)
	East Web	NO	NO				
	West Web	NO	NO				
3-HighBars-9”	Joint	9.5 in.	B	Values not relevant because clamping assembly was not utilized during the test of this specimen			
	East Web	NO	NO				
4-Deep-9”	Joint	11.5 in.	B	10.3 in	11.3 in.	0.008 in. (B)	0.014in. (B)
	East Web	10.75 in.	B				
	West Web	10.75 in.	A				
5-No.6Bars-9”	Joint	7.5 in.	B	NA	8.3 in	NA	0.014 in. (B)
	East Web	7 in.	<0.002				
	West Web	NO	NO				
6-Frosch-4.5”	Joint	8 in.	B	7.3 in.	7.3 in	0.006 in. (A)	0.010 in. (B)
	East Web	2.25 in.	A				
	West Web	0.75 in.	<0.002				
7-Control2-9”	Joint	NO	NO	7.3 in.	7.3 in.	0.014 in. (B)	0.008 in. (B)
	Joint	NO	NO				
	East Web	NO	NO				
	West Web	NO	NO				

[1]The height of crack was measured from the reference line, defined in Figure 6.7.2; only “upward” values are recorded here

[2]The width of crack was documented by crack classification, as defined in Table 6.7.1

[3]The crack length measured on the face of the specimens was taken as the maximum crack length observed prior to cracking at the vertical web interface, see Section 6.6.5. Values are adjusted to match reference line defined in Figure 6.7.2

[4]The crack width measured on the face of the specimen was taken as the maximum crack width observed prior to cracking at the vertical web interface, see Figures 6.6.6-6.6.7

[5]”NO” represents “No reflective cracks observed”

Most of the specimens with a total section depth of 14 in. had a maximum observed crack height of approximately 7- ½ in., which corresponded to a crack length of 8.2 in. once the chamfer length was taken into account as discussed in Section 6.6.5, which correlated well with the visually observed data on the two faces of the specimens. Cracking was visually identified in all

of the subassemblage specimens with the exception of SSMBLG7-Control2. The width of the crack near the joint region was generally a Class B crack, which has a relatively wide range of crack widths (i.e.: 0.008 in. $\leq$ W < 0.023 in.) and corresponded well to the crack widths observed on the origin and end faces of the subassemblages during testing. The only core to develop a Class C crack, crack width larger than 0.023 in., was SSMBLG1-Control1, in which no specific perturbation in the history of the specimen was known to be the cause.

Cracking or separation of the CIP concrete at the vertical precast web interface was observed on nearly every specimen. The presence of cracking at these locations was not known to exist in field applications of the PCSSS, and was attributed to the subassemblage test setup which induced flexural stresses in the joint region. The results discussed in Section 6.6 do not include measurements or recorded data after the presence of cracking at the vertical web interface was detected, therefore the introduction of cracking at the vertical web was not expected to influence the results in Section 6.6.

An additional core specimen was removed near the joint of SSMBLG7-Control2 after no cracking was identified in any of the three original cores. Investigation of the fourth core did not reveal any cracking in the subassemblage specimen, however cracking was visible on the end faces of the specimen during laboratory testing.

Chapter 7: Conclusions and Recommendations

7.0 Introduction

Several numerical and experimental investigations were completed and reviewed during the NCHRP 10-71 project related to issues of importance to the design and performance of precast composite slab span system (PCSSS) bridges. The results from each of these parts of the study were synthesized to develop a relevant design guide for precast composite slab span bridges. The following sections provide a brief summary of the results that were obtained during these studies.

Numerical studies included an investigation of bursting and spalling stresses in the end zones of precast inverted-T sections, effects of spacing of transverse reinforcement in the joint region, and an investigation of the applicability of the AASHTO (2010) specifications for slab-type bridges to the design of PCSSS bridges for live load distribution factors and for consideration of effects of skewed supports.

Experimental studies were completed on two large-scale laboratory bridge specimens, including a Concept 1 two-span continuous bridge and a Concept 2 simply-supported bridge specimen. The Concept 1 laboratory bridge included variations in a number of parameters including precast flange depth and end zone reinforcement details. It was also instrumented in a study by the Minnesota Department of Transportation (Mn/DOT) to investigate the effects of restraint moment and potential development of reflective cracking (Smith et al. 2008). The Concept 1 laboratory bridge was made available to the NCHRP 10-71 project for further study. In the NCHRP 10-71 study, the performance of both bridge specimens was investigated under various types of loading, including cyclic loading to simulate traffic, loading to simulate environmental effects, as well as to investigate load transfer between adjacent precast panels (both longitudinally and transversely).

One of the keys to the effectiveness of the PCSSS bridge, which also makes it unique relative to slab-type bridges, is the need to control potential reflective cracking in the cast-in-place (CIP) concrete above the longitudinal joint between the adjacent precast flanges. A significant effort in the project was devoted to the investigation of crack control reinforcement and the simulation of potential crack development which was noted in a field instrumented PCSSS in Center City Minnesota. The Concept 1 specimen included No. 6 transverse hooked reinforcement embedded into the precast webs to provide load transfer and crack control in the joint region, as well as No. 5 cage stirrups which contributed to the crack control reinforcement. The nominal maximum spacing between transverse reinforcement was 12 in. (similar to the detail of the Center City

Bridge). The Concept 2 specimen included No. 4 embedded hooked reinforcement in the west half of the simple span, while No. 4 straight embedded bars mechanically connected to reinforcement in the precast webs were provided in the east half span. No. 3 cage stirrups were staggered in the Concept 2 laboratory bridge relative to the transverse reinforcement spaced at 18 in. to provide a maximum spacing of 9 in. between transverse reinforcement.

In addition to the two large-scale laboratory bridge specimens, six subassemblage specimens were tested to investigate the relative performance of various reflective crack control reinforcement details. The subassemblage specimens were loaded to flexurally induce cracking above the longitudinal joint between the precast flanges. The size, quantity, and location of cracking were documented through a range of quasi-static and cyclic load tests.

The culmination of the NCHRP 10-71 was the development of a design guide and examples which is included in Appendices A and B for application to PCSSS bridges. The following sections provide a summary of the investigation and conclusions from the components of the study. The order of the topics focuses on issues related to the precast inverted-T element of the bridge and progresses to system issues.

7.1. Bursting, Splitting and Spalling Stresses

The AASHTO (2007) specification included design procedures to address bursting stresses at the ends of precast prestressed concrete beams due to the effects of the development of prestress, which were likely developed specifically for I-girders. These guidelines required large amounts of vertical reinforcement to be placed within a distance of $h/4$ from the end of the member. The shallow section depths of inverted-T precast beams resulted in limited area for the placement of vertical reinforcement, which led to significant congestion.

Significant changes to the specification in regards to end zone stresses have been incorporated since 2007, specifically in the terminology related to end zone stresses. The 2008 interim AASHTO LRFD specification indicate that “bursting” has been replaced with “splitting” in terms of the resistance of pretensioned anchorage zones, and also represented a wider range of precast member shapes (i.e., not necessarily developed specifically for I-girders), as opposed to the specifications up to and including the 2007 LRFD specifications. The 2008 Interim specifications relaxed the placement requirements for wide-shallow sections, by allowing the designer to spread the end zone reinforcement, termed “splitting” reinforcement over a larger distance. In the case of pretensioned solid or voided slabs, the designer can substitute the section width for “*h*,” rather

than using the section depth for "*h*." According to the NCHRP 10-71 study, this may not be appropriate when trying to control spalling stresses. In addition, the terminology for the reinforcement described in this section of the AASHTO specifications should be termed "spalling" reinforcement rather than "splitting" or "bursting" reinforcement.

Experimental and numerical studies were completed in the NCHRP 10-71 study to investigate the effects of end zone stresses on the precast prestressed inverted-T sections used in the PCSSS. The experimental results from the Concept 1 and 2 laboratory bridge investigations indicated that the 12 in. deep concrete sections had sufficient strength to resist tensile stresses induced in the transfer zone of the precast inverted-T sections at the time of release. Four unique end regions of the Concept 1 laboratory bridge specimen precast members, did not exhibit any evidence of cracking in those regions, even where vertical reinforcement was not provided in the end zones of those specimens. These findings were corroborated with the results of numerical studies that showed certain inverted-T members did not require spalling reinforcement, specifically those members with depths less than 22 in. for which the expected concrete strength was larger than the expected vertical tensile stresses due to the development of prestress.

It was also found that for deep inverted-T sections, in particular, the existing requirements specified by the LRFD specification (AASHTO 2010) may be unconservative. Larger amounts of spalling reinforcement than specified by AASHTO 2010 were found to be required through a numerical study. It was also found that the reinforcement should be placed as close to the end of the member as possible (i.e., within *h*/4 of the end of the member, where "*h*" represents the depth of the member). The end region was the most critical region for the reinforcement to be located to address spalling stresses, even for the case of wide sections.

7.2. Restraint Moment

It is important to consider the effects of restraint moment in the design of PCSSS or design the systems as a series of simple spans. The current specification allows that, when the age of the girder is at least 90 days at the time of continuity, the computation of restraint moments is not required (AASHTO 2010 Article 5.14.1.4.4). The reasoning lies in the fact that, when the girder has aged beyond 90 days, the positive restraint moments caused by the precast beams due to time-dependent effects are minimal, and the negative restraint moments that may be generated can be accommodated by the negative moment reinforcement over the piers.

In the case of PCSSS bridges made continuous by casting the CIP concrete on relatively young girders (e.g., 7 to 14 days old) to complete the continuous composite bridge system, the effects of positive restraint moments should be considered. In these cases the positive restraint moments due to time-dependent effects are typically dominated by the creep of the precast sections. It is recommended that the resulting positive time-dependent restraint moments developed at the piers be computed using the P-method.

Research completed during the Mn/DOT study by Smith et al. (2008) and the current study has shown that restraint moments that develop due to thermal gradients applied to the section are significant, and should be considered in either case (i.e., whether or not time-dependent effects generate positive or negative restraint moments). The positive restraint moment effects attributed to the design thermal gradients can be an order of magnitude larger in some climates than the positive restraint moments due to time-dependent effects. The thermal gradients provided by the AASHTO 2010 specification should be taken into consideration by calculating the resulting expected curvatures of each span treated as simply supported. Subsequent derivation of the resulting restraint moments due to the thermal gradient effects is summarized in Section 3.3. The development of positive restraint moments due to thermal gradient effects would also be expected to be significant in continuous monolithic slab span systems, and should be considered during design. There may be little or no economic gain in continuity because of the large thermal restraint moments that develop and in some cases, continuity may require additional reinforcement in the precast sections (i.e., larger than would be required for a simply-supported design).

7.3. Live Load Distribution Factors

Numerical modeling was combined with observations from a live load truck test on the Center City Bridge along with load distribution tests on the laboratory bridge specimens (i.e., Concept 1 and Concept 2) to determine the applicability of current live load distribution factors in the AASHTO LRFD (2010) specification for slab-type bridges to the PCSSS.

The numerical models illustrated that the longitudinal curvatures measured in the precast slab span system with a reflective crack extending to within 3 in. of the extreme compression fiber and a tandem load greater than that which could be physically applied in the field resulted in longitudinal curvatures which were only 84 percent of the longitudinal curvatures predicted using the AASHTO LRFD (2010) load distribution factors for monolithic concrete slab span bridges,

suggesting that PCSSS-type superstructures could reasonably and conservatively be designed using the current live load distribution factors for monolithic slab-type bridges.

Furthermore, the live load truck tests on the Center City Bridge suggested that the measured longitudinal curvatures were approximately three times less than those calculated using monolithic slab span equations. In addition, the measured longitudinal curvatures were consistently conservative when compared to monolithic slab span FEM models. The conservatism in the factors for monolithic slab span bridges was sufficient to cover the cases of the PCSSS bridges even considering the potential effects of reflective cracking as discussed above.

Load distribution tests on Span 2 of the Concept 1 laboratory bridge and the Concept 2 laboratory bridge included an investigation of the transverse load distribution between adjacent precast panels. For each specimen, loading was applied to the south precast panel, and the longitudinal curvatures in the north and south precast panels were calculated based on measured longitudinal strains located throughout the depth of each section. The longitudinal curvatures were measured at various times throughout the range of testing that occurred on each specimen, and therefore provided an estimate of the curvatures of the sections before cracking was induced near the precast joint, as well as after traffic fatigue loading and loading to simulate cracking along the longitudinal precast joint due to environmental effects. The test was designed such that a reduction in the ability of the PCSSS to transfer load to adjacent precast panels would be indicated by a relative reduction in the measured longitudinal curvature of the unloaded panel.

Both Span 2 of the Concept 1 laboratory bridge and the Concept 2, laboratory bridge showed good load transfer capabilities across the longitudinal joint during intermittent tests conducted throughout the investigation of the laboratory bridge specimens to extend the reflective crack. In both cases, little variation in the measured longitudinal curvatures was observed in the unloaded panels, which suggested that load was effectively transferred across the longitudinal joint from the loaded panel despite the presence and increase in the size of reflective cracking induced in/near the joint.

In summary, the numerical and experimental studies in regards to live load distribution factors indicated that the PCSSS was well represented by monolithic FEM models, suggesting that the discontinuity at the precast joint did not significantly affect the load distribution characteristics of the system. Also, the performance of the large-scale laboratory bridge specimens reinforced the notion that the system provided sufficient transverse load distribution, with and without the presence of reflective cracking near the joint region.

7.4. Skew

Numerical modeling was applied to simply-supported monolithic and jointed (to simulate PCSSS discontinuity at the adjacent precast flange interface) bridge models with skewed supports ranging from 0 to 45 degrees. Three independent load cases were investigated, which included a 35 kip load individually applied over a 12 by 12 in. patch at both quarter points and at midspan for each model. For each load case, the largest horizontal shear stress in the plane above the precast joint nearest the loading was determined. The maximum shear stress from these three load cases defined envelopes for the monolithic and jointed models that varied with skew angle. This maximum horizontal shear stress envelope remained relatively constant through the range of skew angles considered for both jointed and monolithic models. With increasing skew angle, the shear stress envelope increased by approximately 15% for the monolithic models and by less than 10% for the jointed models. The small variation and consistency between the models considering a joint between precast sections with a 3 in. flange and a monolithic structure suggested that the effect of the joint in precast composite slab span construction was not expected to significantly affect the performance of the system in skewed applications, and the design of skewed PCSSS bridges could be completed assuming a monolithic slab span system.

7.5. Composite Action and Horizontal Shear Strength

To conclude the laboratory tests, the large-scale bridge specimens were loaded to near ultimate levels of load to investigate the ability for the precast slab span sections to remain composite with the CIP concrete topping. Placement of reinforcement for horizontal shear was observed to be difficult and time consuming for the fabricator, especially when finishing the top web surfaces. Furthermore, the reinforcement extending from the precast webs for horizontal shear extended out of the precast section with minimal clearance between the hook and the precast web surface to avoid interference with placement of the deck reinforcement in the field. In initial field applications of the PCSSS, the low clearance of this horizontal shear reinforcement may have limited its effectiveness because aggregate was unable to flow below the returned stirrups. In addition, past research by Naito et al. (2006) suggested that concrete girders loaded to induce positive moments in the section without horizontal shear ties were observed to achieve sufficiently large levels of horizontal shear stress and remain composite.

Span 2 of the Concept 2 laboratory bridge was designed with the same horizontal shear layout utilized in the Center City Bridge, which satisfied the design requirements of AAHSTO (2005). Span 1 of the Concept 1 laboratory bridge was designed with fewer horizontal shear ties than were used in Span 2 and in the Center City Bridge, and which did not satisfy the minimum horizontal shear reinforcement requirements of the LRFD specification (AASHTO 2005). The minimum horizontal shear reinforcement requirements have not been modified between the 2005 and 2010 versions of the AASHTO specification. The Concept 2 laboratory bridge was designed and constructed with no horizontal shear ties. In both bridges, the surface condition of the precast member was roughened to a surface consistent with a 1/4 in. rake.

In the tests on both spans of the Concept 1 laboratory bridge and on the Concept 2 laboratory bridge, the sections were observed to remain composite well beyond service load levels, through the full range of loading to the maximum capacity of the loading system, which was in excess of the predicted nominal capacity of the Concept 1 and 2 bridges.

The longitudinal strains measured during the tests on the Concept 2 laboratory bridge (which had no horizontal shear ties) indicated linear distributions through the cross sections. The Kent and Park model (1971) was used to determine the corresponding compressive stress distribution in the CIP section assuming unconfined concrete models. Integrating the nonlinear stress distribution, resulted in an estimate of the maximum compression force achieved in the slab during loading to the ultimate capacity. The horizontal shear stress estimated in the system at the precast-CIP interface was subsequently calculated by dividing the total compression force by half of the center to center of bearing span length and the total width of the bridge structure, and was determined to be 135 psi.

The results of the laboratory tests suggest that the AASHTO LRFD specification should allow for the design of precast slab span structures without horizontal shear ties, and allow for the development of a maximum factored horizontal shear stress of 135 psi in sections with intentionally roughened surfaces (i.e., 1/4 in. rake) unreinforced for horizontal shear.

7.6. Control of Reflective Cracking across Longitudinal Joint between Precast Flanges

Control of reflective cracking was investigated through the development and testing of two large-scale laboratory bridge specimens (Concept 1 and Concept 2 laboratory bridges), as well as through a series of subassemblage tests.

Reflective cracking was intentionally induced in the Concept 1 and Concept 2 large-scale laboratory specimens to investigate the performance of the PCSSS through a range of loading that was designed to simulate both fatigue performance due to vehicular loading, as well as the influence of environmental effects. Two million cycles of fatigue loading were applied near the longitudinal precast joint with a patch load to simulate tire traffic on both spans of the Concept 1 laboratory bridge, as well as on the Concept 2 simply-supported laboratory bridge. The magnitude of measured transverse strain under loading to simulate traffic was on the order of 30με, which was much less than the strains measured in the Center City field bridge after cracking was observed. Therefore, in each case, a reflective crack was introduced near the precast joint region by inducing transverse strains above the horizontal precast flange-CIP interface to replicate strain measurements (i.e., approximately 160 με) observed in a field application of a PCSSS bridge in Center City, Minnesota, that were attributed to reflective cracking resulting from thermal gradient effects. Reflective cracking was induced in each specimen after the completion of one million fatigue cycles and then the laboratory bridge specimens were subjected to an additional one million cycles of simulated traffic loading. This enabled investigation of the fatigue performance of the virgin and cracked systems. In the Concept 2 laboratory bridge, reflective cracking was induced only in the east half span (i.e., associated with straight embedded transverse bars), despite equal loading simultaneously applied at the quarter points of both half spans.

During both the first (i.e., uncracked) and second (i.e., after cracking to approximately 160 με) million cycles of traffic loading, little degradation of the joint was observed in either of the large-scale bridge specimens. The resiliency of the system under simulated traffic load suggested that the PCSSS would provide a durable bridge solution even with the presence of reflective cracking.

Because traffic loading was observed to promote little to no degradation of the system, additional tests were conducted to simulate the large increases in transverse strains that had been measured in the Center City Bridge suspected to be the result of daily fluctuations due to thermal gradient effects. To simulate thermal gradient effects in the laboratory, mechanical loading was applied over the precast joint to induce nominal strains on the order of 180με (target level A) and 300 με (target level B), which corresponded to approximate magnitudes measured in the Center City Bridge. To simulate the repeated yearly effects of daily fluctuations of the thermal gradients, a total of 15,000 cycles of load were applied to induce each of the target level strains (except in the Concept 2 laboratory bridge, where the loading beam fractured after 5000 cycles of load to target level B). The 15,000 cycles at the target strain levels (A and B) each corresponded to

approximately 100 years of environmental effects, conservatively assuming thermal gradients large enough to induce the target strain levels would be expected to occur 150 days a year.

Transverse strains measured under a 35 kip patch load, to simulate the adjacent wheel loads of two truck tires, were documented at various times during the environmental effect simulation for both spans of the Concept 1 laboratory bridge, as well as the Concept 2 laboratory bridge to investigate potential degradation of the joint during these tests. For each specimen, measured increases in the transverse strains under the 35 kip patch load were observed as an increasing number of cycles to induce the target-level strains were completed. After the cycles to the target-level strain B (i.e., 300 με) were completed (i.e., 15,000 cycles for the Concept 1 bridge and 5000 cycles for the Concept 2 bridge), the increases in strains due to the application of the 35 kip patch load were approximately 34, 6, and 23 percent for Spans 1 and 2 of the Concept 1 laboratory bridge, and the east (i.e., straight embedded transverse bars) quarter point of the Concept 2 laboratory bridge, respectively. Degradation of the joint in Span 2 of the Concept 1 laboratory bridge was expected to be most severe because the precast flange was thicker than the remaining specimens causing the transverse reinforcement to be located higher in the section and therefore intercept the reflective cracking at a higher depth, and also because the instrumentation was located higher in the section, and therefore strains measured in Span 2 would have been larger if they had been measured lower in the section, at the same approximate depths as in Span 1 of the Concept 1 laboratory bridge and the Concept 2 laboratory bridge. Also documented during the environmental effect simulation was the rate of degradation of the joint under the loads required to induce strains of target-level strain B (approximately 300 με). It was observed that the increase in the strain occurred quickly during the first few thousand cycles, and then tended to stabilize.

The performance of both spans of the Concept 1 laboratory bridge and the Concept 2 laboratory bridge was observed to adequately control cracking in the precast joint region throughout loading to simulate traffic and environmental effects related to the thermal gradient.

Reflective cracking was also monitored throughout the range of testing for seven subassemblage specimens to quantify the relative performance of the respective design details for reflective crack control in each specimen. A primary metric recorded during these tests was the width and stability of the observed cracks throughout the range of applied loads. The ability for each specimen to control the width of cracking was desirable, as large cracks were expected to cause degradation of the longitudinal joint region including providing a potential avenue for the ingress of moisture and chlorides.

Each of the subassemblage specimens performed adequately throughout the range of loading, though variations in the extent of cracking indicated some relative differences. The two specimens with the largest reinforcement ratios, SSMBLG5-No.6Bars (ρ_{cr}=0.0061, as defined in Figure 5.1.2) and SSMBLG6-Frosch (ρ_{cr}=0.0052), performed well relative to the remaining specimens. In these two specimens, measured crack widths were consistently smaller than the remaining specimens. SSMBLG7-Control2 also indicated better than average performance through visual observations, however the analysis of the embedment instrumentation suggested that the behavior of this specimen was similar to the specimens in the group not including SSMBLG5-No.6Bars and SSMBLG6-Frosch. The behavior of SSMBLG7-Control2 was attributed to a relatively smooth precast flange surface achieved prior to the placement of the CIP concrete (which was done in anticipation of studying a debonded flange surface, which was abandoned to allow for a second control specimen to be tested). The relatively smooth flange surface was expected to better distribute transverse stresses across the precast flanges in the joint region, thereby reducing the potential stress concentration at the interface between the adjacent precast flanges which created a longitudinal joint, however it was observed via an analysis of the horizontal crack propagation using the concrete embedment resistive strain gages that a single crack was present internally in the specimen, suggesting that the smooth flange surface did not distribute the transverse stress adequately well so as to promote the development of multiple cracks. A completely debonded surface, however, was not expected to be desirable, as it would likely promote delamination of the horizontal precast flange-CIP interface, which was expected to promote cracking at the vertical precast web, where cage reinforcement was not present to aid in the control of cracking.

In the subassemblage tests, the best performing specimens, SSMBLG5-No.6Bars and SSMBLG6-Frosch, had the largest amounts of steel as noted above (ρ_{cr} of 0.0061 and 0.0052, respectively). Although SSMBLG6-Frosch was named after the Frosch et al. (2006) recommendations, the reinforcement ratio of the SSMBLG5-No.6Bars specimen more closely correlated with that of the Frosch recommendations for crack control. SSMBLG5-No.6Bars had No. 6 transverse hooks spaced at 18 in., which was supplemented with No. 3 bars spaced at 18 in. in a cage that was staggered relative to the transverse hooks such that the maximum spacing was 9 in. to provide crack control over the longitudinal joint region between the precast flanges. SSMBLG6-Frosch was fabricated with No. 4 transverse hooks spaced at 18 in., supplemented with No. 3 bars spaced at 4.5 in. in a cage that was offset around the transverse bars. The maximum spacing in the SSMBLG6-Frosch specimen was 4.5 in., and narrowed in the region where the cage

reinforcement bounded the transverse hooks. The tight spacing of the SSMBLG6-Frosch specimen required careful construction tolerances. In the subassemblage study, the maximum transverse 9 in. spacing for crack control appeared to be sufficient as long as enough reinforcement was provided to ensure that the reinforcement did not yield upon cracking. This was evident through the good performance of both of these specimens.

The maximum transverse reinforcement spacing was further investigated by evaluating the performance of the Concept 1 and 2 laboratory bridges which provided more realistic boundary conditions in the longitudinal joint region above the precast flanges. In this study, it was found that the 9 in. maximum transverse reinforcement spacing provided in the Concept 2 laboratory bridge did not correlate with an improvement in the control of cracking near the longitudinal trough area relative to the 12 in. maximum spacing provided in the Concept 1 spans, and therefore an economical design may favor 12 in. transverse reinforcement spacing to 9 in. spacing with no expected reduction in performance. An increase in the maximum transverse reinforcement spacing to 18 in. is not recommended, primarily because cracking in SSMBLG2-NoCage (which was reinforced with only transverse No. 4 bars spaced at 18 in.) was generally largest and crack widths increased with the least increase in the applied load relative to the other subassemblage specimens which had transverse reinforcement spacings on the order of 9 in. (except for the SSMBLG6-Frosch which had the 4.5 in. spacing), which were observed to provide acceptable crack control.

Furthermore, little difference was observed between the performance of the sections of the Concept 1 laboratory bridge where reflective cracking was observed, with No. 6 transverse hooked bars, and the performance of the Concept 2 laboratory bridge where reflective cracking was observed, with No. 4 transverse hooks. There was, however, a noticeable increase in the relative performance of SSMBLG5-No.6Bars and SSMBLG1-Control1, in which the only nominal difference was the larger bars in the former specimen. Because the increased performance observed in SSMBLG5-No.6Bars, which was on the order of SSMBLG6-Frosch, was achieved with larger bars and a maximum transverse reinforcement spacing of 9 in., it was suggested that a design with No. 6 bars and less cage reinforcement was likely to be more economical and easier to implement in the field than the closely spaced reinforcement cage provided in SSMBLG6-Frosch.

7.7. PCSSS Design Recommendations

The research completed during the NCHRP 10-71 study resulted in the development of a comprehensive design guide for the design and construction of precast composite slab span system bridges. The design guide in reference to PCSSS was developed based on previous work by the researchers (Smith et al. 2008, Eriksson 2008) summarized in Chapter 3; numerical studies to investigate the performance of the PCSSS details, as well as considering the system as a whole as described in Chapter 4; and an extensive large-scale laboratory research program summarized in Chapters 5-6. The design guide includes proposed modifications to the AASHTO LRFD 2010 Bridge Design Specification, as well as the AASHTO LRFD Bridge Construction Specifications.

The design guide developed during the NCHRP 10-71 study is included in Appendix A.

References

AASHTO, 1961, *Interim Specifications: Standard Specifications for Highway Bridges*, Washington, DC

AASHTO, 1994, *AASHTO LRFD Bridge Design Specifications 1st Edition*, Washington, DC

AASHTO, 1997, *Standard Specifications for Highway Bridges 16th Edition*, American Association of State Highway Officials, Washington, DC

AASHTO, 2005, *AASHTO LRFD Bridge Design Specifications 3rd Edition*, Washington, DC

AASHTO, 2010, *AASHTO LRFD Bridge Design Specifications 5th Edition*, Washington, DC

ACI 308.1, 1998, *Standard Specification for Curing Concrete*. American Concrete Institute (ACI), Farmington Hills, MI

ACI 224, 2001, *Control of Cracking in Concrete Structures*. American Concrete Institute (ACI) Committee 224, Farmington Hills, MI

ACI 318, 2008, *Building Code Requirements for Structural Concrete and Commentary*, Farmington Hills, MI

Anderson, A.R., *Systems Concepts for Precast and Prestressed Concrete Bridge Construction*, Highway Research Board Special Report, Issue No. 132. 1972. Highway Research Board, Washington D.C., pp. 9-21

ASTM C36, 2009, *Test Method for Compressive Strength of Cylindrical Concrete Specimens*. American Society for Testing Materials, West Conshohocken, PA

ASTM C78, 2009, *Standard Test Method for Flexural Strength of Concrete (Using Simple Beam with Third-Point Loading)*. American Society for Testing Materials, West Conshohocken, PA

ASTM C469, 2002, *Standard Test Method for Static Modulus of Elasticity and Poisson's Ratio of Concrete in Compression*. American Society of Testing Materials, West Conshohocken, PA

Barker, R., and Puckett, J., *Design of Highway Bridges: An LRFD Approach, 2nd Edition*, 2007. Wiley and Sons, New Jersey

Base, B.D., *An Investigation of Transmission Length in Pre-tensioned Concrete*. Portland Cement Association Research Report No. 5, 1958

Bell, C., Shield, C.K., French. C.W., *Application of Precast Decks and other Elements to Bridge Structures*. Mn/DOT Technical Report No. MN/RC 2006-37, 2006. Minnesota Department of Transportation, Saint Paul, MN

Cici, P. (2010). Personal Correspondence

Blackman, D., *Evaluation of Design Methods for the Control of Early Age Bridge Deck Cracking*, Master's Thesis, 2002, Purdue University, West Lafayette, IN

Endicott, W.A., *'Instant' Bridges Keep Traffic on the Move*, Ascent. 1993. Precast/Prestressed Concrete

Institute, Chicago, IL., pp. 26-28

Erikkson, W.D., *Vertical Tensile Stresses in End Regions of Precast Composite Slab-Span Systems and Restraint Moments*, Master's Thesis, May 2008. University of Minnesota-Twin Cities Graduate School, Minneapolis, MN.

Freyermuth, C.L., *Design of Continuous Highway Bridges with Precast, Prestressed Concrete Girders*. Journal of the Prestressed Concrete Institute 14(2), 1969. pp. 14-39

Fountain, R.S., *A Field Inspection of Prestressed Concrete Bridges*. Portland Cement Association (PCA), 1963.

Frosch, R.J., Bice, J.K., Erickson, J.B., *Field Investigation of a Concrete Deck Designed by the AASHTO Empirical Method: The Control of Deck Cracking*, Indiana Department of Transportation Technical Report FHWA/IN/JTRP-2006/32. September 2006. Indiana Department of Transportation, Indianapolis, IN

Gergely, P., Sozen, M.A., Seiss, C.P., *The Effect of Reinforcement on Anchorage Zone Cracks in Prestressed Concrete Members*, Structural Research Series No. 271, 1963. University of Illinois

Hagen, K. "Development and Construction of Mn/DOT Precast Slab System." PCI National Bridge Conference. October 18, 2005.

Hawkins, N.M., Shahawy, M., *Anchorage Zone Stresses in Prestressed Concrete Beams,* Structural Research Series No. 207, 1960. University of Illinois

Hedegaard, B., (2010). Personal Correspondence

INDOT, 1999, *Standard Specifications*, Indiana Department of Transportation, Indianapolis, IN

Issa, M.A., Yousif, A.A., Kaspar, I.I., Khayyat, S.Y., *Field Performance of Full Depth Precast Concrete Panels in Bridge Deck Reconstruction,* PCI Journal, Vol. 40, No. 1, May-June 1995. Precast/Prestressed Concrete Institute, Chicago, IL, pp. 82-105

Le, Quoc Thanh Chau, "Transverse Cracking in Bridge Decks: Parametric Study." Master's Thesis, 1998. University of Minnesota-Twin Cities Graduate School, Minneapolis, MN

Marshall, W.T., Mattock, A.H., *Control of Horizontal Cracking in Ends of Pretensioned Prestressed Concrete Girders*, Journal of the Prestressed Concrete Institute, 7(5), 1962, pp. 56-74

Merwin, D.P., *Prestressed Concrete Bridge Built in One Weekend*, Ascent, Vol. 13(3). August 2003.

Precast/Prestressed Concrete Institute, Chicago, IL., pp. 32-34

Molnau, K., Dimaculangan, M.C., "Inverted T Design." LRFD Bridge Design Workshop, June 12, 2007

Naito, C., Deschenes, D., *Horizontal Shear Capacity of Composite Concrete Beams without Ties*, Proceedings, Prestressed/Precast Concrete Institute (PCI) National Bridge Conference, 2006. Grapevine, TX

Park, R., Priestley, M.J.N., Gill, W.D., "Ductility of Square Confined Concrete Columns." *Journal of the Structural Division*, ASCE, Vol. 108, No. ST4, April 1982, pp. 929-950

Piccinin, R., Schultz, A., French, C., Shield, C., "The MN/DOT Inverted T-System: Parametric Studies for Preliminary Design". Submitted to the *PCI Journal*, Precast/Prestressed Concrete Institute. 2008

Piccinin, R., 2008. Personal Correspondence

Radabaugh, R.D., *Investigation of Early Age Bridge Deck Cracking*, Master's Thesis, 2001. Purdue University, West Lafayette, IN

Saenz, L.P., "Equations for the Stress-Strain Curve of Concrete." *ACI Journal Proceedings*, Vol. 61, No. 22, September 1964, pp. 1229-1235

SAS Inc., 2004, *ANSYS Version 9.0*, Swanson Analysis Systems, Houston, PA

Smith, M.J., Eriksson, W.D., Shield, C.K., French, C.W., *Monitoring and Analysis of Mn/DOT Precast Composite Slab Span System (PCSSS)*, Mn/DOT Technical Report No. MN/RC 2008-41. September 2008. Minnesota Department of Transportation, Saint Paul, MN.

Suttikan, C., "A Generalized Solution for Time-Dependent Response and Strength of Noncomposite and Composite Prestressed Concrete Beams." University of Texas at Austin, 1978

Tadros, M.K., Baishya, M.C., *Rapid Replacement of Bridge Decks*, NCHRP Report No. 407, National Cooperative Highway Research Program, Transportation Research Board, Washington, DC, 1998

Tokerud, R., *Precast Prestressed Concrete Bridges for Low-volume Roads*, PCI Journal. 1979. Precast/Prestressed Concrete Institute, Chicago, IL.

Uijl, J.A.d., *Tensile Stresses in the Transmission Zones of Hollow-Core Slabs Prestressed with Pretensioned Strands Report 5-83-10*, The Netherlands: Delft University of Technology Department of Civil Engineering, 1983

Wallace, J.W., BIAX – *A Computer Program for the Analysis of Reinforced Concrete Sections*. University of California at Berkeley, 1989

Zia, P., Preston, H.K., Scott, N.L., and Workman, E.B., *Estimating Prestress Losses*. Concrete International, June 1979. pp. 32-38

Appendix A

NCHRP 10-71 Design Guide

Project No. 10-71 **Copy No.___**

Cast-in-Place Concrete Connections for Precast Deck Systems

Proposed
Design Recommendations

including recommended changes to
AASHTO LRFD Bridge Design Specifications and
AASHTO LRFD Bridge Construction Specifications

Prepared for
National Cooperative Highway Research Program
Transportation Research Board
of The National Academies

C.E. French, C.K. Shield, D. Klaseus, M. Smith, W. Eriksson
University of Minnesota – Twin Cities
and
Z. J. Ma, Peng Zhu, Samuel Lewis, Cheryl E. Chapman
University of Tennessee – Knoxville

January 2011

ACKNOWLEDGMENT OF SPONSORSHIP

This work was sponsored by the American Association of State Highway and Transportation Officials, in cooperation with the Federal Highway Administration, and was conducted in the National Cooperative Highway Research Program, which is administered by the Transportation Research Board of the National Academies.

ACKNOWLEDGMENTS

The design recommendations presented herein were developed under NCHRP 10-71 Cast-in-Place Concrete Connections for Precast Deck Systems by investigators from the Department of Civil Engineering at the University of Minnesota, the Department of Civil and Environmental Engineering, University of Tennessee – Knoxville, Eriksson Technologies, Inc., Berger/ABAM Engineers, Inc., Concrete Technology Corp., and Central Pre-Mix Prestress Co. The University of Minnesota was the contractor for this study.

The principal authors of this report are Catherine French, Carol Shield, David Klaseus, Matthew Smith, and Whitney Eriksson, University of Minnesota, and Z. John Ma and Peng Zhu, Samuel Lewis, Cheryl E. Chapman of the University of Tennessee Knoxville. Gratitude is also expressed to Brock Hedegaard, Roberto Piccinin, Max Halverson, Ben Dymond, and Professor Arturo Schultz of the University of Minnesota for their contributions to the project. The research team also gratefully acknowledges the input provided by the NCHRP research panel and program directors.

Foreword

Strong momentum exists for the growing use of precast elements in bridge construction as a means to speed construction and minimize disruption to traffic and commerce. Precast construction also offers higher quality control compared to on-site concrete casting and can reduce the impact of bridge construction on the environment through the elimination of formwork. Two recent NCHRP projects have focused on the investigation of precast decked systems: NCHRP 12-65 Full-Depth, Precast-Concrete Bridge Deck Panel Systems and NCHRP 12-69 Design and Construction Guidelines for Long-Span Decked Precast, Prestressed Concrete Girder Bridges. NCHRP 12-65 addressed the development of transverse and longitudinal connections between full-depth, precast-concrete bridge deck panels, with emphasis on systems without overlays and without post tensioning through the connection. NCHRP 12-69 addressed I-beam, bulb-tee, or multi-stemmed girders with integral decks cast and prestressed with the girder.

This report contains the design recommendations which have been developed as an outcome of project NCHRP 10-71 Cast-in-Place Reinforced Connections for Precast Deck Systems. The focus of this project has been the development of specifications, guidelines, and examples for the design and construction of durable cast-in-place (CIP) reinforced concrete connections for precast deck systems that emulate monolithic construction. The typical sequence of erecting bridge superstructures in the United States is to erect the precast prestressed concrete or steel beams, place either temporary formwork or stay-in-place formwork such as steel or concrete panels, place deck reinforcement, cast deck concrete, and remove formwork if necessary. This project focused on systems that eliminate the need to place and remove formwork thus accelerating on-site construction and improving safety.

The three systems considered in NCHRP 10-71 to accomplish these objectives were identified during the 2004 Prefabricated Bridge Elements and Systems International Scanning tour (International Scanning Study Team, 2005). The scanning tour visited France, Belgium, Japan, and the Netherlands with eleven participants representing FHWA, State Departments of Transportation, National Association of County Engineers, industry, and academia. The study team developed a series of recommendations related to prefabricated elements and systems to be used for superstructure systems, along with substructure systems and movement systems for rapid replacement and construction. Three of the superstructure systems were identified to be specifically addressed in NCHRP 10-71. These systems included: (1) a precast composite slab-span system (PCSSS) for short to moderate span structures, (2) full depth prefabricated concrete decks, and (3) deck joint closure details (e.g., bulb-tee flange connections) for precast prestressed concrete girder systems for long span structures. Each system uses precast elements that are brought to the construction site ready to be set in place and quickly joined together. Depending on the system, the connections are either transverse (across the width of the bridge) or longitudinal (along the length of the bridge); however, practices differ in detailing the transverse and longitudinal connections.

The design recommendations contained herein are divided into two sections. Section 1 contains the recommendations for precast composite slab-span system (PCSSS) bridges. These recommendations encompass the entire design of the system, as the connections are integral with the performance of the entire composite system. Section 2 contains the recommendations for the longitudinal and transverse joints of the decked bulb-tee and precast panel systems. This study was focused only on the design of the cast-in-place joints within these systems, rather than the systems themselves. The design recommendations for the systems have been covered

elsewhere through recommendations developed in conjunction with NCHRP 12-65 and 12-69 and are not repeated herein. In addition to the detailing requirements for these connections, however, performance requirements were developed for the closure pour materials to be used with these connections, which are included herein.

Table of Contents

List of Figures

List of Tables

Section 1: Precast Composite Slab-Span System

1.0 Introduction to Design Recommendations for PCSSS Bridge Systems

This section contains design recommendations to facilitate the adaptation and use of precast composite slab span system (PCSSS) bridges. The Minnesota Department of Transportation (Mn/DOT) developed the initial implementation of PCSSS bridges in the US as an outcome of a *2004 Prefabricated Bridge Elements and Systems International Scanning Tour* (International Scanning Study Team, 2005). The PCSSS, based on the French Poutre Dalle system, is an efficient section for short to moderate span structures. Precast inverted-T panel elements are readily assembled at the construction site and serve as formwork for the cast-in-place concrete which acts compositely with the panels. Transverse reinforcement protruding from the precast webs serves as transverse load distribution reinforcement and also serves as crack control reinforcement in conjunction with a drop-in cage that is placed in the trough over the longitudinal joint between adjacent precast webs.

The recommendations contained herein are based on a comprehensive study that includes information from the field performance of PCSSS bridges and the results of the NCHRP 10-71 study on *Cast-in-Place Concrete Connections for Precast Deck Systems*. The NCHRP study included large-scale laboratory tests on two-span and simple-span PCSSS bridges, as well as, seven subassemblage tests. The two-span and simple-span large-scale bridge specimens provided an opportunity to investigate different cross-sectional details and associated aspects of bridge behavior. These include the effect of flange thickness and type and quantity of transverse joint reinforcement on reflective crack control; horizontal shear transfer reinforcement on composite action; and bursting reinforcement on crack control at release. The seven subassemblages provided an opportunity to investigate variations in crack control reinforcement across the longitudinal joint between the precast flanges.

1.1. Design Recommendations

The proposed design recommendations for the PCSSS are outlined in the following sections based on the controlling behavior. Significant research effort was concentrated on systems constructed using a 12 in. deep precast inverted T-section panel with cast-in-place (CIP) topping measuring 6 in. deep on top of the precast webs. This composite system provides an efficient design for spans in the range of 20 ft. to 31 ft. While the proposed design recommendations herein are generally applicable to sections of all depths, sample calculations included in this discussion refer to sections constructed with a 12 in. deep precast panel; Figure 1.1.1 shows a cross section of a single 12 in. deep precast member with all relevant dimensions required for calculations contained herein. The maximum span length for efficient application of PCSSS bridges is just over 60 ft.

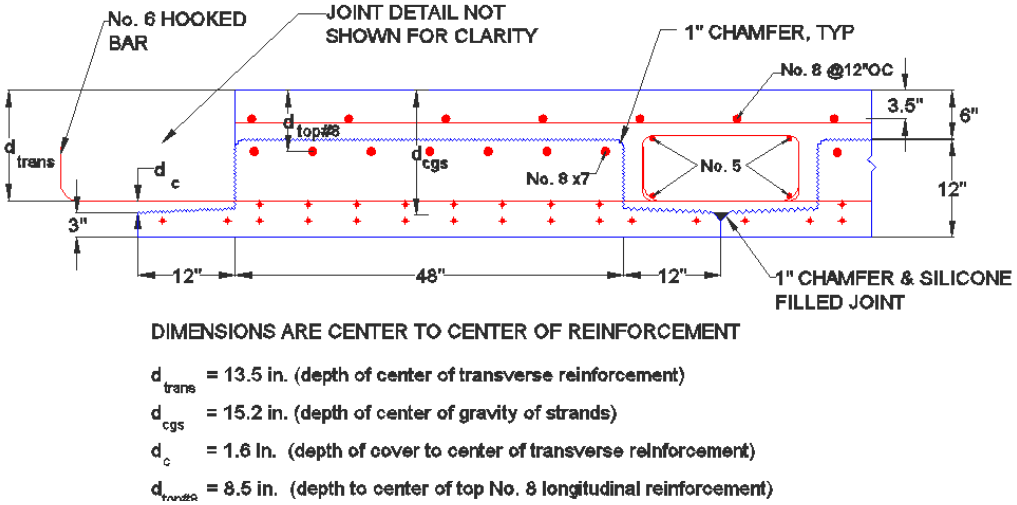

Figure 1.1.1: Typical 18 in. total depth PCSSS cross section and relevant dimensions

Because of the jointed nature of the precast portion of the PCSSS system created by the discontinuity between flanges of adjacent inverted shallow T-sections, and because the continuity of the PCSSS system is provided by cast-in-place (CIP) concrete, rather than through the use of post-tensioning, it is recognized that cracking will likely be initiated in these systems through restrained shrinkage and environmental effects. Consequently, it is important to recognize the existence of such cracking for all design parameters. An important aspect of the design is the control of such cracking through transverse reinforcement located across the joint region in the trough between adjacent precast web sections. It should be noted that CIP systems, which the PCSSS is intended to emulate, are also expected to develop cracks due to restrained shrinkage and environmental effects, as well as due to load effects. In the case of PCSSS bridges, it may be possible to more readily predict locations where cracking due to restraint is likely to occur and apply reinforcement in those regions to control the cracking.

The following design recommendations consist of both proposed modifications to current specifications, generally defined in the 2010 AASHTO LRFD Bridge Design Specifications (5th Edition), as well as general design and construction practices that should be observed by the designer. Anytime AASHTO (2010) is shown in the text, it is meant to reference the 2010 AASHTO LRFD Bridge Design Specifications, unless otherwise noted. Other specifications used in this document include the 2008 ACI 318 Building Code Requirement for Structural Concrete, which is referenced as ACI 318-08 in the text. In the case of modifications to current AASHTO (2010) specifications, proposed additions and deletions to the specification are shown with underline and strikethrough notation, respectively.

It is proposed that a new definition be added for Precast Composite Slab Span Systems in AASHTO (2010) 5.2 as shown below:

AASHTO (2010) Article **5.2 DEFINITIONS**

Post-Tensioning Duct—A form device used to provide a path for post-tensioning tendons or bars in hardened concrete.

.

.

.

Precast Composite Slab Span System— A type of superstructure in which shallow precast prestressed inverted T-sections are made composite with cast-in-place concrete to form a composite slab bridge. The individual precast prestressed inverted T-sections are considered beam elements until made composite with the cast-in-place concrete and are joined transversely with spliced bars that extend from the precast webs. The spliced bars also provide crack control reinforcement in conjunction with a supplemental cage.

Precast Members—Concrete elements cast in a location other than their final position.

.

.

.

1.1.1. Precast Prestressed Inverted-T Design

To better address the design of precast prestressed inverted T-sections incorporated in PCSSS bridges, specifications suggested for modification include AASHTO (2010) Articles 5.14.1.2.2, C5.14.1.2.2, and 5.14.1.2.4

In the initial implementation of PCSSS bridges in the State of Minnesota, the flanges of the precast inverted T-sections were 5.25 in. deep. In the next generation of PCSSS bridges, it was recommended that the flange thickness be decreased to 3 in. for two reasons: (1) to reduce the discontinuity between the adjacent flanges (which acts like a crack between adjacent panels); and (2) to lower the transverse reinforcement that crosses the interface between adjacent panels which better facilitates crack control and the effectiveness of the reinforcement for transverse load transfer. The reduced 3 in. flange depth was deemed to be sufficiently robust for transportation and handling purposes during construction. To investigate the effect of the flange thickness in the NCHRP 10-71 study, the flange thickness was 5.25 in. in one span of the Concept 1 laboratory bridge specimen and 3 in. in the other span as well as in the Concept 2 bridge and the subassemblage specimens.

The flange thickness is measured at the longitudinal joint, while a taper increases the thickness by 1/4 in. at the vertical web. The flange must provide adequate flexural capacity to hold the wet CIP concrete during construction and associated construction loads. A practical upper bound can be investigated with the 22 in. deep precast section with a 6 in. deep CIP deck, the 3 in. thick flange provides sufficient flexural and shear capacity during construction when the compressive strength of the precast concrete at erection is taken to be 6,000 psi. For this

reason, it is recommended that the flange thickness provided for the inverted-T precast sections be 3 in. at the joint, and taper to 3 1/4 in. at the precast web.

A 1 in. 45 degree chamfer shall be included in the top of the flanges at the precast joint, to provide a channel for a silicone caulk to be applied prior to placement of the CIP concrete. The silicone provides an elastic interface between the PC and CIP concrete at the discontinuity created by the precast joint, and seals the joint so wet concrete doesn't leak through the joint. In addition, a 1 in. chamfer shall be included on the top web corners of the PC member, which removes the potential for a sharp, 90 degree corner at that location. Figure 1.1.1 illustrates the chamfer locations.

Two geometric design constraints that should remain fixed for the design of the precast prestressed inverted-T sections, irrespective of the span length, include the thickness of the flange (i.e., 3 in. tapered up to 3 1/4 in.), and the width of the flange (i.e., 12 in.). Changes to the width of the web of the precast inverted-T section may be required depending on the constraints of a specific project. Issues to consider in selecting the web width include hauling and crane limitations in transporting and placing the precast elements, as well as the availability of appropriate formwork from the precast Fabricator. Longer spans (in excess of 31 ft.) would require deeper precast sections and additional prestress. A precast section thinner than 12 in. should be used with caution, as the investigation of thinner sections was not completed during the NCHRP 10-71 study.

To address these issues associated with the design of the precast inverted-T portion of the PCSSS, the following recommendations in AASHTO (2010) should be modified as indicated below.

AASHTO (2010) Article **5.14.1.2 Precast Beams**

5.14.1.2.1 Preservice Conditions

The preservice conditions of prestressed girders for shipping and erection shall be the responsibility of the contractor.

5.14.1.2.2 Extreme Dimensions

The thickness of any part of precast concrete beams shall not be less than:

top flange……..2.0 in.
web, non post-tensioned……5.0 in.
web, post-tensioned……6.5 in.
bottom flange, non inverted-T……..5.0 in.
bottom flange, inverted-T for precast composite slab-span system……3.0 in.

The width of the bottom flange extension of precast concrete inverted-T beams used for precast composite slab-span systems shall be 12.0 in., unless it can be shown that the distance between webs in the precast composite slab-span

system is sufficient to accommodate the development of the spliced transverse reinforcement, the supplemental cage for crack control, and the spacing of the bottom longitudinal bars in the case of continuous span systems that require reinforcement for positive restraint moment.

The maximum dimensions and weight of precast members manufactured at an offsite casting yard shall conform to local hauling restrictions.

C5.14.1.2.2

The 2.0-in. minimum dimension relates to bulb-T and double-T types of girders on which cast-in-place decks are used. The 5.0-in and 6.5-in. web thicknesses have been successfully used by contractors experienced in working to close tolerances. The 5.0-in. limit for bottom flange thickness normally relates to box-type sections, while the 3.0-in. limit for bottom flange thickness specifically relates to inverted-T type sections with 12.0-in. wide flange extensions for use in precast composite slab-span systems. It is suggested that the bottom flange be tapered from 3.0-in. at the joint to 3.25-in. at the vertical web face of the precast member for precast concrete inverted-T beams used for precast composite slab-span systems to facilitate form removal.

The width of the bottom flange for inverted-T type sections is specified at 12.0-in. to ensure (1) adequate development of the transverse reinforcement spliced in the longitudinal closure joint, (2) adequate space to accommodate cage for supplemental crack control reinforcement, and (3) adequate spacing to accommodate longitudinal reinforcement located in single layer in bottom of cage to provide resistance to positive restraint moments in continuous systems where necessary. Increases in the bottom flange width are not recommended, because the minimum thickness of 3.0-in. of the bottom flange may not be adequate to resist construction loads when the flange is wider than 12.0-in. Increasing the thickness of the bottom flange of inverted-T type sections is not recommended as close proximity of the transverse reinforcement to the bottom of the section is preferred.

…

Total structure depth for the PCSSS shall conform to Article 2.5.2.6.3 of the AASHTO (2010) specification without modification, which provides minimum section depths for serviceability requirements. The PCSSS shall be considered a prestressed concrete slab superstructure, as specified in Table 2.5.2.6.3-1 of the specification. As given by AASHTO (2010), for precast concrete slab superstructures, the minimum depths, including the deck, are 0.030*L* and 0.027*L* for simple and continuous spans, respectively. Furthermore, both equations are capped at 6.5

in. and the span length, *L*, and resulting section depth are both in units of ft. For a simple span, the required minimum section depth for a 31 ft. and 65 ft. span would be 11.2 in. and 23.4 in., respectively, which are smaller than the required section dimensions for strength.

Furthermore, the designer should specify a smooth flange surface. As observed in the second control subassemblage specimen, the smooth flange performed better than many of the other specimens. The smoothness of the flange may help to distribute the transverse loads more uniformly over the width of the longitudinal closure joint. The smooth flange also facilitates the removal of formwork for the precast Fabricator.

The reinforcement provided for confinement of the tendons shall conform to AASHTO (2010) Article 5.10.10.2 as written.

The design of the bearing and connection details at both the end and continuous supports for the PCSSS was motivated by three primary characteristics. First, the PCSSS should be designed such that even and uniform bearing across the full width of the precast inverted-T panel is achieved at the ends of the members, ideally through an elastomeric bearing pad as defined by *AASHTO 2009 Interim LRFD Bridge Construction Specifications Article 18.2* and of sufficient dimension to support the factored loads. The bearing pad should extend across the full width of the PCSSS bridge system, less 6 in. to provide a drip setback. Second, a method for relieving restrained shrinkage at the supports should be considered, such as through the use of a bond breaker between the pier cap and CIP closure pour. Finally, a means of transferring the compression force effectively between adjacent spans at a continuous support should be considered. During the current study, a 10 in. flange blockout was utilized near the continuous support to facilitate the development of negative moment at the pier by providing integral CIP concrete within the compression zone of the beam in the joint regions. The 10 in. flange blockout is illustrated in a plan and cross-sectional view of a continuous pier in Figures 1.1.2 and 1.1.3, respectively. The bearing pads are shown in Figure 1.1.2 with diamond hatching, and are not included below the 24 in. trough region, thereby allowing the CIP concrete to be placed directly against the pier cap in these locations, though a bond breaker, when utilized, would separate the interface between the pier cap and CIP concrete.

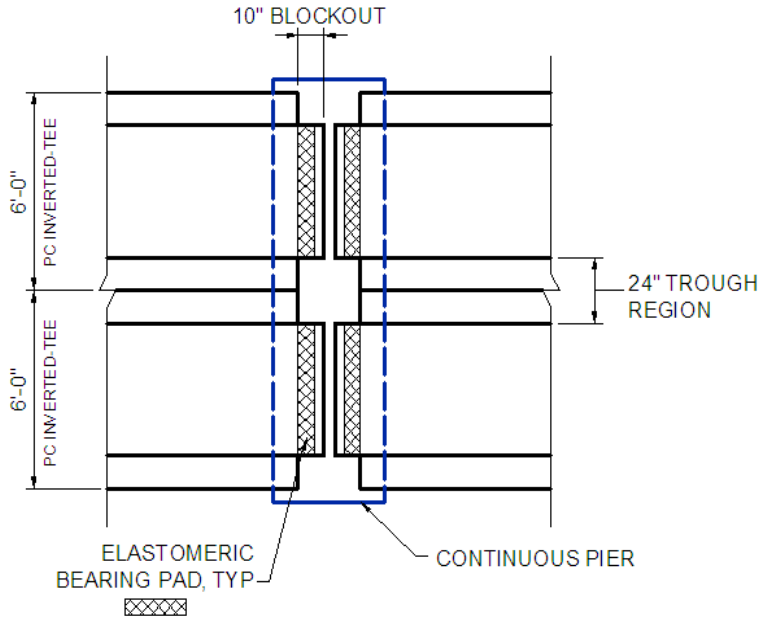

Figure 1.1.2: Plan view of a PCSSS flange blockout at a continuous pier to facilitate the development of negative moment at the pier

A cross-sectional view of the PCSSS and support at a continuous pier is shown in Figure 1.1.3. As in the previous figure, the bearing pad material is shown with a diamond hatching. Also shown is a polystyrene foam in the regions between the precast inverted-T members and the pier, which provided containment for the CIP concrete during the closure pour, but was relatively crushable and was therefore not expected to significantly affect the location of center of bearing.

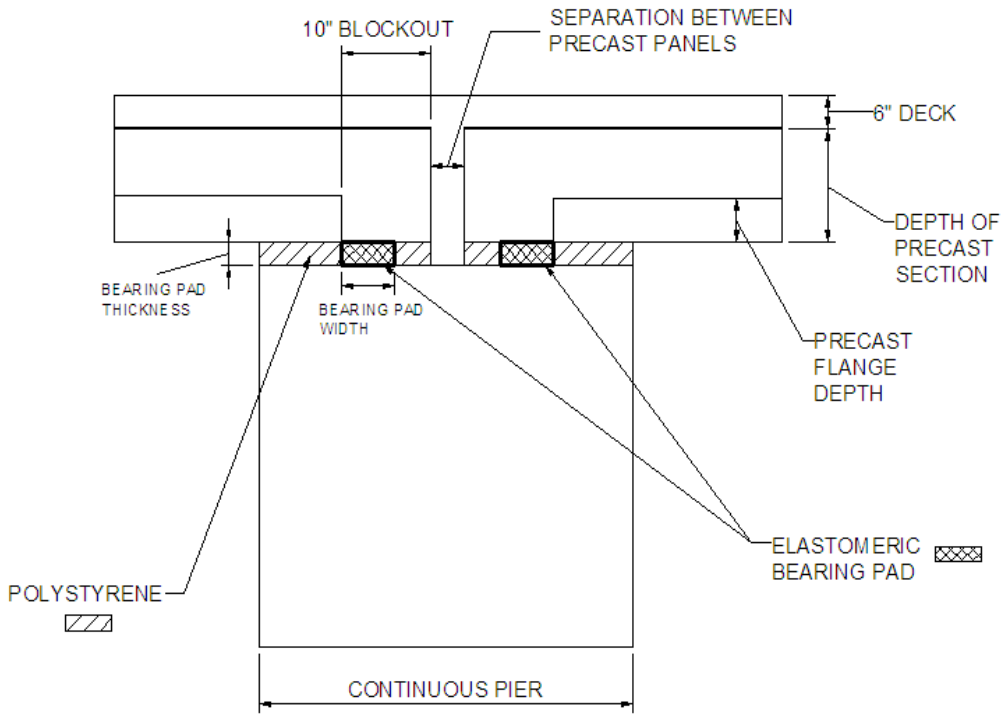

Figure 1.1.3: Cross-sectional view of a PCSSS and support at a continuous pier illustrating the 10 in. flange blockout and general bearing details

Vertical dowels shall be installed in the pier cap and embedded in the CIP closure pour to provide a positive connection between the superstructure and substructure. The ideal location of the vertical dowels is such that they lie in a line along the length of the pier cap that bisects the area created between the ends of longitudinally adjacent precast panels at a continuous pier. Where there is insufficient clearance between adjacent precast panels for the installation of the vertical reinforcement, the dowels may be placed in the area created by the flange blockouts in the trough area between inverted-T members. A review of the PCSSS construction documents utilized in the construction of Mn/DOT Bridge 13004 in Center City, Minnesota revealed that the vertical dowels consisted of No. 5 bars at 12 in. on center, although an equal area of reinforcement grouped in the blockout locations was expected to be a satisfactory alternative where there was insufficient clearance between the ends of the precast members. It is recommended that the dowels be stainless steel for durability, and that they be wrapped (e.g., with ½ in. pipe insulation) above the pier or abutment cap to reduce the amount of restrained shrinkage in the transverse direction.

To address these issues associated with the bearing detail under the precast beam at the abutment and pier of the PCSSS, the following recommendations in AASHTO (2010) should be modified as indicated below.

AASHTO (2010) Article *5.14.1.2.4 Detail Design*

> All details of reinforcement, connections, bearing seats, inserts, or anchors for diaphragms, concrete cover, openings, and fabrication and erection tolerances shall be shown in the contract documents. For any details left to the

Contractor's choice, such as prestressing materials or methods, the submittal and review of working drawings shall be required.

For precast composite slab span construction, continuous bearing shall consist of an elastomeric bearing device of sufficient dimension to support the factored loads.

The effects of restrained shrinkage in the transverse direction on the CIP closure pour shall be considered, and where feasible, a means of relieving restrained shrinkage at the supports shall be employed.

At continuous supports of precast composite slab span bridge construction, a means of facilitating the development of negative moment at the pier by providing integral CIP concrete within the compression zone of the beam in the joint region shall be provided.

Vertical dowels, or equivalent, shall be installed in the pier cap and embedded within the CIP closure pour to provide a positive connection between the superstructure and substructure, and where surface cracking near the continuous piers it to be expected, the dowel reinforcement shall be fabricated from a corrosion resistant material.

C5.14.1.2.4

AASHTO LRFD Bridge Construction Specifications include general requirements pertaining to the preparation and review of working drawings, but the contract documents should specifically indicate when they are required.

Article 18.2 of the *AASHTO 2009 Interim LRFD Bridge Construction Specifications* provides information relevant to the properties of the elastomeric bearing pad.

Restrained shrinkage caused by restraint at the supports may increase the transverse tensile stresses near the precast joint region and subsequently promote or advance reflective cracking. A bond breaker (i.e., plastic sheet) provided between the pier cap and CIP closure pour may reduce the restrained shrinkage near the joint region. The application of foam pipe insulation to vertical dowels emanating from the pier cap and embedded in the CIP concrete is expected to reduce the effects of restrained shrinkage due to the dowel reinforcement and should also be considered.

A flange block out at the end of precast composite slab span members at continuous piers offers a means of providing contiguous CIP concrete in the joint region to facilitate the compressive reaction in the negative moment region of a PCSSS bridge. Research and current design methodology suggest that a 10 in. blockout, measured from the end of the beam was sufficient to accommodate the development of negative moment at the continuous pier. The

blockout shall be incorporated into the precast member during fabrication, and not by means of cutting after fabrication of the members.

1.1.2. Bursting, Splitting and Spalling Forces

An evaluation of the end zone forces in the prestressed inverted T-section was completed by Eriksson (2008) which resulted in suggested modifications to AASHTO (2010) Article 5.10.10.1.

For years, the AASHTO specification included requirements for reinforcement to control "bursting" at the ends of prestressed beams due to the effects of the transfer of prestress from the reinforcement into the concrete. The original specifications were developed to control "spalling" stresses in I-girders, and were mislabeled in the code as "bursting" stresses. The guidelines required the placement of large amounts of vertical reinforcement within a distance of *h*/4 from the end of the member, where *h* is the depth of the member. The shallow section depths of inverted-T precast beams result in limited area for the placement of vertical reinforcement, which leads to significant congestion.

Experimental and numerical studies were completed to investigate the effects of spalling and bursting on the inverted-T sections used in PCSSS. The experimental tests on 12 in. deep inverted T-sections used indicated that the concrete had sufficient strength to resist tensile stresses induced in the transfer zone at release regardless of the reinforcement provided, suggesting that vertical reinforcement was not required in the end zones of those specimens.

Furthermore, numerical studies conducted as part of the investigation supported that certain inverted-T members did not require spalling or bursting reinforcement, specifically those with member depths less than 22 in. and which satisfied the expectation that the concrete tensile strength was larger than the stress developed due to the transfer of prestress. Through the numerical studies, vertical reinforcement was found to be required to control the spalling stresses in deeper sections. The requirement for the vertical reinforcement to be provided within *h/4* from the end of the member (where *h* is the depth of the member) was determined to be the most critical region for the reinforcement to be located.

In the current AASHTO (2010) provisions, the term "bursting" has been replaced with "splitting," although the correct terminology that should be used is "spalling." Bursting and splitting stresses occur along the transfer length of the strand, whereas spalling stresses tend to occur at the end of the member. Although not specifically addressed in AASHTO, the confinement requirements of AASHTO (2010) 5.10.10.2 should help control the bursting and splitting stresses that develop in the transfer length region.

AASHTO (2010) Article **5.10.10 Pretensioned Anchorage Zones**

5.10.10.1 ~~Splitting~~ Spalling Resistance

For all sections other than rectangular slabs and shallow inverted-T sections with heights less than 22 in, the ~~splitting~~ spalling resistance of pretensioned anchorage zones provided by reinforcement in the ends of pretensioned beams shall be taken as:

$$P_r = f_s A_s$$

(5.10.10.1-1)

where:

f_s = stress in steel not to exceed 20 ksi

A_s = total area of reinforcement located within the distance h/4 from the end of the beam (in.^{2})

h = overall dimension of precast member in the direction in which ~~splitting~~ spalling resistance is being evaluated (in.)

The resistance shall not be less than four percent of the total prestressing force at transfer.

For pretensioned I-girders or bulb tees, …

.

.

.

… from the end of each web.

In pretensioned anchorage zones of rectangular slabs and shallow inverted-T sections with heights less than 22 in., vertical reinforcement in the end zones is not required if:

$$\sigma_s < f_r$$

(~~5.10.10~~.1-2)

where:

$$\sigma_s = \frac{P}{A}\left(0.1206\frac{e^2}{h\,d_b} - 0.0256\right) \geq 0$$

$$f_r = 0.23\sqrt{f_{ci}'}$$

σ_s = maximum spalling stress on the end face (ksi)

f_r = direct tensile strength as defined by Article C5.4.2.7 (ksi)

P = prestressing force at transfer (kip)

A = gross cross-sectional area of concrete (in.^{2})

e = strand eccentricity (in.)

h = overall depth of precast member (in.)

d_b = prestressing strand diameter (in.)

f_{ci}' = concrete compressive strength at transfer (ksi)

Where end zone vertical reinforcement is required, it shall be located within the horizontal distance h/4 from the end of the beam, and shall be determined as:

$$A_s = \frac{P\left(0.02\frac{e^2}{h\,d_b} - 0.01\right)}{f_s} \quad (5.10.10.1\text{-}3)$$

where:

A_s = total area of reinforcement located within the distance h/4 from the end of the beam (in.^{2})

The resistance shall not be less than four percent of the total prestressing force at transfer.

In all cases, the reinforcement shall be as close to the end of the beam as practicable.

Reinforcement used to satisfy this requirement can also be used to satisfy other design requirements.

C5.10.10.1

The primary purpose of the choice of the 20-ksi steel stress limit for this provision is crack control.

Spalling ~~Splitting~~ resistance is of prime importance in relatively thin portions of pretensioned members that are tall or wide, such as the webs of I-girders and the webs and flanges of box and tub girders. ~~Prestressing steel that is well distributed in such portions will reduce the splitting forces, while steel that is banded or concentrated at both ends of a member will require increased splitting resistance.~~

For pretensioned slab members with well-distributed prestressing steel across the width of the member, tensile zones can form in the vertical direction of the member as the section depth increases. This is likely due to the additional depth over which the stress must spread before the stresses are well distributed in the section in the case of members with large eccentricity to depth ratios. ~~the width of the member is greater than the depth. A tensile zone is then formed in the horizontal direction perpendicular to the centerline member.~~

For tub and box girders, prestressing strands are located in both the bottom flange and webs. Tensile zones are then formed in both the vertical and horizontal directions in the webs and flanges. Reinforcement is required in both directions to resist ~~the~~ spalling and splitting forces, respectively. Prestressing steel that is well distributed in such portions will reduce the splitting forces, while steel that is banded or concentrated at both ends of a member will require increased splitting resistance.

Experience has shown that the provisions of this article generally control cracking in the end regions of pretensioned members satisfactorily; however, more reinforcement than required by this Article may be necessary under certain conditions. Figures C5.10.10.1-1 and C5.10.10.1-2 show examples of spalling and splitting reinforcement for tub girders and voided slabs.

Changes should be made to the labeling in Figures C5.10.10.1-1 and C5.10.10.1-2 to denote reinforcement which is providing spalling resistance and reinforcement which is providing splitting resistance. Note that the tensile stresses due to bursting/splitting occur along the transfer length region and thus the location of the reinforcement to handle these stresses may need to be distributed differently from that used to resist spalling stresses.

1.1.3. Restraint Moment

Specifications suggested for modification to address restraint moment issues for continuous PCSSS bridges include AASHTO (2010) Article 5.14.1.4.2, 5.14.1.4.4

Restraint moments can be generated in continuous composite systems due to differential time-dependent effects (i.e., creep and shrinkage) between the precast and CIP topping and thermal gradient effects through the cross section due to solar radiation. The effects of both positive and negative restraint moments must be considered for the PCSSS. When CIP is cast on a precast element that is relatively old (i.e., may have been stored in a precasting yard for several months before being placed), much of the creep and shrinkage of the precast element will have occurred prior to casting the CIP topping. In this case, negative restraint moments would be expected to result due to the shrinkage of the CIP placed on the seasoned precast element. Negative restraint moments will cause cracking at the top of the section at the pier, and can therefore be controlled through longitudinal reinforcement near the top of the member which is generally supplied by the deck, and possibly supplemental, reinforcement. When the CIP is cast on a young element, the shrinkage of the CIP and precast may be expected to be relatively similar; however, the precast section will undergo shortening due to creep effects that generally result in positive restraint moments. Cracking due to positive restraint moment will occur near the bottom of the section at the pier. The reinforcement provided to resist positive restraint moment in the PCSSS must be provided in the trough area between precast panels, which limits the available area and disbursement (i.e., the reinforcement must be grouped in the troughs and not be spread out over the width of the system) of reinforcement to resist positive restraint moments.

Significant research was completed by Smith et al. (2008) and Eriksson (2008) on the restraint moment effects for continuous precast composite slab span systems. Smith et al. (2008) monitored the restraint moment in the Concept 1 laboratory bridge for a period of 250 days after continuity was made by determining the reactions measured with load cells at the outside piers of the specimen. In addition, Smith monitored one of the initial implementations of the PCSSS in Minnesota, the Center City Bridge, which was instrumented by Mn/DOT to investigate load distribution and the potential development of reflective cracking. Gages located at the pier indicated that cracking initiated due to the effects of positive restraint moment. The crack was observed to occur as the bridge underwent its first large thermal gradient effects due to solar radiation in the spring. As a consequence, it was suspected that the behavior was driven by thermal gradients in the bridge superstructure where the solar radiation heated the top of the bridge. This caused the individual spans of the bridge to camber which generated positive restraint moments. Eriksson (2008, pp. 56) stated, “Because [the] time-dependent effects on [the day the crack was observed] should not have varied significantly from the previous day, researchers speculated thermal effects may have played a role in the crack development. Based on this conjecture, both time-dependent and thermal gradient effects on restraint moment were investigated analytically.” Eriksson (2008) completed a parametric study to investigate the effects of differential shrinkage, creep, and thermal gradient effects on the development of restraint moments.

In an effort to predict the restraint moment in a section based on the time-dependent properties of the system, Eriksson completed a numerical parametric study using Pbeam, which is a fiber-based finite element code developed by Suttikan at the University of Texas in 1978 (Suttikan, 1978). The program allows for inputs including material strength, age, creep,

shrinkage, steel relaxation, dead loads and support conditions. The program provides output in the form of stresses, strains, reactions and deformations at user specified time intervals (Suttikan 1978). Furthermore, Eriksson utilized a modified version of Pbeam created by Le (1998), called TPbeam, which incorporates thermal gradient in the analysis. After finding that, when using functions based on measured quantities for the input values (i.e., creep, shrinkage, concrete strength gain with age, etc.), Pbeam predicted restraint moments that corresponded reasonably well with the measured results from the Concept 1 laboratory specimen, Eriksson utilized both Pbeam and TPbeam to conduct a parametric study to determine reasonable bounds for expected restraint moments in PCSSS bridges. In general, the purpose of the parametric study was to predict the maximum positive and negative restraint moments that would be expected in PCSSS bridges. Precast strengths of 6 ksi and 12.9 ksi were used with assumed continuity dates of 7, 28, 60, and 90 days to develop an expected envelope of the positive and negative restraint moments.

Because of the difficulty in providing reinforcement for positive restraint moment due to the geometry of the PCSSS, the necessity to design for such moments was of interest. Eriksson found that, “positive restraint moment cracking due to time-dependent effects is not expected [for PCSSS] for spans between 20 and 50 ft.” This conclusion was based on a finite element study that considered only time-dependent effects. It should be noted in design that AASHTO (2010) 5.14.1.4.5 requires that the stress at the bottom of the diaphragm be compressive in order to take advantage of full continuity, considering all load effects. The check is made assuming that the concrete section cannot carry any tension (i.e., section may already be cracked at the pier due to positive moment).

Eriksson found that positive restraint moment generally induced at the pier was due to creep of the precast member, therefore increasing the age of the precast member at continuity will reduce the positive restraint moment due to time-dependent effects in the section. The thermal gradient due to solar radiation has the same effect as placing CIP on a young precast section. Eriksson (2008) found that the positive restraint moments caused by thermal effects induced restraint moments that were two to seven times larger than the positive restraint moments caused by time-dependent effects. As a consequence, positive restraint moment cracking due to thermal gradient effects was expected to occur in nearly all of the designs studied.

Based on the findings by Eriksson (2008), it is important to consider the effects of thermal gradient in the positive restraint moment design for continuous PCSSS bridges. Because the use of Pbeam or TPbeam by bridge designers would be impractical, an analytical method is described below which should be applied to calculate the restraint moment caused by a temperature gradient as defined by AASHTO LRFD (2010) Article 3.12.3. The total restraint moment at a given pier should be calculated as the sum of restraint moments generated by a thermal gradient and time-dependent effects.

AASHTO (2010) Article 3.12.3 provides general guidelines for design of thermal gradients based on regional zones, but indicates temperature gradient should be evaluated on a project specific basis. Judgment is reserved for experienced designers indicating thermal gradient can be neglected if previous structures have not experienced distress. These basic guidelines provide little guidance regarding when thermal gradients are important. Based on the fiber-based finite element model results from Pbeam and TPbeam and the suspected positive moment crack in the Center City Bridge, thermal effects have a significant effect on the development of positive restraint moments and should be considered in the restraint moment design.

Restraint moment design for time-dependent properties is complicated by the need to investigate the interaction of the variation in time-dependent effects over time. The PCA and P-method both provide options for how to design for restraint moments due to time-dependent effects. However, design for restraint moments caused by thermal effects does not include the time variation and should be summed with restraint moments due to time-dependent effects.

Barker and Puckett (2007) provide a hand calculation for determining the restraint moment due to the thermal effects. Assuming the beam is a simple span between supports, apply the design thermal gradient to the section and calculate the resulting curvature in the beam. The curvature from a temperature gradient can be expressed as

$$\varphi = \frac{\alpha}{I} \int T(y) \cdot y \cdot dA \qquad (1.1.1)$$

where α is the coefficient of thermal expansion, *T(y)* is the temperature gradient (°F) through the depth *y* of the member (in.), and *I* is the moment of inertia of the entire cross section (in.^{4}) (Barker and Puckett, 2007) This equation is also found in AASHTO (2010) Article C4.6.6.

The end rotation (θ) can be found by integrating the curvature over half the length of the span. Then, the restraint moment, or the moment restraining the rotation, can be found using the three-moment equation. The equation assumes pinned end supports and is expressed as

$$M = 3 \cdot \theta \cdot \frac{E \cdot I}{L} \qquad (1.1.2)$$

where θ is the rotation, *E* is the elastic modulus (for the composite system), and *L* is the span length.

The moment, *M*, is the restraint moment at the pier of a continuous system to resist the rotations induced by the thermal gradient. If the span lengths on each side of the pier are not equal, then the different spans will induce different moments at the pier (i.e., the rotation would be different, leading to different moments). To use this analysis method, continuity of slope at the pier is necessary. The restraint moments induced by thermal gradients in each span can be calculated using Equation (1.1.2) and the design should be for the largest restraint moment. The effects of thermal gradients and time-dependent effects can be calculated independently and then combined with the appropriate load factors.

Using the above methodology for prediction of the thermally induced restraint moments in the 20 ft. and 50 ft. span beams in the parametric study conducted by Eriksson (2008) provided conservative results as compared to the TPbeam results. The hand calculations overpredicted the calculated positive restraint moment by a range of 20 to 40 percent. The calculations agreed with TPbeam results that the highest ratio of positive restraint moment induced by a thermal gradient to the cracking moment (i.e., 2.9) was for the 20 ft. span with 12.9 ksi concrete. The shorter span with greater strength had the greatest stiffness and the least flexibility of the sections studied. Consequently, the 50 ft. span with 6 ksi concrete, the most flexible section studied had the lowest ratio of positive restraint moment induced by thermal gradient to cracking moment (i.e., 0.95).

If the above design method provides undesirable results, there are a few other options to decrease the positive restraint moment effects. By decreasing time-dependent effects, the combination of thermal effects and time dependent effects would be reduced. Increasing the specified concrete compressive strength of the precast member would increase the stiffness and decrease the creep in the member, which would decrease the positive restraint moments. Providing 90-day girder age at continuity would decrease the time-dependent effects of the

positive restraint moment and eliminate the need for calculation of positive restraint moment due to time-dependent effects based on AASHTO (2010) Article 5.14.1.4.4.

For all cases of PCSSS design, the effectiveness of the continuity connection at the pier must be checked according to AASHTO 5.14.1.4.5. This continuity check requires that the sum of all post-continuity dead loads, restraint moments, half live load, and half thermal gradient, result in net compression at the bottom of the diaphragm. It is recommended that the live load stress used in this check be the stress at the pier associated with the maximum positive moment on the live load envelope. If the continuity check is not satisfied, the system is not fully effective and partial continuity must be considered.

If the above methods do not provide a reasonable design, then the benefits from continuity should be neglected in design and the system should be designed as a series of simple spans. The design of the PCSSS as a simple span while still providing reinforcing steel in the trough region over the pier would not be conservative. The positive moment reinforcement over the pier would generate restraint effects that must be considered in design.

AASHTO (2010) Article 5.14.1.4.2 provides guidance in the design of restraint moments for bridges composed of simple span precast girders made continuous.

AASHTO (2010) Article *5.14.1.4.2 Restraint Moments*

> The bridge shall be designed for restraint moments that may develop because of time-dependent, thermal gradient, or other deformations, except as allowed in Article 5.14.1.4.4.
>
> Restraint moments shall not be included in any combination when the effect of the restraint moment is to reduce the total moment.
>
> For precast composite slab span construction made continuous, reinforcement provided for positive restraint moment must be included in the longitudinal trough region across the pier.

AASHTO (2010) Article *5.14.1.4.4 Age of Girder When Continuity Is Established*

> The minimum age of the precast girder when continuity is established should be specified in the contract documents. This age shall be used for calculating restraint moments due to creep and shrinkage. If no age is specified, a reasonable, but conservative estimate of the time continuity is established shall be used for all calculations of restraint moments.
>
> The following simplification may be applied if acceptable to the Owner and if the contract documents require a minimum girder age of at least 90 days when continuity is established:
>
> - Positive restraint moments caused by girder creep and shrinkage and deck slab shrinkage may be taken to be zero.

- Computation of time-dependent restraint moments shall not be required.

- Positive restraint moments caused by thermal gradients must be taken into consideration for PCSSS bridges made continuous.

- A positive moment connection shall be provided with a factored resistance, φMn, ~~not less than 1.2 M_{cr},~~ as specified in Article 5.14.1.4.9. For all systems with the exception of PCSSS, the factored resistance, φMn, shall not be not less than 1.2 M_{cr}.

For other ages at continuity, the age-related design parameters should be determined from the literature, approved by the Owner, and documented in the contract documents.

1.1.4. Live Load Distribution Factors and Skew Effects

The applicability of the current live load distribution factors, specifically those designated for cast-in-place slab span bridges, to the PCSSS was investigated during the NCHRP 10-71 study. Numerical modeling was combined with observations from a live load truck test on the Center City Bridge along with load distribution tests on the laboratory bridge specimens.

Numerical models were run to investigate the effect of potential discontinuities generated in PCSSS bridges due to the development of precast-CIP interface separation or reflective cracks on live load distribution relative to the live load distribution obtained for monolithic slab-span systems for single tandem and double tandem loading cases. In the case of the double tandem loading, the load scenario was an extreme case, where a double wheel patch load was placed over the joint (i.e., tandems were assumed to be spaced much closer together than physically constitutes two 12ft. lanes of loading.

The PCSSS cases investigated included CIP bonded only to the sides and top of the panel webs (i.e., the CIP was left unbonded from the panel flanges) to simulate the separation of the flanges from the CIP above the longitudinal joints. In addition, runs were conducted to investigate the effect of the discontinuity along the longitudinal joint between the precast flanges, with the CIP assumed to be bonded to the top of the flanges. A model was also run to investigate the effect of a potential reflective crack that extended to approximately the elastic neutral axis depth of the section in transverse bending (i.e., 3 in. below the top surface of the CIP in an 18 in. deep PCSSS).

Although the curvatures obtained for the PCSSS models were larger than those obtained for the corresponding CIP slab-span models, the design curvatures predicted using AASHTO LRFD (2010) exceeded those obtained from the finite element models for all cases. The numerical models illustrated that even in the case of the PCSSS with a reflective crack assumed to extend to within 3 in. of the extreme compression fiber and tandem load greater than could be physically applied to the lane, the longitudinal curvatures were only 84 percent of the longitudinal curvatures

predicted using the AASHTO LRFD (2010) load distribution factors for monolithic concrete slab-span bridges. This suggests that the live load distribution factors for PCSSS type superstructures could reasonably and conservatively be designed using the current live load distribution factors for monolithic slab span bridges.

Furthermore, the live load truck tests on the Center City Bridge suggested that the measured longitudinal curvatures were approximately three times less than those calculated using the monolithic slab span equations. Additionally, the measured longitudinal curvatures were consistently conservative when compared to monolithic slab span FEM models.

Because the numerical study and laboratory results consistently suggested that the PCSSS could be conservatively designed as a solid slab-span bridge system, as specified in AASHTO (2010) Article 4.6.2.3., it is recommended that the PCSSS be designed according to the slab-span effective lane width provisions for determination of the longitudinal design moments.

Numerical modeling was also utilized to investigate the effects of skew on PCSSS bridges through a simply-supported bridge model with skewed supports ranging from 0 to 45 degrees. The primary behavior under investigation was the maximum horizontal shear induced above the precast joint. Three load cases were considered with patch loads centered along the outside panel: midspan, quarter span near acute angle, quarter span near obtuse angle. The longitudinal stress measured in the jointed and monolithic models remained relatively constant through the range of skew angles considered. For lower angles or no skew, the load at the obtuse quarter span controlled among the tested load cases, while for larger skew angles, the midspan load case controlled. Differences between the results for the PCSSS and monolithic CIP case were subtle. At no skew, the horizontal shear stress in the precast joint model was slightly higher than that of the monolithic section, likely due to the reduction in sectional area to carry the shear; while at higher skews, the monolithic model horizontal shear stress was higher than that of the PCSSS, possibly due to better load transfer across the longitudinal joint of the monolithic system.

The small variation and consistency between the models considering a 3 in. joint between the flanges in the PCSSS and a monolithic structure suggest that the effect of the precast joint in PCSSS construction was not expected to significantly affect the performance of the system in skewed applications. The design of skewed PCSSS bridges may be completed assuming a monolithic slab-span system in accordance with AASHTO LRFD (2010), where the longitudinal force effects for slab-span bridges can be reduced by a factor of *r* given a skew angle θ by Eq. 4.6.2.3-3. This relationship has been shown to perform well for monolithic slab-span systems.

Because the precast joint detail of the PCSSS does not significantly change the load transfer across the width of the bridge, it is recommended that the AASHTO LRFD (2010) skew design for slab-span systems be applied to PCSSS.

AASHTO (2010) Article **4.6.2.3 Equivalent Strip Widths for Slab Type Bridges**

This Article shall be applied to the types of cross sections shown schematically in Table 1. For the purpose of this Article, cast-in-place voided slab and precast composite slab-span system (PCSSS) bridges may be considered as slab bridges.

The equivalent width of longitudinal strips per lane for both shear and moment with one lane, i.e., two lines of wheels, loaded may be determined as:

$$E = 10.0 + 5.0\sqrt{L_1 W_1} \quad (4.6.2.3\text{-}1)$$

The equivalent width of longitudinal strips per lane for both shear and moment with more than one lane loaded may be determined as:

$$E = 84.0\ 0 + 1.44\sqrt{L_1 W_1} \ \leq \frac{12.0W}{N_L} \quad (4.6.2.3\text{-}2)$$

where:

E = equivalent width (in.)

L_1 = modified span length taken equal to the lesser of the actual span length or 60.0 (ft.)

W_1 = modified edge-to-edge width of bridge taken to be equal to the lesser of the actual width or 60.0 for multilane loading, or 30.0 for single-lane loading (ft.)

W = physical edge-to-edge width of bridge (ft.)

N_L = number of design lanes as specified in Article 3.6.1.1.1

For skewed bridges, the longitudinal force effects may be reduced by the factor *r*:

$$r = 1.05 - 0.25\tan\theta \ \leq 1.00 \quad (4.6.2.3\text{-}3)$$

where:

θ = skew angle (degrees)

1.1.5. Transverse Load Distribution

To address transverse load distribution requirements for PCSSS bridges, suggested specification modifications include AASHTO (2010) Article 5.14.4.3.3e.

To emulate the satisfactory performance of CIP slab-span systems, precast composite slab-span systems require load transfer between adjacent precast panels. The nature of the design of the precast system, specifically the presence of the discontinuity produced at the flange interfaces, creates a longitudinal joint between panels and requires that adequate transverse load transfer be provided across the joint. The effectiveness of the transverse reinforcement is improved if the flange thickness of the precast sections is minimized. This enables the transverse reinforcement to be placed lower within the cross section increasing its effective depth.

In the case of transverse load distribution, as well as crack control, it is prudent to define the reinforcement ratio based on the amount of concrete near the transverse load distribution reinforcement. In the NCHRP 10-71 study, the depth of concrete considered in the definition of the transverse load distribution reinforcement ratio included the CIP concrete between the top of the precast flanges and the top of the deck. In the case of the 12 in. deep precast section, the depth considered was 15 in. (i.e., 12 in. deep precast section + 6 in. thick deck - 3 in. flange thickness). The total area of reinforcement used in the reinforcement ratio determination should include only the transverse reinforcement terminating in 90^0 hooks that extend through

the precast webs and lap with companion hooked bars protruding from the adjacent precast webs. This lapped reinforcement provides continuity across the longitudinal joints. A single bar should be used in the transverse load distribution reinforcement calculation because the lapped bars must transfer load to each other between the adjacent panels. The reinforcement and depth of concrete considered in the calculation of the reinforcement ratio for load transfer per unit length is highlighted in yellow in Figure 1.1.4.

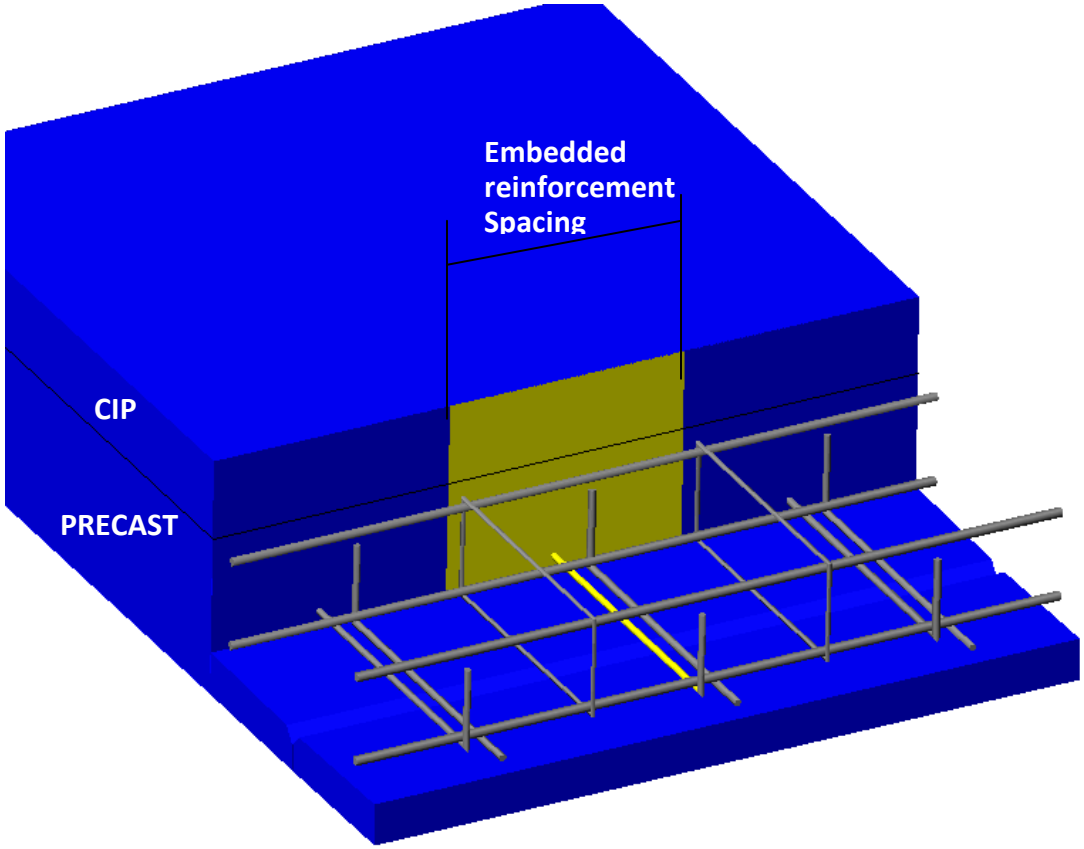

Figure 1.1.4: reinforcement and depth of concrete considered in calculation of the reinforcement ratio for transverse load transfer (highlighted in yellow)

The AASHTO 2010 LRFD Bridge Design Specifications provide guidance in the design of reinforcement for the transverse load distribution in CIP concrete bridge superstructures. Article 5.14.4.1 states that the transverse reinforcement be selected based on the longitudinal flexural reinforcement and the span length. Specifically, the transverse mild reinforcement is computed as a percentage of the total longitudinal flexural reinforcement considering both mild and prestressed longitudinal reinforcement. In the case of prestressed construction, the ratio of the strand stress to the mild reinforcement strength (taken to be 60 ksi in the specification) is taken into account. The calculation for the transverse load reinforcement for mild and prestressed reinforcement is given in AASHTO (2010) equations 5.14.4.1-1 and 5.14.4.1-2, respectively shown below.

- For longitudinal reinforced concrete construction:

  $$k_{mild} = \frac{100}{\sqrt{L}} \leq 50\%$$ (LRFD 5.14.4.1-1)

- For longitudinal prestressed construction

$$k_{ps} = \frac{100}{\sqrt{L}} * \frac{f_{pe}}{60} \leq 50\% \qquad \text{(LRFD 5.14.4.1-2)}$$

where:

k_{mild} = percent of longitudinal mild flexural reinforcement

k_{ps} = percent of longitudinal prestressed flexural reinforcement

L = span length [ft]

f_{pe} = effective stress in prestressing strand [ksi]

The application of equation 5.14.4.1-2 to spans in the range of 20 ft. to 31 ft. resulted in required transverse reinforcement proportions of 65 percent and 52 percent, respectively, when the effective strand stress was taken to be 175 ksi. In both cases, the proportion of transverse reinforcement would be capped at 50 percent.

The amount of longitudinal reinforcement to be considered in proportioning the transverse reinforcement shall include only the primary prestressing strand unless longitudinal mild reinforcement is included as the primary tensile reinforcement; longitudinal mild reinforcement located in the precast flanges may be neglected when present.

A primary disparity in the application of AASHTO (2010) Article 5.14.4.1 to the PCSSS is the difference in depth of the longitudinal and transverse reinforcement. In CIP slab systems, the transverse reinforcement is generally located immediately above the single longitudinal reinforcement layer. In contrast, the PCSSS is constructed such that the centroid of the longitudinal reinforcement may be significantly different than that of the transverse reinforcement. The longitudinal strands are usually located as low as possible within the section depth to maximize strand eccentricity and effectiveness in providing positive moment resistance, whereas the depth of the transverse reinforcement is constrained by requiring sufficient clearance below the bar and the top surface of the flange which limits its effective depth.

The difference between the effective depths of the longitudinal and transverse reinforcement layers is dependent on the number of layers of prestressing strand used in the design and the thickness of the flange. For this reason, it is suggested that the reduction in the effectiveness of the transverse reinforcement be taken into consideration through increasing the required transverse reinforcement by the ratio of the longitudinal to transverse reinforcement effective depths. Because only the prestressing reinforcement is likely to have a larger effective depth compared to that of the transverse reinforcement, an adjustment to increase the required transverse reinforcement for this effect need only be considered for the tendons; the larger effective depth of the transverse reinforcement relative to the centroid of the longitudinal mild reinforcement is conservatively ignored. In the case of a typical 12 in. deep section, the ratio of the effective depth of longitudinal to transverse reinforcement is 1.13 [i.e., (depth of center of gravity of strand)/(effective depth of transverse reinforcement)= 15.2 / 13.5 = 1.126 ≈ 1.13]. The required transverse load distribution reinforcement can be calculated by combining the separate proportions determined relative to the prestressed longitudinal reinforcement and mild longitudinal reinforcement, respectively. The relationship between the longitudinal flexural reinforcement and transverse load distribution reinforcement for the PCSSS can be defined based on the AASHTO (2010) requirement, as shown in equation 1.1.3.

$$A_{tld} = k_{mild}\, A_{l-mild} + \alpha\, k_{ps}\, A_{l-ps} \quad (1.1.3)$$

where:

A_{tld} = area required for transverse load distribution reinforcement [in^2]

$A_{l\text{-}mild}$ = area of longitudinal mild flexural reinforcement [in^2]

$A_{l\text{-}ps}$ = area of longitudinal prestressed flexural reinforcement [in^2]

$\alpha = d_{cgs} / d_{trans} \geq 1.0$

d_{cgs} = depth of center of gravity of prestressed reinforcement [in.]

d_{trans} = depth of center of gravity of transverse reinforcement [in.]

For transverse bar spacing between 12 in. and 18 in., the required bar sizes to satisfy the demands outlined in the previous paragraph would be No. 5 or No. 6 bars for a 12 in. deep precast section with spans between 20 ft. and 31 ft., which are reasonably acceptable bar sizes for bridge construction.

The transverse bars must be designed to be continuous throughout the width of the bridge. The continuity of the reinforcement through the width of the precast member can be achieved either through the use of embedded hooked reinforcement extending through the width of the precast member and protruding across the longitudinal joints, or by separate embedded reinforcement and hooked bars mechanically anchored to the precast member. The transverse bars should terminate with a standard hook, as specified in AASHTO (2010) Article 5.10.2.1 (hook extension of 12 times diameter of the bar), and the hook should extend vertically upward. The transverse reinforcement should extend through the trough area such that the reinforcement terminates as near to the vertical web face of the adjacent precast member as possible, and should never terminate farther than 2.0 in. clear from the vertical precast web of an adjacent panel. For a No. 6 standard hook developed in tension in 4 ksi concrete, the development length is 11.9 in., suggesting that the 22 in. (24 in. width joint – 2.0 in. maximum clear distance) is sufficient to fully develop the reinforcement.

The adjacent transverse load distribution reinforcement was considered to be most accurately represented in the current specification by a contact lap splice. Therefore, the maximum stagger between adjacent transversely load distribution reinforcement should be limited by AASHTO (2010) Article 5.11.5.2, which limits the transverse spacing to one fifth of the lap splice length or 6 in., whichever is less.

Both the Concept 1 and Concept 2 laboratory bridges displayed good load distribution characteristics before and after the introduction of a reflective crack near the precast joint. The 18 in. maximum spacing and reinforcement ratio of 0.0007 (No. 4 bars at 18 in. spacing = .2in^2/ft * 12in/18in / (15in * 12in)) of the transverse bars in the Concept 2 specimen provided a more economical design compared to the Concept 1 specimen, with a maximum spacing of 12 in. and reinforcement ratio of 0.0024 (No. 6 bars at 12 in. spacing = .44in^2/ft / (15in * 12in)). The 18 in. transverse hook spacing may be preferred by fabricators because it requires fewer perforations of their formwork to allow for the embedded transverse bars.

Article 5.14.4.3.3 of the 2010 Interim LRFD Design Specification specifically addresses shear-flexure transfer joints in precast deck bridges; for CIP closure joints, part 'e' of this Article applies.

AASHTO (2010) *Article 5.14.4.3.3e Load Transfer in Cast-in-Place Closure Joint*

Concrete in the closure joint should have strength comparable to that of the precast components; however, this need not be the case in precast-composite slab-span systems. The width of the longitudinal closure joint shall be large enough to accommodate development of the reinforcement in the joint, but in no case shall the width of the joint be less than 12.0 in.

The following additional requirements apply to precast-composite slab-span systems:

The transverse reinforcement for load transfer shall be adequately embedded or mechanically anchored and continuously extend through the supporting precast component.

The amount of bottom transverse load distribution reinforcement per unit length of span shall be determined as in Article 5.14.4.1 by combining the percentages calculated based on longitudinal reinforcing steel and longitudinal prestressing steel divided by the precast inverted-T member width. The percentage based on the longitudinal prestressing steel shall be adjusted by the factor α. The longitudinal mild steel reinforcement in the precast flanges need not be included in the percentage calculation based on longitudinal mild reinforcement.

where:

$\alpha = d_{cgs} / d_{trans} \geq 1.0$

d_{cgs} = depth of center of gravity of prestressed reinforcement (in.)

d_{trans} = depth of transverse reinforcement (in.)

The transverse reinforcement shall be provided such that all load developed in the closure pour can be fully transferred to either, or both, of the adjacent precast sections; therefore the calculated required transverse reinforcement must be provided in each precast section. The transverse load distribution reinforcement shall be installed such that lapping bars from adjacent precast panels in a common closure joint be laterally spaced with a minimum nominal clear spacing of the greater of (1 in., d_b, 4/3 * aggregate size) between the lapped bars. A tolerance in the lateral placement of the transverse hooks of 1/4 in. is acceptable.

The transverse load distribution reinforcement shall be considered to be a lap splice, and thereby conform to Article 5.11.5.2.

The transverse load distribution reinforcement shall be evenly distributed throughout the span, with the reinforcement protruding from a given precast unit spaced at no more than 18.0 in.

C5.14.4.3.3e

Research on precast-composite slab-span systems has shown adequate performance where typical concrete deck mixes are cast on the precast inverted-T sections. The CIP concrete provides the closure pour material in the trough region above the adjacent precast flanges and is contiguously cast the thickness of a typical deck across the bridge to encase the deck reinforcement.

1.1.6. Reflective Crack Control

Suggested specifications to be modified to address reflective crack control include AASHTO (2010) Article 5.7.3.4, 5.14.4.3.3f, 5.14.4.3.3g.

Reflective cracking originating at the longitudinal joint between adjacent precast flanges can be controlled through the addition of a drop-in reinforcing cage in combination with the transverse load distribution reinforcement. It is to be noted that the drop-in cage is only effective in controlling cracks that develop in the vicinity over the longitudinal joint. Cracks that might form at the interface between the CIP and precast web interface would only be restrained by the reinforcement provided for transverse load distribution (i.e., hooked bars protruding from the precast webs). In the vicinity of the longitudinal joint, the reinforcement ratio and spacing required for crack control is based on the sum of the two types of reinforcement (i.e., drop-in reinforcing cage and transverse hooked bars protruding from the precast webs). The reinforcement ratio provided for crack control considers the lower leg of the cage hoops as well as both of the adjacent lapped transverse bars provided for load transfer. The reinforcement and depth of concrete considered in the calculation of the reinforcement ratio for crack control is highlighted in Figure 1.1.5.

The reinforcement spacing provided for crack control is defined as the maximum spacing between the reinforcement crossing the joint, regardless of whether it is part of the drop-in cage or the transverse hooked bars. Therefore, offsetting of the reinforcement cage from the transverse bars wherever possible will reduce the reinforcement spacing provided for crack control; reduction in the spacing of the transverse reinforcement provided an observed benefit in the crack control capabilities of the subassemblage specimens in the NCHRP 10-71 study.

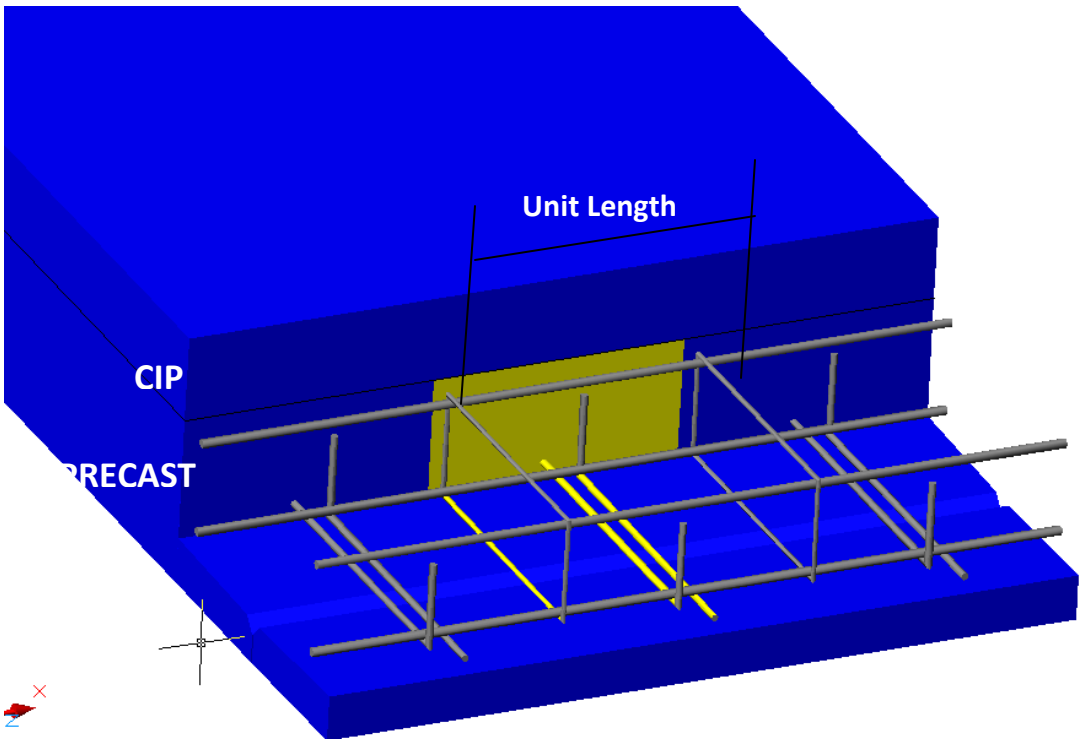

Figure 1.1.5: Reinforcement and depth of concrete considered in the calculation of the reinforcement ratio for crack control (highlighted in yellow)

Three useful resources that provide insight into the design of reinforcement for crack control include AASHTO (2010), ACI 318-08, and Frosch et al. (2006) The AASHTO (2010) and ACI 318-08 specifications provide spacing requirements for flexural reinforcement and shrinkage and temperature reinforcement. Frosch, et al. provides guidelines for the spacing and reinforcement ratio required for crack control in bridge decks. The design requirements for each are summarized in Table 1.1.1. Both AASHTO (2010) and ACI 318-08 provide maximum spacing of 18 in. and a minimum ratio of the area of flexural and shrinkage and temperature reinforcement to the area of the gross section of 0.0018.

Table 1.1.1[1]: Spacing and reinforcement ratio limits for flexural and crack control reinforcement

Reinforcement Type	Reinforcement Design Limits	Source	Article in Spec.
Crack control and shrinkage and temperature	$s < \frac{700\gamma_e}{\beta_s * f_{ss}} - 2 * d_c, \quad where \quad \beta_s = 1 + \frac{d_c}{0.7 * (h - d_c)}$	AASHTO (2010)	5.7.3.4
	$s \leq \min(1.5h, 18\ in.)$		5.10.3.2
Shrinkage and temperature	$A_{sAASHTO} \geq \frac{1.30\ bh}{2(b+h)f_y}; \quad 0.11 \leq A_{sAASHTO} \leq 0.60$		5.10.8
Crack control and shrinkage and temperature	$s < 15 * \frac{40000}{f_s} - 2.5 * c_c$	ACI 318-08	10.6.4
Shrinkage and temperature	$A_{sACI} = \ 0.0018bh \ \ (when\ using\ Gr.60\ bars)$		7.12.2.1
	$s \leq \min(5h, 18\ in.)$		7.12.2.2
Crack control	$s < 9 * \left(2.5 - \frac{c_c}{2}\right) \leq 9in$	Frosch et al. (2006)	
	$\rho_{Frosch} = 6\frac{\sqrt{f_c'}}{f_y}$		

[1]Variables in Table 1.1.1 are defined as follows:

$\gamma_e = 1.0$ for Class 1(No corrosion concerns); 0.75 for Class 2 (Corrosion concerns)

$f_{ss} =$ Stress in reinforcement at service [ksi]

$d_c =$ Depth of concrete cover measured from tension fiber of concrete to center of reinforcement, defined by AASHTO (2010)Section 5.7.3.4 [in.]

$c_c =$ Depth of concrete cover measured from tension fiber of concrete to face of reinforcement, defined by ACI $318-08$ Section 10.6.4 [in.]

$h =$ Total section depth [in]

$A_{sAASHTO} =$ Area of reinforcement in each direction and each face [in.^{2}/ft.]

$A_{sACI} =$ Area of shrinkage and temperature reinforcement [in.^{2}]

$b =$ Least width of component section [in.]

$f_s =$ Stress in reinforcement at service [psi]

$f_c' = 28-$ day concrete compressive strength [psi]

$f_y =$ Reinforcement yield strength [psi]

$\rho_{Frosch} =$ Reinforcement ratio defined by Frosch et al. (2006). Equivalent to: area of reinforcement /gross area of section [dim]

The spacing requirements outlined in Table 1.1.1 depends on the depth of cover provided. AASHTO (2010) defines the depth of cover, d_c, as the distance between the extreme tension fiber of concrete to the center of the flexural reinforcement located closest thereto, while ACI 318-08 defines the depth of concrete cover, c_c, as the distance from the tension fiber of concrete to the face of the reinforcement. Furthermore, Frosch et al. define the depth of cover analogously to ACI 318-08, with the clear distance to the face of the reinforcement. In the case of the transverse reinforcement used for crack control, the depth of cover can be defined in two reasonable ways, depending on whether or not the thickness of the precast flange is considered, as illustrated in Figure 1.1.6. The depth of cover is always measured at the precast joint. The depth of cover for the reference section illustrated in Figure 1.1.1, defined by AASHTO (2010) and ACI 318-08 is 4.6 in. (3.25 in. + 1 in. clear + 0.3125 in.) and 4.25 in. (3.25 in. + 1 in. clear) when the flange is included in the calculation, respectively. When the flange is excluded in the calculation, the depth of cover is 1.6 in. (4.6 in. – 3 in.) and 1.25 in. (4.25 in. – 3 in.) as defined by AASHTO (2010) and ACI 318-08, respectively. When the precast flange is included in the calculation, the spacing requirements are difficult to satisfy, with spacing values ranging from negative values calculated via the AASHTO (2010) equation to 4.4 in. using the equation provided by ACI 318-08. Excluding the flange produces more reasonable spacing values, ranging from 8.3 in. (assuming Class 2 corrosion concerns) to 11.9 in. based on the AASHTO (2010) and ACI 318-08 equations, respectively. Because the crack control reinforcement is located in the CIP above the gap between the adjacent precast flanges, it could be reasoned, that the depth of the flange should not be considered in the calculation of the crack control reinforcement spacing.

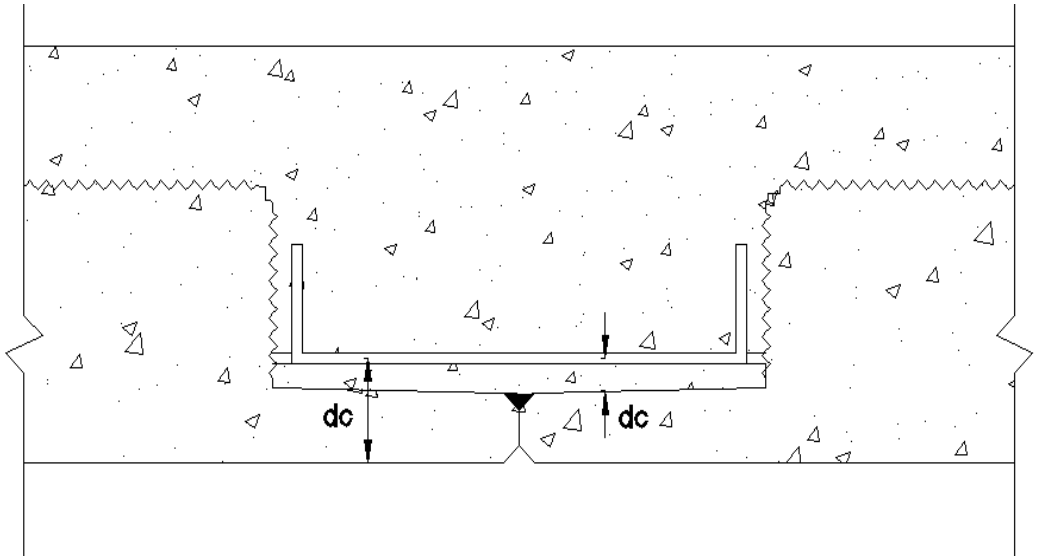

Figure 1.1.6[1]: Variation in magnitude of assumed depth of cover depending on inclusion/exclusion of precast flange measured to center of reinforcement, as defined by AASHTO (2010)

[1]The depth of cover is always measured at the joint; the annotations in Figure 1.1.6 are shown offset for clarity.

Several variations in the spacing and reinforcement ratio provided for crack control were considered in the NCRHP 10-71 study. In the Concept 1 large-scale laboratory bridge specimen, the transverse crack control reinforcement was designed to reflect that of the original Mn/DOT implementation of the PCSSS in Center City, MN. One of the two spans had the same flange depth as the Center City Bridge (i.e., 5.25 in.), and the other span had a reduced flange thickness to reduce the discontinuity between the precast flanges (i.e., 3 in.). The Concept 2 large-scale simply-supported bridge specimen and subassemblage tests were designed to investigate variations in the reinforcement spacing and reinforcement ratios for crack control. The selected configurations, summarized in Table 1.1.2 for each of the laboratory test specimens, provided an opportunity to investigate the range of requirements specified among the three design guidelines outlined above. The smallest reinforcement ratio selected for the study was 0.0025 (among the 12 in. deep sections), which was associated with the maximum spacing and minimum reinforcement size for the transverse hooks (i.e., No. 4 bars) considered to be feasible from a constructability standpoint. The cage reinforcement was fabricated with No. 3 closed stirrups which represented a practical lower bound reinforcement size for the cage.

Table 1.1.2: Crack control reinforcement parameters in the laboratory test specimens

Specimen	Transverse Bar Spacing [in.]	Cage Spacing [in.]	Reinforcement Ratio[1] [%]	Effective Maximum Bar Spacing[2] [in.]
Concept 1, Span 1	12	12	0.0110	12
Concept 1, Span 2	12	12	0.0147	12
Concept 2 Bridge	18	18	0.0031	9
SSMBLG1-Control1	18	18	0.0031	9
SSMBLG2-NoCage	18	NA	0.0025	18
SSMBLG3-HighBars	18	18	0.0031	9
SSMBLG4-DeepSection	18	18	0.0022	9
SSMBLG5-No.6Bars	18	18	0.0061[3]	9
SSMBLG6-Frosch	18	4.5	0.0052[3]	4.5
SSMBLG7-Control2	18	18	0.0031	9

[1]This is the reinforcement ratio defined for crack control

[2]The effective maximum bar spacing is based on the combined transverse bar and cage configuration.

[3]Note that the reinforcement ratio for the SSMBLG5-No.6Bars was actually closer to that of the Frosch et al. (2006) requirements than was the reinforcement ratio for the SSMBLG6-Frosch specimen.

Both the Concept 1 and Concept 2 laboratory bridge specimens provided sufficient crack control throughout the duration of all laboratory testing. Both specimens performed relatively similarly, with comparable increases in the transverse strain over the joint before and after cracking, as well as before and after cycling. In the continuous Concept 1 bridge, cracking in the exterior half span of the test span was always greater than on the interior half span towards the center support. The interior half span was supported on 15 in. of a 42 in. wide concrete pier and the exterior half spans were supported on 12 in. of a 12 in. wide flange section. Due to the continuous nature of the two-span Concept 1 bridge, this phenomenon was expected (i.e., the center pier provided greater restraint to the transverse cracking).

Because both laboratory bridge specimens provided adequate crack control through the duration of testing, both configurations can reasonably be utilized in future designs. The AASHTO (2010) equation provides an adequate measure of the required reinforcement spacing for crack control, however an upper limit is recommended. The good crack control performance of the Concept 1 bridge suggests that the 12 in. maximum spacing is known to produce good results. Therefore, it is recommended that the AASHTO (2010) equation be bounded to a maximum spacing of 12 in.

It is suggested that all transverse bars protruding from the precast members terminate in standard hook, as specified in Section 1.1.5.

AASHTO (2010) **Article 5.7.3.4 Control of Cracking by Distribution of Reinforcement**

The provisions specified herein shall apply to the reinforcement of all concrete components, except that of deck slabs designed in accordance with Article 9.7.2, in which tension in the cross-section exceeds 80 percent of the modulus of rupture, specified in Article 5.4.2.6, at applicable service limit state load combination specified in Table 3.4.1-1.

The spacing *s* of mild steel reinforcement in the layer closest to the tension face shall satisfy the following:

$$s \leq \frac{700\,\gamma_e}{\beta_s\, f_{ss}} - 2d_c$$

(5.7.3.4-1)

in which:

$$\beta_s = 1 + \frac{d_c}{0.7(h - d_c)}$$

where:

γ_e = exposure factor
= 1.00 for Class 1 exposure condition
= 0.75 for Class 2 exposure condition

d_c = thickness of concrete cover measured from extreme tension fiber to center of the flexural reinforcement located closest thereto (in.)

f_{ss} = tensile stress in steel reinforcement at the service limit state (ksi)

h = overall thickness or depth of the component (in.)

Class 1 exposure condition applies when cracks can be tolerated due to reduced concerns of appearance and/or corrosion. Class 2 exposure condition applies to transverse design of segmental concrete box girders for any loads applied prior to attaining full nominal concrete strength and when there is increased concern of appearance and/or corrosion.

In the computation of d_c, the actual concrete cover thickness is to be used. For the design of the transverse reinforcement located in the longitudinal closure joint of precast composite slab-span superstructures, d_c shall be taken as the distance between the extreme tension fiber of the cast-in-place concrete in

the trough and the center of the transverse reinforcement in the closure joint, thereby neglecting the thickness of the precast flange.

When computing the actual stress in the steel reinforcement, axial tension effects shall be considered, while axial compression effects may be considered.

The minimum and maximum spacing of reinforcement shall also comply with the provisions of Articles 5.10.3.1 and 5.10.3.2, respectively.

…

The reinforcement ratio presented by Frosch provides a good basis for the development of an adequate reinforcement ratio for crack control in the longitudinal joint region of precast slab span bridge systems. Frosch et al. (2006) suggests that at the initiation of cracking in the section, adequate reinforcement should be provided to transfer all load from the concrete to the reinforcement.

The presence of a reinforcing cage located in the longitudinal trough between inverted-T sections shall be required in all PCSSS bridge systems. The lack of a cage was investigated during the subassemblage tests and was found to perform poorly relative to the other specimens tested, especially in terms of crack widths and lengths measured on the faces of the specimen. Furthermore, all PCSSS bridges constructed in the field have been built with cage reinforcement, and therefore no information regarding the large-scale in-service performance of a bridge system without a cage was available. Therefore, cage reinforcement shall be provided in each trough region between each precast member, and the transverse reinforcement in the cage shall consist of no less than No. 4 bars spaced at 12 in.

The cage stirrups may be designed in two primary configurations, but in both cases the bottom of the stirrup shall coincide with the depth of the transverse reinforcement for load transfer. The depth of the stirrup may be such that the top horizontal leg is flush with the top of the precast web, or preferably, the depth of the stirrup is minimized (i.e., the depth of the stirrup is the minimum bend diameter for the bar size used or is such to provide adequate room to tie the four longitudinal No. 5 bars inside the stirrup). The minimized stirrup depth allows the top horizontal leg of the stirrup increased potential to intercept a reflective crack earlier. The width of the stirrup in the trough shall be similar to the width of the precast hooks, and shall be as wide as possible while allowing for adequate clearance for the longitudinal cage reinforcement inside of the transverse hooks.

It is suggested that a separate section is designated for reinforcement requirements for crack control, which will be designated as AASHTO (2010) Article 5.14.4.3.3f. The current Article 5.14.4.3.3f shall be moved to 5.14.4.3.3g.

AASHTO (2009) Article ~~5.14.4.3.3f~~ *5.14.4.3.3g Structural Overlay*

Where a structural overlay is used to qualify for improved load distribution as provided in Articles 4.6.2.2.2 and 4.6.2.2.3, the thickness of structural concrete overlay shall not be less than 4.5 in. An isotropic layer of

reinforcement shall be provided in accordance with the requirements of Article 5.10.8. The top surface of the precast components shall be roughened.

AASHTO (2010) *Article 5.14.4.3.3f Reflective Crack Control in Cast-in-Place Closure Joint for Precast Composite Slab-Span Systems*

Transverse reinforcement for crack control shall be placed near the extreme tension face in the cast-in-place closure joint. Transverse reinforcement may be provided by both the reinforcement present for transverse load transfer, as specified in Article 5.14.4.3.3e, as well as through the use of a reinforcing cage consisting of vertical closed stirrups. Transverse reinforcement shall be provided to satisfy:

$$\rho_{cr} = \frac{6\sqrt{f_c'}}{f_y} \quad \text{(5.14.4.3.3f-1)}$$

where:

ρ_{cr} = reinforcement ratio of the section for crack control (%)

f_c' = 28 – day concrete compressive strength (psi)

f_y = yield stress in the reinforcement (psi)

The reinforcement ratio of the section for crack control, ρ_{cr}, shall be calculated considering all load transfer reinforcement and the lower horizontal leg of the cage stirrup crossing the longitudinal joint. The area of concrete considered in the calculation shall be only the cast-in-place concrete between the top of the precast flange and the top of the precast web. The reinforcement ratio for crack control shall be taken as:

$$\rho_{cr} = \frac{A_{trans-cr}}{12(h_{pc} - d_{flange})} \quad \text{(5.14.4.3.3f-2)}$$

where:

$A_{trans-cr}$ = area of transverse reinforcement for crack control. Consists of all reinforcement

traversing the longitudinal joint per unit length (in^2./ft.)

h_{pc} = overall depth of the precast section (in.)

d_{flange} = depth of the precast flange (in.)

A minimum reinforcing cage is required in all sections, and shall consist of no less than No. 4 closed stirrups spaced at 12 in. One longitudinal bar shall be provided in each interior corner of the stirrup for anchorage.

C5.14.4.3.3f

The vertical closed stirrups provided in the reinforcement cage should be configured such that the bottom horizontal stirrup leg is located at approximately the same depth as the transverse load distribution reinforcement. The vertical depth of the top horizontal stirrup leg should be minimized where possible, as the minimized stirrup depth allows the top horizontal leg to intercept potential reflective cracking at a lower depth. The width of the stirrups in the reinforcement cage should be maximized while ensuring minimum bar spacing clearances are met between the cage and the vertical precast web faces.

1.1.7. Composite Action

To address composite action in PCSSS, specifications suggested for modification include AASHTO (2010) Articles 5.8.4.3, and 5.8.4.4

Composite action was maintained throughout the extent of the ultimate loading tests on each of the two spans of the Concept 1 laboratory bridge specimen and the simple-span Concept 2 laboratory bridge specimen. It should be noted that in the Concept 2 bridge, the section relied on only the composite action of the roughened concrete surface; there was no horizontal shear steel that crossed the interface. Both bridge specimens had a standard raked finish on the top horizontal surface of the precast web. Furthermore, each specimen had a roughened diamond pattern with approximately 1/8 in. to 1/4 in. perturbations on the vertical web surfaces of the precast panels. Likewise, the East span of the Concept 1 bridge, which was constructed with the 5 1/4 in. thick precast flange, also had the tops of the precast flanges roughened with the same diamond pattern. The ability of the Concept 2 specimen to maintain composite action suggests that PCSSS bridges can provide adequate horizontal shear strength in the absence of supplemental reinforcement across the precast-CIP concrete interface. The wide precast web sections provided a sufficiently large area such that horizontal forces could be effectively transferred between the CIP and precast units. Furthermore, Kovach and Naito (2008) suggested that concrete beams without horizontal shear reinforcement can conservatively provide 300 psi of horizontal shear resistance at service conditions with a broom or rake finish. The 2010 AASHTO LRFD specification suggests that an intentionally roughened surface can be expected to achieve 240 psi of horizontal shear resistance, which was increased from 100 psi in the 2005 specification. However, the 2010 specification still requires minimum horizontal shear reinforcement.

The compressive force that was transferred between the CIP and precast sections was measured to be 2088 kips in the Concept 2 bridge at the maximum load available to be applied to the section by integrating the strain from three longitudinal strain gages between the neutral axis and the top of the section. The stress in the section was calculated using the modified Kent-Park concrete stress-strain relationship assuming no confinement reinforcement, while using

measured values for the maximum concrete compressive strength and a corresponding concrete strain assumed to be 0.002 at the maximum compressive stress. The horizontal shear stress developed at this condition was calculated by dividing the total compressive force at mid-span by the full width of the deck and half of the center to center of bearing span length, resulting in a measured horizontal shear stress of 135 psi. The width of the deck was taken as 10 ft., and included the area above the precast trough.

Because the Concept 2 bridge specimen, which had no horizontal shear reinforcement, developed a horizontal shear stress of 135 psi, it is recommended that the specification allow for sections to develop a horizontal shear stress of 135 psi with no horizontal shear reinforcement. The $K_1$and K_2 values, which provide upper bound estimates of the horizontal shear capacity of a given section, selected to be used in the proposed specification modifications are simply the smallest, or most conservative of the existing K_1 and K_2 values. Because these were developed specifically for composite beams with horizontal shear reinforcement, even the selected values may not be appropriate. However, these values provide a maximum horizontal shear force that is at least a factor of two larger than the horizontal shear force that would be developed by the full 6 in. deep deck constructed with 10 ksi concrete at ultimate (i.e., assuming that the section were reinforced such that it were required to fully transfer Whitney's stress block through the full 6 in. depth of the CIP deck).

AASHTO (2010) Article **5.8.4 Interface Shear Transfer – Shear Friction**

5.8.4.1 General

Interface shear transfer shall be considered across a given plane at:

- An existing or potential crack,
- An interface between dissimilar materials,
- An interface between two concretes cast at different times, or
- The interface between different elements of the cross-section

…

The nominal shear resistance of the interface plane shall be taken as:

$$V_{ni} = c\,A_{cv} + \mu(A_{vf}\,f_y + P_c) \qquad (5.8.4.1\text{-}3)$$

where:

A_{cv} = area of concrete considered to be engaged in interface shear transfer (in.^{2})

A_{vf} = area of interface shear reinforcement crossing the shear plane within the area A_{cv} (in.^{2})

c = cohesion factor specified in Article 5.8.4.3 (ksi)

μ = friction factor specified in Article 5.8.4.3 (dim.)

f_y = yield stress of reinforcement but design value not to exceed 60 (ksi)

P_c = permanent net compressive force normal to the shear plane; if force is tensile, P_c = 0.0 (kip)

…

5.8.4.3 Cohesion and Friction Factors

The following values shall be taken for cohesion, *c*, and friction factor, μ:

…

For normal-weight concrete placed against a clean concrete surface, free of laitance, with surface intentionally roughened to an amplitude of 0.25 in.:

c = 0.24 ksi
μ = 1.0
K_1 = 0.25
K_2 = 1.5 ksi

For concrete placed against a clean concrete surface, free of laitance, but not intentionally roughened:

c = 0.075 ksi
μ = 0.6
K_1 = 0.2
K_2 = 0.8 ksi

For normal-weight concrete placed against a clean concrete surface, free of laitance, with surface intentionally roughened to an amplitude of 0.25 in. and no interface shear reinforcement provided crossing the shear plane up to the minimum required A_{vf} in Eq. 5.8.4.4-1:

c = 0.135 ksi
μ = 1.0
K_1 = 0.2
K_2 = 0.8 ksi

…

5.8.4.4 Minimum Area of Interface Shear Reinforcement

Except as provided herein, the cross-sectional area of the interface shear reinforcement, A_{vf}, crossing the interface area, A_{cv}, shall satisfy:

$$A_{vf} \geq \frac{0.05\ A_{cv}}{f_y}$$

(5.8.4.4-1)

For a cast-in-place concrete slab on clean concrete girder surfaces free of laitance, the following provisions shall apply:

The minimum interface shear reinforcement, A_{vf}, need not exceed the lesser of the amount determined using Eq. 1 and the amount needed to resist $1.33V_{ui}$ / ϕ as determined using Eq. 5.8.4.1-3.

The minimum reinforcement provisions specified herein shall be waived for girder/slab interfaces with surface roughened to an amplitude of 0.25 in. where the factored interface shear stress, v_{ui} of Eq. 5.8.4.2-1, is less than 0.210 ksi, and all vertical (transverse) shear reinforcement required by the provisions of Article 5.8.1.1 is extended across the interface and adequately anchored in the slab.

For the cast-in-place concrete of precast-composite slab-span systems that is cast on clean precast inverted-T surfaces free of laitance, with a surface intentionally roughened to an amplitude of 1/4 in., the minimum reinforcement provisions specified herein shall be waived.

C5.14.4.3.3f

.

.

.

With respect to a girder/slab interface, the intent is that the portion of the reinforcement required to resist vertical shear which is extended into the slab also serves
as interface shear reinforcement.

In the case of precast-composite slab-span systems, research (*French et al. 2010*) has shown that transverse reinforcement was not required across the CIP-precast interface in order to achieve composite action. Similar results were obtained in studies by Naito et al. (2008).

1.2.Construction Specification Recommendations

The 2009 Interim AASHTO LRFD Bridge Construction Specification (AASHTO 2009) provides guidance for the construction of most bridge superstructures and supporting elements. The PCSSS requires a somewhat unique method of construction and erection which are important to achieve the desired performance of the system. The following sections outline changes to the AASHTO construction specifications in the same manner as utilized in the sections above; proposed modifications to the specification are shown with additions and deletions shown in underline and strikethrough notation, respectively.

1.2.1. Sequence of Placement

Suggested specifications to be modified to address sequence of placement include AASHTO Construction Specification (2009) Article 8.7.2.2

The CIP portion of the inverted-T sections should be poured in a single lift. It is likely that if, for whatever reason, the CIP was placed in two pours, a construction joint would be created in the trough area flush with the top of the precast webs; this type of joint will limit the ability for the section to maintain composite action, as this coincides with the plane separating the precast and CIP concrete.

8.7.2.2 Superstructures

Unless otherwise permitted, no concrete shall be placed …

…

Concrete for box girders may be placed in two or three separate operations consisting of the bottom slab, girder stems, and top slab. In either case, the bottom slab shall be placed first and, unless otherwise permitted by the Engineer, the top slab shall not be placed until the girder stems have been in place for at least five days.

Cast-in-place concrete for the closure pour and deck of composite inverted-T precast slab span structures shall be placed in a single operation.

1.2.2. Construction Joints

There are two primary contact surfaces in the joints of PCSSS bridges. These are the horizontal and vertical surfaces of the precast web and flanges that are in contact with the CIP concrete. All surfaces that will be in contact with CIP concrete during a closure pour must be pre-wetted prior to the placement of concrete, as described in Article 8.8.2, to ensure adequate bond will be achieved between the precast and CIP surfaces. No changes to this section are required; however, to reduce the stress discontinuity at the longitudinal joint between the precast elements, consideration can be given to debonding or "softening" a portion of the CIP-precast flange interface in the vicinity of the longitudinal joint. Extending the debonding across the entire flange width should be avoided as it could lead to reflective cracks initiating at the CIP-precast web interface where the crack control reinforcement consists of only the transverse load distribution reinforcement (i.e., the crack would miss the cage in the trough).

8.8.2 Bonding

Unless otherwise specified in the contract documents, horizontal joints may be made without keys, and vertical joints shall be constructed with shear keys. …

…

All construction joints shall be cleaned of surface laitance, curing compound, and other foreign materials before fresh concrete is placed against the surface of the joint. Abrasive blast or other approved methods shall be used to clean horizontal construction joints to the extent that clean aggregate is exposed. All construction joints shall be flushed with water and allowed to dry to a surface dry condition immediately prior to placing concrete.

1.2.3. Special Requirements for PCSSS Bridges

Specifications suggested for modification to address PCSSS construction include AASHTO Construction Specification (2009) Article 8.17

There are several special requirements unique to PCSSS construction that must be considered. It is useful to provide a new Article in the bridge construction specifications that specifically addresses PCSSS construction. It is recommended that this be Article 8.17: Special Requirements for PCSSS Bridges.

8.17.1 Sequence of Placement

The PCSSS system shall conform to Article 8.7.2.2.

8.17.2 Construction Joints

All construction joints shall be prepared pursuant to Article 8.8.2.

8.17.2.1 Longitudinal Precast Construction Joint

The top longitudinal edge of the precast flanges shall be formed with a 1 in. 45 degree chamfer (measured along the length of the chamfer) to produce a channel 1.4 in. wide by 0.7 in. deep at the precast joint. A silicone caulk, or bonding agent, must be utilized to fill the chamfer between adjacent precast panels. The agent must provide adequate ductility such that cracking does not initiate in the silicone when the panels separate by a total of 1/4 in. at the joint and must remain adequately bonded to the precast members.

The bonding agent must be placed in the chamfer of the joint sufficiently early such that it has fully cured based on Manufacturer's specifications prior to the application of CIP concrete.

8.17.3 Transverse Load Distribution Reinforcement

Transverse reinforcement must be provided to ensure load transfer between adjacent precast panels. All reinforcement for load transfer must be securely anchored or embedded to the respective precast panel. Furthermore, the transverse reinforcement must extend completely through the width of the precast member.

In the case of transverse load distribution reinforcement terminating in a standard hook, the hook shall be oriented vertically regardless of whether the bar is embedded or mechanically to the precast member.

Transverse load distribution reinforcement protruding from adjacent precast panels shall be nominally spaced to provide a minimum clear spacing of the greater of (1 in., d_b, 4/3 * aggregate size) between lapped bars, after erection, with a maximum allowable lateral tolerance of 1/2 in. at each set of transverse bars.

8.17.4 Reinforcing Cage

The reinforcing cage shall be constructed such that the stirrups are oriented vertically after construction. The stirrups shall be installed such that the overlapping closed loop portion of the stirrup alternates between the left and right side of the trough area.

Unless otherwise specified in the contract documents, the reinforcing cage shall be offset from the embedded transverse hooks such that the maximum spacing between transverse reinforcement is minimized.

8.17.5 Bearing Devices

Uniform bearing shall be provided under the full area of contact between the precast composite beams and the pier caps by means of an elastomeric bearing pad of sufficient dimension to support the factored loads in accordance with Article 18.2. The bearing pad should extend along the full width of the PCSSS bridge system, less 6 in. for a drip setback. A crushable membrane shall be provided in areas directly between the precast member and pier cap not supported by the elastomeric bearing pad to prevent the egress of CIP concrete during the closure pour. When the CIP concrete and pier cap are to be separated by a bond breaker to reduce the potential for restrained shrinkage, a layer of plastic sheeting can be used to provide the bond breaker.

Details at continuous piers must be provided to ensure proper construction practices. Longitudinally adjacent precast members meeting at continuous piers must be sufficiently separated such that CIP concrete can be placed between the end faces of the members. A

minimum separation of 4 in. is recommended, which provides adequate clearance for placement and vibration of the CIP concrete. Furthermore, vertical dowels, adequately embedded in the pier cap, shall be provided in the area between longitudinally adjacent members to provide a pin connection with the piers. No. 5 vertical dowels spaced at 12 in. were provided in the Mn/DOT implementation of the PCSSS bridge in Center City; no problems have been observed in the connection between the pier caps and superstructure. It should be noted that more reinforcement may be required to ensure integrity of the connection at the pier for PCSSS bridges located in seismic regions. The use of PCSSS bridges in seismic regions was out of the scope of the NCHRP 10-71 project.

These connection details might be revisited in the future to investigate whether separation of the PCSSS with the bridge pier might be desirable to reduce the potential effects of restrained shrinkage in the longitudinal joint between the precast flanges across the width of the bridge.

8.17.6 Connections at Continuous Piers

Vertical dowels, or equivalent, shall be installed in the pier cap and embedded in the CIP closure pour to provide a positive connection between the superstructure and substructure, and when surface cracking near the continuous piers it to be reasonably expected, the dowel reinforcement shall be fabricated from a corrosion resistant material.

Longitudinally adjacent precast panels meeting at a continuous pier shall be installed such that there is a space no less than 4.0 in. between the beam ends of the adjacent panels, and shall be located equidistant from the vertical dowels. The elastomeric bearing pad is not to be present in the space between adjacent panels, thereby allowing the CIP concrete to fill that region.

References for Precast Slab Span System

AASHTO (2010), *AASHTO LRFD Bridge Design Specifications,* 5th edition, Washington D.C.

AASHTO (2009), *AASHTO LRFD Bridge Construction Specifications,* 2nd edition, Washington D.C., 2009 Interim

ACI 318-08. *Building Code Requirements for Structural Concrete (ACI318-08) and Commentary (ACIR-08).* Farmington Hills, MI. 2008.

Barker, R., and Puckett, J. *Design of Highway Bridges: An LRFD Approach*, 2nd edition, New Jersey: Wiley and Sons, 2007.

Eriksson, W., "Vertical Tensile Stresses in End Regions of Precast Composite Slab-Span Systems and Restraint Moments". M.S., University of Minnesota, 2008

Frosch, R.J., Bice, J.K., Erickson, J.B. "Field Investigation of a Concrete Deck Designed by the AASHTO Empirical Method: The Control of Deck Cracking". *Indiana Department of Transportation Technical Report FHWA/IN/JTRP-2006/32*. September 2006.

International Scanning Study Team, Ralls, M., Tang, B., Bhide, S., Brecto, B., Calvert, E., Capers, H., Dorgan, D., Matsumoto, E., Napier, C., Nickas, W., Russell, H., "Prefabricated Bridge Elements and Systems in Japan and Europe". Federal Highway Administration Report Number FHWA-PL-05-003, 2005

Kovach, J.D., Naito, C. "Horizontal Shear Capacity of Composite Concrete Beams without Interface Ties". *Advanced Technology for Large Structural Systems (ATLSS) Report No. 08-05.*June, 2008.

Le, Quoc Thanh Chau, "Transverse cracking in bridge decks: Parametric study." M.S., University of Minnesota, 1998.

Smith, M., Eriksson, W., Shield, C., French, C., "Monitoring and Analysis of Mn/DOT Precast Composite Slab Span System (PCSSS)". *Minnesota Department of Transportation Technical Report No. MN/RC 2008-41.* September 2008

Suttikan, C., "A Generalized Solution for Time-Dependent Response and Strength of Noncomposite and Composite Prestressed Concrete Beams." University of Texas at Austin, 1978.

Appendix B

Center City Field Bridge Instrumentation Designation, Nominal, and Measured Locations

The instrumentation in the Center City Bridge was documented in MnDOT Report 2006-37 (Bell et al. 2006). However, the instrument locations given were nominal, and the measured instrument locations are given in Table B.1. The measurements that differed from the MnDOT report are highlighted, italicized, and bold. The instrument designation convention is given in Figure B.1. The origin and sign convention of the strain gage measurements is given in Figure B.2. Web #1 was located between Joints #1 and 2, and Web #2 was located between Joints #2 and 3. The center of Joints 1, 2, and 3 were located at 128.5, 200.5 and 272.2 in., respectively from the parapet (i.e., measured distance "Y" in Figure B.1).

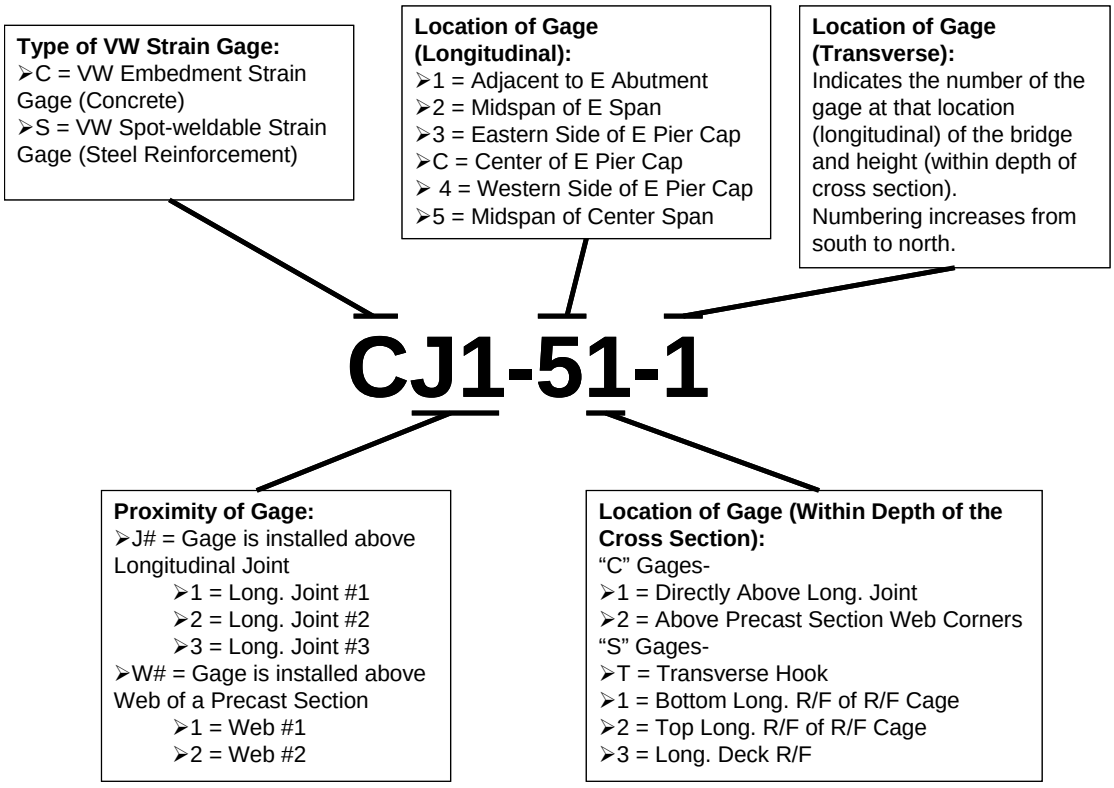

Figure B.1: Center City Bridge instrumentation designation

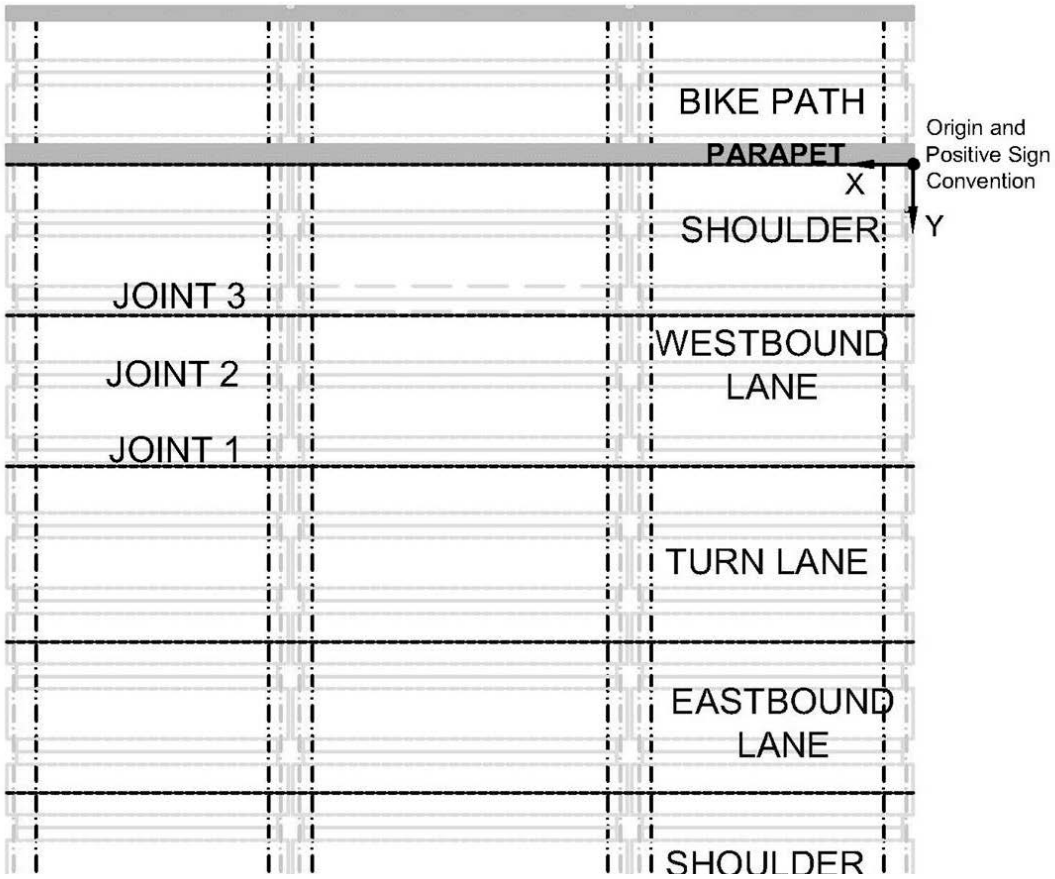

Figure B.2: Center City Bridge measurement origin and sign convention

Table B.1: Nominal and measured locations of longitudinal spot-weldable strain gages in the Center City Bridge

	Nominal (Mn/DOT 2006-37)			Measured		
Instrument	**X**	**Y**	**Z**	**X**	**Y**	**Z**
SJ1-51-1	429	264	9	429.00	***263.25***	***8.75***
SJ1-52-1	429	264	12.5	429.00	***263.25***	***12.00***
SJ1-53-1	427.5	276.5	15.5	427.50	***276.25***	***15.00***
SJ1-53-2	427.5	263.5	15.5	427.50	***264.50***	***15.00***
SJ1-41-1	290	268.5	9	290.00	***268.75***	9.00
SJ1-43-1	290	280	15.5	290.00	280.00	***15.00***
SJ1-43-2	290	268.5	15.5	290.00	268.50	***15.00***
SJ1-C1-1	271	268.5	9	271.00	***269.50***	9.00
SJ1-C3-1	271	268.5	15.5	271.00	268.50	***14.00***
SJ1-C3-2	271	296	15.5	271.00	296.00	***14.00***
SJ1-31-1	252	268.5	9	252.00	268.50	9.00
SJ1-33-1	251	280	15.5	***250.00***	280.00	***15.00***
SJ1-33-2	250	269.5	15.5	***249.00***	269.50	***15.00***
SJ1-21-1	128.5	264	9	128.50	264.00	9.00
SJ1-22-1	128.5	264	12.5	128.50	264.00	***13.00***
SJ1-23-1	130	261.5	15.5	130.00	261.50	15.50
SJ1-11-1	22	264	9	22.00	***264.25***	9.00
SJ1-12-1	22	264	12.5	22.00	***264.25***	***13.00***
SJ1-13-1	21	261.5	15.5	21.00	261.50	15.50
SJ2-51-1	427.5	192	9	427.50	***191.50***	9.00
SJ2-52-1	427.5	192	12.5	427.50	***191.50***	12.50
SJ2-53-1	426.5	193.5	15.5	426.50	193.50	***14.75***
SJ2-41-1	289.5	198	9	289.50	***198.25***	9.00
SJ2-43-1	291.5	197	15.5	291.50	197.00	***15.25***
SJ3-41-1	287	124.5	9	***287.50***	124.50	9.00
SJ3-43-1	286	124	15.5	***285.00***	124.00	***15.00***
SW1-43-1	292.5	249.5	15.5	292.50	249.50	***14.50***
SW1-43-2	292.5	236	15.5	292.50	236.00	***14.50***
SW1-43-3	292.5	225	15.5	***292.00***	225.00	***14.50***
SW2-43-1	291	177.5	15.5	***291.50***	***177.75***	***14.50***
SW2-43-2	291	165.5	15.5	291.00	165.50	***14.50***
SW2-43-3	291	154.5	15.5	291.00	***154.25***	***14.50***

Table B.2: Nominal and measured locations of transverse spot-weldable strain gages in the Center City Bridge

	Nominal (Mn/DOT 2006-37)			Measured		
Instrument	**X**	**Y**	**Z**	**X**	**Y**	**Z**
SJ1-5T-1	434	278.5	7	434.00	278.50	7.00
SJ1-5T-2	432.5	276.5	7	***432.25***	276.50	7.00
SJ1-5T-3	434	274.5	7	434.00	274.50	7.00
SJ1-5T-4	432.5	272.5	7	***432.25***	272.50	7.00
SJ1-5T-5	434	270.5	7	434.00	270.50	7.00
SJ1-5T-6	432.5	268.5	7	***432.25***	268.50	7.00
SJ1-5T-7	434	266.5	7	434.00	266.50	7.00
SJ2-5T-1	434	206.5	7	434.00	206.50	7.00
SJ2-5T-2	432.5	204.5	7	***433.00***	204.50	7.00
SJ2-5T-3	434	202.5	7	434.00	202.50	7.00
SJ2-5T-4	432.5	200.5	7	***433.00***	200.50	7.00
SJ2-5T-5	434	198.5	7	434.00	198.50	7.00
SJ2-5T-6	432.5	196.5	7	***433.00***	196.50	7.00
SJ2-5T-7	434	194.5	7	434.00	194.50	7.00
SJ3-5T-1	434	134.5	7	434.00	134.50	7.00
SJ3-5T-2	432.5	132.5	7	432.50	132.50	7.00
SJ3-5T-3	434	130.5	7	434.00	130.50	7.00
SJ3-5T-4	432.5	128.5	7	432.50	128.50	7.00
SJ3-5T-5	434	126.5	7	434.00	126.50	7.00
SJ3-5T-6	432.5	124.5	7	432.50	124.50	7.00
SJ3-5T-7	434	122.5	7	434.00	122.50	7.00

Table B.3: Nominal and measured locations of transverse concrete embedment strain gages in the Center City Bridge

	Nominal (Mn/DOT 2006-37)			Measured		
Instrument	**X**	**Y**	**Z**	**X**	**Y**	**Z**
CJ1-51-1	438	278.5	8.5	438.00	278.50	***8.25***
CJ1-51-2	438	275.5	8.5	438.00	275.50	***8.25***
CJ1-51-3	438	272.5	8.5	438.00	272.50	***8.25***
CJ1-51-4	438	269.5	8.5	438.00	269.50	***8.25***
CJ1-51-5	438	266.5	8.5	438.00	266.50	***8.25***
CJ2-51-1	438	206.5	8.5	***439.00***	206.50	***8.25***
CJ2-51-2	438	203.5	8.5	***439.00***	203.50	***8.25***
CJ2-51-3	438	200.5	8.5	***439.00***	200.50	***8.25***
CJ2-51-4	438	197.5	8.5	***439.00***	197.50	***8.25***
CJ2-51-5	438	194.5	8.5	***439.00***	194.50	***8.25***
CJ3-51-1	438	134.5	8.5	***438.50***	134.50	***8.25***
CJ3-51-2	438	131.5	8.5	***438.50***	131.50	***8.25***
CJ3-51-3	438	128.5	8.5	***438.50***	128.50	***8.25***
CJ3-51-4	438	125.5	8.5	***438.50***	125.50	***8.25***
CJ3-53-5	438	122.5	8.5	***438.50***	122.50	***8.25***
CJ1-53-1	438	293	13.5	***437.00***	293.00	13.50
CJ1-53-2	438	288.5	13.5	***437.00***	288.50	13.50
CJ1-53-3	438	284	13.5	***437.00***	284.00	13.50
CJ1-53-4	438	279.5	13.5	***437.00***	279.50	13.50
CJ1-53-5	438	275	13.5	***437.00***	275.00	13.50
CJ1-53-6	438	270.5	13.5	***437.00***	270.50	13.50
CJ1-53-7	438	266	13.5	***437.00***	266.00	13.50
CJ1-53-8	438	261.5	13.5	***437.00***	261.50	13.50
CJ1-53-9	438	257	13.5	***437.00***	257.00	13.50
CJ1-53-10	438	252.5	13.5	***437.00***	252.50	13.50
CJ2-53-1	438	221	13.5	438.00	221.00	13.50
CJ2-53-2	438	216.5	13.5	438.00	216.50	13.50
CJ2-53-3	438	212	13.5	438.00	212.00	13.50
CJ2-53-4	438	207.5	13.5	438.00	207.50	13.50
CJ2-53-5	438	203	13.5	438.00	203.00	13.50
CJ2-53-6	438	198.5	13.5	438.00	198.50	13.50
CJ2-53-7	438	194	13.5	438.00	194.00	13.50
CJ2-53-8	438	189.5	13.5	438.00	189.50	13.50
CJ2-53-9	438	185	13.5	438.00	185.00	13.50
CJ2-53-10	438	180.5	13.5	438.00	180.50	13.50
CJ3-53-1	438	149	13.5	***439.00***	149.00	13.50
CJ3-53-2	438	144.5	13.5	***439.00***	144.50	13.50
CJ3-53-3	438	140	13.5	***439.00***	140.00	13.50
CJ3-53-4	438	135.5	13.5	***439.00***	135.50	13.50
CJ3-53-5	438	131	13.5	***439.00***	131.00	13.50
CJ3-53-6	438	126.5	13.5	***439.00***	126.50	13.50
CJ3-53-7	438	122	13.5	***439.00***	122.00	13.50
CJ3-53-8	438	117.5	13.5	***439.00***	117.50	13.50
CJ3-53-9	438	113	13.5	***439.00***	113.00	13.50
CJ3-53-10	438	108.5	13.5	***439.00***	108.50	13.50

Appendix C

Concept 1 Large-Scale Laboratory Bridge Instrumentation Designation and Measured Locations

C.1 Concept 1 Laboratory Specimen Instrumentation Designation

The instrumentation for the concept 1 laboratory specimen was labeled as described in this section as documented by Smith et al. (2008). An example designation is given in Figure C.1.

1. The first character indicated the type of gage.
   - C = VW concrete embedment gage
   - F = Strand resistive gage
   - M = Polyester Mold concrete resistive gage
   - P = Polyester Wire surface resistive gage
   - R = Rosette concrete resistive gage
   - S = VW spot-weldable gage
   - V = 120Ω waterproof resistive gage
   - W = 350Ω waterproof resistive gage

2. The second character indicated the span in which the gage was located.
   - 1 = West span
   - 2 = East span
   - D = CL Pier

3. The third character indicated the precast section within the span in which the gage was located.
   - N = North precast section
   - S = South precast section
   - J = Joint

There was a hyphen after the third character.

4. The fourth character indicated the position of the gage along the precast section.
   - 1 = Pinned end of the beam
   - 2 = Outer quarter point
   - 3 = Midspan
   - 4 = Inner quarter point
   - 5 = Continuous end of the beam

5. The fifth character indicated where the gage was located in the depth of the cross section.

Longitudinal Curvature Gages:

Flange Region

- 1 = Gage on strand
- 2 = Gage at bottom of R/F cage
- 3 = Gage on deck steel

Web Region

- 1 = Gage on strand
- 2 = Gage on mild R/F in beam
- 3 = Gage on deck steel

Composite Action Gages (Additional to those used for longitudinal curvature):

Flange Region

- 5 = Gage at top of R/F cage

Web Region

- 4 = Gage half-way between strand and mild R/F

Prestress Loss Gages:

- 1 = Center of Gravity of Strands

Transverse Gages:

- 1 = Gage over flange
- 2 = Gage over web corner

Bursting Gages:

- M = Mid-height of web

6. The sixth character indicated the orientation of the gage.

- L = Longitudinal
- T = Transverse
- V = Vertical

There was a hyphen after the sixth character.

7. The seventh character indicated the number of the gage at that position. For transverse gages, the numbering increased from south to north. For longitudinal gages, the numbering

increased from the outside of the specimen to the middle of the specimen. For bursting rebar gages, the numbering increased from the stirrup closest to the face of the beam toward the center of the precast section.

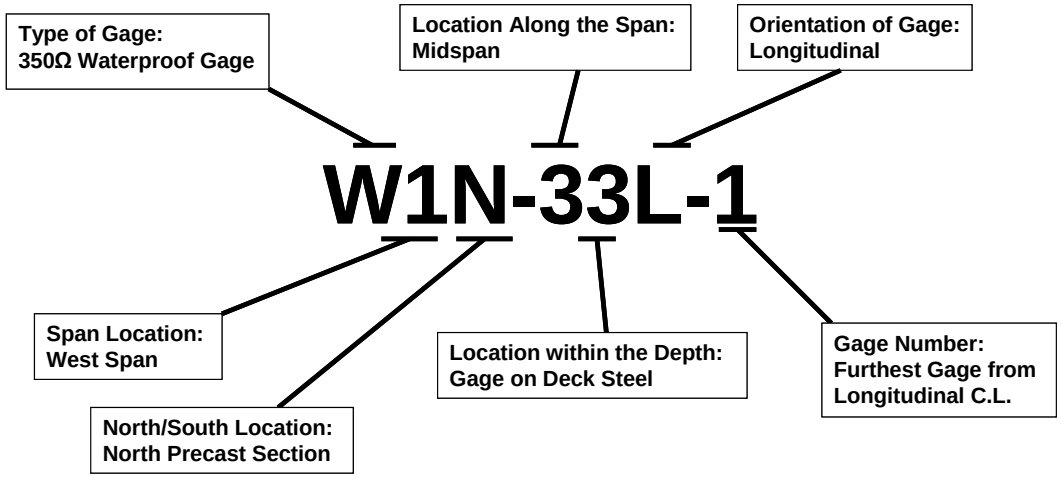

Figure C.1: Concept 1 Laboratory specimen strain gage designation example (Smith et al., 2008)

C.2 Measured Locations of Concept 1 Laboratory Specimen Instrumentation

All of the instrumentation in the laboratory specimen was measured to the nearest ¼ in. The sign convention of the gage ordinates is shown in Figure C.2. The X axis was measured in the E-W direction from the centerline of the pier (E positive); Y was measured in the N-S direction from the joint (N positive); the Z axis was measured in the vertical direction from the bottom of the precast sections (upward positive). The measurements are given in Table C.1.

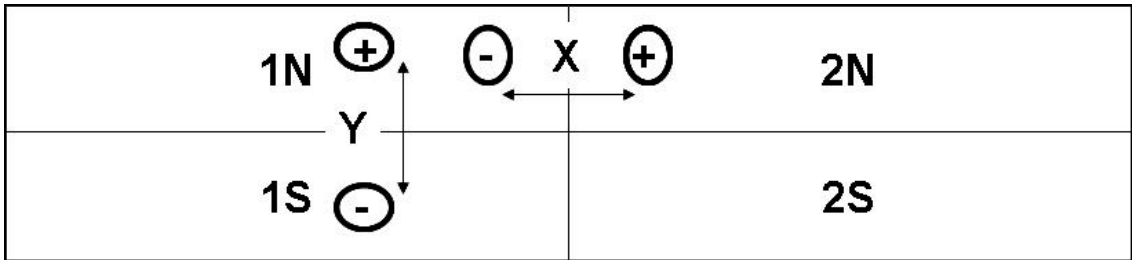

Figure C.2: Sign convention for the strain gage location measurements in the Concept 1 Laboratory Bridge (Smith et al., 2008)

TableC.1: Measured global gage locations for instruments in the concept 1 laboratory bridge specimen (in.)

X from CL pier (E+);Y from joint (N+); Z from top of flange/web			
Gage	X	Y	Z
M1J-11T-1	-255	-9.5	3
M1J-11T-2	-257.5	-5.5	3
M1J-11T-3	-255	0	3
M1J-11T-4	-257.5	5.5	3
M1J-11T-5	-255	9.5	3
M1J-12T-1	-253.5	-18.5	11.25
M1J-12T-2	-251	-14.5	11.25
M1J-12T-3	-253.5	-10.5	11.25
M1J-12T-4	-251	-6.5	11.25
M1J-12T-5	-253.5	-2.5	11.25
M1J-12T-6	-251	2.5	11.25
M1J-12T-7	-253.5	6.5	11.25
M1J-12T-8	-251	10.5	11.25
M1J-12T-9	-253.5	14.5	11.25
M1J-12T-10	-251	18.5	11.25
M1J-21T-1	-194.5	-9.5	4
M1J-21T-2	-197.5	-5.5	4
M1J-21T-3	-194.5	0	4
M1J-21T-4	-197.5	5.5	4
M1J-21T-5	-194.5	9.5	4
M1J-31T-1	-134	-9.5	3
M1J-31T-2	-136.5	-5.5	3

X from CL pier (E+);Y from joint (N+); Z from top of flange/web			
Gage	X	Y	Z
M1J-31T-3	-134	0	3
M1J-31T-4	-136.5	5.5	3
M1J-31T-5	-134	9.5	3
M1J-32T-1	-134.5	-18.5	11
M1J-32T-2	-132	-14.5	11
M1J-32T-3	-134.5	-10.5	11
M1J-32T-4	-132	-6.5	11
M1J-32T-5	-134.5	-2.5	11
M1J-32T-6	-132	2.5	11
M1J-32T-7	-134.5	6.5	11
M1J-32T-8	-132	10.5	11
M1J-32T-9	-134.5	14.5	11
M1J-32T-10	-132	18.5	11
M1J-41T-1	74	-9.5	3
M1J-41T-2	76.5	-5.5	3
M1J-41T-3	74	0	3
M1J-41T-4	76.5	5.5	3
M1J-41T-5	74	9.5	3
M1J-51T-1	26	-9.5	3
M1J-51T-2	29	-5.5	3
M1J-51T-3	26	0	3
M1J-51T-4	29	5.5	3

X from CL pier (E+);Y from joint (N+); Z from top of flange/web			
Gage	X	Y	Z
M1J-51T-5	26	9.5	3
M1J-52T-1	-27.5	-18.5	11
M1J-52T-2	-25	-14.5	11
M1J-52T-3	-27.5	-10.5	11
M1J-52T-4	-25	-6.5	11
M1J-52T-5	-27.5	-2.5	11
M1J-52T-6	-25	2.5	11
M1J-52T-7	-27.5	6.5	11
M1J-52T-8	-25	10.5	11
M1J-52T-9	-27.5	14.5	11
M1J-52T-10	-25	18.5	11
M2J-11T-1	257.75	-9.5	2
M2J-11T-2	255	-5.5	2
M2J-11T-3	257.75	0	2
M2J-11T-4	255	5.5	2
M2J-11T-5	257.75	9.5	2
M2J-12T-1	255	-18.5	8.5
M2J-12T-2	257.5	-14.5	8.5
M2J-12T-3	255	-10.5	8.5
M2J-12T-4	257.5	-6.5	8.5
M2J-12T-5	255	-2.5	8.5
M2J-12T-6	257.5	2.5	8.5

X from CL pier (E+);Y from joint (N+); Z from top of flange/web			
Gage	X	Y	Z
M2J-12T-7	255	6.5	8.5
M2J-12T-8	257.5	10.5	8.5
M2J-12T-9	255	14.5	8.5
M2J-12T-10	257.5	18.5	8.5
M2J-21T-1	198	-9.5	1.25
M2J-21T-2	195.5	-5.5	1.25
M2J-21T-3	198	0	1.25
M2J-21T-4	195.5	5.5	1.25
M2J-21T-5	198	9.5	1.25
M2J-31T-1	147.5	-9.5	2
M2J-31T-2	145	-5.5	2
M2J-31T-3	147.5	0	2
M2J-31T-4	145	5.5	2
M2J-31T-5	147.5	9.5	2
M2J-32T-1	134	-18.5	8.25
M2J-32T-2	136.5	-14.5	8.25
M2J-32T-3	134	-10.5	8.25
M2J-32T-4	136.5	-6.5	8.25
M2J-32T-5	134	-2.5	8.25
M2J-32T-6	136.5	2.5	8.25
M2J-32T-7	134	6.5	8.25
M2J-32T-8	136.5	10.5	8.25

X from CL pier (E+);Y from joint (N+); Z from top of flange/web			
Gage	X	Y	Z
C1J-11T-1	-243.5	0	3
C1J-21T-1	-183.5	0	3.5
C1J-31T-1	-123.5	0	3
C1J-41T-1	-64.5	0	3
C1J-51T-1	-15	0	3.5
C2J-11T-1	244.5	0	2
C2J-21T-1	207.5	0	2
C2J-31T-1	134.5	-8.5	1.75
C2J-31T-2	136.5	-5.5	1.75
C2J-31T-3	134.5	0	1.75
C2J-31T-4	136.5	5.5	1.75
C2J-31T-5	134.5	8.5	1.75
C2J-41T-1	87.5	0	2
C2J-51T-1	16.5	0	2
S1J-21T-1	-192	0	3.5
S1J-31T-1	-132.5	0	2.75
S1J-41T-1	-72.5	0	3.75
S1J-51T-1	-24	0	3.5
S2J-21T-1	202	0	1.75
S2J-31T-1	141.5	0	1.75
S2J-41T-1	81.5	0	1.75

X from CL pier (E+);Y from joint (N+); Z from top of flange/web			
Gage	X	Y	Z
M2J-32T-9	134	14.5	8.25
M2J-32T-10	136.5	18.5	8.25
M2J-41T-1	77.75	-9.5	2.25
M2J-41T-2	75	-5.5	2.25
M2J-41T-3	77.75	0	2.25
M2J-41T-4	75	5.5	2.25
M2J-41T-5	77.75	9.5	2.25
M2J-51T-1	30	-9.5	1.5
M2J-51T-2	27	-5.5	1.5
M2J-51T-3	30	0	1.5
M2J-51T-4	27	5.5	1.5
M2J-51T-5	30	9.5	1.5
M2J-52T-1	25	-18.5	8.5
M2J-52T-2	27.5	-14.5	8.5
M2J-52T-3	25	-10.5	8.5
M2J-52T-4	27.5	-6.5	8.5
M2J-52T-5	25	-2.5	8.5
M2J-52T-6	27.5	2.5	8.5
M2J-52T-7	25	6.5	8.5
M2J-52T-8	27.5	10.5	8.5
M2J-52T-9	25	14.5	8.5
M2J-52T-10	27.5	18.5	8.5

X from CL pier (E+);Y from joint (N+); Z from top of flange/web			
Gage	X	Y	Z
W1N-22L-3	-196.5	8	8
W1N-23L-1	-196	45.5	14.5
W1N-23L-2	-195	20.5	14.5
W1N-23L-3	-195	3.75	15
W1N-32L-3	-137.5	8	8
W1N-33L-1	-138	45.25	14.5
W1N-33L-2	-137	20.5	14.25
W1N-33L-3	-137	4	14.75
W1N-42L-3	-77.5	8	7.5
W1N-43L-1	-79	44.75	14.5
W1N-43L-2	-78	19.75	14.25
W1N-43L-3	-78	3.5	14.75
W1N-52L-4	-20.5	3.25	5
W1N-53L-1	-20.5	2.25	14.25
W1N-53L-2	-20.5	2.25	14.25
W1N-53L-3	-20.5	2.5	14.5
W1N-53L-4	-20.5	12	15
W1S-22L-3	-196.5	-8	8
W1S-23L-1	-196	-42.5	14.5
W1S-23L-2	-196	-18.5	14.5
W1S-23L-3	-195	-4.5	15
W1S-32L-3	-137.5	-8.5	8

X from CL pier (E+);Y from joint (N+); Z from top of flange/web			
Gage	X	Y	Z
W2N-43L-2	79	20.5	14.25
W2N-43L-3	79	2.75	14
W2N-52L-4	19	3	8.25
W2N-53L-1	20	56.75	14
W2N-53L-2	19	39	14.25
W2N-53L-3	21	19.5	14.5
W2N-53L-4	21	2.75	14.5
W2S-22L-3	197.5	6.5	8.75
W2S-23L-1	196	-42.5	14.5
W2S-23L-2	195	-18.5	14.75
W2S-23L-3	195	-5	14.5
W2S-32L-3	137.5	-8	9
W2S-33L-1	137	-42	14.5
W2S-33L-2	137	-18	14.5
W2S-33L-3	137	-5	14
W2S-42L-3	77.5	7.5	8.25
W2S-43L-1	78	-41.5	14.5
W2S-43L-2	78	-17.5	14.5
W2S-43L-3	79	-4.5	14.25
W2S-52L-4	19	-2.5	8.25
W2S-53L-1	22	-58.25	14.5
W2S-53L-2	22	-37.5	14.25

X from CL pier (E+);Y from joint (N+); Z from top of flange/web			
Gage	X	Y	Z
W1S-33L-1	-138	-42.75	14.25
W1S-33L-2	-138	-18.5	14.25
W1S-33L-3	-138	-4.5	14.75
W1S-42L-3	-77.5	-8	7
W1S-43L-1	-79	-42.5	14.5
W1S-43L-2	-79	-19	14.25
W1S-43L-3	-78	-4.5	114.5
W1S-52L-4	-20.5	-2.25	7.75
W1S-53L-1	-17	-58.25	14.25
W1S-53L-2	-17	-38	14.25
W1S-53L-3	-17	-22	14.25
W1S-53L-4	-19	-4.5	15
W2N-22L-3	197.5	-8.75	9
W2N-23L-1	196	44.5	14.5
W2N-23L-2	196	20	14.5
W2N-23L-3	196	2.25	14.25
W2N-32L-3	137.5	-9	9
W2N-33L-1	137	45	14.5
W2N-33L-2	138	20	14
W2N-33L-3	138	2.5	14
W2N-42L-3	77.5	-8	8.75
W2N-43L-1	79	45	14.5

X from CL pier (E+);Y from joint (N+); Z from top of flange/web			
Gage	X	Y	Z
W2S-53L-3	24	-21.5	14.25
W2S-53L-4	19	-4	14.75
W1N-35L-3	-137.5	8	15.25
W1S-35L-3	-137.5	-8.5	15.25
W2N-35L-3	137.5	-9	15.25
W2N-35L-3	137.5	8.5	11.75

X from CL pier (E+);Y from joint (N+); Z from bottom of section			
Gage	X	Y	Z
F2N-21L-1	198	44	1.75
F2N-21L-2	199	21	1.75
F2N-21L-3	198	3.5	2
F2N-31L-1	136.75	45	1.75
F2N-31L-2	136.5	21	1.75
F2N-31L-3	136.5	3.75	2
F2N-41L-1	79.5	44.25	2
F2N-41L-2	80	21.25	1.75
F2N-41L-3	78.5	3.75	2
F2N-51L-1	21	57	2.25
F2N-51L-2	19.5	39	2
F2N-51L-3	20.25	21	2
F2N-51L-4	20.75	3.5	2
M2N-52-1	22	53	8.5
M2N-52-2	22.5	39.5	9
M2N-52-3	22.5	17.75	9.25

X from CL pier (E+);Y from joint (N+); Z from bottom of section			
Gage	X	Y	Z
M1N-34L-2	-136	22	6.25
C1N-31L-1	-137.5	36	2.5
C1N-31L-2	-134	7	1.5
F1N-1MV-1a	-269.5	58.25	6.75
F1N-1MV-2a	-267.5	58.25	6.75
W1N-5MV-1b	-4.75	57.5	6.5
W1N-22L-1	-197	42.5	9.5
W1N-22L-2	-197	21.5	9.5
W1N-32L-1	-137	43	9
W1N-32L-2	-136	22	9.25
W1N-42L-1	-80	42.5	9.25
W1N-42L-2	-80	21.5	9.5
W1N-52L-1	-22.5	55	9.5
W1N-52L-2	-21.5	36	9.5
W1N-52L-3	-23	22	9.25

X from CL pier (E+);Y from joint (N+); Z from bottom of section			
Gage	X	Y	Z
F1S-21L-1	-196.5	-44	1.75
F1S-21L-2	-197	-21	1.75
F1S-21L-3	-196.5	-3	2
F1S-31L-1	-138.5	-44.5	1.75
F1S-31L-2	-138	-21	1.75
F1S-31L-3	-138	-3	2
F1S-41L-1	-78.5	-39.25	1.75
F1S-41L-2	-79.5	-21	1.75
F1S-41L-3	-79	-3	2
F1S-51L-1	-21	-57	2.25
F1S-51L-2	-20	-38.5	2
F1S-51L-3	-21	-21	1.75
F1S-51L-4	-19	-3	2
W1S-1MV-1c	-269	-49.5	7.5
W1S-1MV-1d	-269.25	-58	5.5
W1S-1MV-2c	-267	-49.5	7.5
W1S-1MV-2d	-267.25	-58	5.5
W1S-5MV-1a	-4.75	-58	5.75
W1S-5MV-2a	-6	-58	5.75

X from CL pier (E+);Y from joint (N+); Z from bottom of section			
Gage	X	Y	Z
W1S-22L-1	-197	-42.25	9
W1S-22L-2	-197	-21.5	9.25
W1S-32L-1	-139	-42.5	8.75
W1S-32L-2	-137.5	-21.5	9.25
W1S-42L-1	-78.75	-43	8.75
W1S-42L-2	-79.75	-21.5	9.5
W1S-52L-1	-20	-55.5	9
W1S-52L-2	-19.5	-36	9.25
W1S-52L-3	-18.5	-21.5	9.5
M1S-34L-2	-137.5	-21	7
C1S-31L-1	-139	-36	2.75
C1S-31L-2	-143	-6.75	1.75
M1S-52L-1	-20.5	-52.5	9
M1S-52L-2	-20.5	-39.5	9.25
M1S-52L-3	-18.5	-19	9.25

X from CL pier (E+);Y from joint (N+); Z from bottom of section			
Gage	X	Y	Z
F2N-21L-1	198	44	1.75
F2N-21L-2	199	21	1.75
F2N-21L-3	198	3.5	2
F2N-31L-1	136.75	45	1.75
F2N-31L-2	136.5	21	1.75
F2N-31L-3	136.5	3.75	2
F2N-41L-1	79.5	44.25	2
F2N-41L-2	80	21.25	1.75
F2N-41L-3	78.5	3.75	2
F2N-51L-1	21	57	2.25
F2N-51L-2	19.5	39	2
F2N-51L-3	20.25	21	2
F2N-51L-4	20.75	3.5	2
M2N-52-1	22	53	8.5
M2N-52-2	22.5	39.5	9
M2N-52-3	22.5	17.75	9.25

X from CL pier (E+);Y from joint (N+); Z from bottom of section			
Gage	X	Y	Z
W2N-22L-1	198	43	10
W2N-22L-2	198	22	10
W2N-32L-1	135.5	43	9.5
W2N-32L-2	135.75	21.5	9.5
W2N-42L-1	80	41.75	9.5
W2N-42L-2	79.5	21.25	9.5
W2N-52L-1	21.5	55.5	9.5
W2N-52L-2	22.75	35.25	9.5
W2N-52L-3	24	20.5	9.5
M2N-34L-2	136.5	21.5	6
W2N-5MV-1a	3.5	58	5.5
W2N-5MV-2a	7.5	58	5.5
W2N-1MV-1b	269.5	58	6
C2N-31L-1	136.75	36.5	2.75
C2N-31L-2	136.75	7	2.75

X from CL pier (E+);Y from joint (N+); Z from bottom of section			
Gage	X	Y	Z
F2S-21L-1	197.5	-45	1.75
F2S-21L-2	198.5	-21	1.75
F2S-21L-3	199	-3.5	2
F2S-31L-1	139.5	-45	2
F2S-31L-2	140	-21	1.75
F2S-31L-3	141.5	-3.25	2
F2S-41L-1	79	-44.75	1.75
F2S-41L-2	79.5	-21	1.75
F2S-41L-3	79.5	-3	2
F2S-51L-1	23	-57	2
F2S-51L-2	22.5	-45.25	2
F2S-51L-3	22.5	-21.25	1.75
F2S-51L-4	22.5	-3	2
W2S-22L-1	198	-43	9
W2S-22L-2	197.75	-22	9.25
W2S-32L-1	138.5	-42.25	9.25
W2S-32L-2	139.5	-21.5	9.25
W2S-42L-1	19	-42	9.25
W2S-42L-2	79.5	-21.25	9.5
W2S-52L-1	23.5	-56	9.25
W2S-52L-2	23.5	-36	9.5
W2S-52L-3	23.5	-21.5	9.5

X from CL pier (E+);Y from joint (N+); Z from bottom of section			
Gage	X	Y	Z
M2S-34L-2	138.5	-21.5	5.5
C2S-31L-1	140.5	-36	2.75
C2S-31L-2	141	-7	2.5
W2S-1MV-1a	168.5	-58	6
W2S-1MV-2a	266.5	-58	6.25
W2S-5MV-1c	5.25	-49	7
W2S-5MV-1d	5.5	-58	7.25
W2S-5MV-2c	7.5	-49	7
W2S-5MV-2d	7.5	-58	7.25
M2S-52L-1	20	-53.5	9.25
M2S-52L-2	20	-39.5	9.5
M2s-52L-3	20	-18.5	9.5

X from pier end of beam; Y from joint side of beam; Z from bottom of beam			
Gage	X	Y	Z
R1N-11L-1	266.25	60	7
R1N-11V-1	266.25	60	7
R1N-11S-1	266.25	60	7
R1N-51L-1	2.75	60	6.5
R1N-51V-1	2.75	60	6.5
R1N-51S-1	2.75	60	6.5
R1S-11L-1	266.75	60	6.25
R1S-11V-1	266.75	60	6.25
R1S-11S-1	266.75	60	6.25
R1S-51L-1	3.25	60	6.25
R1S-51V-1	3.25	60	6.25
R1S-51S-1	3.25	60	6.25
R2N-51L-1	2.5	60	7.5
R2N-51V-1	2.5	60	7.5
R2N-51S-1	2.5	60	7.5
R2N-11L-1	267.5	60	7
R2N-11V-1	267.5	60	7
R2N-11S-1	267.5	60	7
R2S-11L-1	265	60	7
R2S-11V-1	265	60	7
R2S-11S-1	265	60	7
R2S-51L-1	2.75	60	7.25
R2S-51V-1	2.75	60	7.25
R2S-51S-1	2.75	60	7.25

X from pier end of beam; Y from joint side of beam; Z from bottom of beam			
Gage	X	Y	Z
F1N-1MV-1a	267	58.25	6.75
F1N-1MV-2a	265	58.25	6.75
W1N-5MV-1b	2.25	57.5	6.5
W1S-1MV-1c	266.5	49.5	7.5
W1S-1MV-1d	266.75	58	5.5
W1S-1MV-2c	264.5	49.5	7.5
W1S-1MV-2d	264.75	58	5.5
W1S-5MV-1a	2.25	58	5.75
W1S-5MV-2a	3.5	58	5.75
W2N-5MV-1a	1	58	5.5
W2N-5MV-2a	5	58	5.5
W2N-1MV-1b	267	58	6
W2S-1MV-1a	266	58	6
W2S-1MV-2a	264	58	6.25
W2S-5MV-1c	2.75	49	7
W2S-5MV-1d	3	58	7.25
W2S-5MV-2c	5	49	7
W2S-5MV-2d	5	58	7.25

Appendix D

Concept 2 Large-Scale Laboratory Bridge Instrumentation Designation, Nominal, and Measured Locations

D.1 Concept 2 Laboratory Specimen Instrumentation Designation

The instrumentation for the concept 2 laboratory specimen was labeled as described in this section. An example designation is given in Figure D.1.

1. The first character indicated the type of gage.
   - C = VW concrete embedment gage
   - T = Strand resistive gage
   - M = Polyester Mold concrete resistive gage
   - P = Polyester Wire surface resistive gage
   - S = VW spot-weldable gage
   - V = 120Ω waterproof resistive gage
   - W = 350Ω waterproof resistive gage

2. The second character indicated the span number. There was only one span in this bridge, however this digit was maintained to facilitate comparison with the instrumentation in the Concept 1 bridge. This value was 1 for every instrument in the Concept 2 bridge.

3. The third character indicated the precast section within the span in which the gage was located.
   - N = North precast section
   - S = South precast section
   - J = Joint

There was a hyphen after the third character.

4. The fourth character indicated the position of the gage along the precast section.
   - 1.0 = East end of span
   - 1.5 = 1/8th point of the span
   - 2.0 = 1/4 point of the span
   - 2.5 = 3/8th point of the span
   - 3.0 = 1/2 point, or mid-span
   - 3.5 = 5/8th point of the span
   - 4.0 = 3/4 point of the span
   - 4.5 = 7/8th point of the span
   - 5.0 = West end of the span

There was a hyphen separating the fourth and fifth characters

5. The fifth character indicated where the gage was located in the depth of the cross section. Numerical values representing the depth start at the bottom of the section and increase towards the top of the section.

a.) For longitudinal instrumentation:

i. 0.5 = Gage was located on the bottom face of the precast unit
ii. 1.0 = Gage was located on the bottom prestressing strand
iii. 2.0 = Gage was located above the precast flange
iv. 2.5 = Gage was located below the precast web
v. 3.0 = Gage was located above the precast web
vi. 3.5 = Gage was located near the top surface of the member

b.) For transverse instrumentation:

i. 1.0 = Gage was located above precast flange at same depth as transverse hooked reinforcement
ii. 1.5 = Gage was located at mid-height of cage stirrup
iii. 2.0 = Gage was located above precast web

6. The sixth character indicated the orientation of the gage.

- L = Longitudinal
- T = Transverse

There was a hyphen after the sixth character.

7. The seventh character indicated the number of the gage at that position.

a.) For longitudinal instrumentation

i. 1 = For gages located closest to the outside flange (farthest away from the interior precast joint)

iii. n = For gages located nearest to the inside joint

b.) For transverse instrumentation

i. 1 = For gage located farthest south in gage group

iii. n = For gage located farthest north in gage group

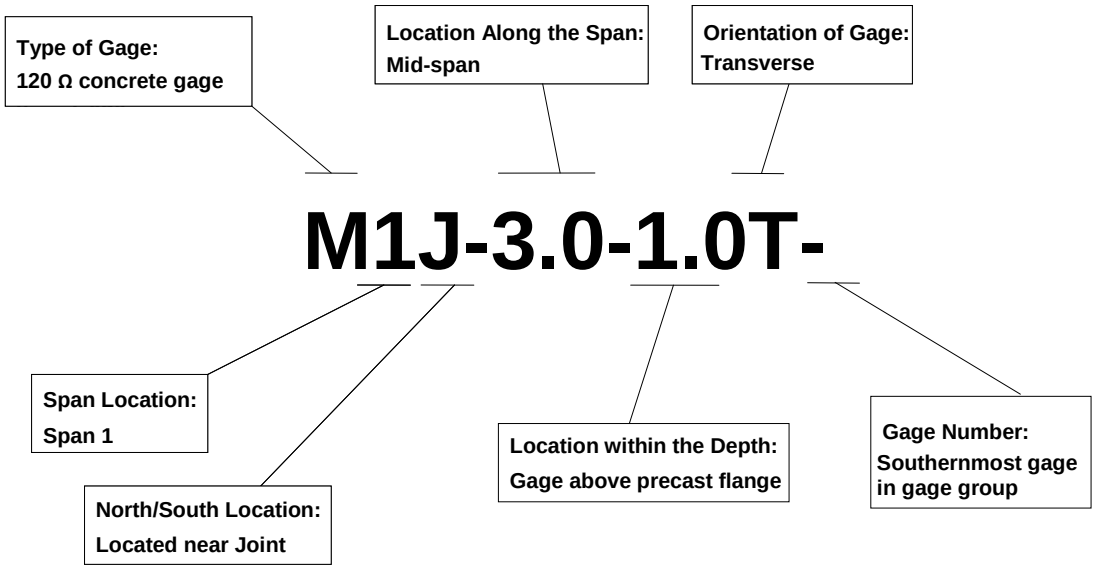

Figure D.1: Concept 2 Laboratory specimen strain gage designation example

D.2 Measured Locations of Concept 2 Laboratory Specimen Instrumentation

All of the instrumentation in the laboratory specimen was measured to the nearest ¼ in. The sign convention of the gage ordinates is shown in Figure D.2. The X axis was measured in the E-W direction from the centerline of the pier (E positive), which was located 2 in. from the end face of the precast unit and corresponded to the center of the concrete pier. The instrumentation in the Concept 2 bridge was designed to correspond with the naming convention utilized in the Concept 1 bridge, where there was a 4 in. gap between the two spans at the concrete pier. The Y ordinate was measured in the N-S direction from the joint (N positive); the Z axis was measured in the vertical direction from the bottom of the precast sections (upward positive). The measurements are given in Table D.1.

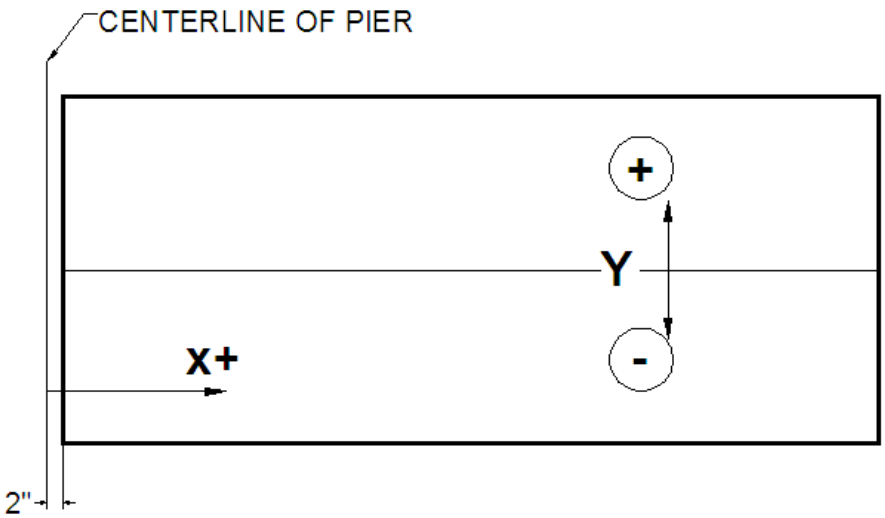

Figure D.2: Sign convention for the strain gage location measurements in the Concept 1 Laboratory Bridge

Table D.1: Global gage locations for instruments in the Concept 2 laboratory bridge specimen (in.)

X from CL pier (E+); Y from joint (N+); Z from bottom of section						
	Nominal Locations			Measured Locations		
Gage	X	Y	Z	X	Y	Z
7/8th point of the span						
T1J-4.5a-1.0T-1	51.75	0	4.5	52.25	0	4.75
M1J-4.5b-1.0T-1	49	0	4.5	49.25	0	4.75
M1J-4.5c-1.0T-1	45	-4.5	4.5	46	-4.5	4
M1J-4.5c-1.0T-2	42.5	0	4.5	42.25	0	4.75
M1J-4.5c-1.0T-3	45	4.5	4.5	45.75	4.5	4.25
M1J-4.5c-1.5T-1	45	-4.5	8.0	46	-4.5	8.25
M1J-4.5c-1.5T-2	42.5	0	8.0	42.25	0	8.5
M1J-4.5c-1.5T-3	45	4.5	8.0	46.25	4.5	8.5
M1J-4.5d-1.0T-1	38.75	0	4.5	39.25	0	4.25
T1J-4.5e-1.0T-1	35.75	0	4.5	34.5	0	4.75
3/4 point of the span (west quarter point)						
M1J-4.0-1.0T-1	81	-4.5	4.5	81.25	-4.5	4
M1J-4.0-1.0T-2	78.5	0	4.5	77.75	0	4
M1J-4.0-1.0T-3	81	4.5	4.5	81.5	4.5	4.25
M1J-4.0-1.5T-1	81	-4.5	8.0	81.5	-4.5	7.25
M1J-4.0-1.5T-2	78.5	0	8.0	78.25	0	7.75
M1J-4.0-1.5T-3	81	4.5	8.0	80.75	4.5	7.75
M1J-4.0-2.0T-1	81	-4.5	14.0	81.5	-4.5	13.75
M1J-4.0-2.0T-2	78.5	0	14.0	78.25	0	13.5
M1J-4.0-2.0T-3	81	4.5	14.0	81.75	4.5	13.75
S1J-4.0-1.0T-1	70.5	0	4.5	75.25	0	4.75
C1J-4.0-1.0T-1	75	0	4.5	76.5	0	4.5
5/8th point of the span						
T1J-3.5a-1.0T-1	105.75	0	4.5	105.75	0	4.75
M1J-3.5b-1.0T-1	103	0	4.5	103.25	0	4.5
M1J-3.5c-1.0T-1	99	-4.5	4.5	99.75	-4.5	4.25
M1J-3.5c-1.0T-2	96.5	0	4.5	96.75	0	4
M1J-3.5c-1.0T-3	99	4.5	4.5	99.5	4.5	4.25
M1J-3.5c-1.5T-1	99	-4.5	8.0	100	-4.5	7.5
M1J-3.5c-1.5T-2	96.5	0	8.0	96.5	0	7.5
M1J-3.5c-1.5T-3	99	4.5	8.0	100	4.5	8.5
M1J-3.5d-1.0T-1	92.75	0	4.5	92.5	0	4
T1J-3.5e-1.0T-1	89.75	0	4.5	89.75	0	4.75

X from CL pier (E+); Y from joint (N+); Z from bottom of section						
	Nominal Locations			Measured Locations		
Gage	X	Y	Z	X	Y	Z
1/2 point of the span (midspan)						
M1J-3.0-1.0T-1	135.75	-4.5	4.5	136.5	-4.5	4.5
M1J-3.0-1.0T-2	133.25	0	4.5	133.25	0	4.5
M1J-3.0-1.0T-3	135.75	4.5	4.5	136.5	4.5	4.75
M1J-3.0-1.5T-1	135.75	-4.5	8.0	136.75	-4.5	7.75
M1J-3.0-1.5T-2	133.25	0	8.0	133.25	0	8.25
M1J-3.0-1.5T-3	135.75	4.5	8.0	136.75	4.5	8
M1J-3.0-2.0T-1	135.75	-4.5	14.0	136.75	-4.5	13.5
M1J-3.0-2.0T-2	133.25	0	14.0	133.5	0	14
M1J-3.0-2.0T-3	135.75	4.5	14.0	136.25	4.5	13.5
S1J-3.0-1.0T-1	141.75	0	4.5	139.5	0	5
C1J-3.0-1.0T-1	137.5	0	4.5	134.5	0	4.25
3/8th point of the span						
T1J-2.5a-1.0T-1	177.75	0	4.5	178.25	0	4.75
M1J-2.5b-1.0T-1	175	0	4.5	175.5	0	4.5
M1J-2.5c-1.0T-1	171	-4.5	4.5	171	-4.5	4.25
M1J-2.5c-1.0T-2	168.5	0	4.5	168	0	4.5
M1J-2.5c-1.0T-3	171	4.5	4.5	171	4.5	4.5
M1J-2.5c-1.5T-1	171	-4.5	8.0	171	-4.5	8
M1J-2.5c-1.5T-2	168.75	0	8.0	167.75	0	8.5
M1J-2.5c-1.5T-3	171	4.5	8.0	170.75	4.5	8.25
M1J-2.5d-1.0T-1	164.75	0	4.5	165	0	4.75
T1J-2.5ae-1.0T-1	161.75	0	4.5	162	0	4.75
1/4 point of the span (east quarter point)						
M1J-2.0-1.0T-1	189	-4.5	4.5	189.25	-4.5	4
M1J-2.0-1.0T-2	186.5	0	4.5	187.75	0	4.25
M1J-2.0-1.0T-3	189	4.5	4.5	189.25	4.5	4.25
M1J-2.0-1.5T-1	189	-4.5	8.0	189.25	-4.5	8
M1J-2.0-1.5T-2	186.5	0	8.0	186.75	0	8
M1J-2.0-1.5T-3	189	4.5	8.0	189.5	4.5	7.5
M1J-2.0-2.0T-1	189	-4.5	14.0	190.5	4.5	13.75
M1J-2.0-2.0T-2	186.5	0	14.0	187	0	13.75
M1J-2.0-2.0T-3	189	4.5	14.0	190.25	-4.5	13.5
S1J-2.0-1.0T-1	196	0	4.5	200.75	0	5
C1J-2.0-1.0T-1	193	0	4.5	185	0	4.25

X from CL pier (E+); Y from joint (N+); Z from bottom of section						
	Nominal Locations			Measured Locations		
Gage	X	Y	Z	X	Y	Z
1/8th point of the span						
T1J-1.5a-1.0T-1	232.25	0	4.5	233.5	0	4.75
M1J-1.5b-1.0T-1	229	0	4.5	229.25	0	4
M1J-1.5c-1.0T-1	225	-4.5	4.5	226.5	-4.5	4.25
M1J-1.5c-1.0T-2	222.5	0	4.5	222.5	0	4.5
M1J-1.5c-1.0T-3	225	4.5	4.5	226.25	4.5	4.25
M1J-1.5c-1.5T-1	225	-4.5	8.0	227	-4.5	8.5
M1J-1.5c-1.5T-2	222.5	0	8.0	222.5	0	8.75
M1J-1.5c-1.5T-3	225	4.5	8.0	226.75	4.5	8
M1J-1.5d-1.0T-1	218.75	0	4.5	219.25	0	4.5
T1J-1.5e-1.0T-1	215.5	0	4.5	215.75	0	4.75

X from CL pier (E+); Y from joint (N+); Z from bottom of section						
	Nominal Locations			Actual Locations		
Gage	X	Y	Z	X	Y	Z
M1N-3.5-3.0L-2	104.5	21	14.0	110	23	13.75
M1N-3.5-3.5L-2	104.5	21	16.0	111.5	23	15.5
M1N-3.5-2.0L-2	104.5	21	5.0	108	22.5	4.75
M1N-3.5-2.5L-2	104.5	21	9.5	108.75	22.25	9.5
M1N-3.5-3.0L-1	106	44	14.0	110.5	44.5	13.5
M1N-3.5-3.5L-1	106	44	16.0	110.5	44.5	15.5
M1N-3.5-2.0L-1	106	44	5.0	107.75	44.25	4.75
M1N-3.5-2.5L-1	106	44	9.5	108	44	9.75
M1N-3.5-2.0L-3	106	3	4.5	106.5	4	6
M1N-3.5-2.5L-3	106	3	8.0	106.5	4	10.5
M1N-3.5-3.0L-3	106	3	14.0	109.5	4	14
M1N-3.5-3.5L-3	106	3	16.0	110	4	15.5
M1N-2.0-3.0L-2	181.5	21	14.0	181.75	21.5	13.5
M1N-2.0-3.5L-2	181.5	21	16.0	181.75	21.5	15.5
M1N-2.0-2.0L-2	181.5	21	5.0	182	21	4.5
M1N-2.0-2.5L-2	181.5	21	9.5	182.5	21	9.25
M1N-2.0-3.0L-1	181.5	45	14.0	182	45.75	13.5
M1N-2.0-3.5L-1	181.5	45	16.0	182.5	45.75	15.5
M1N-2.0-2.0L-1	181.5	45	5.0	182.25	45.25	4.75
M1N-2.0-2.5L-1	181.5	45	9.5	182.5	45	9.5
M1N-2.0-2.0L-3	181.5	3	4.5	182.5	1.75	6.25
M1N-2.0-2.5L-3	181.5	3	8.0	182.5	2.25	10.25
M1N-2.0-3.0L-3	181.5	3	14.0	182.5	3	14
M1N-2.0-3.5L-3	181.5	3	16.0	182.5	3	15.5
M1S-3.5-3.0L-2	107.5	21	14.0	111	22.75	13.25
M1S-3.5-3.5L-2	107.5	21	16.0	111	22.75	15.25
M1S-2.0-2.0L-2	107.5	21	5.0	107	21.25	5.5
M1S-2.0-2.5L-2	107.5	21	9.5	107.75	21.75	9.75

Appendix E

Large-Scale Laboratory Bridge and Subassemblage Core Analysis

E.1 Introduction to Coring Analysis

Several core samples were removed from the large-scale bridge and subassemblage specimens to investigate the presence of internal reflective cracking. The cores were analyzed initially by the naked eye, and subsequently with the aid of a microscope. Prior to being examined, the cores were prepped, which included rinsing them lightly under water, wiping them gently to remove any remaining sludge from the coring process, and patting them dry with paper towels. The cores were reassembled if broken in multiple sections, and the general characteristics of the core were documented (e.g. core height, diameter, and number of sections). The cores were initially examined without the use of the stereomicroscope. Any readily visible cracks observed using only a magnifying glass and a bright light were marked, which will be described later in this section. When it became too difficult to observe the crack by this method, the cores were placed under the viewing objective of the stereomicroscope and examined further for cracks.

The stereomicroscope employed to examine the cores was an Olympus Stereomicroscope SZX12, made available for use by the University of Minnesota's Institute of Technology Characterization Facility. In addition, an Olympus DP10 digital camera was used to take photos of specimens under the viewing objective. The stereomicroscope level of magnification used to examine the cores ranged between 2.1X to 27X magnification. The cores were first typically examined using a magnifying glass before being placed under the stereomicroscope. When a crack was identified, the core was placed under the microscope and the entire visible length of the crack was located using a magnification anywhere from 10X to 27X. To assist in locating the cracks, telescoping lights were positioned such that the cracks were easier to locate. Figure E.1 shows the stereomicroscope and indicates where the digital camera and telescoping lights were mounted.

Once a crack was identified under the microscope, it was marked using a dotted line of red ink along the visible length of the crack, as shown in Figure E.2. A crack gage was used to measure the crack widths along the length of the crack. The measured crack widths were indicated on the surface of the core with pencil, as shown in Figure E.3, along the length of the crack according to the crack width classification categories defined in Table E.1. The orientation, depth, and type of the crack were documented on a supplementary form. During examination of the cores, visible cracks were the only item of the core that was located and marked. In addition, the examination also included looking for indications of potential crack location. Most commonly, these notes referred to location and orientation of an inclined plane between two sections of a broken core because these planes may indicate that a crack was present prior to the sections breaking apart.

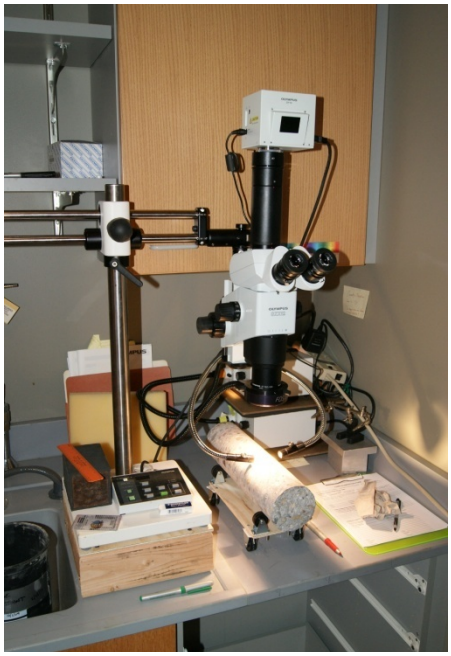

Figure E1: Photograph of Olympus Stereomicroscope SZX12 used for core analysis

Figure E2: Identified crack marked on core specimen using red ink

Figure E3: Crack widths marked on core specimen in pencil

Table E1: Crack width classification categories

Crack Classification	Crack Width (W)
0.002[1]	W < 0.002”
A	0.002” ≤ W < 0.008”
B	0.008” ≤ W < 0.023”
C	0.023” ≤ W < 0.200”
D	W ≥ 0.200”

[1]Cracks classified as having width < 0.002” are shown simply with a “2” in Table G2.

E2: Tabulation of Cracking in Cores

Cracking was tabulated for each core specimen. Reflective cracking was measured from a reference line that corresponded with the precast flange – CIP interface, as shown in Figure E4. The tabulated crack measurements are outlined in Table E2.

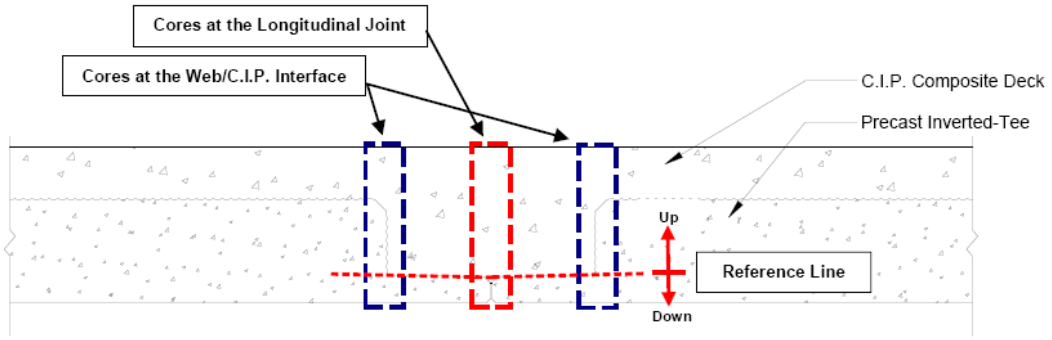

Figure E4: Location of reference line for measurement of vertical location of cracking in core specimens

Table E2: Tablation of characteristics of core samples

Core Designation					Core Characteristics	Reflective Crack Characteristics			
Specimen[1]	X-Coord.[2]	Y-Coord.[3]	Location of Core	Side of Longitudinal Joint	Core Diameter	Distance from Longitudinal Joint or Web/C.I.P. interface	Side of Core	Depth of Crack[4]	Width of Crack[5]
C1-S1	26	0	Longitudinal Joint	N/A	2 ¾" S.C.[6]	N.O.[7]	N.O.[7]	N.O.[7]	N.O.[7]
C1-S1	134	0	Longitudinal Joint	N/A	2 ¾" S.C.[6]	N.O.[7]	N.O.[7]	N.O.[7]	N.O.[7]
C1-S1	192	2	Longitudinal Joint	North	2 ¾" S.C.[6]	N.O.[7]	N.O.[7]	N.O.[7]	N.O.[7]
C1-S1	197.5	0	Longitudinal Joint	N/A	2 ¾" S.C.[6]	1/8" South 1/8" South	West East	2 ¾" (up) 1 ¼" (up)	**A**: 0"-1 ¼"; 2: 1 ¼"-2 ¾" 2: 0"-1 ¼"
C1-S1	-194.5	0	Longitudinal Joint	N/A	1 ¾"	½" North ½" North	West East	Undefined[8]	Undefined[8]
C1-S2	74	0	Longitudinal Joint	N/A	1 ¾"	N.O.[7]	N.O.[7]	N.O.[7]	N.O.[7]
C1-S2	146	0	Longitudinal Joint	N/A	1 ¾"	N.O.[7]	N.O.[7]	N.O.[7]	N.O.[7]
C1-S2	195.5	0	Longitudinal Joint	N/A	1 ¾"	N.O.[7]	N.O.[7]	N.O.[7]	N.O.[7]
C1-S2	198	0	Longitudinal Joint	N/A	1 ¾"	N.O.[7]	N.O.[7]	N.O.[7]	N.O.[7]
C2-2.0	193	0	Longitudinal Joint	N/A	3 ¾"	N.O.[7]	N.O.[7]	N.O.[7]	N.O.[7]
C2-2.0	193	12	Web/C.I.P. Interface	North	3 ¾"	0" 0"	West East	3 ¼" 1 ½"	2: ¼"-1"; **A**: 1"-2 ¼"; 2: 2 ¼"-3 ½" 2: 1 ¼" – 1 ½"
C2-2.0	193	12	Web/C.I.P. Interface	South	3 ¾"	0"	North	(0")[9]	2: (entire length)
C2-4.0	76	0	Longitudinal Joint	N/A	3 ¾"	N.O.[7]	N.O.[7]	N.O.[7]	N.O.[7]
C2-4.0	76	12	Web/C.I.P. Interface	North	3 ¾"	N.O.[7]	N.O.[7]	N.O.[7]	N.O.[7]
C2-4.0	76	12	Web/C.I.P. Interface	South	3 ¾"	N.O.[7]	N.O.[7]	N.O.[7]	N.O.[7]

Core Designation					Core Characteristics	Reflective Crack Characteristics			
Specimen[1]	X-Coord.[2]	Y-Coord.[3]	Location of Core	Side of Longitudinal Joint	Core Diameter	Distance from Longitudinal Joint or Web/C.I.P. interface	Side of Core	Depth of Crack[4]	Width of Crack[5]
SSMBLG 1	31.5	0	Longitudinal Joint	N/A	2 ¾"	¾" East 1 ¼" East	North South	7 ½" (up) 6" (up)	(North) **C**: 0"-1"; **B**: 1"-2"; **A**: 2"-3 ½"; **B**: 3 ½"-4 ½"; **A**: 4 ½"-5"; **2**: 5"-7 ½" (South) **C**: 0"-1"; **B**: 1"-1 ¼"; **2**: 1 ¼"-1 ½"; **A**: 1 ½"-1 ¾"; **C**: 1 ¾"-2 ¼"; **B**: 2 ¼"-2 ¾"; **A**: 2 ¾"-3 ½"; **B**: 3 ½"-4 ½"; **A**: 4 ½"-5"; **2**: 5"-6"
SSMBLG 1	31.5	12	Web/C.I.P. Interface	East	2 ¾"	0" 0"	North South	7" (up); 3"(down) 7" (up); 3"(down)	**A**: 0"-¾"; **2**: ¾"-7" (up); **A**: 0"-1"; **B**: 1"-3" (down) **A**: 0"-1"; **2**: 1"-7" (up); **B**: 0"-3" (down)
SSMBLG 1	31.5	12	Web/C.I.P. Interface	West	2 ¾"	N.O.[7]	N.O.[7]	N.O.[7]	N.O.[7]
SSMBLG 2	33.5	0	Longitudinal Joint	N/A	2 ¾"	¾" West ¾" West	North South	7 ¼" 7"	**B**: 0"-2 ¼"; **A**: 2 ¼"-3 ¼"; **2**: 3 ¼"-4"; **A**: 4"-7 ¼" **B**: 0"-2" **A**: 2"- 2 ¾"; **B**: 2 ¾"-3 ¼"; **A**: 3 ¼"-5 ¾"; **2**: 5 ¾"-7"
SSMBLG 2	33.5	12	Web/C.I.P. Interface	East	2 ¾"	N.O.[7]	N.O.[7]	N.O.[7]	N.O.[7]
SSMBLG 2	33.5	12	Web/C.I.P. Interface	West	2 ¾"	N.O.[7]	N.O.[7]	N.O.[7]	N.O.[7]
SSMBLG 3	28	0	Longitudinal Joint	N/A	2 ¾"	¾" (West) 1" (West)	North South	9 ½" 9 ¼"	***B.P.[10]: 0"-6 ½"***; **A**: 6 ½"- 8 ½"; **2**: 8 ½"- 9 ½" ***B.P.[10]: 0"-6 ½"***; **A**: 6 ½"- 7"; **B**: 7"-8 ½"; **A**: 8 ½"- 8 ¼"; **2**: 8 ¾"- 9 ¼"
SSMBLG 3	28	12	Web/C.I.P. Interface	West	2 ¾"	N.O.[7]	N.O.[7]	N.O.[7]	N.O.[7]
SSMBLG 4	31.5	0	Longitudinal Joint	N/A	2 ¾"	1" West 1 ¾" West	North South	11 ¼" 10 ¾"	(North) **A**: 0"- ½"; **B**: ½"-1 ½"; **A**: 1 ½"-3 ½"; **B**: 3 ½"-7 ¼"; **2**: 7 ¼"-8 ¾"; **A**: 8 ¾"-9"; **2**: 9"-11 ¼" (South) **B**: 0"-1 ¼"; **A**: 1 ¼"-1 ¾"; **B**: 1 ¾"-5"; **A**: 5"-5 ½"; **B**: 5 ½"-7 ¼"; **2**: 7 ¼"-8"; **A**: 8"-8 ¾"; **2**: 8 ¼"-10 ¾"
SSMBLG 4	31.5	12	Web/C.I.P. Interface	East	2 ¾"	¼" West ¼" West	North South	10 ¼" (up), 3" (down) 10 ¾" (up), 3" (down)	***BP[10]: 0"-6"***; **A**: 6"-6 ½"; **2**: 6 ½"-10 ¼" (up); ***B.P.[10]: 0"-3"***; **B**: 1"-2 ½" (down) ***B.P.[10]: 0"-6"***; **A**: 6"-7 ¾"; **2**: 7 ¾"-10 ¾" (up); ***B.P.[10]: 0"-3"*** (down)
SSMBLG 4	31.5	12	Web/C.I.P. Interface	West	2 ¾"	0" 0"	North South	10 ¾" 10 ¾"	***B.P.[10]: 0"-10 ¾"***; **2**: 10 ¼"-10 ¾" ***B.P.[10]: 0"-9 ½"***; **A**: 9 ½"-10"; **2**: 10"-10 ¾"
SSMBLG 5	28	1	Longitudinal Joint	East	2 ¾"	1 ½" East 1 ¾" East	North South	7 ½" 4"	**B**: 0"- ½"; **A**: ½"-1 ¼"; **B**: 1 ¼"-1 ¾"; **A**: 1 ¾"-4"; **2**: 4"-7 ½" **A**: 0"- ½"; **B**: ½"-1 ½"; **A**: 1 ½"-2 ¾"; **2**: 2 ¾"-4"
SSMBLG 5	31.5	0	Longitudinal Joint	N/A	2 ¾"	N.O.[7]	N.O.[7]	N.O.[7]	N.O.[7]
SSMBLG 5	31.5	12	Web/C.I.P. Interface	East	2 ¾"	0" 0"	North South	7" (up); 1 ½" (down) 7" (up); ¾" (down)	**2**: 0"-7" (up); **2**: 0"-1 ½" (down) **2**: 0"-7" (up); **2**: 0"-¾" (down)
SSMBLG 5	31.5	12	Web/C.I.P. Interface	West	2 ¾"	0" 0"	North South	1" (down) 1" (down)	**A**: 0"- ½"; **2**: ½"-1" **A**: 0"- ½"; **2**: ½"-1"

Core Designation					Core Characteristics	Reflective Crack Characteristics			
Specimen[1]	X-Coord.[2]	Y-Coord.[3]	Location of Core	Side of Longitudinal Joint	Core Diameter	Distance from Longitudinal Joint or Web/C.I.P. interface	Side of Core	Depth of Crack[4]	Width of Crack[5]
SSMBLG 6	32	0	Longitudinal Joint	N/A	2 ¾"	¾" East 1 ½" East	North South	1 ¾" 2 ¾"	2: 0"-1 ¾" **A**: 0"-1 ¾"; 2: 1 ¾"-2 ¼"
SSMBLG 6	32	12	Web/C.I.P. Interface	East	2 ¾"	0" 0"	North South	8" (up); 2" (down) 7" (up); 1 ½" (down)	(North) **B**: 0"-2 ½"; **A**: 2 ½"-4 ½"; 2: 4 ½"-8" (up); **B**: 0"-1 ½"; 2: 1 ½"-2" (down) (South) **B**: 0"-1 ¼"; **A**: 1 ¼"-4 ¼"; 2: 4 ¼"-7" (up); **B**: 0"-1 ½" (down)
SSMBLG 6	32	12	Web/C.I.P. Interface	West	2 ¾"	0" 0"	North South	¾" ¾"	2: 0"- ¾" 2: 0"- ¾"
SSMBLG 7	28.5	0	Longitudinal Joint	N/A	2 ¾"	N.O.[7]	N.O.[7]	N.O.[7]	N.O.[7]
SSMBLG 7	31.5	0	Longitudinal Joint	N/A	2 ¾"	N.O.[7]	N.O.[7]	N.O.[7]	N.O.[7]
SSMBLG 7	31.5	12	Web/C.I.P. Interface	East	2 ¾"	N.O.[7]	N.O.[7]	N.O.[7]	N.O.[7]
SSMBLG 7	31.5	12	Web/C.I.P. Interface	West	2 ¾"	N.O.[7]	N.O.[7]	N.O.[7]	N.O.[7]

[1] C1" represents "Concept 1 Bridge Specimen"; "S1" represents "Span 1"; "S2" represents "Span 2"; SSMBLG" represents "Subassemblage Bridge Specimen"

[2] Distance along the longitudinal joint referenced from side of specimen, (inches)

[3] Distance perpendicular to and referenced from the longitudinal joint (inches)

[4] Depth of crack measured up (unless specified otherwise) from the reference line indicated in the Longitudinal Joint Elevation Figure.

[5] Width of crack, classifications (bold font) defined by Table XY, ranging between depths from the reference point defined on the Bridge Specimen - Longitudinal Joint Elevation Figure.

[6] "S.C." indicates that core was split into two half-diameter cores due to a "Saw Cut" made during the demolition of the bridge specimen

[7] "N.O." represents "No Reflective Cracks Observed"

[8] Reflective crack is continuous with shrinkage crack from surface, so beginning and end points are undefined

[9] Reflective crack lies along precast flange/C.I.P. interface (i.e. reflective crack has no vertical depth)

[10] "B.P." represents that this is actually a "Break Plane" between two sections of the core that is likely to have been a reflective crack prior to breaking apart. It is not an in-situ reflective crack.

.

Appendix F

Subassemblage Sectional Calculations and Analyses

F.1: Subassemblage Specimen Design Calculations and Analyses

The subassemblage specimens utilized during the current study were primarily considered to provide a comparison of the benefits of particular crack control details relative to one another. To provide an understanding of the expected behavior of each specimen based on its individual measured material properties, geometry, and reinforcement details, a detailed analytical investigation was completed. The relevant calculations are outlined below.

Sectional calculations for subassemblage specimens

Specimen dimensions and variables are defined in plan and elevation views of the subassemblage specimens in Figures F.1 and F.2, respectively. As shown in Figure F.1, each subassemblage specimen was 120 in. “long”, which corresponded with the span length during the load tests while the width of each specimen, which was measured parallel to the longitudinal precast joint, ranged from 62.75 in. to 67.25 in. The origin of each specimen, for reference regarding the instrumentation and reinforcement placement, as well as general documentation, was located on the bottom of the section, directly at the precast joint. The origin corresponded with the end of each specimen nearest the embedded transverse reinforcement that was spaced a clear distance of 3 in. from the face, which was consistent among each of the seven subassemblage specimens, and is also shown in Figure F.2.

As illustrated in Figure F.2, the total section depth is composed of the precast member depth, which was either 12 in. or 16 in., plus a 2 in. thick deck for all specimens other than SSMBLG3-HighBars, which had a 2 in. thick deck near the joint region, and tapered to 3-1/2 in. a distance of 15 in. in either direction from the joint.

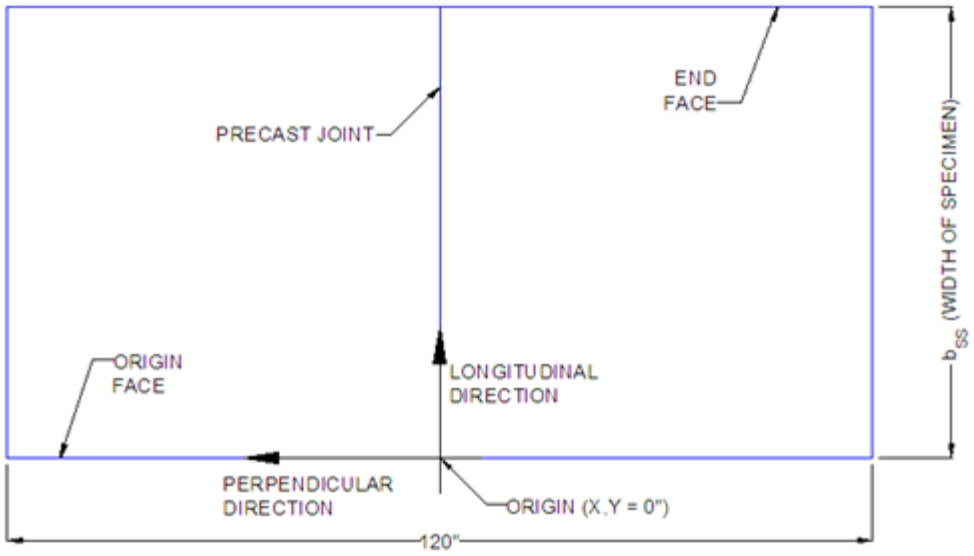

Figure F1: Plan view of subassemblage specimens

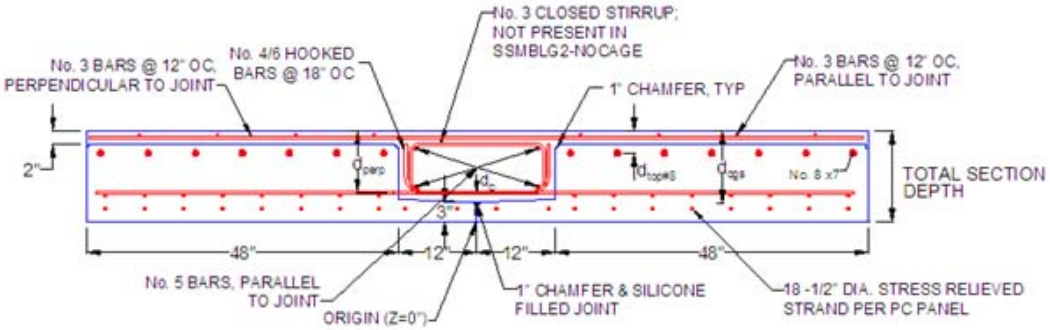

(a) Subassemblage section view perpendicular to joint

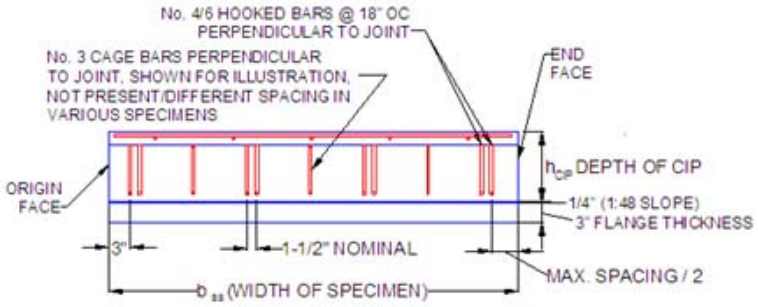

(b) Subassemblage section view parallel to joint

Figure F2: Subassemblage specimen section views

Note: The index number in each array represents the subassemblage specimen number. For example, subassemblage 1 will always be represented as the first entry in any array variable

Useful units:

$kip := 1000lbf$ $ksi := \frac{kip}{in^2}$ Specimen range variable: $i := 1 .. 7$

Specimen naming includes specimen number - description - maximum distance between perpendicular reinforcement immediately above the precast joint

$Specimens_i :=$

"1-Control1-9in."
"2-NoCage-18in."
"3-HighBars-9in."
"4-Deep-9in."
"5-No.6Bars-9in."
"6-Frosch-4.5in."
"7-Control2-9in."

Material Properties

Measured material properties have been documented herein. Values were measured on the first day of laboratory testing for each specimen

CIP Elastic modulus: tensile strength via 3 point beam test: concrete compressive strength:

$E_{cSS_i} :=$

4740ksi
5633ksi
3933ksi
4703ksi
4112ksi
5270ksi
4194ksi

$f_{t_i} :=$

.840ksi
.746ksi
.678ksi
.757ksi
.609ksi
.806ksi
.732ksi

$f_{c_i} :=$

6552psi
6577psi
4726psi
7151psi
5204psi
6898psi
7005psi

Steel elastic modulus: $E_s := 29000ksi$

Specimen and reinforcement geometry and layout

A_{shook} equals the area of a single perpendicular hooked bar

A_{scage} equals the area of all horizintally oriented legs of the stirrups in the cage at a given level, i.e.: all the horizontal legs of the stirrups at the bottom of the trough

b_{ss} equals nominal width, perpendicular to joint, of specimen

h_{cip} equals the nominal depth of CIP concrete between top of precast flange at the joint and the top of the specimen

d_{shook} equals the nominal depth of the hooks oriented perpendicular to joint, measured from top of specimen to center of reinforcement, also used as depth of lower horizontal leg of cage reinforcement

$d_{toplegofcage}$ equals the nominal depth of the center of the top horizontal leg of the cage reinforcement from the top of the specimen

d_{sdeck} equals the nominal depth of the center of the deck reinforcement oriented perpendidcular to the joint from the top of the speceimen

$A_{shook_i} :=$

$.2in^2$
$.2in^2$
$.2in^2$
$.2in^2$
$.44in^2$
$.2in^2$
$.2in^2$

$A_{scage_i} :=$

$.33in^2$
$0in^2$
$.33in^2$
$.33in^2$
$.33in^2$
$1.43in^2$
$.33in^2$

Area of No. 3 mild reinforcement:

$A_3 := 0.11in^2$

$b_{ss_i} :=$

62.75in
67.25in
62.75in
62.75in
62.75in
64.0in
62.75in

$h_{cip_i} :=$

11in
11in
11in
15in
11in
11in
11in

$d_{shook_i} :=$

9.75in
9.75in
7in
13.75in
9.6875in
9.75in
9.75in

$d_{sdeck} := 1.5625in$

$d_{toplegofcage} := 2.25in$

Location of uncracked and cracked netural axis

Method of transformed sections is utilized to calculate neutral axis (NA) location, the modular ratio is the ratio of the elastic modulus of the steel to the elastic modulus of the concrete

$$n_i := \frac{E_s}{E_{cSS_i}} \qquad n = \begin{pmatrix} 6.1 \\ 5.1 \\ 7.4 \\ 6.2 \\ 7.1 \\ 5.5 \\ 6.9 \end{pmatrix}$$

Depth of neutral axis is measured from top surface of each specien, as follows:

$$A_{total} \cdot \bar{x} = \sum_i \left[(n - 1) A_s \cdot d_s + A_{concrete} \cdot d_{concrete} \right]$$

Black box in upper right corner of equation indicates that the equation is not evaluated; only shown for illustration of method of calculation

Uncracked

$$x_{uncracked_i} := \frac{\frac{b_{ss_i} \cdot \left(h_{cip_i}\right)^2}{2} + \left(n_i - 1\right) \cdot \left[\begin{pmatrix} 8\, A_{shook_i} + A_{scage_i} \end{pmatrix} \cdot d_{shook_i} + A_{scage_i} \cdot d_{toplegofcage} \cdots \right]}{b_{ss_i} \cdot h_{cip_i} + \left(n_i - 1\right) \cdot \left(8\, A_{shook_i} + 2\, A_{scage_i} + 5 A_3\right)}$$

$$x_{uncracked} = \begin{pmatrix} 5.54 \\ 5.53 \\ 5.5 \\ 7.54 \\ 5.61 \\ 5.54 \\ 5.54 \end{pmatrix} \cdot in$$

Cracked

Neutral axis depth is calculated as above; the depth of the concrete in compression is equal to the neutral axis depth, therefore a quadratic equation must be solved. The coefficients of the quadratic equation are as follows:

The cracked transformed section is shown in Figure 3:

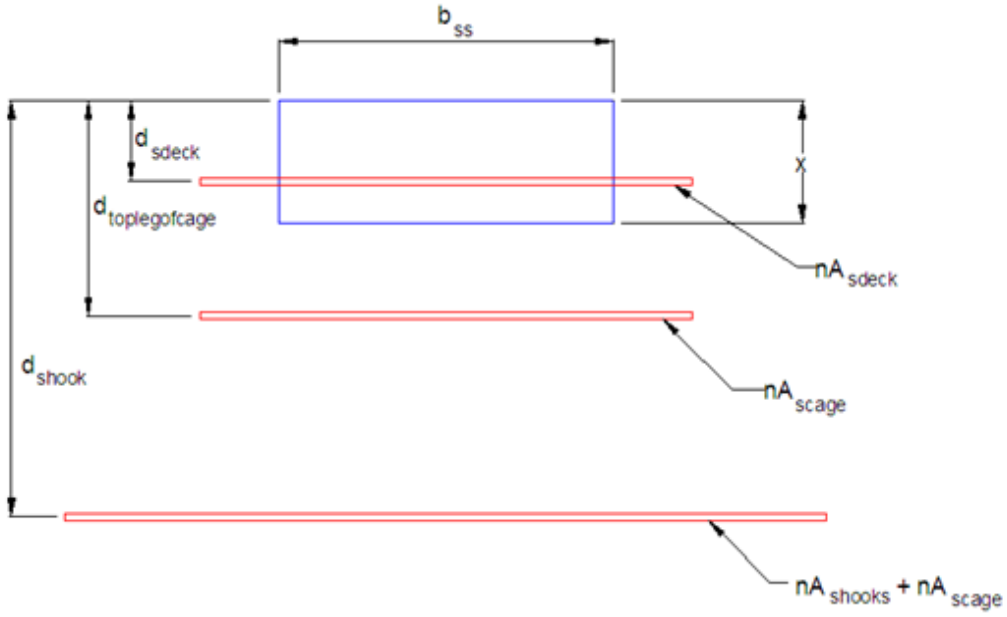

Figure F3: Cracked transformed section, with neutral axis, *x*, measured from top of section

The area of the deck reinforcement should be subtracted from the total area of the section by multiplying by (n-1) if x is greater than d_{sdeck}, but should not be subtracted if x less than d_{sdeck}. Assume that the netural axis is larger than the depth of the deck reinforcement:

quadratic equation for neutral axis depth (x): $Ax^2 + Bx + C = 0$

$$A = \frac{b_{ss_i}}{2}$$

$$B = n_i \cdot \left(8\, A_{shook_i} + 2\, A_{scage_i}\right) + \left(n_i - 1\right) \cdot 5 \cdot A_3$$

$$C = -\left[n_i \cdot \left(8\, A_{shook_i} + A_{scage_i}\right) \cdot d_{shook_i} + n_i \cdot A_{scage_i} \cdot d_{toplegofcage} + \left(n_i - 1\right) \cdot 5 \cdot A_3 \cdot d_{sdeck}\right]$$

The polyroots function is used to evaluate the parabolic function for each specimen. The polyroots function takes the coefficients A,B, and C and returns, for a parabolic function, two roots. Let the matrix *Coeffs* be the matrix of coefficients, with each column representing a subassemblage specimen:

$$\text{Coeffs} := \left| \begin{array}{l} M \leftarrow 0 \\ \text{for } i \in 1..7 \\ \quad \left| \begin{array}{l} M_{3,i} \leftarrow \dfrac{b_{ss_i}}{2} \\ M_{2,i} \leftarrow \left[n_i \cdot \left(8\,A_{shook_i} + 2\,A_{scage_i} \right) + \left(n_i - 1 \right) \cdot \left(5A_3 \right) \right] \cdot \dfrac{1}{in} \\ M_{1,i} \leftarrow -\left[\begin{array}{l} n_i \cdot \left[\left(8\,A_{shook_i} + A_{scage_i} \right) \cdot d_{shook_i} \right] + n_i \cdot \left(A_{scage_i} \cdot d_{toplegofcage} \right) \cdots \\ + \left(n_i - 1 \right) \cdot 5A_3 \cdot d_{sdeck} \end{array} \right] \cdot \dfrac{1}{in^2} \end{array} \right. \\ \text{return } M \end{array} \right.$$

$$\text{Coeffs} = \begin{pmatrix} -124.1 & -83.9 & -110.6 & -172.7 & -273.5 & -184.1 & -140.3 \\ 16.6 & 10.5 & 20.2 & 16.8 & 32.8 & 27 & 18.9 \\ 31.4 & 33.6 & 31.4 & 31.4 & 31.4 & 32 & 31.4 \end{pmatrix} \cdot in$$

<-- constant term
<-- linear term
<-- parabolic term

Evaluating the polyroots function returns two roots, the second root, denoted by the subscript 2 after the polyroots function, is the positive root for each case, which is saved to the variable $x_{cracked}$

$$x_{cracked_i} := \text{polyroots}\left(\text{Coeffs}^{\langle i \rangle} \right)_2 \cdot in$$

$$x_{cracked} = \begin{pmatrix} 1.74 \\ 1.43 \\ 1.58 \\ 2.09 \\ 2.48 \\ 2.01 \\ 1.84 \end{pmatrix} \cdot in$$

Check assumption that the depth of the deck reinforcement is less than the depth of the neutral axis:

$$NAcheck_i := \left| \begin{array}{ll} \text{"OK"} & \text{if } x_{cracked_i} > d_{sdeck} \\ \text{"NG"} & \text{if } x_{cracked_i} < d_{sdeck} \end{array} \right.$$

$$d_{sdeck} = 1.563 \cdot in$$

$$NAcheck = \begin{pmatrix} \text{"OK"} \\ \text{"NG"} \\ \text{"OK"} \\ \text{"OK"} \\ \text{"OK"} \\ \text{"OK"} \\ \text{"OK"} \end{pmatrix}$$

Reclaculate the depth of the neutral axis with the area of the deck reinforcement not subtracted from the total area of the section when the deck reinforcement is below the neutral axis depth

$$\begin{aligned}
&\text{Coeffs} := \left|\begin{array}{l}
M \leftarrow 0 \\
\text{for } i \in 1..7 \\
\quad \left|\begin{array}{l}
M_{3,i} \leftarrow \dfrac{b_{ss_i}}{2} \\
M_{2,i} \leftarrow \left[n_i \cdot \left(8\,A_{shook_i} + 2\,A_{scage_i}\right) + \left|\begin{array}{ll} \left(n_i \cdot 5A_3\right) & \text{if } x_{cracked_i} < d_{sdeck} \\ \left[\left(n_i - 1\right)\cdot 5\cdot A_3\right] & \text{if } x_{cracked_i} > d_{sdeck} \end{array}\right| \right] \cdot \dfrac{1}{in} \\
M_{1,i} \leftarrow -\left[n_i \cdot \left[\left(8\,A_{shook_i} + A_{scage_i}\right)\cdot d_{shook_i}\right] + n_i \cdot \left(A_{scage_i} \cdot d_{toplegofcage}\right) \cdots \right] \cdot \dfrac{1}{in^2} \\
\qquad + \left|\begin{array}{ll} \left(n_i \cdot 5\cdot A_3 \cdot d_{sdeck}\right) & \text{if } x_{cracked_i} < d_{sdeck} \\ \left[\left(n_i - 1\right)\cdot 5\cdot A_3 \cdot d_{sdeck}\right] & \text{if } x_{cracked_i} > d_{sdeck} \end{array}\right|
\end{array}\right. \\
&\text{return } M
\end{array}\right.
\end{aligned}$$

$$\text{Coeffs} = \begin{pmatrix} -124.1 & -84.7 & -110.6 & -172.7 & -273.5 & -184.1 & -140.3 \\ 16.6 & 11.1 & 20.2 & 16.8 & 32.8 & 27 & 18.9 \\ 31.4 & 33.6 & 31.4 & 31.4 & 31.4 & 32 & 31.4 \end{pmatrix} \cdot in$$

<-- constant term
<-- linear term
<-- parabolic term

Evaluating the polyroots function returns two roots, the second root, denoted by the subscript 2 after the polyroots function, is the positive root for each case, which is saved to the variable $x_{cracked}$

$$x_{cracked_i} := \text{polyroots}\left(\text{Coeffs}^{\langle i \rangle}\right)_2 \cdot in$$

$$x_{cracked} = \begin{pmatrix} 1.74 \\ 1.43 \\ 1.58 \\ 2.09 \\ 2.48 \\ 2.01 \\ 1.84 \end{pmatrix} \cdot in$$

Moment of Inertia

The moment of inertia of the section is the moment of inertia of the individual components about centroid of component plus area of component multiplied by the distance to centroid of section squared (parallel axis theorem). Assume reinforcement contributes only the portion defined by the parallel axis theorem:

$$I_{section} = \sum_{components} I_{component} + A_{component} \cdot distance^2$$

Uncracked

$$I_{uncracked_i} := \frac{1}{12} b_{ss_i} \cdot \left(h_{cip_i}\right)^3 + b_{ss_i} \cdot h_{cip_i} \cdot \left(\left| \frac{h_{cip_i}}{2} - x_{uncracked_i} \right|\right)^2 \cdots + \left(n_i - 1\right) \left[\begin{array}{l} 8\, A_{shook_i} \left(\left| d_{shook_i} - x_{uncracked_i} \right| \right)^2 \cdots \\ + \left(A_{scage}\right)_i \left(\left| d_{shook_i} - x_{uncracked_i} \right| \right)^2 \cdots \\ + A_{scage_i} \cdot \left(\left| d_{toplegofcage} - x_{uncracked_i} \right| \right)^2 \cdots \\ + 5 \cdot A_3 \cdot \left(\left| d_{sdeck} - x_{uncracked_i} \right| \right)^2 \end{array} \right]$$

$$I_{uncracked} = \begin{pmatrix} 7199 \\ 7614 \\ 7064 \\ 18184 \\ 7433 \\ 7450 \\ 7236 \end{pmatrix} \cdot in^4$$

Cracked

$$I_{cracked_i} := \frac{1}{12} b_{ss_i} \left(x_{cracked_i}\right)^3 + b_{ss_i} \cdot x_{cracked_i} \cdot \left(\left| \frac{x_{cracked_i}}{2} - x_{cracked_i} \right|\right)^2 \dots$$
$$+ n_i \cdot \left[8 A_{shook_i} \cdot \left(\left| d_{shook_i} - x_{cracked_i} \right|\right)^2 + A_{scage_i} \cdot \left(\left| d_{shook_i} - x_{cracked_i} \right|\right)^2 \dots \right] \dots$$
$$+ A_{scage_i} \cdot \left(\left| d_{toplegofcage} - x_{cracked_i} \right|\right)^2$$
$$+ \begin{cases} \left[n_i \cdot 5 \cdot A_3 \cdot \left(\left| d_{sdeck} - x_{cracked_i} \right|\right)^2 \right] & \text{if } x_{cracked_i} < d_{sdeck} \\ \left[\left(n_i - 1\right) \cdot 5 \cdot A_3 \cdot \left(\left| d_{sdeck} - x_{cracked_i} \right|\right)^2 \right] & \text{if } x_{cracked_i} > d_{sdeck} \end{cases}$$

$$I_{cracked} = \begin{pmatrix} 868 \\ 636 \\ 502 \\ 1810 \\ 1732 \\ 1173 \\ 966 \end{pmatrix} \cdot in^4$$

Curvature

$$M_{crack_i} := \frac{f_{t_i} \cdot I_{uncracked_i}}{h_{cip_i} - x_{uncracked_i}} \qquad M_{crack} = \begin{pmatrix} 1107 \\ 1038 \\ 870 \\ 1845 \\ 840 \\ 1099 \\ 970 \end{pmatrix} \cdot in \cdot kip$$

Flexural capacity of specimen. Because the transverse hooks are not continuous into both adjacent precast sections, consider only half of the transverse hooks and none of the reinforcing cage

Calculate β_1 for each specimen, β_1 is a function of the concrete strength, rounded to the nearest thousand:

$$rounded\_f_{c_i} := round\left(f_{c_i} \cdot \frac{1}{psi}, -3\right) \qquad rounded\_f_{c_i} = \begin{pmatrix} 7000 \\ 7000 \\ 5000 \\ 7000 \\ 5000 \\ 7000 \\ 7000 \end{pmatrix}$$

$$\beta 1_i := \begin{cases} 0.85 & \text{if } rounded\_f_{c_i} \le 4000 \\ \left[0.85 - 0.05 \cdot \frac{\left(rounded\_f_{c_i} - 4000\right)}{1000}\right] & \text{if } rounded\_f_{c_i} > 4000 \\ 0.65 & \text{if } rounded\_f_{c_i} > 8000 \end{cases} \qquad \beta 1 = \begin{pmatrix} 0.70 \\ 0.70 \\ 0.80 \\ 0.70 \\ 0.80 \\ 0.70 \\ 0.70 \end{pmatrix}$$

$$M_{flexure_i} := 4\, A_{shook_i} \cdot 60ksi \cdot \left(d_{shook_i} - \frac{\beta 1_i \cdot x_{cracked_i}}{2}\right) \qquad M_{flexure} = \begin{pmatrix} 439 \\ 444 \\ 306 \\ 625 \\ 918 \\ 434 \\ 437 \end{pmatrix} \cdot in \cdot kip$$

$$\phi_{uncracked_i} := \frac{M_{crack_i}}{E_{cSS_i} \cdot I_{uncracked_i}} \qquad \phi_{uncracked} = \begin{pmatrix} 0.000032 \\ 0.000024 \\ 0.000031 \\ 0.000022 \\ 0.000027 \\ 0.000028 \\ 0.000032 \end{pmatrix} \cdot \frac{1}{in}$$

The same moment is applied immediately before and after cracking:

$$\phi_{cracked_i} := \frac{M_{crack_i}}{E_{cSS_i} \cdot I_{cracked_i}} \qquad \phi_{cracked} = \begin{pmatrix} 0.000269 \\ 0.00029 \\ 0.000441 \\ 0.000217 \\ 0.000118 \\ 0.000178 \\ 0.00024 \end{pmatrix} \cdot \frac{1}{in}$$

Compare results, normalized by the Control 1 specimen:

$$\frac{x_{uncracked_i}}{x_{uncracked_1}} = \begin{pmatrix} 1.000 \\ 0.998 \\ 0.993 \\ 1.362 \\ 1.013 \\ 1.000 \\ 1.001 \end{pmatrix} \qquad \frac{x_{cracked_i}}{x_{cracked_1}} = \begin{pmatrix} 1.000 \\ 0.822 \\ 0.909 \\ 1.203 \\ 1.422 \\ 1.157 \\ 1.054 \end{pmatrix}$$

$$\frac{I_{uncracked_i}}{I_{uncracked_1}} = \begin{pmatrix} 1.000 \\ 1.058 \\ 0.981 \\ 2.526 \\ 1.032 \\ 1.035 \\ 1.005 \end{pmatrix} \qquad \frac{I_{cracked_i}}{I_{cracked_1}} = \begin{pmatrix} 1.000 \\ 0.732 \\ 0.578 \\ 2.084 \\ 1.995 \\ 1.351 \\ 1.112 \end{pmatrix}$$

$$\frac{\phi_{uncracked_i}}{\phi_{uncracked_1}} = \begin{pmatrix} 1.000 \\ 0.746 \\ 0.966 \\ 0.665 \\ 0.847 \\ 0.863 \\ 0.986 \end{pmatrix} \qquad \frac{\phi_{cracked_i}}{\phi_{cracked_1}} = \begin{pmatrix} 1.000 \\ 1.077 \\ 1.641 \\ 0.806 \\ 0.438 \\ 0.661 \\ 0.891 \end{pmatrix}$$

Appendix G

Subassemblage Instrumentation Designation, Nominal, and Measured Locations

G.1 Subassemblage Specimen Instrumentation Designation

The instrumentation for the subassemblage specimens was labeled as described in this section. An example designation is given in Figure G.1.

1. The first character indicated the specimen and type of gage. The specimen was labeled as SSLGX, where 'X' was the specimen number. The gage types are listed below:

- C = VW concrete embedment gage
- T = Steel resistive gage
- M = Polyester Mold concrete resistive gage
- S = VW spot-weldable gage

There was a hyphen after the first character.

2. The second character indicated the position of the gage along the length of the precast joint

- 2.0 = Origin face of specimen
- 3.0 = 1/2 point, or middle of specimen measured along length of joint

There was a hyphen separating the fourth and fifth characters

3. The third character indicated where the gage was located in the depth of the cross section. Numerical values representing the depth start at the bottom of the section and increase towards the top of the section.

i. 1.0 = Gage was located above precast flange at same depth as transverse hooked reinforcement
ii. 1.5 = Gage was located at mid-height of cage stirrup
iii. 2.0 = Gage was located above precast web

4. The fourth character indicated the orientation of the gage. All gages were oriented transversely, or perpendicular to the precast joint.

- T = Transverse

There was a hyphen after the sixth character.

7. The seventh character indicated the number of the gage at that position.

ii. 1 = For gage located farthest south in gage group

iv. n = For gage located farthest north in gage group

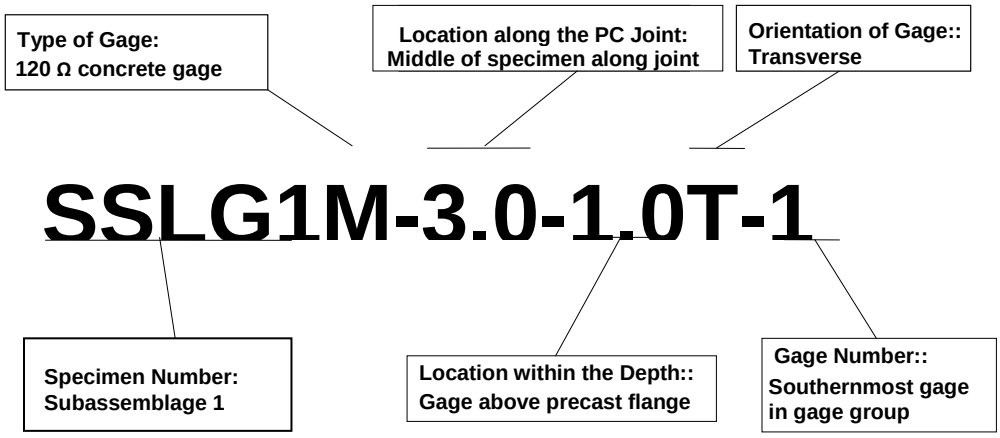

Figure G.1: Subassemblage specimen strain gage designation example

G.2 Measured Locations of Subassemblage Specimen Instrumentation

All of the instrumentation in the subassemblage specimens was measured to the nearest ¼ in. The sign convention of the gage ordinates is shown in Figure G.2. The X axis (which was defined to be the North direction) was measured along the length of the precast joint from the origin face, which was defined to be the face where the transverse hooked reinforcement was always 3 in. away; Y was measured in the E-W direction from the joint (W positive); the Z axis was measured in the vertical direction from the bottom of the precast sections (upward positive). The measurements are given in Table G.1.

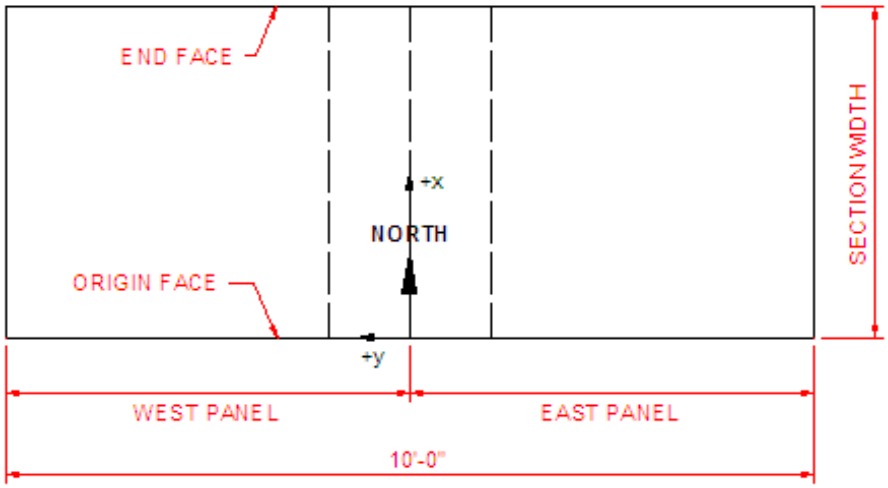

Figure G.2: Sign convention for the strain gage location measurements in the Concept 1 Laboratory Bridge

Table G.1: Nominal and measured instrumentation locations in the subassemblage specimens

X from edge (N+); Y from joint (W+); Z from bottom of section						
Gage	Nominal Locations			Measured Locations		
	X	Y	Z	X	Y	Z
Resistive gages located near middle cross section						
SSLG1M-3.0-1.0T-1	33.5	-4.5	4.5	33.25	-4.5	4.25
SSLG1M-3.0-1.0T-2	30.5	0	4.5	29.5	0	4.25
SSLG1M-3.0-1.0T-3	33.5	4.5	4.5	33	4.5	4
SSLG1M-3.0-1.5T-1	33.5	-4.5	8	33.5	-4.5	9
SSLG1M-3.0-1.5T-2	30.5	0	8	29.5	0	9.25
SSLG1M-3.0-1.5T-3	33.5	4.5	8	33.25	4.5	9.25
SSLG1M-3.0-2.0T-1	33.5	-4.5	14	33.5	-4.5	11.75
SSLG1M-3.0-2.0T-2	30.5	0	14	28.75	0	12
SSLG1M-3.0-2.0T-3	33.5	4.5	14	33.5	4.5	12
Resistive gages located near origin cross section						
SSLG1Ta-2.0-1.0T-1	23	0	4.5	23	0	4
SSLG1Mb-2.0-1.0T-1	18	0	4.5	18	0	4.25
SSLG1Mc-2.0-1.0T-1	15.5	-4.5	4.5	16.25	-4.5	4.25
SSLG1Mc-2.0-1.0T-2	12.5	0	4.5	12.75	0	4.25
SSLG1Mc-2.0-1.0T-3	15.5	4.5	4.5	16.25	4.5	4.25
SSLG1Mc-2.0-1.5T-1	15.5	-4.5	8	16.75	-4.5	8.25
SSLG1Mc-2.0-1.5T-2	12.5	0	8	12.5	0	9.25
SSLG1Mc-2.0-1.5T-3	15.5	4.5	8	16.5	4.5	8.5
SSLG1Md-2.0-1.0T-1	9	0	4.5	9	0	4.25
SSLG1Te-2.0-1.0T-1	5	0	4.5	5	0	4
Vibrating wire gage located near middle cross section						
SSLG1C-3.0-1.0T-1	34	0	4.5	34.25	0	4.5

X from edge (N+); Y from joint (W+); Z from bottom of section						
Gage	Nominal Locations			Measured Locations		
	X	Y	Z	X	Y	Z
Gages located near middle cross section						
SSLG2M-3.0-1.0T-1	33.5	-4.5	4.5	33.75	-4.5	4.5
SSLG2M-3.0-1.0T-2	30.5	0	4.5	30.75	0	4.75
SSLG2M-3.0-1.0T-3	33.5	4.5	4.5	33.5	4.5	4.5
SSLG2M-3.0-1.5T-1	33.5	-4.5	8	33.5	-4.5	6.75
SSLG2M-3.0-1.5T-2	30.5	0	8	30.5	0	6.25
SSLG2M-3.0-1.5T-3	33.5	4.5	8	33.5	4.5	6.5
SSLG2M-3.0-2.0T-1	33.5	-4.5	14	33.75	-4.5	9.75
SSLG2M-3.0-2.0T-2	30.5	0	14	21	0	9.5
SSLG2M-3.0-2.0T-3	33.5	4.5	14	33.5	4.5	9.5
Gages located near origin cross section						
SSLG2Ta-2.0-1.0T-1	23	0	4.5	22.75	0	4
SSLG2Mb-2.0-1.0T-1	18	0	4.5	18.75	0	4.25
SSLG2Mc-2.0-1.0T-1	15.5	-4.5	4.5	15.5	-4.5	4.5
SSLG2Mc-2.0-1.0T-2	12.5	0	4.5	12.25	0	4.25
SSLG2Mc-2.0-1.0T-3	15.5	4.5	4.5	15	4.5	4.25
SSLG2Mc-2.0-1.5T-1	15.5	-4.5	8	15.75	-4.5	7.25
SSLG2Mc-2.0-1.5T-2	12.5	0	8	12.5	0	7.25
SSLG2Mc-2.0-1.5T-3	15.5	4.5	8	15.25	4.5	7.25
SSLG2Md-2.0-1.0T-1	9	0	4.5	8.75	0	4.5
SSLG2Te-2.0-1.0T-1	5	0	4.5	4.75	0	4
Vibrating wire gage located near middle cross section						
SSLG2C-3.0-1.0T-1	34	0	4.5	35.5	0	4.5

X from edge (N+); Y from joint (W+); Z from bottom of section						
Gage	Nominal Locations			Measured Locations		
	X	Y	Z	X	Y	Z
Gages located near middle cross section						
SSLG3M-3.0-1.0T-1	33.5	-4.5	4.5	33.5	-4.5	4.25
SSLG3M-3.0-1.0T-2	30.5	0	4.5	29.75	0	4
SSLG3M-3.0-1.0T-3	33.5	4.5	4.5	33	4.5	4.25
SSLG3M-3.0-1.5T-1	33.5	-4.5	8	33.25	-4.5	7.5
SSLG3M-3.0-1.5T-2	30.5	0	8	30.75	0	8.25
SSLG3M-3.0-1.5T-3	33.5	4.5	8	31.75	4.5	8.25
SSLG3M-3.0-2.0T-1	33.5	-4.5	14	33.25	-4.5	13.5
SSLG3M-3.0-2.0T-2	30.5	0	14	29.5	0	14.25
SSLG3M-3.0-2.0T-3	33.5	4.5	14	33.5	4.5	15
Gages located near origin cross section						
SSLG3Ta-2.0-1.0T-1	23	0	4.5	22.5	0	4
SSLG3Mb-2.0-1.0T-1	18	0	4.5	18	0	4.25
SSLG3Mc-2.0-1.0T-1	15.5	-4.5	4.5	15	-4.5	4
SSLG3Mc-2.0-1.0T-2	12.5	0	4.5	13.25	0	4.5
SSLG3Mc-2.0-1.0T-3	15.5	4.5	4.5	15.75	4.5	4.25
SSLG3Mc-2.0-1.5T-1	15.5	-4.5	8	15.5	-4.5	7.75
SSLG3Mc-2.0-1.5T-2	12.5	0	8	13.25	0	8.25
SSLG3Mc-2.0-1.5T-3	15.5	4.5	8	15.75	4.5	8
SSLG3Md-2.0-1.0T-1	9	0	4.5	8.25	0	4.25
SSLG3Te-2.0-1.0T-1	5	0	4.5	5	0	4
Vibrating wire gage located near middle cross section						
SSLG3C-3.0-1.0T-1	34	0	4.5	33.5	0	4.25

X from edge (N+); Y from joint (W+); Z from bottom of section						
Gage	Nominal Locations			Measured Locations		
	X	Y	Z	X	Y	Z
Gages located near middle cross section						
SSLG4M-3.0-1.0T-1	33.5	-4.5	4.5	33.25	-4.5	4.5
SSLG4M-3.0-1.0T-2	30.5	0	4.5	30.5	0	4
SSLG4M-3.0-1.0T-3	33.5	4.5	4.5	33	4.5	4
SSMBLG4M-3.0-1.25T-2a	33.5	0	8	33.5	0	8.25
SSMBLG4M-3.0-1.25T-2b	30.5	0	8	29.75	0	8.25
SSLG4M-3.0-1.5T-1	33.5	-4.5	8	33.5	-4.5	10
SSLG4M-3.0-1.5T-2	30.5	0	8	30	0	10.25
SSLG4M-3.0-1.5T-3	33.5	4.5	8	33.25	4.5	9.75
SSLG4M-3.0-2.0T-1	33.5	-4.5	14	33.25	-4.5	15.5
SSLG4M-3.0-2.0T-2	30.5	0	14	29.75	0	15.74
SSLG4M-3.0-2.0T-3	33.5	4.5	14	33.5	4.5	15.5
Gages located near origin cross section						
SSLG4Ta-2.0-1.0T-1	23	0	4.5	23	0	4.25
SSLG4Mb-2.0-1.0T-1	18	0	4.5	18	0	4.5
SSLG4Mc-2.0-1.0T-1	15.5	-4.5	4.5	15.5	-4.5	4.25
SSLG4Mc-2.0-1.0T-2	12.5	0	4.5	12	0	4.5
SSLG4Mc-2.0-1.0T-3	15.5	4.5	4.5	15.25	4.5	4.5
SSLG4Mc-2.0-1.5T-1	15.5	-4.5	8	16	-4.5	10
SSLG4Mc-2.0-1.5T-2	12.5	0	8	11.25	0	10.5
SSLG4Mc-2.0-1.5T-3	15.5	4.5	8	15.75	4.5	9.75
SSLG4Md-2.0-1.0T-1	9	0	4.5	6.25	0	4.25
SSLG4Te-2.0-1.0T-1	5	0	4.5	4.75	0	4
Vibrating wire gage located near middle cross section						
SSLG4C-3.0-1.0T-1	34	0	4.5	34.75	0	4.5

X from edge (N+); Y from joint (W+); Z from bottom of section						
Gage	Nominal Locations			Measured Locations		
	X	Y	Z	X	Y	Z
Gages located near middle cross section						
SSLG5M-3.0-1.0T-1	33.5	-4.5	4.5	32.75	-4.5	4.25
SSLG5M-3.0-1.0T-2	30.5	0	4.5	31	0	4.25
SSLG5M-3.0-1.0T-3	33.5	4.5	4.5	32.5	4.5	4
SSLG5M-3.0-1.5T-1	33.5	-4.5	8	32.75	-4.5	8.5
SSLG5M-3.0-1.5T-2	30.5	0	8	30.25	0	8.25
SSLG5M-3.0-1.5T-3	33.5	4.5	8	32.5	4.5	8.5
SSLG5M-3.0-2.0T-1	33.5	-4.5	14	32.5	-4.5	13.75
SSLG5M-3.0-2.0T-2	30.5	0	14	29.75	0	14.5
SSLG5M-3.0-2.0T-3	33.5	4.5	14	33.25	4.5	14.5
Gages located near origin cross section						
SSLG5Ta-2.0-1.0T-1	23	0	4.5	23.75	0	4.25
SSLG5Mb-2.0-1.0T-1	18	0	4.5	18.5	0	4.25
SSLG5Mc-2.0-1.0T-1	15.5	-4.5	4.5	15.5	-4.5	4
SSLG5Mc-2.0-1.0T-2	12.5	0	4.5	12.25	0	4.5
SSLG5Mc-2.0-1.0T-3	15.5	4.5	4.5	15.25	4.5	4.25
SSLG5Mc-2.0-1.5T-1	15.5	-4.5	8	15.25	-4.5	8
SSLG5Mc-2.0-1.5T-2	12.5	0	8	12.75	0	8.25
SSLG5Mc-2.0-1.5T-3	15.5	4.5	8	16	4.5	8.25
SSLG5Md-2.0-1.0T-1	9	0	4.5	8.25	0	4.25
SSLG5Te-2.0-1.0T-1	5	0	4.5	4.5	0	4.25
Vibrating wire gage located near middle cross section						
SSLG5C-3.0-1.0T-1	34	0	4.5	34.5	0	4.25

X from edge (N+); Y from joint (W+); Z from bottom of section						
Gage	Nominal Locations			Measured Locations		
	X	Y	Z	X	Y	Z
Gages located near middle cross section						
SSLG6M-3.0-1.0T-1	33.5	-4.5	4.5	34.5	-4.5	4.5
SSLG6M-3.0-1.0T-2	30.5	0	4.5	30.5	0	4.25
SSLG6M-3.0-1.0T-3	33.5	4.5	4.5	34.75	4.5	4.25
SSLG6M-3.0-1.5T-1	33.5	-4.5	8	34.75	-4.5	6
SSLG6M-3.0-1.5T-2	30.5	0	8	30.25	0	7.5
SSLG6M-3.0-1.5T-3	33.5	4.5	8	34.75	4.5	6
SSLG6M-3.0-2.0T-1	33.5	-4.5	14	35	-4.5	11.75
SSLG6M-3.0-2.0T-2	30.5	0	14	31	0	11.75
SSLG6M-3.0-2.0T-3	33.5	4.5	14	35	4.5	11.5
Gages located near origin cross section						
SSLG6Ta-2.0-1.0T-1	23	0	4.5	23	0	4
SSLG6Mb-2.0-1.0T-1	18	0	4.5	18.5	0	4
SSLG6Mc-2.0-1.0T-1	15.5	-4.5	4.5	15	-4.5	4
SSLG6Mc-2.0-1.0T-2	12.5	0	4.5	13	0	4
SSLG6Mc-2.0-1.0T-3	15.5	4.5	4.5	15.25	4.5	4.25
SSLG6Mc-2.0-1.5T-1	15.5	-4.5	8	15.25	-4.5	7.25
SSLG6Mc-2.0-1.5T-2	12.5	0	8	12.5	0	7.5
SSLG6Mc-2.0-1.5T-3	15.5	4.5	8	15.25	4.5	7.75
SSLG6Md-2.0-1.0T-1	9	0	4.5	9.25	0	4
SSLG6Te-2.0-1.0T-1	5	0	4.5	5.25	0	4
Vibrating wire gage located near middle cross section						
SSLG6C-3.0-1.0T-1	34	0	4.5	32.5	0	4.5

X from edge (N+); Y from joint (W+); Z from bottom of section						
Gage	Nominal Locations			Measured Locations		
	X	Y	Z	X	Y	Z
Gages located near middle cross section						
SSLG7M-3.0-1.0T-1	33.5	-4.5	4.5	32.5	-4.5	4.25
SSLG7M-3.0-1.0T-2	30.5	0	4.5	30.25	0	4.5
SSLG7M-3.0-1.0T-3	33.5	4.5	4.5	32.5	4.5	4.25
SSLG7M-3.0-1.5T-1	33.5	-4.5	8	33	-4.5	7.5
SSLG7M-3.0-1.5T-2	30.5	0	8	30.75	0	8.25
SSLG7M-3.0-1.5T-3	33.5	4.5	8	32.5	4.5	8.25
SSLG7M-3.0-2.0T-1	33.5	-4.5	14	32	-4.5	11.75
SSLG7M-3.0-2.0T-2	30.5	0	14	30.5	0	12.25
SSLG7M-3.0-2.0T-3	33.5	4.5	14	32	4.5	12
Gages located near origin cross section						
SSLG7Ta-2.0-1.0T-1	23	0	4.5	23	0	4.25
SSLG7Mb-2.0-1.0T-1	18	0	4.5	17.75	0	4.25
SSLG7Mc-2.0-1.0T-1	15.5	-4.5	4.5	16	-4.5	4.25
SSLG7Mc-2.0-1.0T-2	12.5	0	4.5	12.25	0	4.5
SSLG7Mc-2.0-1.0T-3	15.5	4.5	4.5	16	4.5	4.25
SSLG7Mc-2.0-1.5T-1	15.5	-4.5	8	15.75	-4.5	8
SSLG7Mc-2.0-1.5T-2	12.5	0	8	12.5	0	7.5
SSLG7Mc-2.0-1.5T-3	15.5	4.5	8	16	4.5	7.5
SSLG7Md-2.0-1.0T-1	9	0	4.5	9	0	4.5
SSLG7Te-2.0-1.0T-1	5	0	4.5	5.25	0	4.5
Vibrating wire gage located near middle cross section						
SSLG7C-3.0-1.0T-1	34	0	4.5	34.5	0	4.25